PB-221 488

NUMERICAL THERMAL PLUME MODEL FOR VERTICAL OUTFALLS IN SHALLOW WATER

Donald S. Trent, et al

Oregon State University

Prepared for:

Environmental Protection Agency

March 1973

DISTRIBUTED BY:

NTIS

National Technical Information Service
U. S. DEPARTMENT OF COMMERCE
5285 Port Royal Road, Springfield Va. 22151

EPA-R2-73-162
MARCH 1973
W73-11333

Environmental Protection Technology Series

PB 221 488

Numerical Thermal Plume Model for Vertical Outfalls in Shallow Water

Reproduced by
NATIONAL TECHNICAL
INFORMATION SERVICE
U.S. Department of Commerce
Springfield VA 22151

Office of Research and Monitoring
U.S. Environmental Protection Agency
Washington, D.C. 20460

520

RESEARCH REPORTING SERIES

Research reports of the Office of Research and Monitoring, Environmental Protection Agency, have been grouped into five series. These five broad categories were established to facilitate further development and application of environmental technology. Elimination of traditional grouping was consciously planned to foster technology transfer and a maximum interface in related fields. The five series are:

1. Environmental Health Effects Research
2. Environmental Protection Technology
3. Ecological Research
4. Environmental Monitoring
5. Socioeconomic Environmental Studies

This report has been assigned to the ENVIRONMENTAL PROTECTION TECHNOLOGY series. This series describes research performed to develop and demonstrate instrumentation, equipment and methodology to repair or prevent environmental degradation from point and non-point sources of pollution. This work provides the new or improved technology required for the control and treatment of pollution sources to meet environmental quality standards.

/ ✓

SELECTED WATER RESOURCES ABSTRACTS

INPUT TRANSACTION FORM

1. Report No.

W 73-11333

Numerical Thermal Plume Model for Vertical Outfalls in Shallow Water,

(all caps)

5. Report Date

6.

8. Performing Organization Report No.

D~~onald~~ S. Trent and J~~ames~~ R. Welty

EPA Project 16130 DGM

~~16130 DGM~~

Department of Mechanical Engineering.
Oregon State University,
Corvallis, ~~Oregon~~, [illegible]

13. Type of Report and Period Covered

~~12. Sponsoring Organization Environmental Protection Agency~~

Environmental Protection Agency, Technology Series,
Report ~~Number~~, EPA-R2-73-162, March 1973. 78 p, 215 fig, 12 tab, 113 ref.

A theoretical study of the heat and momentum transfer resulting from a flow of power plant condenser effluent discharged vertically to shallow, quiescent coastal receiving water is presented. The complete partial differential equations governing steady, incompressible, turbulent flow driven by both initial momentum and buoyancy are solved using finite-difference techniques to obtain temperature and velocity distributions in the near field of the thermal discharge.

Turbulent quantities were treated through the use of Reynolds stresses with further simplification utilizing the concept of eddy diffusivities computed by Prandtl's mixing length theory. A Richardson number correlation was used to account for the effects of density gradients on the computed diffusivities.

Results were obtained for over 100 cases, 66 of which are reported, using the computer program presented ~~in this manuscript~~. These results ranged from cases of pure buoyancy to pure momentum and for receiving water depths from 1 to 80 discharge diameters deep. Various computed gross aspects of the flow were compared to published data and found to be in excellent agreement. Data for shallow water plumes and the ensuing lateral spread are not readily available; however, one computed surface temperature distribution was compared to proprietary data and found also to be in reasonable agreement. (EPA)

17a. Descriptors

*Waste ~~heat~~ water disposal, *heated ~~shallow discharge,~~ water, *turbulent ~~buoyant~~ flow, jets, temperature prediction, *thermal pollution, *Outfalls, Model studies, Water pollution control, *Heat transfer

17b. Identifiers

*Plume models

73-162

Copy available from GPO Sup Doc as EP 1.23/2: $4.80 ; microfiche from NTIS as PB 221 465, $0.95.

05B
05G

19. Security Class. (Report)

20. Security Class. (Page)

21. No. of Pages

22. Price

Send To:

WATER RESOURCES SCIENTIFIC INFORMATION CENTER
U.S. DEPARTMENT OF THE INTERIOR
WASHINGTON, D.C. 20240

Author	Oregon State University

ia

EPA-R2-73-162
March 1973

NUMERICAL THERMAL PLUME MODEL
FOR VERTICAL OUTFALLS IN SHALLOW WATER

By

Donald S. Trent
James R. Welty

Project 16130 DGM

Project Officer

Mostafa A. Shirazi
Environmental Protection Agency
National Environmental Research Center
Corvallis, Oregon 97330

Prepared for

OFFICE OF RESEARCH AND MONITORING
U.S. ENVIRONMENTAL PROTECTION AGENCY
WASHINGTON, D.C. 20460

For sale by the Superintendent of Documents, U.S. Government Printing Office, Washington, D.C. 20402
Price $4.80 domestic postpaid or $4.25 GPO Bookstore

EPA Review Notice

This report has been reviewed by the Environmental Protection Agency and approved for publication. Approval does not signify that the contents necessarily reflect the views and policies of the Environmental Protection Agency, nor does mention of trade names or commercial products constitute endorsement or recommendation for use.

ABSTRACT

A theoretical study of the heat and momentum transfer resulting from a flow of power plant condenser effluent discharged vertically to shallow, quiescent coastal receiving water is presented. The complete partial differential equations governing steady, incompressible, turbulent flow driven by both initial momentum and buoyancy are solved using finite-difference techniques to obtain temperature and velocity distributions in the near field of the thermal discharge.

Turbulent quantities were treated through the use of Reynolds stresses with further simplification utilizing the concept of eddy diffusivities computed by Prandtl's mixing length theory. A Richardson number correlation was used to account for the effects of density gradients on the computed diffusivities.

Results were obtained for over 100 cases, 66 of which are reported, using the computer program presented in this manuscript. These results ranged from cases of pure buoyancy to pure momentum and for receiving water depths from 1 to 80 discharge diameters deep. Various computed gross aspects of the flow were compared to published data and found to be in excellent agreement. Data for shallow water plumes and the ensuing lateral spread are not readily available; however, one computed surface temperature distribution was compared to proprietary data and found also to be in **reasonable agreement.**

This report was submitted in fulfillment of Grant No. 16130-DGM between the Environmental Protection Agency and the Department of Mechanical Engineering, Oregon State University.

TABLE OF CONTENTS

Page

CHAPTER 1. INTRODUCTION 1

1.1 Objectives 3

1.2 Summary 4

CHAPTER 2. DISCUSSION OF THERMAL PLUMES AND PROBLEM DESCRIPTION 7

2.1 The Nature of Thermal Plumes in Marine Surroundings 7

2.1.1 Discharge Magnitude 8

2.1.2 Outfall Configuration 10

2.1.3 Hydrodynamic Regimes 12

2.1.4 Oceanographic Effects 15

2.1.4.1 Density Stratification 17

2.1.4.2 Effect of Currents 18

2.1.4.3 Ocean Turbulence 21

2.1.4.4 Air-Sea Interactions 22

2.2 Plume Analysis State-of-the-Art 23

2.2.1 Submerged Outfalls 25

2.2.2 Horizontal Shoreline Outfalls 27

2.3 Work Description 28

CHAPTER 3. TRANSPORT EQUATIONS - GENERAL THEORY 30

3.1 Coordinate System 30

3.2 Conservation Laws 31

3.2.1 Continuity 33

3.2.2 The Equations of Motion for Turbulent Flow 34

3.3 The Boussinesq Approximation 36

Preceding page blank

3.4 The Pressure Equation 39

3.5 Γ Transport 40

3.5.1 Transport of Heat, Salinity and Buoyancy 40

3.6 The Equation of State for Sea Water 45

3.7 Vorticity Transport 47

3.8 Non-dimensional Form of the Equations of Motion 50

3.9 Further Comments on the Concept of "Eddy Viscosity" 53

3.10 Two-Dimensional Forms of the Transport Equations in Rectangular and Axisymmetric Coordinates 56

3.10.1 Two-Dimensional Transport Equations in Rectangular Geometry 58

3.10.2 Two-Dimensional Transport Equations in Axisymmetric Coordinates 62

CHAPTER 4. PLUME THEORY - SIMILARITY SOLUTIONS 65

4.1 General Description 65

4.2 Simplified Equations for a Vertical Plume 67

4.3 Radial Velocity and Temperature Profiles 71

4.3.1 Zone of Established Flow 71

4.3.2 Zone of Flow Establishment 74

4.4 Zone of Flow Establishment 76

4.5 Governing Differential Equations 77

4.5.1 Initial Condition 80

4.5.2 Evaluation of Terms Involving K and λ 81

4.5.3 Homogeneous Receiving Water 82

4.6 Lateral Velocity, u_r 83

CHAPTER 5. FINITE DIFFERENCE MODELS 84

5.1 Physical System for the Vertical Round Port 85

5.2 Governing Differential Equations 87

5.3 Vorticity Equations 90

5.4 Dimensionless Forms 92

5.5 Coordinate Transformation 94

5.6 Finite Difference Grid System 96

5.7 Difference Equations 100

  5.7.1 Stream Function and Velocity 100

  5.7.2 Transport Equations 103

  5.7.3 Summary of Required Difference Equations 108

5.8 Boundary Conditions 109

5.9 Rectangular Coordinates 132

  5.9.1 Governing Differential Equations 132

  5.9.2 Rectangular Difference Equations 135

  5.9.3 Rectangular Boundary Conditions 138

CHAPTER 6. CODE DESCRIPTION AND ORGANIZATION 141

6.1 Computational Procedure

6.2 Executive Program and Subroutine Description 143

6.3 Flow Charts 151

CHAPTER 7. CODE VERIFICATION AND NUMERICAL EXPERIMENTS 163

7.1 Deep Water Plumes 164

  7.1.1 The Momentum Jet 171

    7.1.1.1 Centerline Velocity and Concentration for Momentum Jets 172

    7.1.1.2 Spread of the Momentum Jet 189

    7.1.1.3 Radial Distribution of Vertical Velocity, Concentrations and Vorticity for the Momentum Jet 192

7.1.1.4 Distribution of Radial Velocity for the Momentum Jet 201

7.1.1.5 Typical Contours and Three-Dimensional Plots for a Momentum Jet 207

7.1.2 Two Cases of Pure Buoyancy 207

7.1.2.1 Centerline Velocity and Temperature 207

7.1.2.2 Spread of the Pure Buoyant Plume 218

7.1.2.3 Radial Distribution of Vertical Velocity, Temperature and Vorticity for Pure Buoyancy 220

7.1.2.4 Radial Velocity and Entrainment for Pure Buoyancy 228

7.1.3 Mixed Flow - Forced Plumes 237

7.1.3.1 Centerline Velocity and Temperature for Forced Plumes 237

7.1.3.2 Rate of Spread and Entrainment 251

7.2 Transport Coefficients 253

7.2.1 The Radial Transport Coefficient, ϵ_r 266

7.2.2 The Vertical Transport Coefficient, ϵ_Z 284

7.3 Numerical Stability and Convergence 298

7.3.1 Numerical Stability 299

7.3.2 Convergence 304

CHAPTER 8. NUMERICAL EXPERIMENTS FOR SHALLOW WATER CASES 319

8.1 Modeling the Vertical Eddy Diffisivity Multiplier, FZ 319

8.2 Results for Homogeneous Receiving Water 10 Port Diameters Deep 325

8.3 Results for Homogeneous Receiving Water 5 Port Diameters Deep 340

8.4 Results for Two Different Methods of Computing FZ 346

8.5 Numerical Experiments Involving Ambient Stratification 355

8.6 Discharge at Very Shallow Depth 376

8.7 Comparison with Field Data 382

CHAPTER 9. CONCLUSIONS 384

BIBLIOGRAPHY 389

APPENDIX A - CONVECTIVE TRANSPORT DIFFERENCE APPROXIMATION 400

APPENDIX B - FINITE DIFFERENCES FOR IRREGULAR NODE SPACING 415

APPENDIX C - COORDINATE TRANSFORMATION 419

APPENDIX D - SOME RELATIONSHIPS BETWEEN TIME DEPENDENT AND STEADY STATE NUMERICAL METHODS IN HEAT TRANSFER AND FLUID FLOW 423

APPENDIX E - LISTING OF SYMJET COMPUTER PROGRAM - 1108 VERSION 434

LIST OF TABLES

Table	Title	Page
2.1	Summary of Work Pertinent to Ocean Outfall Plume Analysis	24
3.1	Differential Equations Required for Velocity-Pressure and Vector Potential-Vorticity Methods in Two and Three Dimensions	57
4.1	Values of Terms Involving K and λ	81
7.1	Summary of Momentum Jet Verification Cases ($F_0 \rightarrow \infty$)	166
7.2	Summary of Pure Buoyant Plume Verification Cases ($F_0 = 0$)	168
7.3	Summary of Mixed Flow Verification Cases	169
7.4	Comparison of the Spreading Constant Reported by Various Investigators	191
7.5	Correlation of the Vertical Diffusion Coefficient ε_z with the Local Richardson Number, RI	287
7.6	Values of Vertical Eddy Viscosities in the Sea	290
7.7	Convergence Behavior, 40x33 Grid	308
7.8	Convergence Behavior, 31x34 Grid	312
7.9	Convergence Behavior, 26x25 Grid	314

LIST OF ILLUSTRATIONS

Figure — Page

2.1 Condenser coolant flow rate as a function of temperature rise and plant electric generating capacity (fossil fired plant) 9

2.2 Condenser coolant flow rate as a function of temperature rise and plant electric generating capacity (nuclear plant) 10

2.3 Vertical thermal plume in deep water, illustrating possible flow regimes 13

2.4 Vertical thermal plume in shallow water, illustrating continual transition of the flow field 16

2.5 Possible configuration of a vertical buoyant plume in stratified receiving water 19

2.6 Possible configuration of a buoyant plume in stratified receiving water with cross-current, u_∞ 20

3.1 Rectangular coordinate system 30

3.2 Relationship between the buoyancy parameter, Δ_1 and density disparity, Δ_2 45

4.1 Zone of flow establishment for plumes with large and small densimetric Froude numbers, F_0 66

4.2 Coordinate system for axisymmetric vertical plume 68

4.3 Typical velocity profile in the zone of flow establishment for a momentum jet 75

5.1 Physical system for axisymmetric vertical plume where the bottom boundary is some distance $z_b \neq 0$ above the outfall port 86

5.2 Physical system for shallow water, axisymmetric, vertical plume 88

5.3 Computational grid for difference equations 97

Figure Page

5.4 Typical finite difference cell illustrating indices for Ψ, Ω, Γ, U and V 99

5.5 Typical sea surface boundary and interior cells 115

5.6 Typical centerline boundary and interior cells 118

5.7 Typical inflow boundary and interior cell (deep water only) 120

5.8 Typical inflow boundary and interior cell (shallow water case only) 122

5.9 Typical vertical port side boundary and interior cell (shallow water case only) 125

5.10 Typical bottom boundary and boundary cell 127

5.11 Typical inflow-outflow boundary and interior cells 129

5.12 Physical system for line plume issuing to flowing receiving water 133

7.1 Computational grid for the stream function, Ψ, illustrating the effect of the sinh (ξ) transformation ($\Delta\xi = .14690$, $\Delta Z = 1.0$) 170

7.2 General features of momentum jet centerline velocity (based on Albertson's data) 173

7.3 Comparison of experimental data and similarity solution with computed results for a momentum jet. Centerline velocity and concentration for case 2 175

7.4 Comparison of experimental data and similarity solution with computed results for a momentum jet. Centerline velocity and concentration for case 4 177

7.5 Computed centerline velocity and concentration for momentum jet, case 5 178

Figure		Page
7.6	Comparison of experimental data and similarity solution with computed results for a momentum jet. Centerline velocity and concentration for case 6	179
7.7	Computed centerline velocity and concentration for momentum jet, case 7	181
7.8	Computed centerline velocity and concentration for momentum jet, case 8	183
7.9	Computed centerline velocity and concentration distribution for momentum jet, case 9	184
7.10	Centerline velocity distributions for cases 4, 7, and 9, normalized to $V_o = 1.0$	186
7.11	Centerline velocity and concentration distribution for case 10 (includes effect of large vertical eddy diffusivity)	188
7.12	Shape preserving of velocity profiles computed for an inviscid, rotational fluid (reference case 2)	189
7.13	Computed rate of spread of the momentum jet half-radius, $r_{1/2}$	190
7.14	Radial distribution of normalized vertical velocity for case 2	194
7.15	Normalized radial distribution of axial velocity, momentum jet case 4	195
7.16	Normalized radial distribution of axial velocity case 4	196
7.17	Radial distribution of axial velocity at various elevations case 4	197
7.18	Normalized distribution of axial velocity case 6	198
7.19	Normalized radial concentration distribution, type 1 boundary condition case 2	199

Figure Page

7.20 Normalized radial concentration distribution, type 2 boundary condition, case 4 200

7.21 Radial vorticity distribution for momentum jet type 2 boundary condition, case 4 202

7.22 Radial vorticity distribution for momentum jet at $Z = 15$. A comparison between type 1 and 2 boundary conditions, and the Gaussian distribution 203

7.23 Normalized radial velocity distribution for momentum jet 204

7.24 Vertical distribution of stream function at R_∞, case 6 206

7.25 Streamlines for case 6 -- momentum jet 208

7.26 Isopycnals for case 6 -- momentum jet 209

7.27 Vorticity level lines for case 6 -- momentum jet 210

7.28 3D illustration of stream function -- psi, case number 6 211

7.29 3D illustration of stream function -- psi, case number 6 212

7.30 3D illustration of buoyancy distribution - Δ_1, case number 6 213

7.31 3D illustration of fluid vorticity - omega, case number 6 214

7.32 Computed centerline velocity and temperature excess for case 13. Pure buoyancy, $F_o = 0$ 216

7.33 Computed centerline velocity and temperature excess for case 14. Pure buoyancy, $F_o = 0$ 217

7.34 Computed rate of spread of half-radius, $r_{1/2}/D$. Pure buoyancy, case 14 ($D = 2 r_o$) 219

Figure Page

7.35 Normalized distribution of computed axial velocity. Pure buoyancy, case 13 222

7.36 Normalized radial distribution of axial velocity. Pure buoyancy, case 13 223

7.37 Radial distribution of axial velocity in pure buoyancy, case 13 224

7.38 Normalized radial distribution of axial velocity. Stronger source, pure buoyancy, case 14 225

7.39 Normalized distribution of computed radial temperature excess. Pure buoyancy, case 14 226

7.40 Radial distribution of vorticity. Pure buoyancy, case 14 227

7.41 Normalized radial velocity distributions for pure buoyant plume, case 14 229

7.42 Vertical distribution of stream function at R_∞. Pure buoyancy, case 14 230

7.43 Streamlines for case 14, pure buoyancy 231

7.44 Isotherms for case 14, pure buoyancy, $\Delta T/\Delta T_0$ 232

7.45 Vorticity level lines for case 14, pure buoyancy 233

7.46 3D illustrations of stream function - psi, case number 14 234

7.47 3D illustration of temperature field - ΔT, case number 14 235

7.48 3D illustration of fluid vorticity - omega. Case 14, pure buoyancy 236

7.49 Centerline velocity and buoyancy for cases 15, 16 and 17 240

7.50 Centerline buoyancy distribution for cases 17 and 18 242

Figure | Page

7.51 Centerline velocity and buoyancy for cases 17, 19 and 20 243

7.52 3D illustration of vorticity - omega. Case 17, buoyant plume with running calculation of half radius 245

7.53 3D illustration of vorticity - omega, case number 21 246

7.54 Centerline velocity and buoyancy for cases 22 and 23 247

7.55 Comparison between computed results and similarity solution for $F_0 = 1.0$ 249

7.56 Comparison between computed centerline distributions of velocity and buoyancy for $F_0 = 1000$ and $F_0 \rightarrow \infty$ 250

7.57 Comparison of half-radius spread for various densimetric Froude numbers 252

7.58 Effect of the eddy Prandtl number on half-radius spread 252

7.59 Entrainment trends in mixed flows 254

7.60 Streamlines for case 22 - mixed flow, FO = 46 255

7.61 Isotherms for case 22 - mixed flow, FO = 46 256

7.62 Vorticity level lines for case 22 - mixed flow, FO = 46 257

7.63 3D illustration of stream function - psi. Case 22 - deep water buoyant jet 258

7.64 3D illustration of temperature field - T. Case 22 - deep water buoyant jet 259

7.65 3D illustration of fluid vorticity - omega. Case 22 - deep water buoyant jet 260

Figure		Page
7.66	Regional specification for turbulent eddy coefficient modeling	267
7.67	Computed values of FR for a momentum jet	270
7.68	Computed radial eddy diffusion factors, FR for deep water plumes at various densimetric Froude numbers	271
7.69	Comparison of computation using constant and variable radial eddy transport coefficients	273
7.70	Concentration distribution in the zone of flow establishment	275
7.71	Computed potential core and half radius ($F_o = 46$)	277
7.72	Centerline velocity and temperature distribution for 44 diameter deep outfall	279
7.73	Computed centerline velocity and temperature excess. Cases for 10 diameter deep water	281
7.74	3D illustration of temperature field	283
7.75	Dependence of ε_{zs} on sea state	288
7.76	Correlation of ε_z with density gradient	290
7.77	Observation of flow patterns past the end of a cylinder	300
7.78	Computed flow patterns past the end of a cylinder	300
7.79	Convergence behavior, 40 x 33 grid	309
7.80	Convergence history of V and Γ at selected cells, momentum jet, 40 x 33 grid	311
7.81	Convergence history of U, V and Δ_1 at selected cells 31 x 34 grid	313
7.82	Iteration history for one cell of case 2	316

Figure		Page
8.1	Computed centerline velocity and temperature excess for intermediate depth, cases 48 through 51 (10 diameters deep)	326
8.2	Surface distribution of radial velocity, cases 48 through 51 (see Table 8.1)	327
8.3	Distributions of radial velocity case 50	329
8.4	Maximum radial velocity profiles, cases 48 through 51	330
8.5	Radial velocity profiles at r/D=7.32, cases 48 through 51	331
8.6	Surface temperature excess distribution, cases 48 through 51 (see Table 8.1)	332
8.7	Vertical temperature excess distributions for various radial positions, cases 48 and 50	333
8.8	Streamlines for case 48 - buoyant discharge, FO = 100	333
8.9	Isotherms for case 48 - buoyant discharge, FO = 100	333
8.10	Vorticity level lines for case 48 - buoyant discharge, FO = 100	333
8.11	3D illustration of stream function -- PSI. Case No. 48, intermediate water outfall, surface 10 diameters above port, FO = 100	334
8.12	3D illustration of temperature field -- ΔT. Case No. 48, intermediate water outfall, surface 10 diameters above port, FO = 100	334
8.13	3D illustration of fluid vorticity - OMEGA, Case no. 48, intermediate water outfall, surface 10 diameters above port, FO = 100	334
8.14	Streamlines for case 49 - buoyant discharge, FO = 25	334

Figure	Page
8.15 Isotherms for case 49 - buoyant discharge, FO = 25	335
8.16 Vorticity level lines for case 49 - buoyant discharge, FO = 25	335
8.17 3D illustration of stream function -- PSI. Case No. 49, intermediate water outfall, surface 10 diameters above port, FO = 25	335
8.18 3D illustration of stream function -- PSI. Case No. 49, intermediate water outfall, surface 10 diameters above port, FO = 25	335
8.19 3D illustration of temperature field -- ΔT. Case No. 49, intermediate water outfall, surface 10 diameters above port, FO = 25	336
8.20 3D illustration of fluid vorticity - OMEGA. Case No. 49, intermediate water outfall, surface 10 diameters above port, FO = 25	336
8.21 Streamlines for case 50 - buoyant discharge, FO = 5	336
8.22 Isotherms for case 50 - buoyant discharge, FO = 5	336
8.23 Vorticity level lines for case 50 - buoyant discharge, FO = 5	337
8.24 3D illustration of stream function -- PSI. Case No. 50, intermediate water outfall, surface 10 diameters above port, FO = 5	337
8.25 3D illustration of temperature field -- ΔT. Case No. 50, intermediate water outfall, surface 10 diameters above port, FO = 5	337
8.26 3D illustration of fluid vorticity - OMEGA. Case No. 50, intermediate water outfall, surface 10 diameters above port, FO = 5	337

Figure Page

8.27 Streamlines for case 51 - buoyant discharge, FO = 1 338

8.28 Isotherms for case 51 - buoyant discharge, FO = 1 338

8.29 Vorticity level lines for case 51 - buoyant discharge, FO = 1 338

8.30 3D illustration of stream function -- PSI. Case No. 51, intermediate water outfall, surface 10 diameters above port, FO = 1 338

8.31 3D illustration of temperature field -- ΔT. Case No. 51, intermediate water outfall, surface 10 diameters above port, FO = 1 339

8.32 3D illustration of fluid vorticity - OMEGA. Case No. 51, intermediate water outfall, surface 10 diameters above port, FO = 1 339

8.33 Computed centerline dimensionless velocity and temperature excess for shallow water, cases 52 through 55 (5 diameters deep) 341

8.34 Vertical distribution of radial velocity at various radial positions, case 52 342

8.35 Vertical distribution of temperature excess at various radial positions, case 52 342

8.36 Streamlines for case 52 - buoyant discharge, FO = 1 344

8.37 Isotherms for case 52 - buoyant discharge, FO = 1 344

8.38 Vorticity level lines for case 52 - buoyant discharge, FO = 1 344

8.39 3D illustration of stream function -- PSI. Case No. 55, very shallow water outfall, surface 5 diameters above port, FO = 1 344

8.40 3D illustration of temperature field -- ΔT. Case No. 55, very shallow water outfall, surface 5 diameters above port, FO = 1 345

Figure | Page

8.41 3D illustration of fluid vorticity - OMEGA. Case No. 55, very shallow water outfall, surface 5 diameters above port, FO = 1 345

8.42 Computed radial velocity at surface, cases 58 and 59 348

8.43 Vertical distribution of radial velocity, U, cases 58 and 59 349

8.44 Vertical distribution of radial velocity, U, cases 58 and 59 349

8.45 Streamlines for an axisymmetric, vertical plume, confined by a free surface, case 58 350

8.46 Streamlines for an axisymmetric, vertical plume, confined by a free surface, case 59 351

8.47 Surface temperature excess, ΔT_s, cases 57, 58 and 59 352

8.48 Vertical temperature excess distribution, cases 58 and 59 353

8.49 Vertical temperature excess distribution, cases 58 and 59 353

8.50 Isotherms for an axisymmetric, vertical plume, confined by a free surface, case 59 354

8.51 Ambient temperature profiles for cases 60 through 65 356

8.52 Vertical distribution of radial velocity, case 60 357

8.53 Vertical temperature excess distribution, case 60 357

8.54 Streamlines for an axisymmetric, vertical plume, confined by a free surface, case 60 - intermediate depth, homogeneous ambient, Mamayev, BETA = .4 358

8.55 Isotherms for an axisymmetric, vertical plume, confined by a free surface, case 60 - intermediate depth, homogeneous ambient, Mamayev, BETA = .4 358

Figure		Page
8.56	Vorticity contours axisymmetric, vertical plume, confined by a free surface, case 60 - intermediate depth, homogeneous ambient, Mamayev, BETA = .4	358
8.57	3D illustration of stream function -- PSI, case no. 60	358
8.58	3D illustration of temperature field -- ΔT, case No. 60	359
8.59	3D illustration of fluid vorticity - OMEGA, case No. 60	359
8.60	Vertical distribution of radial velocity, case 61	359
8.61	Vertical excess temperature distribution, case 61	359
8.62	Streamlines for an axisymmetric, vertical plume, confined by a free surface, case 61 - intermediate depth, with 2 degree thermocline, Mamayev	360
8.63	Isotherms for an axisymmetric, vertical plume, confined by a free surface, case 61 - intermediate depth, with 2 degree thermocline, Mamayev	360
8.64	Vorticity contours axisymmetric, vertical plume, confined by a free surface, case 61 - intermediate depth, with 2 degree thermocline, Mamayev	360
8.65	Vertical Distribution of Radial Velocity. Case 61	362
8.66	Vertical Temperature Excess Distribution. Case 61	363
8.67	Surface Temperature Excess, ΔT_S for Cases 60 and 63	364
8.68	Streamlines for an axisymmetric, vertical plume, confined by a free surface. Case 63 - intermediate depth with 4 degree thermocline. Mamayev	365
8.69	Isotherms for an axisymmetric, vertical plume, confined by a free surface. Case 63 - intermediate depth with 4 degree thermocline, Mamayev	365
8.70	Vorticity contours axisymmetric, vertical plume, confined by a free surface. Case 63 - intermediate depth with 4 degree thermocline, Mamayev	365

Figure		Page
8.71	3D illustration of stream function -- PSI. Case 63 - intermediate depth with 4 degree thermocline, Mamayev	365
8.72	3D illustration of temperature field -- T. Case 63 - intermediate depth with 4 degree thermocline, Mamayev	366
8.73	3D illustration of fluid vorticity - OMEGA. Case 63 - intermediate depth, with 4 degree thermocline, Mamayev	366
8.74	Vertical distribution of radial velocity. Case 64	368
8.75	Vertical, excess temperature distribution. Case 64	368
8.76	Streamlines for an axisymmetric, vertical plume, confined by a free surface. Case 64 - intermediate depth, with 5 degree thermocline, Mamayev	369
8.77	Isotherms for an axisymmetric, vertical plume, confined by a free surface. Case 64 - intermediate depth, with 5 degree thermocline, Mamayev	369
8.78	Vorticity contours axisymmetric, vertical plume, confined by a free surface. Case 64 - intermediate deptn, with 5 degree thermocline, Mamayev	369
8.79	3D illustration of viscous stream function - Case 64 - intermediate depth, with 5 degree thermocline, Mamayev	369
8.80	3D illustration of temperature field -- ΔT Case 64 - intermediate depth, with 5 degree tnermocline, Mamayev	370
8.81	3D illustration of vorticity -- OMEGA Case 64 - intermediate depth, with 5 degree thermocline, Mamayev	370
8.82	Vertical distribution of radial velocity. Case 65	371
8.83	Vertical, excess temperature distribution. Case 65	372
8.84	Streamlines for an axisymmetric, vertical plume, confined by a free surface, case 65 - intermediate depth, with 5 degree thermocline, Mamayev	373

Figure | Page

8.85 Vorticity contours axisymmetric, vertical plume, confined by a free surface, case 65 - intermediate depth, with 5 degree thermocline, Mamayev 373

8.86 Isotherms for an axisymmetric, vertical plume, confined by a free surface, case 65 - intermediate depth, with 5 degree thermocline, Mamayev 373

8.87 Streamlines for an axisymmetric, vertical plume, confined by a free surface, case 65 - intermediate depth, continued iteration. 373

8.88 Isotherms for an axisymmetric, vertical plume, confined by a free surface, case 65 - intermediate depth, continued iteration. 374

8.89 Vorticity contours axisymmetric, vertical plume, confined by a free surface, case 65 - intermediate depth, continued iteration. 374

8.90 Surface radial velocity, case 66 378

8.91 Surface temperature excess, case 66 378

8.92 Vertical distribution of radial velocity at various radial positions, case 66 379

8.93 Vertical distribution of temperature excess at various radial positions, case 66 379

8.94 Streamlines for case 66 (1.0 dia deep) FO = .111 380

8.95 Isotherms for case 66 (1.0 dia deep) FO = .111 380

8.96 Vorticity for case 66 (1.0 dia deep) FO = .111 380

8.97 3D illustration of fluid vorticity - OMEGA Case 66 380

8.98 3D illustration of stream function -- PSI, Case 66 381

8.99 3D illustration of stream function -- PSI, Case 66 381

8.100 3D illustration of temperature field -- T. Case 66 381

Figure		Page
8.101	3D illustration of temperature field -- ΔT. Case 66	381
8.102	Comparison of computed surface temperature with field data	383
A-1	Finite difference grid system	404
A-2	Values of σ_x and σ_y for a preferred difference scheme	408
A-3	Convective Γ flux for an infinitesimal axisymmetric volume element	410
A-4	Axisymmetric finite difference cell, p, with the four immediate neighbor cells	412
B-1	Irregular spaced grid	415
B-2	Grid layout for vertical differences	417
C-1	Ratio of actual to computed node spacing	422
D-1	Finite difference cell	428

NOMENCLATURE

Variables which are not listed in this nomenclature are defined at the appropriate location within the manuscript. A few variable names have been duplicated; however, the definitions listed below hold throughout the text with duplications defined at the point of use. Dimensions are given in the force-length-time system (F-L-T).

A	Constant used in Chapter 7.
a	Thermal diffusivity, L^2/T
B	Buoyancy parameter defined in Chapter 3.
b	Slot width (slot plume), L
C_1,C_2	Constants
c	Concentration
D	Diameter of outfall port, L
e_i, $\hat{e}$	Unit vector ($i = 1,2,3$)
E	Momentum parameter for plume similarity solution.
f	Coriolis constant, 1/T
FR	Radial eddy momentum diffusivity multiplier
FZ	Vertical eddy momentum diffusivity multiplier
g	Gravitational constant, L/T^2
k	Kinetic energy of turbulent motion, FL
K	Entrainment parameter
ℓ	Characteristic length, L
L	Liebmann acceleration constant
M	Total momentum, FT

$\hat{n}$	Unit surface normal vector
P	Pressure, F/L^2
P^o	Deviatoric pressure (defined in Chapter 3), F/L^2
P'	Fluctuating pressure, F/L^2
Q	Plume entrainment rate, L^2/T
r	Radial coordinate, L
R_{ij}	Reynolds stress tensor, F/L^2
S	Salinity, ppt
t	Time, T
T	Temperature, °C
u	Velocity, L/T
u'	Fluctuating velocity, L/T
$\vec{U}_I$	Irrotational velocity vector, L/T
$\vec{U}_S$	Solenoidal velocity vector, L/T
v	Vertical velocity, L/T
x	horizontal coordinate, L
x_i	General rectangular coordinate, L
Y	Space coordinate, L
z	Vertical coordinate, L

Greek

α	Entrainment constant
β	Constant used in vertical eddy diffusivity model
δ	Convergence criterion
ε	Eddy diffusivity for momentum, L^2/T
ε_γ	Eddy diffusivity for matter, L^2/T
ε_H	Eddy diffusivity for heat, L^2/T
ε_ρ	Eddy diffusivity for density, L^2/T
ζ	Variable defined in Chapter 3.
Θ	Longitude
κ	Thermal conductivity, F/LT^oC
μ	Dynamic viscosity, FT/L^2
ν	Kinematic viscosity, L^2/T
π	3.14159
ρ	Density, FT^2/L^4
ρ'	Fluctuating density, FT^2/L^4
τ	Shear stress
ϕ	Latitude
$\dot{\phi}$	Source or sink term in Γ-transport equation, $1/L^3\ T$
Φ	Scalar potential, L^2/T
Ψ	Stream function, L^2/T
$\vec{\psi}$	Vector potential, L^2/T
ω	vorticity, $1/T$
Ω^*	Earth rotation velocity, $1/T$

Standard Dimensionless Parameters

EU	Euler number, $\Delta P/\frac{1}{2}\rho v_o^2$
F_o, FO	Densimetric Froude number, $\frac{v_o^2}{(\frac{\rho_r-\rho_o}{\rho_o})gD}$
P_r	Prandtl number, ν/κ
PR	Eddy Prandtl number, $\varepsilon/\varepsilon_H$
SC,λ	Eddy Schmidt number, $\varepsilon/\varepsilon_\gamma$
Re	Reynolds number, $\frac{v\ell}{\nu}$
RE	Eddy Reynolds number, $\frac{v\ell}{\varepsilon}$
RI	Local Richardson number, $-\frac{g}{\rho_o}\frac{(d\rho/dZ)}{(du/dZ)^2}$
RI'	Gross Richardson number, $-\frac{g}{\rho_o}\frac{(\Delta\rho/\Delta Z)}{(\Delta u/\Delta Z)^2}$ for the thermal layer.

Dimensionless Parameters Defined in this Manuscript

C	Concentration, c/c_o
E*	Momentum parameter, $\left(\frac{V_m z}{\sqrt{K}}\right)^3$
P*	Pressure, $P^o\rho_r/\Delta P_o$
R	Radial coordinate, r/r_o
R*	Density parameter, $\frac{E^{*1/3}\Delta_{2m}z}{\sqrt{K}\,(1+\lambda)}$

t^*	Time, tv_o/D
U	Radial velocity, u_r/v_o
V	Vertical velocity, u_z/v_o
X	Space coordinate, x/x_o
Z	Vertical coordinate, z/r_o
Ƶ	Vertical coordinate, z/D
Γ	Conservative constituent parameter
Δ_1	Buoyancy parameter, $(\frac{\rho_r-\rho}{\rho_r-\rho_o})$
Δ_2	Density disparity parameter, $(\frac{\rho_\infty-\rho}{\rho_r-\rho_o})$
Δ_3	Salirity parameter, $(\frac{S_r-S}{S_r-S_o})$
ε^*	Eddy diffusivity for momentum, $\varepsilon/\varepsilon_o$
Θ	Temperature parameter, $(\frac{T_o-T}{T_o-T_r})$
ξ	Radial coordinate, $\sinh^{-1}$ (R)
ρ^*	Stratification parameter, $\rho_\infty(Z)/\rho_o$
Ψ	Stream function, $\psi/r_o\, v_o^2$
Ω	Vorticity, $\omega r_o/v_o$
Ω^{**}	Earth rotational velocity, $2\Omega^*/f_o$

Subscripts

The following subscript definitions hold unless otherwise defined in the text.

b	Refers to slot jet width
c	Refers to center, or core
e	Value at end of zone of flow establishment
E	Elliptic partial differential equation
H	Refers to heat
i	Tensor index
j	Tensor index, also computational grid index in the horizontal (radial) direction
k	Tensor index, also computational grid index in the vertical direction
m	Value at jet centerline
max	Maximum value
p	Computational grid index
port	Refers to conditions at outfall port
q	Computational grid index
r	Refers to radial direction, or reference condition for scalar quantities
s	Refers to condition at surface
T	Refers to turbulent conditions, or transport equation
x	Refers to x (horizontal) direction
z	Refers to z (vertical) direction

Greek Subscripts

γ	Refers to a conservative constituent
Δ	Refers to the buoyancy parameter
ρ	Refers to density
Ψ	Refers to the stream function
Ω	Refers to vorticity

Other Subscripts

o	Refers to conditions of or at the outfall
∞	Refers to conditions far removed from the outfall
1/2	Refers to the half-width

Mathematical Notations

$\frac{D}{Dt}$	Substantial derivative
∇^2	Laplacian operator
$\vec{\nabla}$	Gradient operator, del
Δ	Finite-difference operator
$\sum$	Summation except where otherwise specified
δ_{ij}	Kronecker delta function
e_{ijk}	Permulation tensor
Log	Natural logarithm
$\vert\;\vert$	Absolute value
$\hat{}$	Hat, unit vector
$\overline{}$	Overbar, time or space averaging
sinh, cosh, tanh, coth	Hyperbolic functions

A NUMERICAL MODEL FOR PREDICTING ENERGY DISPERSION IN THERMAL PLUMES ISSUING FROM LARGE, VERTICAL OUTFALLS IN SHALLOW COASTAL WATER

CHAPTER 1

INTRODUCTION

The growing demand for electric power in the United States has set the stage for an additional environmental concern; the enormous quantities of waste heat discharged to our natural waterways by existing and planned large thermal power plants. The concern, of course, is the impact of the waste heat on the resident ecosystem. The answer to the underlying question, "are thermal effects a detriment to the environment?", is largely a matter of philosophy since certain species of the flora and fauna are apt to thrive under the altered conditions whereas others would doubtless perish.

The central issue is, however, that these large quantities of discharged waste heat will in fact alter the environment and certain changes in the ecosystem will occur. Just what changes will take place and the nature of the shift in the ecosystem are open to numerous questions. Preservation of species, the impact on the overall food chain, and the encroachment of undesirable species are certainly compromising aspects. These questions and many others of equal importance are certainly not unattended, but the interaction of the ecosystem with the environment and the complexity of ecodynamics as influenced by artificial shifts in the environment presents an analytical and empirical task to arrive at reliable predictive methods of monumental proportions.

Although the ultimate concern of so-called "thermal pollution" lies in the ecological impact, it is necessary as a first step to assess the receiving water temperature changes. Prediction of the temperature distribution in natural waters is in itself a formidable task owing to the complexity of such natural phenomena as hydrodynamics, dispersion, and atmospheric interaction (transport processes). To date, no analytical or empirical tool has been devised to predict thermal distributions with any degree of confidence for general situations. The state-of-the-art has been developed along the lines of applying the most appropriate simplified analytical or empirical model to an immediate situation. Unfortunately, some situations are complicated to the extent that simplified methods are a hopeless exercise and can lead to a valueless or grossly overrestrictive assessment.

Such complexities lead to methods involving more elaborate numerical models or physical scale modeling. In this work, we take the former approach, that of numerical modeling.

As is pointed out in Chapter 2, previous analytical plume modeling efforts have dealt primarily in two areas which are:

- The initial mixing zone where, in certain cases, similarity solutions apply, and
- The far field where heat transfer is governed by turbulent diffusion and atmospheric interchange.

The past research has largely neglected an area of prime importance, that being the near field of large, vertical outfalls in shallow coastal waters. This neglect is in part due to the complexity of the flow region in question and the fact that it is a new problem. The near thermal field for such outfalls is, nevertheless, a very important aspect of plume analysis, and is in need of analytical attention.

1.1 Objectives

The primary objective of the work contained in this thesis is the investigation and application of finite-difference methods in analyzing the dispersion of thermal effluents issuing from large single port vertical outfalls in shallow coastal receiving water. Such systems are typical of several existing and/or planned thermal power plant reject-heat discharge systems. This analysis, constitutes research needed for future thermal discharge management. Since we are interested primarily in the hydrodynamics and energy transport for a shallow water, vertically confined plume, simplified analytical methods cannot be applied with confidence. Physical modeling holds some promise as an alternative to numerical modeling, at least in the near field and in the absence of stratification. Since the numerical modeling devised in this study was a considerable effort in itself, physical modeling was not attempted. Verification of the numerical techniques was rather carried out by testing the computer program for several cases that could be checked with data published in the literature.

The secondary objective of the work was to develop a computer program for analytical study of the above mentioned outfall systems which would also include use of similarly solutions where applicable, along with the more elaborate numerical techniques.

1.2 Summary

In the initial scoping of the vertical plume problem it was planned to investigate both the transient and steady state operation of the outfall system. Initially, several transient cases were run which were academically quite interesting but it was soon ascertained that the application of steady flow techniques was more efficient in obtaining the desired results--the quasi-steady flow distributions. Consequently, the transient techniques were abandoned. In general, the scope of the study encompasses nearly all of the real quasi-steady flow complication expected in actual situations which conform to axisymmetric assumptions. The most notable complication is that of plume induced turbulence.

One exception to the modeling of observed phenomena was the surface boil; the surface was assumed flat and free-slip in all instances. This assumption averted the problem of modeling a distorted surface which is thought to be of small importance to the overall plume characteristics. Other complications accounted for include the possible existence of a potential core, ambient stratification, and non-homogeneous, anisotropic turbulence in both the vertical rise and lateral plume spreading. Flows for the entire range of densimetric Froude numbers were investigated, including cases of pure natural convection.

The solution method deemed most practical for purposes of this study was the stream function-vorticity, finite-difference approach, in axisymmetric coordinates. The transport equations were used in their conservative forms and special upstream differencing techniques were employed for the convective terms.

The finite-difference computation technique verification study was carried out for three deep water flow categories:

- pure momentum jets,
- pure buoyant plumes, and
- forced plumes where both initial momentum and buoyancy play important roles.

Results from this portion of the study were compared to data reported in the literature or valid similarity solutions. These comparisons involved:

- centerline distributions of velocity and buoyancy (or temperature),
- spread of the half-radius,
- radial distributions of vertical velocity and buoyancy (or temperature),
- radial velocities,
- entrainment trends, and
- eddy diffusivities.

The effects of several different computational aspects were included which involved effects of the:

- boundary conditions and their computation,
- various models for eddy diffusivities,
- Prandtl (or Schmidt) number effects,
- Richardson number modification of vertical diffusivities,
- potential core,
- ambient turbulence,
- vertical turbulence within the plume, and
- various factors involving numerical stability and convergence.

The general results of this portion of the study showed excellent agreement with experimental data where the eddy diffusivities are well modeled. Plume generated turbulence was modeled using Prandtl's mixing length hypothesis in all cases.

In Chapter 8 the plume model is extended to shallow water cases. Verification is not presented since there are no readily available appropriate or reliable data.* Here we rely on the extensive verification study of Chapter 7 mentioned above.

---

*Verification of the surface temperature distribution was obtained for one case. The data is proprietary, hence no details of operating conditions are disclosed.

CHAPTER 2

DISCUSSION OF THERMAL PLUMES AND PROBLEM DESCRIPTION

The dynamical behavior of heated water issuing to the marine environment from an ocean outfall is influenced by a number of variables which fall into two general categories. The first of these categories encompasses engineered variables such as outfall design, effluent temperature, etc; and, the second, those variables which we cannot control, such as the oceanographic and meteorlogical parameters. In this chapter, we shall illustrate and discuss how ambient and engineered variables influence the gross behavior of a thermal plume, briefly discuss the analytical "state-of-the-art," and qualitatively describe the problem undertaken in this research.

2.1 The Nature of Thermal Plumes in Marine Surroundings

In the following discussion the terms jet flow and plume flow will be used, and to avoid confusion it is appropriate to outline the meaning of each at this time. A convective flow in a free environment caused solely by buoyancy is commonly called a simple plume. In this case, the general pattern of motion is caused by a density disparity between the flow and the surrounding environment. Such instances are atmospheric thermal and the smoke plumes generated by field fires. A jet, on the other hand, is characterized by source flow inertia where the flow may not involve a density difference.

The flow which is of primary concern in this discussion is a combination of the above where both initial momentum and buoyancy have significant influence on the flow behavior. Such a flow might be termed a forced plume. However, in this work the flow field will be called a thermal plume or plume. Reference will be made to jet flow from time to time, which will imply that conditions near the outfall, where initial momentum dominates the dynamic behavior, is the subject of discussion or that the effluent is neutrally buoyant.

A temperature difference is not the only factor which must be considered as a buoyancy source in a thermal plume. Differential salt concentration is certainly a factor. Salinity differences must be considered if the power plant condenser coolant is drawn from an estuary and rejected off-coast,in which case, the effluent would most likely be less saline than the receiving water and contribute to the overall buoyant force.

2.1.1 Discharge Magnitude

The volumetric flow rate required by a thermal power station depends on plant size, steam cycle thermodynamic efficiency, and coolant temperature rise. Typical installations range from 1000 to 2000 Mw_e and operate at a coolant temperature rise between 15 and 20 ^{o}F. Plant efficiency depends largely on whether the heat source is nuclear or fossil. The steam cycle thermodynamic efficiency for a typical fossil fired plant will be in the neighborhood of 42% for optimum conditions, whereas typical efficiency for a modern nuclear plant operating under similar conditions is about 32%. Hence, the nuclear plant will reject about 50% more heat than a fossil fired plant having the same net electrical output.

The condenser coolant volumetric flow rate required by power stations in the 1000 to 2000 Mw_e range is impressive by any standards, regardless of whether the plant is nuclear or fossil fired. Figures 2.1 and 2.2 illustrate this fact. It is possible that in the future a particular site will consist of a number of individual units. Thus the cooling load on a certain ocean locale may result from the production of perhaps 10 Gw_e.

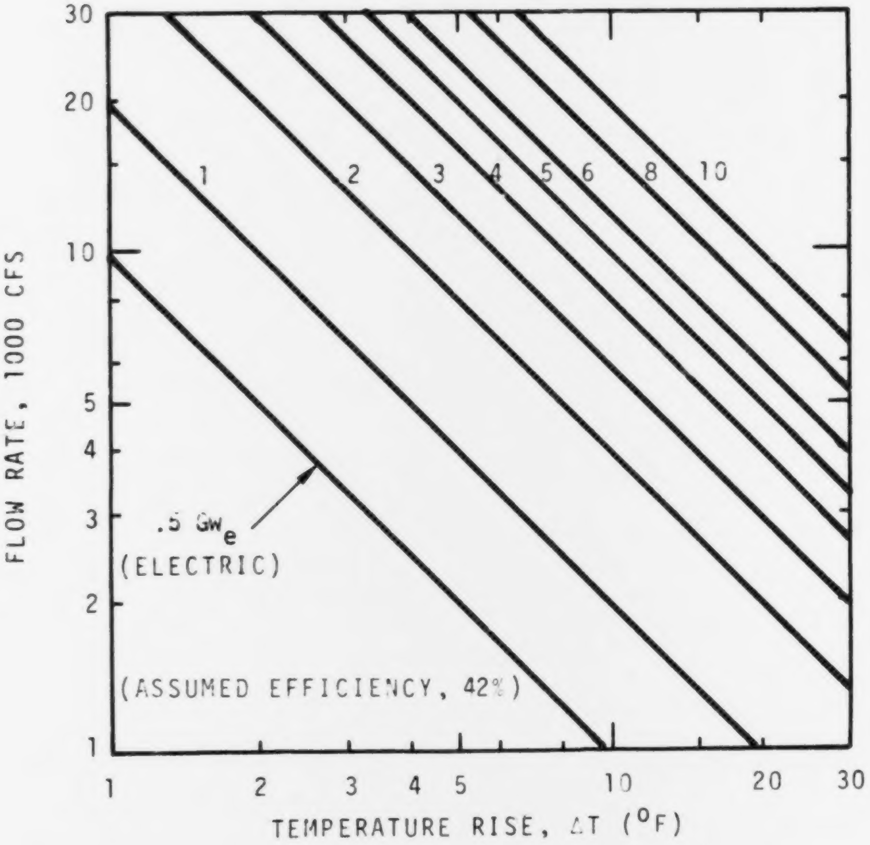

Figure 2.1 Condenser Coolant Flow Rate as a Function of Temperature Rise and Plant Electric Generating Capacity (Fossil Fired Plant)

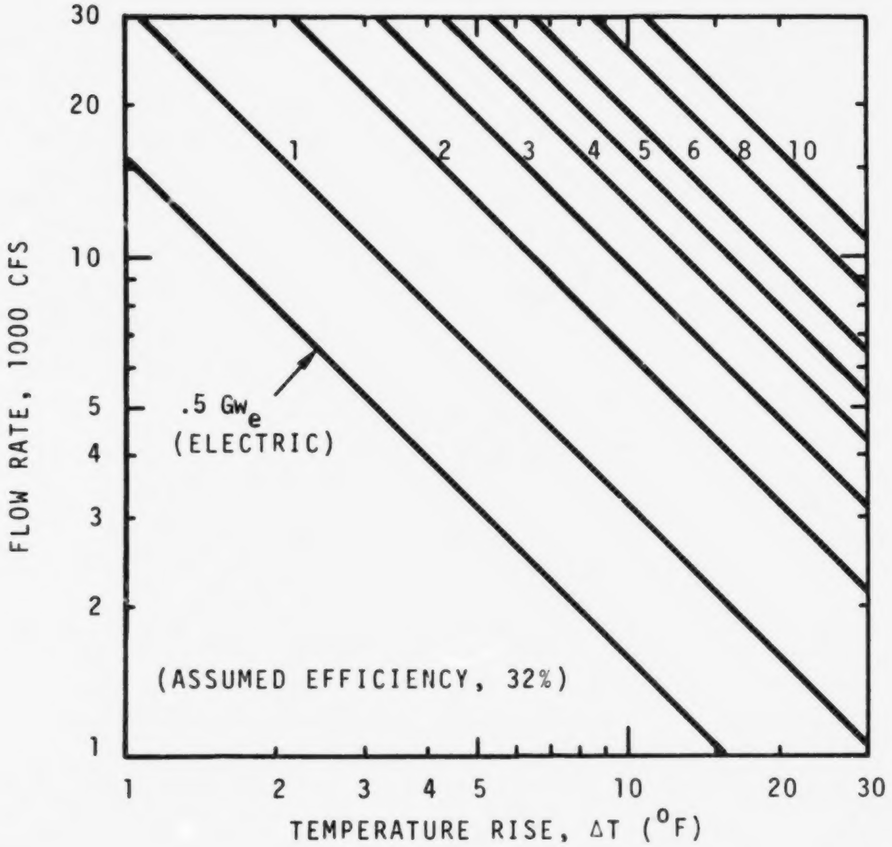

Figure 2.2 Condenser Coolant Flow Rate as a Function of Temperature Rise and Plant Electric Generating Capacity (Nuclear Plant)

2.1.2 Outfall Configuration

Condenser coolant may be rejected to the ocean either at the shoreline or offshore through a submerged outfall.

The shoreline discharge may be either by canal or conduit. Examples of such existing systems are the following fossil fired plants owned by Pacific Gas and Electric [113].

1) Contra Costa, 1298 Mw_e, rejecting heat to the San Francisco Bay Delta.

2) Pittsburgh, 1340 Mw_e, rejecting heat to the San Francisco Bay Delta.

3) Morro Bay, 1030 Mw_e, rejecting heat to the Pacific Ocean.

Numerous other examples might be cited since the shoreline outfall system has widespread use.

Submerged, offshore outfalls may be designed in two general fashions:

1) a single port (dual in some cases) outlet situated either vertical or horizontal, or

2) a diffuser section at the end of the pipeline consisting of numerous ports. The diffuser is typical of municipal waste outfalls.

Some examples of large vertical port outfalls are:

1) Moss Landing fossil fired plant. Reject heat from 1500 Mw_e generation, discharged about 800 feet offshore. Dual ports.

2) San Onofre nuclear plant. Reject heat from approximately 450 Mw_e generation, discharged through a 14-foot diameter pipe 2600 feet offshore, about 15 feet below sea surface.

3) Redondo Beach fossil fired plant. Reject heat from 1612 Mw_e generation. Two offshore outfall systems: a) two 10-foot diameter pipes discharging vertically about 2100 feet offshore; and b) a single 14-foot diameter pipe discharging vertically 300 feet off, about 16 feet beneath water surface.

4) El Segundo fossil fired plant. Reject heat from 1020 Mw_e generation. Two offshore outfall systems: a) two 10-foot diameter pipes, discharging 2100 feet offshore, vertically, 20 feet beneath ocean surface; and b) two 12-foot diameter pipes, discharging 2070 feet offshore, vertically, 20 feet beneath ocean surface.

To this author's knowledge, no large power plant uses diffusers for offshore ocean discharge at present, although such a system is proposed for the Shoreham plant [95], discharging to Long Island Sound.

2.1.3 Hydrodynamic Regimes

Experimental observations of forced plumes issuing from submerged ports have revealed the existence of four distinct flow regimes, as follows (Figure 2.3):

- Zone of flow establishment (jet flow)
- Zone of established flow (mixed flow)
- Transition from established to drift flow, and
- Zone of drift flow.

The zone of flow establishment is in effect a transition zone from pipe flow to an established forced plume. Consider fluid issuing from an outfall port of diameter D (Figure 2.3), to the surrounding ocean, with a turbulent velocity profile. For the sake of analysis, this profile is usually assumed uniform with velocity v_0. Immediately the velocity begins to deteriorate at the flow boundary as a result of turbulent mixing with the surrounding ocean water. This region of mixing spreads both inward toward the center of the plume and outward into the sur-

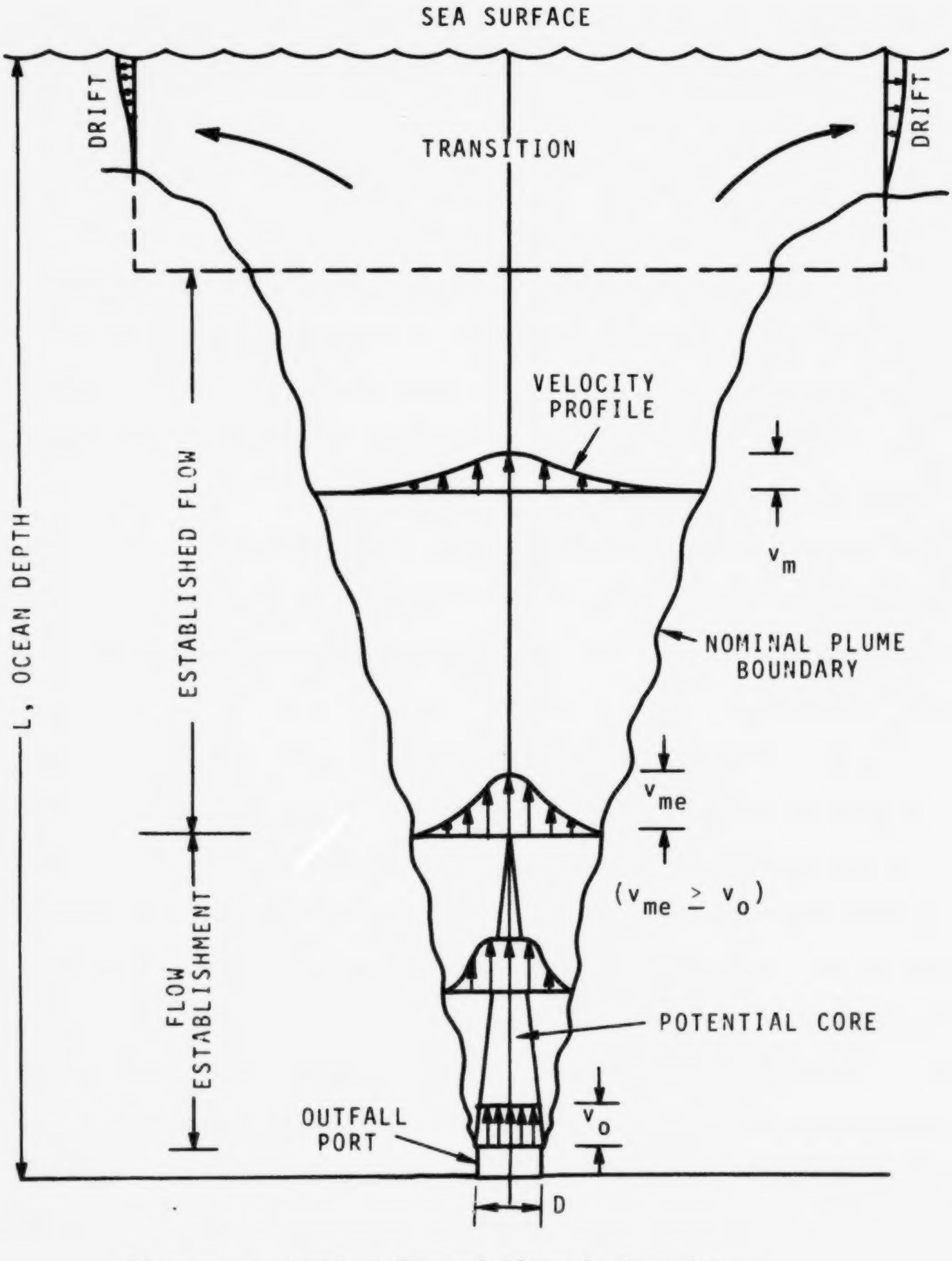
SEA SURFACE
DRIFT
TRANSITION
DRIFT
VELOCITY PROFILE
v_m
L, OCEAN DEPTH
ESTABLISHED FLOW
NOMINAL PLUME BOUNDARY
v_{me}
$(v_{me} \geq v_o)$
FLOW ESTABLISHMENT
POTENTIAL CORE
OUTFALL PORT
v_o
D

Figure 2.3 Vertical Thermal Plume in Deep Water, Illustrating Possible Flow Regimes

roundings. Within a short distance, z_e, from the outfall port, the interchange of momentum due to mixing has spread to the center of the plume. At this point, it is generally assumed that the plume vertical velocity profile is fully developed, or established.

In the zone of established flow, velocity profiles are approximately similar at all axial locations and the driving force may be either initial momentum, buoyancy, or both (mixed flow). As distance from the outfall increases, the effective width of the plume and the amount of plume flow increases as a result of lateral mixing or turbulent diffusion (commonly called entrainment). Momentum of the plume at successive cross-sections is changing according to the density difference between the plume and surroundings. Maximum velocity, v_m, of the plume will decrease, except if the buoyancy is large compared to initial momentum, in which case the maximum velocity may increase momentarily near the outfall.

The transition from established flow to drift flow is caused by the plume encountering the ocean surface or by the plume attaining a neutrally buoyant condition in a density stratified sea. Here velocity profiles change drastically with essentially all mean vertical motion vanishing. The motion at the transition zone termination may be dominated by prevailing ocean currents.

In the zone of drift flow, prevailing ocean currents will generally dominate the plume motion, although a lateral density flow will persist if the plume is situated on the ocean surface with buoyancy. Lateral mixing is dominated by ocean turbulence, whereas vertical mixing depends on both the plume and environment driving forces.

Under certain conditions, all of the above hydrodynamic regimes will not prevail. For instance, in the case of a large diameter port issuing in shallow water, the zone of established flow will most likely be absent. This situation is usually termed a "confined plume" (Figure 1.4) and the hydrodynamics are characterized by a continuous transition from pipe flow to drift flow.

An example of a typical confined plume is the thermal effluent of the Southern California Edison power plant located at San Onofre, California, discharging approximately 15 feet beneath the sea surface. The port is vertical and 14 feet in diameter. Based on experiments by Albertson, et al. [4] concerning neutrally buoyant jets, this depth is less than the length for flow establishment.

For shoreline outfalls, the same flow regimes exist. However, the zone of established flow may be less distinct depending on the relative magnitudes of initial momentum and buoyancy (initial densimetric Froude number). This zone will assert itself if buoyancy is small or initial momentum is large. In the case of small initial momentum and moderate or large buoyancy, the initial mixing zone will be a continuous transition from the outfall to drift flow without established flow in the sense of similar velocity profiles.

2.1.4 Oceanographic Effects

The nature of the surrounding ocean can have a dramatic effect on the behavior of a thermal plume. Probably the most influential of these oceanographic variables are the following:

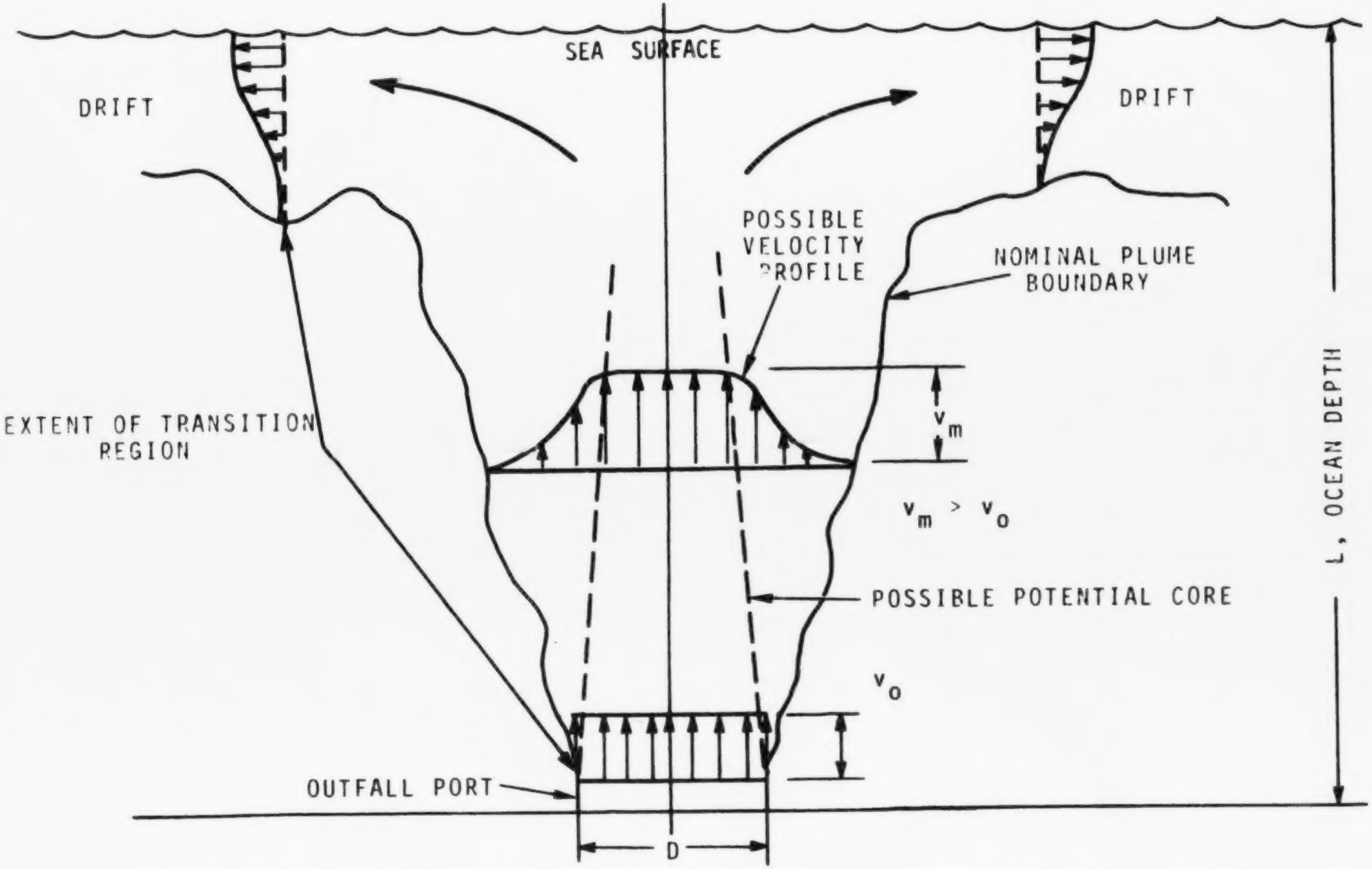
SEA SURFACE
DRIFT
DRIFT
POSSIBLE VELOCITY PROFILE
NOMINAL PLUME BOUNDARY
EXTENT OF TRANSITION REGION
v_m
$v_m > v_o$
L, OCEAN DEPTH
POSSIBLE POTENTIAL CORE
v_o
OUTFALL PORT
D

Figure 2.4 Vertical Thermal Plume in Shallow Water, Illustrating Continual Transition of the Flow Field

- density stratification,
- currents, and
- turbulence.

2.1.4.1 Density Stratification

In all discussions concerning ambient density stratification, stable stratification is implied. One effect of stratification is stabilization of the ambient flow field insofar as vertical convection and mixing are concerned. However, the discussion in this chapter will be confined to the direct effect of limitation of height of rise for plumes issuing from submerged outfalls.

The maximum height that the thermal plane will attain (and whether the plume will reach the surface or not) depends largely on the ambient density structure. Obviously, this discussion does not apply to confined plumes, but to cases where the outfall port size is small compared to the ocean depth, as for example, diffuser ports. Both theory and experiment have shown that the plume will always reach the surface if the ocean is homogeneous with respect to density.

The ocean, however, is rarely homogeneous, except perhaps in very shallow coastal waters where good vertical mixing occurs. The reason that a thermal plume may not penetrate to the ocean surface in a density stratified environment is that the plume entrains the heaviest water nearest the outfall. This water causes dilution to some extent and is carried upward with the plume. As the plume ascends, the density difference between the plume and surroundings steadily decreases because the flow is being diluted and cooled through entrainment, and because the density of the surroundings is decreasing upwards.

If the density stratification has sufficient magnitude (among other considerations which will be discussed later), the plume will eventually reach a level of neutral buoyancy some distance below the water surface. At this point the flow continues upward only by virtue of the vertical momentum it possesses at that point. As the plume continues upward, it continues to entrain liquid that is now less dense than the plume flow; hence, the flow is negatively buoyant. Eventually, all upward vertical momentum is lost and, since the plume liquid is denser than the surroundings at that depth, the pollutants will cascade downward around the upward flow.

Small oscillations in the vertical motion will follow and when these oscillations vanish the plume is said to be "trapped" (Figure 2.5). At the trap level all mean motion is horizontal since the flow is neutrally buoyant (assuming that environmental isosteric surfaces are horizontal).

2.1.4.2 Effect of Currents

Currents have a dramatic effect on plume behavior in nearly all flow regimes. The types of currents that might have influence are tidal currents, longshore currents, upwelling, wind driven surface currents, and persistent currents that are peculiar to a certain locale.

The zone of flow establishment is essentially unaffected by cross currents; but, in the zone of established flow (deep water), a cross current will cause the plume to be "bent-over" (Figure 2.6). The most significant effect of this bending is a decrease in the height of rise, also, the dynamics within the plume are changed.

When the plume is bent over, two distinct counter rotating vortices are formed (Figure 2.6). These vortices are quite apparent in atmospheric smoke plumes discharging into a cross wind; the same phenomenon occurs in the ocean.

In the drift flow regime, the plume flow is carried along with the ocean current nearly as though it were the ambient water. Thus, ocean currents play a dominant hydrodynamic role on the eventual fate of the pollutant. Upwelling causes a persistent offshore surface current,

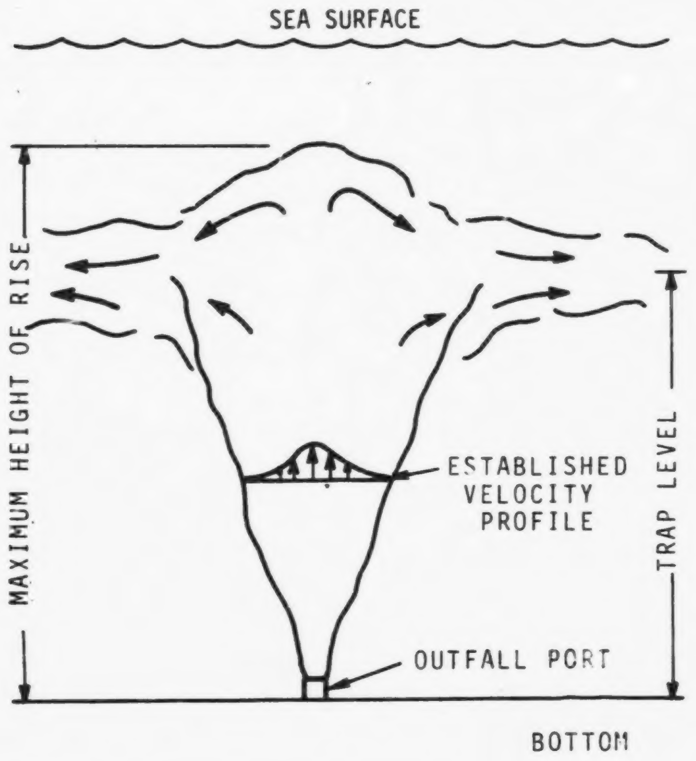
SEA SURFACE
MAXIMUM HEIGHT OF RISE
TRAP LEVEL
ESTABLISHED VELOCITY PROFILE
OUTFALL PORT
BOTTOM

Figure 2.5 Possible Configuration of a Vertical Buoyant Plume in Stratified Receiving Water

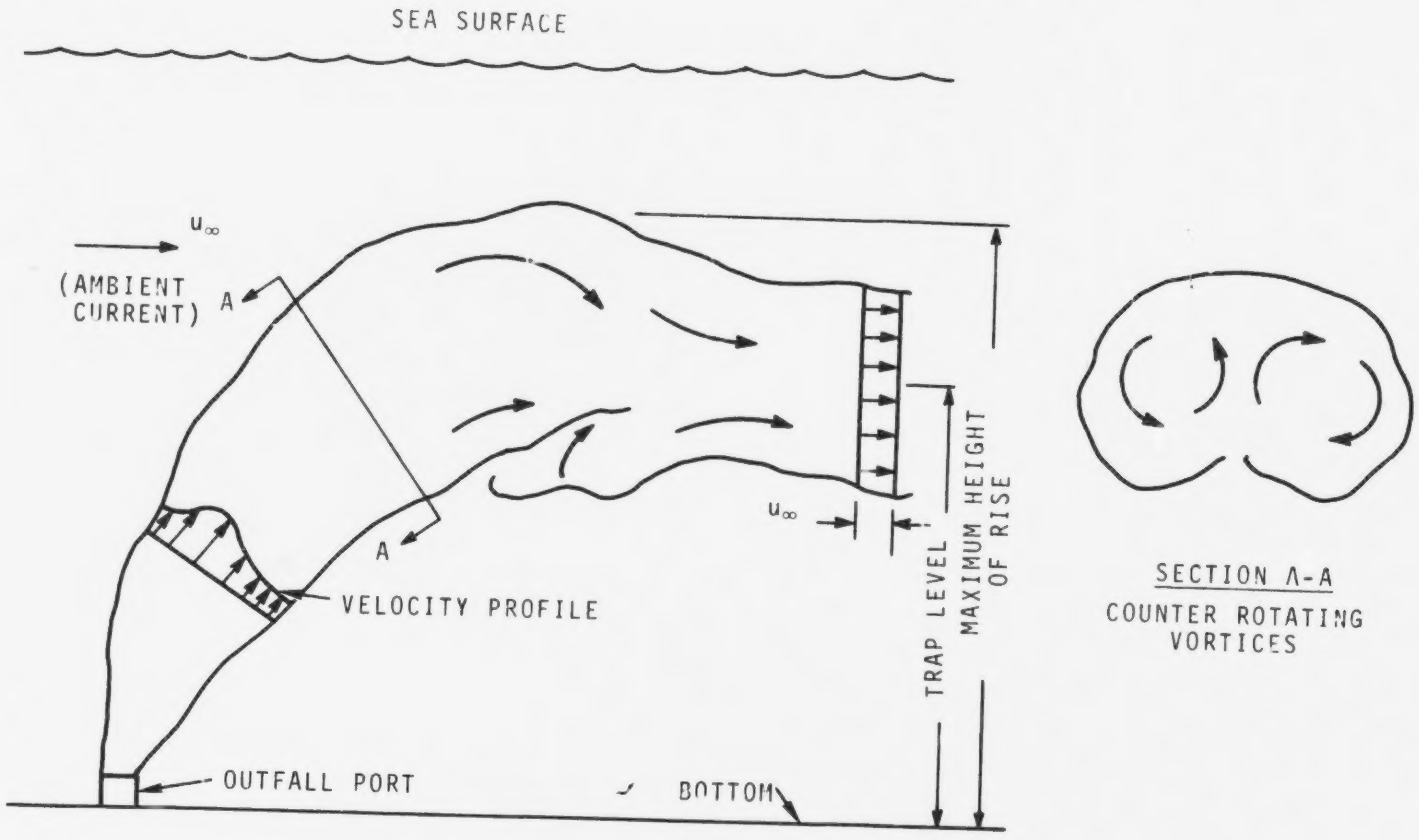
SEA SURFACE
u_∞
(AMBIENT CURRENT)
A
A
VELOCITY PROFILE
OUTFALL PORT
BOTTOM
u_∞
TRAP LEVEL
MAXIMUM HEIGHT OF RISE
SECTION Λ-A
COUNTER ROTATING VORTICES

Figure 2.6 Possible Configuration of a Buoyant Plume in Stratified Receiving Water with Cross-Current, u_∞

thus, a surface plume could be carried out to sea. Wind driven surface currents and tidal currents can cause the pollutant to be carried onshore or out to sea, and longshore currents can cause the pollutant to be distributed along the shoreline.

2.1.4.3 Ocean Turbulence

The origin of oceanic turbulence is not fully understood, although in the surface zone it is probably caused mostly from wind-generated wave action. As such, the turbulence is neither homogenous nor isotropic, and only the gross behavior can be described.

Ocean turbulence has some effect on all regimes of plume flow. Turbulence scales that are on the same size or larger than the plume cross-section will have an effect similar to a crosscurrent, and all scales should have some influence on the plume entrainment rate (although it is thought that the influence is small in all zones except the drift regime, since turbulence generated by the plume dominates the ocean turbulence). In the zone of drift flow scales of motion larger than the flow field result in action similar to oceanic currents, and the pollutant field simply flows along with the turbulent motion. Smaller scales of motion add to the eddy diffusion of the pollutant; thus, as the pollutant field spreads, larger and larger scales of eddy mixing come into play.

Another factor complicating oceanic turbulence is that it is highly anisotropic, at least in the larger scales of motion. Since most oceanic waters are density stratified to some degree (except perhaps in shallow water), vertical mixing is suppressed to a great extent. Thus, a pollution field diluted by eddy diffusion will spread much more rapidly in the lateral direction than in the vertical.

2.1.4.4 Air-Sea Interactions

Wind and heat transfer are the major air-sea interface phenomena which may significantly affect thermal plume dynamics. Wind stress at the sea surface causes two local effects which have previously been mentioned: wind driven surface current, and turbulence. And, on a larger scale, wind is responsible for coastal upwelling. We will only point out these wind stress effects here and refer the interested reader to such references as Neumann and Pierson [63] or Wada [107] for additional details and references.

Heat transfer at the interface is carried on by atmospheric convection, radiation, and evaporation. Evaporation is probably the most significant of these modes and is materially affected by the surface temperature and conditions in the atmospheric boundary layer such as temperature, humidity and turbulence. Again, wind plays an important role here through promotion of atmospheric turbulence and convective currents. Radiation heat transfer depends on the sea surface temperature and albedo, atmospheric conditions such as turbidity, and position of the sun.

The effect of surface heat transfer is more complicated than merely heating or cooling of the plume. For instance, if heat is lost at the surface, convective downcurrents of cooler water may occur, tending to homogenize the plume vertically. If heat is gained at the surface, the plume will become more stable and suppress vertical mixing.

Atmospheric heat transfer will affect the plume dynamics predominately in the drift flow regime when the plume is situated at the surface. The area exposed to the atmosphere in the surface transition (zone 3) is small on a comparative basis and will likely be unaffected by surface heat transfer.

2.2 Plume Analysis State-of-the-Art

There has been a great deal of theoretical and experimental work carried out in the past 20 years or so dealing with the dynamics of buoyant plumes. Most of this work has dealt directly with either atmospheric smoke plumes or ocean plumes caused by submerged offshore industrial and municipal waste outfall systems: (cf. Baumgartner and Trent [12]). Much lesser and more recent efforts have treated horizontal shoreline discharges (cf. Stolzenbach and Harleman [94]). More basic studies concerned with turbulent transport quantities in jet flow have also received much attention.

In this section we will briefly outline the state-of-the-art and past studies dealing with plume calculations. Table 2.1 summarizes a good share of the work related to plume investigations both theoretical and experimental. This table is by no means all inclusive and the particular categories may not be completely descriptive of the work accomplished in the cited references. However, it does serve to illustrate where research emphasis has been placed on problems which are related both directly and indirectly to thermal outfall analysis.

A brief discussion of Table 2.1 will be given separately for submerged and horizontal shoreline outfalls.

TABLE 2.1. SUMMARY OF WORK PERTINENT TO OCEAN OUTFALL PLUME ANALYSIS

			Geometry				Type of Flow			Ambient Condition				Principal Zone Investigated						Solution Methods			2-D Finite Diff.	
Principal Investigator	Ref.	Application	Vertical Round Port	Horizontal, Submerg., Round	Horizontal Shoreline	Relative L/D Ratio*	Momentum Jet	Simple Plume	Forced Plume	Homogeneous	Stratified	Stagnant	Cross-Current	Zone 1	Zone 2	Zone 3	Zone 4	Experimental or Field Data	Analytical	Similarity Sol.	Diffusion Equation	Empirical and/or Dimensional Analysis	Linear Momentum	Vorticity-Stream Function
Albertson	4	Sub. Jets		X		L	X			X		X		X				X	X			X		
Albertson	4	Sub. Jets		X		L	X			X		X			X			X	X	X				
Baines	8	Sub. Jets		X		L	X			X		X		X				X				X		
Hinze	41	Sub. Jets		X		L	X			X		X		X				X						
Schmidt	85	Thermals				L		X		X		X			X			X	X	X				
Rouse	81	Thermals				L		X		X		X			X			X	X	X				
Priestley	73	Plumes	X			L			X	X	X	X			X			X	X	X				
Priestley	74	Plumes	X			L			X	X			X		X		X	X	X					
Morton	60	Thermals				L		X		X		X			X				X	X				
Morton	58	Plumes	X			L			X		X	X			X				X	X				
Abraham	1	Waste Outfall	X	X		L	X		X	X	X	X		X	X			X	X	X				
Abraham	3	Jets				L	X			X		X			X				X	X				
Fan	26	Waste Outfall	X	X		L			X	X	X	X			X			X	X	X				
Fan	27	Waste Outfall	X			L			X	X		X	X		X			X	X	X				
Keffer	50	Plume	X			L			X	X		X	X		X			X	X	X				
Cederwall	17	Waste Outfall	X	X		L			X	X	X	X			X			X	X	X				
Brooks	16	Waste Outfall	X			L			X		X	X			X				X	X		X		
Tomich	99	Jets	X			L	X			X		X			X			X	X				X	
Zeller	112	Thermal Outfall			X				X	X			X		X			X	X	X				
Jen	48	Thermal Outfall			X				X	X		X			X			X	X	X				
Tamai	96	Thermal Outfall			X				X	X		X			X			X	X	X				
Hayashi	38	Thermal Outfall			X				X	X		X			X			X	X	X				
Sharp	88,89	Thermal Outfall			X	L			X	X		X				X		X				X		
Frankel	30	Waste Outfall	X			I			X	X		X			X	X		X				X		
Sami	83	Jets	X				X			X		X		X	X			X						
Stolzenbach	94	Thermal Outfall			X				X	X		X	X	X	X	X		X	X	X		X		
Hart	37	Waste Outfall	X			L			X	X	X	X			X			X						
Bosanquet	14	Waste Outfall		X		L			X	X	X	X			X			X	X	X				
Hoult	45	Plumes	X			L			X	X		X	X	X	X				X	X		X		
Wada	106	Thermal Outfall			X				X	X		X			X	X			X					X
Wada	108	Thermal Outfall			X				X	X		X					X		X					X
Manabe	56	Thermal Outfall			X				X	X							X		X					X
Okubo	64	Dispersion		NA				NA		X							X		X		X			
Okubo	65	Thermals				L		X			X	X			X				X	X				
Leenderste	53	Tidal Hydraulics		NA				NA		X							X	X	X				X	
Ramsey	75	Heated Jet	X						X	X			X	X	X	X		X						
Fay	29	Plumes	X			L			X	X		X	X	X	X			X				X		
Murota	62	Jets	X			I	X			X		X		X	X	X		X				X		
Masch	57	Tidal Hydraulics		NA				NA		X							X	X	X				X	
Fox	28	Plumes	X			L			X	X	X	X			X			X	X	X				
Murgai	61	Thermals				L		X		X	X	X			X				X	X				
Hirst	44	Plumes	X		X	L			X	X	X	X	X		X				X	X				
Schmidt	86	Smoke Plumes	X			L			X		X	X	X		X				X	X		X		
Hirst	43	Plumes	X	X		L			X	X	X	X	X	X					X	X		X		
Scorer	87	Plumes	X			L			X	X		X	X		X				X			X		
Morton	59	Plumes	X			L			X	X	X	X			X				X	X				
Csanady	22	Plumes	X			L		X		X	X		X		X				X		X			
Anwar	5	Waste Outfall	X	X		L			X	X		X			X			X	X	X				
Abraham	2	Waste Outfall	X			L			X	X		X			X				X	X				
Turner	102	Waste Outfall	X			L			X	X		X		X	X	X		X	X	X				
Rawn	76	Waste Outfall		X		L			X	X		X			X			X				X		
Harremoes	36	Waste Outfall		X		L			X															
Tulin	101	Waste Outfall	X			L			X	X	X	X	X		X	X			X	X				
Baumgartner	11	Waste Outfall	X			L			X		X	X			X			X	X	X				

*The L/D ratio applies only to submerged outfalls: S, L/D ≤5, I, 5<L/D<15, L, L/D 15.

2.2.1 Submerged Outfalls

For submerged outfalls the depth of discharge dictates the method of analysis. Deep water cases are substantially simpler to analyze than the shallow water counterparts (at least in the absence of cross currents) which is a result of the applicability of similarity solutions. Similarity analysis has expedited the theoretical analysis in this zone and resulted in mathematical models that are sufficiently accurate for engineering calculations.

Zone 1 has received substantial attention but is of minor importance in deep water analysis because it is a relatively short-distance effect (approximately six port diameters or less). Most of the work involving this zone has been carried out in the absence of buoyant forces. Abraham [1] presents a mathematical model for cases where buoyant forces have a significant affect on the zone length. Recently, Hirst [43] has presented a more thorough analysis.

There has been essentially no theoretical work done for zone 3 of the deep water plume (i.e., near the surface or in the region of the maximum height of rise). It is generally assumed that the similarity solutions of zone 2 hold in zone 3; but, this is a very poor assumption. Frankel and Cumming [30] have shown through experiment that this is the case. Sharp [88,89] has experimentally investigated the surface spread of a hot water plume, and Murota and Muraoki [62] have investigated the effect of a free surface on plume hydrodynamics.

Very little theoretical work has been done on deep water plumes in the presence of a crosscurrent. This lack of effort is undoubtedly a result of the solution difficulty since similarity principles are not strictly valid for this case. However, Fan [26] has treated the crossflow problem for a vertical plume using similarity assumptions and obtained reasonable results. There are serious theoretical questions concerning the use of similarity profiles in the presence of a crosscurrent. Hirst [44] presents analysis for crosscurrents which includes a stratified ambient medium. Various experimental studies coupled with dimensional analysis have been carried out for the crossflow problem, but as yet no generally proven computational model has been published which relates details of the plume dynamics.

Deep water plume analysis is particularly applicable to waste outfalls having small ports, common to diffuser systems. Typical submerged thermal outfalls such as those off the Southern California coast cited by Zeller and Rulifson [113] utilize very large, vertical single ports. The amount of receiving water between the port and sea surface may be on the order of 1-3 port diameters. No published theoretical studies have treated plumes with such L/D ratios. In this case zone 2 does not exist and there is no delineation between zones 1 and 3. All that may be said is that the flow undergoes a transition from pipe flow to drift flow.

The following general conclusions are made concerning submerged outfall state-of-the-art computational models.

1. Acceptable computational models are available for deep water plumes except for;
    - Zone 3, the surface or maximum-height-of-rise transition zone, and

- plumes issuing in crosscurrent (existing models to be proven).

2. There is no acceptable computation model or technique available for shallow water plumes such as those typical of large thermal power plant outfalls.

2.2.2 Horizontal Shoreline Outfalls

Horizontal shoreline discharge is also utilized by a number of thermal power plants throughout the United States. Table 2.1 illustrates that there has been only modest effort made to analyze this problem. From a mathematical modeling standpoint the horizontal surface discharge of a thermal plume is extremely complex since the phenomena involved are inherently three-dimensional (the same is true for horizontal submerged ports in shallow water, and the case of a crosscurrent in deep water).

In spite of the three-dimensional aspects of the shoreline plume, various solutions have been formed using similarity princples (e.g., Zeller [112], Jen, et al. [48], Hayashi, et al. [38], Tamai, et al.[96] and Stolzenbach, et al. [94]. Except for the work of Stolzenbach, none of these methods are, in this author's opinion, acceptable for engineering computations. Before a completely acceptable model is constructed for general application, three-dimension flow characteristics will need to be accounted for in some manner along with crosscurrent effects.

2.3 Work Description

The previous section delineates several areas of outfall analysis which need attention. As a practical matter it is not feasible to incorporate all of these areas into a general mathematical model which would apply to all outfall configurations and oceanographic conditions.

The scope of this manuscript is limited to vertical plumes. We are primarily interested in large single port vertical thermal outfalls issuing in shallow water (Figure 2.4). Typical existing configurations are those located at Moss Landing, San Onofre and Redondo Beach, cited earlier. However, the ultimate objective of the work is to provide a complete program which mathematically models the temperature and velocity distribution in a vertical thermal plume, from outfall port to the drift flow regime (zone 4), regardless of ocean depth. The transition region, as defined here, refers to any part of the flow field for shallow water plumes. This region is the portion of the program which must be treated by finite-difference techniques and constitutes the principle effort of this work.

In addition we also set down the difference equations appropriate for a line plume, but do not include these in the modeling program.

In summary, the work covered by this manuscript deals with the problem of mathematically modeling velocity and temperature distributions in the locale of vertical thermal outfalls. The techniques for analysis are as follows:

- Shallow water plumes : finite-differences

- Deep water plumes

1. Zone 1 : existing empirical
2. Zone 2 : similarity solution
3. Zone 3 : finite-differences

The primary task described in this manuscript is the finite-difference application to the confined plume and computation of the entire flow field dynamics for zones I, II, and III. The circulation of the ambient is also included. Although there have been various related studies, none have dealt with the numerical solution of a confined, vertical plume and radial surface spread. Tomich [99] numerically modeled the compressible free jet problem, Ma and Ong [55] investigated an impulsively started momentum jet, but paid little attention to the more complicated features of the dynamics. Recently, Pai and Hsieh [68] have carried out numerical work with laminar jets.

CHAPTER 3

TRANSPORT EQUATIONS - GENERAL THEORY

In this chapter the fundamental laws and equations which govern marine hydrodynamics and energy transport are set down. We begin by considering the fundamental equations for laminar, incompressible flow and modify these equations so they are appropriate for marine considerations.

These equations are written in various forms which are appropriate for later discussion concerning theory review, similarity solutions, and numerical considerations.

3.1 Coordinate System

The governing differential equations are given in Cartesian tensoral form with coordinates x_i (Figure 3.1). For analysis of the local sea, the geopotential surface is assumed to be flat.

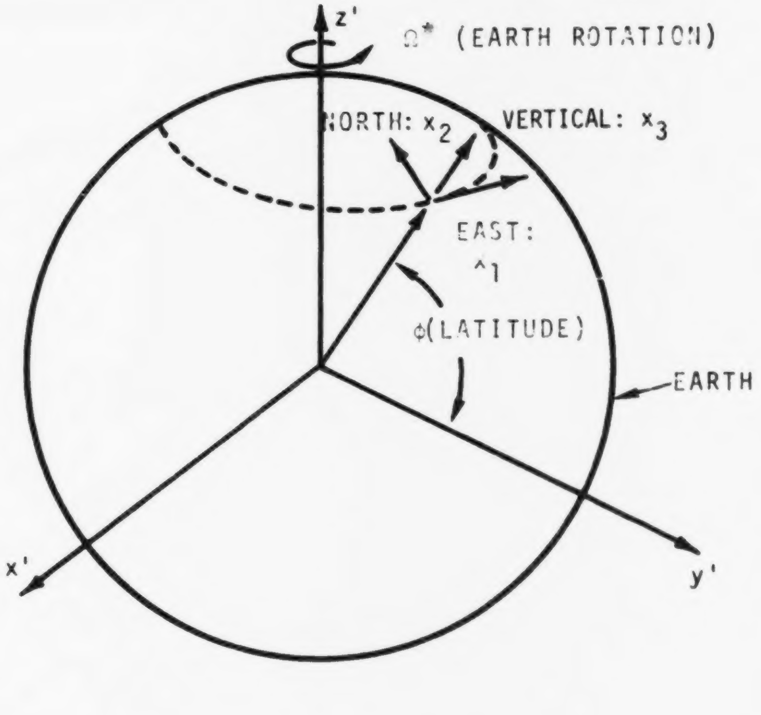

Figure 3.1
Rectangular Coordinate System

3.2 Conservation Laws

The differential equations governing the heat and momentum transport of a thermal plume in the oceanic environment may be derived from the following physical laws:

- Continuity (conservation of mass)
- Newton's Second Law (conservation of momentum), and
- The first law of thermodynamics (conservation of energy)

In addition, an appropriate equation of state is needed to relate sea water density in terms of local temperature and salinity.

Detailed derivation of the primitive conservation equations will not be discussed here but may be found in such texts dealing with fluid dynamics (cf. Bird, Stewart and Lightfoot [13], Welty, Wicks and Wilson [115], Hinze [40]). A few modifications of the standard form of the conservation equations must be made so that they apply in general to a thermal plume in the sea. These modifications are chiefly concerned with turbulent approximations, incorporation of coriolis effects, and the Boussinesq approximation concerning small density variations. Additional detail concerning these approximations may be found in standard references dealing with marine hydrodynamics (cf. Hill [39], Phillips [70]) and the general subject of turbulence (e.g. Hinze [40]).

The primitive equations appropriate for our analysis are presented in Cartesian tensoral form[1] as follows:

---

[1] Einsteinian notation is used where repeated indices imply summation over all three index values (i = 1,2,3).

Continuity:

$$\frac{D\rho}{Dt} + \rho \frac{\partial u_i}{\partial x_i} = 0. \qquad (3.1)$$

The operator D/Dt in the above equation is the substantial derivative and has the usual meaning:

$$\frac{D}{Dt} = \frac{\partial}{\partial t} + u_j \frac{\partial}{\partial x_j} ,$$

where t is time and u_j is velocity along the j^{th} coordinate. In Equation (3.1) the quantity ρ is density.

Momentum:

$$\rho \frac{Du_i}{Dt} + e_{ijk} 2\rho u_k \Omega_j^* = - \frac{\partial P}{\partial x_i} - \rho g \delta_{i3} + \frac{\partial \tau_{ij}}{\partial x_j} \qquad (3.2)$$

where Ω_j^* is the component of planetary angular velocity along the j^{th} coordinate, P is pressure, g is the local gravitational constant and τ_{ij} is the fluid molecular stress tensor. The symbol e_{ijk} is the usual cartesian permutation tensor which takes values of zero if any two of the three subscript are identical, +1 for even permutations and -1 for odd permutations. The symbol δ_{ij} is the Kronecker delta which is equal to 1 when i = j, and otherwise 0. Coriolis effects are incorporated into the momentum equation by the term $e_{ijk} 2\rho u_k \Omega_j^*$ and, according to the specified coordinate system, (Figure 3.1) gravitational forces act only along the x_3 direction; hence, $\delta_{ij} = \delta_{i3}$.

In any fluid dynamic system, variations of density may cause fluid motion due to the action of gravity. In the ocean, these density variations may be caused by temperature differences and variation of local salt content, or concentrations of other materials whether in solution or not. Hence, in lieu of the heat transport equation we will consider at this point a transport equation for a general scalar quantity, Γ, where Γ may be heat, salinity or other dilute transferable constituents. The Γ transport equation is:

$$\frac{D\Gamma}{Dt} = \frac{\partial}{\partial x_i}\left(\kappa_\gamma \frac{\partial \Gamma}{\partial x_i}\right) + \dot{\phi} . \tag{3.3}$$

Constituent sources, sinks and dissipative mechanisms are incorporated in the term $\dot{\phi}$ and the symbol κ_γ is the molecular diffusion coefficient for the Γ quantity.

3.2.1 Continuity

In the ocean, and especially in the case of the thermal plume, the density field, ρ, varies with both space and time,

$$\rho = \rho(x_i,t). \tag{3.4}$$

However, essentially all density variation is caused by distributions of heat content, salinity, etc., as opposed to compressibility effects (i.e. high speed compressible effects). The local density anomaly is very small compared to the local value of density, and the conservation of mass (Equation 3.1) may be approximated with sufficient accuracy by the volume continuity equation

$$\frac{\partial u_i}{\partial x_i} = 0. \tag{3.5}$$

We point out here that although $\frac{\partial \rho}{\partial x_i} = 0$ may be an acceptable approximation with regard to mass conservation, this quantity cannot be ignored in the momentum equation (see Section 3.3), and is precisely the coupling between momentum transport and Γ transport.

3.2.2 The Equations of Motion for Turbulent Flow

Within the framework of assumptions concerning continuous fluid properties, constant gravitational force, and negligible earth curvature, the momentum transport equations (3.2) are valid regardless of the nature of the flow or fluid. The usual additional assumptions in hydrodynamics are that the fluid is Newtonian, incompressible and that Stokes viscosity relationships are a valid description of the fluid stress rate-of-strain (cf. Welty et al.). Thus, the stress terms (Equation 3.2), τ_{ij}, may be replaced by

$$\tau_{ij} = \mu \frac{\partial u_i}{\partial x_j} , \qquad (3.6)$$

where μ is dynamic viscosity.

For the purpose of treating turbulent flow, it is assumed that the velocity components, u_i, pressure, P, and density, ρ, are composed of mean or average parts and superimposed random fluctuating parts (cf. Hinze [40]). Symbolically,

$$u_i = \overline{u}_i + u'_i ,$$

$$P = \overline{P} + P' , \text{ and}$$

$$\rho = \overline{\rho} + \rho' ,$$

where the overbar represents mean of values and the prime, random values. These definitions are substituted into the equations of motion and the result is time averaged term-by-term over a sufficiently long period of time to obtain

$$\bar{\rho}\left[\frac{D\bar{u}_i}{Dt} + \frac{\partial}{\partial x_j}(\overline{u'_i u'_j}) + 2e_{ijk}\Omega^*_j\bar{u}_k\right] = -\frac{\partial\bar{P}}{\partial x_i} - \bar{\rho}g\delta_{i3} + \frac{\partial\bar{\tau}_{ij}}{\partial x_j}{}^{1} \qquad (3.7)$$

which is seen to be identical in the mean motion with Equation (3.2) except for the appearance of the term

$$\frac{\partial}{\partial x_j}(\overline{u'_i u'_j}).$$

A new quantity is now defined:

$$R_{ij} = -\rho\,\overline{u'_i u'_j}, \qquad (3.8)$$

which is called the Reynolds stress. Finally the complete equations of motion in the rotating Earth reference frame are written as

$$\rho\left(\frac{Du_i}{Dt} + 2e_{ijk}\Omega^*_j u_k\right) = -\frac{\partial P}{\partial x_i} - \rho g\delta_{i3} + \frac{\partial}{\partial x_j}(\tau_{ij} + R_{ij}) \qquad (3.9)$$

for the mean flow. Here the overbars denoting average quantities have been omitted since mean, or average, quantities are implied. The turbulent stress terms may be related to mean flow quantities through the Prandtl mixing length theorem (cf. Neumann and Pierson [63]) to obtain

---

[1] Terms envolving fluctuations of pressure and density have been ignored.

$$R_{ij} = -\overline{\rho u'_i u'_j} = \rho\varepsilon_{ij}\frac{\partial u_i}{\partial x_j} \ . \tag{3.10}$$

Hence, using Equations (3.6) and (3.10) in (3.9) yields

$$\rho\left(\frac{Du_i}{Dt} + 2e_{ijk}\Omega^*_j u_k\right) = -\frac{\partial P}{\partial x_i} - \rho g\delta_{i3} + \frac{\partial}{\partial x_j}\left[\rho(\nu + \varepsilon_{\underline{ij}})\frac{\partial u_i}{\partial x_j}\right]^1 , \tag{3.11}$$

where ε_{ij} is the eddy diffusion coefficient for momentum, a second order tensor, and ν is kinematic viscosity.

In the case of a thermal plume, $\varepsilon_{ij} >> \nu$ except where velocity gradients are small and the flow has strong stratification. We will assume that ε_{ij} includes molecular viscous effects and write the momentum equations as

$$\rho\left(\frac{Du_i}{Dt} + 2e_{ijk}\Omega^*_j u_k\right) = -\frac{\partial P}{\partial x_i} - \rho g\delta_{i3} + \frac{\partial}{\partial x_i}\left(\rho\varepsilon_{\underline{ij}}\frac{\partial u_i}{\partial x_j}\right) . \tag{3.12}$$

3.3 The Boussinesq Approximation

In this work, four quantities of density are defined as follows:

- $\rho = \rho(x_i,t)$, the density at a point in the thermal plume.
- $\rho = \rho_\infty(x_3)$, the density distribution which would exist in the local sea in the absence of the plume.
- $\rho_r =$ Constant, a reference density for the receiving water.
- $\rho_o =$ Constant, the density of the effluent issuing from the outfall port.

---

[1] The summation convention for repeated tensoral indices does not apply to underscored indices in this text.

The density distribution of the reference ocean, $\rho_\infty(x_3)$, is assumed to be independent of time and vary with x_3 alone.

Buoyant forces on a fluid element are established by the density difference

$$\Delta\rho = \rho - \rho_\infty .^{1} \tag{3.13}$$

So that,

$$\rho = \rho_\infty + \Delta\rho . \tag{3.14}$$

According to the Boussinesq approximation, (cf. Phillips [70]) when density variations, $\Delta\rho$, are small,(i.e. $|\Delta\rho/\rho| << 1$) these variations may be ignored as they influence inertial and viscous terms in the equations of motion, but must be accounted for in the gravitational term. In view of Equation (3.14), the equations of motion may be written

$$\frac{Du_i}{Dt} + 2e_{ijk}\Omega_j^* u_k = - \frac{1}{\rho_r}\frac{\partial P}{\partial x_i} - \left(\frac{\Delta\rho + \rho_\infty}{\rho_r}\right) g\delta_{3i} + \frac{\partial}{\partial x_j}\left(\varepsilon_{\underline{\underline{ij}}}\frac{\partial u_i}{\partial x_j}\right) \tag{3.15}$$

Now, let P^o be the pressure difference between a point in the plume and outside the plume located on the same geopotential surface, so that

$$P^o = \frac{P - P_\infty}{\rho_r} = \frac{P}{\rho_r} - g\int_{x_3}^{0} \frac{\rho_\infty}{\rho_r}\, dx . \tag{3.16}$$

---

[1] Hereafter, we will refer to $\rho_\infty(x_3)$ as simply ρ_∞, keeping in mind the dependence on x_3.

Here, we have assumed that the pressure distribution in the reference ocean is hydrostatic. Hence, Equation (3.15) may be reduced to:

$$\frac{Du_i}{Dt} + 2e_{ijk}\Omega^*_j u_k = -\frac{\partial P^\circ}{\partial x_i} + \left(\frac{\rho_\infty - \rho}{\rho_r}\right) g\delta_{i3} + \frac{\partial}{\partial x_j}\left(\epsilon_{\underline{ij}}\frac{\partial u_i}{\partial x_j}\right) \quad (3.17)$$

Equation (3.17) is the so-called "advective" form of the equations of motion. This name has become popular among oceanographers and meterologists and is so called because the convective terms are expressed in the form $u_j \partial u_i/\partial x_j$.

The convective terms may be written in slightly different form by noting that

$$\frac{\partial u_j u_i}{\partial x_j} = u_j \frac{\partial u_i}{\partial x_j} + u_i \frac{\partial u_j}{\partial x_j} .$$

However, by Equation (3.5)

$$u_j \frac{\partial u_j}{\partial x_j} = 0,$$

so that for an incompressible flow

$$u_j \frac{\partial u_i}{\partial x_j} \equiv \frac{\partial u_j u_i}{\partial x_j}$$

Thus, Equation (3.17) may also be expressed as

$$\frac{\partial u_i}{\partial t} + \frac{\partial u_j u_i}{\partial x_j} + 2e_{ijk}\Omega^*_j u_k = -\frac{\partial P^\circ}{\partial x_i} + \left[\frac{\rho_\infty - \rho}{\rho_r}\right] g\delta_{i3} + \frac{\partial}{\partial x_j}\left[\epsilon_{\underline{ij}} \frac{\partial u_i}{\partial x_j}\right] \quad (3.18)$$

which is called the "conservative" form of the equations of motion.

3.4 The Pressure Equation

Equation (3.17), or (3.18) contains four unknown quantities; u_1, u_2, u_3, and P^o. Since only three scalar equations are involved, an additional relationship is required.

An equation for pressure, P^o, may be derived by taking the divergence of Equation (3.17). This operation yields:

$$\frac{\partial}{\partial t}\left(\frac{\partial u_i}{\partial x_i}\right) + \left(\frac{\partial u_j}{\partial x_i}\right)\left(\frac{\partial u_i}{\partial x_j}\right) + u_j \frac{\partial}{\partial x_j}\left(\frac{\partial u_i}{\partial x_i}\right) + 2e_{ijk}\Omega^{*}_{j}\frac{\partial u_k}{\partial x_i} +$$

$$\frac{\partial^2 P^\circ}{\partial x_i \partial x_i} + \frac{g}{\rho_r}\frac{\partial(\rho_\infty - \rho)}{\partial x_3} - \frac{\partial}{\partial x_i}\left[\frac{\partial}{\partial x_j}\varepsilon_{\underline{ij}}\frac{\partial u_i}{\partial x_j}\right] = 0. \tag{3.19}$$

By continuity

$$\frac{\partial u_i}{\partial x_i} = 0, \tag{3.20}$$

so that Equation (3.19) is reduced to

$$\frac{\partial^2 p^\circ}{\partial x_i \partial x_i} = -\left(\frac{\partial u_j}{\partial x_i}\right)\left(\frac{\partial u_i}{\partial x_j}\right) - 2e_{ijk}\Omega^{*}_{j}\frac{\partial u_k}{\partial x_i} + \frac{\partial B}{\partial x_3}$$

$$+ \frac{\partial}{\partial x_j}\left[\left(\frac{\partial \varepsilon_{\underline{ij}}}{\partial x_i}\right)\left(\frac{\partial u_i}{\partial x_j}\right)\right], \tag{3.21}$$

where B is the buoyancy parameter, defined as

$$B = \frac{g}{\rho_r}(\rho_\infty - \rho) \tag{3.22}$$

For the case where coriolis forces are neglected and quantities involving derivatives of eddy viscosity are small compared to other terms, the presssure equation is

$$\frac{\partial^2 p^\circ}{\partial x_i \, \partial x_i} = -\left(\frac{\partial u_i}{\partial x_j}\right)\left(\frac{\partial u_j}{\partial x_i}\right) + \frac{\partial B}{\partial x_3} \; . \tag{3.23}$$

3.5 Γ Transport

The Γ transport Equation (3.3) may be modified for turbulent flow by considering the transported quantity, Γ, to be composed of a mean part, $\bar{\Gamma}$, and a fluctuating part, Γ', or

$$\Gamma = \bar{\Gamma} + \Gamma' .$$

Then in a manner analogous to the method applied to the equations of motion, the turbulent Γ transport equation becomes

$$\frac{D\Gamma}{Dt} = \frac{\partial}{\partial x_i}\left(\varepsilon_{\gamma \underline{j}} \frac{\partial \Gamma}{\partial x_j}\right) + \dot{\Phi} \, , \tag{3.24}$$

Where $\varepsilon_{\gamma j}$ is the eddy diffusion coefficient and is assumed to include molecular effects.

3.5.1 Transport of Heat, Salinity and Buoyancy

Letting Γ = T, in Equation (3.24), where T is temperature, the heat transport equation is

$$\frac{DT}{Dt} = \frac{\partial}{\partial x_j}\left(\varepsilon_{Hj} \frac{\partial T}{\partial x_i}\right) . \tag{3.25}$$

In this case $\dot{\Phi}$ corresponds to heat sources and sinks and/or viscous dissipation. Since none of these effects are significant in an ocean plume, $\dot{\Phi}$ is neglected. The quantity ε_{Hj} is the turbulent heat diffusion coefficient and is assumed to include molecular effects. For salt transport, we let $\Gamma = S$, when S is salinity; hence,

$$\frac{DS}{Dt} = \frac{\partial}{\partial x_j} \left(\varepsilon_{Sj} \frac{\partial S}{\partial x_j} \right). \qquad (3.26)$$

Salinity is a conservative property, thus $\dot{\Phi}$ is omitted. The quantity ε_{Sj} is the combined molecular and turbulent mass diffusion coefficient.

The equations for heat and salinity transport are coupled to the Equations of motion (3.17) or (3.18) through the buoyancy term $(\rho_\infty - \rho)/\rho_r$. For that matter, any Γ constituent, which when transported in the system of interest causes density variations to occur, is coupled in the same fashion. Thus, it is not the absolute value of temperature, salinity, etc., which is important to the system dynamics, but resulting density variations in a lateral plane caused by the transport of these quantities. For this reason it is necessary only to deal with the transport of buoyancy in analyzing the dynamical behavior of the system. However, we must solve the equation for heat or salinity transport (in a system where differences of salinity and temperature are the causes of density variations) in order to establish the magnitude of temperature and salt content, and to treat certain boundary conditions. Once the density and temperature (or salinity) distribution is known, salinity (or temperature) may be calculated from an equation of state for sea water.

A "density transport" equation may be derived by combining Equations (3.25) and (3.26) [assuming that an equation of state, $\rho = \rho(S,T)$ holds] after the independent variables, T and S, have been changed to ρ Hence,

$$\frac{D\rho}{Dt} = \frac{\partial}{\partial x_j} \left(\varepsilon_{\rho j} \frac{\partial \rho}{\partial x_j}\right) + \varepsilon_{\rho j} \frac{1}{\rho}\left(\frac{\partial \zeta}{\partial x_j}\right) \cdot \left(\frac{\partial \rho}{\partial x_j}\right), \qquad (3.27)$$

where

$$\zeta = \frac{\partial T}{\partial \rho} + \frac{\partial S}{\partial \rho} \qquad (3.28)$$

A buoyancy parameter may be defined as

$$\Delta_1 = \frac{\rho_r - \rho}{\rho_r - \rho_o}$$

and the appropriate transport equation for Δ_1 is

$$\frac{D\Delta_1}{Dt} = \frac{\partial}{\partial x_j} \left(\varepsilon_{\rho j} \frac{\partial \Delta_1}{\partial x_j}\right) + \varepsilon_{\rho j}\left(\frac{\partial \zeta}{\partial x_j}\right) \cdot \left(\frac{\partial \Delta_1}{\partial x_j}\right). \qquad (3.29)$$

A second parameter Δ_2 which incorporates ρ_∞ may be defined as

$$\Delta_2 = \Delta_1 - \left(\frac{\rho_r - \rho_\infty}{\rho_r - \rho_o}\right) = \frac{\rho_\infty - \rho}{\rho_r - \rho_o} . \qquad (3.30)$$

The transport of Δ_2 is described by

$$\frac{D\Delta_2}{Dt} - u_3\frac{\partial\rho^*_\infty}{\partial x_3} = \frac{\partial}{\partial x_j}\left(\varepsilon_{\rho j}\frac{\partial\Delta_2}{\partial x_j}\right) - \frac{\partial}{\partial x_3}\left(\varepsilon_{\rho 3}\frac{\partial\rho'_\infty}{\partial x_3}\right)$$

$$+ \varepsilon_{\rho j}\frac{1}{\rho}\left(\frac{\partial\zeta}{\partial x_j}\right)\cdot\left(\frac{\partial\rho}{\partial x_j}\right) , \qquad (3.31)$$

where $\rho^*_\infty = \rho_\infty/(\rho_r - \rho_o)$

If density is a linear function of both temperature and salinity, that

$\rho - \rho_o = -a\ (T - T_o) + b(S-S_o)$,

then ζ = constant and $\partial\zeta/\partial x_j = 0$.

Equations (3.27), (3.29) and (3.21) become

$$\frac{D\rho}{Dt} = \frac{\partial}{\partial x_j}\left(\varepsilon_{\rho j}\frac{\partial\rho}{\partial x_j}\right) , \qquad (3.32)$$

$$\frac{D\Delta_1}{Dt} = \frac{\partial}{\partial x_j}\left(\varepsilon_{\rho j}\frac{\partial\Delta_1}{\partial x_j}\right) , \text{ and} \qquad (3.33)$$

$$\frac{D\Delta_2}{Dt} - u_3\frac{\partial\rho^*_\infty}{\partial x_3} = \frac{\partial}{\partial x_j}\left(\varepsilon_{\rho j}\frac{\partial\Delta_2}{\partial x_j}\right) - \frac{\partial}{\partial x_3}\left(\varepsilon_{\rho 3}\frac{\partial\rho^*_\infty}{\partial x_3}\right), \qquad (3.34)$$

respectively.

The quantity ζ, is seen to be a correction term which accounts for nonlinearities in the equation of state, $\rho = \rho\ (S,T)$. As it turns out, sea water density does vary approximately linearly with salinity (See Section 3.6) so that $\rho = f\ (T)$ for constant S.

In the remainder of this manuscript, Δ_1 and Δ_2 will be referred to as

- $\Delta_1 = \dfrac{\rho_r - \rho}{\rho_r - \rho_o}$, buoyancy parameter,
- $\Delta_2 = \dfrac{\rho_\infty(x_3) - \rho}{\rho_r - \rho_o} = \Delta_1 - \Delta_1\big|_\infty$, density disparity parameter.

The motivation for defining two buoyancy quantities is that it is more convenient to use Δ_1 in the numerical analysis (Chapter 5), whereas Δ_2 is convenient for similarity analysis. For consideration of salinity transport, a third buoyancy term is defined as

$$\Delta_3 = \frac{S_r - S}{S_r - S_o},$$

where S_r and S_o are the reference and outfall effluent salinities, respectively.

Figure 3.2 illustrates the relationship between the quantities and Δ_1 and Δ_2 at elevation X_3 = constant.

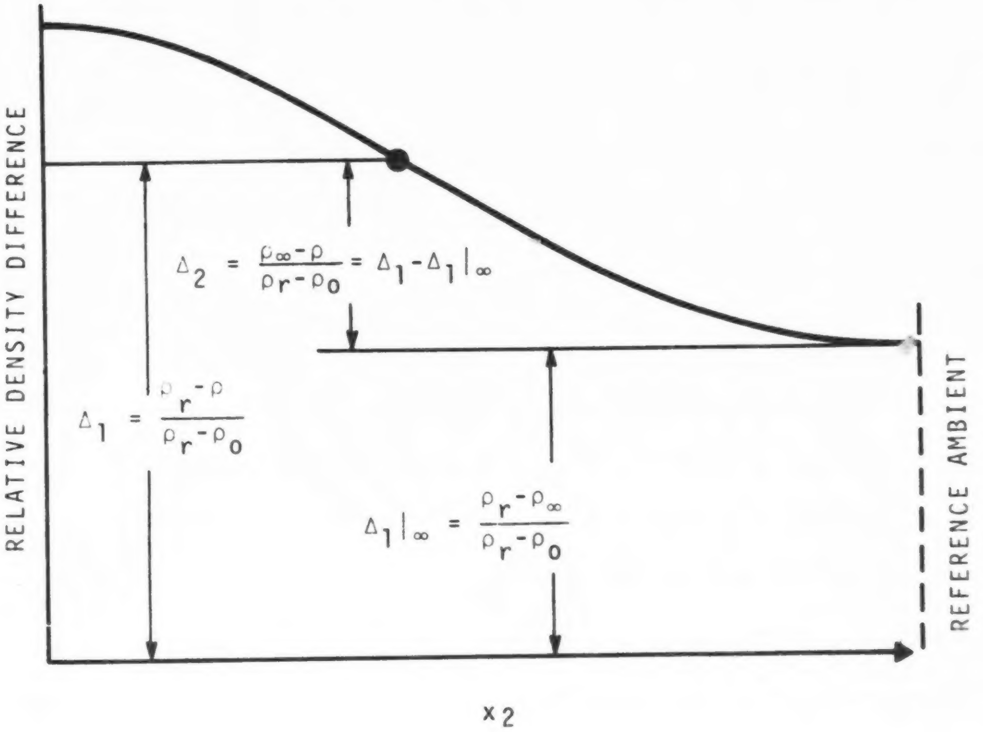
RELATIVE DENSITY DIFFERENCE
$\Delta_2 = \frac{\rho_\infty - \rho}{\rho_r - \rho_o} = \Delta_1 - \Delta_1|_\infty$
$\Delta_1 = \frac{\rho_r - \rho}{\rho_r - \rho_o}$
$\Delta_1|_\infty = \frac{\rho_r - \rho_\infty}{\rho_r - \rho_o}$
REFERENCE AMBIENT
x_2

Figure 3.2 Relationship Between the Buoyancy Parameter, Δ_1 and Density Disparity, Δ_2

3.6 The Equation of State for Sea Water

The density of sea water is a function of pressure, temperature and salinity, in the absence of other pollutants. Hence, the equation of state has the form

$$\rho = \rho(P,S,T). \tag{3.35}$$

Since we are dealing only with rather shallow water on an oceanographic scale, pressure effects are negligible; therefore,

$$\rho = \rho(S,T). \tag{3.36}$$

If other contaminants, having concentration, C, are present, then

$$\rho = \rho(S,T,C) \ . \tag{3.37}$$

In this work, we will deal only with Equation (3.36).

Since density variations are small in the sea, oceanographers deal with a modified density called sigma-t, defined as

$$\sigma_t = (\rho - 1) \times 1000,$$

which has cgs units and is a measure of the deviation in density from 1.0 gm/ml. The equation of state in general use by oceanographers may be found in U.S. Navy Hydrographic Office publication number 615 [103] (or in Hill [39]) and has the form:

$$\sigma_t = \Sigma_t + (\sigma_o + .1324)\ [1 - A_t + B_t\ (\sigma_o - .1324)] \tag{3.38}$$

where

$$\Sigma_t = \frac{(T - 3.98)^2}{503.370} \times \frac{T + 283}{T + 67.26} \ ,$$

$$A_t = 10^{-3} T(4.7867 - .098185T + .0010843T^2)$$

$$B_t = 10^{-6} T(18.030 - .8164T + .01667T^2)$$

$$\sigma_o = -.093 + .8149S - .000482S^2 + .0000068S^2.$$

In the above equations, T is in degrees Celsius, and salinity in parts per thousand. The quantity σ_0 is the density of sea water, in sigma-t units at zero pressure and temperature. σ_0 is usually expressed in terms of chlorine content instead of salinity, S, but for purposes here, salinity will suffice.

3.7 Vorticity Transport - An Alternate Approach

In dealing with geophysical fluid dynamic problems it is frequently difficult, if not impossible, to set realistic boundary conditions required for the solution of Equation (3.21). Pressure, and consequently associated boundary conditions, may be eliminated entirely from consideration by introducing the quantity, vorticity.

A brief summary of the general theory will be presented here for a homogeneous, isotropic turbulent flow field (i.e., $\varepsilon_{ij} = \varepsilon =$ constant) in three dimension. Additional information concerning vorticity transport may be found in Batchelor [10].

As demonstrated by Batchelor, a conservative fluid velocity field may be defined by vector addition of an irrotational contribution, u_I and a solenoidal contribution u_S, or

$$\vec{u} = \vec{u}_I + \vec{u}_S. \tag{3.39}$$

The solenoidal part satisfies

$$\nabla \cdot \vec{u}_S = 0$$

whereas the irrotational part satisfies

$$\nabla \times \vec{u}_I = 0.$$

In addition the irrotational part of the velocity field, u_I, may be described in terms of a scalar potential Φ so that

$$\vec{u}_I = \nabla\Phi$$

and the solenoidal part in terms of a vector potential, $\vec{\Psi}$, or

$$\vec{u}_S = \nabla \times \vec{\Psi} .$$

Hence, the total velocity field is described by the vector and scalar potential as

$$\vec{u} = \nabla\Phi + \nabla \times \vec{\Psi}. \tag{3.40}$$

Vorticity, $\vec{\omega}$, is defined as

$$\vec{\omega} = \nabla \times \vec{u}.$$

Taking the curl of Equation (3.40) and use of the above expression for vorticity, yields

$$\vec{\omega} = \nabla \times (\nabla\times\vec{\Psi}). \tag{3.41}$$

However, by vector identity

$$\nabla \times (\nabla\times\vec{\Psi}) = \nabla(\nabla\cdot\vec{\Psi}) - \nabla^2\vec{\Psi} ,$$

which for an incompressible flow gives

$$\nabla^2\vec{\Psi} = -\vec{\omega} \tag{3.42}$$

since $\nabla\cdot\vec{\Psi} = 0$.

Equation (3.42) is a Poisson type partial differential equation relating the vector potential to the distribution of vorticity in the flow field.

The divergence of Equation (3.40) gives

$$\nabla^2\Phi = \nabla \cdot \vec{u}$$

In view of the incompressibility condition,

$$\nabla \cdot \vec{u} = 0,$$

and satisfies LaPlace's equation

$$\nabla^2\Phi = 0. \tag{3.43}$$

Hence, the velocity field may be established through solution of Equations (3.42), (3.43) and (3.40).

Hirasaki and Hellums [42] have shown that Equation (3.43) is extremely useful for the purpose of prescribing inflow-outflow boundary conditions in a three dimensional velocity field. In fact, they have demonstrated that the flux boundary condition may be prescribed entirely by the scalar potential, Φ (velocity potential), or u_I. Hence, one is permitted to set tangential components of $\vec{\Psi} = 0$ and the normal derivative of $\vec{\Psi} = 0$ at all boundaries. The utility of this theory lies in the fact that vector potential boundary condition may be intractable without consideration of the scalar potential, Φ. One exception is the case of flow in a closed system where the boundary conditions on $\vec{\Psi}$ remain as described above and since there is no boundary mass flux, $\nabla\Phi = 0$ everywhere (cf. Aziz [7]).

An equation for vorticity transport may be derived by taking the curl of the Equations of motions (3.17) (after setting $\varepsilon_{ij} = \varepsilon$). This operation yields

$$\frac{D\vec{\omega}}{Dt} = (\vec{\zeta} + \vec{\omega}) \cdot \nabla\vec{u} + \nabla \times B\hat{e}_3 + \varepsilon\nabla^2\vec{\omega} \tag{3.44}$$

where $\hat{e}_3$ is a unit vector in the vertical direction.

The vorticity transportation equation was simplified appreciably by assuming a homogeneous, isotropic turbulence field. If the turbulence field were not treated as such, numerous terms involving the gradient of ε_{ij} would appear. These terms will be investigated in Section 3.10, which covers two-dimensional flow fields. The two dimensional counterpart to Equation (3.44) is

$$\frac{D\vec{\omega}}{Dt} = \nabla \times B\hat{e}_3 + \varepsilon \nabla^2 \vec{\omega} , \tag{3.45}$$

where one coordinate is vertical (x_3) and the other lies in the lateral plane.

3.8 Non-dimensional Form of the Equations of Motion

A non-dimensional formulation of the equations of motion permits the investigation of the magnitude of the various forces exerted on a fluid element in terms of similarity parameters. The importance of the various parameters may then be analyzed on an order-of-magnitude basis and the results used to justify simplification of the governing equations under certain flow conditions. To this end, we define the following dimensionless variables:

$$\left.\begin{aligned}
U_i &= u_i/v_o, \\
p^* &= p^o \rho_r/\Delta P_o, \\
\Omega_j^{**} &= 2\Omega_j^*/f_o, \\
t^* &= t v_o/D, \\
X_i &= x_i/D, \\
\varepsilon_{ij}^* &= \varepsilon_{ij}/\varepsilon_o.
\end{aligned}\right\} \tag{3.46}$$

In the above,

v_o - reference velocity (for the thermal plume we will use the effluent velocity at the outfall port),

ΔP_o - reference dynamic pressure (may be taken as $1/2\ \rho_o v_o^2$)

f_o - characteristic coriolis parameter

D - characteristic length (may be taken as the outfall port diameter)

ε_o - characteristic eddy diffusion coefficient for momentum (may be set to Cv_oD, where C is a constant).

Substituting the set (3.46) into Equation (3.18) yields,

$$\frac{\partial U_i}{\partial t^*} + \frac{\partial U_j U_i}{\partial X_j} + e_{ijk}\left(\frac{f_o D}{v_o}\right)\Omega_j^{**} U_k = -\left(\frac{\Delta P_o}{\rho_r v_o^2}\right)\frac{\partial P^*}{\partial X_i}$$

$$+\left(\frac{\rho_\infty - \rho}{\rho_r}\right)\frac{gD}{v_o^2}\,\delta_{i3} + \left(\frac{\varepsilon_o}{v_o D}\right)\frac{\partial}{\partial X_j}\left(\varepsilon_{\underline{ij}}^{*}\ \frac{\partial U_i}{\partial X_j}\right) \qquad (3.47)$$

The dimensionless groups in Equation (3.47) are:

$\dfrac{v_o^2}{f_o D}$ = Ro, Rossby number (ratio of inertial forces to coriolis forces),

$\dfrac{\rho_r v_o^2}{\Delta P_o}$ = Eu, Euler number (ratio of inertial forces to pressure forces),

$\dfrac{v_o^2}{\left(\frac{\rho_\infty - \rho}{\rho_r}\right) gD}$ = F_o, densimetric Froude number (ratio of inertial forces to internal buoyant forces).

$\frac{v_o D}{\varepsilon_o}$ = Re_T, turbulent Reynolds number (ratio of inertial forces to turbulent shear forces).

In terms of the above similarity parameters Equation (3.47) becomes:

$$\frac{\partial U_i}{\partial t^*} + \frac{\partial U_i U_j}{\partial X_j} + \frac{1}{Ro} e_{ijk} \Omega_j^{**} U_k = - \frac{1}{Eu} \frac{\partial P^*}{\partial X_i} + \frac{1}{F_o} \delta_{i3} + \frac{1}{Re_T} \frac{\partial}{\partial X_j} \left(\varepsilon^*_{\underline{ij}} \frac{\partial U_i}{\partial X_j} \right) \tag{3.48}$$

Equation (3.48) represents a gross non-dimensionalization. Ideally, we should treat each component of momentum separately and use length scales which correspond to the particular coordinates. However, for purposes here the form of Equation (3.48) is sufficient.

At middle latitudes, the characteristic coriolis parameter, f_o, is approximately equal to 10^{-4}, and v_o/D has magnitude on the order of 1 for a large outfall part. Hence, the Rossby number for the thermal plume is on the order of 10,000. Where smaller ports are considered v_o/D may be from 10 to 100, giving Rossby numbers from 10^5 to 10^6. The densimetric Froude number, F_o, for a large thermal outfall will be on the order of 10-50 and the reference Reynolds number Re_T will be of the same order. Also, we cannot neglect pressure effects. All other terms are on the order of 1 except eddy coefficients in some portions of the flow field. Hence, it follows that for a thermal plume and the scales of motion to be considered here, the coriolis term is sufficiently small to neglect by virtue of the apparaent size of the Rossby number. In consideration to follow we will deal with the equations of motion in the general form of

$$\frac{\partial U_i}{\partial t^*} + \frac{\partial U_j U_i}{\partial X_j} = - \frac{1}{Eu} \frac{\partial P^*}{\partial X_i} + \frac{1}{F_o} \delta_{i3}$$

$$+ \frac{1}{Re_T} \frac{\partial}{\partial X_j} \left(\varepsilon^*_{ij} \frac{\partial U_i}{\partial X_j} \right), \qquad (3.49)$$

and dimensional variations of the same.

3.9 Further Comments on the Concept of "Eddy Viscosity"

In Section 3.22, we introduced velocity fluctuation, u_j', as a means of describing turbulent flow. Without the coriolis term, Equation (3.9) is known as Reynolds' equation, after Osborne Reynolds [78] who first expressed the turbulent equations of motion in this fashion. Reynolds' equation for the mean flow differs from the laminar flow counterpart only by the Reynolds stress terms, R_{ij}.

The Reynolds equation represents a vast simplification (at least outwardly) of extremely complex flow conditions. However, the task still remains in relating the turbulent or "apparent" stresses to mean flow quantities.

Boussinesq (cf. Hinze [40]) was evidently the first to use the concept of "apparent" viscosity, in his studies of two-dimensional flow. He assumed that turbulent stress, τ_e could be expressed in a manner analogous to molecular viscous stress or

$$\tau_e = -\rho \, \overline{u'v'} = \varepsilon \frac{du}{dy} \, . \qquad (3.50)$$

In the above, ε is the "apparent" or eddy viscosity, u' and v' are x and y components of the velocity fluctuation, respectively, and u is the mean velocity in the x direction.

Prandtl [72] introduced the concept of "mixing lengths" to describe the turbulent exchange coefficient. This idea was motivated by the mean free path concept of molecular motion and has turned out to be a fruitful hypothesis in spite of obvious physical questions.

The idea of mixing length theory is that a small parcel of fluid containing any transferrable property is transported, unchanged, by velocity fluctuation from one position, a distance ℓ to a new position where it is absorbed in the flow field. The distance ℓ is the mixing length.

Let $u_1(x_1,x_2,x_3)$ be the mean velocity at the origin of the exchanged fluid parcel, and $u_1(x_1 + \ell_1,x_2 + \ell_2,x_3 + \ell_3)$ be the mean velocity at the absorbed position. Then the velocity fluctuation is (cf. Neumann and Pierson).

$$u_1(x_1,x_2,x_3) - u_1(x_1 + \ell_1,x_2 + \ell_2,x_3 + \ell_3)$$

$$- \ \ell_1 \frac{\partial u_1}{\partial x_1} - \ell_2 \frac{\partial u_1}{\partial x_2} - \ell_3 \frac{\partial u_1}{\partial x_3} \quad .$$

Then

$$\begin{aligned} u'_{1(1)} &= - \ell_1 \frac{\partial u_1}{\partial x_1} \\ u'_{1(2)} &= - \ell_2 \frac{\partial u_1}{\partial x_2} \qquad (3.51) \\ u'_{1(3)} &= - \ell_3 \frac{\partial u_1}{\partial x_3} \end{aligned}$$

Here, the fluctuating velocity $u'_{i(j)}$ is shown as a second order tensor where the subscript j indicates the particular turbulent component of u'_i. Hence, in a somewhat nebulous fashion:

$$R_{ij} = -\bar{\rho}(\overline{u'_{i(j)} \cdot u'_j}) = \varepsilon_{ij} \frac{\partial u_i}{\partial x_j} . \qquad (3.52)$$

Mixing length theory is rather unsatisfying because of the physical basis; nevertheless, it does accomplish the purpose of relating mean flow behavior to the Reynolds stresses. Actually, the concept of an eddy viscosity requires a fourth order tensor quantity (Hinze, Pond [71]) to satisfy theoretical treatment of the Reynolds stresses. Such a quantity would be completely unmanageable from a practical standpoint. Even the second order tensor ε_{ij} is difficult, if not impossible, to calculate from measurable quantities such as frictional forces and velocity gradients.

Hot wire and laser techniques offer a method for direct measurement of the fluctuating velocities and hence correlation of the Reynolds stresses through statistics. However, statistical theory has not yet provided a means for evaluating ε_{ij} in practical engineering calculations.

As a result of our lack of understanding and inability to calculate or measure ε_{ij}, further assumptions must be made. In the ocean we must deal with at least two values of eddy viscosity, a lateral value and a vertical one. Gross measurements have shown that these two values are vastly different. Fofonoff (cf. Hill) suggests using a form from Saint-Guily which gives

$$R_{ij} = -\bar{\rho}\overline{(u_i' \cdot u_j')} \doteq \varepsilon_j \frac{\partial u_i}{\partial x_j} + \varepsilon_i \frac{\partial u_i}{\partial x_i}, \qquad (3.53)$$

where ϵ_j is the lateral eddy viscosity for i,j≠3 and the vertical for i,j=3.

For the work presented in this thesis, we will use three components given by ε_j.

3.10 Two-Dimensional Forms of the Transport Equations in Rectangular and Axisymetric Coordinates

In the previous sections of this chapter, the appropriate differential equations for solving the thermal plume problem in three-space were layed out. Ideally, we would prefer to solve the plume problem in this manner since the nature of the flow is distinctly three-dimensional. However, computational requirements necessary to obtain proper resolution of desired quantities in three dimensions are prohibitive from a practical standpoint in view of available computer hardware and economics.

Two-dimensional considerations which demand significantly less computation time and computer capacity, are appropriate in cases where flow symmetry is approximately realized. Such cases are the vertical plume and line thermal investigated in this thesis. Hopefully, computation economics will permit practical, three-dimensional engineering calculations in the near future, thus avoiding certain restrictions inherent with two-dimensional approximations. Table 3.1 gives a summary of general requirements for two- and three-dimensional forms of the velocity-pressure and Vorticity-Vector potential equations.

TABLE 3.1. DIFFERENTIAL EQUATIONS REQUIRED FOR VELOCITY-PRESSURE AND VECTOR POTENTIAL-VORTICITY METHODS IN TWO AND THREE DIMENSIONS

		Velocity-Pressure Equation Set		Vector Potential-Vorticity Equation Set	
		3-Dim. i=1,2,3	2-Dim. i=1,2	3-Dim. i=1,2,3	2-Dim. i=1,2
U_1	Parabolic	X	X		
U_2	Parabolic	X	X		
U_3	Parabolic	X			
p^0	Elliptic	X	X		
Γ	Parabolic (1 or more)	X	X	X	X
ω_1	Parabolic			X	
ω_2	Parabolic			X	
ω_3	Parabolic			X	X
Ψ_1	Elliptic			X	
Ψ_2	Elliptic			X	
Ψ_3	Elliptic			X	X
Φ	Elliptic			(X)*	
Total of Required Equations (minimum)		5	4	7(8)	3

*Used only in the case of open boundaries.

3.10.1 Two-Dimensional Transport Equations in Rectangular Geometry

The two-dimensional rectangular coordinate system which will be considered in this study is defined as a plane normal to the geopotential surface (Figure 3.1). The two coordinates are defined as x and z, where x is in the x_1, x_2 plane, with no particular orientation, and z is aligned with the vertical x_3 axis. Corresponding velocity components u and v are in the x and z directions, respectively.

Velocity-Pressure Equations:

The velocity-pressure equations are as follows.

Continuity:

$$\frac{\partial u}{\partial x} + \frac{\partial v}{\partial z} = 0 \tag{3.54}$$

Momentum transport:

x-direction,

$$\frac{Du}{Dt} = -\frac{\partial P^o}{\partial x} + \frac{\partial}{\partial x}\left(\varepsilon_X \frac{\partial u}{\partial x}\right) + \frac{\partial}{\partial z}\left(\varepsilon_Z \frac{\partial u}{\partial z}\right), \tag{3.55}$$

$$\frac{Dv}{Dt} = -\frac{\partial P^o}{\partial z} + B + \frac{\partial}{\partial x}\left(\varepsilon_X \frac{\partial v}{\partial x}\right) + \frac{\partial}{\partial z}\left(\varepsilon_Z \frac{\partial v}{\partial z}\right). \tag{3.56}$$

In the above momentum transport equations, ε_X is the lateral eddy diffusivity coefficient and ε_Z is the corresponding vertical value. The substantial derivative is given in two dimensions as

$$\frac{D}{Dt} = u\frac{\partial}{\partial x} + v\frac{\partial}{\partial z}.$$

Constituent transport:

$$\frac{D\Gamma}{Dt} = \frac{\partial}{\partial x}\left(\varepsilon_{\gamma X} \frac{\partial \Gamma}{\partial x}\right) + \frac{\partial}{\partial z}\left(\varepsilon_{\gamma Z} \frac{\partial \Gamma}{\partial z}\right). \tag{3.57}$$

Equations for the transport of specific constituents such as Δ_1, Δ_2, S, etc. will be developed where appropriate.

The appropriate pressure equation may be obtained from Equation (3.20) by letting i=2,3 and j=2,3. Hence

$$\begin{aligned}\nabla^2 p^o = &-\left\{\left(\frac{\partial u}{\partial x}\right)^2 + 2\left(\frac{\partial v}{\partial x}\right)\left(\frac{\partial u}{\partial z}\right) + \left(\frac{\partial v}{\partial z}\right)^2\right\} + \frac{\partial B}{\partial z}\\ &+ \frac{\partial}{\partial x}\left[\left(\frac{\partial \varepsilon_x}{\partial x}\right)\left(\frac{\partial u}{\partial x}\right)\right] + \frac{\partial}{\partial z}\left[\left(\frac{\partial \varepsilon_z}{\partial x}\right)\left(\frac{\partial u}{\partial z}\right)\right]\\ &+ \frac{\partial}{\partial x}\left[\left(\frac{\partial \varepsilon_x}{\partial z}\right)\left(\frac{\partial v}{\partial x}\right)\right] + \frac{\partial}{\partial z}\left[\left(\frac{\partial \varepsilon_z}{\partial z}\right)\left(\frac{\partial v}{\partial z}\right)\right],\end{aligned} \tag{3.58}$$

where $\nabla^2 = \frac{\partial^2}{\partial x^2} + \frac{\partial^2}{\partial z^2}$.

If turbulent contributions are neglected,

$$\nabla^2 p^o = -\left\{\left(\frac{\partial u}{\partial x}\right)^2 + 2\left(\frac{\partial v}{\partial x}\right)\left(\frac{\partial u}{\partial z}\right) + \left(\frac{\partial v}{\partial z}\right)^2\right\} + \frac{\partial B}{\partial z} \tag{3.59}$$

Recall that by Equation (3.16),

$$p^o = P/\rho_r - g\int_z^0 \rho_\infty/\rho_r\, dz,$$

The most notable work in obtaining numerical solution to the laminar form of the velocity-pressure equations given above was performed at the Los Alamos Scientific Laboratory by Welch and colleagues (cf. the "MAC Method" [109]). Based on these pioneering efforts at LASL, numerous other investigations have employed MAC techniques to viscous flow problems [6, 23, 46]. Pagnani [67] applied the MAC techniques successfully to natural circulation in an enclosed cell.

Stream Function - Vorticity Equations:

An expression for the stream function in (x-z) coordinates may be obtained by considering only the x_3 component of the vector Equation (3.43), or

$$\nabla^2 \Psi = -\omega, \tag{3.60}$$

where: ψ (stream function) = Ψ_3 and $\omega = \omega_3$.

Velocity relationships are obtained by using only the Ψ_3 component of Equation (3.40)

$$\vec{u} = \nabla \times (\psi \hat{e}_z) \tag{3.61}$$

which yields

$$u = -\frac{\partial \psi}{\partial z} \tag{3.62}$$

$$v = \frac{\partial \psi}{\partial x} . \tag{3.63}$$

If the eddy diffusivity ϵ_{ij} is constant, Equation (3.45) may be used to obtain ω_3 as

$$\frac{D\omega}{Dt} = -\frac{\partial B}{\partial x} + \epsilon \nabla^2 \omega \tag{3.64}$$

where again we let $\omega = \omega_3$.

However, in general we must consider the two anisotropic, nonhomogeneous components ϵ_x and ϵ_z. In this case, numerous terms involving derivatives of ϵ_x and ϵ_y appear. The vorticity equations are derived for this case by cross differentiating Equations (3.54) and (3.56), then subtracting the latter result from the former to obtain

$$\begin{aligned}\frac{D\omega}{Dt} = & - \frac{\partial B}{\partial x} + \varepsilon_x \frac{\partial^2 \omega}{\partial x^2} + \varepsilon_z \frac{\partial^2 \omega}{\partial z^2} \\ & + \frac{\partial \varepsilon_x}{\partial z} \cdot \frac{\partial^2 u}{\partial x^2} + \frac{\partial \varepsilon_z}{\partial z} \cdot \frac{\partial^2 u}{\partial z^2} - \frac{\partial \varepsilon_x}{\partial x} \cdot \frac{\partial^2 v}{\partial x^2} - \frac{\partial \varepsilon_z}{\partial x} \cdot \frac{\partial^2 v}{\partial z^2} \\ & + \frac{\partial}{\partial z} \left(\frac{\partial \varepsilon_x}{\partial x} \cdot \frac{\partial u}{\partial x} + \frac{\partial \varepsilon_z}{\partial z} \cdot \frac{\partial u}{\partial z} \right) \\ & - \frac{\partial}{\partial x} \left(\frac{\partial \varepsilon_x}{\partial x} \cdot \frac{\partial v}{\partial x} + \frac{\partial \varepsilon_z}{\partial z} \cdot \frac{\partial v}{\partial z} \right) \end{aligned} \tag{3.65}$$

If the structure of the turbulent field is homogeneous, and isotropic, Equation (3.65) simplifies to

$$\frac{D\omega}{Dt} = - \frac{\partial B}{\partial x} + \varepsilon_x \frac{\partial^2 \omega}{\partial x^2} + \varepsilon_z \frac{\partial^2 \omega}{\partial z^2} . \tag{3.66}$$

Stream function-vorticity transport solution methods have been employed for a number of years by oceanographers in computing such geophysical phenomena as western boundary currents (e.g. the Kuro Shio and the Gulf Stream, cf. Neumann and Pierson). But these techniques have become popular in engineering application only in the past few years, a result due in part to the recognition that these methods are extremely well adapted to problems involving natural convection. Solution to the laminar form of the stream function - vorticity equations given above have been carried out by a number of researchers [7, 31, 82, 100, 104, 106, 108, 111]. The most notable work being carried out on the turbulent form of the equations is at the Imperial College by Spalding and colleagues [69, 82, 90, 91, 92, 93].

3.10.2 Two-Dimensional Transport Equations in Axisymmetric Coordinates

Again referring to Figure 3.1, the axisymmetric coordinate system is oriented such that the radial coordinate, r, may be considered a rotating line in the x_1, x_2 plane. The vertical coordinate, z, is again aligned with the x_3 direction, normal to a geopotential surface.

Velocity-Pressure Equations:

The velocity-pressure equations are as follows:

Continuity:

$$\frac{1}{r}\frac{\partial u_r r}{\partial r} + \frac{\partial v}{\partial z} = 0, \qquad (3.67)$$

where u_r is the radial velocity.

Momentum transport:

r - direction,

$$\frac{Du_r}{Dt} = -\frac{\partial P^o}{\partial r} + \frac{\partial}{\partial r}\left(\frac{\varepsilon_r}{r}\frac{\partial u_r r}{\partial r}\right) + \frac{\partial}{\partial z}\left(\varepsilon_z \frac{\partial u_r}{\partial z}\right). \qquad (3.68)$$

The substantial derivative in axisymmetric coordinates is:

$$\frac{D}{Dt} = \frac{\partial}{\partial t} + u_r \frac{\partial}{\partial r} + v\frac{\partial}{\partial z} \qquad (3.69)$$

z-direction:

$$\frac{Dv}{Dt} = -\frac{\partial P^o}{\partial z} + B + \frac{1}{r}\frac{\partial}{\partial r}\left(r\varepsilon_r \frac{\partial v}{\partial r}\right) + \frac{\partial}{\partial z}\left(\varepsilon_z \frac{\partial v}{\partial z}\right). \qquad (3.70)$$

In the above equations, ε_r is the radial eddy diffusivity coefficient for momentum.

Constituent transport:

$$\frac{D\Gamma}{Dt} = \frac{1}{r}\frac{\partial}{\partial r}\left(r\varepsilon_{\gamma r}\frac{\partial\Gamma}{\partial r}\right) + \frac{\partial}{\partial z}\left(\varepsilon_{\gamma z}\frac{\partial\Gamma}{\partial z}\right) . \tag{3.71}$$

where $\varepsilon_{\gamma r}$ is the radial coefficient for turbulent Γ diffusivity.

The pressure equation may be derived by differentiating Equations (3.69) and (3.70), then adding these two results to Equation (3.68). Hence,

$$\nabla^2 p^o = \frac{\partial B}{\partial z} - \left\{\left(\frac{u}{r}\right)^2 + \left(\frac{\partial u}{\partial r}\right)^2 + \left(\frac{\partial v}{\partial z}\right)^2 + 2\,\frac{\partial u}{\partial z}\cdot\frac{\partial v}{\partial r}\right\} \tag{3.72}$$

where the operator

$$\nabla^2 = \frac{\partial^2}{\partial r^2} + \frac{1}{r}\frac{\partial}{\partial r} + \frac{\partial^2}{\partial z^2} . \tag{3.73}$$

Vorticity in (r-z) coordinates is given as

$$\omega = \frac{\partial u_r}{\partial z} - \frac{\partial v}{\partial r} . \tag{3.74}$$

Also we define a stream function ψ according to

$$u_r = -\frac{1}{r}\frac{\partial\psi}{\partial z} \tag{3.75}$$

and

$$v = \frac{1}{r}\frac{\partial\psi}{\partial r} . \tag{3.76}$$

Substitution of Equations (3.75) and (3.76) into Equation (3.74) yields

$$\frac{\partial^2\psi}{\partial r^2} - \frac{1}{r}\frac{\partial\psi}{\partial r} + \frac{\partial^2\psi}{\partial z^2} = - r\omega \qquad (3.77)$$

for the stream function Ψ. Note that Equation (3.77) is not the usual Laplacian for (r-z) coordinates (e.g. Equation 3.73).

The vorticity transport equation is derived by cross-differentiating Equations (3.68) and (3.70) and then subtracting the latter result from the former. This operation leads to

$$\begin{aligned}
\frac{\partial\omega}{\partial t} + \frac{\partial u_r\omega}{\partial r} + \frac{\partial v\omega}{\partial z} &= - \frac{\partial B}{\partial r} \\
&+ \varepsilon_r \frac{\partial}{\partial r}\left[\frac{1}{r}\frac{\partial \omega r}{\partial r}\right] + \varepsilon_z \frac{\partial^2\omega}{\partial z^2} \\
&+ \frac{\partial}{\partial z}\left[\frac{1}{r}\frac{\partial u_r r}{\partial r} \cdot \frac{\partial\varepsilon_r}{\partial r} + \frac{\partial u_r}{\partial z} \cdot \frac{\partial\varepsilon_z}{\partial z}\right] + \frac{\partial\varepsilon_r}{\partial z} \cdot \frac{\partial}{\partial r}\left[\frac{1}{r}\frac{\partial u_r r}{\partial r}\right] \\
&+ \frac{\partial\varepsilon_z}{\partial z} \cdot \frac{\partial^2 u_r}{\partial z^2} - \frac{\partial}{\partial r}\left[\frac{\partial v}{\partial r} \cdot \frac{\partial\varepsilon_r}{\partial r} + \frac{\partial v}{\partial z} \quad \frac{\partial\varepsilon_z}{\partial z}\right] \\
&- \frac{\partial\varepsilon_r}{\partial r} \cdot \left[\frac{\partial^2 v}{\partial r^2} + \frac{1}{r}\frac{\partial v}{\partial r}\right] + \frac{\partial\varepsilon_z}{\partial r} \cdot \frac{\partial^2 v}{\partial z^2} \qquad (3.78)
\end{aligned}$$

If the turbulent structure of the flow field is homogeneous, and isotropic, derivatives of ε_r and ε_z vanish and the vorticity transport equation becomes

$$\frac{\partial\omega}{\partial t} + \frac{\partial u_r\omega}{\partial r} + \frac{\partial v\omega}{\partial z} = - \frac{\partial B}{\partial r} + \varepsilon_r \frac{\partial}{\partial r}\left(\frac{1}{r}\frac{\partial \omega r}{\partial r}\right) + \varepsilon_z \frac{\partial^2\omega}{\partial z^2} . \qquad (3.79)$$

CHAPTER 4

PLUME THEORY - SIMILARITY SOLUTIONS

As an integral part of the thermal plume dispersion program, this chapter is concerned with flow regimes 1 and 2, which may adequately be described by empirical correlations and similarity solutions.

4.1 General Description

The zone of "flow establishment" (Figure 2.3) is a region of transition from essentially a pipe flow at the outfall orifice to a fully developed velocity profile some distance downstream. This situation occurs only in deep water, and when velocity profiles become fully developed, the flow field is said to be "established." This zone is characterized by velocity profiles which are very similar in shape at each axial location.

The zone of flow establishment is a region of intense turbulent mixing between the plume flow and surrounding water. The mixing process which starts at the periphery of the outfall port spreads inward toward the center of the plume and outward into the surroundings. Eventually mixing will spread to the plume centerline where the centerline velocity will begin rapid diminution. Upstream from this point, flow in an approximate conical section is relatively unaffected by the mixing process. This zone is called the "potential core" and is characterized by relatively flat velocity profiles at all axial locations.

Figure 4.1 illustrates a precise change from one flow regime to the next. In reality, however, before the velocity field becomes

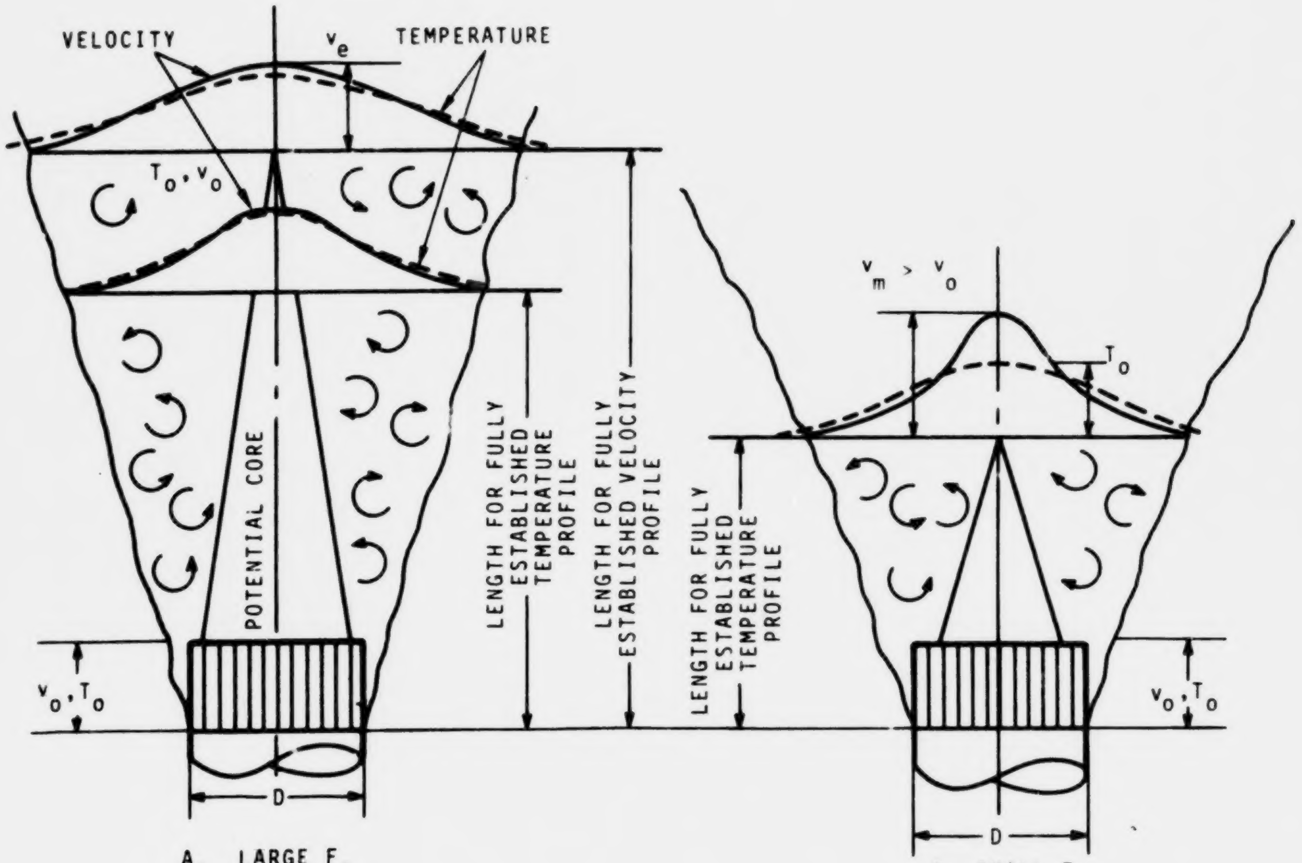

VELOCITY
v_e
TEMPERATURE
T_o, v_o
POTENTIAL CORE
LENGTH FOR FULLY ESTABLISHED TEMPERATURE PROFILE
LENGTH FOR FULLY ESTABLISHED VELOCITY PROFILE
v_o, T_o
D
$v_m > v_o$
T_o
LENGTH FOR FULLY ESTABLISHED TEMPERATURE PROFILE
v_o, T_o
D

A. LARGE F_o

B. SMALL F_o

Figure 4.1. Zone of flow establishment for plumes with large and small densimetric Froude numbers, F_o.

fully established in the sense of similar velocity profiles, the centerline velocity will begin to deteriorate giving a transition zone between the two regimes. This transition is apparent from the data of Albertson et al. [4]. Although Murota and Muraoki [62] have proposed a correlation for this zone, according to Hinze [40] this distance is relatively short and is generally excluded from analysis.

In the case of a momentum jet (neutrally buoyant flow, or $F_0 \to \infty$) velocity in the potential core is that of the issuing jet and analysis is based on the assumption that momentum is conserved at each axial cross-section. However, in the case of buoyant plumes, momentum is generated by the density disparity and velocity will actually increase in the potential core (as indicated in Figure 4.2B).

As mentioned previously, the zone of established flow is typified by velocity profiles which have nearly the same shape at all axial locations. For this reason similarity analysis has played an important role in analysis of this flow regime. Numerous experimental and analytical studies have been carried out for both the momentum jet and buoyant plume in the absence of restraining boundaries.

In this manuscript, the work of Albertson and Abraham [1] is used for modeling Zone 1, and Abraham's work for the established flow regime is extended for the analysis of Zone 2.

4.2 Simplified Equations for a Vertical Plume

Governing equations for a vertical plume issuing from a round port are more convenient to derive in axisymmetric coordinates. Thus, with reference to Figure 2.3 and the coordinate system given in

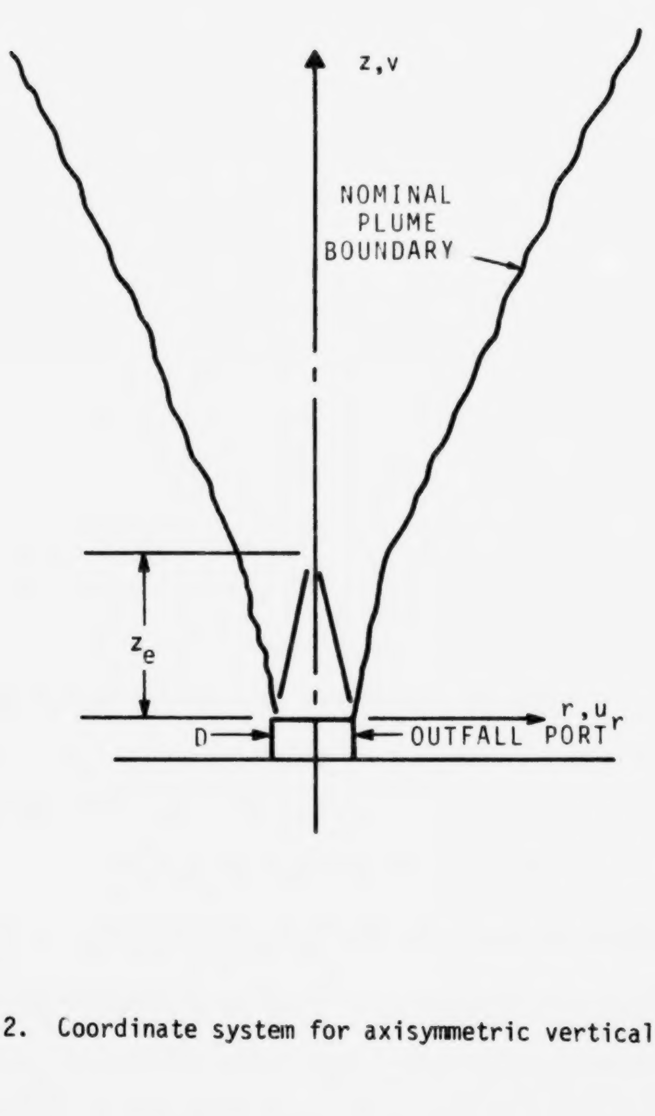
z,v
NOMINAL
PLUME
BOUNDARY
z_e
r, u_r
D
OUTFALL PORT

Figure 4.2. Coordinate system for axisymmetric vertical plume.

Figure 4.2, the following assumptions are posed:

- steady flow
- flow is axisymmetric
- coriolis effects are neglected
- flow field is assumed hydrostatic throughout: $\frac{\partial p^o}{\partial z} = 0$
- density difference between the plume and surroundings is assumed small compared to the density at any point in the flow field: $|\rho_\infty - \rho| << \rho$
- plume is fully turbulent
- eddy transport of momentum and heat is only effective in the lateral direction (normal to jet axis)
- molecular heat conduction and viscosity are ignored.

With the above simplifications and assumptions it is possible to disregard a number of terms in cylindrical governing Equations (3.69) through (3.73) and arrive at the following equation set:

Continuity:

$$\frac{1}{r} \frac{\partial (u_r r)}{\partial r} + \frac{\partial v}{\partial z} = 0. \tag{4.1}$$

Momentum:

Employing "order of magnitude" analysis common to boundary layer theory (e.g. Schlichting [84])and incorporating previous assumptions, we see a need for the z-direction momentum Equation (3.72) only. This equation reduces to

$$v \frac{\partial v}{\partial z} + u_r \frac{\partial v}{\partial r} = \left(\frac{\rho_\infty - \rho}{\rho_0}\right) g - \frac{1}{\rho_0 r} \frac{\partial}{\partial r} (r\tau_{rz}), \tag{4.2}$$

where τ_{rz} is the turbulent shear stress.

Energy transport may be accounted for by the appropriate axisymmetric form of the density transport Equation (3.34) or

$$u_r \frac{\partial \Delta_2}{\partial r} + v \frac{\partial \Delta_2}{\partial z} - v \frac{\partial \rho_\infty^*}{\partial z} = \frac{1}{r} \frac{\partial}{\partial r} \left\{ \varepsilon_{Hr} \frac{\partial \Delta_2}{\partial r} \right\}. \tag{4.3}$$

For salinity we use Equation (3.71), with $\Gamma = \Delta_3$,

$$u_r \frac{\partial \Delta_3}{\partial r} + v \frac{\partial \Delta_3}{\partial z} = \frac{1}{r} \frac{\partial}{\partial r} \left\{ \varepsilon_{Sr} \frac{\partial \Delta_3}{\partial r} \right\}, \tag{4.4}$$

with the buoyancy parameter, Δ_3, defined as

$$\Delta_3 = \frac{S_r - S}{S_r - S_0} . \tag{4.5}$$

Using the continuity relationship Equation (4.1), Equations (4.2), (4.3) and (4.4) may be rearranged to yield the following:

$$\frac{\partial v^2}{\partial z} + \frac{1}{r} \frac{\partial}{\partial r} (ru_r v) = \left(\frac{\rho_\infty - \rho}{\rho_0}\right) g - \frac{1}{\rho_0 r} \frac{\partial}{\partial r} (r\tau_{rz}). \tag{4.6}$$

$$\frac{\partial v\Delta_2}{\partial z} + \frac{1}{r} \frac{\partial}{\partial r} (ru_r \Delta_2) - v \frac{\partial \rho^*_\infty}{\partial z} = \frac{1}{r} \frac{\partial}{\partial r} \left\{ \varepsilon_{Hr} \frac{\partial \Delta_2}{\partial r} \right\}, \tag{4.7}$$

$$\frac{\partial}{\partial z}(v\Delta_3) + \frac{1}{r}\frac{\partial}{\partial r}(ru_r\Delta_3) = \frac{1}{r}\frac{\partial}{\partial r}\left\{\varepsilon_S r \frac{\partial\Delta_3}{\partial r}\right\}, \qquad (4.8)$$

respectively.

4.3 Radial Velocity and Temperature Profiles

A large amount of experimental work has been carried out in the past concerning radial velocity and temperature profiles for free jets. Earlier work was concerned primarily with momentum jets. Schmidt [85] in 1941 was evidently the first to consider the mechanics of convective plumes, such as convective currents over fires, etc. Schmidt's work was reported in the German literature, and apparently because of the war, went unnoticed until Rouse et al. [81] carried out similar work in the early 1950's. Since then a number of researchers [8, 26, 41, 77, 83] have investigated velocity profiles and associated transport coefficients for both momentum jets and buoyant plumes.

4.3.1 Zone of Established Flow

The experimental studies have established that velocity and temperature profiles are approximately similar at all axial locations in the zone of established flow for all vertical plumes in a stagnant, free environment. Also, profiles are nearly Gaussian and may be adequately described by the normal distribution curve:

$$v(r,z) = v_m e^{-\frac{1}{2}\left(\frac{r}{\sigma}\right)^2} \qquad (4.9)$$

for velocity, and

$$\theta(r,z) = \theta_m e^{-\frac{\lambda}{2}\left(\frac{r}{\sigma}\right)^2} \tag{4.10}$$

for the temperature distribution. In the above equations the subscript m refers to condition at the plume centerline, λ is the eddy Prandtl number, and σ is the standard deviation.

The standard deviation has been found to relate to the vertical coordinate, z, by

$$\sigma^2 = \frac{1}{2}\,\frac{z}{K}^2 \tag{4.11}$$

where K is an experimental entrainment parameter. Hence,

$$v(r,z) = v_m e^{-K\left(\frac{r}{z}\right)^2} \tag{4.12}$$

and

$$\theta(r,z) = \theta_m e^{-K\lambda\left(\frac{r}{z}\right)^2}. \tag{4.13}$$

It is important to remember that these profiles have no theoretical basis and are merely the result of curve fitting.

The values K and λ must be determined by measurement and have been found to depend on the extent of buoyancy. For instance, in the case of a simple plume (pure buoyancy, $F_0=0$) Schmidt found that

$K = 48$

$\lambda = 1.2$.

The data of Rouse yields

$K = 96$

and

$\lambda = .74$

for a buoyant point source. Abraham in his analysis of a simple plume used values

$$K = 92$$

and

$$\lambda = .74.$$

For the momentum jet case, (neutral buoyancy) Albertson found

$$K = 77.$$

Abraham used

$$\lambda = .80$$

for this case.

Baines [8] observed in his investigations that the initial Reynolds number affected the results. He found the following best fit for his experimental results:

$$v(r,z) = v_m e^{-K \left(\frac{r}{z}\right)^N} \tag{4.14}$$

where $K = 43.3$ and $N = 1.82$ for $R_e = 2.1\text{x}10^4$, and $K = 64.4$ and $N = 1.84$ for $R_e = 7\text{x}10^4$.

Where values for K and λ are needed in the present work, the following are used:

simple plume (pure buoyancy, or $F_o \to 0$),

$K = 92$

$\lambda = .74$, and

momentum jet (neutral buoyancy, or $F_o \to \infty$),

$K = 77$

$\lambda = .80$

4.3.2 Zone of Flow Establishment

Figure 4.3 illustrates a typical velocity distribution in this zone. Albertson estimated this distribution for a momentum jet by assuming a flat profile across the potential core and a Gaussian distribution for the mixing zone. Albertson derived an integral expression for momentum flux across a lateral plane in this zone by integrating Equation (4.6) with $\rho_\infty = \rho$, for $r = 0$ to $r \to \infty$, or

$$\frac{M}{M_o} = \frac{\int_0^\infty v^2 dA}{v_o^2 \; A_o} = 1. \tag{4.15}$$

The quantity M is total momentum flux crossing a plane normal to the mean flow and A is cross-sectional area. Thus, Equation (4.15) states that momentum is conserved with $M_o = v_o^2 A_o$ the momentum source strength. By letting $C_1 = \sigma/z$, the momentum flux relationship above yields

$$\frac{z_e}{D} = \frac{1}{2C_1} \tag{4.16}$$

where C_1 is an experimental constant. By approximating the potential core diameter, D_c, according to

$$\frac{D_c}{D} = 1 - \frac{z}{z_e} \tag{4.17}$$

the mean velocity distribution in this region takes the form

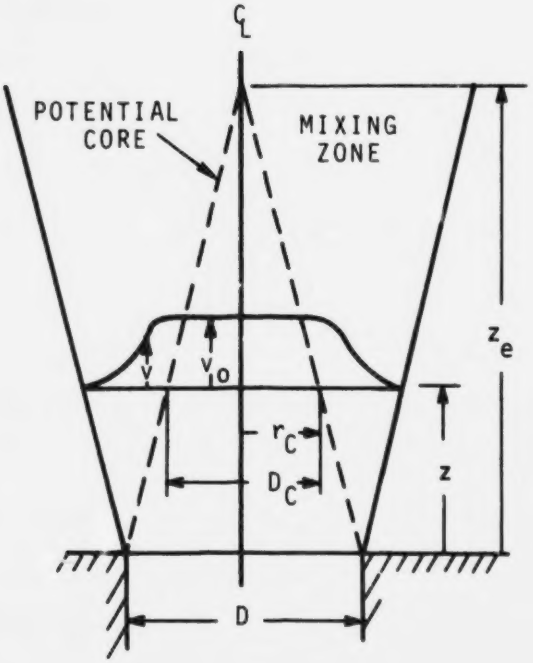
℄
POTENTIAL CORE
MIXING ZONE
v
v_o
r_c
D_c
z
z_e
D

Figure 4.3. Typical velocity profile in the zone of flow establishment for a momentum jet.

$$\frac{v}{v_0} = \exp \left\{ - \frac{1}{2C_1^2} \left[C_1 + \left(\frac{r-D/2}{z} \right)^2 \right] \right\} . \qquad (4.18)$$

Equation (4.18) above will be used in the following work when a velocity distribution near the outfall port is required. Note that this equation is not correct for buoyant plumes since density differences have been ignored. However, very near the outfall port (say one port diameter downstream), inertial effects are assumed to dominate the flow behavior regardless of the degree of buoyancy. Evaluation of the empirical constant C_1 and the length z_e are dealt with in the next section.

4.4 Zone of Flow Establishment

For a plume issuing from a small diameter port in deep water the length for flow establishment, z_e, has relatively small influence on conditions far downstream except as it enters in the established flow solutions as a boundary condition. On the other hand, for large outfall ports, the theoretical zone may extend over a good portion of the flow field, or even to the ocean surface. In this section, we will discuss methods for evaluating z_e in deep water for both the neutrally buoyant and buoyant cases.

Many experiments have been carried out by various investigators in an effort to establish the length of the potential core for turbulent round jets issuing into stagnant fluids. Good reviews of this work are given by Hinze [40] and by Gaunter, Livingwood, and Haycak [32]. Gaunter et al. in their review, state that values for z_e/D vary from about 4.7 to 7.7. For instance, Albertson et al. found that $z_e = 6.2$ for their work. Baines reports that jet Reynolds number had considerable effect on z_e/D for his experiments. In fact for $Re_o = 1.4\times10^4$, $z_e/D = 5$ and for $Re_o = 10^5$, $z_e/D = 7$.

Where buoyancy affects the potential core length, Abraham bases z_e on the concentration distribution. Hence, z_e for concentration is given by

$$\frac{1.42}{F_o}\left(\frac{z_e}{D}\right)^3 + \left(\frac{z_e}{D}\right)^2 - \frac{(1+\lambda)^2 K}{8} = 0 \qquad (4.19)$$

where λ and K take values .8 and 77, respectively. The limiting value of z_e/D in Equation (4.19) for $F_o \to \infty$ is approximately 5.6. The value of z_e/D for concentration profile establishment is about 10% less than the value of 6.2 for velocity profiles found by Albertson.

4.5 Governing Differential Equations

To derive the equations governing the dynamics of a vertical plume in Zone 3 we integrate Equations (4.6),(4.7) and (4.8), in a lateral plane, from $r = 0$ to $r \to \infty$. Thus, the following expressions apply as indicated,

Vertical momentum transport:

$$\frac{d}{dz}\int_0^\infty v^2 r\,dr = \int_0^\infty \left(\frac{\rho_\infty - \rho}{\rho_o}\right) g r\,dr \qquad (4.20)$$

Density disparity transport:

$$\frac{d}{dz}\int_0^\infty v\Delta_2 rdr \; - \; \frac{\partial \rho_\infty^*}{\partial z}\int_0^\infty vrdr \; = \; 0 \tag{4.21}$$

Salinity or concentration transport:

$$\frac{d}{dz}\int_0^\infty v\Delta_3 rdr = 0 \, . \tag{4.22}$$

Equation (4.20) may be written in terms of Δ_2 by rearranging the gravitational contribution to yield,

$$\frac{d}{dz}\int_0^\infty v^2 rdr = g\left(\frac{\rho_r - \rho_o}{\rho_o}\right)\int_0^\infty \Delta_2 rdr \tag{4.23}$$

Integration of Equations (4.21) through (4.23) may be completed by utilizing profiles given by Equations (4.12) and(4.13) (4.13) for Δ_1 and Δ_2. Hence, the resulting expressions are

Vertical momentum:

$$\frac{d}{dz}\left\{\frac{v_m^3 z^3}{K^{3/2}}\right\} = 3g\left(\frac{\rho_r - \rho_o}{\rho_o}\right)\frac{v_m \Delta_{2m} z^3}{\lambda K^{3/2}} \tag{4.24}$$

Density disparity:

$$\frac{d}{dz}\left\{\frac{v_m \Delta_{2m} z^2}{K(\lambda + 1)}\right\} = \frac{v_m z^2}{K} \quad \frac{d\rho_\infty^*}{dz} \tag{4.25}$$

Salinity or concentration:

$$\frac{v_{m_1} z^2}{K(\lambda + 1)} = \frac{D^2 v_o \Delta_{3o}}{4} \tag{4.26}$$

Cast in dimensionless form, the above equations become

$$\frac{dE^*}{d\mathcal{Z}} = \frac{3}{F_o} \left(\frac{1+\lambda}{\lambda\sqrt{K}}\right) \mathcal{Z}R^*, \tag{4.27}$$

$$\frac{dR^*}{d\mathcal{Z}} = \frac{\mathcal{Z}}{\sqrt{K}} E^{*1/3} \frac{d\rho_\infty^*}{d\mathcal{Z}} \tag{4.28}$$

$$\Delta_{1m} = \frac{\sqrt{K}(1+\lambda)}{4} \frac{1}{E^{*1/3}\mathcal{Z}} \tag{4.29}$$

where,

$$\mathcal{Z} = z/D$$

$$V_m = v_m/v_o$$

$$E^* = \left(\frac{V_m\mathcal{Z}}{\sqrt{K}}\right)^3 \tag{4.30}$$

$$R^* = \frac{E^{*1/3} \Delta_{2m}\mathcal{Z}}{\sqrt{K}\,(1+\lambda)}\text{ , and} \tag{4.31}$$

$$\Delta_{1o} = 1.$$

4.5.1 Initial Condition

The solutions of Equations (4.27) and (4.28) are begun at $Z = Z_e$, or in the beginning of the established flow regime. Abraham's relationship (4.19) may be used to evaluate this distance for the entire range of densimetric Froude numbers, F_o. Once Z_e is known, the initial values E^*_e and R^*_e may be established. We assume that ambient stratification may be neglected over Z_e, then

$$\Delta_2 \Big|_{Z=Z_e} = 1, \text{ and}$$

$$\frac{d\rho_\infty^*}{dZ} \Big|_{Z=Z_e} = 0 .$$

Hence, by Equations (4.30) and (4.31)

$$R_e^* = \frac{1}{4} . \tag{4.32}$$

The initial value of E* may be found by considering Equation (4.30). For large initial Froude numbers ($F_o \to \infty$) $V_{me} \to 1$, so that

$$E_e^* = \left(\frac{Z_e}{\sqrt{K}}\right)^3 . \tag{4.33}$$

However, for low F_o, V_{me} is typically larger than 1 and unknown. To avoid estimation of V_{me}, we use Equations (4.29) and (4.30) with $\Delta_{2me} = 1$, to obtain

$$E_e^* = \left[\frac{\sqrt{K}(1 + \lambda)}{4Z_e}\right]. \tag{4.34}$$

For large F_o, Equation (4.34) reduces to

$$E_e^* = \frac{\sqrt{2}}{4} ; \tag{4.35}$$

in which case $Z_e = 5.6$. This result agrees with Equation (4.19).

4.5.2 Evaluation of Terms Involving K and λ

Listed in Table 4.1 below are limiting values of K and λ as suggested by Abraham along with limiting and mean values of terms involving K and λ.

TABLE 4.1 VALUES OF TERMS INVOLVING K AND λ

Term	Momentum Jet ($F_o \rightarrow \infty$)	Simple Plume ($F_o \rightarrow 0$)	Mean Value	Max. Error (%)
K	77	92		
λ	.80	.74		
$\frac{1+\lambda}{\lambda\sqrt{K}}$	.256	.245	1/4	2.4%
$\frac{1}{\sqrt{K}}$	.114	.104	.109	4.8%
$\frac{4}{\sqrt{K}(\lambda+1)}$	.253	.239	.245	2.9%

Using convenient values for the above terms, the governing equations and initial conditions are:

$$\frac{dE^*}{dZ} = \frac{3}{4F_o} Z R^*, \tag{4.36}$$

$$\frac{dR^*}{dZ} = .11 Z E^{*\,1/3} \frac{d\rho_\infty^*}{dZ} , \qquad (4.37)$$

$$\Delta_{1m} = \frac{4}{Z\ E^{*\ 1/3}} , \qquad (4.38)$$

and the initial conditions are:

$$E_e^* = \frac{64}{Z_e^{\ 3}} \qquad (4.39)$$

$$R_e^* = 1/4 . \qquad (4.40)$$

4.5.3 Homogeneous Receiving Water

For the case of homogeneous receiving water the above equations may be solved analytically since $d\rho_\infty/dZ = 0$. Therefore, from Equation (4.37)

$$R^* = 1/4, \qquad (4.41)$$

and Equation (4.36) becomes

$$\frac{dE^*}{dZ} = \frac{3Z}{16F_o} . \qquad (4.42)$$

Equation (4.42) may be integrated immediately to yield

$$E^* = \left\{ \frac{64}{Z_e^3} + \frac{3}{32F_o} [Z^2 - Z_e^{\ 2}] \right\} . \qquad (4.43)$$

Centerline concentration is then given by Equation (4.41) as

$$\Delta_{1m} = \left\{ \frac{Z^3}{64} \left[\frac{64}{Z_e^{\ 3}} + \frac{3}{32F_o} (Z^2 - Z_e^{\ 2}) \right] \right\}^{-1/3} . \qquad (4.44)$$

Apparently, the stratified case must be solved numerically.

4.6 Lateral Velocity, u_r

Once the plume centerline velocity, v, has been calculated, and the lateral distribution of axial velocity has been established, it is a simple matter to calculate u_r from the continuity equation,

$$\frac{1}{r} \frac{\partial(ru_r)}{\partial r} + \frac{\partial v}{\partial r} = 0 . \tag{4.45}$$

Since v(r,z) is known, Equation (4.45) may be written as

$$\frac{d}{dr} [u_r r] = rf(v) \tag{4.46}$$

or

$$u_r = \frac{1}{r} \int_0^r f(v)\, xdx. \tag{4.47}$$

CHAPTER 5

FINITE-DIFFERENCE MODELS

The finite-difference models developed in this chapter are applicable to the following two situations:

- Vertical round ports issuing into quiescent receiving water, and
- Line plumes which may include ambient current effects.

From a practical standpoint, the vertical round port in shallow water is of foremost importance because this configuration is typical of present and planned installations. The line thermal model would find application in analyses of the plume which develops over a diffuser line once the individual round plumes have interferred with one another.

The numerical models are formed in two dimensions for steady flow conditions. In the case of a vertical round plume, a two-dimensional model will not accommodate any ambient cross flow which would destroy the plume symmetry. Hence, the solution is strictly valid only during slack tide conditions in the absence of prevailing local currents. However, cross currents, tidal or otherwise, have little effect on the initial mixing (near-port locale) of plume flow from large outfalls in shallow water. The reason for this is that the effluent momentum dominates the ambient flow. At the San Onofre outfall, data show that isotherms in the near vicinity of the outfall are reasonably concentric even in the presence of tidal currents [24]. In view of available data it appears that a two-dimensional axisymmetric model for the vertical round plume should give adequate results for the initial mixing region, in spite of ambient cross flow.

The line thermal model may accommodate ambient flow perpendicular to the plume since in this case the phenomenon remains two-dimensional. End affects are, of course, ignored in this case.

Difference models are based on the vorticity-stream function equation described in Chapter 3. Where the finite-difference solution is started some distance above the outfall port, boundary conditions are obtained from available data or similarity solutions as described in Chapter 4. As indicated by Table 3.1, the minimum number of equations required is three. We will also consider salinity transport so that four partial differential equations are required, these being one Poisson type equation for the stream function and a total of three transport equations for vorticity and two Γ constituents.

5.1 Physical System for the Vertical Round Port

The physical system of primary concern is a large, single port, submerged vertical thermal outfall issuing to stagnant receiving water. Figure 5.1 illustrates this system in axisymmetric coordinates (r, z). Later, conditions for a line plume will be discussed in an appropriate cartesian coordinate system. The receiving water has depth, L, and is assumed stratified with density $\rho_\infty(z)$. Flow enters the system along the bottom boundary ($z = z_b$) with some known velocity and temperature distribution. In all cases to be analyzed the inflow will occur only over a small portion of this boundary, which extends from the plume centerline to a point r_b, the nominal plume boundary. For the shallow water cases, $r_b = R_0$ the outfall port radius

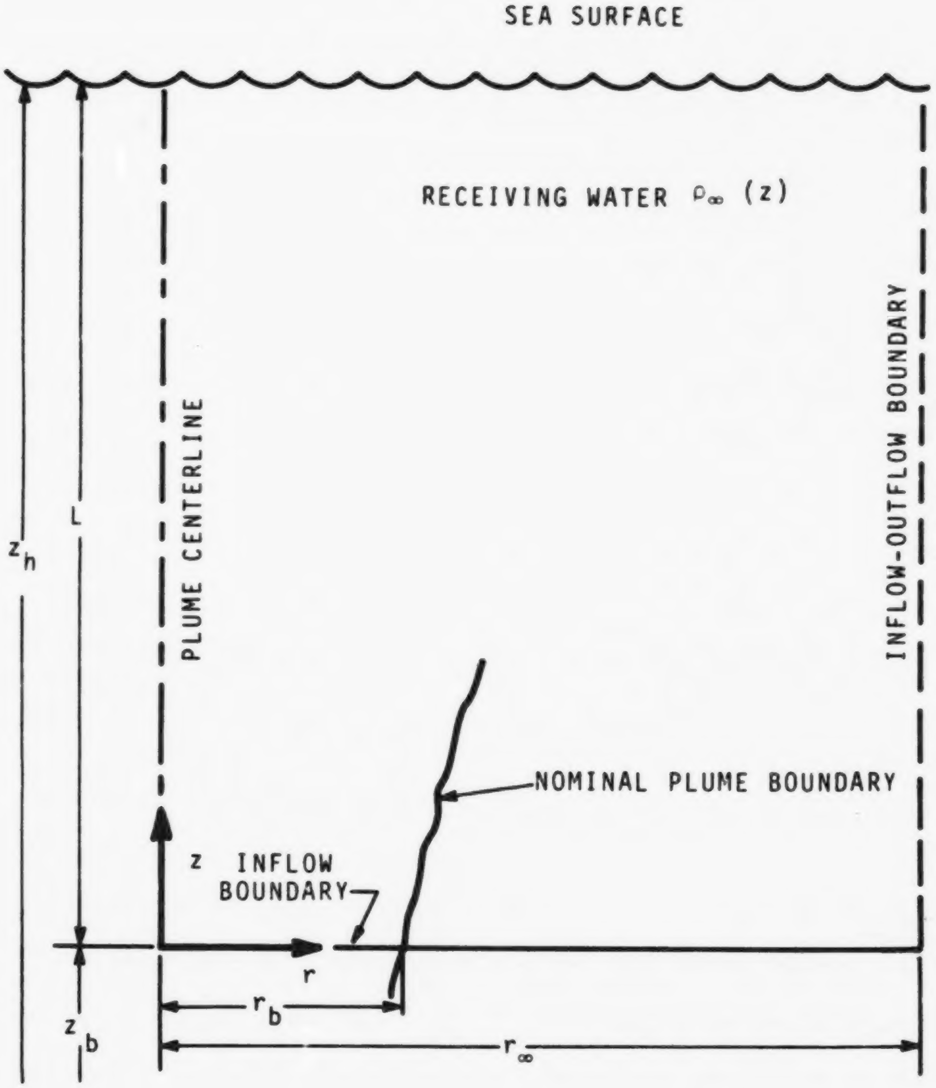
SEA SURFACE
RECEIVING WATER ρ_∞ (z)
PLUME CENTERLINE
INFLOW-OUTFLOW BOUNDARY
(FREE-FLOW)
z_h
L
NOMINAL PLUME BOUNDARY
z
INFLOW
BOUNDARY
r
r_b
z_b
r_∞

Figure 5.1 Physical System for Axisymmetric Vertical Plume where the Bottom Boundary is Some Distance $z_b \neq 0$ Above the Outfall Port

(Figure 5.2). It is assumed that no flow crosses that portion of the bottom boundary extending from r_b to r_∞.

The plume centerline and ocean surface form no-flow boundaries, or a reference streamline. A free-slip condition is assumed at the ocean surface, but this surface is not allowed to distort vertically. The flow boundary condition at $r = r_\infty$ is free except that streamlines are assumed to have constant slope. Flow will both enter and exit over portions of this boundary; the exact distribution is a part of the numerical computation. The mean velocity might be assumed wholly horizontal since r_∞ is a large distance compared to r_b, and since density stratification will impede vertical flow. This assumption would lead to level streamlines.

For shallow water geometry, (Figure 5.2) the ocean bottom is assumed flat and $z_b = 0$. The port side and ocean floor are assumed no-slip boundaries.

5.2 Governing Differential Equations

For incompressible, turbulent flow in axisymmetric coordinates, the differential equations describing continuity, linear momentum and buoyancy transport were given in Section 3.10.2 and are reiterated below.

Continuity:

$$\frac{1}{r} \frac{\partial ur}{\partial r} + \frac{\partial v}{\partial z} = 0, \tag{5.1}$$

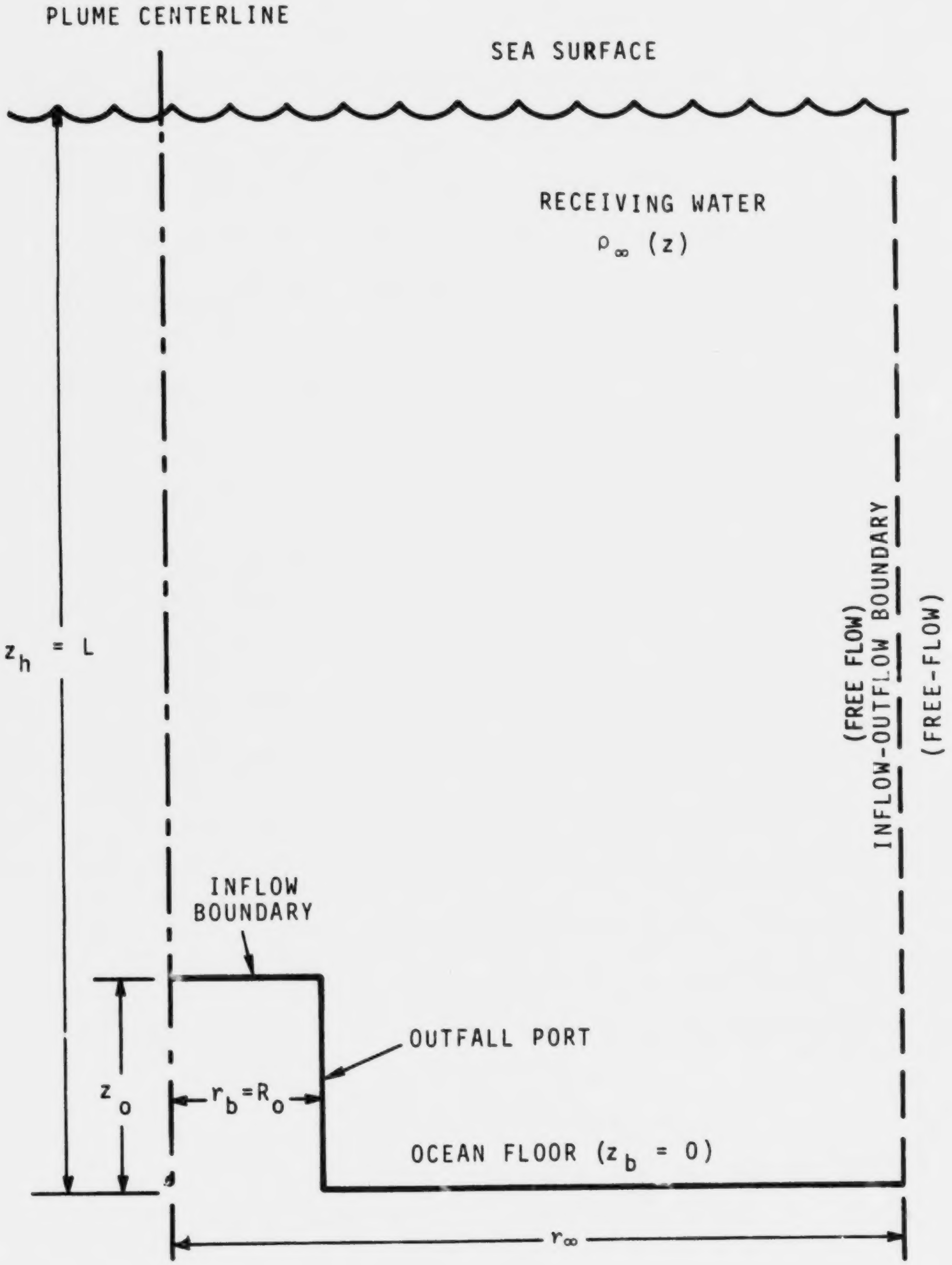
PLUME CENTERLINE
SEA SURFACE
RECEIVING WATER
ρ∞ (z)
(FREE FLOW)
INFLOW-OUTFLOW BOUNDARY
(FREE-FLOW)
z_h = L
INFLOW
BOUNDARY
OUTFALL PORT
z_o
r_b=R_o
OCEAN FLOOR (z_b = 0)
r∞

Figure 5.2 Physical System for Shallow Water, Axisymmetric, Vertical Plume

where u and v are radial and vertical velocity components, respectively (note that u is used instead of u_r as in Section 3.10.2).

Momentum transport:

r = direction,

$$\frac{Du}{Dt} = - \frac{\partial P^o}{\partial r} + \varepsilon_r \frac{\partial}{\partial r} \left[\frac{1}{r} \frac{\partial ur}{\partial r} \right] + \varepsilon_z \frac{\partial^2 u}{\partial z^2} . \qquad (5.2)$$

z = direction,

$$\frac{Dv}{Dt} = - \frac{\partial P^o}{\partial z} + \left(\frac{\rho_\infty - \rho}{\rho_o}\right) g + \frac{\varepsilon_r}{r} \cdot \frac{\partial}{\partial r} \left(r \frac{\partial v}{\partial r}\right) + \varepsilon_z \frac{\partial^2 v}{\partial z^2} \qquad (5.3)$$

In Equations (5.2) and (5.3) above, derivatives of ε_r and ε_z have been ignored.

Buoyancy transport:

In lieu of the energy equation, the transport equation for Δ_1 is considered,

$$\frac{D\Delta_1}{Dt} = \frac{\varepsilon_{\rho r}}{r} \frac{\partial}{\partial r} \left(r \frac{\partial \Delta_1}{\partial r}\right) + \varepsilon_{\rho z} \frac{\partial^2 \Delta_1}{\partial z^2} , \qquad (5.4)$$

where again derivatives of the eddy buoyancy diffusivities, $\varepsilon_{\rho r}$ and $\varepsilon_{\rho z}$ have been ignored. The buoyancy parameter, Δ_1, as defined in chapter 3 is

$$\Delta_1 = \frac{\rho_r - \rho}{\rho_r - \rho_o}$$

5.3 Vorticity Equations

For the problem at hand, it is more convenient to deal with vorticity transport rather than linear momentum transport. In dealing with vorticity, we need not be concerned about pressure and need to consider one less partial differential equation. The appropriate vorticity-stream function equations were given in Section 3.10.2 and as a matter of convenience are listed below.

Stream function, ψ:

$$\frac{\partial^2 \psi}{\partial r^2} - \frac{1}{r}\frac{\partial \psi}{\partial r} + \frac{\partial^2 \psi}{\partial z^2} = - r\omega \tag{5.5}$$

Vorticity, ω:

$$\frac{\partial \omega}{\partial t} + \frac{\partial u\omega}{\partial r} + \frac{\partial v\omega}{\partial z} = - \frac{\partial B}{\partial r} + \varepsilon_r \frac{\partial}{\partial r}\left(\frac{1}{r}\frac{\partial \omega r}{\partial r}\right) + \varepsilon_z \frac{\partial^2 \omega}{\partial z^2} , \tag{3.79}$$

where vorticity is defined as

$$\omega = \frac{\partial u}{\partial z} - \frac{\partial v}{\partial r} . \tag{3.74}$$

Once having solved for the stream function distribution (Equation 5.5) the velocity field is found by the relationships,

$$u = - \frac{1}{r}\frac{\partial \psi}{\partial z} \tag{5.6}$$

and

$$v = \frac{1}{r}\frac{\partial \psi}{\partial r} . \tag{5.7}$$

In the remainder of this work we will consider only steady flow. Hence, the vorticity transport Equation (3.81) has the form

$$\frac{\partial u\omega}{\partial r} + \frac{\partial v\omega}{\partial z} = - \frac{g}{\rho_o} \frac{\partial(\rho_\infty - \rho)}{\partial r} + \varepsilon_r \frac{\partial}{\partial r} \left(\frac{1}{r} \frac{\partial \omega r}{\partial r} \right) + \varepsilon_z \frac{\partial^2 \omega}{\partial z^2} \qquad (5.8)$$

where B has been replaced by the definition Equation (3.22). Steady flow transport of the buoyancy parameter Δ_1 is given by

$$\frac{1}{r} \frac{\partial(ru\Delta_1)}{\partial r} + \frac{\partial(v\Delta_1)}{\partial z} = \frac{\varepsilon_{\rho r}}{r} \frac{\partial}{\partial r} \left(r \frac{\partial \Delta_1}{\partial r} \right) + \varepsilon_{\rho z} \frac{\partial^2 \Delta_1}{\partial z^2} \qquad (5.9)$$

The convective terms in Equation (5.9) are in "conservative" form which was obtained from Equation (5.4) through the use of the continuity Equation (5.1).

In summary, the equations to be solved for the axisymmetric plume dispersion are (5.4), (5.8) and (5.9) along with (5.5) and (5.6). Equation (3.76) will be considered to evaluate vorticity boundary conditions. To account for salinity transport (if applicable) a second Equation (5.9) will be solved with Δ_1 defined as a salinity parameter, Δ_3, where

$$\Delta_3 = \frac{S_r - S}{S_r - S_o} \quad .$$

Temperature distributions may be calculated from the Equation of State (3.38) once Δ_1 and Δ_3 have been established. Hereafter only the conservative form of the transport equations will be considered. Although the pressure distribution is not considered in this work, it could be calculated through Equation (3.74).

5.4 Dimensionless Forms

To cast the governing equations in dimensionless form consider the following dimensionless variables:

$R = r/r_o$,

$Z = z/r_o$, [1]

$U = u/v_o$,

$V = v/v_o$,

$\Psi = \psi/(r_o^2 v_o)$,

$\Omega = \omega/(v_o/r_o)$;

and, the dimensionless parameters:

$$RE_r = \frac{r_o v_o}{\varepsilon_r} \text{ , (radial, turbulent Reynolds number)}$$

$$RE_z = \frac{r_o v_o}{\varepsilon_z} \text{ , (vertical, turbulent Reynolds number)}$$

$$PR_r = \frac{\varepsilon_r}{k_r} \text{ , (radial, turbulent Prandtl number)}$$

$$PR_z = \frac{\varepsilon_z}{k_z} \text{ , (vertical, turbulent Prandtl number)}$$

$$F_o = \frac{v_o^2}{\frac{\rho_r - \rho_o}{\rho_o} \; 2 \; r_o g} \text{ (densimetric Froude number).}$$

---

[1] Note that a second dimensionless vertical distance is used in this manuscript defined as $\mathcal{Z} = z/D$ and should not be confused with Z.

In the above definitions r_0 is the outfall port radius and v_0 is the effluent velocity issuing from the port.

With these variables, the system of governing equations is written as

stream function:

$$\frac{\partial^2 \Psi}{\partial R^2} - \frac{1}{R}\frac{\partial \Psi}{\partial R} + \frac{\partial^2 \Psi}{\partial Z^2} = - R\Omega, \tag{5.10}$$

vorticity:

Note that in Equation (5.8) the Boussinesq term may be rewritten as

$$- \frac{g}{\rho_0}\frac{\partial(\rho_\infty - \rho)}{\partial r} = - \frac{g}{\rho_0}\frac{(\rho_r - \rho)}{\partial r} + \frac{g}{\rho_0}\frac{\partial(\rho_r - \rho_\infty)}{\partial r},$$

since ρ_∞ is a function of Z alone. Hence,

$$\frac{\partial}{\partial R}(U\Omega) + \frac{\partial}{\partial Z}(V\Omega) = - \frac{1}{2F_0}\frac{\partial \Delta_1}{R} +$$

$$\frac{1}{RE_r}\left(\frac{\partial^2 \Omega}{\partial R^2} + \frac{1}{R}\frac{\partial \Omega}{\partial R} - \frac{\Omega}{R^2}\right) + \frac{1}{RE_z}\frac{\partial^2 \Omega}{\partial Z^2}, \tag{5.11}$$

buoyancy parameter:

$$\frac{1}{R}\frac{\partial}{\partial R}(RU\Delta_1) + \frac{\partial}{\partial Z}(V\Delta_1) =$$

$$\frac{1}{RE_r PR_z}\left(\frac{\partial^2 \Delta_1}{\partial R^2} + \frac{1}{R}\frac{\partial \Delta_1}{\partial R}\right) + \frac{1}{RE_z PR_z}\frac{\partial^2 \Delta_1}{\partial Z^2} \tag{5.12}$$

along with

$$U = -\frac{1}{R}\frac{\partial\Psi}{\partial Z} \quad , \tag{5.13}$$

and

$$V = \frac{1}{R}\;\frac{\partial\Psi}{\partial R} \quad . \tag{5.14}$$

5.5 Coordinate Transformation

When solving partial differential equations numerically, it is desirable to have fine grid space resolution where large derivatives of the dependent variables are expected. In the present problem, a fine grid spacing is needed in the radial direction near the outfall port and plume centerline. At large distances from the centerline, large grid spacing may be used since radial changes in the dependent variables are expected to be small. To this end, a non-linear transformation is employed on the radial coordinate, of the form

$$R = \sinh \xi \ . \tag{5.15}$$

This transformation has the desirable properties:

$$R \simeq \xi, \quad \Delta R \simeq \Delta\xi \qquad \text{for small } R,$$

and

$$R \simeq \frac{1}{2}e^{\xi}, \ \Delta R \simeq \frac{\Delta\xi}{2}\ e^{\xi} \qquad \text{for large } R.$$

In terms of transformed coordinates, the governing equations are:

stream function:

$$\operatorname{sech}^2\xi \left[\frac{\partial^2\Psi}{\partial\xi^2} - (\tanh\xi + \coth\xi)\frac{\partial\Psi}{\partial\xi}\right] + \frac{\partial^2\Psi}{\partial Z^2} = -\sinh\xi\,\Omega \quad . \tag{5.16}$$

vorticity:

$$\operatorname{sech} \xi \cdot \frac{\partial(U\Omega)}{\partial \xi} + \frac{\partial(V\Omega)}{\partial Z} = - \left(\frac{\operatorname{sech} \xi}{2\ F_o}\right) \frac{\partial \Gamma}{\partial \xi}$$

$$+ \frac{\operatorname{sech}^2 \xi}{RE_r} \left[\frac{\partial^2 \Omega}{\partial \xi^2} + \left(\frac{\operatorname{sech}^2 \xi}{\tanh \xi}\right) \cdot \frac{\partial \Omega}{\partial \xi} - \Omega \coth^2 \xi\right]$$

$$+ \frac{1}{Re_z} \cdot \frac{\partial^2 \Omega}{\partial Z^2} \quad . \tag{5.17}$$

buoyancy parameter:

$$\left(\frac{\operatorname{sech} \xi}{\sinh \xi}\right) \cdot \frac{\partial}{\partial \xi} \left[\left(\sinh \xi\right) U\Gamma\right] + \frac{\partial(V\Gamma)}{\partial Z} = \frac{\operatorname{sech}^2 \xi}{RE_r\ PR_r} \cdot \left[\frac{\partial^2 \Gamma}{\partial \xi^2} + \frac{\operatorname{sech}^2}{\tanh \xi} \cdot \frac{\partial \Gamma}{\partial \xi}\right]$$

$$+ \frac{1}{RE_z\ PR_z} \cdot \frac{\partial^2 \Gamma}{\partial Z^2} \quad . \tag{5.18}$$

Transformed expressions for velocity are given by:

$$U = - \frac{1}{\sinh \xi} \cdot \frac{\partial \Psi}{\partial Z} \tag{5.19}$$

$$V = \frac{\operatorname{sech} \xi}{\sinh \xi} \cdot \frac{\partial \Psi}{\partial \xi} \tag{5.20}$$

Finite-difference calculations will be based on even increments of the transformation coordinate, ξ.

In the vertical direction, fine resolution is needed in the region where the plume spreads laterally. In all thermal plume cases of interest, this region is in the vicinity of the receiving water surface. However, for other pollutants, such as municipal and industrial wastes, lateral spread may take place below the surface and pollutant concentration information is needed in the vicinity of this plane. Since methods presented here are also applicable to these pollutant plumes, a fine grid arrangement near the surface is not specified as a general case. Rather, the vertical grid spacing will be treated as node-wise variable and exact specification left to the discretion of the computer program user.

5.6 Finite-Difference Grid System

The finite-difference grid layout consists of two grid systems. One grid is used to calculate the stream function, Ψ, which provides information to compute velocity components, U and V. This system coincides with the physical boundaries and is illustrated by the wider lines on Figure 5.3. The stream function is calculated at the interior intersection points designated by the solid round symbols. Solid box symbols represent boundary points.

Velocities are not calculated at these same points. The U components are computed at vertical midpoints which are designated by open circle symbols; whereas, the V components are computed at horizontal midpoints (ξ coordinate) and designated by open box symbols. In this

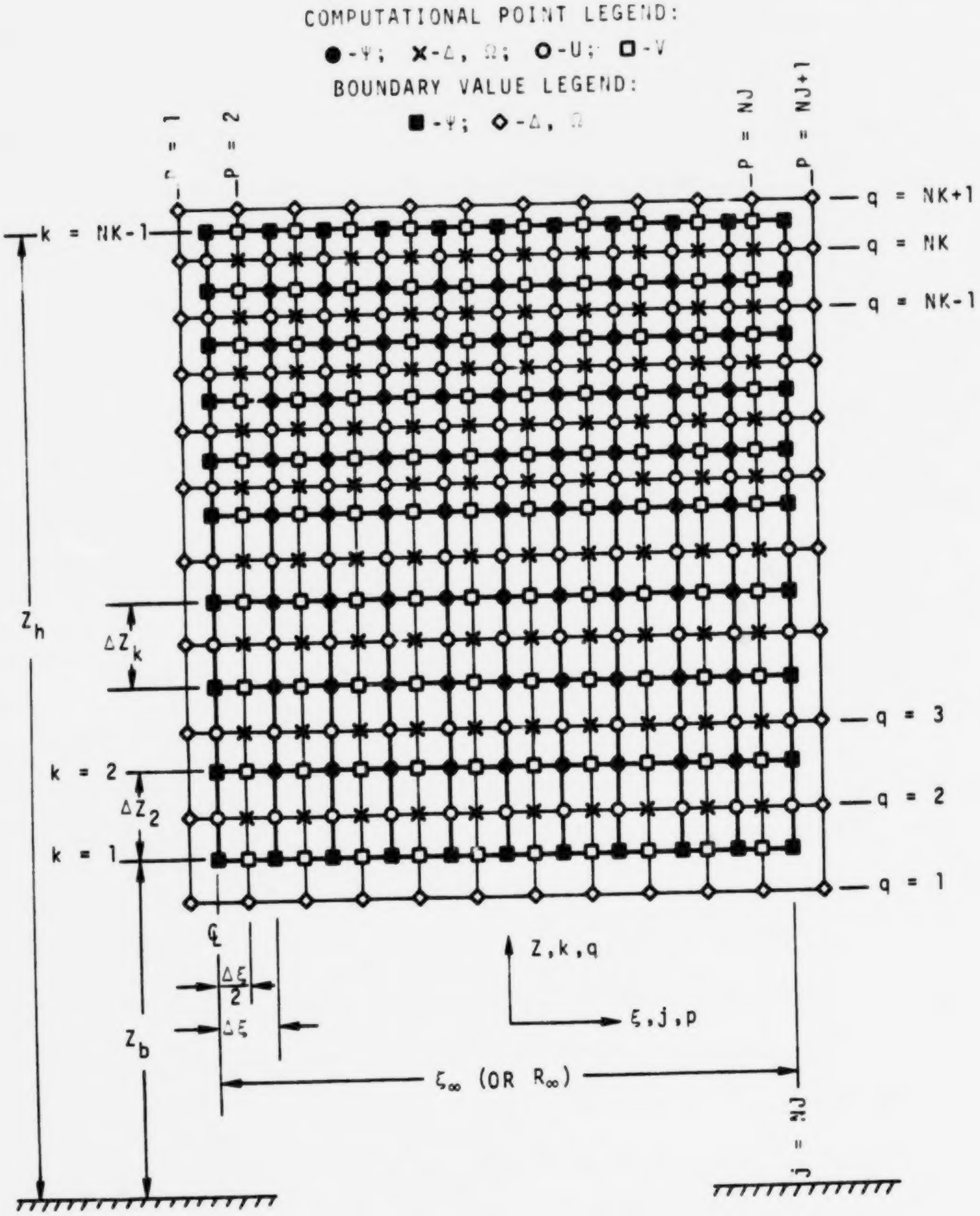
COMPUTATIONAL POINT LEGEND:
●-Ψ; ✱-Δ, Ω; ○-U; □-V
BOUNDARY VALUE LEGEND:
■-Ψ; ◇-Δ, Ω
p = 1
p = 2
p = NJ
p = NJ+1
q = NK+1
q = NK
q = NK-1
k = NK-1
Z_h
ΔZ_k
q = 3
k = 2
ΔZ_2
q = 2
k = 1
q = 1
℄
Δξ/2
Δξ
Z_b
Z,k,q
ξ,j,p
ξ_∞ (OR R_∞)
j = NJ

Figure 5.3 Computational Grid for Difference Equations

manner, the stream function grid layout defines a system of cells with the stream function, Ψ, computed at each corner point (or set by boundary conditions, as the case may be) and velocities defined at the center of the cell face (see Figure 5.4).

The second grid system is used to calculate vorticity, Ω, and buoyancy parameter, Δ_1, (also Δ_3) and is illustrated in Figures 5.3 and 5.4 by the narrow lines. This layout completely overlaps the grid (and physical system) with interior intersection points centered in the cells defined by the Ψ grid system. These interior grid points are indicated by crosses with boundary values at cross-and-box points.

The reason this staggered grid system is used is for computational convenience in treating boundary conditions and to permit convective transport terms to be evaluated at cell faces.

In Figure 5.3, the Ψ grid system is sized by NJ and NK grid points in the ξ (or R) direction and vertical direction, respectively. The Ω, Δ_1 system has size NJ + 1 and NK + 1 in the respective directions. Points on the Ψ grid are indicated by j, k, whereas points on the Ω, Δ_1 grid are indicated by p, q. In this figure, Z_b defines the bottom boundary of the stream function grid (physical boundary) and Z_h the top (sea surface). Vertical spacing for the system is defined by ΔZ_k and may be variable. Grid spacing along the ξ coordinate is even, designated by $\Delta\xi$. System boundary points for the Ω, Δ_1 grid are located at $Z_b - \frac{1}{2}\,\Delta Z_2$ for the bottom $Z_h + \frac{1}{2}\,\Delta Z_{NK-1}$ at the top, $-\frac{1}{2}\,\Delta\xi$ on the left and $\xi_\infty + \frac{1}{2}\,\Delta\xi$ at the right boundary, where ξ_∞ is the assumed right hand physical boundary. Figure 5.4 also illustrates

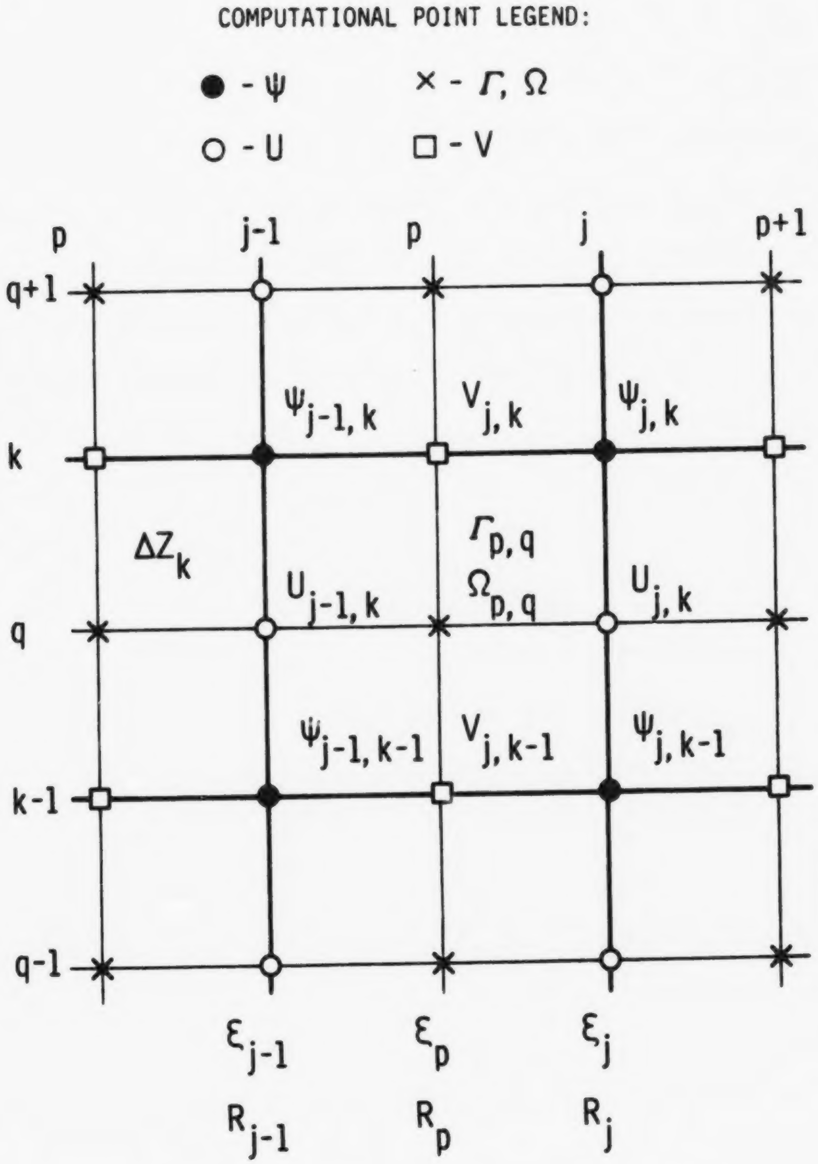
COMPUTATIONAL POINT LEGEND:
● - ψ
× - Γ, Ω
○ - U
□ - V
p
j-1
p
j
p+1
q+1
k
q
k-1
q-1
ψj-1, k
Vj, k
ψj, k
ΔZk
Γp, q
Ωp, q
Uj-1, k
Uj, k
ψj-1, k-1
Vj, k-1
ψj, k-1
εj-1
εp
εj
Rj-1
Rp
Rj

Figure 5.4 Typical Finite Difference Cell Illustrating Indices for Ψ, Ω, Γ, U and V

indices, computed quantities, cell size and radial distances for a typical interior cell.

5.7 Difference Equations

Standard difference representation is used wherever possible in this work. Central differences are used for both first and second partials except for convective terms where a special donor-cell method is used. Techniques for uneven spacing are used for the vertical differences.

5.7.1 Stream Function and Velocity

Consider the stream function grid system illustrated in Figures 5.3 and 5.4. The finite difference representation of Equation (5.16) based on central differences for both first and second partials is as follows:

$$
\begin{aligned}
2 \left[\frac{\operatorname{sech}^2 \xi_j}{\Delta\xi^2} + \frac{1}{\Delta Z_k \Delta Z_{k+1}} \right] \Psi_{j,k} = {} \\
& + \frac{\operatorname{sech}^2 \xi_j}{\Delta\xi^2} \cdot \left[1 + \left(\tanh \xi_j + \coth \xi_j \right) \cdot \frac{\Delta\xi}{2} \right] \Psi_{j-1,k} \\
& + \frac{\operatorname{sech}^2 \xi_j}{\Delta\xi^2} \cdot \left[1 - \left(\tanh \xi_j + \coth \xi_j \right) \cdot \frac{\Delta\xi}{2} \right] \Psi_{j+1,k} \\
& + \frac{2}{\Delta Z_{k+1} \left[\Delta Z_{k+1} + \Delta Z_k \right]} \cdot \Psi_{j,k+1} \\
& + \frac{2}{\Delta Z_k \left[\Delta Z_{k+1} + \Delta Z_k \right]} \cdot \Psi_{j,k-1} + \bar{\Omega}_{j,k} \sinh \xi_j \quad .
\end{aligned}
\tag{5.21}
$$

In the above difference equation, the quantity $\bar{\Omega}_{j,k}$ is the average value of Ω at point (j,k), hence the overbar. This average value must be used since $\Omega_{p,q}$ does not lie on the Ψ computational grid points. Vorticity is averaged for the four cells neighboring point (j,k) as follows:

$$\bar{\Omega}_{j,k} = \bar{\Omega}_1 + \frac{\Delta Z_k}{\Delta Z_k + \Delta Z_{k+1}} (\bar{\Omega}_2 - \bar{\Omega}_1), \tag{5.22}$$

where

$$\bar{\Omega}_1 = \Omega_{p,q} + \frac{1}{4} (\Omega_{p+1,q} - \Omega_{p-1,q}),$$

and

$$\bar{\Omega}_2 = \Omega_{p,q+1} + \frac{1}{4} (\Omega_{p+1,q+1} - \Omega_{p-1,q+1}).$$

Velocity is calculated in first-order manner as

$$U_{j,k} = \frac{-1}{\sinh \xi_j \ \Delta Z_k} (\Psi_{j,k} - \Psi_{j,k-1}) \tag{5.23}$$

and

$$V_{j,k} = \frac{\operatorname{sech} \xi_p}{\sinh \xi_p \Delta\xi} (\Psi_{j,k} - \Psi_{j-1,k}). \tag{5.24}$$

Thus far, we have discussed differencing the governing equations only in transformed radial coordinate, ξ. To permit more versatile computation we also include provision for calculation directly in (R,Z) coordinates. This is easily done by collapsing the hyperbolic functions so that

$$\sinh \xi \rightarrow \xi = R, \text{ (also set } \tanh \xi = 0)$$

and

$$\cosh \xi \rightarrow 1$$

giving

$$\Delta\xi = \Delta R.$$

Hence, for linear radial coordinates Equations (5.21), (5.22), (5.23) and (5.24) collapse to

$$\begin{aligned} 2\left(\frac{1}{\Delta R^2} + \frac{1}{\Delta Z_k \, \Delta Z_{k+1}}\right) \Psi_{j,k} = {} & \frac{1}{\Delta R^2}\left(1 - \frac{1}{2j}\right) \Psi_{j+1,k} \\ & + \frac{1}{\Delta R^2}\left(1 + \frac{1}{2j}\right)\Psi_{j-1,k} \\ & + \frac{2}{\Delta Z_{k+1}\left(\Delta Z_{k+1} + \Delta Z_k\right)} \Psi_{j,k+1} \\ & + \frac{2}{\Delta Z_k\left(\Delta Z_{k+1} + \Delta Z_k\right)} \Psi_{j,k-1} \\ & + j\Delta R \, \bar{\Omega}_{j,k} \end{aligned} \qquad (5.25)$$

Velocity:

R-component

$$U_{j,k} = \frac{-1}{j\Delta R \Delta Z_k} \left(\Psi_{j,k} - \Psi_{j,k-1}\right) \qquad (5.26)$$

Z-component

$$V_{j,k} = \frac{1}{(j-\frac{1}{2})\Delta R^2} \left(\Psi_{j,k} - \Psi_{j-1,k}\right). \qquad (5.27)$$

In Equations (5.25) through (5.27) sinh ξ_j is replaced by $j\Delta R$ and sinh ξ_p by $(j - \frac{1}{2})\,\Delta R$.

5.7.2 Transport Equations

Except for the convective transport terms, central differences are used to approximate all derivatives in the transport Equations (5.17) and (5.18). Special consideration is given the convective terms which involves basing numerical approximations on transport integral techniques (see Appendix A).

Referring to the p,q grid system illustrated in Figures 5.3 and 5.4 the difference representation of the steady flow vorticity transport Equation (5.17) is written as (after collecting terms)

$$\left\{\frac{2}{RE_z \Delta Z_k} \cdot \left[\frac{1}{\Delta Z_k + \Delta Z_{k+1}} + \frac{1}{\Delta Z_k + \Delta Z_{k-1}}\right] + \frac{\operatorname{sech}\ \xi_p}{RE_r \Delta\xi^2} \cdot \left[2 + \Delta\xi^2 \coth^2 \xi_p\right]\right.$$

$$+ \frac{\operatorname{sech}\ \xi_p}{2\Delta\xi} \cdot \left[|U_{j,k}| + U_{j,k} + |U_{j-1,k}| - U_{j-1,k}\right]$$

$$\left. + \frac{1}{2\Delta Z_k} \cdot \left[|V_{j,k}| + V_{j,k} + |V_{j,k-1}| - V_{j,k-1}\right]\right\} \Omega_{p,q}$$

$$= \left\{\frac{\operatorname{sech}\ \xi_p}{2\Delta\xi} \cdot \left[|U_{j-1,k}| + U_{j-1,k}\right] + \frac{\operatorname{sech}^2 \xi_p}{RE_r \Delta\xi^2} \cdot \left[1 - \frac{\Delta\xi}{2} \frac{\operatorname{sech}^2 \xi_p}{\tanh\ \xi_p}\right]\right\} \Omega_{p-1,q}$$

Equation (5.28) continued on next page.

$$+\left\{\frac{\operatorname{sech}\xi_p}{2\Delta\xi}\cdot\left[|U_{j,k}| - U_{j,k}\right] + \frac{\operatorname{sech}^2\xi_p}{RE_r\Delta\xi^2}\cdot\left[1 + \frac{\Delta\xi}{2}\,\frac{\operatorname{sech}^2\xi_p}{\tanh\xi_p}\right]\right\}\Omega_{p+1,q}$$

$$+\left\{\frac{1}{2\Delta Z_k}\cdot\left[|V_{j,k-1}| + V_{j,k-1}\right] + \frac{2}{RE_z\Delta Z_k}\cdot\left[\frac{1}{\Delta Z_k+\Delta Z_{k-1}}\right]\right\}\Omega_{p,q-1}$$

$$+\left\{\frac{1}{2\Delta Z_k}\cdot\left[|V_{j,k}| - V_{j,k}\right] + \frac{2}{RE_z\Delta Z_k}\cdot\left[\frac{1}{\Delta Z_k+\Delta Z_{k+1}}\right]\right\}\Omega_{p,q+1} \tag{5.28}$$

$$-\frac{\operatorname{sech}\xi_p}{4F_o\Delta\xi}\cdot\left[\Delta 1_{p+1,q} - \Delta 1_{p-1,q}\right] \quad .$$

The turbulent Reynolds numbers, RE_r and RE_z, in the above difference equation are point variables of the form $RE_r(p,q)$ and $RE_z\,(p,q)$. Derivatives of these quantities are neglected in the above equations but are accounted for in the computations.

Equation (5.28) may be collapsed to radial coordinates in the same fashion as illustrated in Section 5.7.1. Hence, in non-transformed radial coordinates the vorticity transport difference equation, after collecting terms, is (note that numerically $p = j-1/2$)

$$\Bigg[\frac{2}{RE_z \Delta Z_k} \left\{\frac{1}{\Delta Z_k + Z_{k+1}} + \frac{1}{\Delta Z_k + \Delta Z_{k-1}}\right\} + \frac{1}{RE_r \Delta R^2}\left(2 + \frac{1}{p^2}\right)$$

$$+ \frac{1}{2\Delta R}\Big(|U_{j,k}| + U_{j,k} + |U_{j-1,k}| - U_{j-1,k}\Big)$$

$$+ \frac{1}{2\Delta Z_k}\Big(|V_{j,k}| + |V_{j,k} + |V_{j,k-1}| - V_{j,k-1}\Big)\Bigg] \Omega_{p,q}$$

$$= \Bigg[\frac{1}{2\Delta R}\Big(|U_{j-1,k}| + U_{j-1,k}\Big) + \frac{1}{RE_r \Delta R^2}\left(1 - \frac{1}{2p}\right)\Bigg] \Omega_{p-1,q}$$

$$+ \Bigg[\frac{1}{2\Delta R}\Big(|U_{j,k}| - U_{j,k}\Big) + \frac{1}{RE_r \Delta R^2}\left(1 + \frac{1}{2p}\right)\Bigg] \Omega_{p+1,q}$$

$$+ \Bigg[\frac{1}{2\Delta Z_k}\Big(|V_{j,k-1}| + V_{j,k-1}\Big) + \frac{2}{RE_z \Delta Z_k}\left(\frac{1}{\Delta Z_k + \Delta Z_{k-1}}\right)\Bigg] \Omega_{p,q-1}$$

$$+ \Bigg[\frac{1}{2\Delta Z_k}\Big(|V_{j,k}| - V_{j,k}\Big) + \frac{2}{RE_z \Delta Z_k}\left(\frac{1}{\Delta Z_k + \Delta Z_{k+1}}\right)\Bigg] . \Omega_{p,q+1}$$

$$- \frac{1}{4F_o \Delta R}\Big(\Delta_{p+1,q} - \Delta_{p-1,q}\Big) \quad . \tag{5.29}$$

The convective terms are formed in a manner such that vorticity convected out of cell (p,q) has the value $\Omega_{p,q}$ and vorticity flowing into the same cell is convected in with the value of the cell where it originated, regardless of the directional sense of fluid motion. This character of convective transport is essential in properly conserving the transported quantity and in avoiding certain computational difficulties.

The difference formulation of the buoyancy equation after collecting terms is written as

$$
\begin{aligned}
&\left\{\frac{2}{PR_z RE_z \Delta Z_k} \cdot \left[\frac{1}{\Delta Z_{k+1}+\Delta Z_k} + \frac{1}{\Delta Z_{k-1}+\Delta Z_k}\right] + \frac{2\,\mathrm{sech}^2\,\xi_p}{PR_r RE_r \Delta\xi^2} + \frac{\sinh\,\xi_j \cdot \mathrm{sech}\,\xi_p}{2\Delta\xi\,\sinh\xi_p}\right. \\
&\quad \cdot \left[|U_{j,k}| + U_{j,k}\right] + \frac{\sinh\,\xi_{j-1} \cdot \mathrm{sech}\,\xi_p}{2\Delta\xi\,\sinh\xi_p} \cdot \left[|U_{j-1,k}| - U_{j-1,k}\right] \\
&\quad \left. + \frac{1}{2\Delta Z_k}\left[|V_{j,k}| + V_{j,k} + |V_{j,k-1}| - V_{j,k-1}\right]\right\}\Delta 1_{p,q} \\
&= \left\{\frac{\sinh\xi_{j-1} \cdot \mathrm{sech}\,\xi_p}{2\Delta\xi\,\sinh\,\xi_p} \cdot \left[|U_{j-1,k}| + U_{j-1,k}\right] + \frac{\mathrm{sech}^2\,\xi_p}{PR_r RE_r \Delta\xi^2}\right. \\
&\quad \left. \cdot \left[1 - \frac{\Delta\xi}{2}\,\frac{\mathrm{sech}^2\,\xi_p}{\tanh\,\xi_p}\right]\right\}\Delta 1_{p-1,q} + \left\{\frac{\sinh\xi_j \cdot \sinh\,\xi_p}{2\Delta\xi\,\sinh\,\xi_p}\right. \\
&\quad \left. \cdot \left[|U_{j,k}| - U_{j,k}\right] + \frac{\mathrm{sech}^2\,\xi_p}{PR_r RE_r \Delta\xi^2} \cdot \left[1 + \frac{\Delta\xi}{2}\,\frac{\mathrm{sech}^2\,\xi_p}{\tanh\,\xi_p}\right]\right\}\Delta 1_{p+1,q} \\
&\quad + \left\{\frac{1}{2\Delta Z_k} \cdot \left[|V_{j,k-1}| + V_{j,k-1}\right] + \frac{2}{PR_z RE_z \Delta Z_k} \cdot \left[\frac{1}{\Delta Z_{k-1}+\Delta Z_k}\right]\right\}\Delta 1_{p,q-1} \\
&\quad + \left\{\frac{1}{2\Delta Z_k} \cdot \left[|V_{j,k}| - V_{j,k}\right] + \frac{2}{PR_z RE_z \Delta Z_k} \cdot \left[\frac{1}{\Delta Z_{k+1}+\Delta Z_k}\right]\right\}\Delta 1_{p,q+1} \quad .
\end{aligned}
\tag{5.30}
$$

In linear radial coordinates, Equation (5.30) reduces to

$$\begin{aligned}
&\Bigg[\frac{2}{PR_zRE_z\Delta Z_k}\left(\frac{1}{\Delta Z_{k+1}+\Delta Z_k} + \frac{1}{\Delta Z_{k-1}+\Delta Z_k}\right) \\
&+ \frac{2}{PR_rRE_r\Delta R^2} + \frac{j}{2p\Delta R}\left(|U_{j,k}| + U_{j,k}\right) + \frac{j-1}{2p\Delta R}\cdot\left(|U|_{j-1,k}U_{j-1,k}\right) \\
&+ \frac{1}{2\Delta Z_k}\left(|V_{j,k}| + V_{j,k} + |V_{j,k-1}| - V_{j,k-1}\right)\Bigg]\Delta 1_{p,q} \\
&= \left[\frac{j-1}{2p\Delta R}\left(|U_{j-1,k}| + U_{j-1,k}\right) + \frac{1}{PR_rRE_r\Delta R^2}\left(1 - \frac{1}{2p}\right)\right]\Delta 1_{p-1,q} \\
&+ \left[\frac{j}{2p\Delta R}\left(|U_{j,k}| - U_{j,k}\right) + \frac{1}{PR_rRE_r\Delta R^2}\left(1 + \frac{1}{2p}\right)\right]\Delta 1_{p+1,q} \\
&+ \left[\frac{1}{2\Delta Z_k}\left(|V_{j,k-1}| + V_{j,k-1}\right) + \frac{2}{PR_zRE_z\Delta Z_k}\left(\frac{1}{\Delta Z_{k-1}+\Delta Z_k}\right)\right]\Delta 1_{p,q-1} \\
&+ \left[\frac{1}{2\Delta Z_k}\left(|V_{j,k}| - V_{j,k}\right) + \frac{1}{PR_zRE_z\Delta Z_k}\left(\frac{1}{\Delta Z_{k+1}+\Delta Z_k}\right)\right]\Delta 1_{p,q+1}\ . \qquad (5.31)
\end{aligned}$$

The Δ_3 transport difference equation corresponding to Equations (5.30) and (5.31) are obtained simply by replacing Δ_1 with Δ_3 and noting that the eddy Schmidt number, SC, should be used in the case of material transport, instead of the eddy Prandtl number, PR. Materials other than salt may be treated in a similar fashion.

5.7.3 Summary of required difference equations

The difference equations to be solved are:

Transformed coordinates (ξ, Z),

Ψ - Equation (5.21)

Ω - Equation (5.28)

Δ_1 - Equation (5.30)

Δ_3 - Equation (5.30)

U - Equation (5.23)

V - Equation (5.24)

Linear Coordinates (R, Z)

Ψ - Equation (5.25)

Ω - Equation (5.29)

Δ_1 - Equation (5.31)

Δ_3 - Equation (5.31)

U - Equation (5.26)

V - Equation (5.27)

5.7.4 Vertical Grid Space Restrictions

Although the vertical grid spacing is variable, there are three locations where an exception is expedient for the treatment of boundary conditions (Section 5.8). These exceptions are as follows:

1. At the grid system bottom boundary $\Delta Z_2 = \Delta Z_1$
2. At the sea surface $\Delta Z_{NK+1} = \Delta Z_{NK}$

where $Z_h = \sum_{k=2}^{NK} \Delta Z_K$

3. At the level of the plume inflow boundary

$$\Delta Z_{KP} = \Delta Z_{KP+1} = \Delta Z_{KP+2}$$

where KP is the grid boundary location.

These exceptions place no serious limitation on vertical grid spacing and are incorporated only to expedite computer bookkeeping in treating the various boundary conditions.

5.8 Boundary Conditions

Attention is now focused on evaluation of boundary conditions necessary to carry out solution of the equation sets summarized in Section 5.7.3.

Referring to Figures 5.1 and 5.2, the sea surface ($Z = Z_h$) is considered a free-slip boundary which is vertically rigid. A specified flow enters the bottom inflow boundary where $R \leq R_o$. Depending on the water depth, this boundary may constitute the outfall port orifice (shallow water case, see Figure 5.2) or an arbitrary lateral plane through the plume (deep water case, see Figure 5.1) at elevation $Z = Z_b$. In the former case, the port geometry must be considered along with the ocean floor. The radial velocity distribution, V_o, depends on R and the port side and ocean floor are no-slip surfaces. In the latter instance, the velocity distribution is obtained either directly from data (hydraulic model or prototype) or calculated by the similarity techniques described in Chapter 4. Outside the plume nominal boundary (Figure 5.1) the bottom boundary is assumed slip-free.

Surface heat transfer is neglected in this study since the sea surface area is relatively small and surface heat exchange will have very little effect on the overall temperature distribution. Boundary condition sets a and b given below refer to the physical systems shown in Figures 5.1 (deep water) and 5.2 (shallow water) respectively. To eliminate confusion, the boundary conditions are stated in terms of R (in lieu of the transformed coordinate, ξ).

1. Sea Surface ($0 \leq R \leq R_\infty$, $Z = Z_h$)

   a. $\Psi = \text{Constant} = \Psi_1$,

   $$\Omega = 0 \qquad (5.32)$$

   $$\frac{\partial \Delta_1}{\partial Z} = 0 \text{ (adiabatic condition)}$$

   $$\frac{\partial \Delta_3}{\Delta Z} = 0$$

   b. Same as above.

2. Plume Centerline

   a. $R = 0$, $Z_b \leq Z \leq Z_h$

   $$\Psi = \text{Constant} = \Psi_1$$

   $$\Omega = 0 \qquad (5.33)$$

   $$\frac{\partial \Delta_1}{\partial R} = 0$$

   $$\frac{\partial \Delta_3}{\partial R} = 0$$

   b. $R = 0$, $Z_o \leq Z \leq Z_h$

   Same as above.

3. Inflow Boundary

a. $Z = Z_b,\ 0 \leq R \leq R_b$

$$\Psi = \Psi_1 + \int_o^R V(R,Z_b)RdR \tag{5.34}$$

$$\Omega = \frac{\partial U}{\partial Z} - \frac{\partial V}{\partial R}$$

$$\Delta_1 = \Delta_{1_b}$$

$$\Delta_3 = \Delta_{3_b}$$

b. $Z = Z_o,\ 0 \leq R \leq R_o$

$$\Psi = \Psi_1 + \int_o^R V(R,Z_o)RdR \tag{5.35}$$

$$\Omega = \frac{\partial U}{\partial Z} - \frac{\partial V}{\partial R}$$

$$\Delta_1 = \Delta_{1_o}$$

$$\Delta_3 = \Delta_{3_o}$$

4. Port Side ($R = R_o,\ Z_b = 0 \leq Z \leq Z_o$)

a. Not applicable

b. $\Psi = \psi_1 + \dfrac{V_oR_o}{2} = \Psi_1 + \dfrac{1}{2} = \Psi_2$

Where the reference velocity, $V_o = 1$.

$$\Omega = -\frac{\partial V}{\partial R} \text{ (no slip)} \tag{5.36}$$

$$\frac{\partial \Delta_1}{\partial R} = 0$$

$$\frac{\partial \Delta_3}{\partial R} = 0$$

5. Bottom Boundary

a. $Z = Z_b,\ R_b \leq R \leq R_\infty$

$$\Psi = \Psi_1 + \int_0^{R_b} V(R,Z_b)RdR = \Psi_2 \qquad (5.37)$$

$$\Omega = 0$$

$$\frac{\partial \Delta_1}{\partial Z} = 0$$

$$\frac{\partial \Delta_3}{\partial Z} = 0$$

b. $Z = Z_b = 0,\ R_0 \leq R \leq R_\infty$

$$\Psi = \Psi_1 + \frac{1}{2} = \Psi_2$$

$$\Omega = \frac{\partial U}{\partial Z} \text{ (no slip)} \qquad (5.38)$$

$$\frac{\partial \Delta_1}{\partial Z} = 0$$

$$\frac{\partial \Delta_3}{\partial Z} = 0$$

6. Inflow-Outflow Boundary ($R = R_\infty,\ Z_b \leq Z \leq Z_h$)

The distance to the inflow-outflow (or free-flow) boundary, R_∞, must be chosen in advance and this distance must be large enough such that boundary conditions listed below prevail approximately.

a. $\frac{\partial \Psi}{\partial R} = 0$; or $\frac{\partial^2 \Psi}{\partial R^2} = 0$

Meaning that streamlines are level, or the streamlines do not change slope, respectively.

$$\Omega = \frac{\partial U}{\partial Z} - \frac{\partial V}{\partial R}, \qquad (5.39)$$

$$\Delta_1 = \frac{\rho_r - \rho_\infty}{\rho_r - \rho_0} \qquad \text{(Ambient condition)},$$

$$\Delta_3 = \frac{S_r - S_\infty}{S_r - S_0} \qquad \text{(Ambient condition)}$$

The conditions on Δ_1 and Δ_3 are valid so long as convection dominates the transport at the boundary and upstream differencing is used.

Now consider the difference form of these equations. Again, refer to Figure 5.3 and note that boundary values for the (j,k) grid (Ψgrid) fall on the boundary of the physical system; whereas, on the (p,q) grid (grid for Ω, Δ_1 and Δ_3) the boundary cells are fictitious in that they fall outside of the physical system. These cells are for the purpose of obtaining specific conditions at the real boundary. Again conditions a and b refer to cases given in Figures 5.1 and 5.2, respectively. The difference forms are given in terms of the transformed variable, ξ, for computer application.

1. Sea Surface ($k = NK$, $q = Nq + 1$)

   a. Deep Water (Refer to Figure 5.5)

Velocity:

$U_{j,NK+1} = U_{j,NK}$ (Free Slip) (5.40.1)

$V_{j,NK} = 0$ (5.40.2)

Stream Function:

$\Psi_{j,NK} = 1$ (Arbitrary) (5.40.3)

Vorticity:

Let Ω_s be the vorticity at point (p, Nk). By the free slip velocity condition above and the fact $V_{j,Nk} = 0$,

$$\Omega_s = \left(\frac{\partial U}{\partial Z} - \frac{\partial V}{\partial R} \right)\Big|_{NK} = 0.$$

Hence, Ω_s is the nodewise average value at Z_h, or

$$\Omega_s = \frac{1}{2} (\Omega_{p,Nq} + \Omega_{p,Nq+1}) = 0,$$

so that

$\Omega_{p,Nq+1} = - \Omega_{p,Nq}$. (5.40.4)

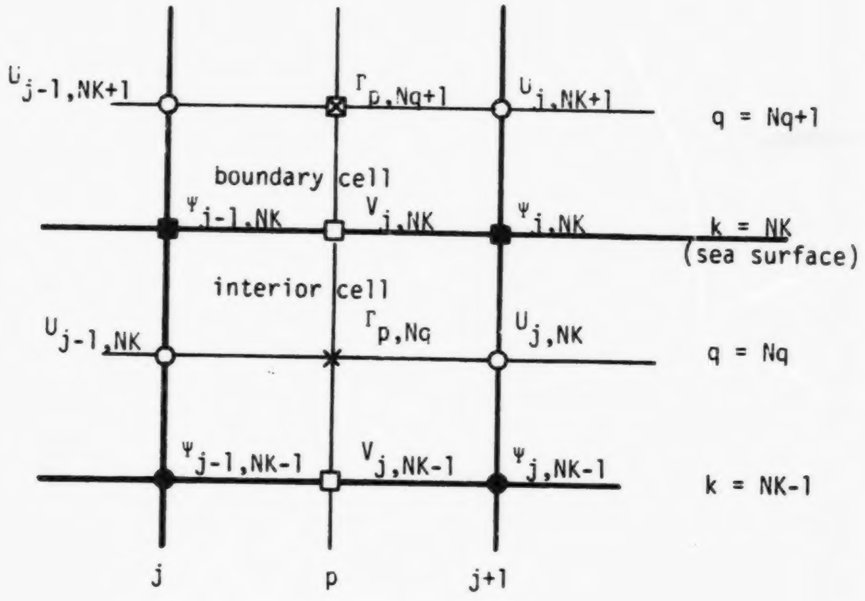
$U_{j-1,NK+1}$
$\Gamma_{p,Nq+1}$
$U_{j,NK+1}$
q = Nq+1
boundary cell
$\Psi_{j-1,NK}$
$V_{j,NK}$
$\Psi_{j,NK}$
k = NK
(sea surface)
interior cell
$U_{j-1,NK}$
$\Gamma_{p,Nq}$
$U_{j,NK}$
q = Nq
$\Psi_{j-1,NK-1}$
$V_{j,NK-1}$
$\Psi_{j,NK-1}$
k = NK-1
j
p
j+1

Figure 5.5 Typical Sea Surface Boundary and Interior Cells

[$\Gamma_{p,q}$ indicate any of the cell centered quantities Ω, Δ_1 and Δ_3.]

Buoyancy:

Since the adiabatic condition prohibits heat transport across the surface,

$$\left.\frac{\partial \Delta_1}{\partial Z}\right|_{Z_h} = 0,$$

Hence,

$$\frac{1}{\Delta Z_{NK}} (\Delta_{1p,Nq+1} - \Delta_{1p,Nq}) = 0, \qquad (5.40.5)$$

or

$$\Delta_{1p,Nq+1} = \Delta_{1p,Nq}.$$

Salinity:

Likewise,

$$\Delta_{3p,Nq+1} = \Delta_{3p,Nq} \quad . \qquad (5.40.6)$$

b. Shallow Water

Same as deep water case above.

2. Plume Centerline (R = 0)

a. Deep Water Case (Refer to Figure 5.6)

Velocity:

$U_{1,k} = U_{2,k}$ (velocity gradient vanishes) (5.41.1)

$V_{1,k} = 0$. (5.41.2)

Stream Function:

$\Psi_{1,k} = 1$ (Must be consistent with condition 1.a). (5.41.3)

Vorticity:

From the conditions on velocity given above, the centerline vorticity, $\Omega_{\text{℄}} = 0$, or averaging across the centerline,

$$\Omega_{\text{℄}} = 1/2\ (\Omega_{1,q} + \Omega_{2,q}) = 0 .$$

Hence,

$\Omega_{1,q} = - \Omega_{2,q}$. (5.41.4)

Buoyancy:

At the centerline, the buoyancy gradient must vanish.

Hence,

$$\frac{1}{\Delta\xi} (\Delta T_{2,k} - \Delta T_{1,k}) = 0,$$

or

$\Delta T_{1,k} = \Delta T_{2,k}$. (5.41.5)

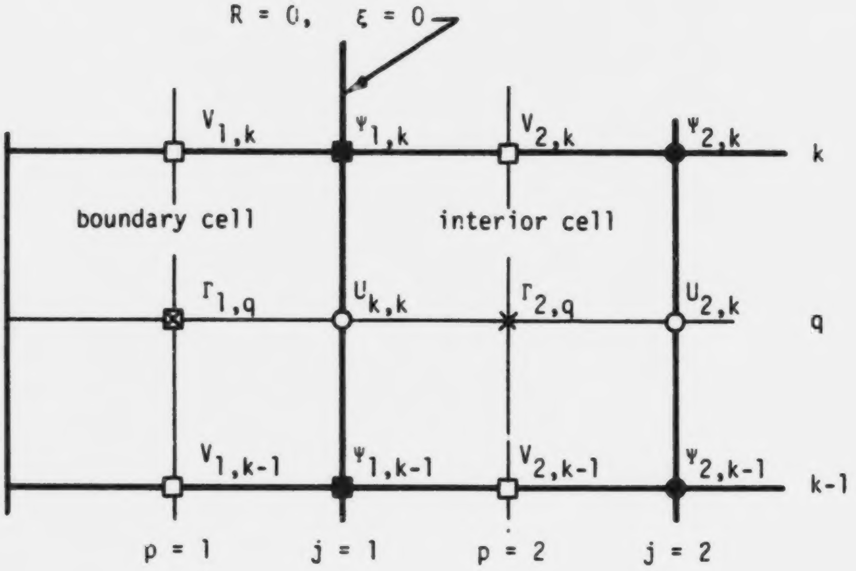
R = 0, ξ = 0
V1,k
Ψ1,k
V2,k
Ψ2,k
k
boundary cell
interior cell
Γ1,q
Uk,k
Γ2,q
U2,k
q
V1,k-1
Ψ1,k-1
V2,k-1
Ψ2,k-1
k-1
p = 1
j = 1
p = 2
j = 2

Figure 5.6 Typical Centerline Boundary and Interior Cells [$\Gamma_{p,q}$ indicates any of the cell centered quantities, Ω, Δ_1 and Δ_3.]

Salinity:

Since the same conditions hold for salinity and buoyancy transport at the centerline,

$$ {}^{\Delta}3_{1,k} = {}^{\Delta}3_{2,k} \qquad (5.41.6) $$

b. Shallow Water Case

Same as deep water case above.

3. Plume Inflow Boundary

a. Deep Water Case ($Z = Z_b$, $0 \le R \le R_b$;

(Refer to Figure 5.7)

Velocity:

$$ U_{j,1} = U(\xi, Z_b - \frac{1}{2} \Delta Z_1) \qquad (5.42.1) $$

Calculated by methods in Chapter 4.

$$ V_{j,1} = V(\xi, Z_b). \qquad (5.42.2) $$

Data function, or calculated by methods in Chapter 4.

Stream Function:

$$ \Psi_{j,1} = 1 + \sum_{\substack{n=2 \\ p=2}}^{j} V(n,1) \Delta\xi \sinh \xi_p \cosh \xi_p \cdot \qquad (5.42.3) $$

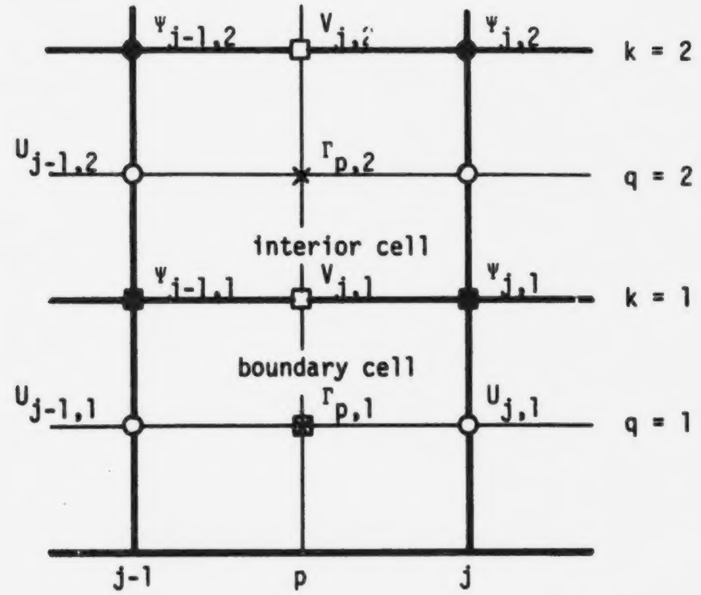

$\Psi_{j-1,2}$
$V_{j,2}$
$\Psi_{j,2}$
k = 2
$U_{j-1,2}$
$\Gamma_{p,2}$
q = 2
interior cell
$\Psi_{j-1,1}$
$V_{j,1}$
$\Psi_{j,1}$
k = 1
boundary cell
$U_{j-1,1}$
$\Gamma_{p,1}$
$U_{j,1}$
q = 1
j-1
p
j

Figure 5.7 Typical Inflow Boundary and Interior Cell (deep water case only).

[$\Gamma_{p,q}$ indicates any of the cell centered quantities Ω, Δ_1 and Δ_3.]

Vorticity:

Vorticity at the inflow boundary, $\Omega_{p,b}$ is calculated from,

$$\Omega_{p,b} = \frac{1}{2}\left(\Omega_{p,2} + \Omega_{p,1}\right) = \left(\frac{\partial U}{\partial Z} - \frac{\partial V}{\partial R}\right)\Big|_{b}$$

Hence,

$$\Omega_{p,1} = - \Omega_{p,2} + \frac{1}{\Delta Z_2}\left[U_{j,2}-U_{j,1} + U_{j-1,2}-U_{j-1,1}\right]$$

$$- \frac{1}{\Delta\xi\cosh\xi_p}\left[V_{j+1,1}-V_{j-1,1}\right]. \qquad (5.42.4)$$

Buoyancy:

$$\Delta_{1_{p,1}} = \Delta_1[(j-1/2)\Delta\xi,\ Z_b-1/2\ \Delta Z_1)]. \qquad (5.42.5)$$

Data, function, or calculated by methods in Chapter 4.

Salinity:

$$\Delta_{3_{p,1}} = \Delta_3[(j-1/2)\Delta\xi,\ Z_b-1/2\ \Delta Z_1)] \qquad (5.42.6)$$

Data, function, or calculated by methods in Chapter 4.

b. Shallow Water Case ($Z=Z_o$, $0\leq R\leq R_o$; Refer to Figure 5.8)

Velocity:

$$U_{j,KP} = 0 \qquad (5.43.1)$$

$$V_{j,KP} = V_o = \text{Constant; or, } V_{j,kp} = V(\xi,Z_b). \qquad (5.43.2)$$

Stream Function:

$$\Psi_{j,KP} = 1 + \Delta\xi\sum_{\substack{n=2\\p=2}}^{j} V(n,KP)\sinh\xi_p\cosh\xi_p \qquad (5.43.3)$$

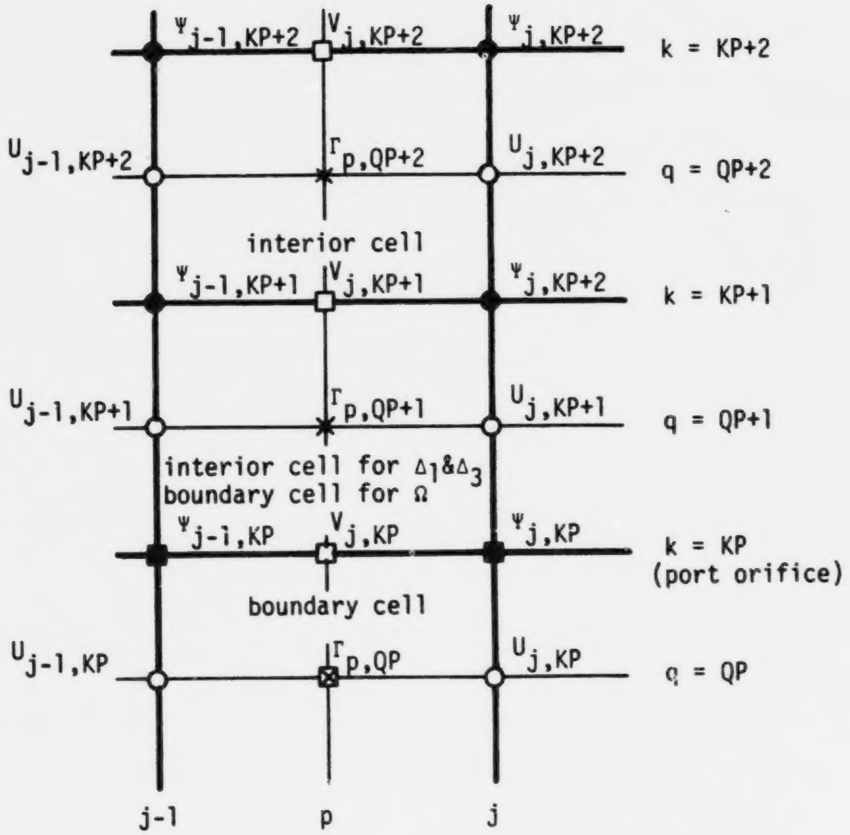

$\Psi_{j-1,KP+2}$
$V_{j,KP+2}$
$\Psi_{j,KP+2}$
k = KP+2
$U_{j-1,KP+2}$
$\Gamma_{p,QP+2}$
$U_{j,KP+2}$
q = QP+2
interior cell
$\Psi_{j-1,KP+1}$
$V_{j,KP+1}$
$\Psi_{j,KP+2}$
k = KP+1
$U_{j-1,KP+1}$
$\Gamma_{p,QP+1}$
$U_{j,KP+1}$
q = QP+1
interior cell for Δ_1&Δ_3
boundary cell for Ω
$\Psi_{j-1,KP}$
$V_{j,KP}$
$\Psi_{j,KP}$
k = KP
(port orifice)
boundary cell
$U_{j-1,KP}$
$\Gamma_{p,QP}$
$U_{j,KP}$
q = QP
j-1
p
j

Figure 5.8 Typical Inflow Boundary and Interior Cell (shallow water case only).
[$\Gamma_{p,q}$ indicates cell centered quantities Ω, Δ_1 and Δ_3.]

Vorticity:

Since in one case, $V_{j,1} = V_0$ is assumed constant over the port radius, we choose to evaluate vorticity at QP+1 , instead of at the port orifice. $\Omega_{p,QP+1}$ will then become the boundary value. Convenience is the primary reason for doing this, because to remain consistent with V_0 = constant, $\Omega_{j,QP}$ is impossible to define correctly at the port edge. This procedure is also helpful in using power law profiles for $V(\xi, Z_b)$ (see Chapter 7). Vorticity at a point (p,k) is given by

$$\Omega_{p,k} = \frac{1}{2}(\Omega_{p,q+1} + \Omega_{p,q}) \quad .$$

Hence,

$$\Omega_{p,q} = -\Omega_{p,q+1} + 2\,\Omega_{p,k}$$

at q = QP + 1,

$$\Omega_{p,QP+1} = -\Omega_{p,QP+2} + \frac{1}{\Delta Z_{KP+1}}[U_{j,KP+2} + U_{j-1,KP+2} - U_{j,KP+1} - U_{j-1,KP+1}] - \frac{1}{\Delta\xi\cosh\xi_p}[V_{j+1,KP+1} - V_{j-1,KP+1}] \qquad (5.43.4)$$

Buoyancy:

$$\Delta_{1_{p,QP}} = \text{Constant} = \Delta_{1_0} \qquad (5.43.5)$$

Salinity:

$$\Delta_{3_{p,QP}} = \text{Constant} = \Delta_{3_0} \qquad (5.43.6)$$

4. Port Vertical Side

a. Deep Water Case - Not applicable

b. Shallow water case ($R = R_o$, $0 \leq Z \leq Z_o$; Refer to Figure 5.9)

Velocity:

$$U_{NP,k} = 0 \tag{5.44.1}$$

$$V_{NP,k} = - V_{NP+1,k} \text{ (No-slip condition).} \tag{5.44.2}$$

Stream Function:

$$\Psi_{NP,k} = 1 + \Delta\xi \sum_{\substack{n=2 \\ p=2}}^{NP} V(n,KP) \sinh \xi_p \cosh \xi_p. \tag{5.44.3}$$

Although the exact value of $\Psi_{NP,k} = 1 + \frac{1}{2} R_o{}^2 V_o$, the difference approximation will lead to a slight deviation.

Vorticity:

$$\Omega_{NP,q} = \frac{1}{2} (\Omega_{MP+1,q} + \Omega_{MP,q}).$$

Hence,

$$\Omega_{MP,q} = - \Omega_{MP+1,q} - \frac{2}{\Delta\xi \cosh \xi_{MP}} (V_{NP+1,k} + V_{NP+1,k-1}). \tag{5.44.4}$$

Buoyancy:

$$\Delta_{1_{MP,q}} = \Delta_{1_{MP+1,q}} \text{ (Adiabatic condition)} \tag{5.44.5}$$

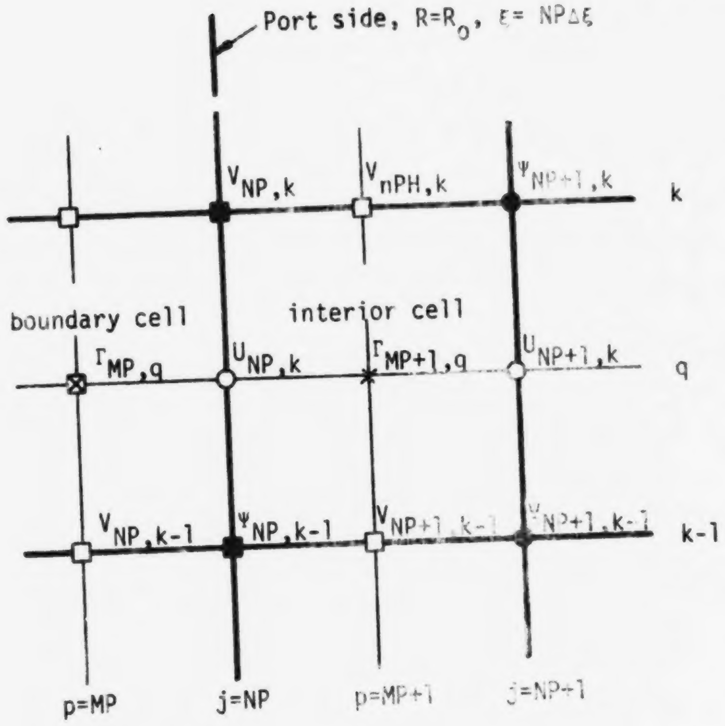
Port side, R=R$_o$, ξ= NPΔξ
V$_{NP,k}$
V$_{nPH,k}$
Ψ$_{NP+1,k}$
k
boundary cell
interior cell
Γ$_{MP,q}$
U$_{NP,k}$
Γ$_{MP+1,q}$
U$_{NP+1,k}$
q
V$_{NP,k-1}$
Ψ$_{NP,k-1}$
V$_{NP+1,k-1}$
Ψ$_{NP+1,k-1}$
k-1
p=MP
j=NP
p=MP+1
j=NP+1

Figure 5.9 Typical Vertical Port Side Boundary and Interior Cell (shallow water case only).

[$\Gamma_{p,q}$ indicates cell centered quantities Ω, Δ_1 and Δ_3.]

Salinity:

$$\Delta_{3_{MP,q}} = \Delta_{3_{MP+1,q}} \qquad (5.44.6)$$

5. Bottom Boundary

a. Deep Water Case ($R_b \leq R \leq R_\infty$, $Z = Z_b$; Refer to Figure 5.10)

Velocity:

$$U_{j,1} = U_{j,2} \text{ (free-slip condition)} \qquad (5.45.1)$$

$$V_{j,1} = 0 \text{ (level stream line condition)} \qquad (5.45.2)$$

Stream Function:

$$\Psi_{j,1} = 1 + \Delta\xi \sum_{\substack{n=2 \\ p=2}}^{NB} V(n,1) \sinh \xi_p \cosh \xi_p, \qquad (5.45.3)$$

where NB is the number of inflow cells to the nominal plume boundary.

Vorticity:

$$\Omega_{p,1} = - \Omega_{p,2} \text{ (free-slip condition)} \qquad (5.45.4)$$

Buoyancy:

$$\Delta_{1_{p,1}} = \Delta_{1_{p,2}} \qquad (5.45.5)$$

Salinity:

$$\Delta_{3_{p,1}} = \Delta_{3_{p,2}} \qquad (5.45.6)$$

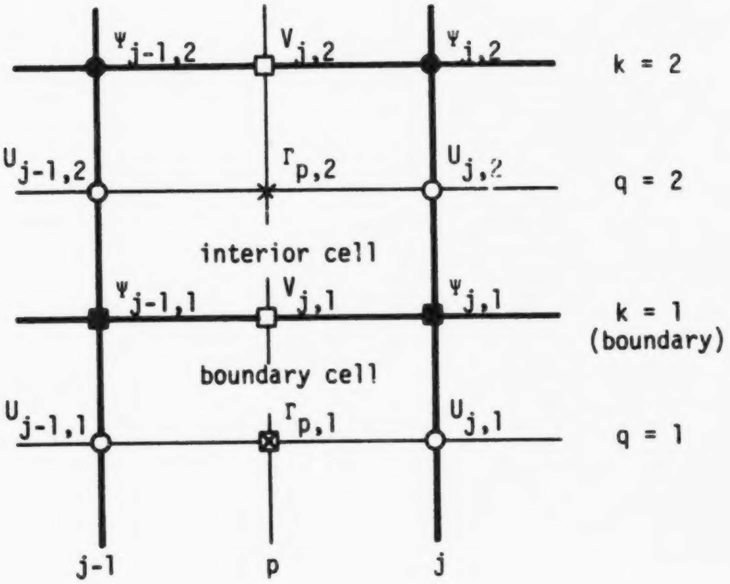
$\Psi_{j-1,2}$
$V_{j,2}$
$\Psi_{j,2}$
k = 2
$U_{j-1,2}$
$\Gamma_{p,2}$
$U_{j,2}$
q = 2
interior cell
$\Psi_{j-1,1}$
$V_{j,1}$
$\Psi_{j,1}$
k = 1
(boundary)
boundary cell
$U_{j-1,1}$
$\Gamma_{p,1}$
$U_{j,1}$
q = 1
j-1
p
j

Figure 5.10 Typical Bottom Boundary and Boundary Cell [$\Gamma_{p,q}$ indicates cell centered quantities Ω, Δ_1 and Δ_3.]

b. Shallow Water Case ($R_o \leq R \leq R_\infty$, $Z = Z_b = 0$;

Refer to Figure 5.10)

Velocity:

$U_{j,1} = - U_{j,2}$ (No-slip condition) (5.46.1)

$V_{j,1} = 0$ (5.46.2)

Stream Function:

$\Psi_{j,1} = 1 + \frac{1}{2} R_o^2 V_o$ (5.46.3)

Vorticity:

$\Omega_{p,1} = - \Omega_{p,2} + \frac{2}{\Delta Z_2} (U_{j,2} + U_{j-1,2})$, (No-slip Condition) (5.46.4)

Buoyancy:

$\Delta_{1_{p,1}} = \Delta_{1_{p,2}}$ (Adiabatic condition) (5.46.5)

Salinity:

$\Delta_{3_{p,1}} = \Delta_{3_{p,2}}$ (5.46.6)

6. Inflow-Outflow Boundary

a. Deep Water Case ($R = R_\infty$, $Z_b \leq Z \leq Z_h$; Refer to Figure 5.11)

$j = NJ$, $p = Np$

Velocity:

$U_{NJ,k} = - \frac{1}{\sinh \varepsilon_{NJ} \Delta Z_k} (\Psi_{NJ,k} - \Psi_{NJ,k-1})$ (5.47.1)

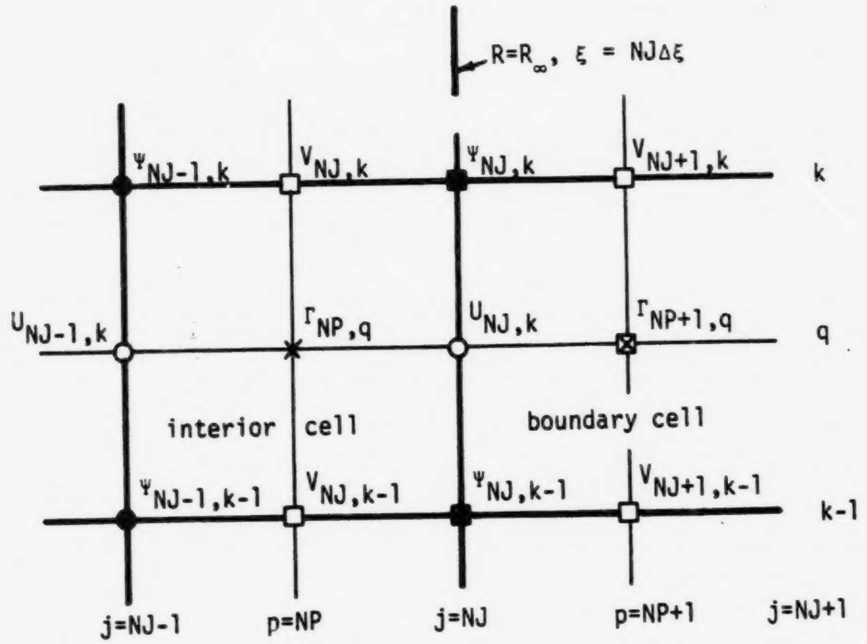
R=R$_\infty$, ξ = NJΔξ
$\Psi_{NJ-1,k}$
$V_{NJ,k}$
$\Psi_{NJ,k}$
$V_{NJ+1,k}$
k
$U_{NJ-1,k}$
$\Gamma_{NP,q}$
$U_{NJ,k}$
$\Gamma_{NP+1,q}$
q
interior cell
boundary cell
$\Psi_{NJ-1,k-1}$
$V_{NJ,k-1}$
$\Psi_{NJ,k-1}$
$V_{NJ+1,k-1}$
k-1
j=NJ-1
p=NP
j=NJ
p=NP+1
j=NJ+1

Figure 5.11 Typical Inflow-Outflow Boundary and Interior Cells
[$\Gamma_{p,q}$ indicates cell centered quantities Ω, Δ_1 and Δ_3.]

$$V_{NJ+1,k} = V_{NJ,k} \qquad (5.47.2)$$

Condition 5.47.2 results follow from the stream function condition given below.

Stream Function:

$$\Psi_{NJ,k} = \Psi_{NJ-1,k} \text{ (Level stream lines)} \qquad (5.47.3)$$

$$\Psi_{NJ,k} = 2\Psi_{NJ-1,k} - \Psi_{NJ-2,k} \text{ (No change of slope)} \qquad (5.74.4)$$

Vorticity:

Since $\frac{\partial V}{\partial R} = 0$ (Equation 5.47.3)

the vorticity, $\Omega_{NP+1,k}$ is given by

$$\Omega_{NP+1,q} = \left.\frac{\partial U}{\partial Z}\right|_{NJ,k}$$

$$\Omega_{NP+1,q} = \frac{1}{2\,\Delta Z_k}\left(\frac{\sinh \xi_{NJ}}{\sinh \xi_{NP+1}}\right)(U_{NJ,k+1} - U_{NJ,k-1}) \qquad (5.47.5)$$

Note that $(\partial U/\partial Z)_{NJ,k}$ has been replaced by a central difference form using even spacing of ΔZ. For the more general case of uneven ΔZ_k, refer to Appendix B .

Buoyancy:

$$\Delta_{1_{NP+1,q}} = \left(\frac{\rho_r - \rho_q}{\rho_r - \rho_o}\right)_{\text{Ambient}} \qquad (5.47.6)$$

Salinity:

$$\Delta_{3_{NP+1,q}} = \left(\frac{S_r - S_q}{S_r - S_o}\right)_{\text{Ambient}} \qquad (5.47.7)$$

6. Shallow Water Case

Same as above.

A number of assumptions and restrictions are involved with the above boundary values. For instance, the sea surface is restricted to remain flat, although visual observation indicates that a slight "boil" will occur at the plume centerline. At the bottom boundary of the deep water case, beyond R_b, it is assumed that there is neither a vertical component of mean velocity nor any change in the horizontal velocity profile. Additionally it is assumed that neither Δ_1 (nor Γ) is diffused across this boundary.

Transported quantities are assumed constant at $R = R_\infty$. Within the framework of the difference scheme, this is a perfectly valid assumption if convective terms, acting normal to this boundary, dominate the diffusion terms. Any quantity convected into the system is assumed to have the ambient value. Stream lines are assumed flat or having constant slope at this point and recirculation of flow out of the system is prohibited.

Many of the above assumptions are a result of ignorance with regard to processes outside the chosen system boundary. Since there is no way of regulating these processes, assumptions based on physical insight are the only viable alternative. Fortunately, the more nebulous assumptions occur at points far removed (at $R = R_\infty$ and bottom boundary) from the region of prime interest. And there is some recourse, in that numerical experiments are possible which give insight to the importance and effect of these assumptions. Results given in Chapter 7 reveal that the boundary specifications at R_∞ have little influence on the numerical solution as long as R_∞ is a reasonable distance from the port (approximately two plume diameters).

5.9 Rectangular Coordinates

The previous sections have dealt exclusively with (R,Z) coordinates or transformed, (ξ,Z) coordinates. In this section we treat the governing differential and difference equations in rectangular (X,Z) coordinates.

Detailed derivation of these forms are omitted; only the results are presented. In contrast to previous considerations neither transformed coordinates or unequal grid spacing will be considered.

The physical problem which we wish to analyze is a two-dimensional line plume that forms over a multiport diffuser line. This condition is approximately realized once the flows from a series of single round ports spread and interfere with one another parallel to the diffuser line. In dealing with the single round port, we were restricted to stagnant environment because any cross-current would destroy the problem symmetry and require a three-dimensional analysis. In the line plume case we may consider environmental velocity components which fall in the (X,Z) plane. Figure 5.12 illustrates the physical system for the line plume considered here.

5.9.1 Governing Differential Equations

Differential equations for the X,Z coordinate system comparable to Equations (5.10), (5.11), (5.12), (5.13), and (5.14) given in

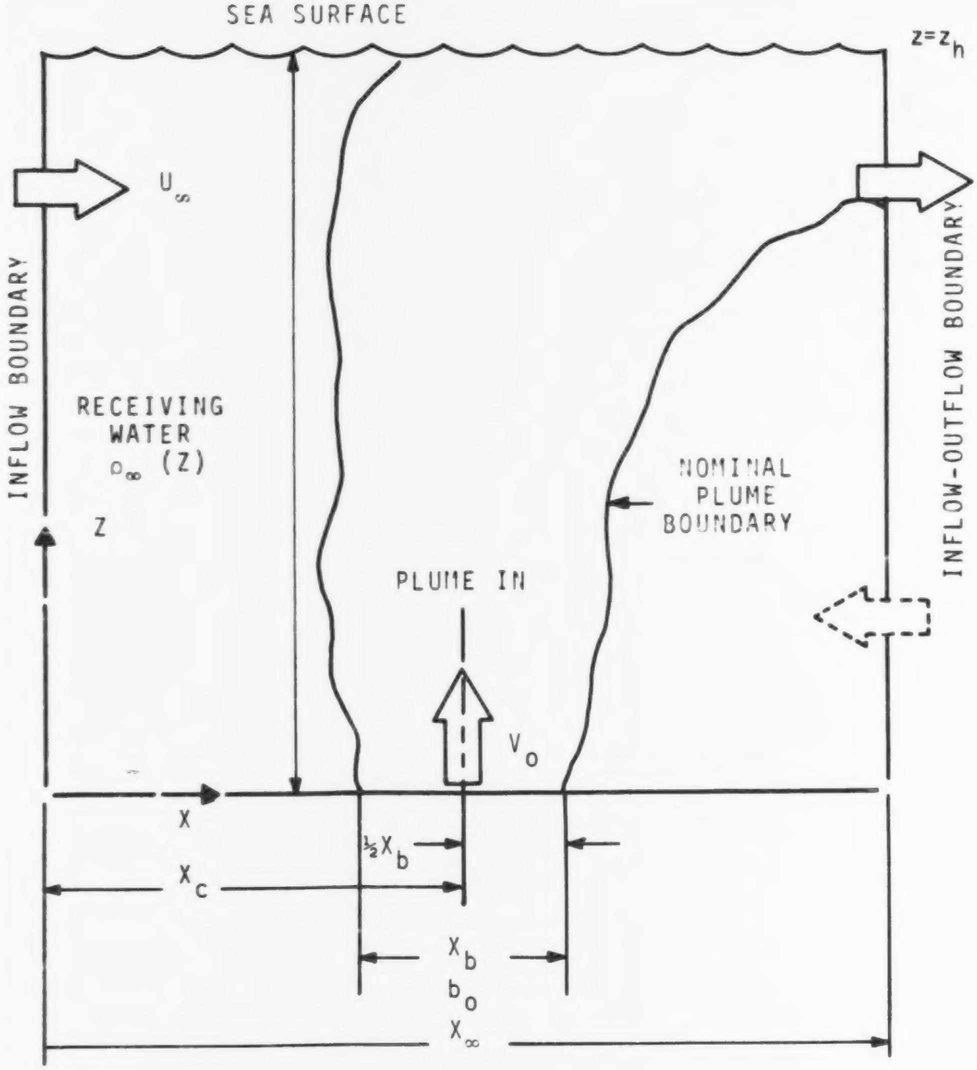
SEA SURFACE
$z=z_h$
U_∞
INFLOW BOUNDARY
RECEIVING WATER
$\rho_\infty(Z)$
Z
NOMINAL PLUME BOUNDARY
INFLOW-OUTFLOW BOUNDARY
PLUME IN
V_o
X
$\frac{1}{2}X_b$
X_c
X_b
b_o
X_∞

Figure 5.12 Physical System for Line Plume Issuing to Flowing Receiving Water

Section 5.4 are:

Stream Function:

$$\frac{\partial^2 \Psi}{\partial X^2} + \frac{\partial^2 \Psi}{\partial Z^2} = - \Omega . \tag{5.48}$$

Vorticity:

$$\frac{\partial}{\partial X} (U\Omega) + \frac{\partial}{\partial Z} (V\Omega) = - \frac{1}{F_o} \frac{\partial \Delta_1}{\partial X} + \frac{1}{RE_x} \frac{\partial^2 \Omega}{\partial X^2} + \frac{1}{RE_z} \frac{\partial^2 \Omega}{\partial Z^2} \tag{5.49}$$

Buoyancy Parameter:

$$\frac{\partial}{\partial X} (U\Delta_1) + \frac{\partial}{\partial Z} (V\Delta_1) = \frac{1}{RE_x PR_x} \frac{\partial^2 \Delta_1}{\partial X^2} + \frac{1}{RE_z PR_z} \frac{\partial^2 \Delta_1}{\partial Z^2} \tag{5.50}$$

Velocity:

$$U = - \frac{\partial \Psi}{\partial Z} \tag{5.51}$$

$$V = \frac{\partial \Psi}{\partial X} \tag{5.52}$$

In the above set of equations,

$X = x/b_o$

$Z = z/b_o$

$U = u/v_o$

$V = v/v_o$

$\Psi = \psi/(b_o v_o)$

$$\Omega = \omega/(v_o/b_o) \ ,$$

where v_o and b_o are reference plume velocity and width, respectively.

Dimensionless parameters are:

$$RE_x = \frac{v_o b_o}{\varepsilon_x}$$

$$RE_z = \frac{v_o b_o}{\varepsilon_z}$$

$$PR_x = \frac{\varepsilon_x}{k_x}$$

$$PR_z = \frac{\varepsilon_z}{k_z}$$

$$F_o = \frac{v_o^2}{\left(\frac{\rho_r - \rho_o}{\rho_o}\right) g b_o}$$

defined as in Section 5.4, keeping in mind that the radial direction is simply the "X" direction in this section.

5.9.2 Rectangular Difference Equations

Rectangular difference equations are formulated on a grid identical to that illustrated in Figures 5.3 and 5.4 with the corresponding change from the ξ coordinate to the X coordinate.

Here we consider only a regular grid, which has spacing ΔX and ΔZ. Difference equations are given below.

Stream Function:

$$\Psi_{j,k} = \frac{\Psi_{j-1,k} + \Psi_{j+1,k}}{2\left(\frac{1}{\Delta X^2} + \frac{1}{\Delta Z^2}\right)\Delta X^2} + \frac{\Psi_{j,k-1} + \Psi_{j,k+1}}{2\left(\frac{1}{\Delta X^2} + \frac{1}{\Delta Z^2}\right)\Delta Z^2}$$

$$+ \frac{\bar{\Omega}_{j,k}}{2\left(\frac{1}{\Delta X^2} + \frac{1}{\Delta Z^2}\right)} \tag{5.55}$$

Vorticity, $\bar{\Omega}_{j,k}$, is the average value for the four surrounding cells (see Figure 5.4) and given as

$$\bar{\Omega}_{j,k} = \frac{1}{4}\left(\Omega_{p,q} + \Omega_{p,q+1} + \Omega_{p+1,q} + \Omega_{p+1,q+1}\right) \tag{5.56}$$

Velocity is calculated by

$$U_{j,k} = -\frac{1}{\Delta Z}\left(\Psi_{j,k} - \Psi_{j,k-1}\right) \tag{5.57}$$

$$V_{j,k} = \frac{1}{\Delta X}\left(\Psi_{j,k} - \Psi_{j-1,k}\right) \tag{5.58}$$

and vorticity by

$$\begin{aligned} &\left[\frac{1}{2\Delta X}\left(|U_{j,k}| + U_{j,k} + |U_{j-1,k}| - U_{j-1,k}\right)\right. \\ &+ \frac{1}{2\Delta Z}\left(|V_{j,k}| + V_{j,k} + |V_{j,k-1}| - V_{j,k-1}\right) \\ &+ \left.\frac{2}{RE_x \Delta X^2} + \frac{2}{RE_z \Delta Z^2}\right] \Omega_{p,q} \quad = \\ &= \left[\frac{1}{2\Delta X}\left(|U_{j-1,k}| + U_{j-1,k}\right) + \frac{1}{RE_x \Delta X^2}\right] \Omega_{p-1,q} \end{aligned}$$

$$+\left[\frac{1}{2\Delta X}\left(|U_{j,k}| - U_{j,k}\right) + \frac{1}{RE_x\Delta X^2}\right]\Omega_{p+1,q}$$

$$+\left[\frac{1}{2\Delta Z}\left(|V_{j,k-1}| + V_{j,k-1}\right) + \frac{1}{RE_z\Delta Z^2}\right]\Omega_{p,q-1}$$

$$+\left[\frac{1}{2\Delta Z}\left(|V_{j,k}| - V_{j,k}\right) + \frac{1}{RE_z\Delta Z^2}\right]\Omega_{p,q+1}$$

$$-\ \frac{1}{2F_o\Delta X}\left(\Delta 1_{p+1,q} - \Delta 1_{p-1,q}\right). \tag{5.59}$$

The buoyancy parameter, Δ_1, is calculated by,

$$\left[\frac{1}{2\Delta X}\left(|U_{j,k}| + U_{j,k} + |U_{j-1,k}| - U_{j-1,k}\right)\right.$$

$$+\ \frac{1}{2\Delta Z}\left(|V_{j,k}| + V_{j,k} + |V_{j,k-1}| - V_{j,k-1}\right)$$

$$\left. +\ \frac{2}{RE_x PR_x\Delta X^2} + \frac{2}{RE_z PR_z\Delta Z^2}\right]\Delta 1_{p,q}$$

$$= \left[\frac{1}{2\Delta X}\left(|U_{j-1,k}| + U_{j-1,k}\right) + \frac{1}{RE_x PR_x\Delta X^2}\right]\Delta 1_{p-1,q}$$

$$+\left[\frac{1}{2\Delta X}\left(|U_{j,k}| + U_{j,k}\right) + \frac{1}{RE_x PR_x\Delta X^2}\right]\Delta 1_{p+1,q}$$

$$+\left[\frac{1}{2\Delta Z}\left(|V_{j,k-1}| + V_{j,k-1}\right) + \frac{1}{RE_z PR_z\Delta Z^2}\right]\Delta 1_{p,q-1}$$

$$+\left[\frac{1}{2\Delta Z}\left(|V_{j,k}| - V_{j,k}\right) + \frac{1}{RE_z PR_z\Delta Z^2}\right]\Delta 1_{p,q+1} \tag{5.60}$$

The salinity or Δ_3 transport equation is given exactly by Equation (5.60) with PR replaced by SC, the eddy Schmidt number.

5.9.3 Rectangular Boundary Conditions

Boundary conditions for the rectangular problem are substantially the same as in the axisymmetric problem. Notable differences are provision for crossflow and lack of problem symmetry.

Referring to Figure 5.12 boundary conditions are as follows:

1. Sea surface ($0 \leq X \leq X_\infty$, $Z = Z_h$)

$$\Psi = \text{constant} = \Psi_1$$

$$\Omega = 0 \text{ (free slip condition)}$$

$$\frac{\partial \Delta_1}{\partial Z} = 0 \text{ (adiabatic condition)}$$

$$\frac{\partial \Delta_3}{\partial Z} = 0$$

2. Inflow boundary ($X = 0$, $Z_b \leq Z \leq Z_h$)

$$\Psi = \Psi_1 - \int_{Z_h}^{Z} U_\infty(Z)\, dZ$$

$$\Omega = \frac{\partial U_\infty}{\partial Z}$$

$$\Delta_1 = \frac{\rho_r - \rho_\infty}{\rho_r - \rho_o}$$

$$\Delta_3 = \frac{S_r - S_\infty}{S_r - S_o}$$

3. Bottom boundary $(0 \leq X \leq X_c - \frac{1}{2} X_b, \ Z = Z_b)$

$$\Psi = \Psi_1 - \int_{Z_h}^{Z_b} U_\infty (Z) \, dZ = \text{constant} = \Psi_2$$

$$\Omega = 0 \text{ (free slip condition)}$$

$$\frac{\partial \Delta_1}{\partial Z} = 0$$

$$\frac{\partial \Delta_3}{\partial Z} = 0$$

4. Plume inflow boundary $(X_c - \frac{1}{2} X_b \leq X \leq X_c + \frac{1}{2} X_b, \ Z = Z_b)$

Assume that V, Δ_1 and Δ_3 are known from data or empirical relationships.

$$\Psi = \Psi_2 + \int_{X_c - \frac{1}{2} X_b}^{X} V_b dX$$

$$\Omega = \frac{\partial U}{\partial Z} - \frac{\partial V}{\partial X}$$

5. Bottom boundary $(X_c + \frac{1}{2} X_b < X \leq X_\infty, \ Z = Z_b)$

$$\Psi = \Psi_2 + \int_{X_c - \frac{1}{2} X_b}^{X_c + \frac{1}{2} X_b} dX = \text{constant} = \Psi_3$$

$$\Omega = 0 \text{ (free slip condition)}$$

$$\frac{\partial \Delta_1}{\partial Z} = 0$$

$$\frac{\partial \Delta_3}{\partial Z} = 0$$

6. Inflow-outflow boundary ($X=X_\infty$, $Z_b \le Z \le Z_h$)

$$\frac{\partial \Psi}{\partial X} = 0$$

$$\Omega = \frac{\partial U}{\partial Z}$$

$$\Delta_1 = \frac{\rho_r - \rho_\infty}{\rho_r - \rho_o}$$

$$\Delta_3 = \frac{S_r - S_\infty}{S_r - S_o}$$

CHAPTER 6

CODE DESCRIPTION AND ORGANIZATION

The computer program described herein obtains the solution of the transformed difference Equations (5.21), (5.23), (5.24), (5.28), and (5.30) for the quantities Ψ, U, V, Ω, and Δ_1, (or Γ), respectively. Through input option one may also obtain these solutions in ordinary radial coordinates (see summary Section 5.7.3). A program which obtains the solutions through the use of the density disparity parameter Δ_2 (as opposed to Δ_1) has been used but is not presented in this manuscript.

The program consists of 20 subroutines and/or functions which in part are managed by an executive routine called "SYMJET". Initially, the code was set up for the Oregon State University CDC 3300 time sharing system. This system, although extremely handy for program development, is too small in terms of available core and too slow for economically treating large problems. The code version presented here is adapted to the Computer Science Corporation Univac 1108 located in Richland, Washington. This version of the code has also been successfully executed on the Control Data Corporation 6600 located in Palo Alto, California, and on the CDC 6400 system at the Battelle Memorial Institute in Columbus, Ohio.

6.1 Computational Procedure

The primary task at hand involves the simultaneous solution of one elliptic partial differential equation for the stream function, Ψ, (Equation 5.21) and two parabolic transport equations for the vorticity, Ω, and the buoyancy, Δ_1, [Equations (5.28) and (5.30), respectively]. Equations for U and V (5.23 and 5.24, respectively) may be considered as auxiliary, but are, nevertheless, essential and need to be solved along with (5.21), (5.28), and (5.30) during iteration. In the case of neutral buoyancy, only Equations (5.21) and (5.28) need to be solved simultaneously.

The iterative procedure is built about the equations for Ψ, Ω, and Δ_1. The technique used in the Gauss-Seidel method for all quantities defined by second order partial differential equations. Liebmann acceleration is employed with the alternatives of both under and over relaxation. Assuming all boundary conditions are set and pertinent variables are initialized, the procedure is as follows:

1. Compute $\Delta_{1p,q}$ and $\Gamma_{p,q}$ using Equation (5.30) based on previously calculated values of $U_{j,k}$,$V_{j,k}$ and appropriate transport coefficients.
2. Compute $\Omega_{p,q}$ using Equation (5.28) and the previously computed values of $U_{j,k}$,$V_{j,k}$, $\Delta_{1p,q}$ and appropriate transport coefficients.
3. Update necessary boundary values for Δ_1, Γ, and Ω.
4. Use the newly computed values of Ω to compute the stream function distribution from Equation (5.21). One or more iterations may be required to arrive at a satisfactory solution for Ψ. Compute a new velocity field $V_{j,k}$ and $U_{j,k}$ from the newly calculated Ψ distribution.

5. If the eddy transport terms are not constant, compute multipliers FR and FZ from new velocity field (for definition of the FR and FZ multiplier, see Chapter 7).
6. Repeat Steps 1 through 5 until a preset convergence criterion is satisfied or a specific number of iterations has been completed.

6.2 Executive Program and Subroutine Description

As mentioned previously, the computer code consists of an executive routine called "SYMJET" and 20 subroutines and/or functions. The following discussion relates the primary duties served by each of these routines.

SYMJET

Executive routine

1. Reads case header and integer case set-up information.
2. Reads alphanumeric data for line printer output array option, plot tape options, isoline interpolation options, and program control.
3. Calls subroutines for data input, problem set-up and initialization, and problem execution. The subroutines called are (in the calling sequence):
    - INPUT
    - READY
    - PLABAK
    - STREAM (for inviscid flow solution)
    - SSCOMP

- INTERP

4. Performs other miscellaneous tasks such as clock initialization, tape rewind, presetting variables, etc.

SUBROUTINE INPUT

General data input routine

1. Reads restart tape if required.
2. Reads remaining input data from cards.
3. Converts portions of input data to appropriate quantities and units (e.g., temperature data to density data).

Subroutine is called once during execution.

SUBROUTINE READY

Problem set-up routine

1. Sets all computed constants.
2. Sets constant boundary conditions.
3. Presets turbulence multipliers.
4. Option to call SUBROUTINE SIMJET.
5. Option to call SUBROUTINE GAUSS.

Subroutine called once during execution.

SUBROUTINE PLABAK

General information and debug output

1. Writes to line printer various computed and input supplied variables and the operation modes of current case.
2. Writes to line printer constant arrays used in the difference equation computations.

Subroutine is called once or not at all at the user's option.

SUBROUTINE STREAM (IT, NSKIP)

Solves for stream function, Ψ

1. Computes the viscous or inviscid stream function (Equation 5.21) by Gauss-Siedel iteration. When called, this subroutine iterates on Ψ (PSI) "IT" times.
2. Upon completion of "IT" iterations the velocity components $U_{j,k}$ and $V_{j,k}$ are computed by the auxiliary Equations (5.23) and (5.24).

For an inviscid flow computation (the inviscid flow solution may be called for the purpose of initializing the viscous flow computation if desired) STREAM is called and returns control to the executive routine. When STREAM is called from SSCOMP, which computes the viscous flow field, control is then returned to SSCOMP. Subroutine STREAM constitutes what is referred to in this manuscript as the "inner iteration loop" (subroutine SSCOMP constitutes the "outer iteration loop") and is called at least once for each "outer iteration".

SUBROUTINE SSCOMP

Computes steady flow solution of all transport equation

1. Solves transport equations for
   - Δ_1
   - Γ and
   - Ω,

   using Gauss-Siedel iteration with Liebmann acceleration (deceleration).

2. Updates boundary values of ζ, Γ, and Ω.
3. Computes convergence rate information and the cell indices having the slowest convergence.
4. Calls subroutine STREAM to compute velocity field.
5. Calls subroutine EDDY to compute eddy transport multipliers as required.
6. Writes out monitor node values.
7. Calls subroutine OUTPUT for either interim or final array output.
8. Generates plot data tape.
9. Computes surface area above T_{amb} in 1 °C increments.
10. Performs a Gamma constituent balance error, $(\Gamma_{in}-\Gamma_{out})/\Gamma_{in}$, for the overall system and then returns control to the executive routine.

This subroutine is referred to as the "outer iteration loop" and is called but once during a case execution. The code spends the majority of the execution time in this routine.

SUBROUTINE EDDY (M)

Computes eddy transport multiplier FR and FZ

1. Computes potential core.
2. Computes plume half radius, $R_{1/2}$ and nominal plume boundary, $R_{.05}$, at each vertical grid point.
3. Computes FR from mixing length theory.

$$FR = V_{max} \cdot R_{1/2}$$

4. Computes FZ based on mixing length theory and incorporates Richardson number modification (computes point Richardson number, RI, and calls function RCHMOD for modifier).

If eddy multipliers are computed based on the velocity distribution, this subroutine is called once during each "outer iteration". Either FR, FZ or both may be computed selectively. (Parameter M in the call list specifies the option). Details of the particular eddy transport models used and regions of applicability are discussed in Chapter 7. Also, this subroutine may be bypassed a set number of iterations for computation stability purposes (discussed in Chapter 7).

SUBROUTINE OUTPUT (MODE)

Primary line printer output call routine

1. The primary purpose of this routine is to call selectively the output array writer subroutine, AROUT, based on the alpha input read in through the executive routine. The arrays and array header Holleriths are aligned in the call list of AROUT. This subroutine may be called selectively for array writing through the input Fortran variable NOUT. That is, every time that the "outer iteration" number is divided by NOUT and yields a whole number, the array writing routine is called. The parameter, MODE, is an output option.
2. The secondary purpose of subroutine OUTPUT is to write out selectively the convergence rate information computed in

subroutine SSCOMP, that is, maximum changes in Ψ, Δ_p and Ω and the nodal location of these changes, during successive iterations. The iteration numbers selected for output are specified by the input Fortran variable NTTY, in the exact manner that NOUT is used in 1. above.

SUBROUTINE AROUT (list)

General array writer

This subroutine is used to write out all computed arrays specified for printing. The appropriate array, header and grid coordinates are aligned in the call list at subroutine OUTPUT. Miscellaneous computations are also performed here as necessary. For instance, if normalized arrays are desired, these are normalized in AROUT and if temperature arrays are required the buoyancy parameter (Δ_1) array is converted to a temperature array through successive calls to function TEMP.

SUBROUTINE INTERP

Calling routine for isoline interpolation

The only job performed by this subroutine is selectively setting up arrays to be interpolated by the general interpolator routine, ISOGEN. Selection is made through input of the Fortran alpha array TERP during execution of the executive routine. The particular array, header and other appropriate data are aligned in the call list of ISOGEN. This subroutine is optionally called through the executive routine following execution of SSCOMP.

SUBROUTINE ISOGEN (list)

General isoline interpolator

The function of ISOGEN is to interpolate a given array, aligned in memory through the subroutine call list, for isolines whose values are selected at input and specified by the Fortran array, ISOLN. For a specific array (say the stream function array) the coordinates of an isoline (streamline) are quadratically interpolated and coordinates printed. Contouring may be accomplished by hand plotting the results. Automated plotting of the computed points would be quite difficult since the points are not ordered.[1]

SUBROUTINE GAUSS (N)

Optionally computes Gaussian distributions for inflow

This subroutine computes Gaussian boundary distributions for V, Δ_1, and Γ in either the zone of flow establishment or the zone of established flow. The particular option is determined by the parameter, N. These computations are based on the Albertson et al. [4] data and theoretical results given by Abraham [1]. The routine is called once from subroutine READY.

SUBROUTINE SIMJET (list)

This routine computes the centerline distributions of V, Δ_2 and Γ from the similarity solutions of a vertical plume given in Chapter 4. For the homogeneous problem, V is calculated from Equation (4.43) and Δ_2 from (4.4). In the case of stratification these quantities are computed from Equations (4.36), (4.37), and (4.38) using the fourth order Runge-Kutta technique. Results from this routine may be used for inflow boundary information in the more elaborate finite-difference method for the confined plume. Calling is through subroutine READY and is performed at most once.

---

[1] Automated contouring is accomplished using a special contouring routine.

FUNCTION SIGMAT (SAL, T, N)

Given the salinity, SAL, and temperature, T, this function computes Sigma-t (σ_t, see Section 3.6) based on algebraic equations given in the U.S. Navy Hydrographic publication number 615 [103] or as given in Hill [39].

FUNCTION TEMP (SALT, SIGMA)

Given the salinity, SALT, and the density in Sigma-t units, SIGMA, this function solves the equations referenced above for the temperature in degrees centigrade by the Newton-Raphson method. The function SIGMAT (SAL, T, N) is repeatedly called during the iteration process.

FUNCTION SANH (X, N)

Hyperbolic sine coordinate transformation function which yields Sinh (X) for N = 1 and X for N = 0 (linear radial coordinates, no transformation).

FUNCTION CASH (X, N)

Hyperbolic cosine transformation function which yields COSH (X) for N = 1, and 1.0 for N = 0.

FUNCTION RCHMOD (N, RICH)

Computes Richardson number (RICH) modification of the vertical eddy viscosity coefficient by one of five different models (option given by N). These models are given in Chapter 7 (cf. Table 7.5).

6.3 Flow Charts

Detailed flow charts of all subroutines in the SYMJET computer code would require an extensive amount of space. For this reason only the main subroutines and the executive program will be illustrated. The charting of these will also be somewhat abbreviated. A partial bibliography of the computer variables may be found in the program listing (Appendix E).

SYMJET FLOW CHART
(Executive Routine)

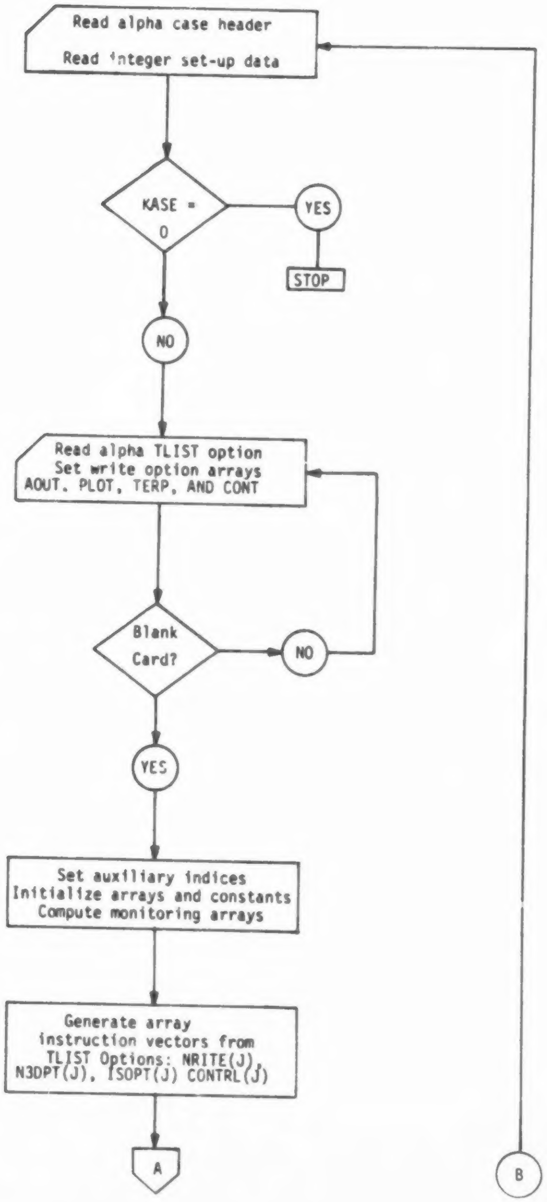
Read alpha case header
Read integer set-up data
KASE = 0
YES
STOP
NO
Read alpha TLIST option
Set write option arrays
AOUT, PLOT, TERP, AND CONT
Blank Card?
NO
YES
Set auxiliary indices
Initialize arrays and constants
Compute monitoring arrays
Generate array instruction vectors from TLIST Options: NRITE(J), N3DPT(J), ISOPT(J) CONTRL(J)
A
B

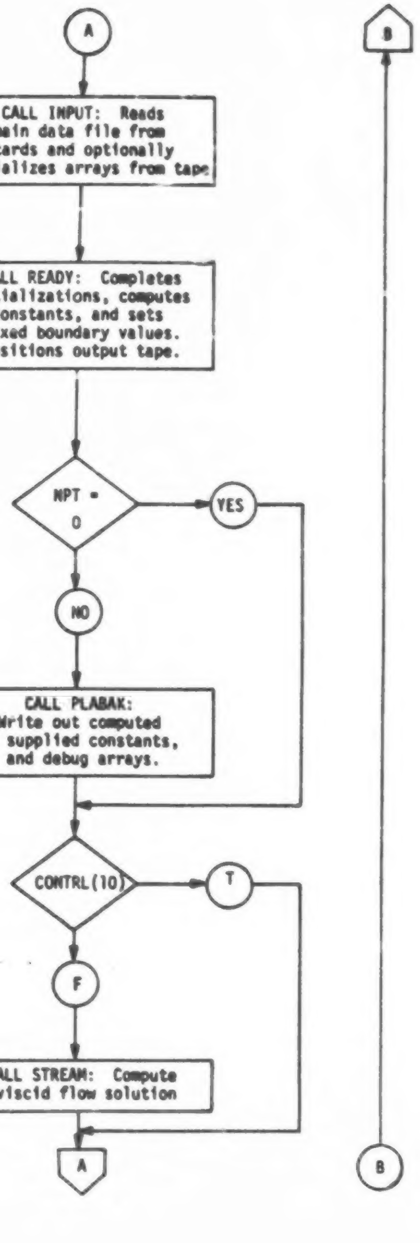
A
B
CALL INPUT: Reads main data file from cards and optionally initializes arrays from tape
CALL READY: Completes initializations, computes constants, and sets fixed boundary values. Positions output tape.
NPT = 0
YES
NO
CALL PLABAK: Write out computed and supplied constants, and debug arrays.
CONTRL(10)
T
F
CALL STREAM: Compute inviscid flow solution
A
B

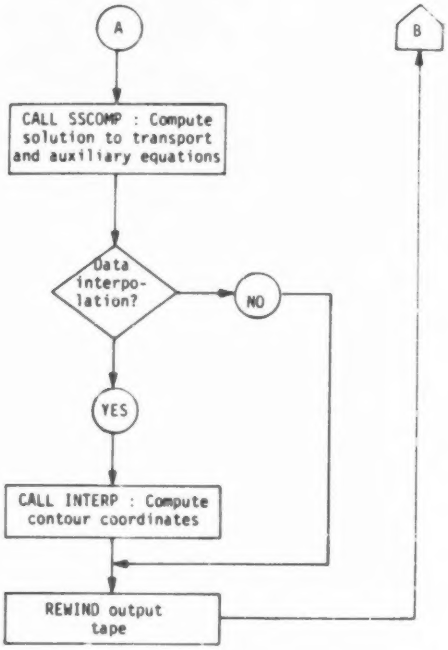
A
B
CALL SSCOMP : Compute solution to transport and auxiliary equations
Data interpolation?
NO
YES
CALL INTERP : Compute contour coordinates
REWIND output tape

SUBROUTINE INPUT FLOW CHART

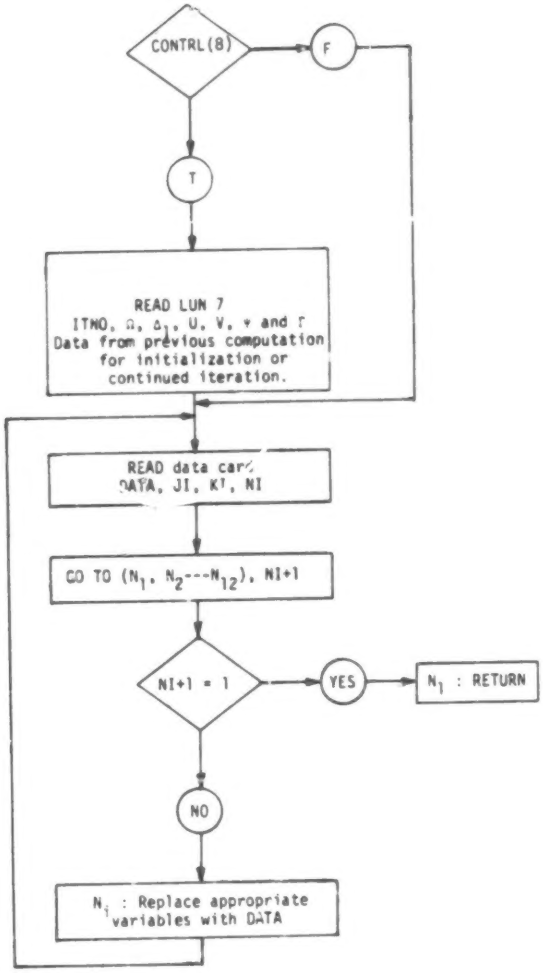
CONTRL(8)
F
T
READ LUN 7
ITNO, Ω, Δ_1, U, V, Ψ and Γ
Data from previous computation for initialization or continued iteration.
READ data card
DATA, JI, KI, NI
GO TO (N_1, N_2---N_{12}), NI+1
NI+1 = 1
YES
N_1 : RETURN
NO
N_i : Replace appropriate variables with DATA

SUBROUTINE READY FLOW CHART

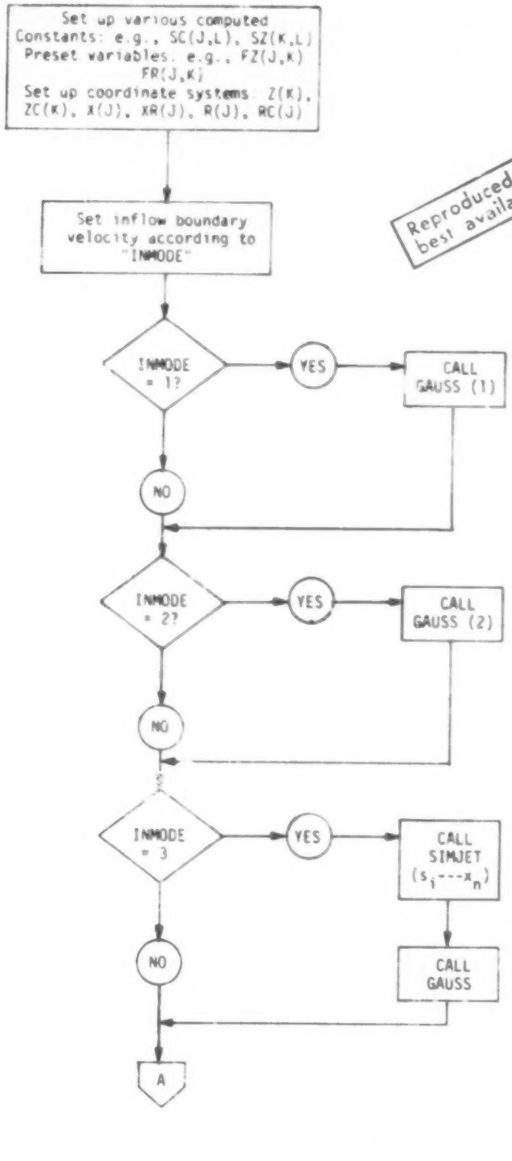
Set up various computed Constants: e.g., SC(J,L), SZ(K,L) Preset variables. e.g., FZ(J,K) FR(J,K) Set up coordinate systems. Z(K), ZC(K), X(J), XR(J), R(J), RC(J)
Set inflow boundary velocity according to "INMODE"
INMODE = 1?
YES
CALL GAUSS (1)
NO
INMODE = 2?
YES
CALL GAUSS (2)
NO
INMODE = 3
YES
CALL SIMJET (s_i---x_n)
CALL GAUSS
NO
A

Reproduced from best available copy.

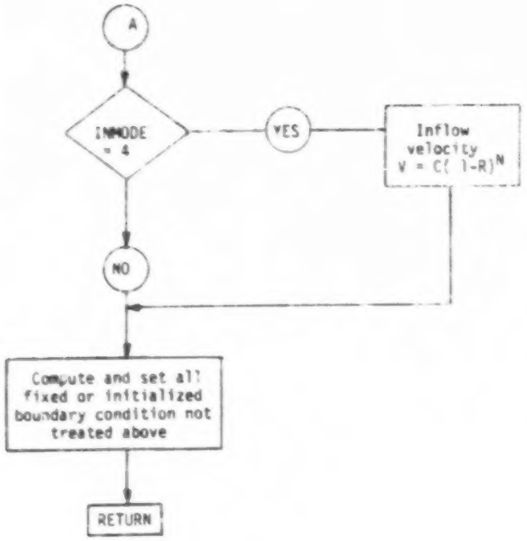
A
INMODE = 4
YES
Inflow velocity V = C(1-R)^N
NO
Compute and set all fixed or initialized boundary condition not treated above
RETURN

SUBROUTINE STREAM FLOW CHART

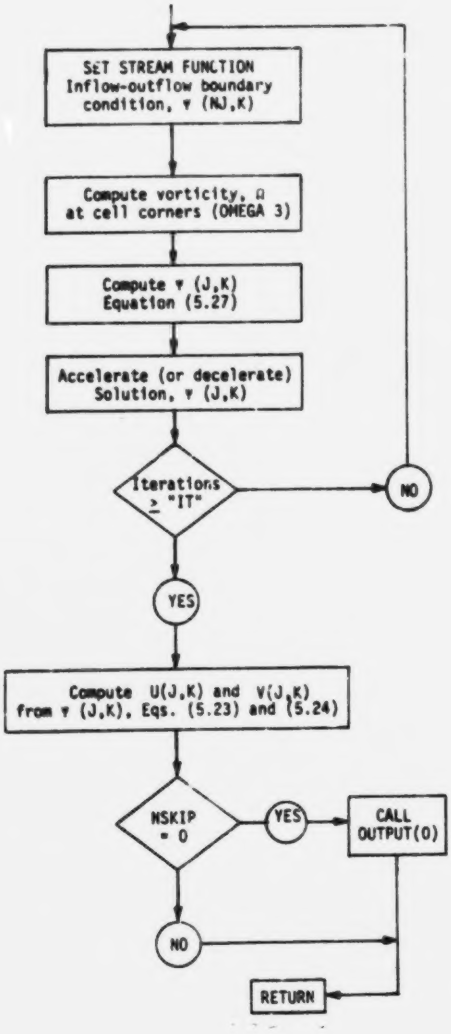
SET STREAM FUNCTION
Inflow-outflow boundary condition, ψ (NJ,K)
Compute vorticity, Ω at cell corners (OMEGA 3)
Compute ψ (J,K) Equation (5.27)
Accelerate (or decelerate) Solution, ψ (J,K)
Iterations ≥ "IT"
NO
YES
Compute U(J,K) and V(J,K) from ψ (J,K), Eqs. (5.23) and (5.24)
NSKIP = 0
YES
CALL OUTPUT(0)
NO
RETURN

SUBROUTINE SSCOMP FLOW CHART

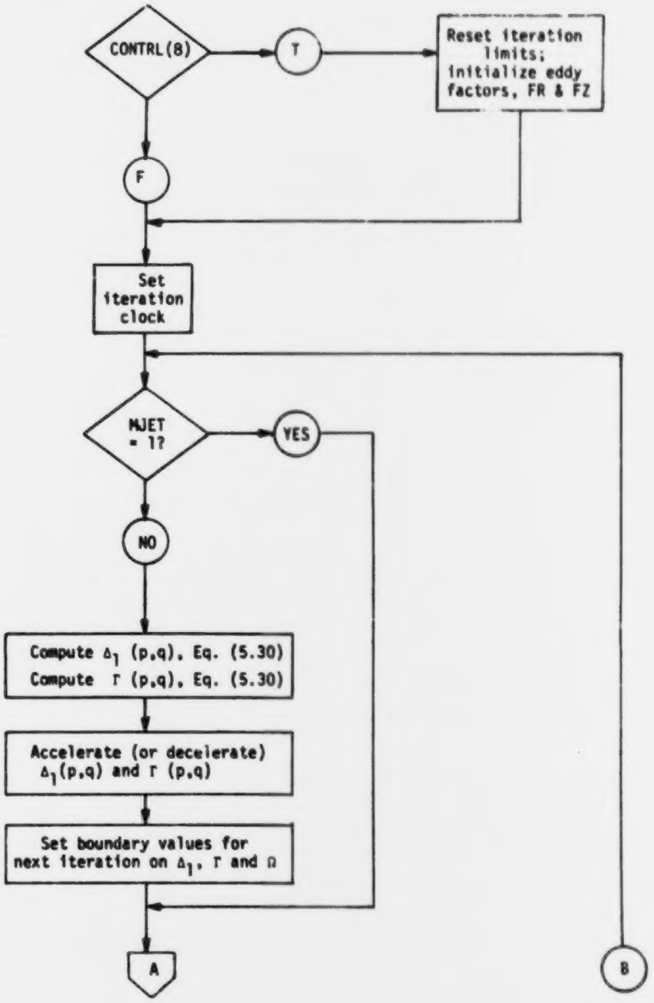
CONTRL(8)
T
Reset iteration limits; initialize eddy factors, FR & FZ
F
Set iteration clock
MJET = 1?
YES
NO
Compute Δ_1 (p,q), Eq. (5.30)
Compute Γ (p,q), Eq. (5.30)
Accelerate (or decelerate) Δ_1(p,q) and Γ (p,q)
Set boundary values for next iteration on Δ_1, Γ and Ω
A
B

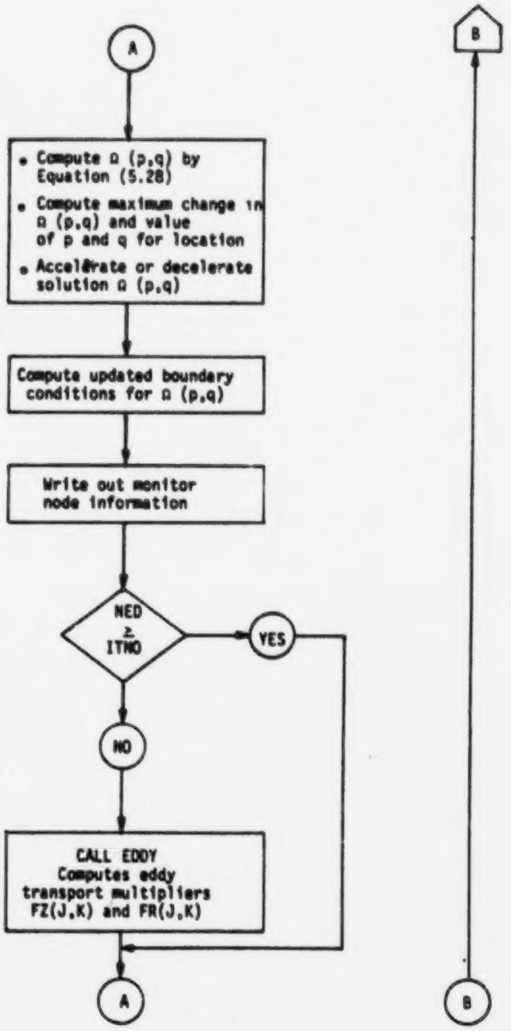
A
Compute Ω (p,q) by Equation (5.28)
Compute maximum change in Ω (p,q) and value of p and q for location
Accelerate or decelerate solution Ω (p,q)
Compute updated boundary conditions for Ω (p,q)
Write out monitor node information
NED ≥ ITNO
YES
NO
CALL EDDY
Computes eddy transport multipliers FZ(J,K) and FR(J,K)
A
B
B

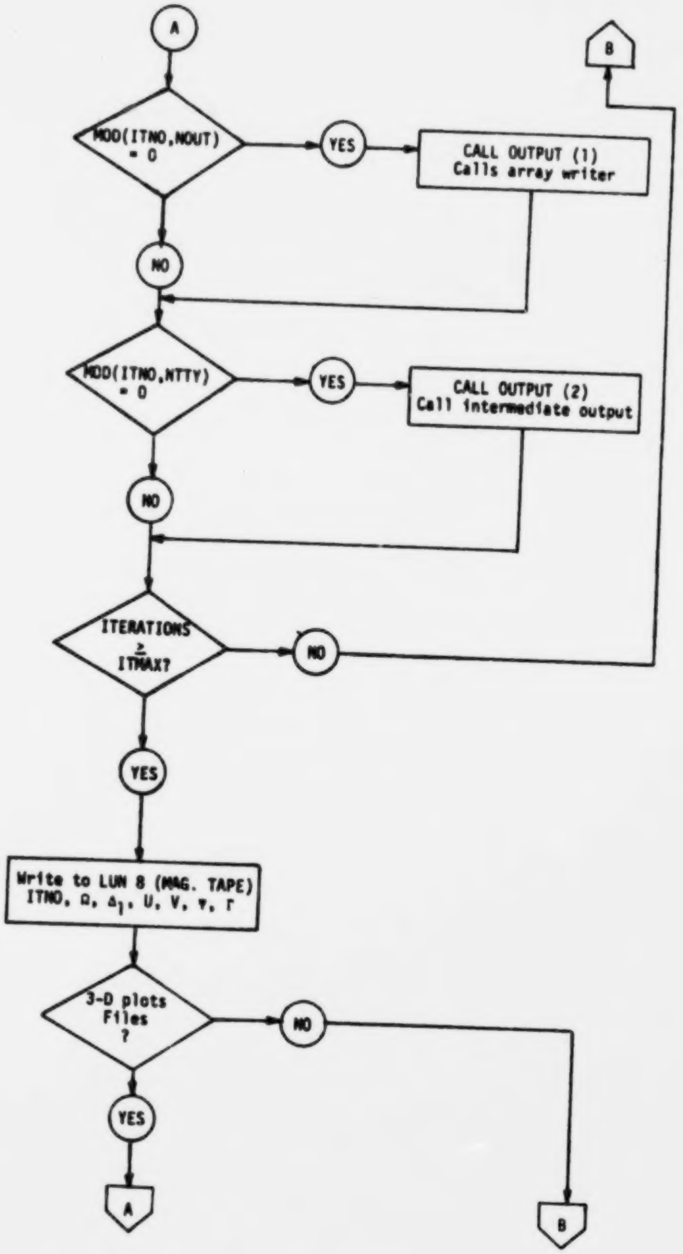
A
B
MOD(ITNO,NOUT) = 0
YES
CALL OUTPUT (1)
Calls array writer
NO
MOD(ITNO,NTTY) = 0
YES
CALL OUTPUT (2)
Call intermediate output
NO
ITERATIONS ≥ ITMAX?
NO
YES
Write to LUN 8 (MAG. TAPE)
ITNO, Ω, Δ_1, U, V, ψ, Γ
3-D plots Files ?
NO
YES
A
B

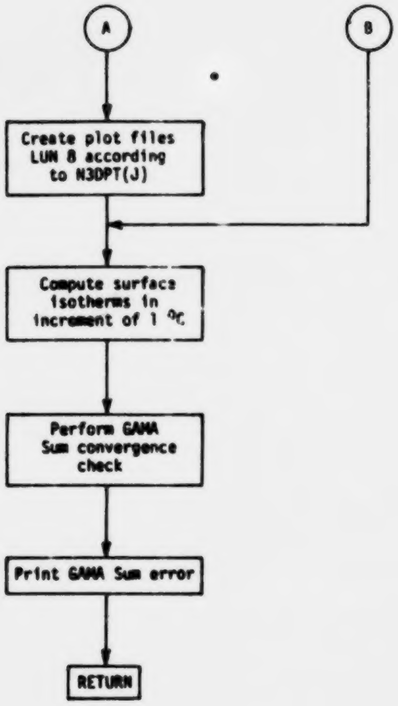
A
B
Create plot files LUN 8 according to N3DPT(J)
Compute surface isotherms in increment of 1 °C
Perform GAMA Sum convergence check
Print GAMA Sum error
RETURN

CHAPTER 7

CODE VERIFICATION AND NUMERICAL EXPERIMENTS

In this chapter we are concerned with verification of the numerical model. Ultimately, the program is to be used in describing the plume resulting from large vertical thermal outfalls in shallow water, and, as previously mentioned, published field data concerning velocity and temperature distributions along with other pertinent data needed for evaluation or verification are essentially non-existent for these cases. Even laboratory data from hydraulic models are scant and steady flow experiments to model quasi-steady oceanic conditions with stratification are essentially impossible.

Verification of the numerical techniques will be carried out by using the code described in Chapter 6 to simulate various problems which have been well studied, both experimentally and analytically, and for which much information has been published in the literature. One such problem which the code can easily handle is the deep water momentum jet. In this case much knowledge has been compiled concerning velocity distributions, concentrations, and turbulence parameters. The computer code can easily handle interacting buoyancy for the same geometry. Although there is a lesser amount of experimental data published in the open literature for buoyancy cases, especially on turbulent parameters, there is enough information for meaningful comparisons with the numerical model.

Once the computer program is verified using this published information, the program can be applied with confidence to conditions of more interest and practical value, such as shallow water and stratified ambient cases. Having checked the program against experimental results for simple cases, we know at least that the numerical procedures are working correctly, although auxiliary models (e.g., turbulence) may not be entirely correct.

Also presented in this chapter are some of the code operating experiences, turbulence modeling, solution convergence and stability, and discussion of some of the more troublesome boundary conditions.

7.1 Deep Water Plumes

By deep water plumes we are implying that the effluent is discharging into a semi-infinite water body, although as a practical matter computational boundaries must be finite. For program verification, we use the following deep water flow categories:

- Momentum Jet - the fluid motion is induced entirely by the effluent initial momentum. Buoyancy is also calculated but is decoupled from the momentum equation and may be used as a measure of concentration. This case is indicated by $F_0 \to \infty$.
- Pure Buoyant Plume - in this instance there is no effluent and, consequently, no initial momentum. The driving force is pure buoyancy caused by a source of heat located in the position of the outfall port. An arbitrary reference velocity is used

along with a length scale that corresponds to a port radius. This case is indicated by $F_o = 0$.

- Mixed Flow - both initial momentum and buoyancy have varying degrees of importance. In this case $0 < F_o < \infty$.

Various cases of the above categories have been checked against available experimental data and similarity solutions. These cases are itemized in Tables 7.1, 7.2, and 7.3.

Four different effluent velocity profiles and concentrations (or temperature) have been used in this work which are:

- Type 1 : Gaussian profiles, established at 4.5 diameters from the port exit,
- Types 2, 3 : Power law velocity profile at the port exit with a constant radial concentration (or temperature) distribution, and
- Type 4 : Constant radial distribution of all quantities at the port exit.

Equations for these profiles are given in Table 7.1.

Figure 7.1 illustrates a typical grid system in R-Z coordinates. Note the effect of the hyperbolic sine transformation in stretching the cell widths as the distance R is increased. The computation grid (ξ,Z-coordinates) has uniform radial cell widths as illustrated in Figure 5.3.

TABLE 7.1. SUMMARY OF MOMENTUM JET VERIFICATION CASES ($F_o \rightarrow \infty$)

$PR_r = .80, \ PR_z = .80$

Case No.	Grid Size	$\Delta\xi$	ΔZ	Z (Surface)	R_∞	Boundary Type[1]	ϵ_r Type[2]	ϵ_z
1	26 x 40	.2	2	43.5	74.2	1	3	.0001
2	35 x 40	.1	2	43.5	14.96	1	1	.0001
3	26 x 40	.2	2	43.5	74.2	1	1	.0001
4	40 x 33	.12591	2	64	67.85	2 N=7	3	.0001
5	40 x 33	.12591	2	64	67.85	3 N=7	3	.0001
6	40 x 33	.12591	2	64	67.85	3 N=10	3	.0001
7	40 x 33	.12591	2	64	67.85	2 N=10	3	.0001
8	40 x 33	.12591	2	64	67.85	3 N=7	4	.0001
9	40 x 33	.12591	2	64	67.85	2 N=6.6	3	.0001
10	40 x 33	.12591	2	64	67.85	3 N=10	3	$\epsilon_z = \epsilon_r$
11	30 x 26	.2	2	43.5	74.2	1	Inviscid Test	
12	30 x 26	.2	2	43.5	74.2	1	Creeping Test	

[1] Inlet velocity profile type:

1. $V(R,Z) = V(0,Z)\ e^{-77(\frac{R}{Z})^2}$
2. $V(R,0) = \frac{(N+1)\ (2N+1)}{2N^2}\ (1-R)^{1/N}$
3. $V(R,0) = (1-R)^{1/N}$
4. $V(R,0) = V_o$ = Constant

[2] Radial eddy viscosity calculation type:

1. $\varepsilon_r = .0295\ r_o v_o$ = Constant
2. $\varepsilon_r = .0256\ r_{1/2} v_m$: Prior specification of $r_{1/2}$ from Gaussian distribution of velocity, v_m calculated iteratively.
3. $\varepsilon_r = .0256\ r_{1/2} v_m$: Iterative calculation of both $r_{1/2}$ and v_m.
4. $\varepsilon_r = .0263\ r_{1/2} v_m$: Same as Type 3.

TABLE 7.2. SUMMARY OF PURE BUOYANT PLUME VERIFICATION CASES (F_o = 0)[1]

$PR_r = .714$, $PR_z = .714$

Case No.	Grid Size	$\Delta\xi$	ΔZ	Z (Surface)	R_∞	ε_r Type[2]	Heat Source Condition[3]
13	40 x 33	.12591	2	64	67.85	3	1
14	40 x 33	.12591	2	64	67.85	3	2

[1] Reference densimetric Froude number is not zero but based on a reference velocity since there is no inflow at the source.

[2] See Table 7.1.

[3] Heat Source Type:

1. Weak Source: Simulated heated plate maintained at $\Delta T = 25\ ^{o}C$.
   Heat transferred to fluid by conduction alone over range $0 < R \leq 1$.

2. Stronger Source: Simulated source in first fluid node to maintain fluid temperature at $\Delta T = 25\ ^{o}C$. Heat transferred by both conduction or convection.

TABLE 7.3. SUMMARY OF MIXED FLOW VERIFICATION CASES

Case No.	Grid Size	$\Delta\xi$	ΔZ	Z (Surface)	R_∞	F_o	Boundary Type[1]	ϵ_r Type[1]	ϵ_{z_o}	PR_r	PR_z
15	26 x 40	.2	2	43.5	74.2	52	1	1	.0001	.714	.714
16	26 x 40	.2	2	43.5	74.2	52	1	2	.0001	.714	.714
17	26 x 40	.2	2	43.5	74.2	52	1	3	.0001	.714	.714
18	26 x 40	.2	4	82.5	74.2	52	1	3	.0001	.714	.714
19	26 x 40	.2	2	43.5	74.2	35	1	3	.0001	.714	.714
20	26 x 40	.2	2	43.5	74.2	106	1	3	.0001	.714	.714
21	26 x 40	.2	2	43.5	74.2	52	1	3	#See Below	.714	.714
22	40 x 33	.12591	2	64	67.85	45.5	$\overset{2}{N=7}$	3	.0001	.714	.714
23	40 x 33	.12591	2	64	67.85	45.5	$\overset{2}{N=7}$	3	.0001	.80	.80
24	40 x 33	.12591	2	64	67.85	1	$\overset{2}{N=7}$	3	.0001	.80	.80
25	40 x 33	.12591	2	64	67.85	1000	$\overset{2}{N=7}$	3	.0001	.80	.80
26	40 x 33	.12591	2	64	67.85	45.5	$\overset{2}{N=10}$	3	.0001	.714	.714
27	40 x 33	.12591	2	64	67.85	45.5	$\overset{2}{N=10}$	3	.0001	.714	.714

[1] See Table 7.1.

#ϵ_{z_o} = 1.0, Gaussian distribution $\epsilon_z = \epsilon_{z_o} e^{-A^2(Z_s-Z)^2}$

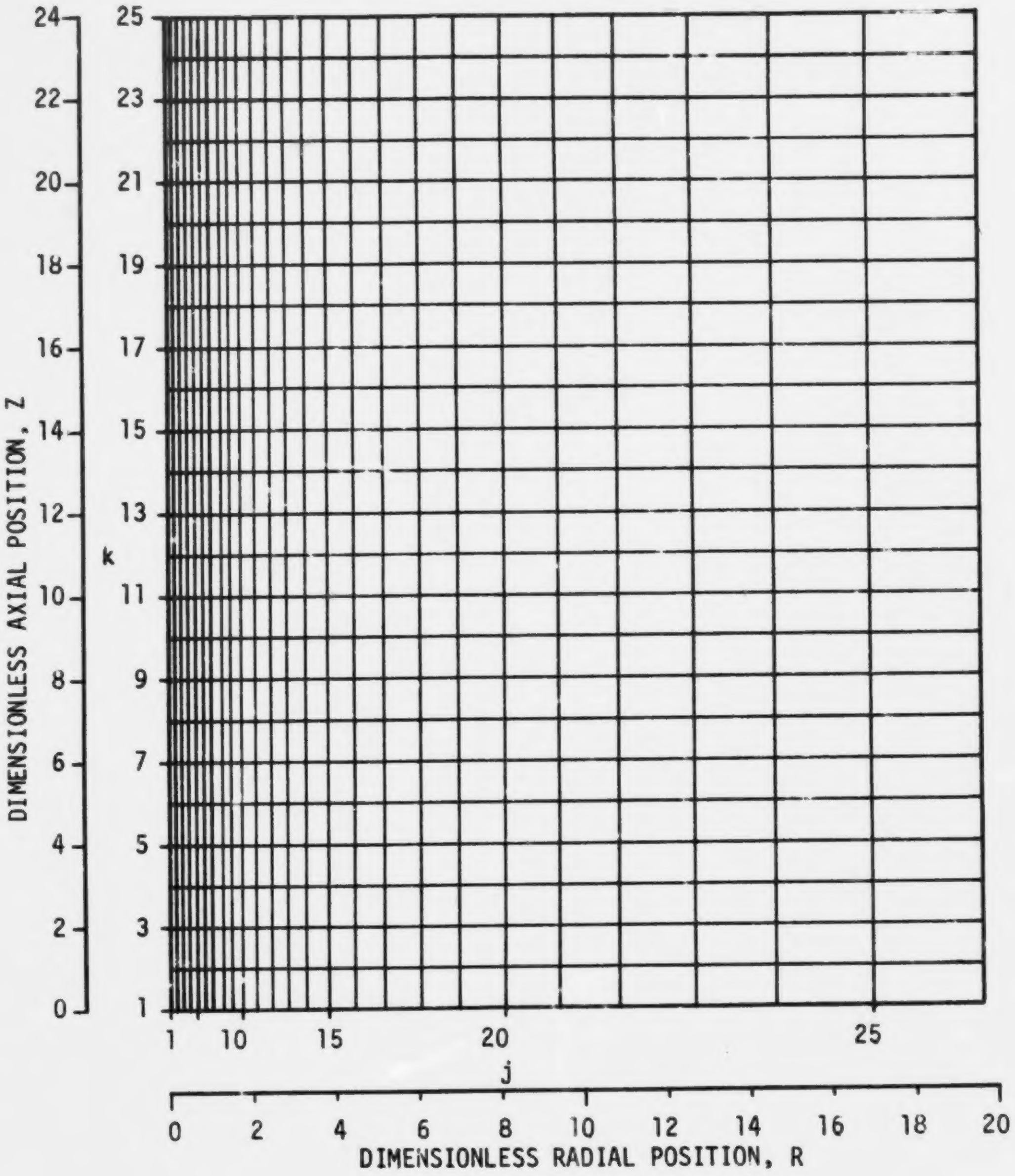
24
22
20
18
16
14
12
10
8
6
4
2
0
DIMENSIONLESS AXIAL POSITION, Z
25
23
21
19
17
15
13
k
11
9
7
5
3
1
1
10
15
20
25
j
0
2
4
6
8
10
12
14
16
18
20
DIMENSIONLESS RADIAL POSITION, R

Figure 7.1. Computational Grid for The Stream Function, Ψ, Illustrating the Effect of the Sinh (ξ) Transformation (Δξ = .14690, ΔZ = 1.0)

7.1.1 The Momentum Jet

A vast amount of information has been gathered concerning the dynamic behavior of momentum jets dating back to Tollmien's [98] work of 1926. Hence, there is sufficient data reported in the literature to check all of the gross aspects of the jet structure computed. In verifying the computational technique with the published data we use the following jet characteristics:

- Centerline velocity and concentration,
- Radial distribution of axial velocity and concentration,
- Rate of jet spread, and
- Radial velocity.

Although there is a vast amount of published data available for verification, the primary data used is from Albertson, et al. [4], Baines [8], Abraham [1] and information obtained from several researcher's published in Chapter 24 of Schlichting's text "Boundary Layer Theory" [84]. Additional information is obtained from reviews by Gauntner et al. [32] and Chapter 6 of Hinze's text "Turbulence" [40].

Some of the relevant restrictions in this section are:

- Vertical turbulence is negligible; one case is run to verify this fact.
- The computational grid system has an impermeable upper boundary. Hence, velocity profiles begin to "feel" the boundary some distance before it is reached.

Aside from the quantitative verification mentioned above, illustrations of streamlines, concentration, and vorticity contours, and three-dimensional plots of the same information are provided for additional qualitative assessment. Table 7.1 summarizes the momentum jet cases run.

7.1.1.1 Centerline Velocity and Concentration for Momentum Jets

A similarity solution for vertical plumes was given in Chapter 4 as

$$E^* = \frac{64}{Z_e^3} + \frac{3}{32F_o}\left(Z^2 - Z_e^2\right) \tag{4.43}$$

In the case of a momentum jet $F_o \rightarrow \infty$ so that,

$$E^* = \frac{64}{Z_e^3} . \tag{7.1}$$

Then by definition

$$\frac{V_m Z}{\sqrt{K}} = \frac{4}{Z_e} \tag{7.2}$$

where again V_m is the centerline velocity, K is related to the plume entrainment (see Table 4.1), numerically equal to 77, and Z_e is the potential core length based on concentration (cf. Abraham [1]).

By Equation (7.2)

$$V_m = \frac{4\sqrt{K}}{Z_e} /Z. \tag{7.3}$$

According to Abraham $Z_e \simeq 5.6$; hence,

$$V_m = 6.2/Z \tag{7.4}$$

which is also the result obtained by Albertson.

Equation (7.4) implies that a plot of the dimensionless centerline velocity, V_m, versus axial distance in port diameters $\bar{z}$ has slope of -1 when plotted to Log-Log scale, and has an intercept of 6.2 on the $\bar{z}$-coordinate when $V_m = 1$. Experiments carried out by Albertson are probably the most frequently quoted data bearing out Equation (7.4). Various other researchers have carried out similar experiments (e.g., Baines, Tollmien and Reichardt [77]). Although there seems to be general agreement that $V_m \sim \bar{z}^{-1}$, there is some disagreement on the potential core length (hence, the constant of proportionality), or the Log-Log plotted intercept value mentioned above. A review of a portion of this work is given by Gauntner. It is noteworthy to point out here that the potential core length (see Figure 4.1) is assumed to be the centerline velocity plot intercept (V_m=1, $\bar{z}$=6.2; see Figure 7.2),

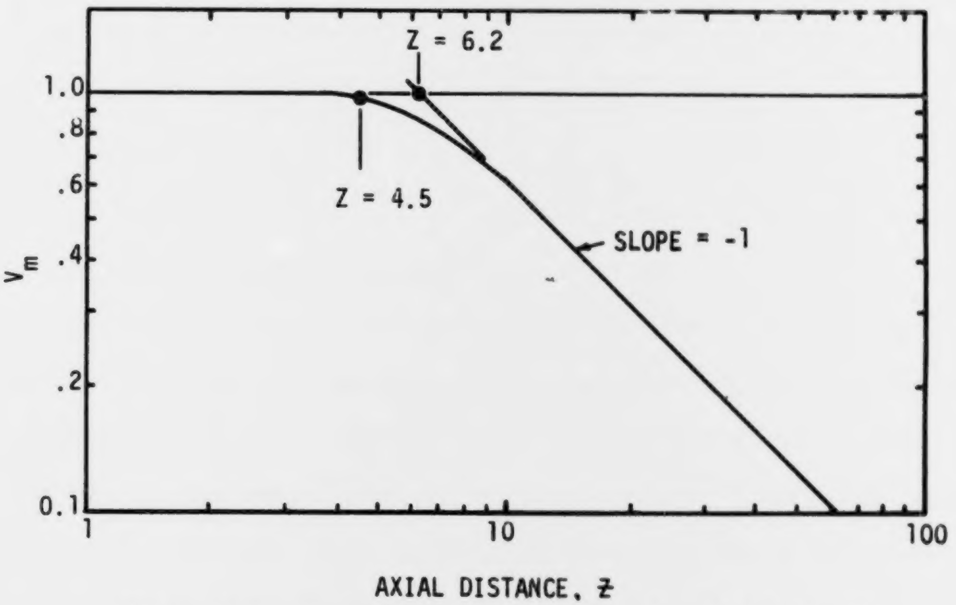

Figure 7.2. General Features of Momentum Jet Centerline Velocity (Based on Albertson's data)

although the actual potential core length may be somewhat smaller. For instance, Albertson measured an actual length of approximately 4.5 whereas their similarity solution is based on 6.2. The reason for using the value 6.2 is that it is more representative of downstream data than 4.5. As a matter of fact, similarity solutions are not valid out to approximately 10 to 12 diameters. In Figure 7.2 , the distance $Z = 4.5$ is the approximate distance where deterioration of centerline velocity is first apparent.

Figure 7.3 illustrates centerline velocity, V_m, and concentration, C_m, comparisons for

- Similarity theory
- Experiment, and
- The present computational technique.

The similarity theory concentration distribution along the centerline is

$$C_m = 5.6/Z \qquad (7.5)$$

as given by Abraham.

Figure 7.3 indicates remarkable agreement between the computed and measured centerline velocity distribution. Concentrations agree with the similarity curve almost identically past $Z \simeq 20$. These results are based on the Type 1 boundary conditions (Section 7.1). Computational runs 1 and 3 also use the Type 1 boundary condition, for different water depths and node spacing; although these cases are not plotted, centerline distributions nearly identical to those depicted in Figure 7.3 were obtained. The only deviation found between experimental and

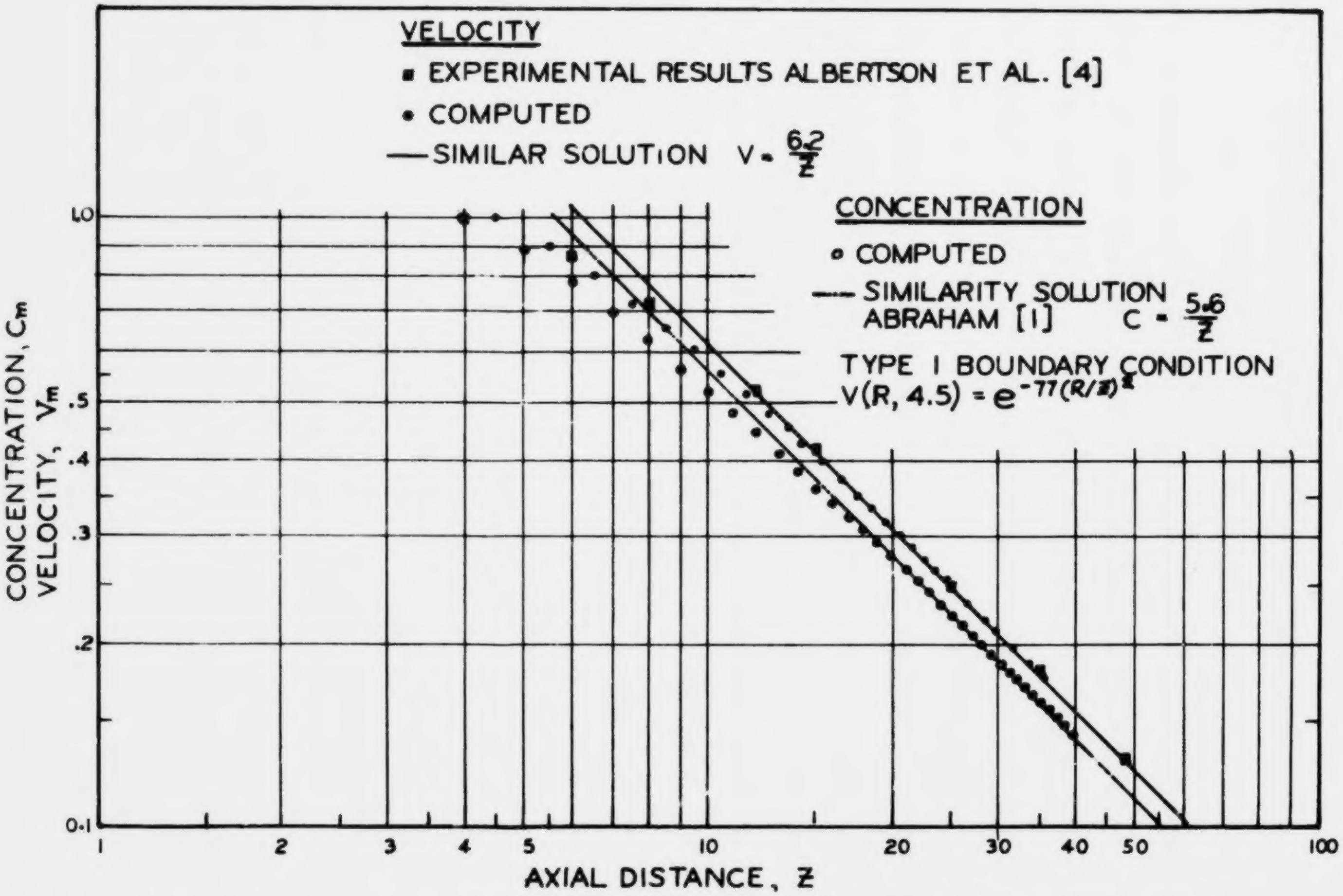

Figure 7.3. Comparison of Experimental Data and Similarity Solution with Computed Results for a Momentum Jet. Centerline Velocity and Concentration for Case 2.

computed centerline velocity in these cases is that a very slight difference in slope was noted, whereby the computed slope was very slightly less steep than -1.

Similar results for Case 4, which uses the Type 2 boundary condition, are given in Figure 7.4. Note that the 1/7 power velocity profile gives a centerline value of 1.22 for an average jet exit velocity of $V_0 = 1$. These centerline velocity results are somewhat higher than Albertson's data, but agree well with the data obtained by Baines for an initial Reynolds number of 7×10^4. Baines contends that there is a Reynolds number effect on the potential core length and offers data which apparently substantiates his assertion. According to Gauntner, this facet of jet theory is apparently still unresolved.

The computed data for this case reveals the relationships:

$$V_m \simeq 7/Z. \tag{7.6}$$

and

$$C_m \simeq 5.1/Z. \tag{7.7}$$

Again, the computed velocity distribution is very slightly less steep than a slope of -1.

Figures 7.5 and 7.6 illustrate centerline velocity and concentration distributions for Cases 5 and 6. Both of these cases again use a Type 2 boundary condition with the inflow velocity distributions given by

$$V(R,0) = (1-R)^{1/N}. \tag{7.8}$$

Case 5 uses N equal to 7 whereas N in Case 6 is equal to 10.

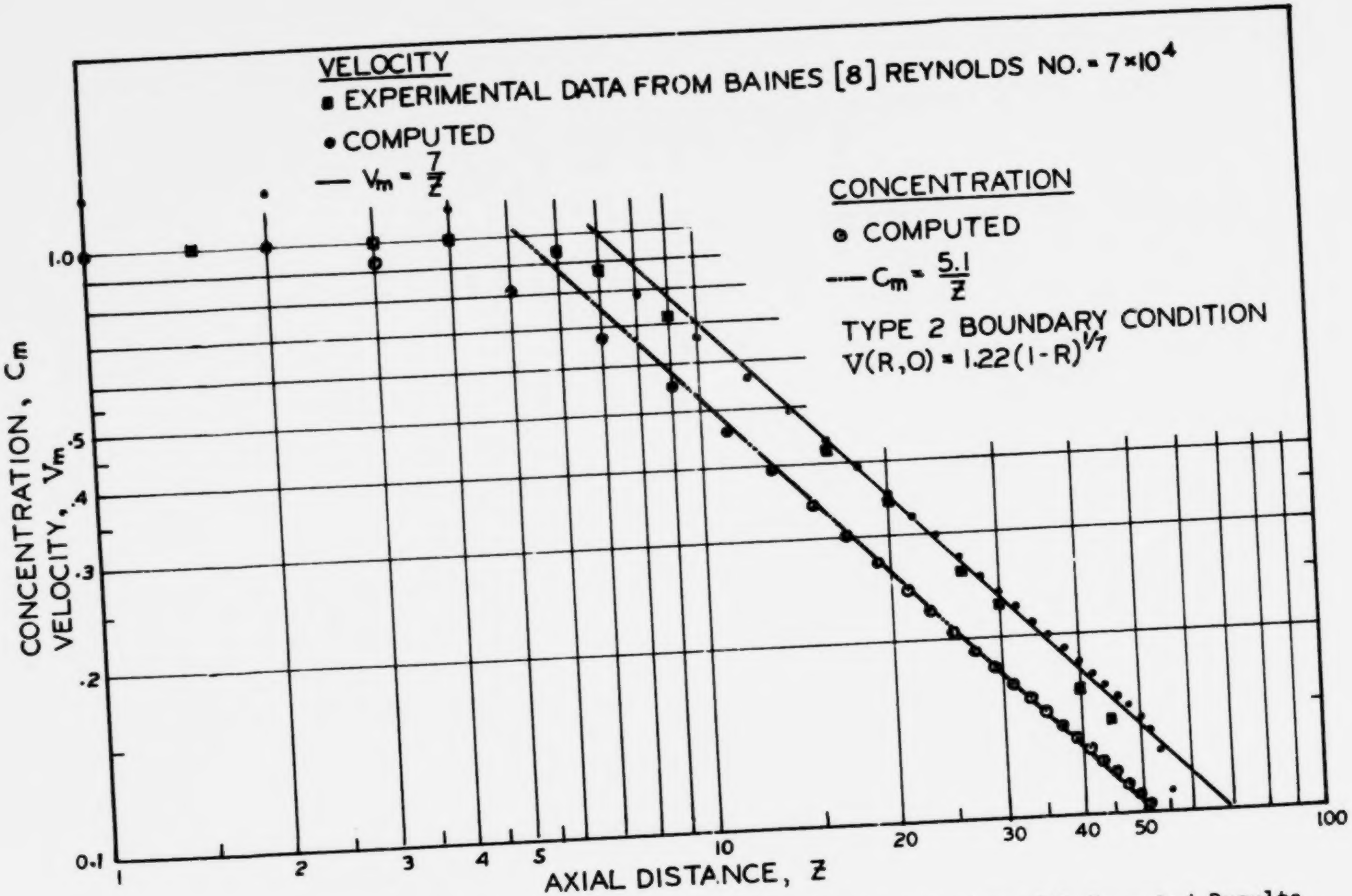

Figure 7.4. Comparison of Experimental Data and Similarity Solution with Computed Results for a Momentum Jet. Centerline Velocity and Concentration for Case 4.

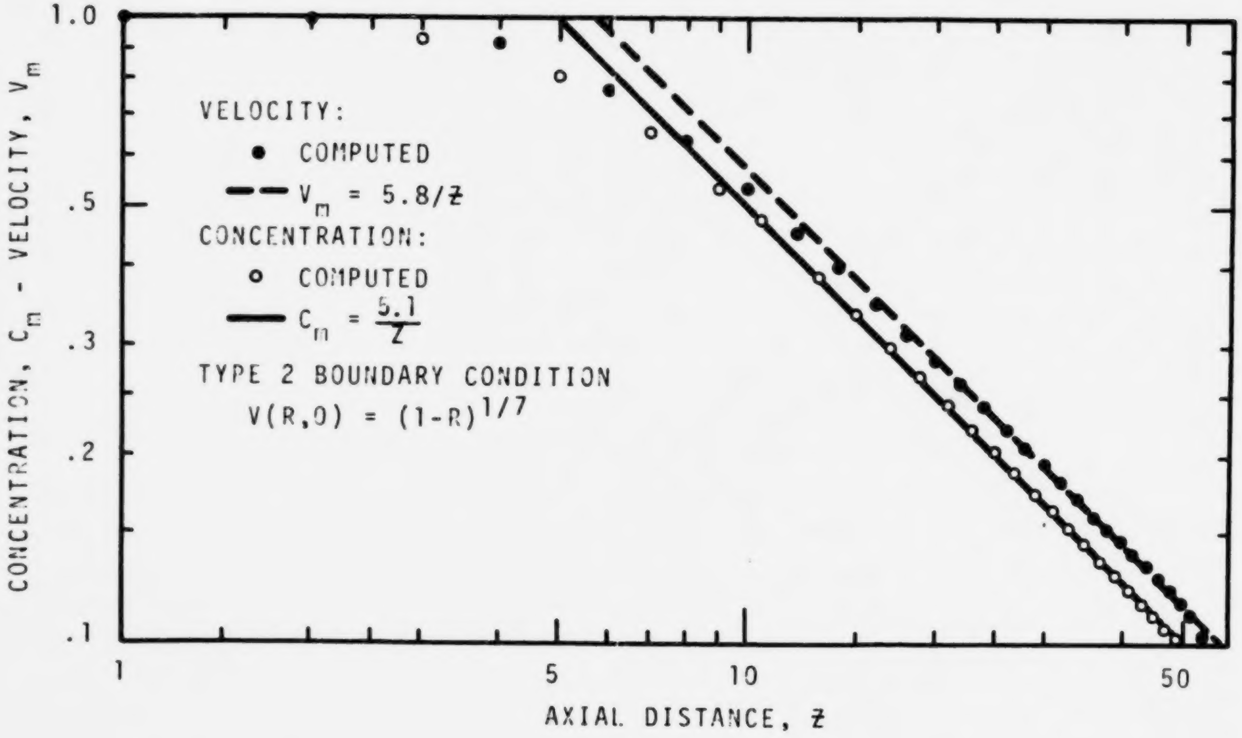

Figure 7.5. Computed Centerline Velocity and Concentration for Momentum Jet, Case 5

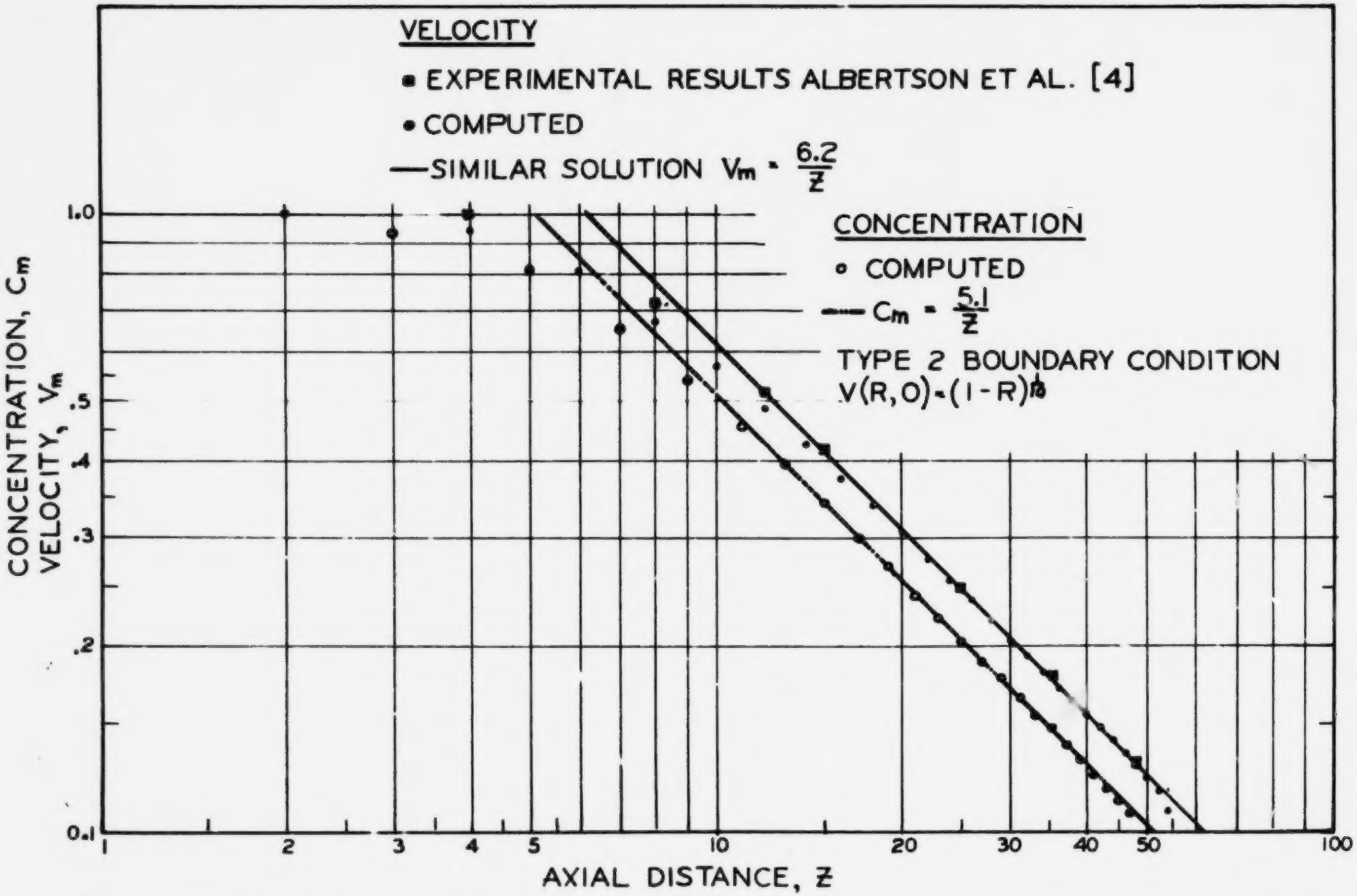

Figure 7.6. Comparison of Experimental Data and Similarity Solution with Computed Results for a Momentum Jet. Centerline Velocity and Concentration for Case 6.

According to Schlichting, these profiles correspond to pipe Reynolds numbers of 1.1×10^5 and 3.2×10^6, respectively. The computing technique shows a marked difference between the asymtotic centerline velocities for these two cases, that is, for large Z,

$$\text{Case 5:} \quad V_m \simeq 5.8/Z \tag{7.9}$$

$$\text{Case 6:} \quad V_m \simeq 6.2/Z \tag{7.10}$$

Although the slope is still approximately -1 and the asymtotic concentration for both cases is given by,

$$C_m \simeq 5.1/Z. \tag{7.11}$$

Note that

$$V(0,0) = 1$$

which results in an average inflow velocity less than unity.

From these results it is tempting to conclude that since the inflow velocity profile has an effect on the -1 slope intercept, a Reynolds number effect on the potential core length is demonstrated. However, it is felt that the lack of finite difference resolution and shortcomings in modeling turbulence in the zone of flow establishment, are sufficient to shadow such a conclusion. Comparing Case 4 where,

$$V(R,0) = 1.22\ (1-R)^{1/7} \tag{7.12a}$$

and Case 7 (Figure 7.7) where

$$V(R,0) = 1.155\ (1-R)^{1/10} \tag{7.12b}$$

reveals asymtotic velocity profiles,

$$V_m \simeq 7/Z \tag{7.13}$$

and concentration

$$C_m \simeq 5.1/Z. \tag{7.14}$$

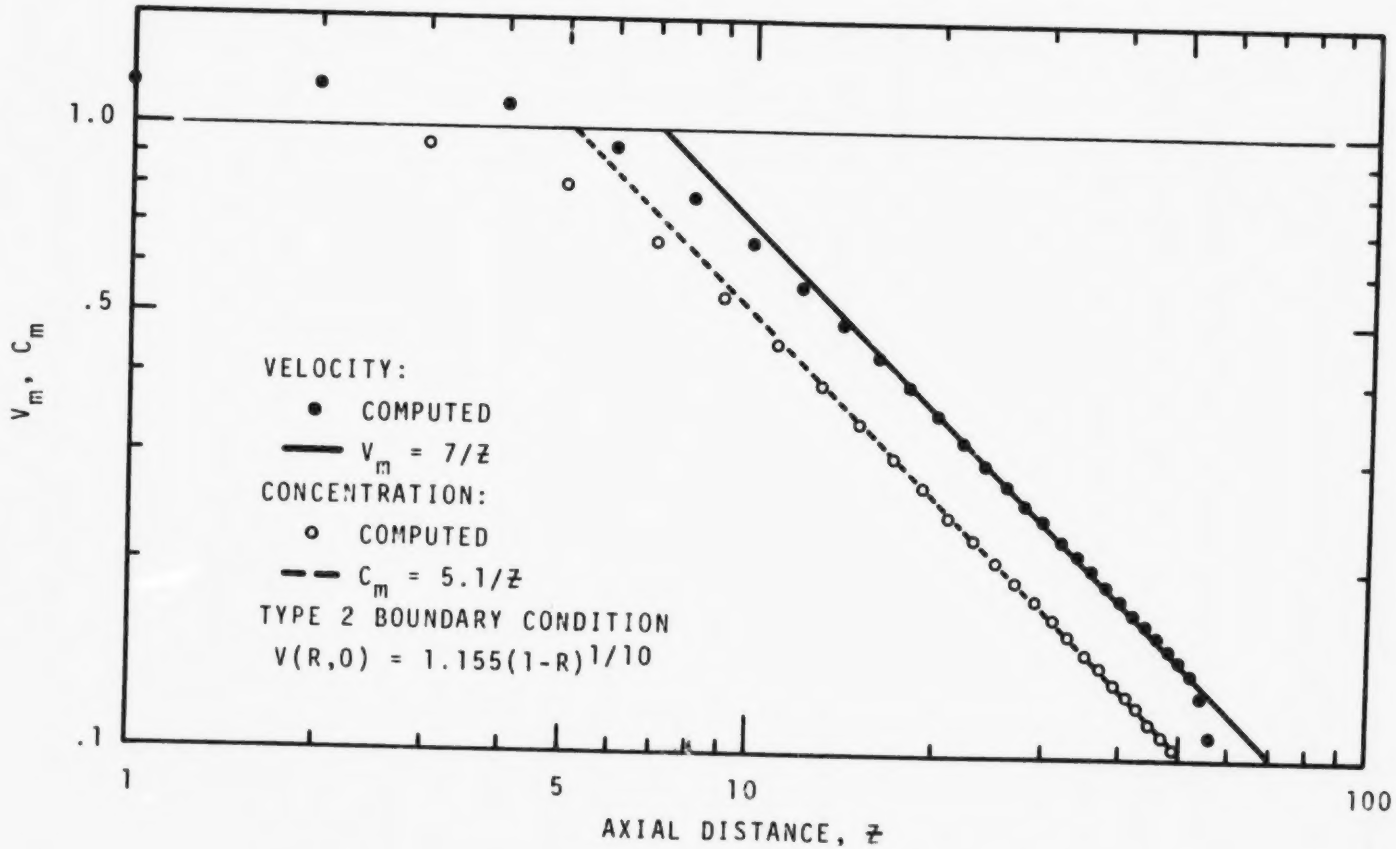

Figure 7.7. Computed Centerline Velocity and Concentration for Momentum Jet, Case 7

It is important to note that the jet exit average velocity in both Cases 5 and 6 is unity whereas it is 1.22 in Case 4 and 1.155 in Case 7.

In all computer runs cited thus far, the radial eddy viscosity has been computed from Prandtl mixing length theory. This particular aspect of the work is discussed in more detail in Section 7.2. Essentially, the eddy viscosity is calculated by

$$\epsilon_r = c\, v_{max}\, r_{1/2}, \tag{7.15}$$

where v_{max} is the centerline velocity, $r_{1/2}$ is the jet half radius and c is a constant having the value .0256 for an axisymmetric momentum jet (cf. Schlichting [84], p. 699); all cases thus far use c = .0256. Case 8 (see Figure 7.8) uses c = .0263 (picked quite arbitrarily and as a fraction is 1/38 = $1/RE_r$) and is to be compared to Case 5, Figure 7.5. The net effect of this change is a slight shift in the velocity slope toward -1 (difficult to see slope shift from compared figures, but numerical results bear out the change). Although the higher value of c appears to yield a velocity slope nearer -1, the value c = .0256 is used for all following computations in this manuscript.

Case 9 (Figure 5.9) represents an additional case using Type 2 boundary conditions with a velocity profile at the jet exit given by

$$V(R,0) = 1.24\,(1-R)^{\frac{1}{6.6}} \quad . \tag{7.16}$$

Note that all cases (4, 7 and 9) use the boundary velocity profile

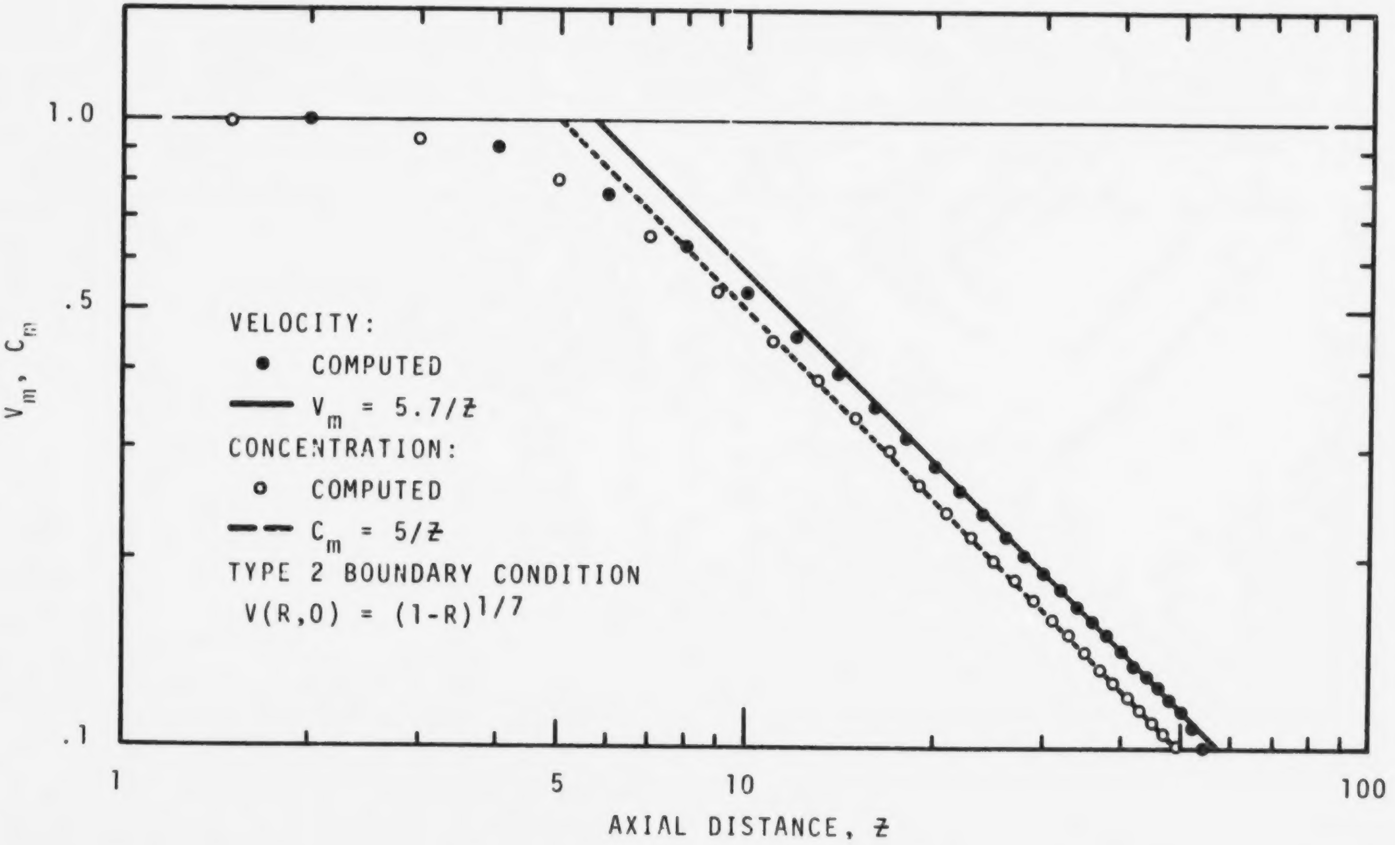

Figure 7.8. Computed Centerline Velocity and Concentration for Momentum Jet, Case 8

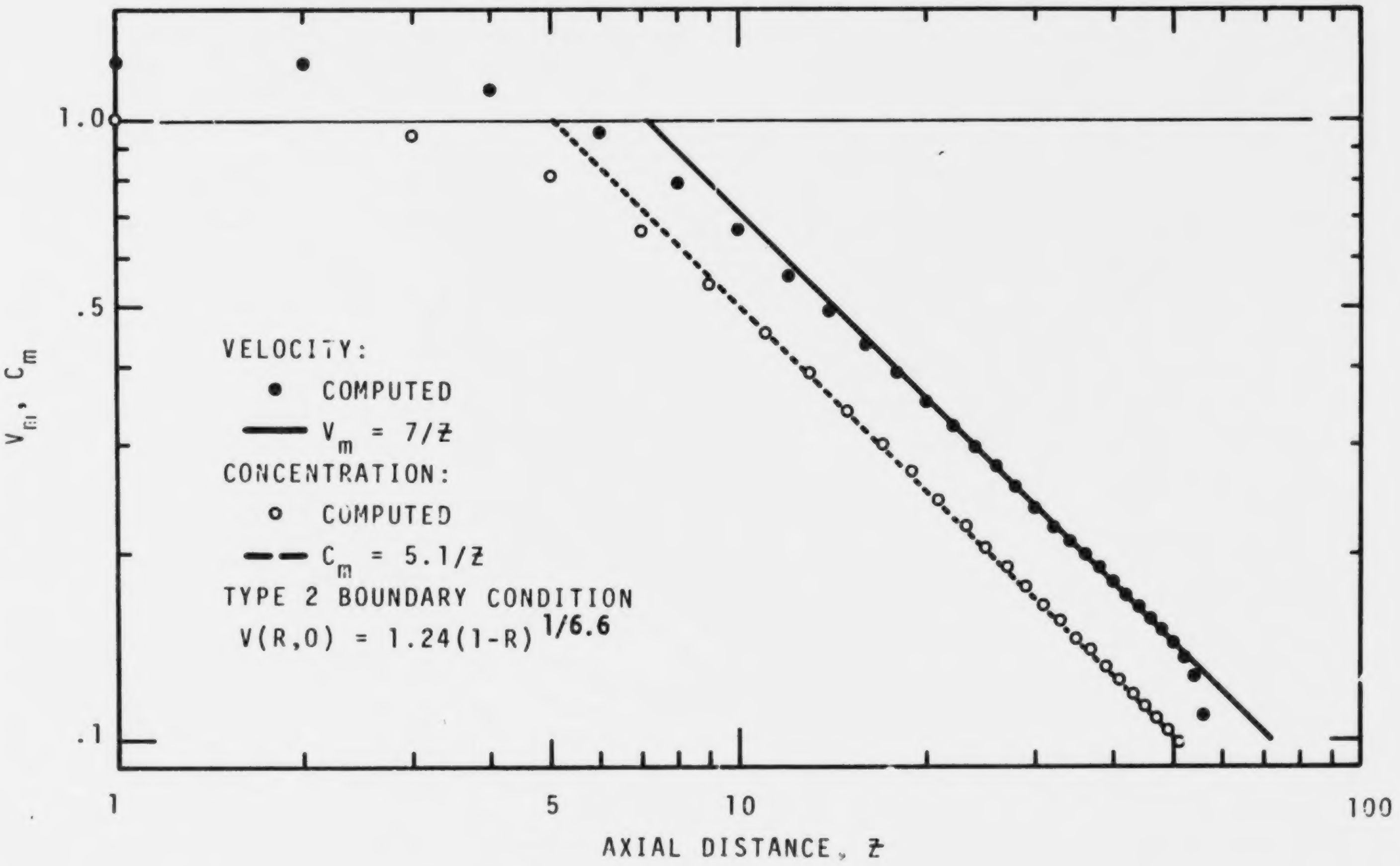

Figure 7.9. Computed Centerline Velocity and Concentration Distribution for Momentum Jet, Case 9

$$V(R,0) = \frac{(N+1)(2N+1)}{2N^2} (1-R)^{\frac{1}{N}} \tag{7.17}$$

for the jet. In all of these cases the asymptotic centerline velocity profiles are essentially identical and represented quite accurately by

$$V_m \simeq 7/Z \tag{7.18}$$

and concentration given by

$$C_m \simeq 5.1/Z. \tag{7.19}$$

Figure 7.10 illustrates these cases where the distribution is normalized by dividing each value by the corresponding value of V(0,0). The net result of this operation is that the solution collapses to the cases using corresponding values of N and where V(R,0) is set by Equation (7.8). Although this result was certainly expected, it serves to illustrate that the computer program is functioning correctly in this sense and to bear out again the velocity profile effect on the asymptotic centerline velocity distribution (Figure 7.10). Computationally, this condition is apparently caused by the differences of the jet exit vorticity distribution.

Vertical eddy diffusion, which should be of minor importance in the jet mainstream, has also been ignored in cases cited to this point. By ignored, it is meant that the value has been set to compare with molecular viscosity which is perhaps three orders of magnitude smaller than the jet induced eddy viscosity. The primary reason for vertical diffusion being set to a very small value in these verification studies

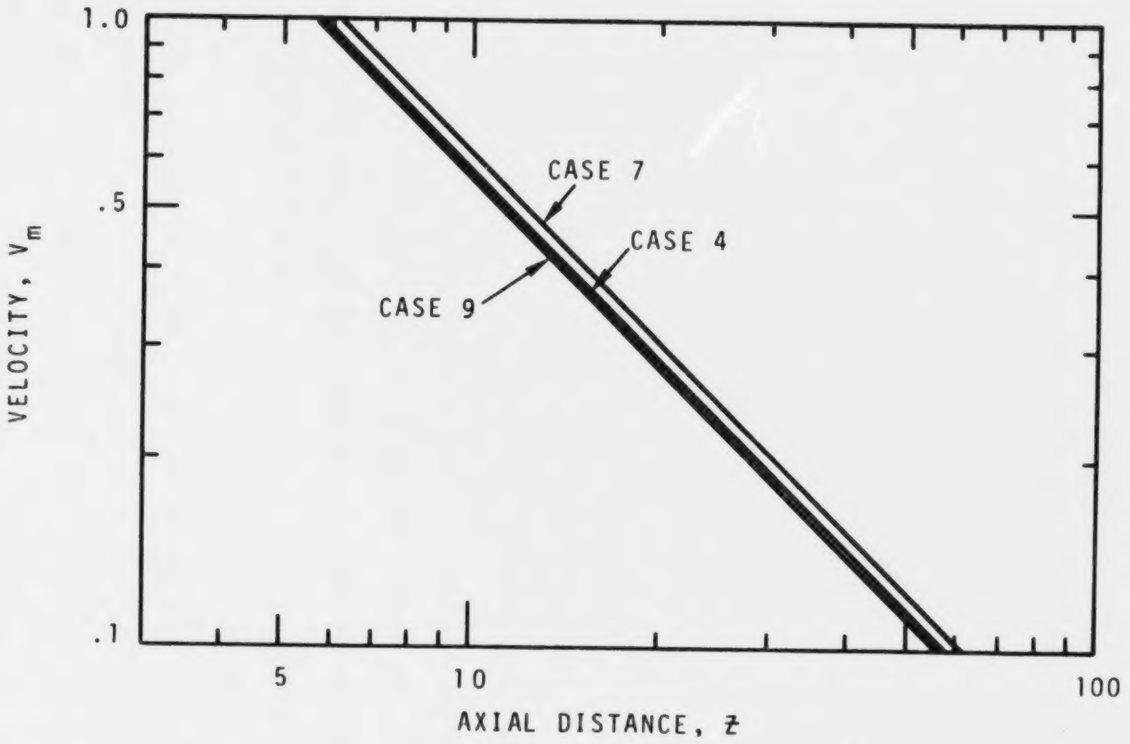

Figure 7.10. Centerline Velocity Distributions for Cases 4, 7, and 9, Normalized to $V_o = 1.0$

is so that vertical entrainment near the surface where the jet is spreading laterally will be minimized.

With a large value of vertical diffusion, in nonstratified media, streamlines outside the jet would be distorted upward because of the vertical entrainment in the lateral spread and would not be a realistic representation of deep water conditions.

In Case 10 (Figure 7.11) the vertical eddy viscosity has been accounted for by setting

$$\varepsilon_z = \varepsilon_r \, .$$

Figure 7.11 is to be compared with Figure 7.5 (Case 6). Case 10 shows a slight increase of centerline velocity over Case 6 which is an effect to be expected if vertical diffusion has any importance, since the shape-preserving vorticity will be transported downstream at a slightly higher rate.

As further discussion of the above statement, Case 11 has been run where the fluid was considered as inviscid, although rotational. The numerical fluid reacted in a manner such that the jet exit velocity profile was completely shape preserved until the surface effects were encountered (see Figure 7.12). Considering the opposite extreme of a hypothetical fluid where vertical diffusion completely dominates radial transport, the same shape preserving nature would exist. Case 11 also served to illustrate the computational stability of the differencing technique used for cases where $Re_r = Re_z \to \infty$.

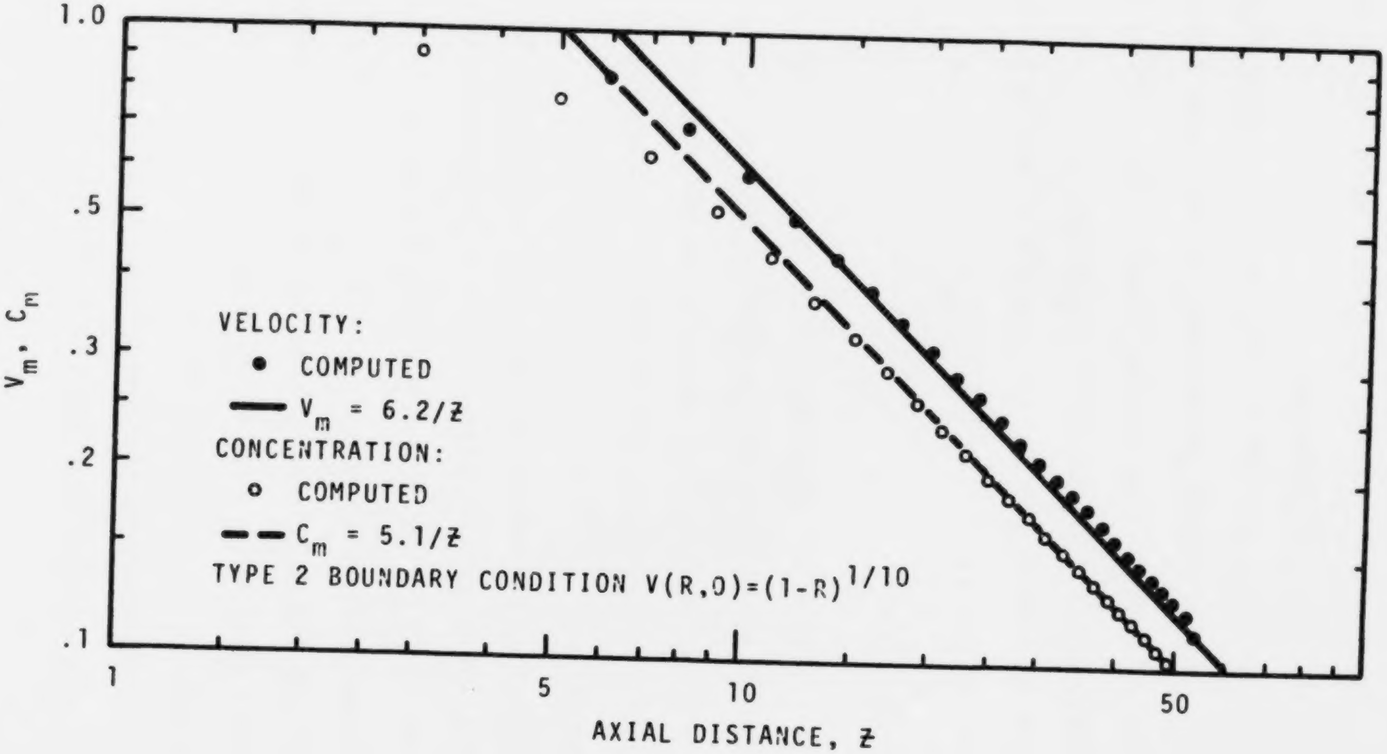

Figure 7.11. Centerline Velocity and Concentration Distribution for Case 10 (Includes effect of large vertical eddy diffusivity.)

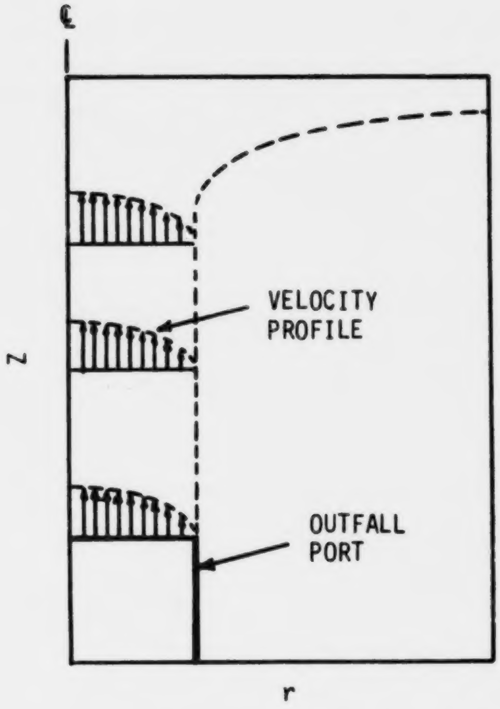

Figure 7.12. Shape Preserving of Velocity Profiles Computed for an Inviscid, Rotational Fluid (Ref. Case 2)

7.1.1.2 Spread of the Momentum Jet

The rate of spread of the half radius, $r_{1/2}$ is illustrated in Figure 7.13-A and compared to measurements in Figure 7.13-B. The computed rate of spread is given by

$$r_{1/2} = C_1 z \tag{7.20}$$

where

$$C_1 = .0875.$$

For the several momentum jet computations carried out, the above equation holds. Table 7.4 compares some of the reported values of C_1.

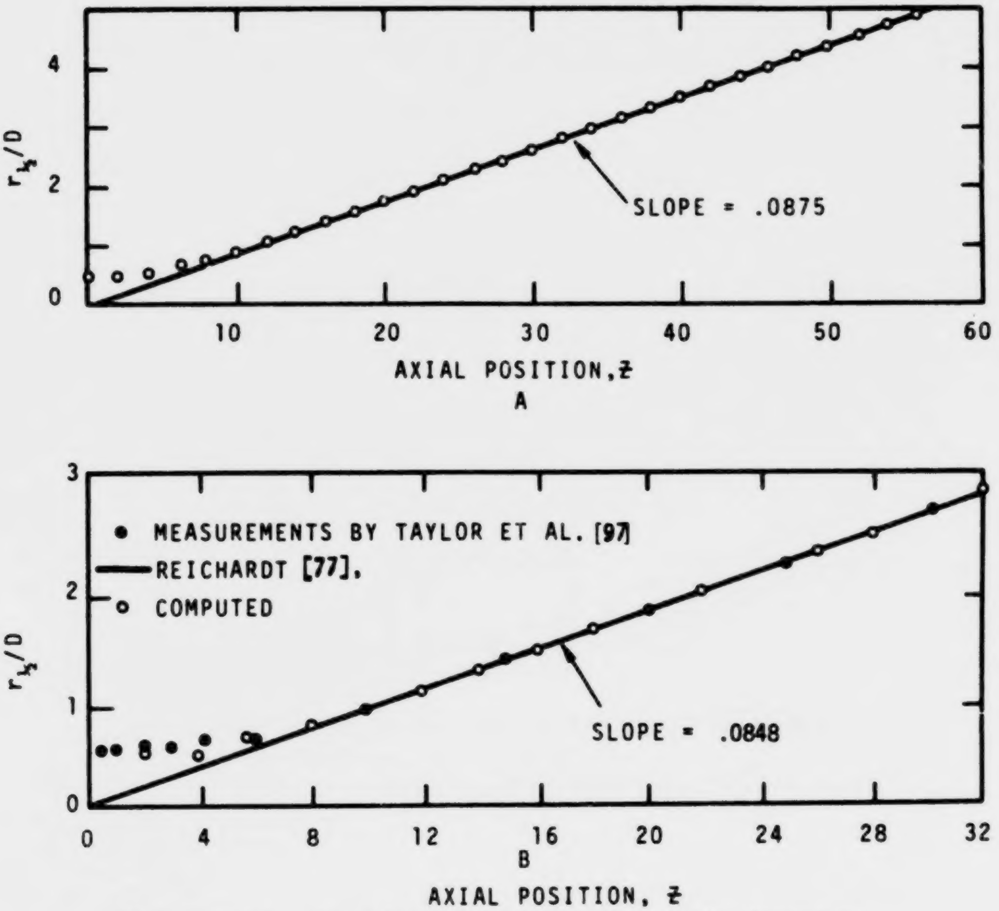

Figure 7.13. Computed Rate of Spread of the Momentum Jet Half-Radius, $r_{1/2}$

TABLE 7.4. COMPARISON OF THE SPREADING CONSTANT REPORTED BY VARIOUS INVESTIGATORS

Investigator	Comment	C_1
Albertson et al. [4]		.095
Baines [8]	Reynolds Number 7×10^4	$\simeq$ .085
Baines [8]	Reynolds Number 2.1×10^4	$\simeq$ .095
Reichardt [77]		.0848
Taylor et al. [97]		.0854
Corrsin and Uberoi [20]*		.0814
Keagy and Weller [49]*		.0888
Present numerical computation		.0875

---

*Based on momentum measurements.

As Table 7.4 indicates, there is no universal agreement of the value for C_1 among the cited investigators. These discrepancies are possibly due to measurement methods and/or flow condition dependence. Again, Baines offered data which tends to confirm the role of the latter. Hence, the computed value of .0875 seems to be a realistic value in view of reported measurement, but cannot be compared as an absolute because of experimental discrepancies. Variations in the half-radius may also be observed from Figure 7.12.

7.1.1.3 Radial Distribution of Vertical Velocity, Concentrations and Vorticity for the Momentum Jet

The radial distribution of vertical velocity for a momentum jet is essentially Gaussian. For instance the data obtained by Albertson is adequate expressed by

$$V = V_m e^{-K(\frac{R}{Z})^2} , \qquad (7.21)$$

where

$K = 77.$

Likewise, concentration distributions are adequately given by

$$C = C_m e^{-\lambda K(\frac{R}{Z})^2} \qquad (7.22)$$

where λ is the eddy Schmidt number and equal to .8. The coefficient K will vary from experiment to experiment similar to the variation in data measured to establish the length of the potential core. As given in Chapter 4, Baines found

$$V = V_m e^{-64.4(\frac{R}{Z})^{1.84}} \qquad (7.23)$$

for a Reynolds number of 7×10^4 and

$$V = V_m e^{-43.3(\frac{R}{Z})^{1.82}} \qquad (7.24)$$

for a Reynolds number of 2.1×10^4. Gortler [34] found K = 100. For a summary of additional experimental data on the value of K one may refer to Abraham [1].

One should bear in mind that the use of the Gaussian distribution has no theoretical basis, but is a result of curve fitting. Figures 7.14 through 7.18 all illustrate the vertical velocity profiles plotted against different coordinates. Figure 7.14 illustrates the distribution of computed velocity for comparison with the data of Albertson for Case 2 which uses the Type 1 boundary condition. Figure 7.15 relates this same type of information for Case 4 compared to the data of Reichardt (cf. Schlichting). Figures 7.14 and 7.15, along with Figure 7.16 (Case 6) provide a comparison with the Gaussian distribution. Computed information shows excellent agreement with the data and essentially the same deviation from the Gaussian curve. Unfortunately, correct numerical modeling at the jet boundary is practically unobtainable because of numerical smearing and inability to correctly model turbulence at the jet boundary. These facets account for deviations at the boundary and the fact that the computed velocity does not attain zero at a finite radius.

Figures 7.16 and 7.18 also bear out the similarity of the computed velocity profiles whereby the computed velocity at elevation Z = 10 shows the only appreciable deviation from complete similarity. Baines' data is also illustrated in Figure 7.15. The various other momentum jet case runs showed, upon spot check, that these curves are typical of all cases run with similar assumptions.

Typical computed concentration profiles are shown in Figures 7.19 and 7.20. Again, as in the case of velocity, striking similarity is evidenced in the radial distributions at all elevations. One noticable fact is the deviation from a Gaussian distribution is more pronounced

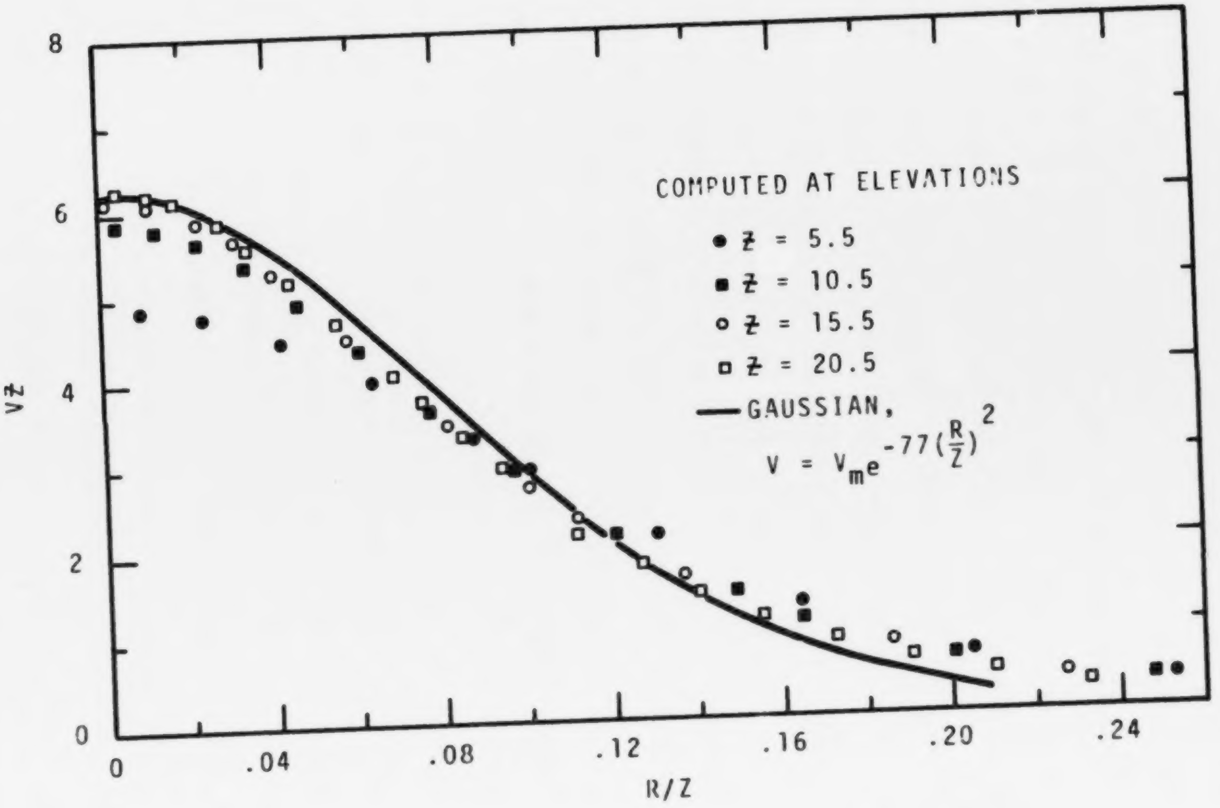

Figure 7.14. Radial Distribution of Normalized Vertical Velocity for Case 2

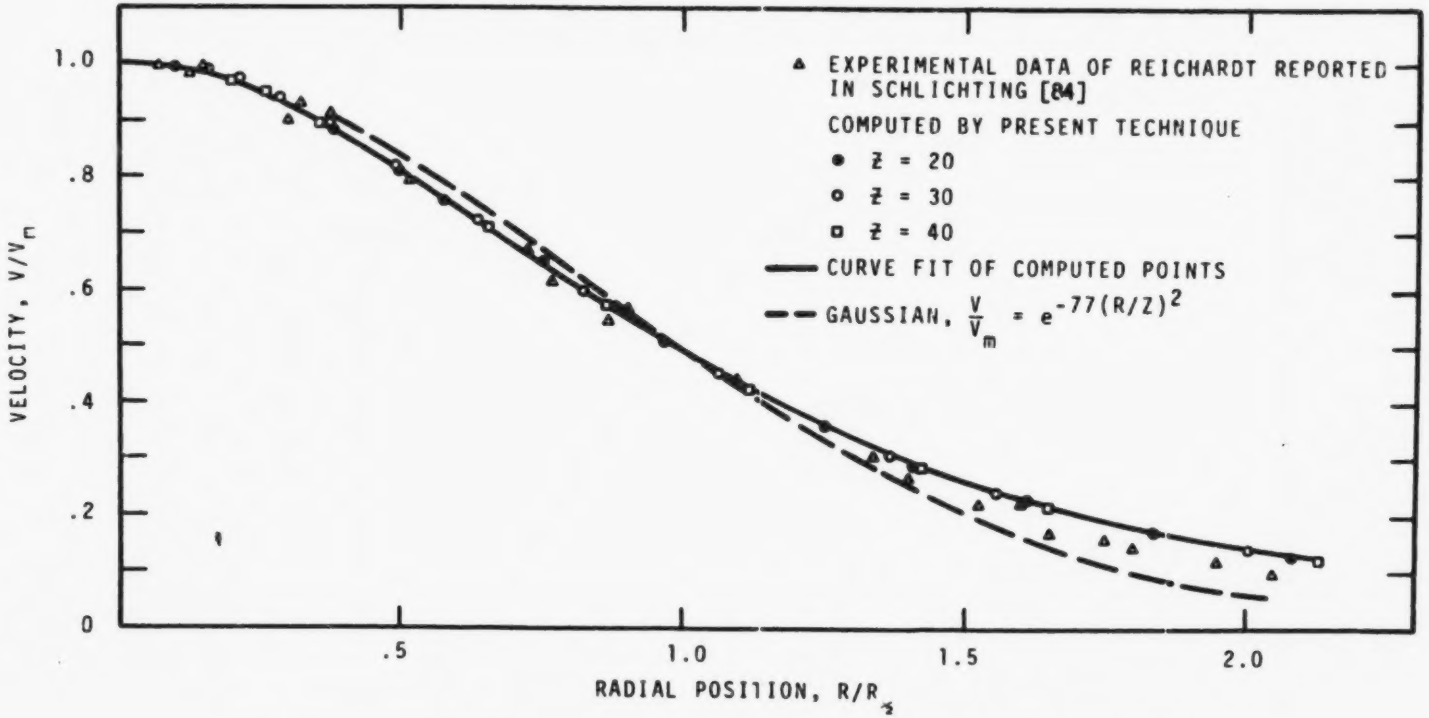

Figure 7.15. Normalized Radial Distribution of Axial Velocity, Momentum Jet Case 4

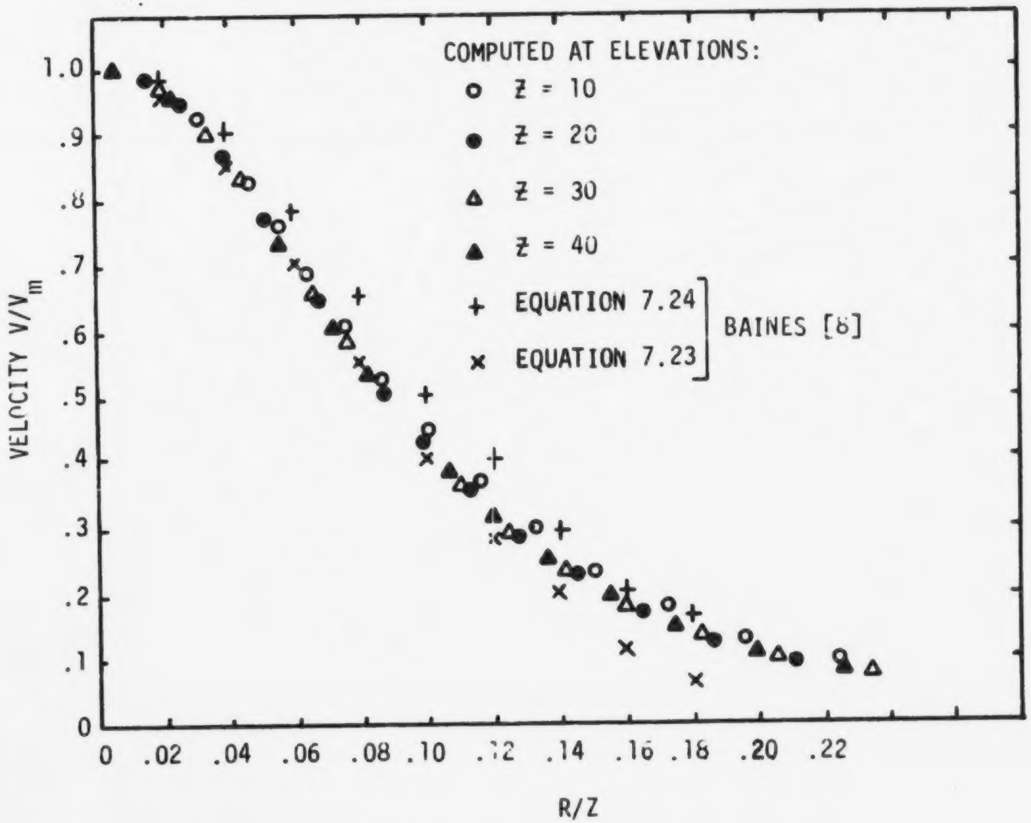

Figure 7.16. Normalized Radial Distribution of Axial Velocity Case 4

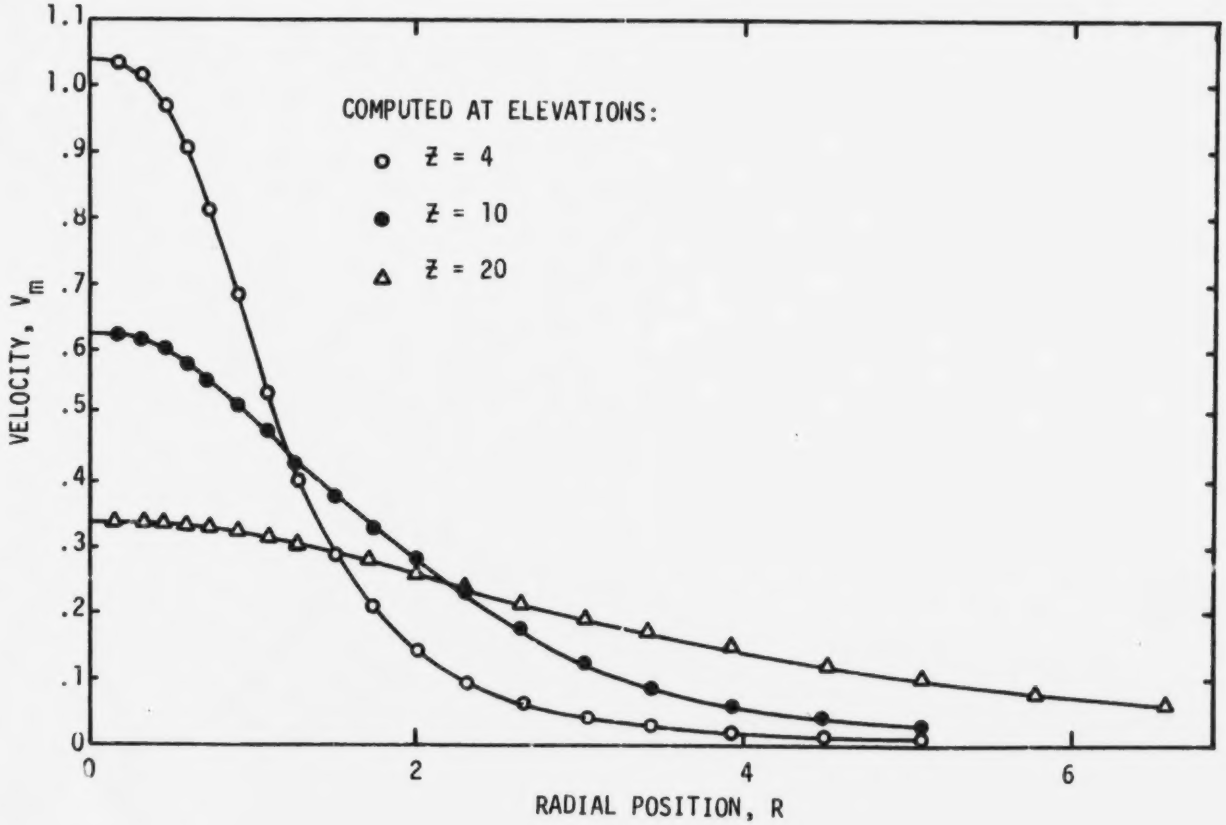

Figure 7.17. Radial Distribution of Axial Velocity at Various Elevations Case 4

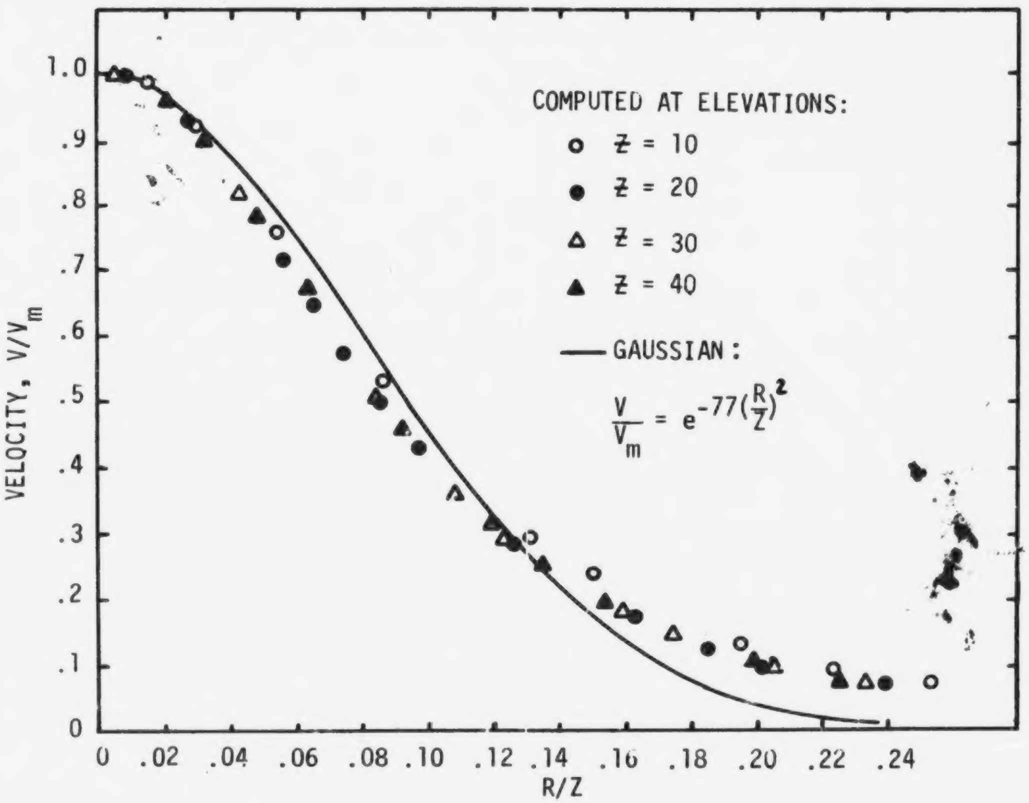

Figure 7.18. Normalized Distribution of Axial Velocity Case 6

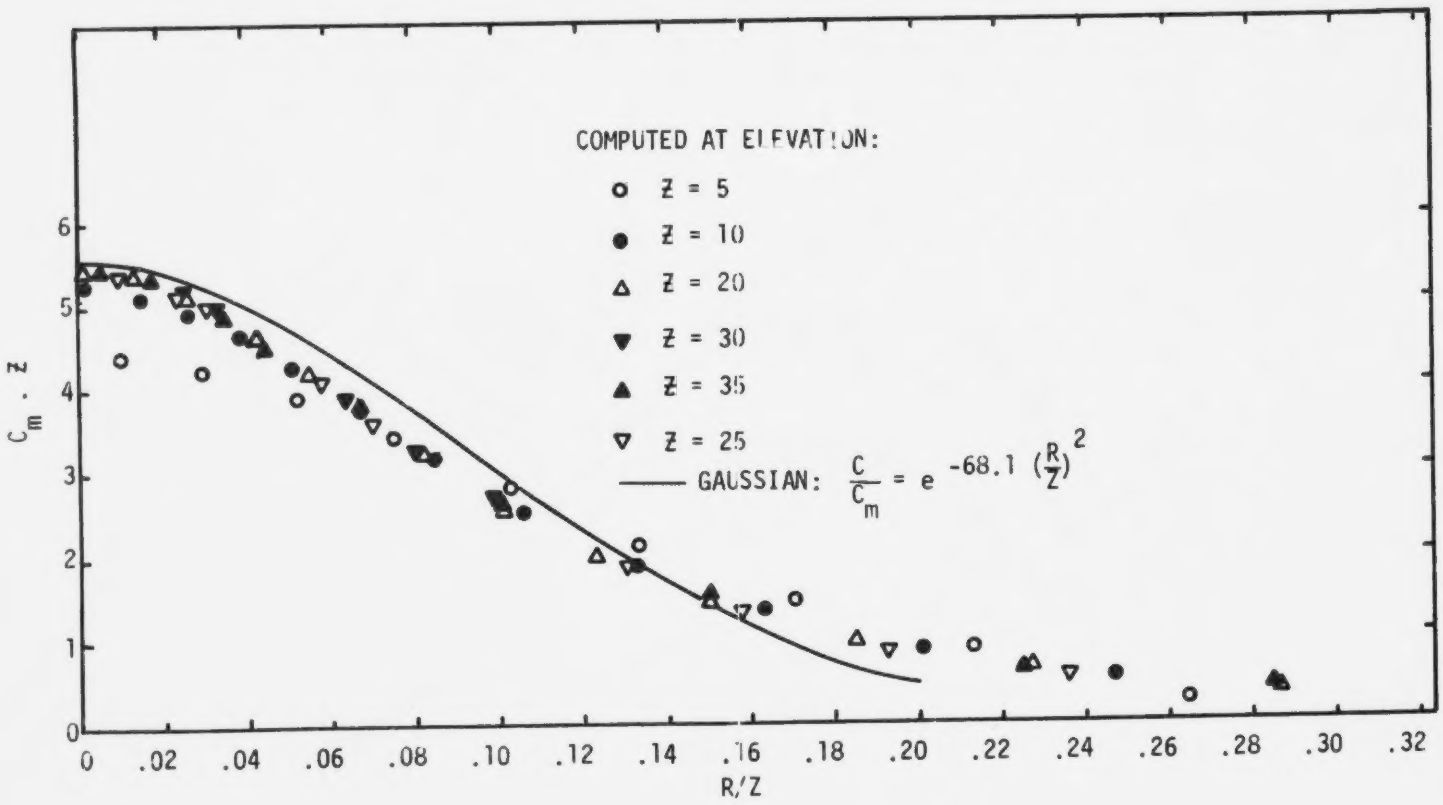

Figure 7.19. Normalized Radial Concentration Distribution, Type 1 Boundary Condition Case 2

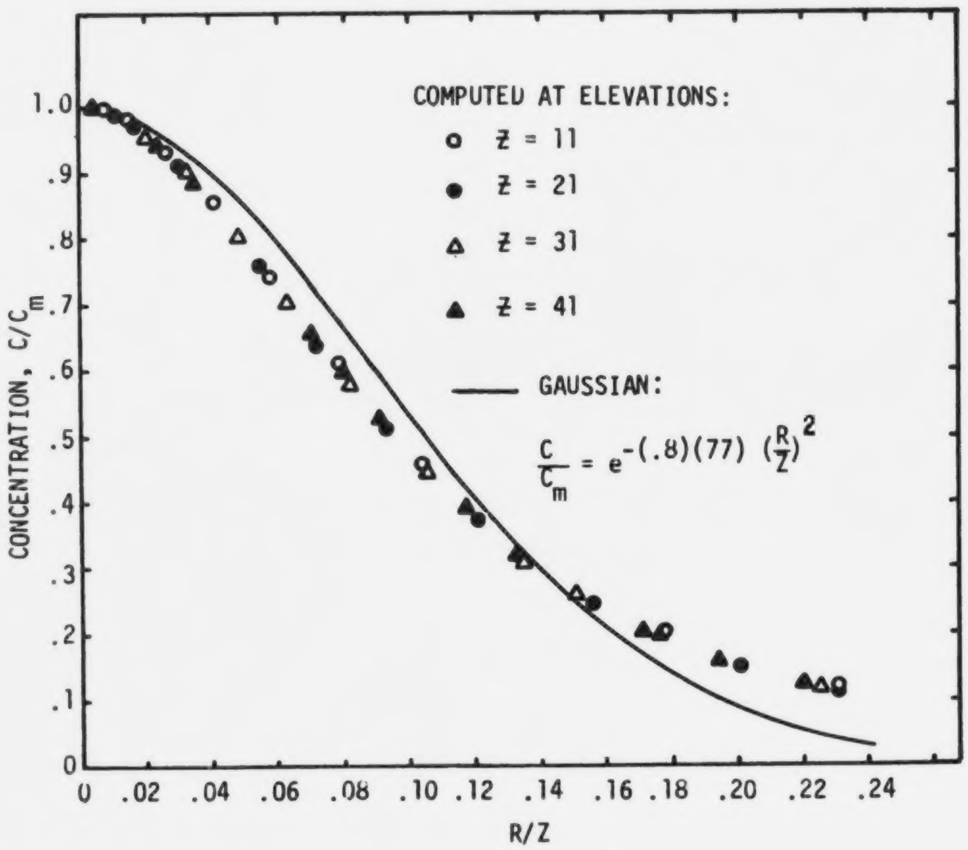

Figure 7.20. Normalized Radial Concentration Distribution, Type 2 Boundary Condition Case 4

for these profiles. As in the case of velocity, concentration is smeared to some extent across the jet boundary.

Figure 7.21 illustrates the vorticity profiles at several locations and Figure 7.22 compares the computed vorticity to the Gaussian vorticity at elevations $\bar{Z} = 11, 31$ and 41. Note that the computed vorticity maxima occur nearer the jet centerline than similar maxima for the Gaussian velocity profile. This fact is also revealed by the experimental velocity data presented in the literature (cf. Figure 7.15).

7.1.1.4 Distribution of Radial Velocity for the Momentum Jet

A typical normalized distributional of radial velocity is illustrated in Figure 7.23 (Case 6). The solid line represents the Albertson et al. theory and the dashed line represents an approximate envelope of their experimental data. Albertson was unable to resolve clearly the difference between the theory and his data. Misinterpretation of the collected data may have been the cause of such a large discrepancy for it hardly seems logical that his theory (based largely on empirical results) could be so far in error. The radial velocities computed in this study show good agreement with Albertson's empirical model, at least over the range of positive velocities. Again, Albertson's data shows gross disagreement with computed and experimental results for the distributions of vertical velocity. The effect of this discrepancy should be revealed most clearly along the jet centerline which is not apparent from results (cf. Figure 7.6).

Figure 7.23 also reveals the similarity of radial velocity. It is difficult to compare computed entrainment rates with the result

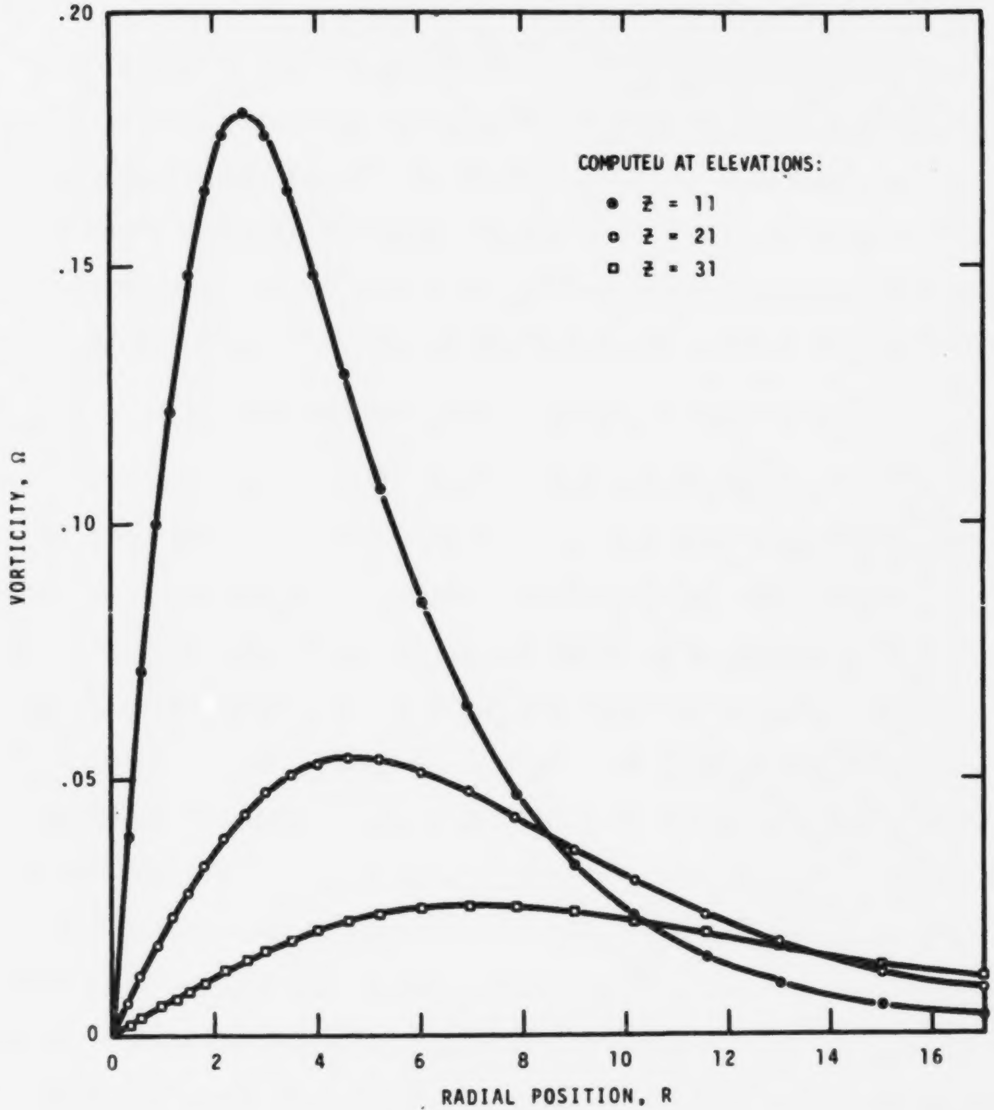

Figure 7.21. Radial Vorticity Distribution for Momentum Jet Type 2 Boundary Condition Case 4

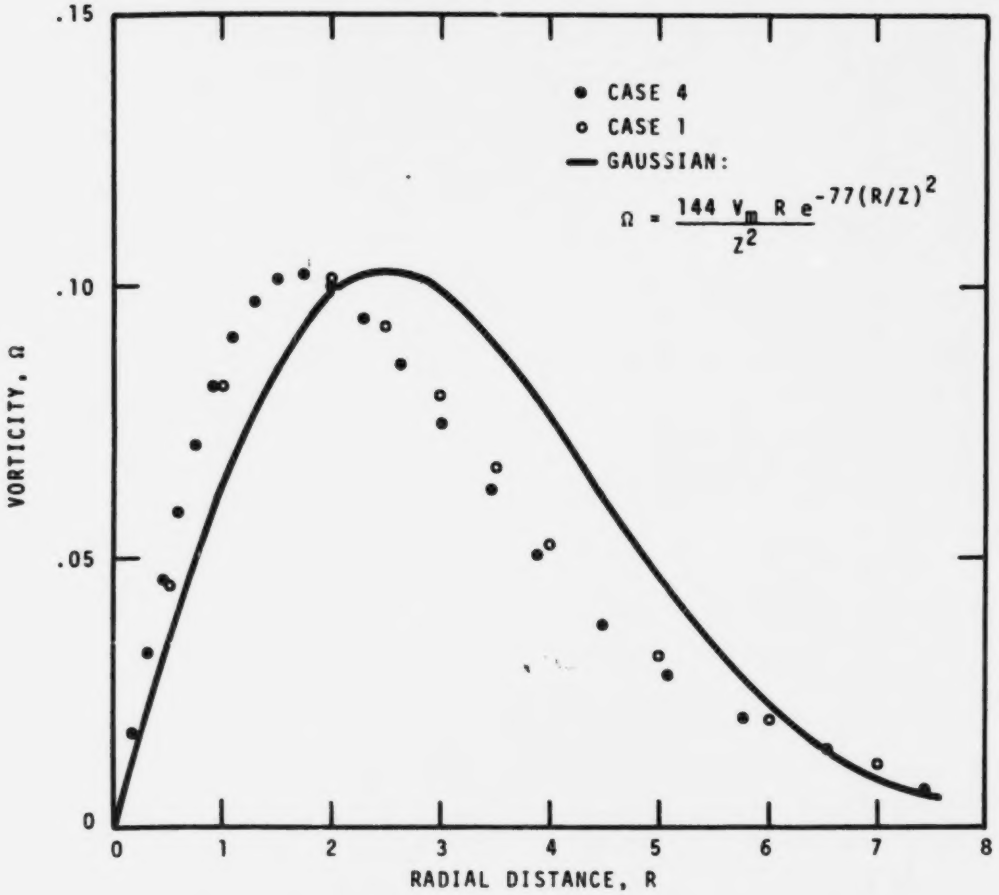

Figure 7.22. Radial Vorticity Distribution for Momentum Jet at $Z = 15$. A Comparison Between Type 1 and 2 Boundary Conditions, and the Gaussian Distribution.

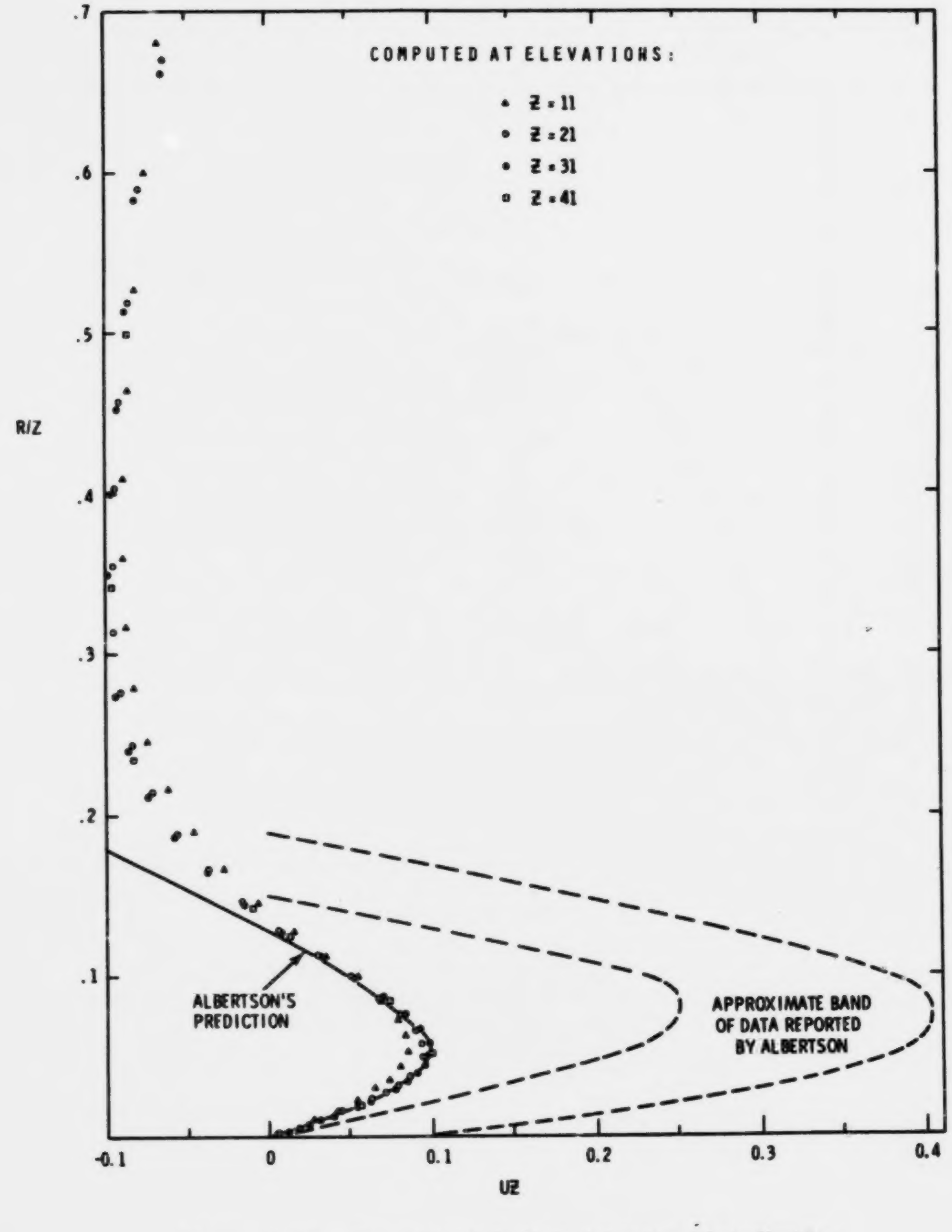

Figure 7.23. Normalized Radial Velocity Distribution for Momentum Jet

given in the literature because we have typically assumed a jet nozzle extending into the fluid, whereas reported data is usually for wall flush jets. In Case 6, this distance is four port diameters. Typical experimental data may be correlated by

$$\frac{Q}{Q_o} = C_1 Z \quad , \tag{7.25}$$

where C_1 is an empirical constant, Q is the total vertical flow at elevation Z, and Q_o is the jet flow. Albertson gives C_1 as .32.

Equation (7.25) indicates a constant entrainment rate for momentum jets, or

$$\frac{dQ}{dZ} = C_1 Q_o . \tag{7.26}$$

Figure 7.24 is a plot of the computed stream function vertical distribution at the inflow-outflow boundary (i.e., $\Psi(R_\infty,Z)$)for Case 6. By definition the differential stream function along this vertical plume is a measure of the entrained flow; that is,

$$\Delta\Psi = - UR\Delta Z. \tag{7.27}$$

The total flow through the plane $Z = 4$ is given by

$$\Psi(R,4) - \Psi(R,0) = 1.919 - 1.0 = .919$$

Based on $Q_o = .919$

$$\frac{Q}{Q_o} = .3(Z-Z_{port}) \tag{7.28}$$

Where $Z_{port} = 4$.

The straight line fit of the computations illustrated in Figure 7.24 is

$$\psi(R_\infty, Z) = .233\ (Z-Z_{port}) + 1.75. \tag{7.29}$$

Then, based on the intercept with $Z = 4$,

$$\frac{Q}{Q_0} = .33\ (Z-Z_{port})\ . \tag{7.30}$$

Hence, using Q_0 as the total of the jet effluent plus entrainment from below the port gives a lateral entrainment rate comparable to the reported work where the fluid issues from a wall-flush jet.

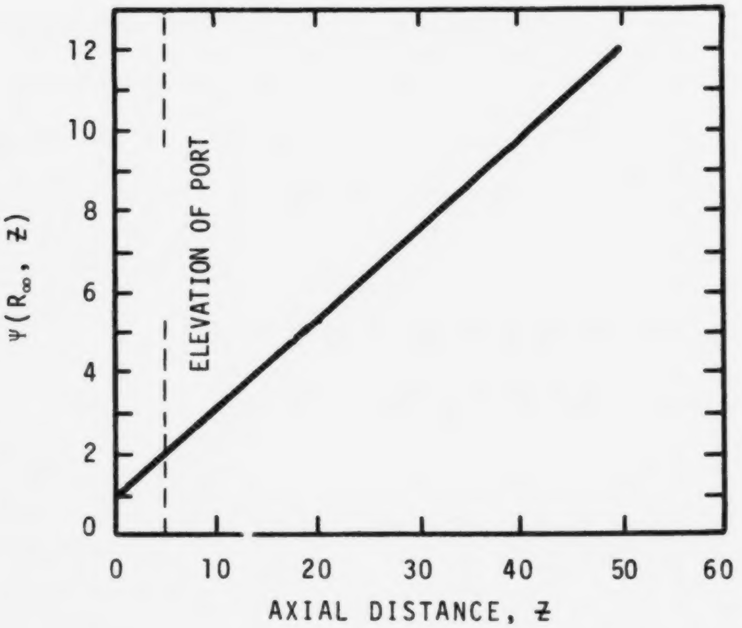

Figure 7.24. Vertical Distribution of Stream Function Ψ, Case 6

7.1.1.5 Typical Contours and Three-Dimensional Plots for a Momentum Jet

Additional information may be obtained by inspecting the level lines and distribution surfaces of the stream function, concentration and vorticity. The centerline and surface streamlines are set at $\Psi = 1.0$. This information is illustrated in Figures 7.25 through 7.31. The three dimensional plots (Figures 7.28 through 7.31) have been arbitrarily scaled to fit a prescribed data box and are valuable for qualitative reasons alone.

7.1.2 Two Cases of Pure Buoyancy

To check the computer program and computational techniques where buoyancy is the sole driving force, two cases were run where the outfall port or jet was replaced by a heat source (see Table 7.2). In the case of pure buoyancy, we are checking the same general features of the plume as in the case of the momentum jet. However, there is much less information published. Here we check the computed

- Centerline velocity and temperature,
- Radial distribution of axial velocity and temperature, and
- Rate of plume spread

for a very weak and intermediate strength buoyant source. Both cases are well within the validity of the Boussinesq approximation. Solution restrictions are the same as those pointed out in Section 7.1.1.

7.1.2.1 Centerline Velocity and Temperature

For a purely buoyant source (and also for effluent cases where $F_0 = 0$) it has been established by Rouse et al. [8]] and Schmidt [85]

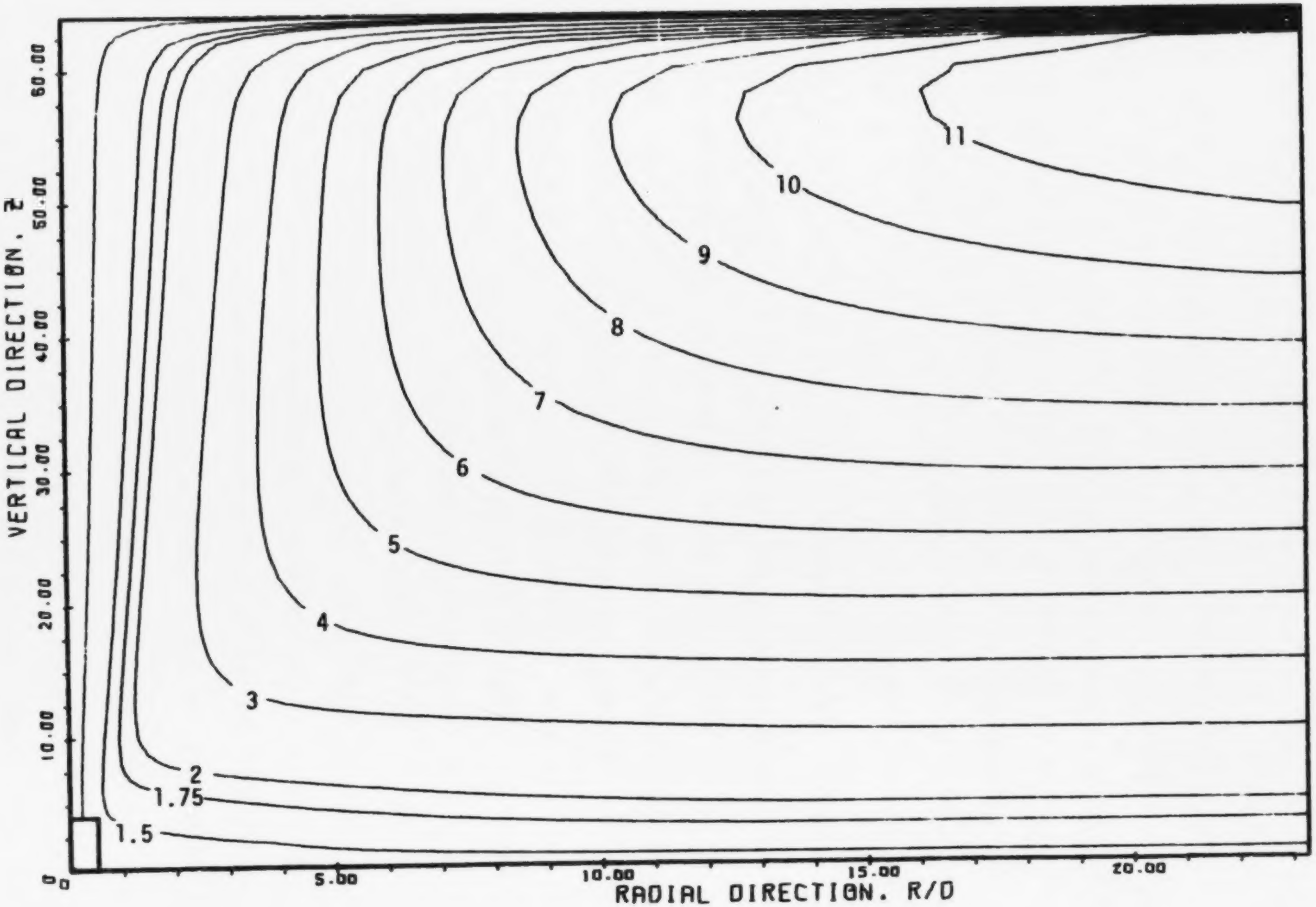

FIGURE 7.25. STREAMLINES FOR CASE 6 -- MOMENTUM JET

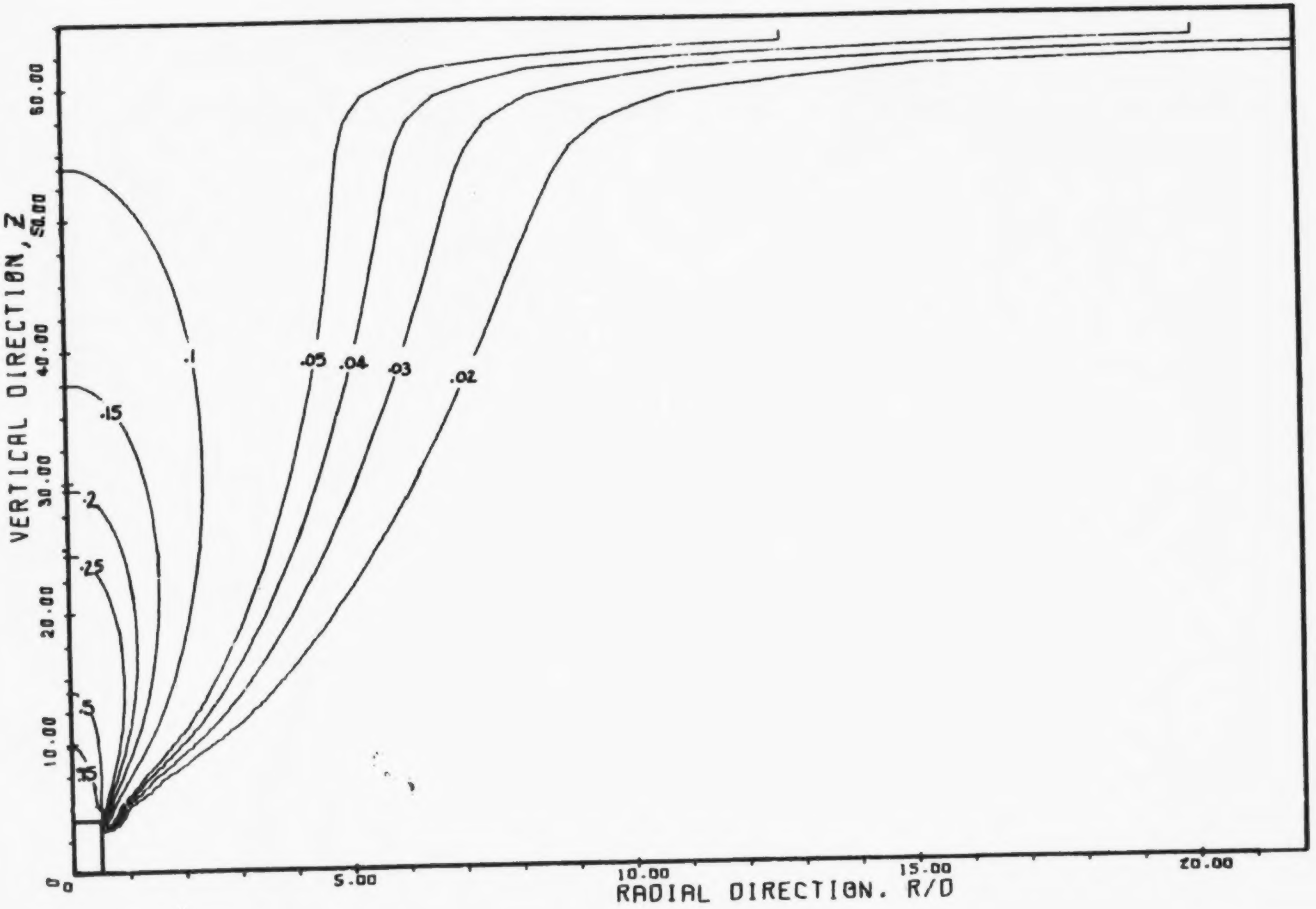

FIGURE 7.26. ISOPYCNALS FOR CASE 6 -- MOMENTUM JET

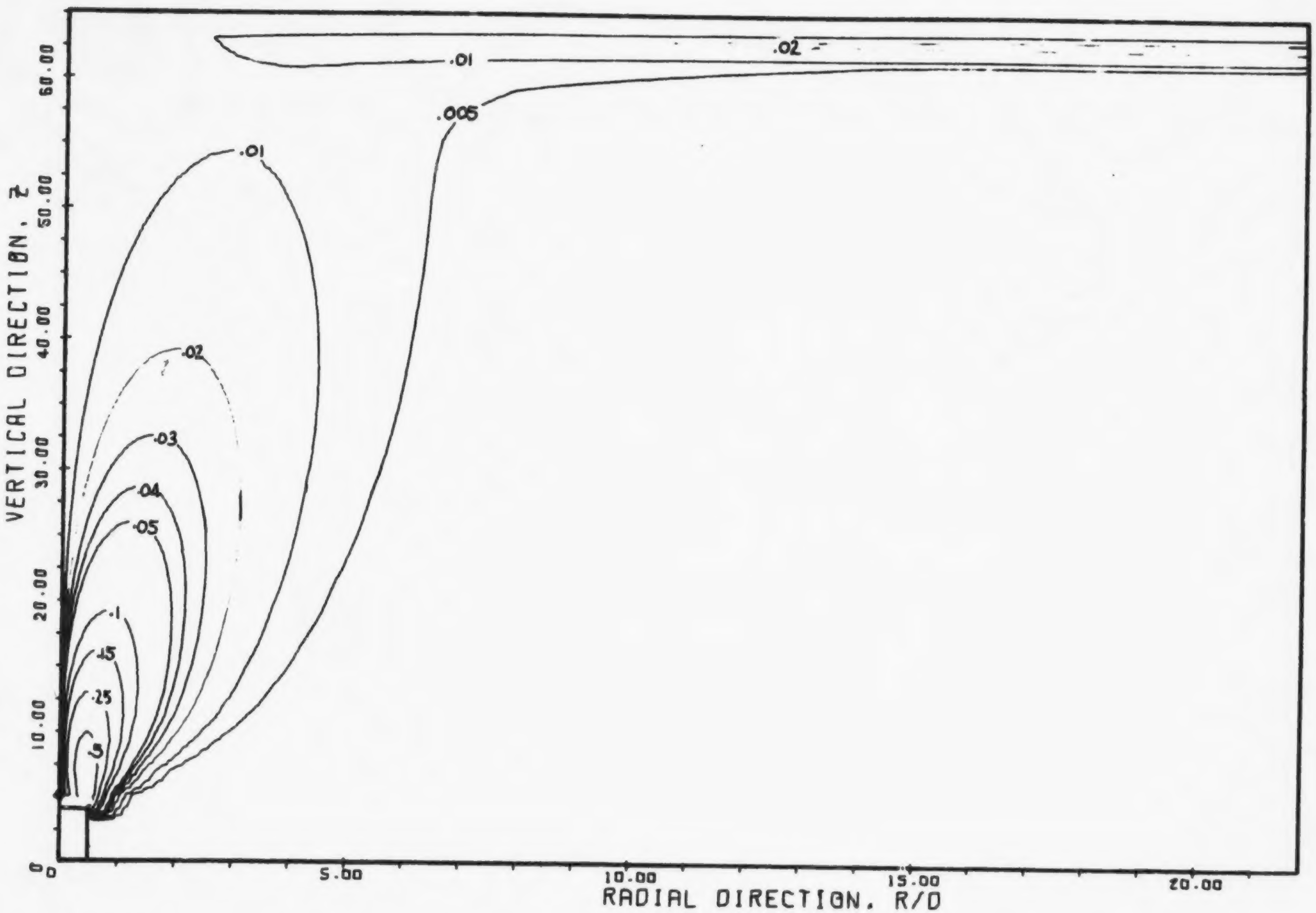

FIGURE 7.27 VORTICITY LEVEL LINES FOR CASE 6 -- MOMENTUM JET

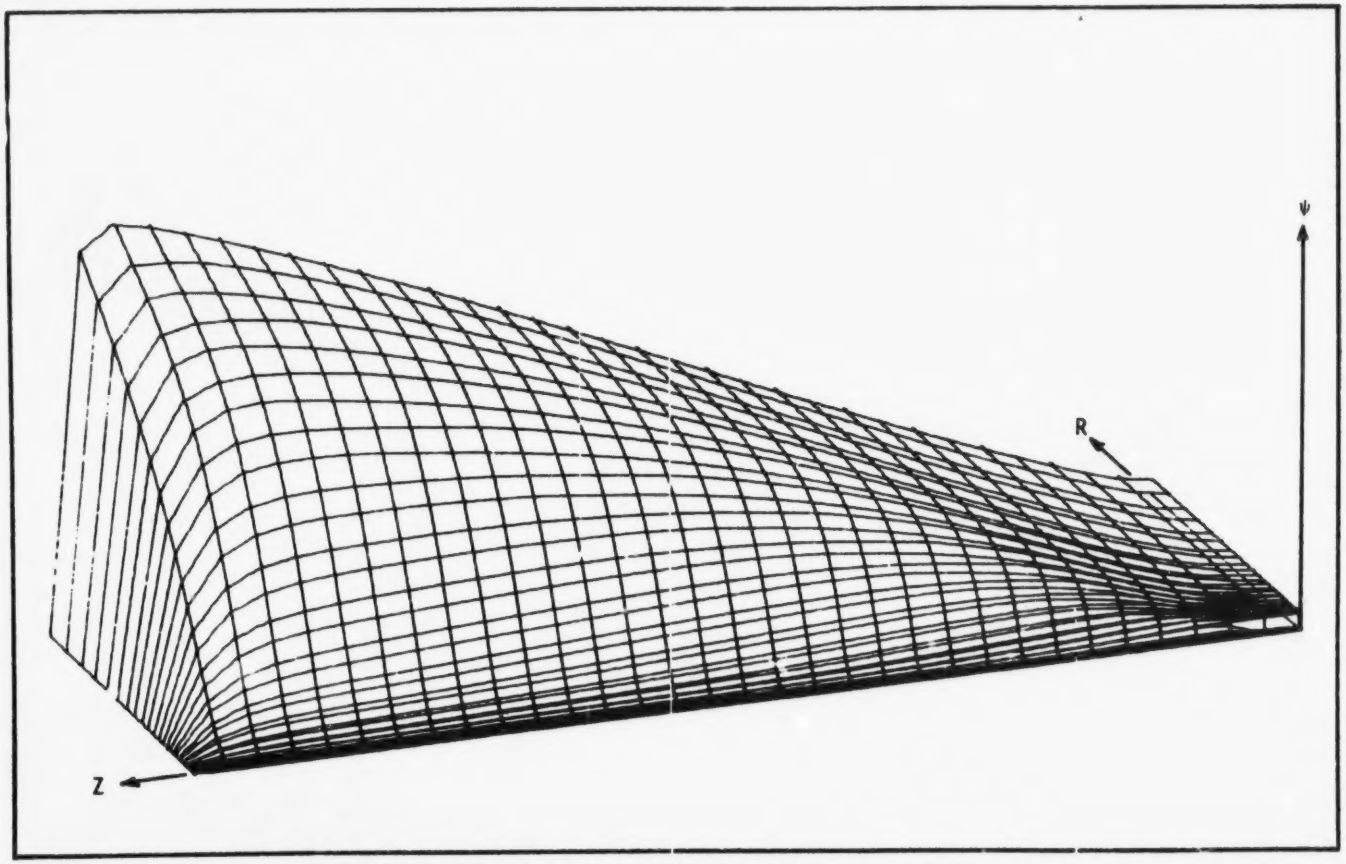

FIGURE 7.28. 3D ILLUSTRATION OF STREAM FUNCTION -- PSI. CASE NO. 6

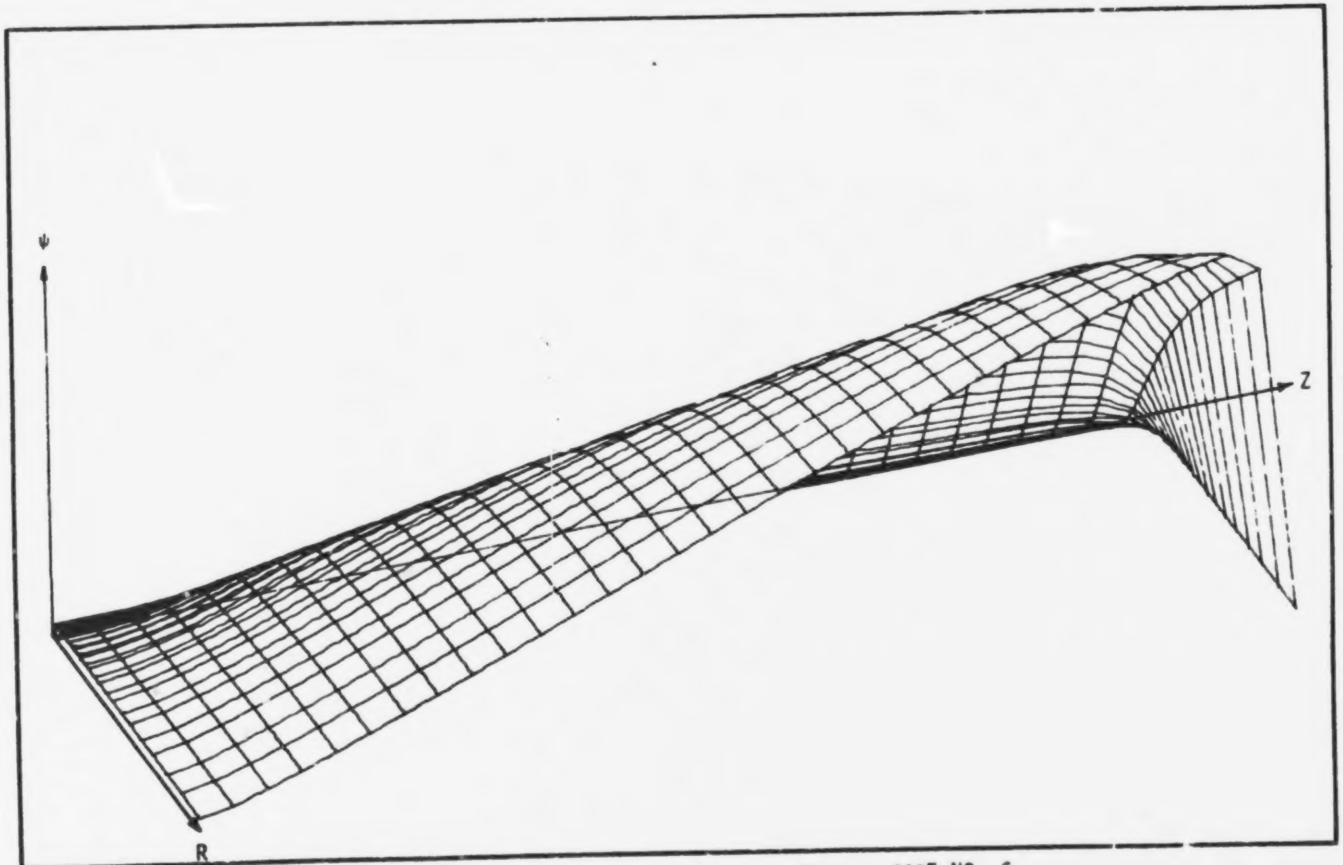

FIGURE 7.29. 3D ILLUSTRATION OF STREAM FUNCTION -- PSI. CASE NO. 6

CASE - DEEP WATER MOMENTUM JET - V(R,0) = (1-R)**(1/10)

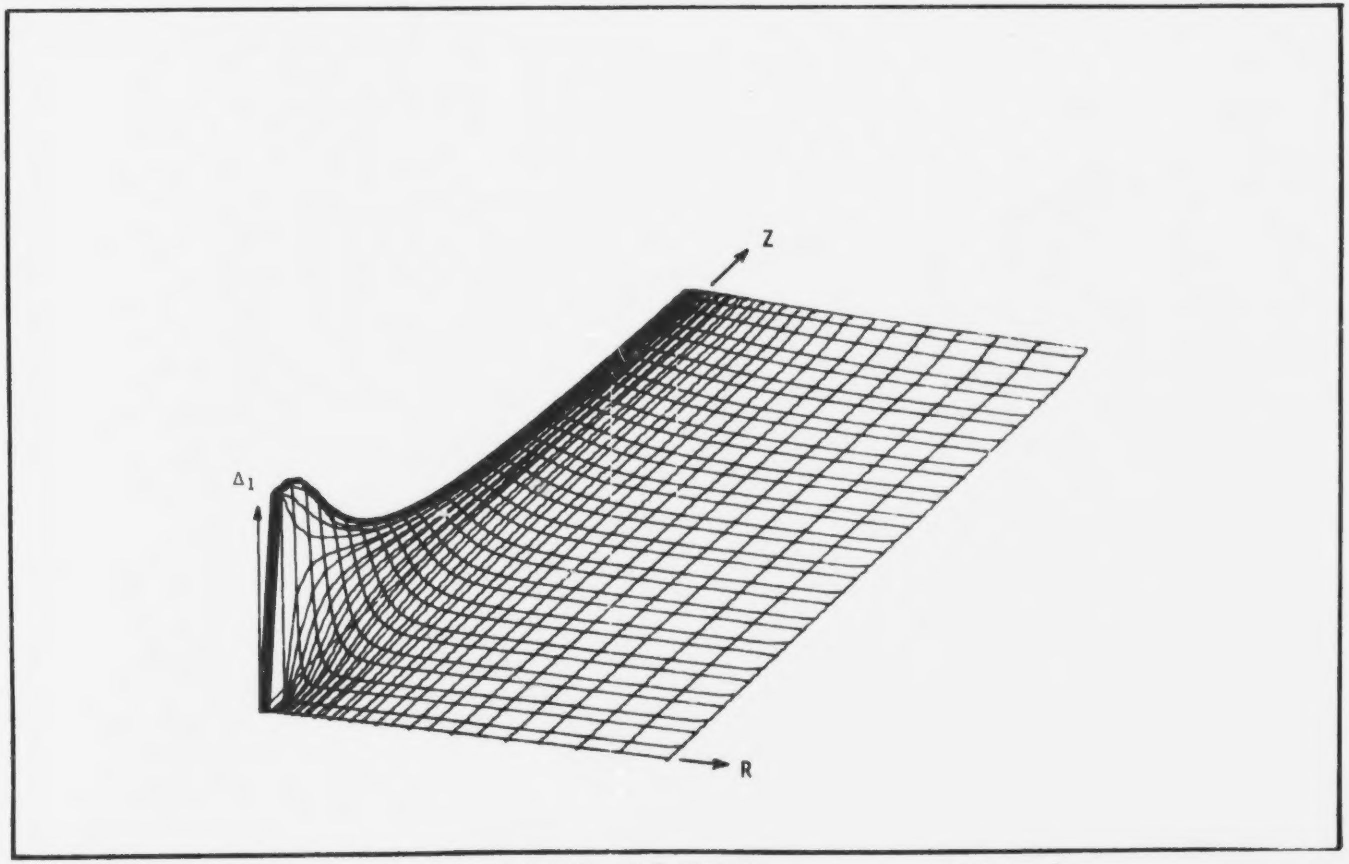

FIGURE 7.30. 3D ILLUSTRATION OF BUOYANCY DISTRIBUTION - Δ_1 CASE NO.6

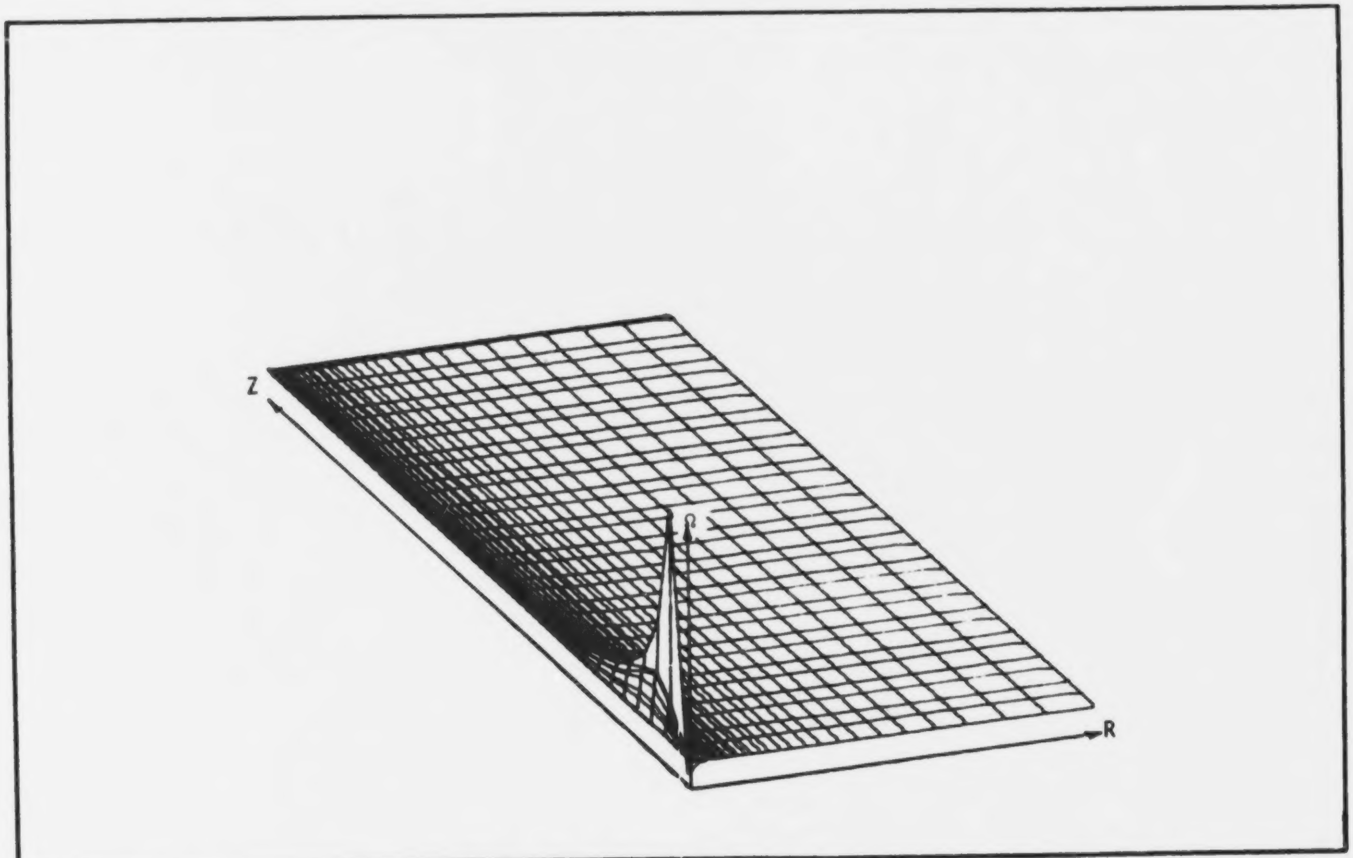

FIGURE 7.31. 3D ILLUSTRATION OF FLUID VORTICTY - OMEGA. CASE NC. 6

that

$$V_m \simeq Z^{-1/3} \tag{7.31}$$

and

$$\Delta T_m \simeq Z^{-5/3} \tag{7.32}$$

In the case of an effluent with little initial momentum and strong buoyancy, Abraham [1] gives

$$V_m = 4.4(F_o Z)^{-1/3} \tag{7.33}$$

$$\Delta T_m = 9.5\ F_o^{\ 1/3}\ Z^{-5/3} \tag{7.34}$$

based on Rouse's data.

Figure 7.32 illustrates the centerline velocity and temperature for Case 13. In this case, the source is very weak and gives a maximum fluid temperature rise of only .95 °C. The maximum velocity is a little above .09 ft/sec occurring at an elevation of about seven source diameters above the source. The flow apparently does not become established until an elevation of 15 to 20 diameters has been reached. Above this approximate region the computed centerline velocity shows decay very closely approximating the -1/3 law given by Equation 7.31. Velocities computed above $Z = 50$ (surface at $Z = 64$) show influence of the free surface.

Temperature decay, on the other hand, begins to follow Equation (7.32) at approximately $Z = 10$ and computed values are extremely close to a - 5/3 slope. However, there is no apparent surface effect on temperature, whereas Case 14 (Figure 7.33) reveals noticeable change

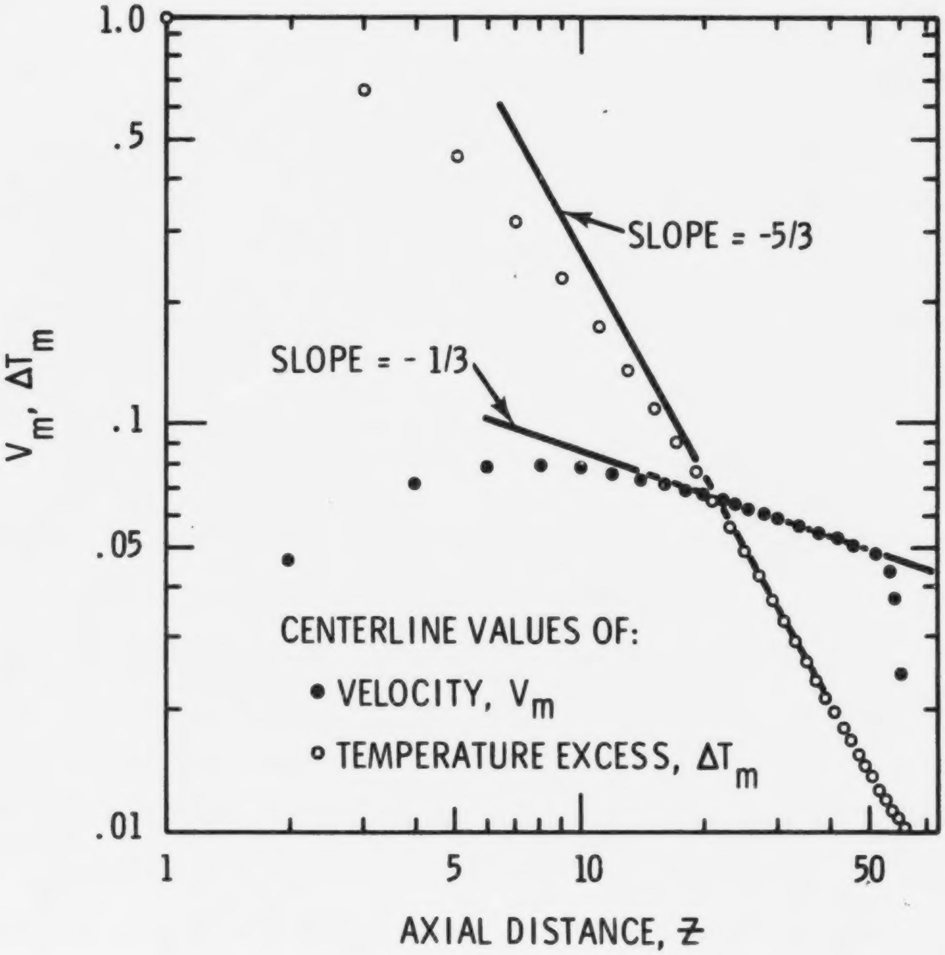

Figure 7.32 Computed Centerline Velocity and Temperature Excess for Case 13. Pure Buoyancy, $F_o = 0$.

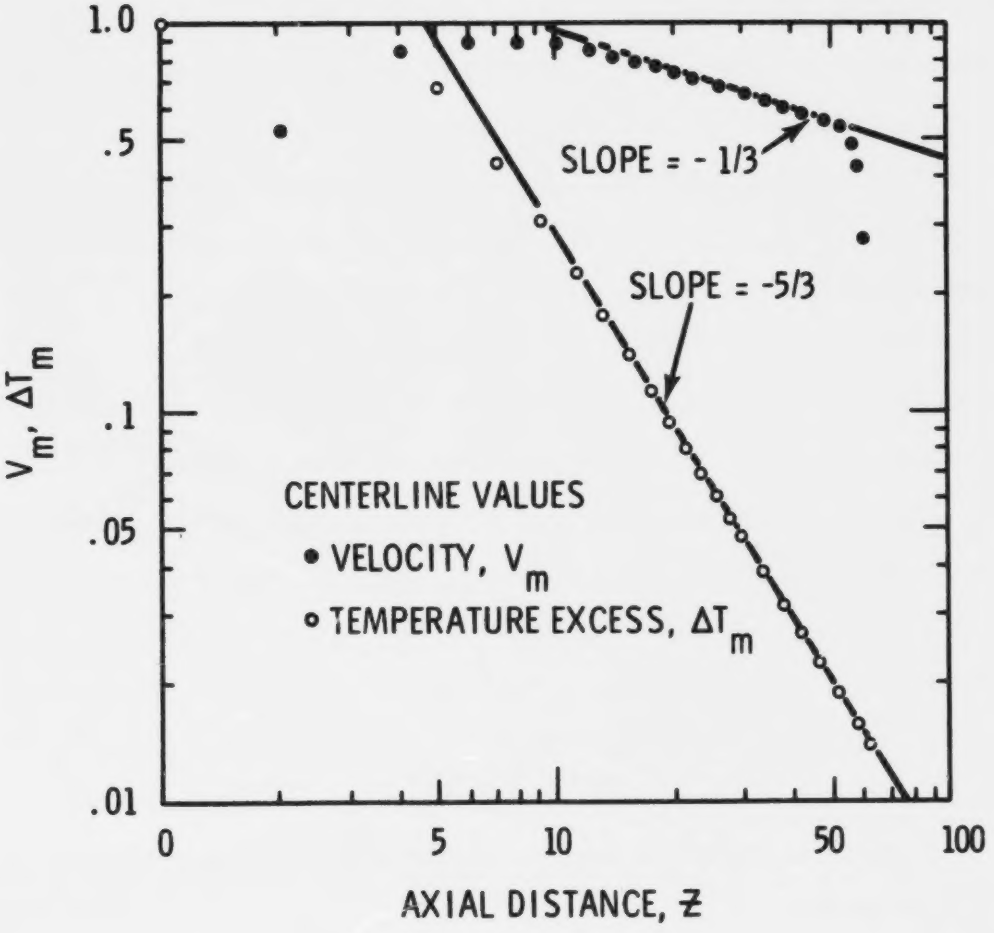

Figure 7.33. Computed Centerline Velocity and Temperature Excess for Case 14. Pure Buoyancy, $F_o = 0$.

in slope near the surface. It is felt that continued iteration would have shown somewhat larger deviation from the -5/3 slope near the surface in both of these cases.

Figure 7.33 (Case 14) illustrates similar results for a situation where the fluid directly in contact with the heat source was maintained at a 25 ^{o}C temperature rise. Under these conditions the maximum velocity was about 0.8 ft/sec occurring at approximately 8 diameters above the source. The shape of the centerline velocity distribution is very nearly the same as in Case 13 and achieves the -1/3 slope at approximately 20 diameters above the source. The temperature distribution, however, shows some differences in that the -5/3 decay is not attained until about 20 diameters and, as mentioned previously, there is demonstrated a marked surface effect. Results for both of these cases could be improved somewhat by continued iteration in the vicinity of the surface. Convergence was slow in this region for both runs, but temperature changes indicated an increased surface effect. Another aspect is that vertical turbulence has been essentially neglected, a poor assumption in the surface effects region. A realistic approximation of vertical turbulence here would also tend to increase the surface temperature.

7.1.2.2 Spread of the Pure Buoyant Plume

The rate of spread of the half radius, $r_{1/2}$, for pure buoyancy is demonstrated in Figure 7.34 for Case 13. Case 14 was found to be essentially identical to Case 13. Based on Rouse's data, Abraham ascertained that the half radius is approximated by

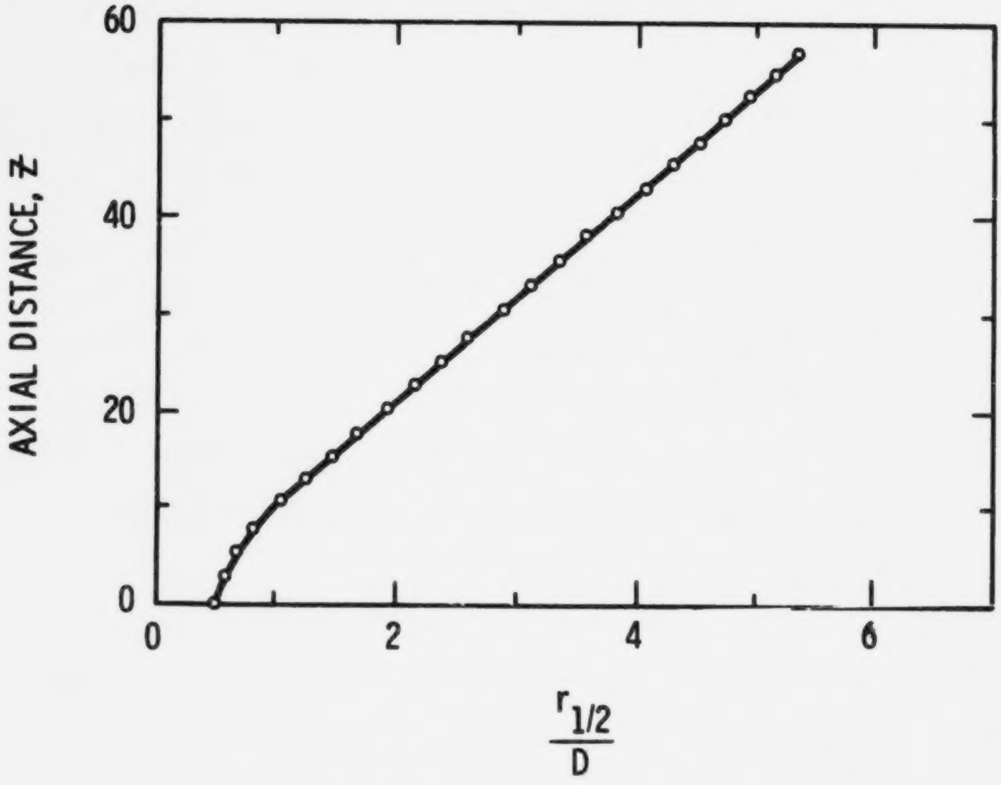

Figure 7.34. Computed Rate of Spread of Half-Radius, $r_{1/2}/D$. Pure Buoyancy, Case 14 ($D=2r_o$)

$$\frac{r_{1/2}}{D} = \sqrt{\frac{.69}{K}}\ Ƶ = .0866\ Ƶ \qquad (7.35)$$

where K = 92.

The data obtained by Rouse revealed K = 96, at least for the selected curve fit. Abraham's theory and experiments yield K = 92, and according to him, no major discrepancy in results is obtained in either case. Figure 7.34 reveals a computed spread of approximately

$.092\, z$. Not only is this rate of spread different from the rate based on a Gaussian profile, but the rate is greater than in the case of pure momentum ($r_{1/2}/D \simeq$ was computed). Gaussian profiles show the opposite to be true. The reason for these discrepancies has not been completely resolved.

Barring difficulties with the computer code, which has been checked, the discrepancy may be caused by incorrect modeling of the turbulence in the presence of buoyancy. It is also possible that the data obtained from flame sources in air may be significantly influenced by effects not accountable through the Boussinesq approximations. That is, the Boussinesq approximation would not be valid for modeling plumes over diffusion flame plumes because of the large density variations compared to the reference density, even though temperature will decay quite rapidly. In both Cases 13 and 14, the density variations may influence the rate of spread and explain the present discrepancy. Additional data for a low Froude number flow case is presented in Section 7.1.3.2.

7.1.2.3 Radial Distribution of Vertical Velocity, Temperature and Vorticity for Pure Buoyancy

The data obtained by Rouse and Schmidt demonstrate that the normal distribution curve again fits the buoyant plume radial profiles quite well.

In this case, data obtained by Rouse gives

$$V = V_m e^{-K(\frac{R}{Z})^2} \qquad (7.36)$$

where K = 96, and

$$\Delta T = T_m e^{-\lambda K(\frac{R}{Z})^2} \qquad (7.37)$$

where

$$\lambda = .74.$$

However, the Gaussian curves used for comparisons here will be based on Abraham's value of K = 92 which yields $\lambda K = 68.1$. As in the case of the momentum jet, these distributions have no theoretical basis, but are a result of curve fitting.

Radial distributions for Case 13 are illustrated in Figures 7.35, 7.36 and 7.37, for various elevations. Computed results show excellent similarity at all elevations except near the source (Figures 7.35 and 7.36).

Figure 7.37 shows the velocity profiles for Case 13 as computed. Figure 7.38 again shows excellent similarity at all elevations except near the source for Case 14.

A normalized temperature profile is illustrated in Figure 7.39 and vorticity at various elevations is plotted in Figure 7.40. One notable feature revealed by Figure 7.39 is that the temperature distribution is in considerably closer agreement with the Gaussian curve in the case of a momentum jet (cf. Figure 7.20).

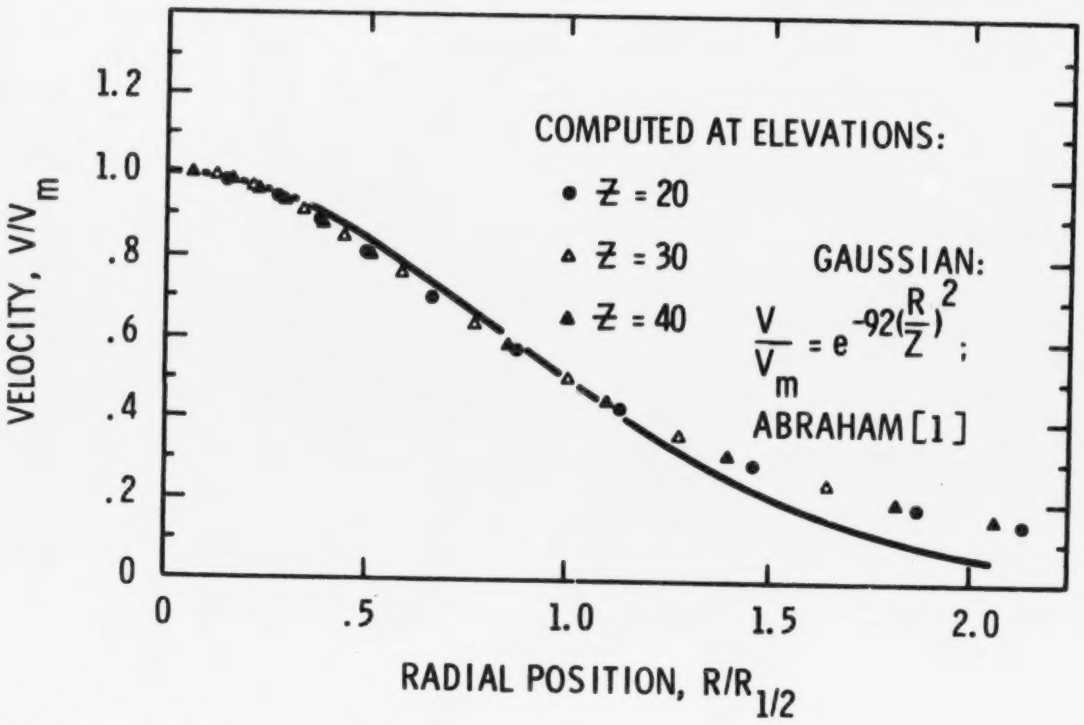

Figure 7.35. Normalized Distribution of Computed Axial Velocity. Pure Buoyancy, Case 13

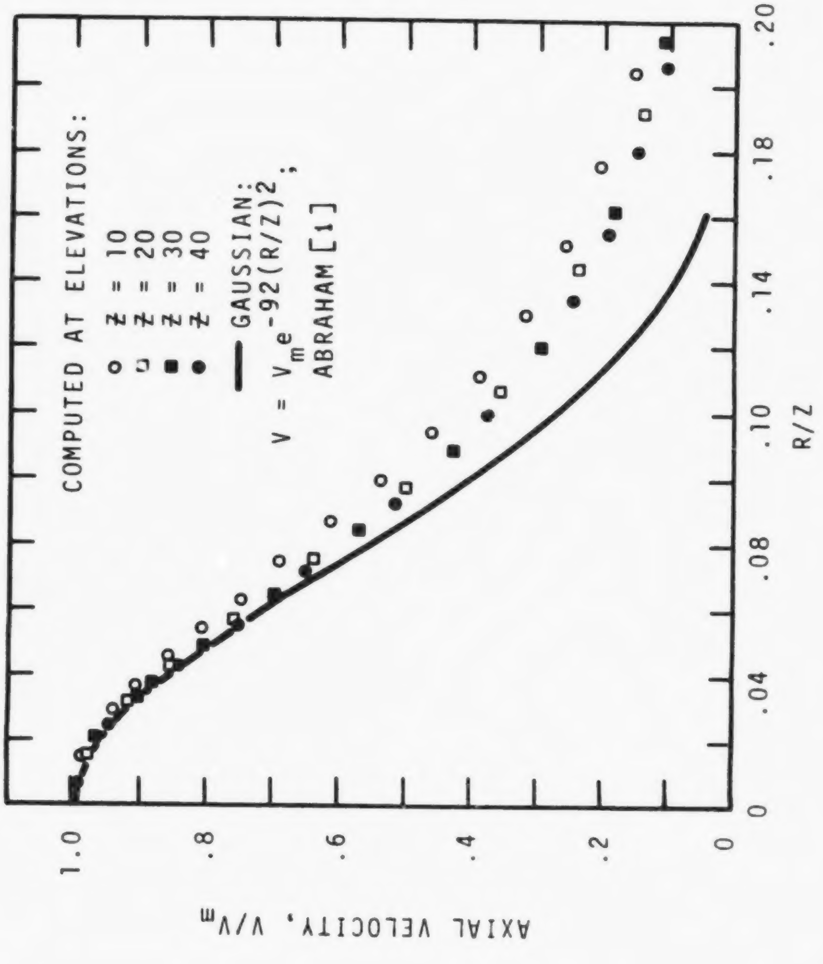

Figure 7.36. Normalized Radial Distribution of Axial Velocity, Pure Buoyancy, Case 13

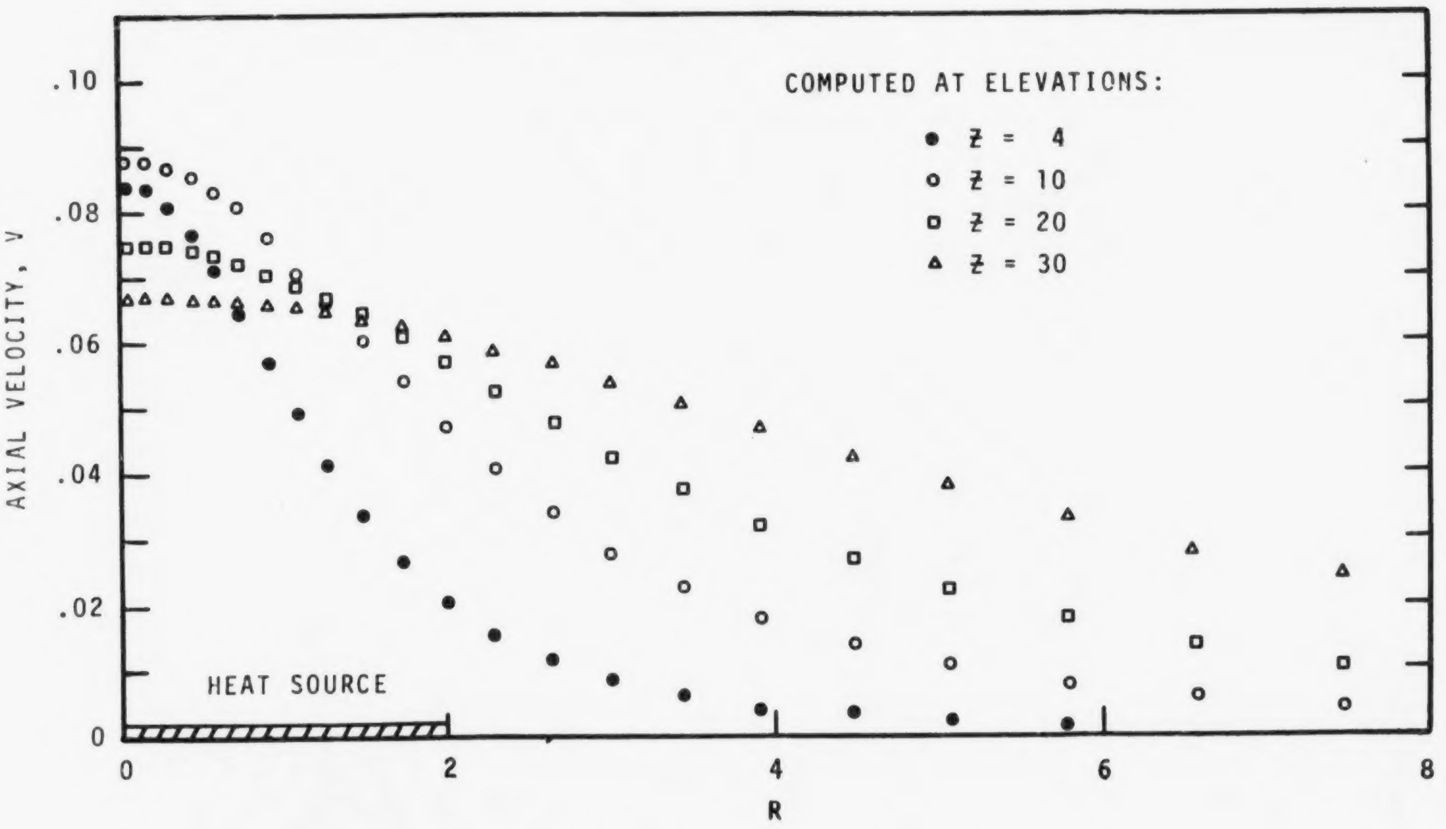

Figure 7.37. Radial Distribution of Axial Velocity in Pure Buoyancy, Case 13

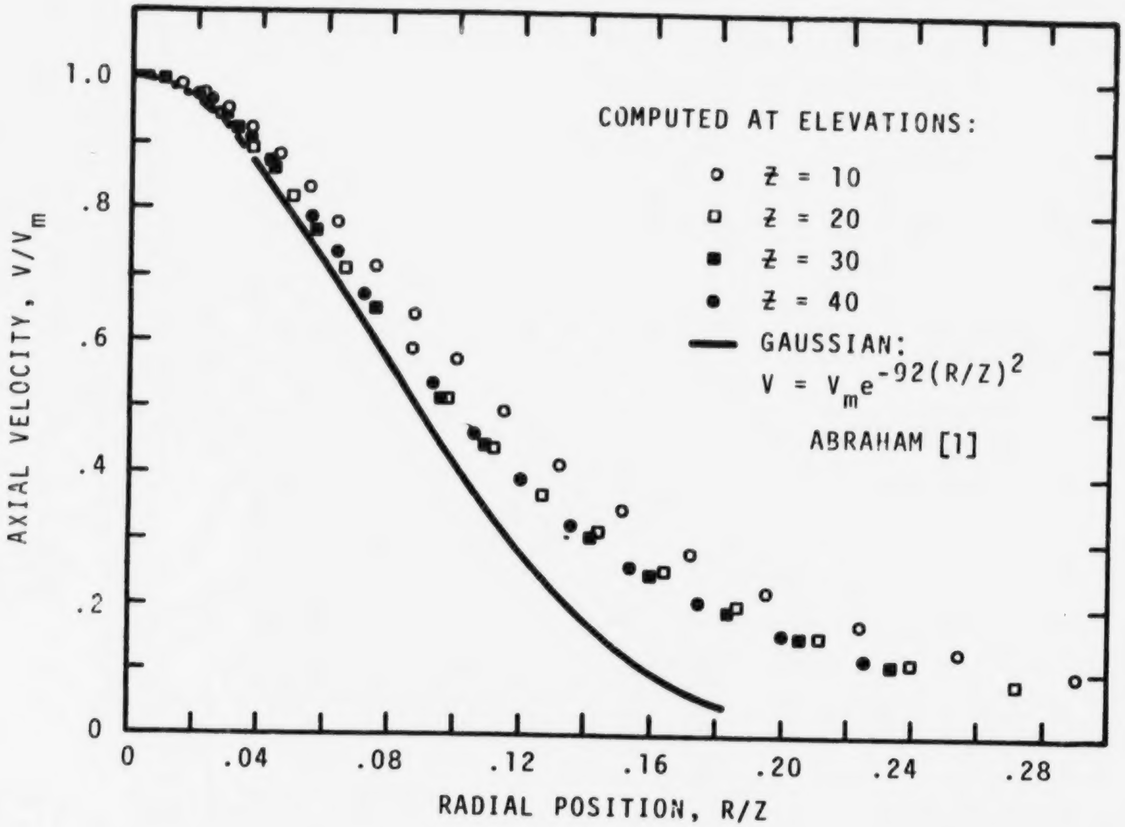

Figure 7.38. Normalized Radial Distribution of Axial Velocity. Stronger Source, Pure Buoyancy, Case 14.

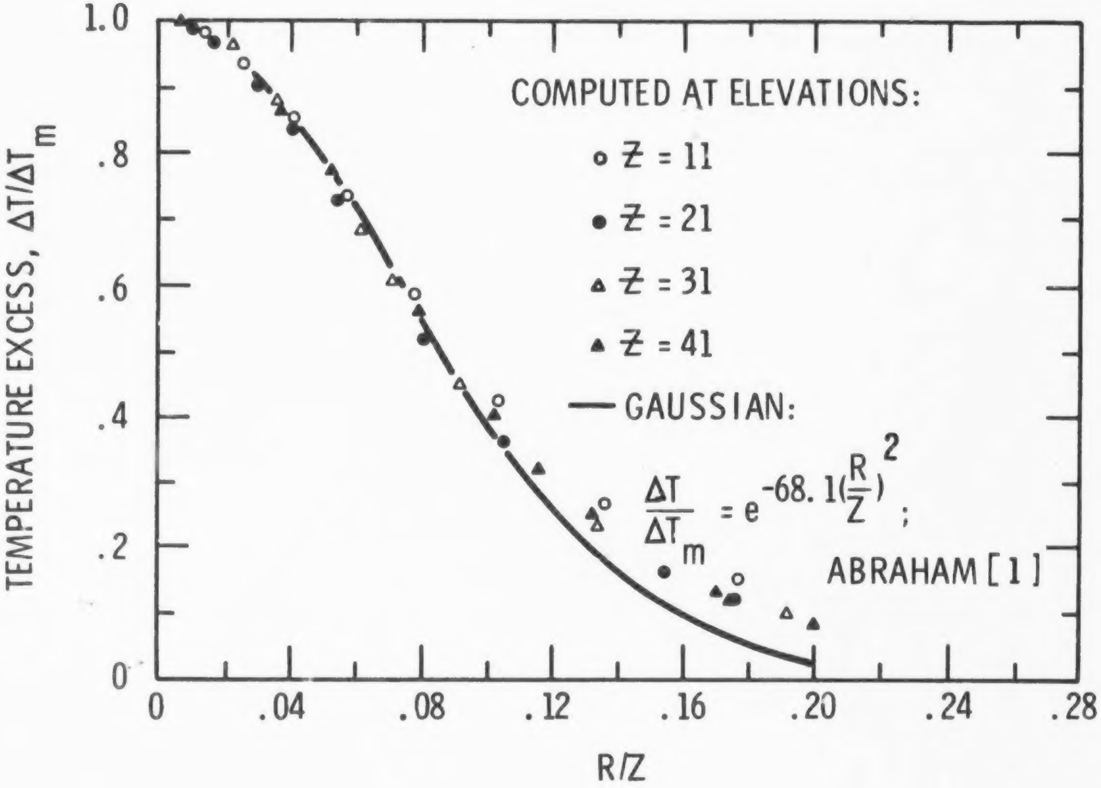

Figure 7.39. Normalized Distribution of Computed Radial Temperature Excess. Pure Buoyancy, Case 14.

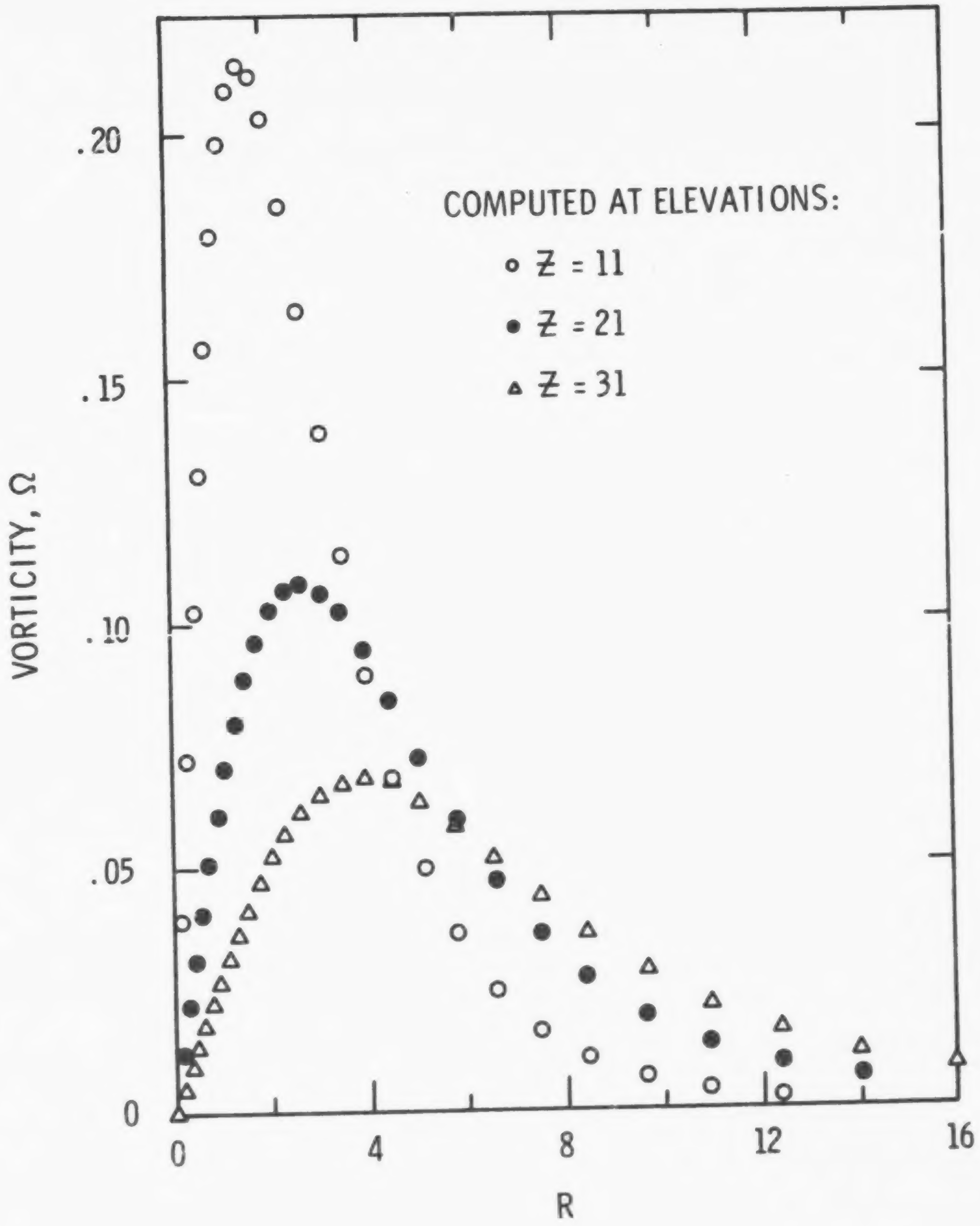

Figure 7.40. Radial Distribution of Vorticity.
Pure Buoyancy, Case 14.

7.1.2.4 Radial Velocity and Entrainment for Pure Buoyancy

The normalized distribution of radial velocity for Case 14 is given in Figure 7.41. As opposed to momentum jet results (Figure 7.23), similarity of the radial flow is not apparent using the coordinates R/Z and $U\bar{Z}$. Also note that, compared to the corresponding momentum jet data, the magnitude of negative radial flow is somewhat larger, indicating an increased radial entrainment rate. Although it has not been plotted, the radial flow below about six source diameters is negative over the entire flow field.

From similarity theory it has been established (cf. Abraham) that

$$\frac{dQ}{d\bar{Z}} = C_1 V_m \bar{Z}. \qquad (7.38)$$

By Equation (7.31)

$$\frac{dQ}{d\bar{Z}} = C_2 \bar{Z}^{2/3}. \qquad (7.39)$$

Then integrating Equation (7.39) yields

$$Q = C_3\, \bar{Z}^{5/3}. \qquad (7.40)$$

The values C_1, C_2 and C_3 are appropriate constants; magnitudes are unimportant since we are interested only in how Q varies with $\bar{Z}$. Figure 7.42 illustrates the value of $\Psi(R_\infty, \bar{Z})$ as a function of $\bar{Z}$, and since $\Psi(R_\infty, \bar{Z})$ is directly proportional to the entrainment Q, this plot reveals the variation of Q with $\bar{Z}$ for pure buoyancy. The computed data in Figure 7.42 is obviously represented by a functional relationship more complicated than Equation (7.40). At lower elevations ($Z \simeq 6$ to 15)

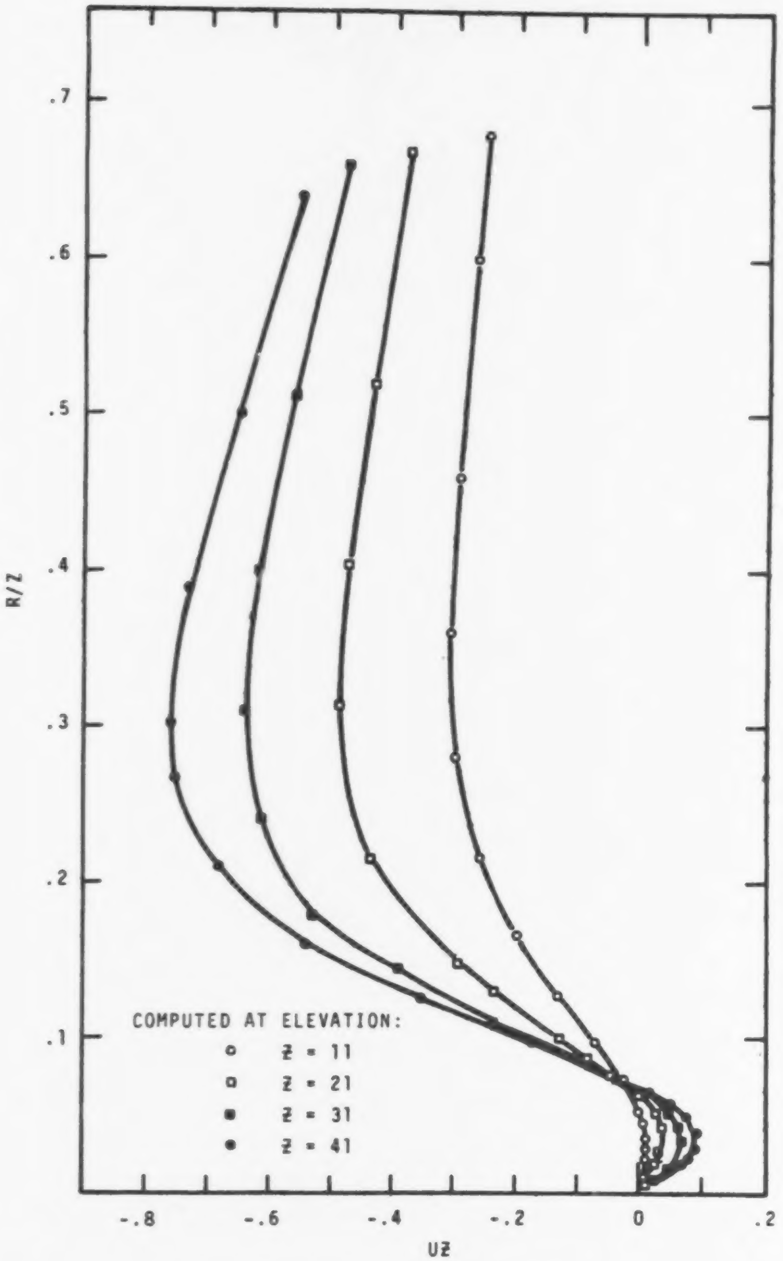

Figure 7.41. Normalized Radial Velocity Distributions for Pure Buoyant Plume, Case 14

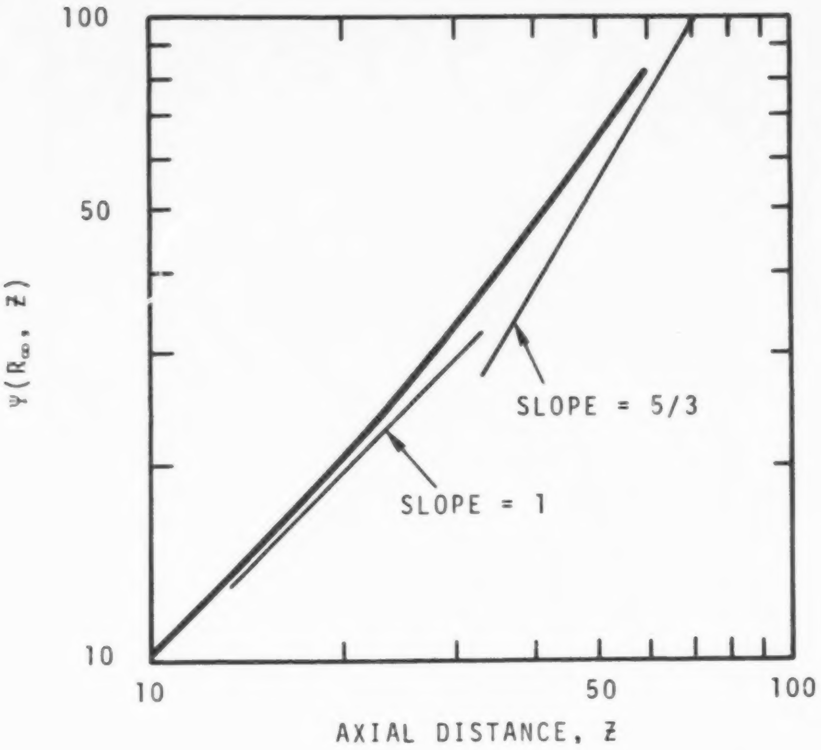

Figure 7.42. Vertical Distribution of Stream Function at R_∞. Pure Buoyancy, Case 14

$$Q \sim \bar{z}. \tag{7.41}$$

Thus, in this range the plume entrains ambient fluid proportional to a momentum jet. The 5/3 slope is never indicated by the data, but Figure 7.42 shows that the entrainment data would apparently approach a 5/3 slope asymtotically for sufficient depth.

Figures 7.43 through 7.45 illustrate streamlines, isotherms and vorticity level lines for Case 14. As in all cases reported, the centerline value of the stream function is 1.0. Three-dimensional illustrations of the same information is displayed in Figures 7.46 - 7.48.

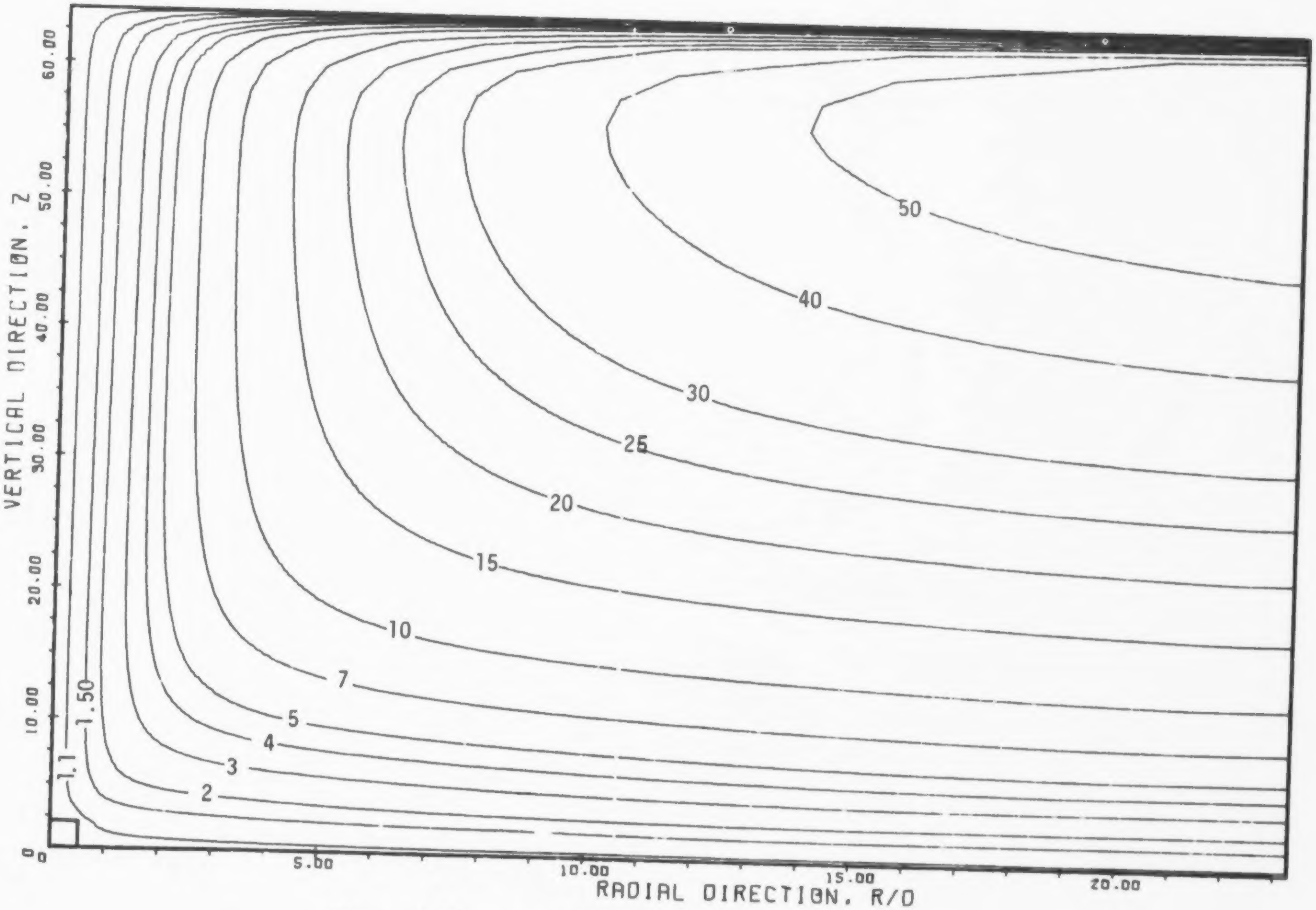

Figure 7.43. Streamlines for Case 14, Pure Buoyancy

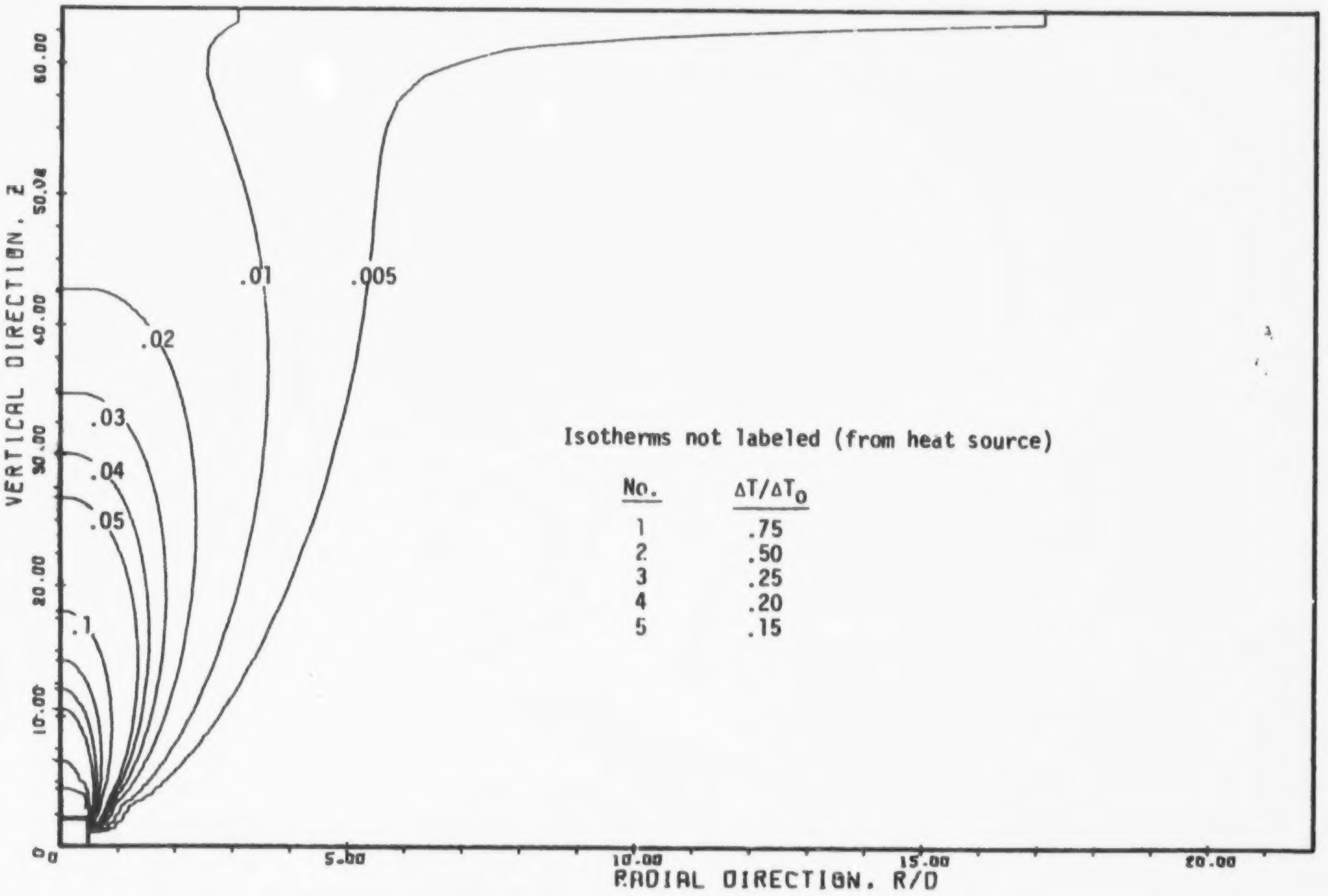

Isotherms not labeled (from heat source)

No.	$\Delta T/\Delta T_o$
1	.75
2	.50
3	.25
4	.20
5	.15

Figure 7.44. Isotherms for Case 14, Pure Buoyancy, $\Delta T/\Delta T_o$

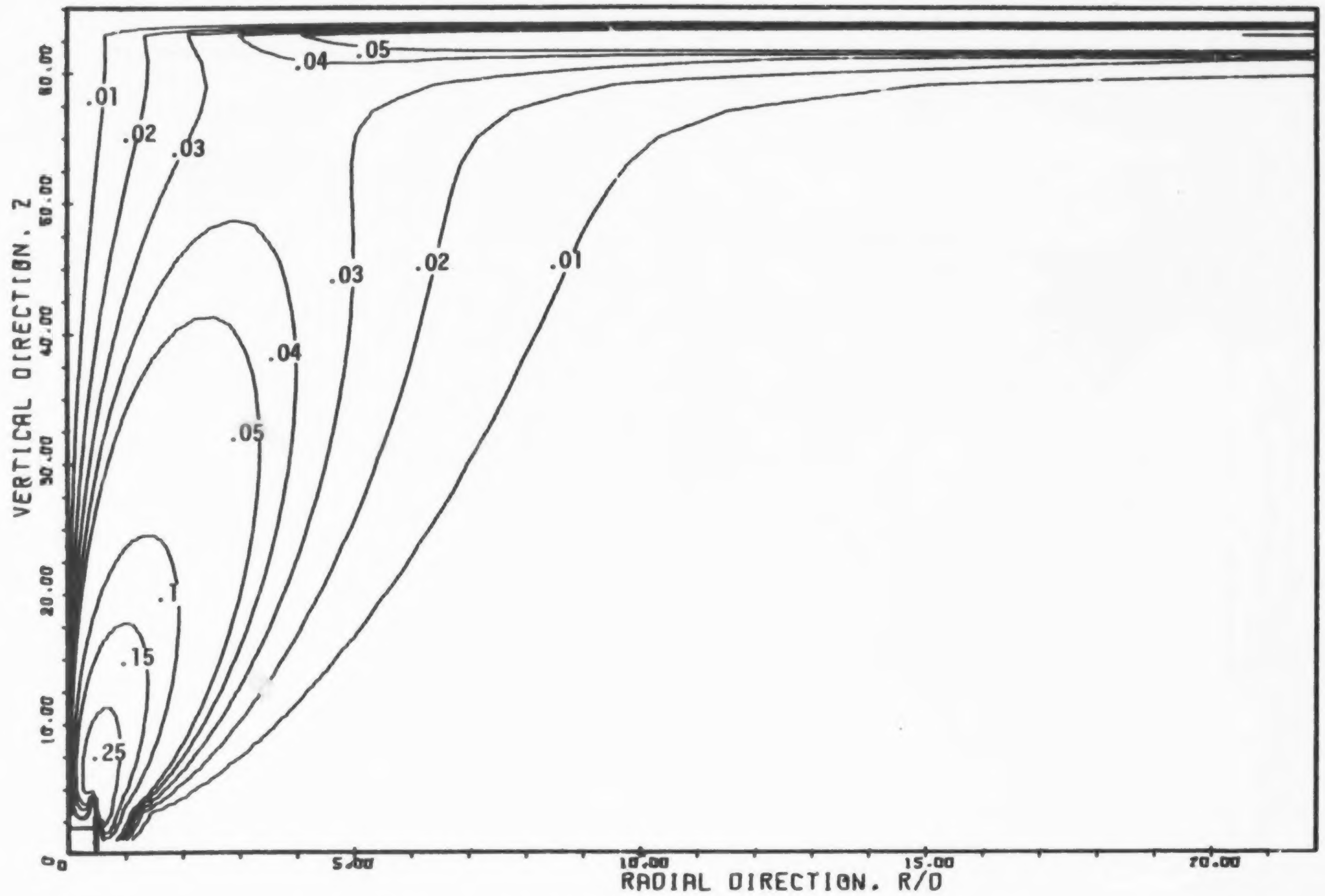

Figure 7.45. Vorticity Level Lines for Case 14, Pure Buoyancy

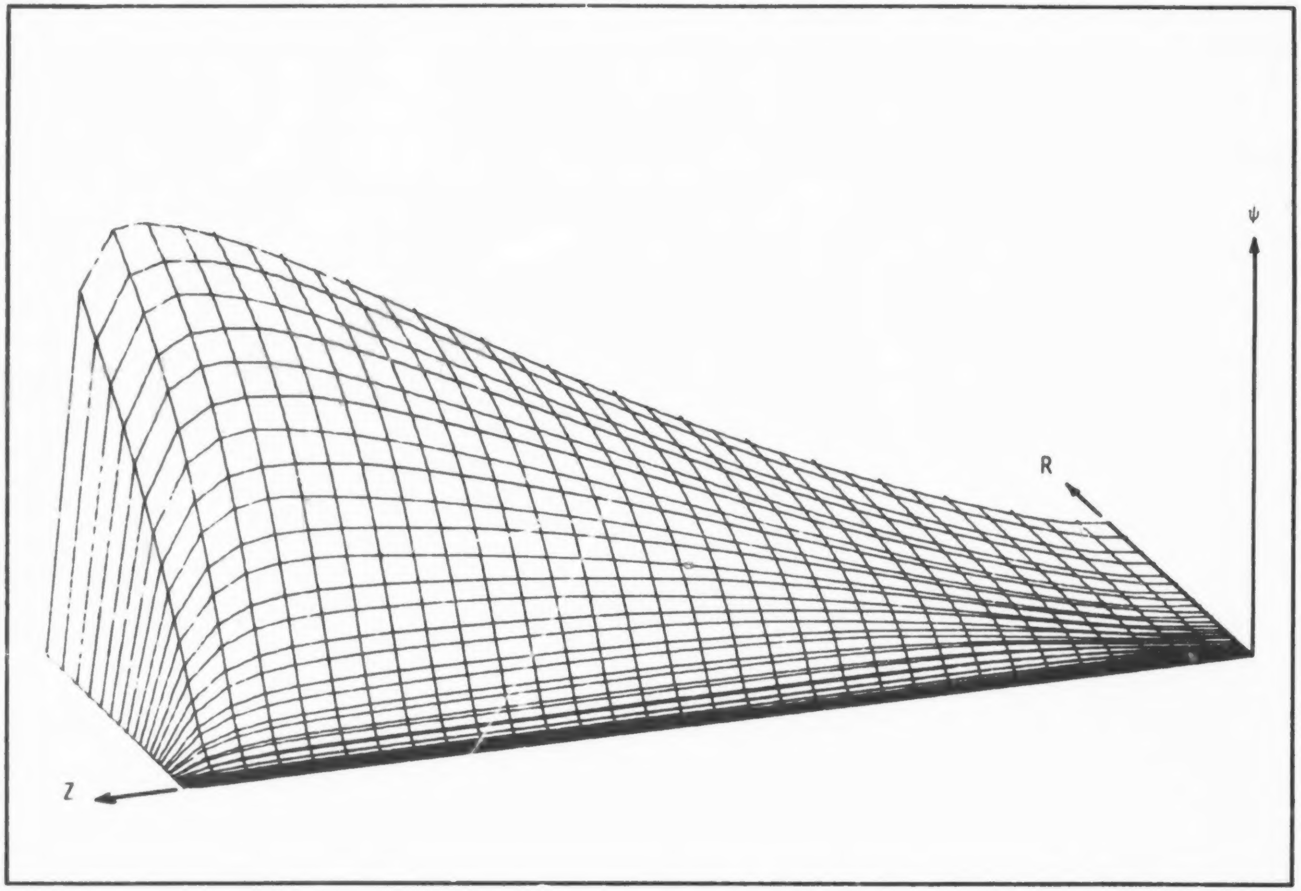

Figure 7.46. 3D Illustration of Stream Function - PSI, Case No. 14.

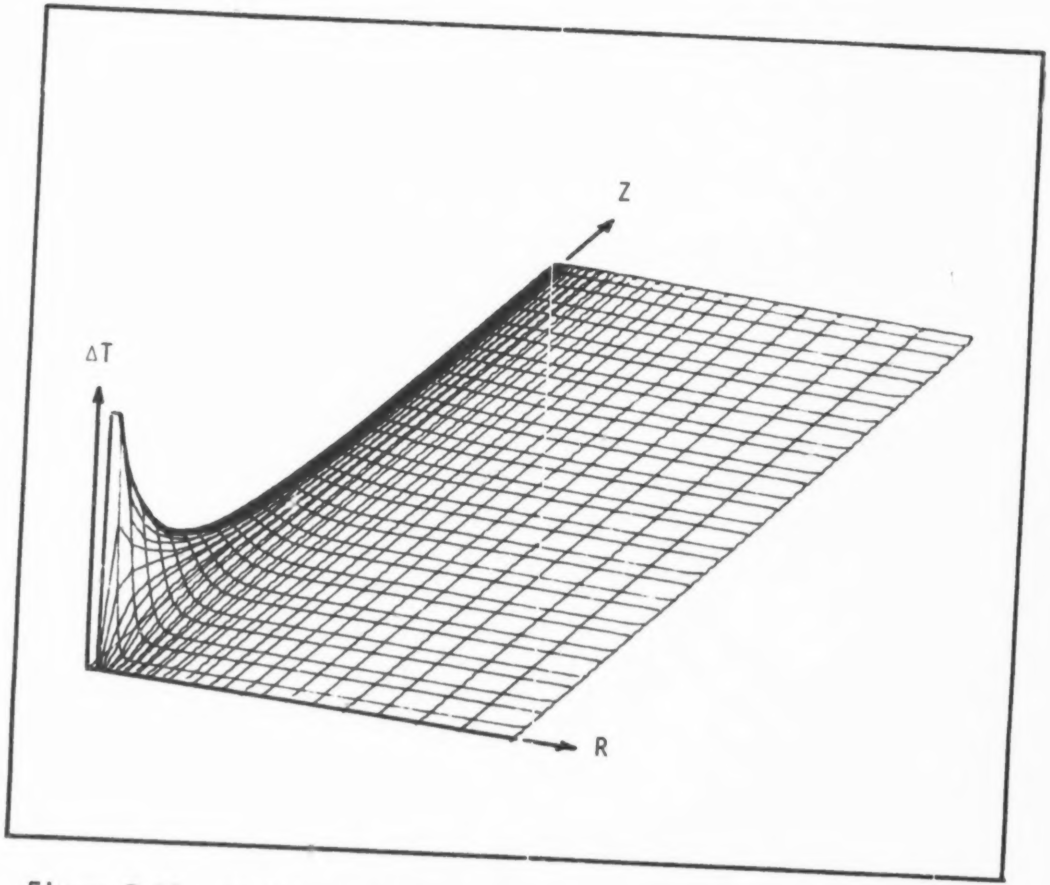

Figure 7.47. 3D Illustration of Temperature Field - ΔT, Case No. 14.

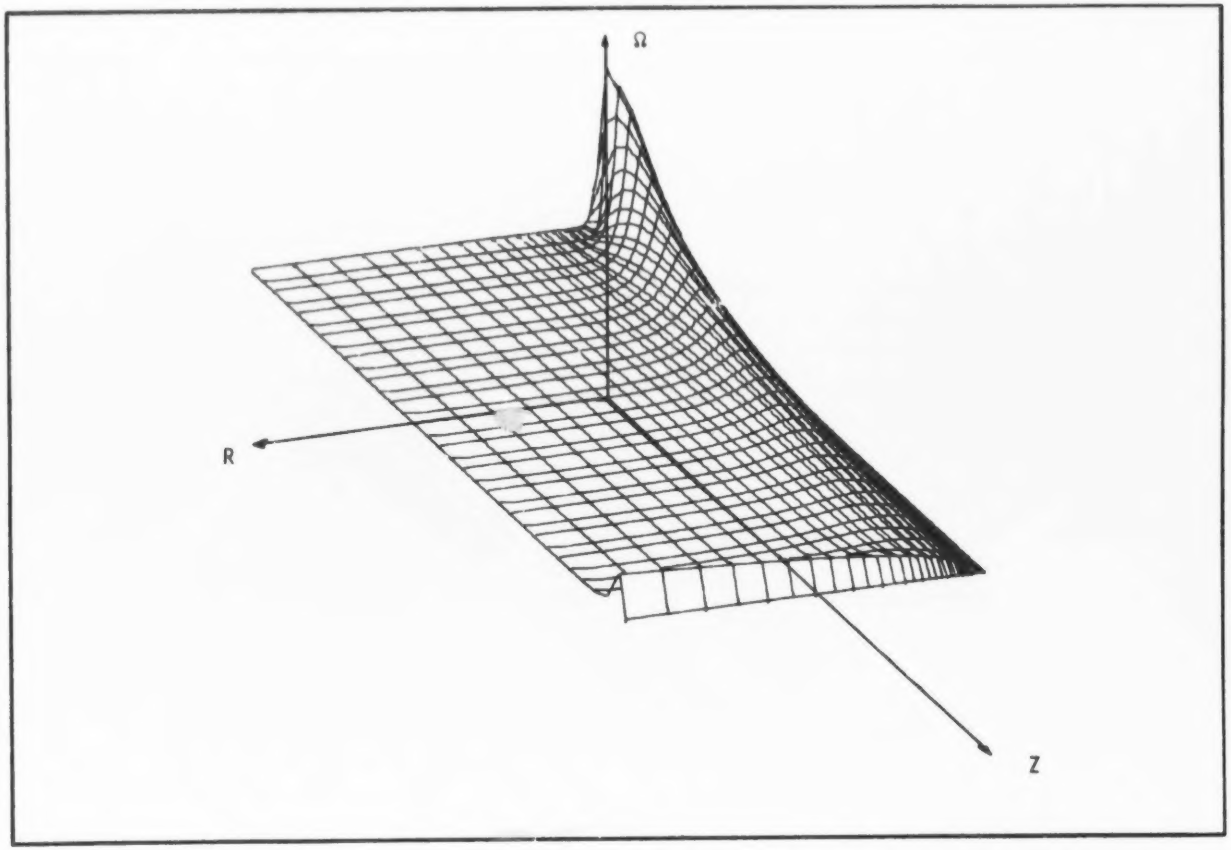

Figure 7.48. 3D Illustration of Fluid Vorticity - Omega, Case 14, Pure Buoyancy. Temperature Difference of Source Maintained at 25 oC.

7.1.3 Mixed Flow - Forced Plumes

In Sections 7.1.1 and 7.1.2 we have checked in some detail the computed flow characteristics at both ends of the dynamic spectrum--pure momentum and pure buoyant flows. This section deals with flows having dynamic characteristics of both which are appropriately classified as "forced plumes' as coined by Morton [58]. Cases used to compare with similarity solutions and experimental data are summarized in Table 7.3. To this end, a variety of effluent boundary conditions have been investigated.

The cases here are too numerous to treat each in full detail so that only the general characteristics of

- Centerline velocity and temperature, and
- Rate of spread and entrainment

will be illustrated, along with selected contour and three-dimensional plots. The similarity solution discussed in Chapter 4 will be used for comparison.

7.1.3.1 Centerline Velocity and Temperature for Forced Plumes

In Chapter 4 the following similarity solution was given for vertical forced plumes:

$$E^* = \frac{64}{z_e^3} + \frac{3}{32F_o}(z^2-z_e^2) \qquad (7.42)$$

and

$$\Delta_{1_m} = \left\{\frac{z^3}{64}\left[\frac{64}{z_e^3} + \frac{3}{32F_o}\;(z^2-z_e^2)\right]\right\}^{-1/3} \qquad (7.43)$$

the variable

$$E^* = \frac{V_m Z^3}{\sqrt{K}} \quad , \qquad (7.44)$$

and Z_e is based on Equation (4.19).

The above equations, except for (7.44), do not reveal variations in the values of K and λ. These values and their effect on the governing equations have been discussed in Chapter 4 and are summarized in Table 4.1. The largest error in velocity is seen to be introduced by $1/\sqrt{K}$ (4.8% deviation from the mean value) but is absorbed in E*.

Equations (7.42) and (7.43) reveal the use of simple fractions which simplify the equations and are very close to the mean values given in Table 4.1. Since these variations are small, and in view of experimental data scatter, it does not seem justified to use more complicated relationships for K and λ as did Abraham, at least for the vertical plume. At any rate, the subject equations yield results that are in good agreement with Abraham's computations and yield excellent agreement with Fan's [27] data concerning the maximum height of rise where stratification is of concern (cf. Baumgartner and Trent [12]). Thus Equations (7.42) and (7.43) will be used to compare with the finite difference results.

Cases 15, 16 and 17 compare the effect of three different methods of computing the radial component of eddy momentum diffusiviity, ε_r. In all cases ε_r is computed from

$$\frac{\varepsilon_r}{v_o r_o} = .0256 \, V_{max} R_{1/2} = .0256 \, FR \qquad (7.45)$$

however, different methods for computing FR are used. A detailed discussion for this computation is given in Section 7.2.

Case 15:

FR = constant = 1.178

Case 16:

$FR = .180\ V_m Z.$

where V_m is the currently calculated value of centerline velocity at elevation Z.

Case 17:

$FR = V_m R_{1/2}$

with running calculation of both V_m and $R_{1/2}$;

all other conditions for these cases remain fixed.

Figure 7.49 illustrates the centerline velocity, V_m, and buoyancy, Δ_{1m}, for these three cases. The significant feature of results shown in this figure is that using a constant value for ε_r (Case 15) gives results with appreciable error in buoyancy (or temperature). The use of a pre-calculated half-radius (mixing length) based on a Gaussian velocity distribution gives somewhat better results (Case 16). The similarity solution is found to give quite accurate results for $Z > 15$-20 and Case 17 shows buoyancy results in excellent agreement with the similarity solution, although the velocity distribution shows a sizable difference. The large discrepancies in both velocity and buoyancy at lower elevations ($Z \gtrsim 10$) are expected since similarity solutions are not valid in this range.

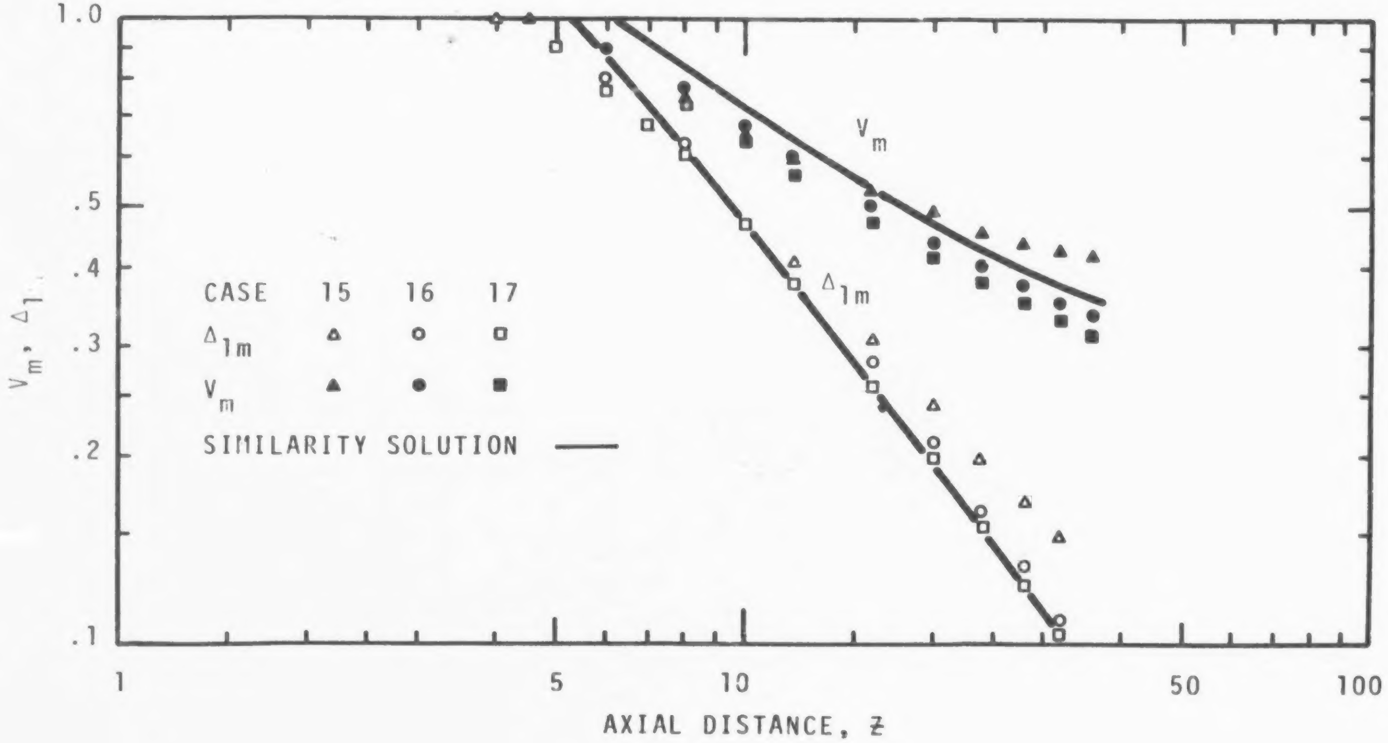

Figure 7.49. Centerline Velocity and Buoyancy for Cases 15, 16 and 17

These three cases also represent progressively more difficult computational problems owing to the non-linearity of the eddy diffusivity.

Case 15, where a constant value of ε_r is used, caused no computational difficulties and is of course the fastest with regard to computer time. This problem is quite similar to the laminar flow plume problem, but ε_r can be several orders of magnitude larger than the counterpart molecular momentum diffusivity. Case 17, where V_m and $R_{1/2}$ are computed iteratively is the most difficult and requires the most computer time. The computational difficulty stems from the fact that velocity profiles at the initiation of the FR computation cannot be too far in error or a numerical instability will result. In addition, the convergence rate is slowed by continuous updating of FR.

Returning to the discussion of momentum jets (Section 7.1.1), only Cases 2 and 3 used ε_r = constant, all other cases used FR calculated as in Case 17. However, in the case of a momentum jet, FR is indeed constant so that any of the three methods for computing ε_r should yield essentially identical results (see Section 7.2). Only in the case where buoyancy is present will variations in FR become apparent, and for this reason, demonstration of results was deferred to cases dealing with mixed flow.

Case 18 is identical to Case 17, except the vertical grid spacing has been doubled giving an overall depth of 82.5 port diameters. Figure 7.50 illustrates centerline buoyancy for the case compared with the results of Case 17 along with the similarity solution. Slightly higher values for buoyancy were calculated in Case 18 compared to

Case 17, an effect of doubling the vertical grid spacing.

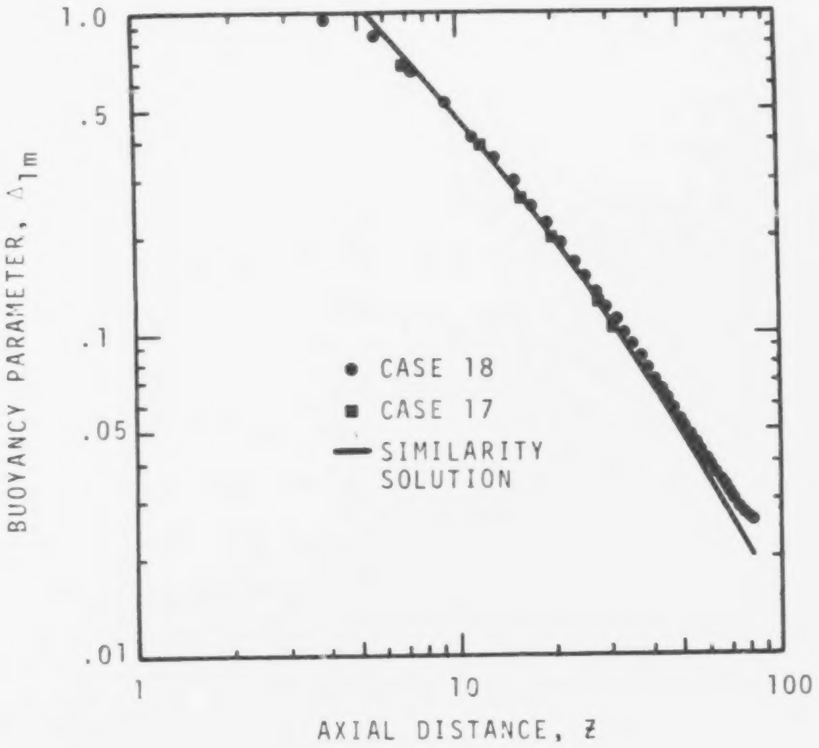

Figure 7.50. Centerline Buoyancy Distribution for Cases 17 and 18

Figure 7.51 illustrates the centerline velocity and buoyancy distributions for Cases 17, 19 and 20 where the densimetric Froude numbers are 52, 35 and 106, respectively. All other variables are fixed for these cases. Case 21 is identical to Case 17 except the vertical eddy momentum diffusivity, ε_z, was assumed to have the form

$$\varepsilon_z = \varepsilon_{zo} e^{-A^2(Z_s - Z)^2} \tag{7.46}$$

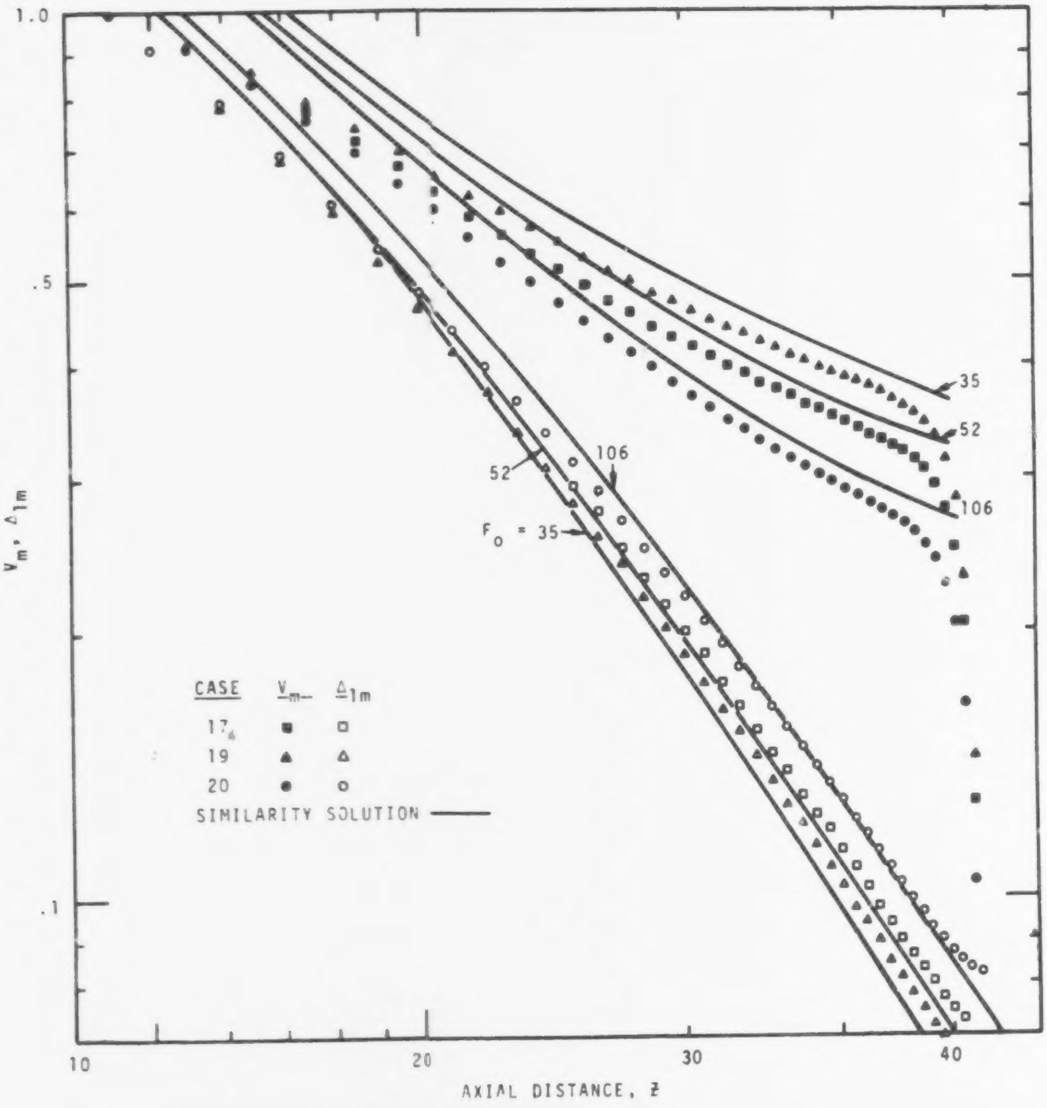

Figure 7.51. Centerline Velocity and Buoyancy for Cases 17, 19 and 20

where A is a constant, Z_s is the surface elevation and ϵ_{z_0} is a reference eddy diffusivity. The objective of this case was to illustrate the effect, on the plume flow, of substantial eddy diffusion confined near the surface. Although the exact values of ϵ_{z_0} and A are of little importance to this end, they have values: $\epsilon_{z_0} = 1$ and $A = .2$. The only significant effects caused by this treatment of ϵ_z are in the radial spread and vertical diffusion of vorticity and radial velocity at the surface. In the case of negligible vertical momentum diffusion, vorticity tends to accummulate in the surface nodes and the mass tends to spread frictionlessly within these surface nodes at high velocities. The presence of significant vertical eddy transport diffuses the vorticity and velocity further downward into the ambient fluid. Figure 7.52 shows a vorticity ridge near the surface for an essentially frictionless flow (Case 17), whereas Figure 7.53 (Case 21) illustrates considerable mitigation of this ridge through vertical diffusion.

Cases 22 and 23 differ from the preceding mixed flow computation in that a Type 2 boundary condition is used with N equal to 7 (refer to Equation 7.17). Various other differences are noted from Table 7.3 (e.g. the Froude number and finite-difference grid). These two cases are identical to one another except the eddy Prandtl number in Case 22 is .714 whereas in Case 23, .80 is used. These computations were performed primarily to determine the effect of the Prandtl number on the rate of spread (Section 7.1.3.2). However, an appreciable effect is also noted on the centerline buoyancy distribution (Figure 7.54), whereas little difference was found in centerline velocity for the two

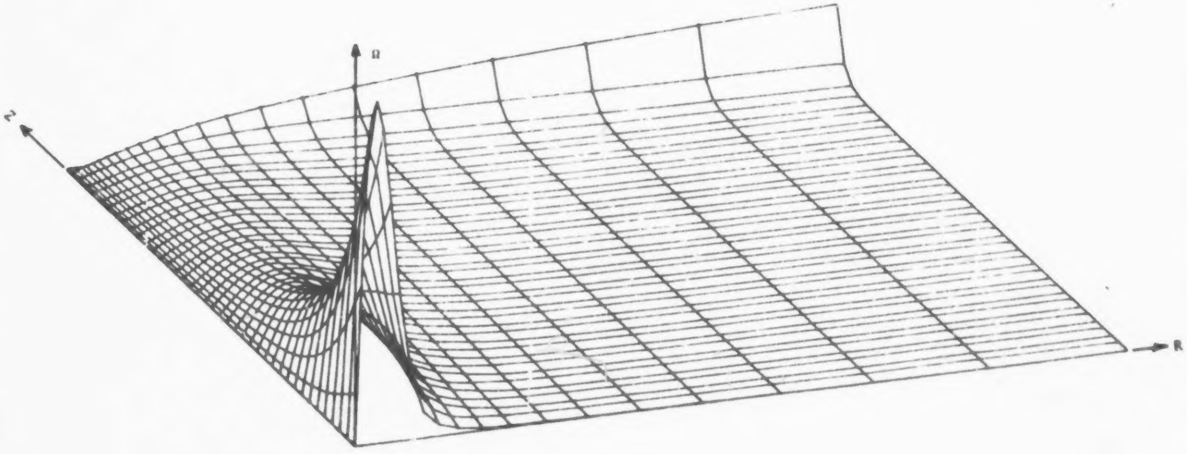

FIGURE 7.52. 3D ILLUSTRATION OF VORTICITY --- OMEGA
CASE 17 --- BUOYANT PLUME WITH RUNNING CALCULATION OF HALF RADIUS

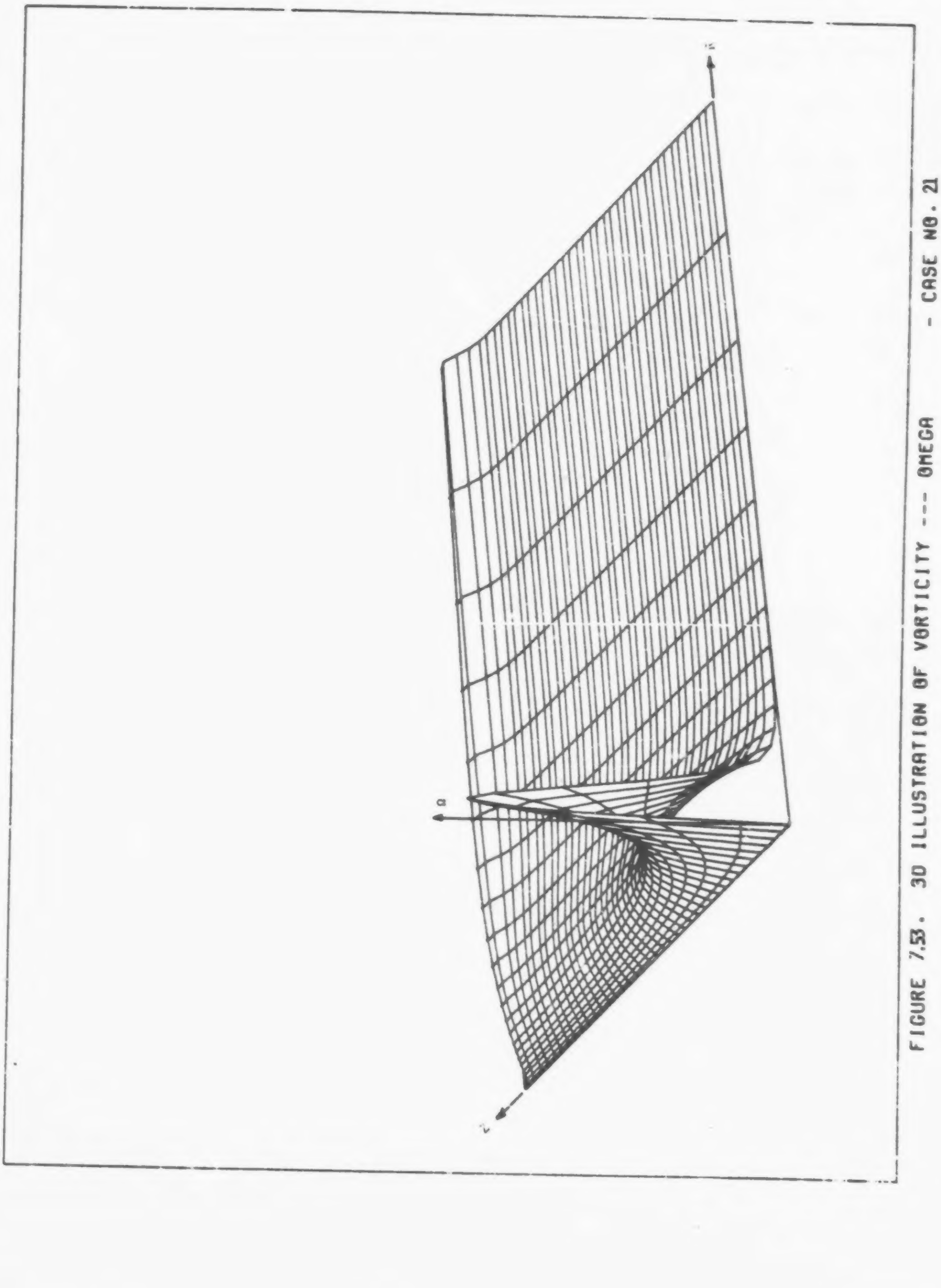

FIGURE 7.53. 3D ILLUSTRATION OF VORTICITY --- OMEGA - CASE NO. 21

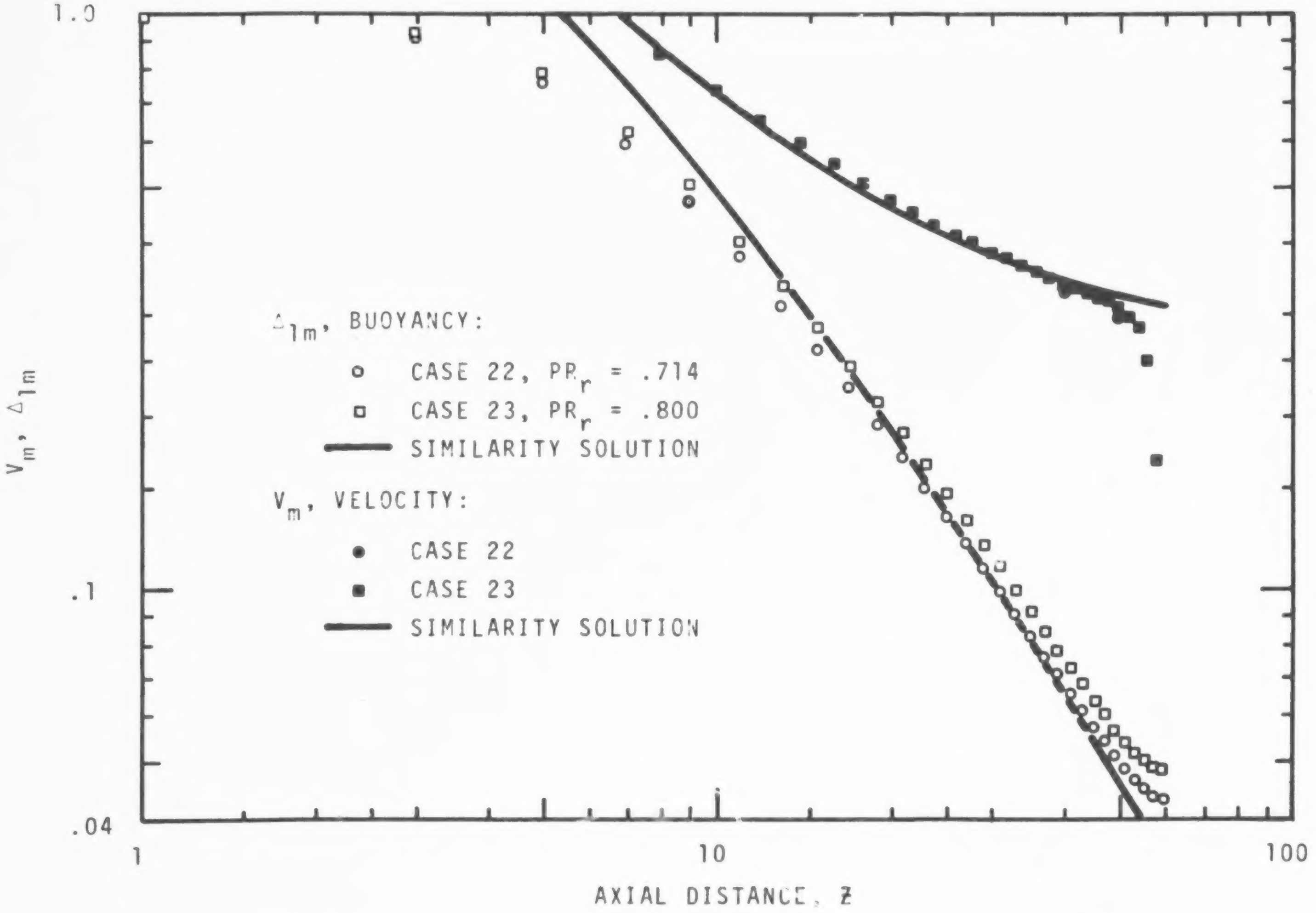

Figure 7.54. Centerline Velocity and Buoyancy for Cases 22 and 23

cases. Since the power law effluent velocity profile is used, with N equal to 7, the maximum centerline velocity is approximately 1.2. This boundary condition indicates much better agreement with the similarity solution for downstream velocity than was obtained using the Gaussian profile (Type 1 boundary condition) in preceding mixed flow cases.

Figure 7.55 shows centerline distributions for Case 24 which is identical to Case 23 except the densimetric Froude number is 1.0 as opposed to 46. Unfortunately, the eddy Prandtl number for this case was not reset to .714 (.8 was used). This error was not discovered until the contents of the restart tape were destroyed; hence, for economic reasons the case was not rerun (cases for very low F_o are slow in converging). However, the slope of the buoyancy curve is essentially identical to the similarity solution and, borrowing the trends of Cases 22 and 23, the buoyancy curves would nearly coincide if PR_r equal to .714 had been used. Also, from Figure 7.54 we would expect no appreciable change in the velocity distribution of Figure 7.55.

Figure 7.55 illustrates that for low F_o, the velocity initially increases due to the large relative buoyancy, reaching a maximum at about 5 diameters downstream. The velocity distribution then tends to a - 1/3 slope as in the case of pure buoyancy. Likewise, the buoyancy distribution tends to a - 5/3 slope as in purely buoyant plumes.

Figure 7.56 illustrates centerline distributions for F_o = 1000 (Case 25) compared to computed results for a momentum jet (Case 4).

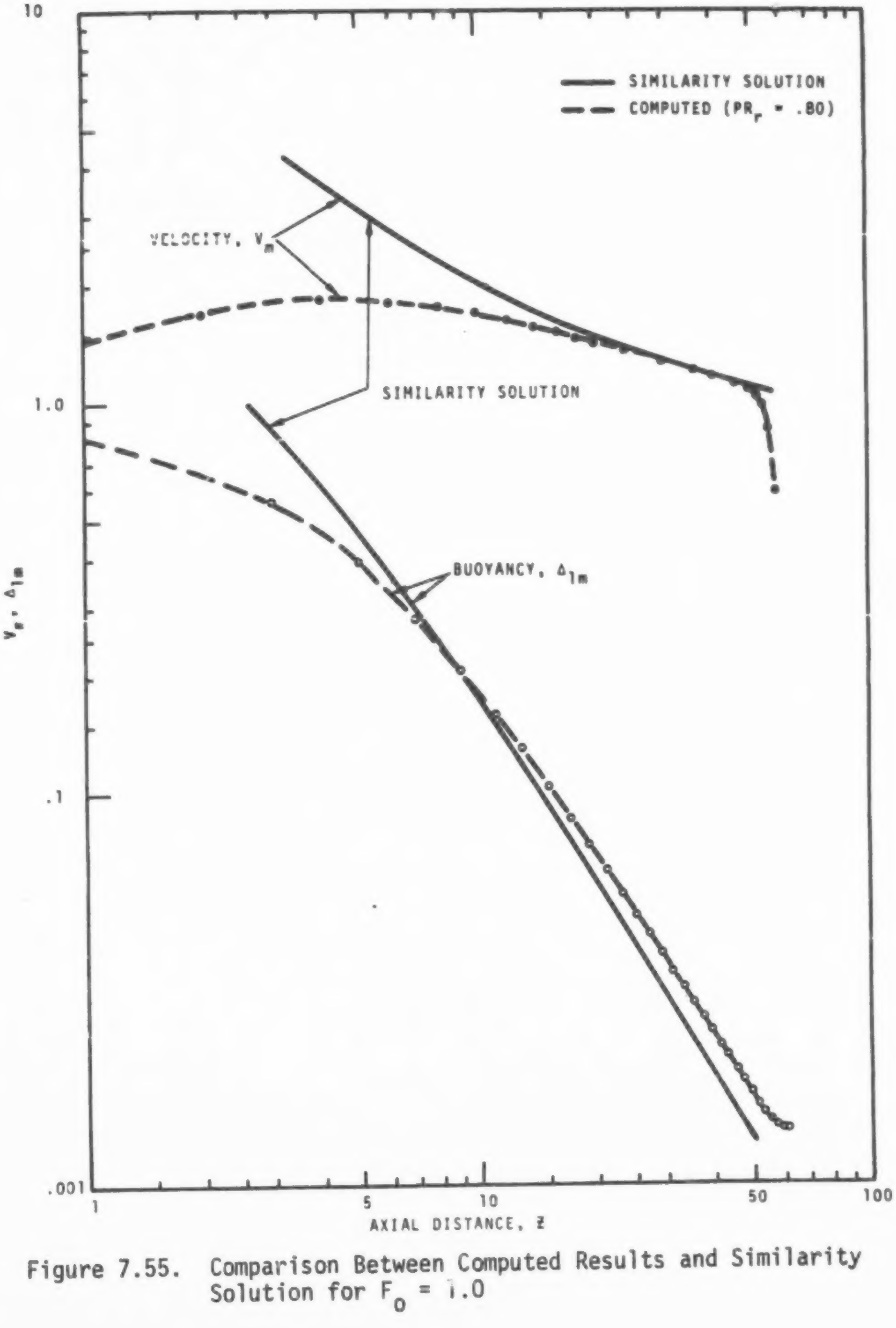

Figure 7.55. Comparison Between Computed Results and Similarity Solution for F_0 = 1.0

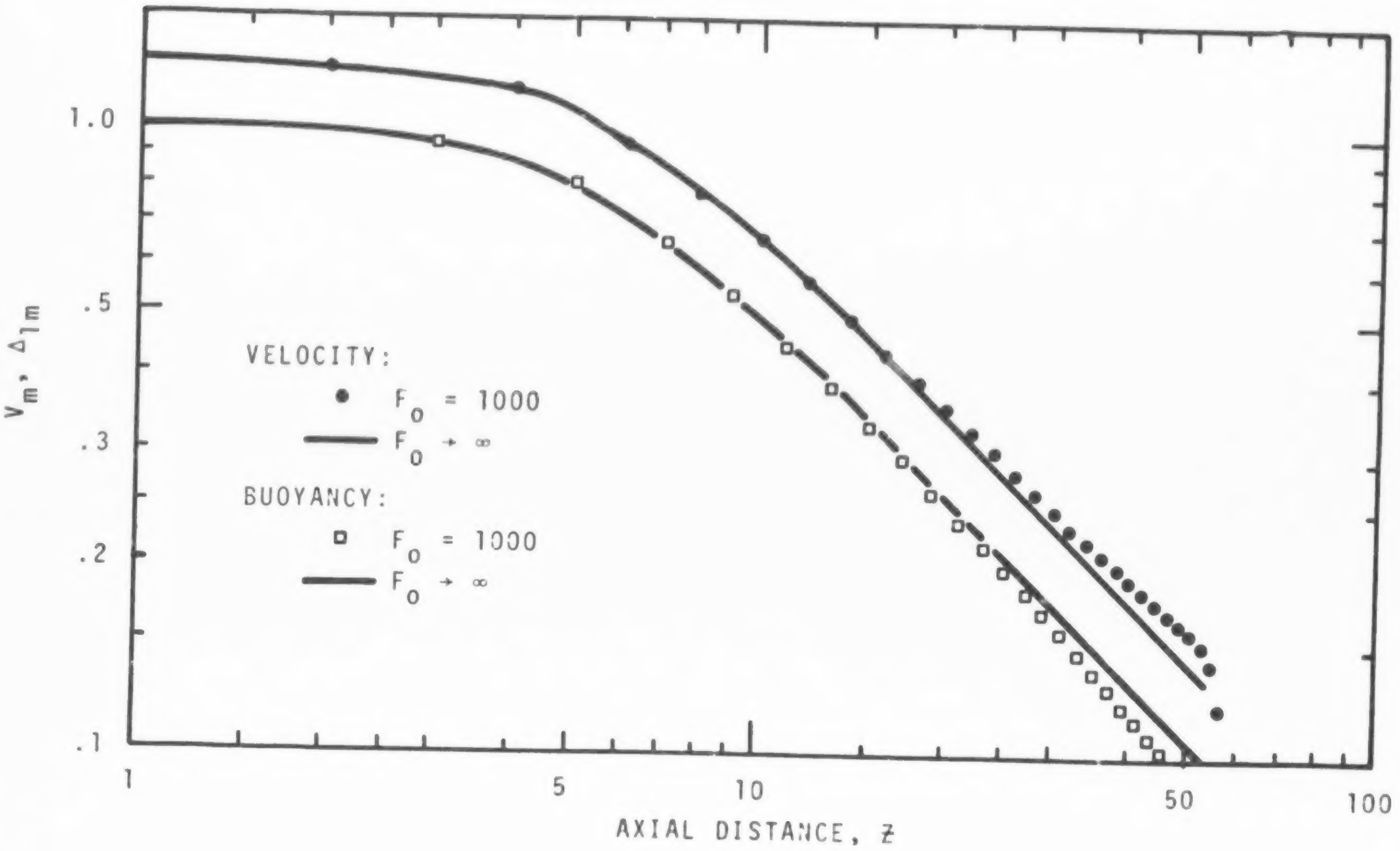

Figure 7.56. Comparison Between Computed Centerline Distributions of Velocity and Buoyancy for $F_o = 1000$ and $F_o \to \infty$

7.1.3.2 Rate of Spread and Entrainment

Results from momentum jet computation revealed that the jet half radius spreads according to

$$r_{1/2} = .0875\ z. \tag{7.47}$$

and pure buoyant plume calculations yielded

$$r_{1/2} \simeq .092\ z. \tag{7.48}$$

Although these results showed a reverse trend from experimental observation, absolute values are not in large disagreement with experiment. Figure 7.57 illustrates the rate of half-radius spread for $F_o = 0, 1, 46$ and ∞. The effect of different eddy Prandtl numbers for $F_o = 46$ is revealed by Figure 7.58 (Cases 22 and 23). As pointed out earlier, the case for $F_o = 1$ was inadvertently run using $PR_r = .8$ and Figure 7.57 shows that this case has the same spread rate as the case where $F_o \rightarrow \infty$. Thus, the fact that one case is dominated by initial inertia and the other by buoyancy seemed to have no effect on the half-radius spread rate. This being a fact of the computational technique then explains why the plume has a larger computed spread rate where $PR_r = .714$ as opposed to $PR_r = .8$. It is expected that had $PR_r = .714$ been used in the $F_o = 1$ computation, the half-radius curve would have coincided with the curve for $F_o = 0$. Case 22 where $F_o = 46$ shows that the half-radius begins to spread as a momentum jet ($Z \leq 10$-12), passes through a transition and then spreads at the same rate as a purely buoyant plume, at far downstream points. Case 23 begins to spread as a momentum jet, then passes through a

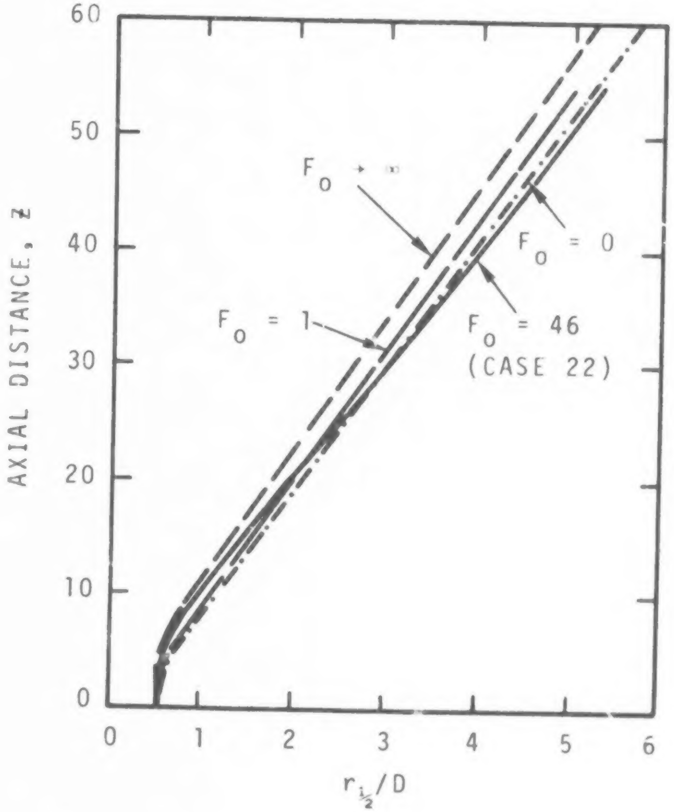

Figure 7.57. Comparison of Half-Radius Spread for Various Densimetric Froude Numbers

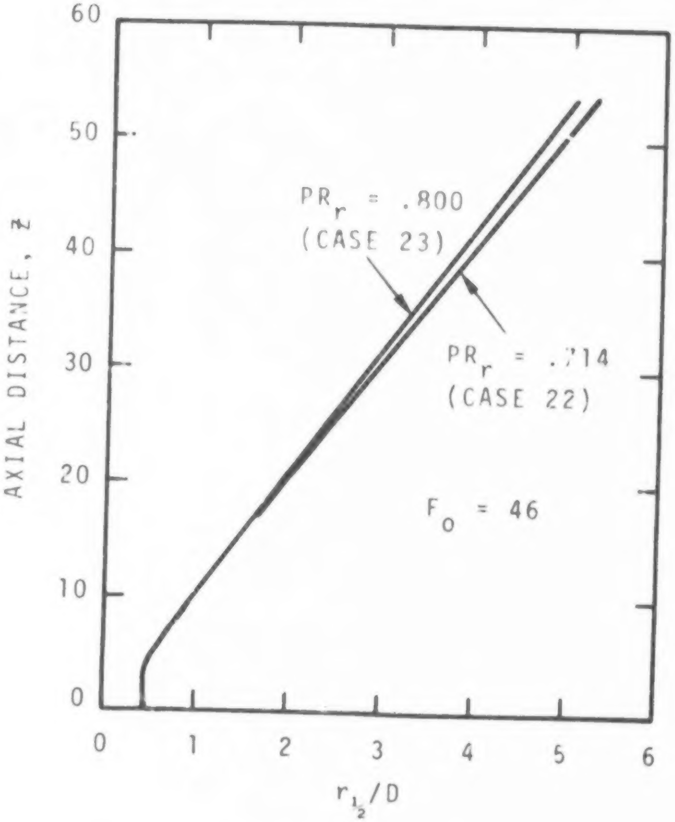

Figure 7.58. Effect of the Eddy Prandtl Number on Half-Radius Spread

transition to a wider spread, and at far downstream points, again spreads like a momentum jet (but wider).

Figure 7.59 shows the variation of $\psi(R_\infty,Z)$, a measure of entrainment, with elevation. Again we cannot expect good correspondence with wall-flush jets at lower elevation since for the cases illustrated the outfall port has finite height above the bottom. At higher elevations we note that for $F_0 = 1000$ a slope of 1 is attained which is appropriate for momentum jets. The case for $F_0 = 1$ has obtained a slope of approximately 1.4 and is increasing. Had the solution been carried to higher elevations, the experimental value of 5/3 would perhaps be attained. For $F_0 = 46$ we find intermediate values of $\psi(R_\infty,Z)$ with the slope tending toward that of the case for $F_0 = 1$. Again the slope is increasing and would perhaps attain the value of 5/3 as in pure buoyancy, at increased axial distance.

Figures 7.60 through 7.62 illustrate streamlines, isotherms and level lines of vorticity, respectively, for Case 22. Figures 7.63 through 7.65 show this same information in three-dimensional plots.

7.2 Transport Coefficients

In obtaining the results presented thus far, we have made use of certain transport coefficient models which describe the required components of radial and vertical turbulent diffusion. This thesis, in the main, is not a study of modeling these coefficients but through necessity one must utilize reasonable methods for modeling these quantities if reliable results are to be obtained. For the momentum jet issuing to a semi-infinite medium, the important transport coefficient models

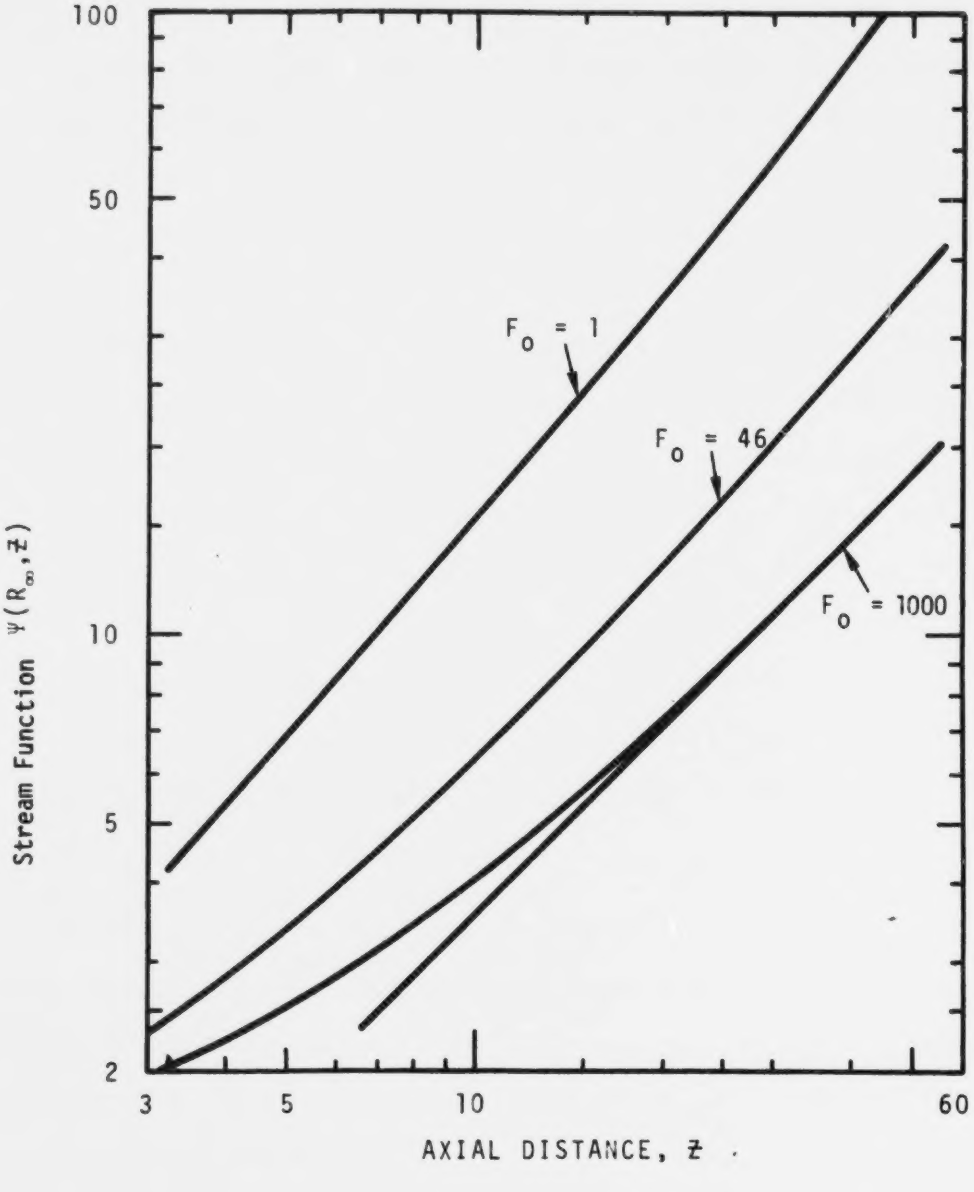

Figure 7.59. Entrainment Trends in Mixed Flows

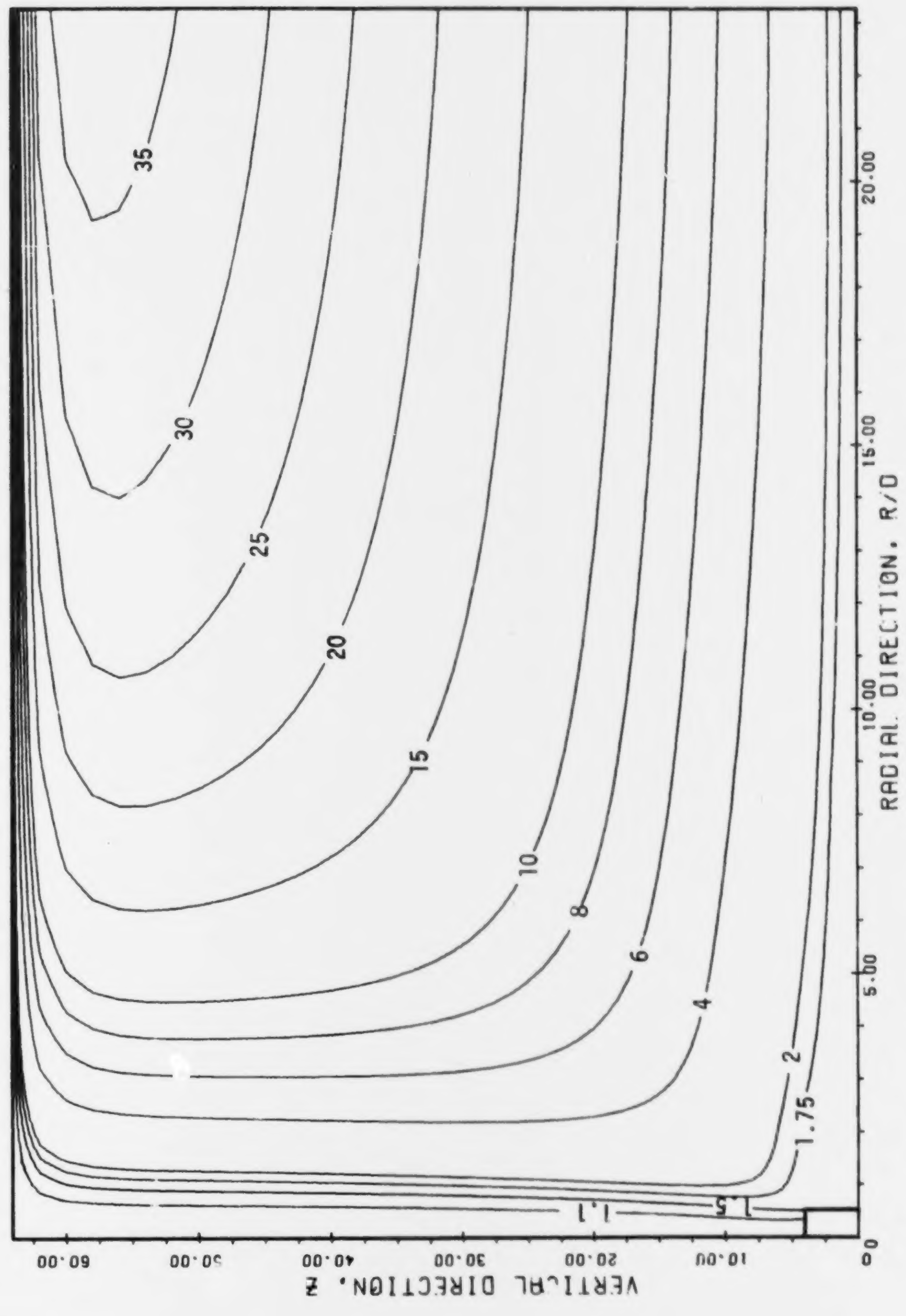

FIGURE 7.60. STREAMLINES FOR CASE 22 - MIXED FLOW. FO = 46

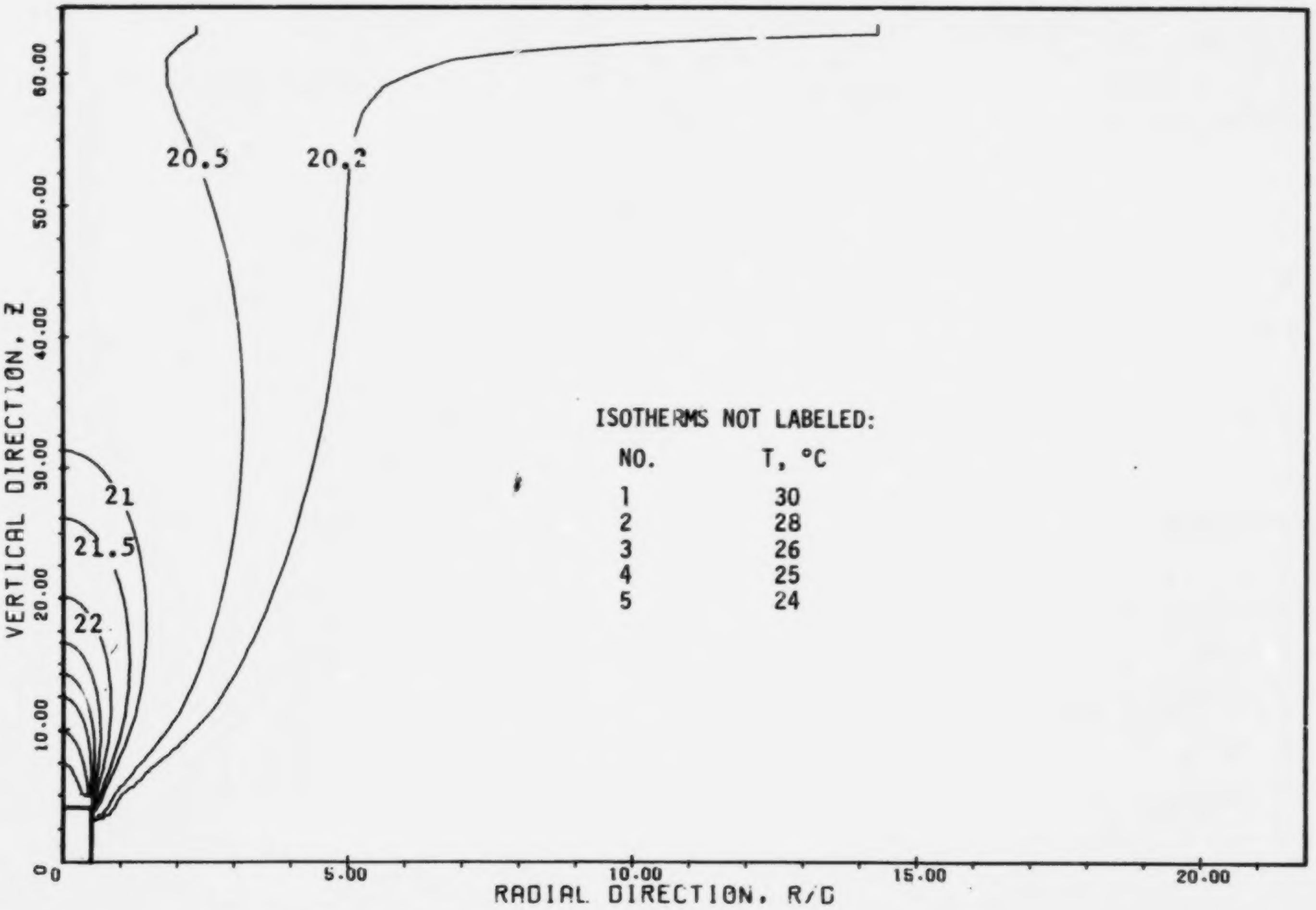

FIGURE 7.61. ISOTHERMS FOR CASE 22 - MIXED FLOW. FO = 46

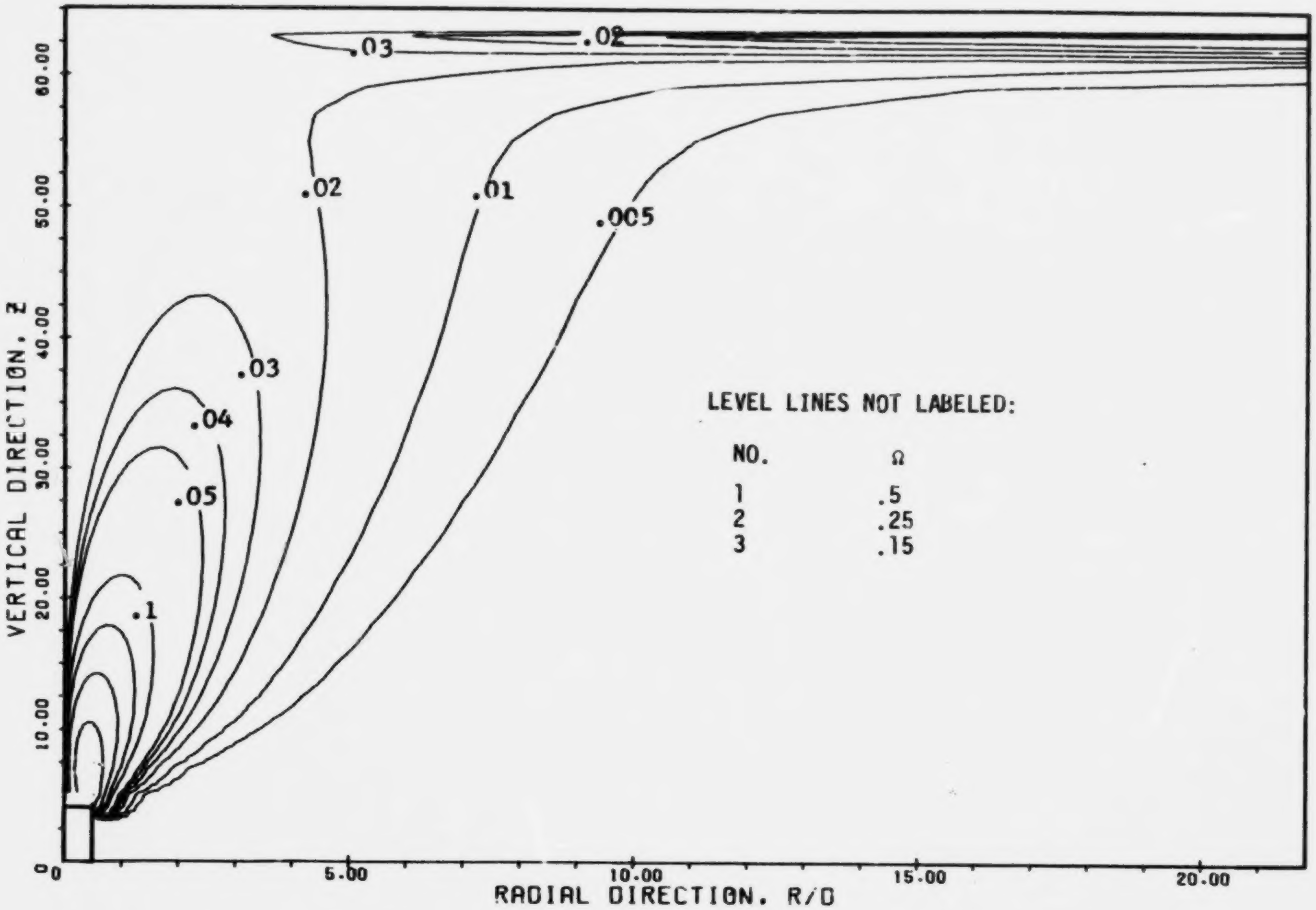

FIGURE 7.62. VORTICITY LEVEL LINES FOR CASE 22 - MIXED FLOW, FO = 46

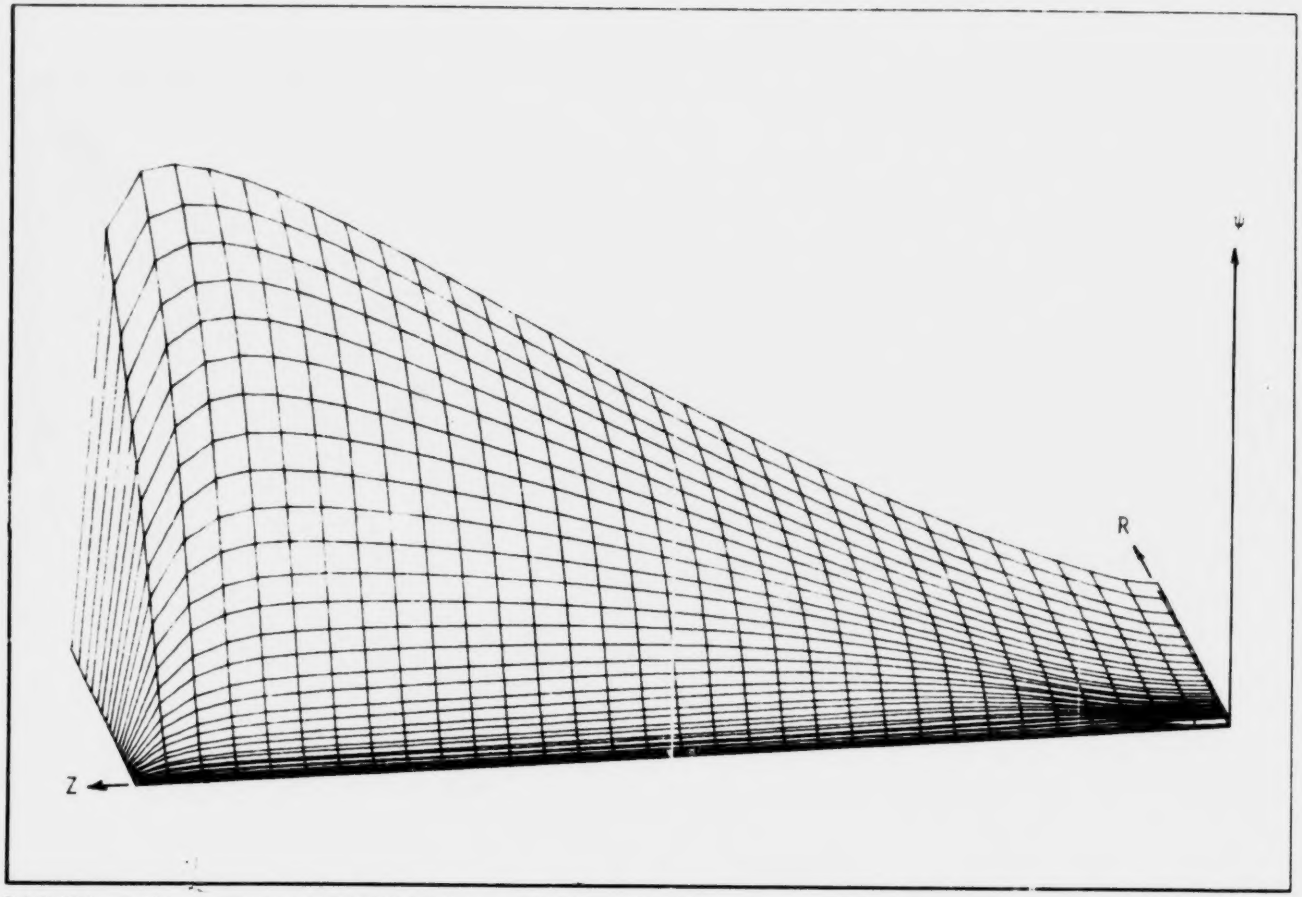

FIGURE 7.63. 3D ILLUSTRATION OF STREAM FUNCTION -- PSI.

CASE 22 - DEEP WATER BUOYANT JET

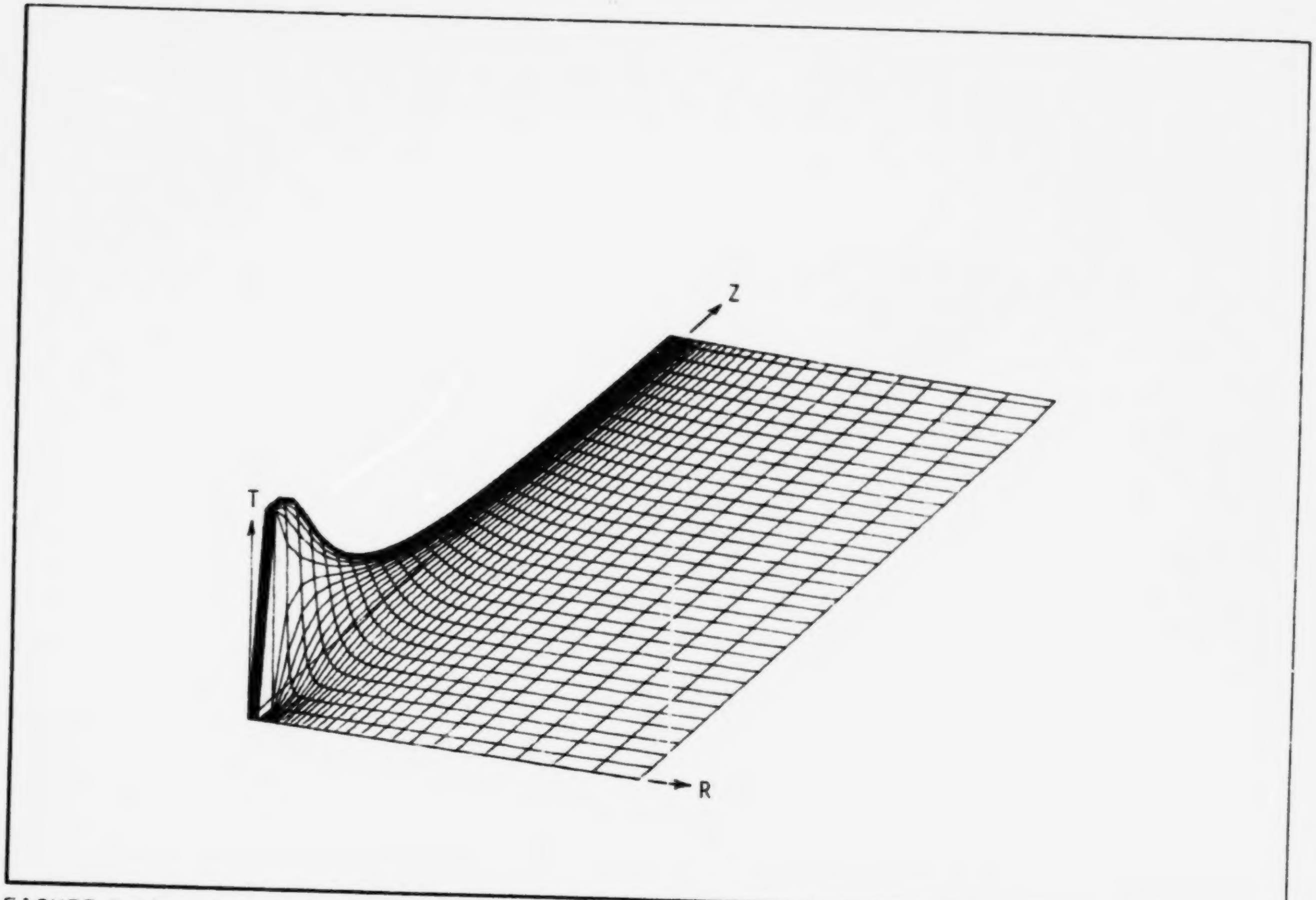

FIGURE 7.64. 3D ILLUSTRATION OF TEMPERATURE FIELD -- T.

CASE 22 - DEEP WATER BUOYANT JET

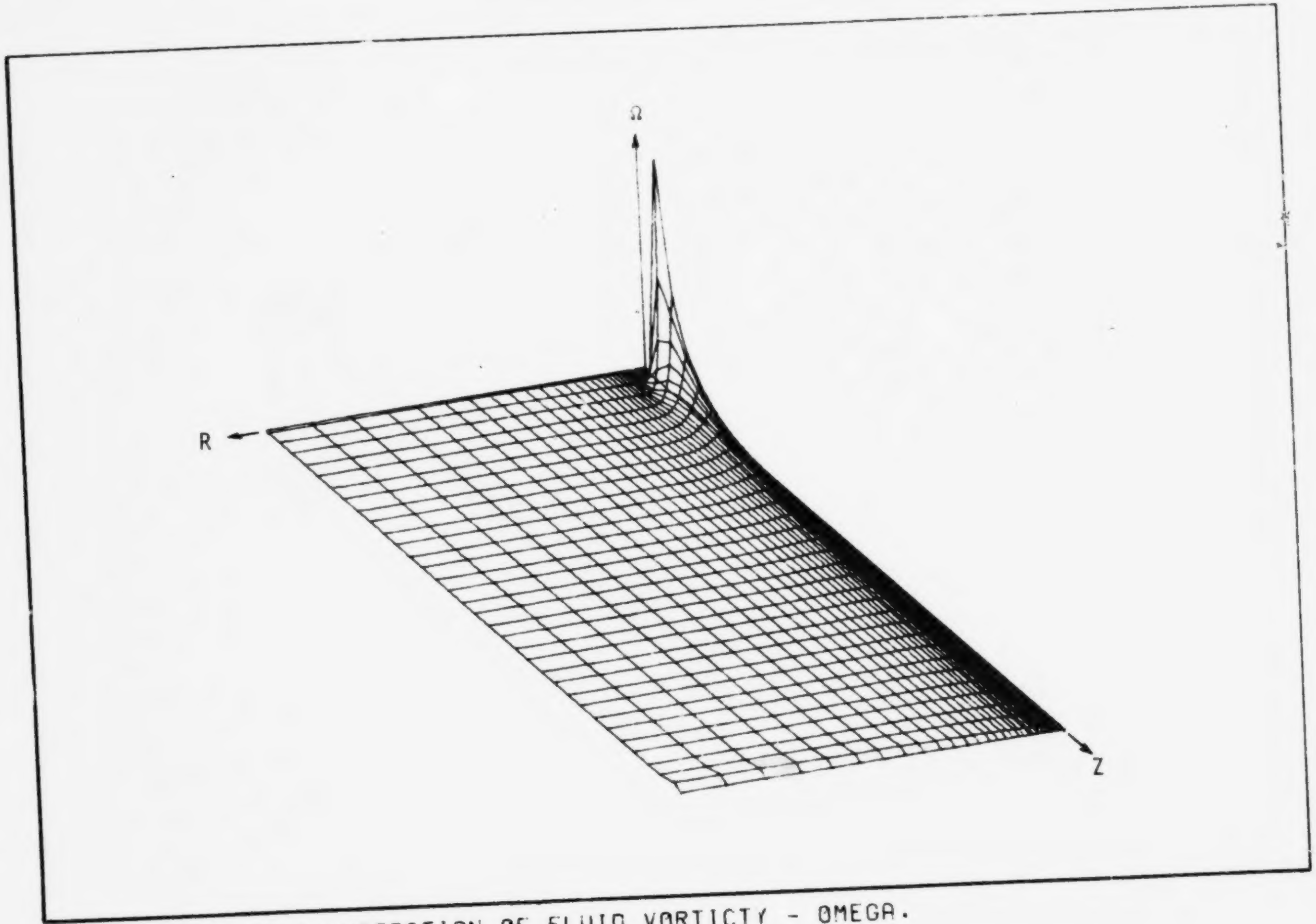

FIGURE 7.65. 3D ILLUSTRATION OF FLUID VORTICTY - OMEGA.

CASE 22 -- DEEP WATER BUOYANT JET

turn out to be trivial since they are constant. However, where buoyancy plays a role and the buoyant surface spread in stratified media is of concern these models are quite complicated and in certain instances (surface spread) the theoretical and experimental efforts are sadly lacking.

In this work it is necessary to model the momentum diffusion coefficients for the radial and vertical directions, ε_r and ε_z, along with the corresponding Prandtl (or Schmidt) numbers, PR_r and PR_z. Turbulence contributions may be considered to fall into the following two categories:

1. that generated by the effluent stream, and
2. the ambient contribution which has origin from
    - wind stress and wave action,
    - shear flow at solid boundaries, and
    - contributions depending on the local history and/or convection across system boundaries.

In general, the effluent generated turbulence will dominate the ambient contribution within the plume except in the surface zone where plume velocities may be low and wind and wave action under a high sea state dominate the effluent induced effects. However, in the circulating portion of the flow field, ambient contributions will dominate.

The turbulence models used in the present work are based on Prandtl's second hypothesis which is appropriately modified to include the influence of stratification. Experience has found that Prandtl's hypothesis may be applied with good results where mean velocity gradients have reasonable magnitude and a mixing length may be easily defined, but breaks down entirely, at least computationally, where velocity gradients are very small, or confused, and the mixing length has dubious interpretation (e.g., the circulating flow). Prandtl's hypothesis, as stated by Schlichting [84], is

$$\tau = \rho\varepsilon_r \frac{\partial v}{\partial r} = \rho C_1 b(v_{max}-v_{min}) \frac{\partial v}{\partial r}$$

where τ is fluid stress, C_1 is an empirical constant, and b is the width of the mixing zone. The eddy diffusivity for momentum ε_r is then

$$\varepsilon_r = C_1 \ell_r (v_{max}-v_{min}) \tag{7.49}$$

where ℓ_r is the mixing length of an axisymmetric plume and assumed to be the width of the half-radius in established flow. An equivalent relationship may be written for ε_z, the vertical component, in the zone of surface spread. In the mainstream of the plume, the usual case is that only one or the other of the transport coefficients will have a significant effect on the flow dynamics. For instance, in the vertical rise, ε_r is of utmost importance ,whereas ε_z may be neglected as a practical matter. However, ε_z is included in the computations, and may in fact be important near the surface where vertical velocity may be small. In the lateral spread, the opposite is true where ε_r has relatively small influence. The value v_{max} in the zone of plume rise is easily defined as the centerline velocity. u_{max} in the lateral spread will occur at the surface for a buoyant flow in homogeneous surroundings. In both cases the maximum velocity has sufficient magnitude compared to velocities outside the plume so that $v_{max} >> v_{min}$ and $u_{max} >> u_{min}$. Hence,

$$\varepsilon_r = C_1 \ell_r v_{max} \tag{7.50}$$

and

$$\varepsilon_z = C_2 \ell_z u_{max}, \tag{7.51}$$

where ℓ_z is an as yet undefined vertical mixing length in the vertical direction. Note, that Equation (7.51) includes no compensation for stratified flow.

Equations (7.50) and (7.51) are adequate for modeling the turbulence inside the plume and are relatively convenient to use, but only because we have prior knowledge of the plume geometry. Outside the plume, in the region of flow induced circulation, these expressions are useless because we have no adequate criterion for mixing lengths and, in fact, velocity gradients may have nothing to do with the primary contribution to the field of turbulence. Fortunately, for the problem at hand, turbulence in the circulating field is of nominal importance, and except for the fact that some degree of viscosity in this region helps to speed the numerical computation, we could assume the fluid as inviscid.

It is recognized that Prandtl's second hypothesis has limited application in the numerical computation of circulating and recirculating fluid flow. Prandtl recognized the shortcomings of this hypothesis in that it could be applied with confidence only to reasonably simple, steady-state flows. Various other investigators also recognized that a more fundamental approach needed to be employed. Such an approach needed to consider such various aspects as

- convection,
- diffusion,
- creation, and
- dissipation

of the turbulence which could be related in some fashion or another to mean flow quantities. Earlier models were based on the transport of turbulent energy. However, these models still depended on the definition of a mixing length to relate the dissipation or decay. Chou [18, 19] sought to overcome this difficulty by introducing a second transport equation for decay scale. Rotta [79,80] developed these ideas even further and set down the transport equations for the complete Reynolds stress tensor.

Based on the pioneering work of Rotta, Spalding [92] and his colleagues at the Imperial College in London, have had considerable success in applying these ideas to generalized numerical computation in recirculating flow fields. Spalding's model for computing turbulence quantities involves transport equations (cf. Reference [93]) for

- k, the kinetic energy of turbulent motion,
- W, which may be considered as the average value of the fluctuations of the fluid vorticity, and
- g, the average value of the square of the fluctuating component of the mass fraction of injected fluid.

Spalding defines a length scale as:

$$\ell = (k/W)^{1/2}, \tag{7.52}$$

hence,

$$\varepsilon = C_3 \rho k^{1/2} \ell. \tag{7.53}$$

Thus, in addition to equations for the stream function, vorticity, buoyancy, and/or other required constituents, transport equations of the following types are also required:

$$\rho u \frac{\partial k}{\partial X} + \rho v \frac{\partial k}{\partial r} - \frac{1}{r} \frac{\partial}{\partial r} \left(\frac{r \varepsilon}{\sigma_1 k} \frac{\partial k}{\partial r}\right)$$

$$= C_4 \rho k^{1/2} \ell \left(\frac{u}{Y}\right)^2 - C_5 \rho \frac{k^{3/2}}{\ell}, \tag{7.54}$$

where the C's are constants defined by Spalding. Similar equations are required for W and g. As testimony to these and similar methods the reader is referred to the following work carried out at the Imperial College: Patankar and Spalding [69], Gosman, Pun, Runchal, Spalding and Wolfshtein [35], Bradshaw and Ferriss [15], and Spalding [89].

Although solving additional transport equation for turbulence quantities, such as Equation (7.54), appears to be a considerable effort in itself, this approach offers a realistic and negotiable compromise to otherwise unapproachable problems in turbulent flow. These, or similar methods have not been employed in the present study, but only because the flow field offered enough a priori knowledge to justify and permit the use of simpler mixing length models.

7.2.1 The Radial Transport Coefficient, ε_r

To model the plume and circulating flow fields, the radial component of eddy diffusion must be modeled throughout the fluid system. To this end, four flow regions are defined which are illustrated in Figure 7.66.

These regions are defined as follows:

Region I: Zone of established plume flow
Region II: Zone of flow establishment
Region III: Circulating ambient
Region IV: Lateral surface spread

Each of these regions has special characteristics and must receive special attention.

Region I

Equation (7.50) relates the radial component of momentum transport as

$$\varepsilon_r = C_1 \ell_r v_{max} \tag{7.55}$$

For Region I (established flow), $C_1 = .0256$, $\ell_r = r_{1/2}$, the plume half-radius, and v_{max} as the centerline velocity. Tomich [99] used a similar relationship for his analysis of a compressible free jet. In dimensionless form

$$\frac{\varepsilon_r}{r_o v_o} = .0256\, R_{1/2} V_{max} \tag{7.56}$$

where

$$R_{1/2} = \frac{r_{1/2}}{r_o}$$

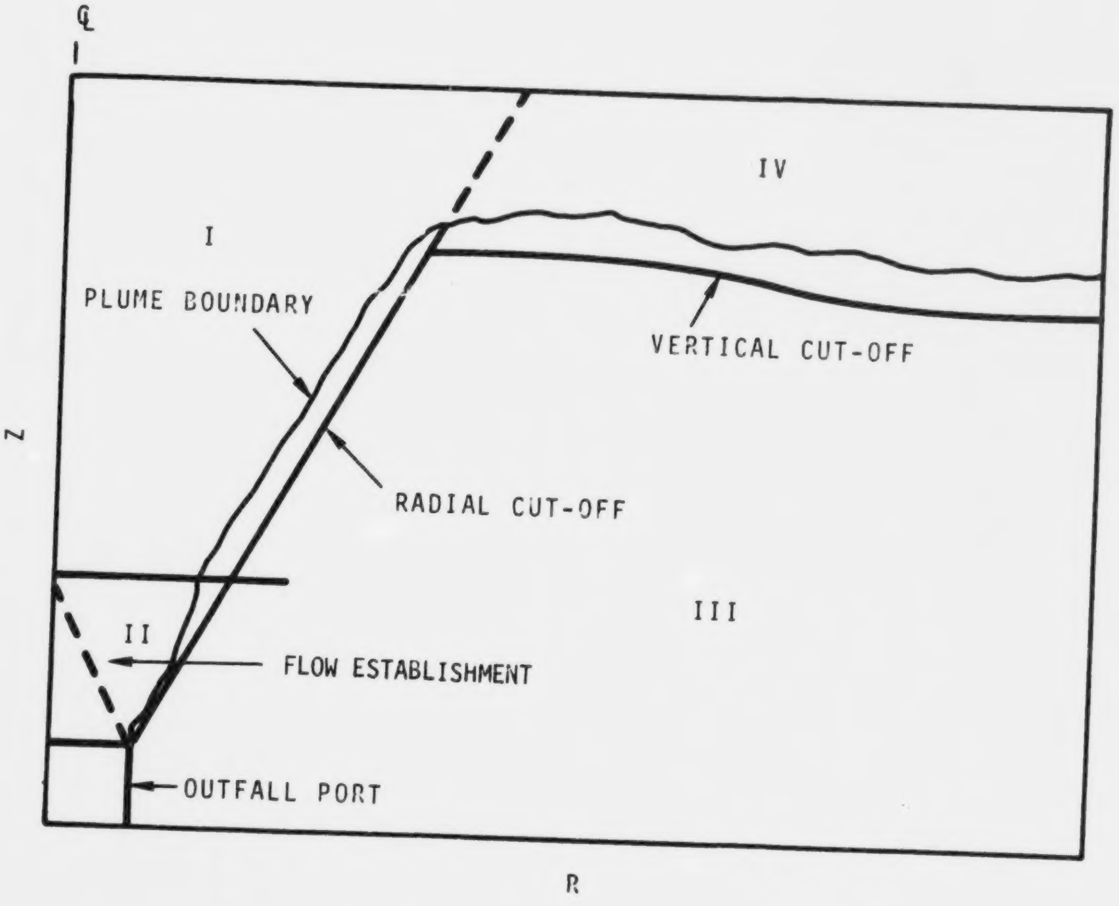

℄
I
II
III
IV
PLUME BOUNDARY
VERTICAL CUT-OFF
RADIAL CUT-OFF
FLOW ESTABLISHMENT
OUTFALL PORT
Z
R

Figure 7.66. Regional Specification for Turbulent Eddy Coefficient Modeling

and

$$V_{max} = \frac{v_{max}}{v_o} \quad .$$

As a reference value for ε_r we set

$$\varepsilon_{r_o} = .0256 \qquad (7.57)$$

where $R_{1/2} = R_o = 1.0$ and $V_{max} = V_o = 1.0$.

So that

$$\frac{\varepsilon_{r_o}}{r_o v_o} = \frac{1}{RE_{r_o}} = .0256.$$

Hence, the reference radial Reynolds number is

$$RE_{r_o} = 39, \qquad (7.58)$$

the value used in all computations except Case 8.

To obtain the point Reynolds number $RE_{r(j,k)}$ (the indices on RE_r will be omitted hereafter with the point value always implied), we define

$$\varepsilon_r = \varepsilon_{r_o} FR_{jk} \qquad (7.59)$$

where, ε_r may be viewed as the point value of eddy diffusivity with subscripts omitted. With the definition Equation (7.59)

$$FR_{jk} = R_{1/2}\ V_{max}, \qquad (7.60)$$

and

$$RE_r = RE_{r_o}/FR_{jk} \quad . \qquad (7.61)$$

For the momentum jet, in the zone of established flow (cf. Section 7.1), it has been established that

$$V_{max} = 12.4/Z \qquad (7.62)$$

and at the half radius

$$\frac{V}{V_{max}} = .5 = e^{-K\left(\frac{R_{1/2}}{Z}\right)^2} \tag{7.63}$$

or

$$\frac{R_{1/2}}{Z} = \sqrt{\frac{\log 2}{K}} \quad . \tag{7.64}$$

Using the value K = 77 from Abraham [1],

$$FR_{jk} = 1.176, \tag{7.65}$$

for a momentum jet (subscripts on FR will be omitted hereafter, with the point value implied).

Equation (7.65) represents an empirical value for FR. Two numerical experiments were carried out for the momentum jet, one case where FR = 1.176 was held constant and the other where FR was computed according to Equation (7.60). The centerline velocity distributions for both cases were found to be essentially identical. Figure 7.67 illustrates the result of iteratively computing $FR = R_{1/2}V_{max}$. In both of these cases a Gaussian profile at $Z = 4.5$ was used for the inflow boundary condition (Type 1 boundary condition - Region II does not enter into compution). Figure 7.68 illustrates FR for cases having varying degrees of buoyancy using the Type 2 inflow boundary condition (power law velocity profile). Note that in this instance FR $\simeq$ 1 for the momentum jet ($F_0 \rightarrow \infty$) and is owed to a slightly higher centerline velocity, the ratio approximately equal to the value of Equation (7.65).

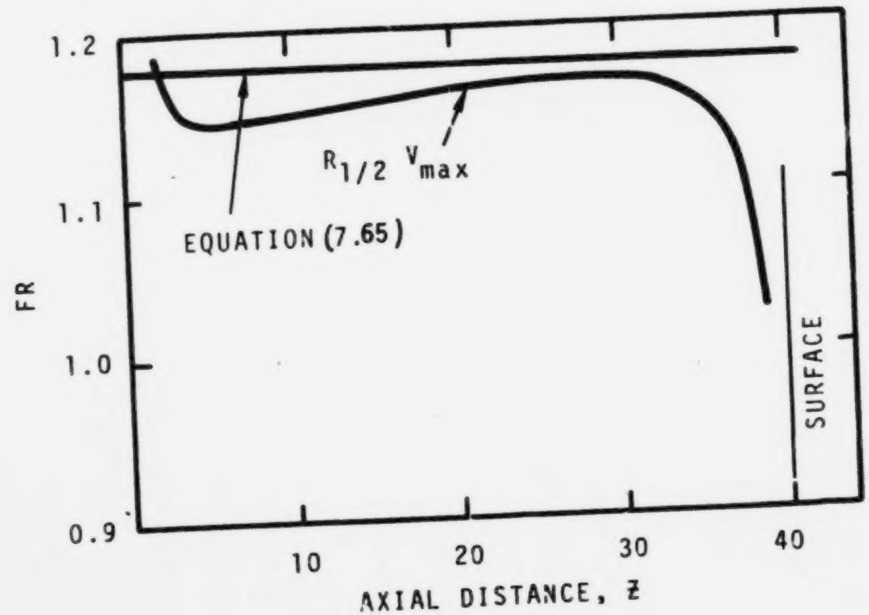

Figure 7.67. Computed Values of FR for a Momentum Jet

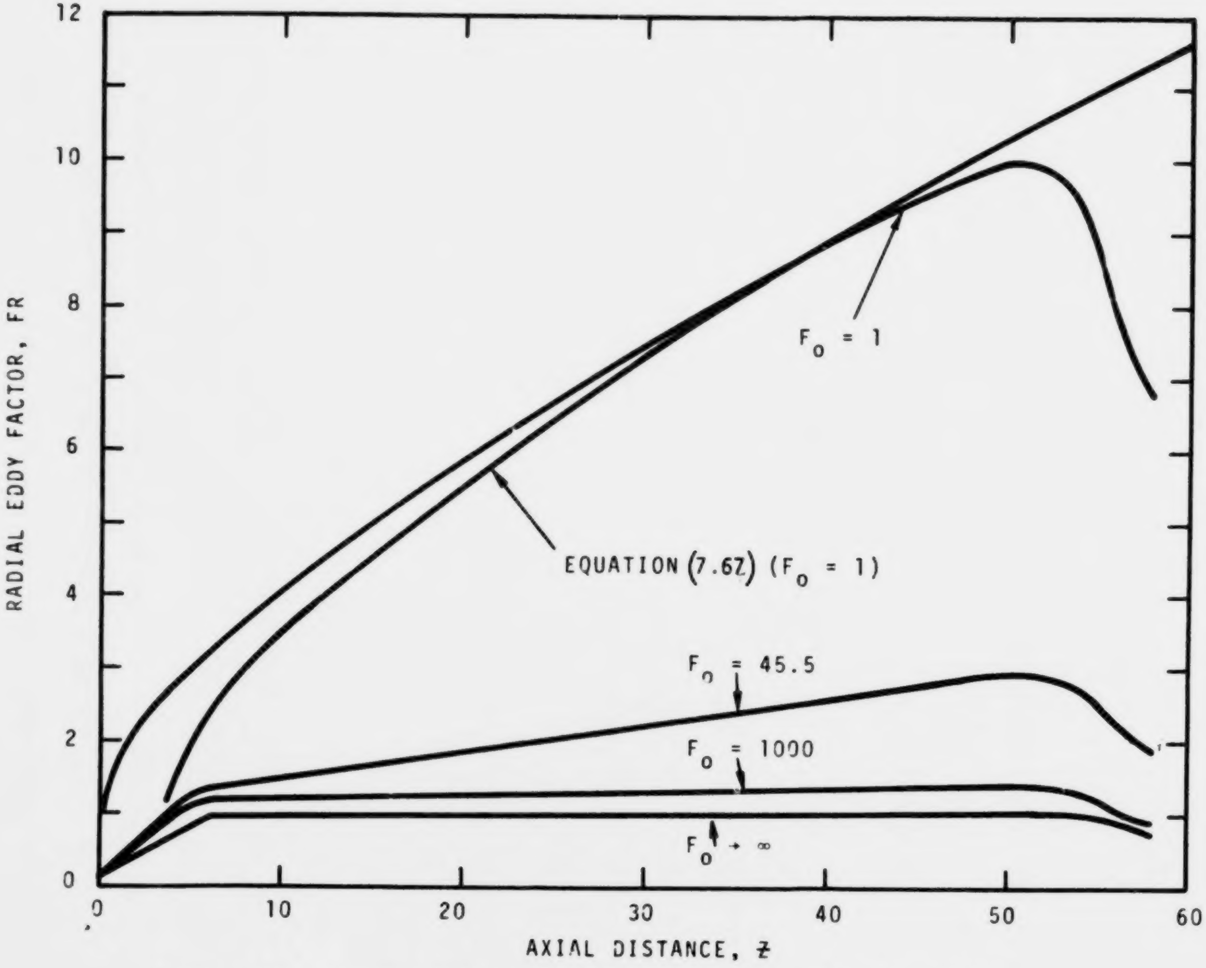

Figure 7.68. Computed Radial Eddy Diffusion Factors, FR for Deep Water Plumes at Various Densimetric Froude Numbers

For the cases dominated by buoyancy, Equation (7.33) gives

$$V_{max} = 4.4\ (F_o Z)^{-1/3}$$

or

$$V_{max} = 4.4(2)^{1/3}(F_o Z)^{-1/3} \qquad (7.66)$$

The radial velocity distribution is again given by Equation (7.63) with K = 92.

In this instance

$$FR = (2)^{1/3} 4.4(F_o Z)^{-1/3} \sqrt{\frac{\log 2}{92}}\ Z,$$

$$FR = \frac{(12)^{1/3}\ 4.4 \sqrt{\frac{\log 2}{92}}}{F_o^{\ 1/3}}\ Z^{2/3}$$

$$FR = \frac{.481}{F_o^{\ 1/3}}\ Z^{2/3}, \qquad (7.67)$$

based on

$$Z = z/r_o.$$

Equation (7.67) is also plotted on Figure 7.68 for comparison of the empirical approximation and computed value of FR for $F_o = 1$.

Aside from merely illustrating how the radial eddy transport coefficient ε_r varies as a function of the degree of buoyancy, Figure 7.69 also reveals that the use of a constant transport coefficient is untenable in buoyant plume flow computations and can lead to order-of-magnitude errors. A numerical experiment was carried out to

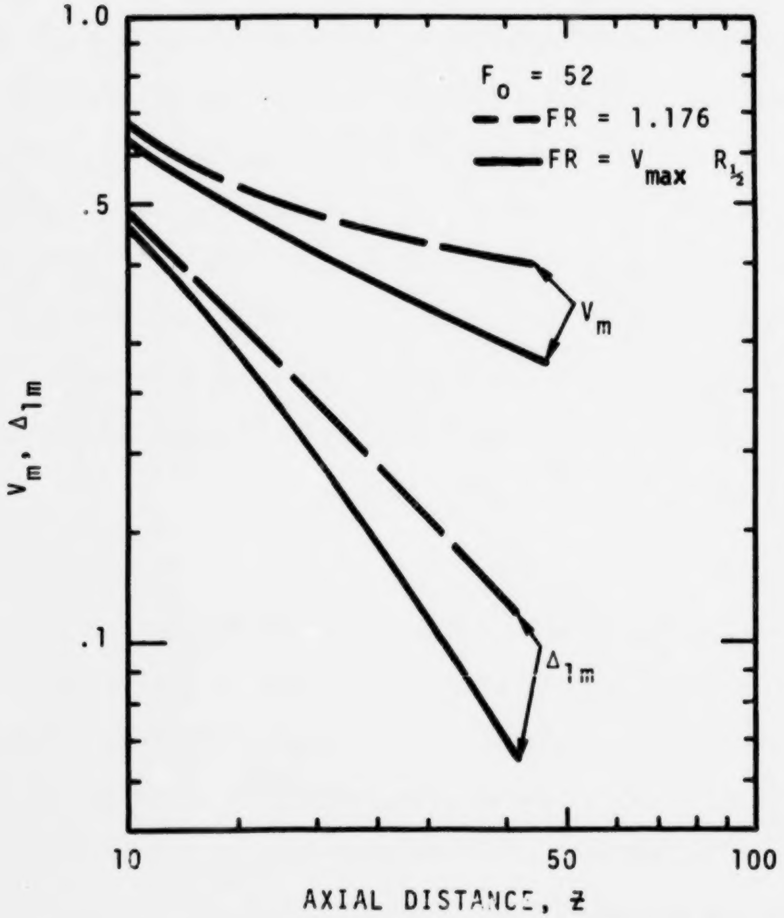

Figure 7.69. Comparison of Computation Using Constant and Variable Radial Eddy Transport Coefficients

ascertain these differences for F_o = 52 using the Type 1 boundary condition. Figure 7.69 illustrates that large errors will occur in both the centerline velocity and buoyancy distribution if ε_r = constant is used. The curves corresponding to Cases 15 (FR = constant) and 16 (FR = $V_{max}R_{1/2}$). Also refer to Figure 7.49.

In the early development of the computer program, how to effect the variable transport computation iteratively was unknown and such attempts led to numerical instability. Although this problem was surmounted later (see Section 7.3 for stability problems related to variable ϵ_r and ϵ_z), as an interim step, the mixing length $R_{1/2}$ was computed prior to computation from similarity assumptions for the given Froude number. With $R_{1/2}$ fixed, FR was computed from Equation (7.60), and eliminated this source of numerical instability. However, the solution was only nominally more accurate than using FR = constant. Hence, this method was adjudged inadequate and, as mentioned earlier, later abandoned.

Region II

The zone of flow establishment is characterized by turbulence regimes (see Figure 7.70), 1) the potential core, a roughly conical region, where mixing is dictated by the convected pipe flow turbulence, and 2) the zone of intense mixing lying outside the potential core, spreading into the ambient, and created by the shear between the effluent and the ambient fluids. A mixing length, ℓ_c, may be philosophically defined as being proportional to the width of the shear region. However, the geometry is difficult to define and the criterion as to the width of the mixing zone is quite arbitrary. Also the length of the mixing zone, Z_e, that is, the point where the zone of intense mixing reaches the plume centerline, is also quite arbitrary and certainly is not defined by a sharp point as Figure 7.70 indicates. Tomich [99] bypassed the mixing length problem in the region by setting ϵ_r = .2 times the value in the established flow regime. For a momentum jet, this value was found to yield downstream results in good agreement with experimental results.

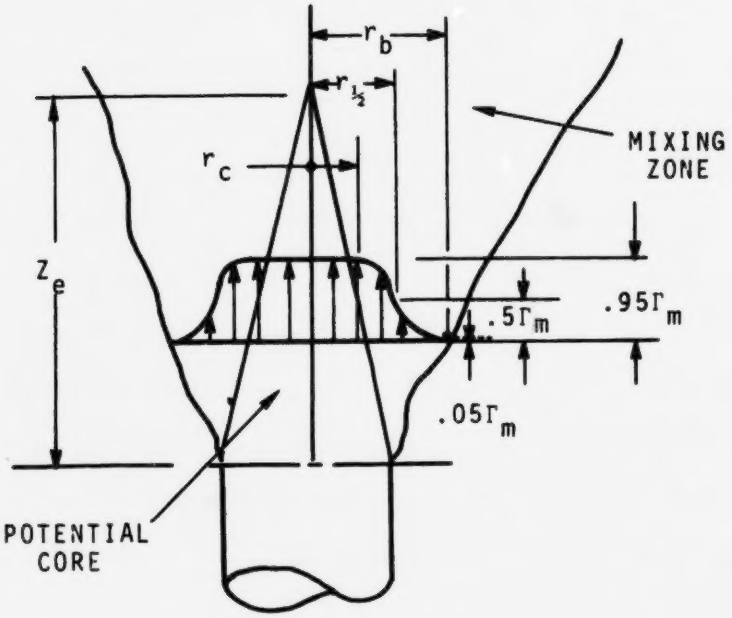
r_b
$r_{½}$
r_c
MIXING ZONE
Z_e
$.5\Gamma_m$
$.95\Gamma_m$
$.05\Gamma_m$
POTENTIAL CORE

Figure 7.70. Concentration Distribution in the Zone of Flow Establishment

In this study, we have not followed Tomich's method since we deal with cases of high relative buoyancy (low densimetric Froude numbers).

To set up a turbulence model for this regime we need:

1) a mixing length, and

2) a definition of the region of application:

- radial region
- vertical extent.

To compute a mixing length, a reasonable criterion is

$$\ell_c = r_{1/2} - r_c$$

where r_c is the radius of the potential core and $r_{1/2}$ is again the half-radius. The transport coefficient is then defined by,

$$\epsilon_{rc} = .0256\ (r_{1/2} - r_c)\ v_{max}. \tag{7.68}$$

Physically, ϵ_{rc} would apply over the region $r_b - r_c$, where r_b is the mixing zone outer boundary.

The next problem then is to define r_c based on some relevant mean flow quantity. In the present work, the concentration profile was used for such a criterion. Velocity could not be used because of power law boundary profiles and because buoyancy tends to distort the velocity profile. The criterion was set as

$$r_c = r_{.95} \tag{7.69}$$

or r_c extended to the point where the concentration was decreased to 95% of the centerline value. The outer boundary was set as

$$r_c = r_{.05} \tag{7.70}$$

or where the concentration had decreased to 5% of the centerline value. The length of the potential core was computed from the criterion

$$z_c = z_{.90} \tag{7.71}$$

where the concentration at the plume centerline is reduced to 90% of the initial value. The numerical model does not account for derivatives resulting from variations in ϵ_r[1], and where convection terms dominate transport, this deletion is valid. However, in the flow establishment region, this treatment can lead to large constituent discrepancies if the gradients of ϵ_r are not accounted for. For this reason and other computational difficulties, ϵ_r has been assumed radially constant at a given elevation, laterally to the plume cut-off.

Based on Equation (7.68) along with criterion Equations (7.69) and (7.71) a typical computed potential core and half-radius is illustrated in Figure 7.71 for $F_0 = 46$. This method for computing the transport coefficient was felt to be unsatisfactory in that the computations were slowed down compared to preset specification, and definition of the potential core appears to have questionable accuracy. However, one fact was established as a result of these experiments in that $R_{1/2} \simeq 1.0$ for all cases run. The method finally used was to define the length, Z_e, based on a criterion similar to Equation (7.71), use a straight line fit between the

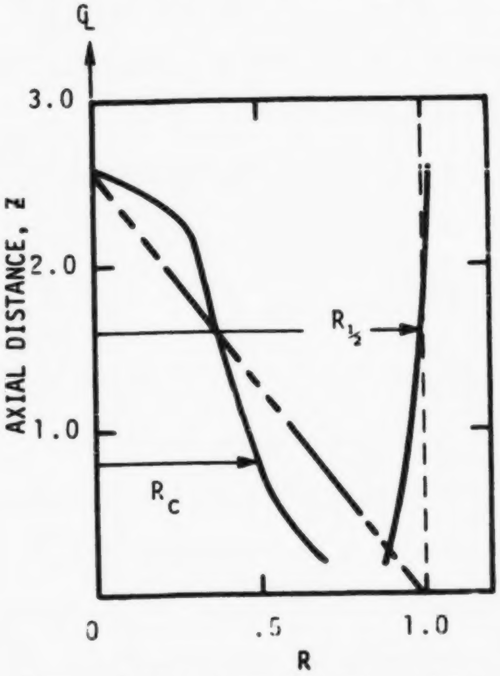

Figure 7.71. Computed Potential Core and Half-Radius $F_0 = 46$

---

[1] Refer to Equations (3.73) and (3.80) and note the computer program does not contain any viscous terms envolving derivatives of ϵ_r. It may be shown that such terms are small except in Region II.

points $(0,Z_e)$ and $(1.0,Z_o)$ to define the potential core, and set $R_{1/2} = 1.0$ up to Z_e (see dashed lines on Figure 7.71). This procedure was found to be satisfactory and added speed to the computation.

The remaining problem, in computing quantities within Region II, is that the computer model treats ε_{rc} constant across a lateral plane, where, in fact, there is considerable variation. Treating ε_{rc} constant in this fashion is to overestimate the diffusion coefficient within the core since the value used is typical of the turbulent mixing region. The net result of this procedure is to effectively reduce the computed core length which can result in downstream errors. One way to bring the computed core length more in line with experimental results concerning the core lenth is to reduce the value of ε_{rc}.

One such model, which is based solely on numerical experiment is given by,

$$\varepsilon_{rc} = .0256\ (r_{1/2}-r_c)(r_{1/2}-r_o)/r_{1/2}\ v_{max} \qquad (7.74)$$

which is the same as Equation (7.68) except for the multiplication factor $(r_{1/2}-r_c)/r_{1/2}$. This factor has the effect of reducing the eddy diffusion, given by Equation (7.68), near the outfall and has decreasing importance as the end of the potential core is approached. This model for radial eddy diffusivity gives good results over the entire range of Froude numbers for deep water plumes (see Figure 7.72) and is the preferred method of computing ε_r. All cases discussed earlier are based on Equation (7.68) where applicable. The case for $F_o = 1$ illustrated in Figure 7.72 may be compared with Figure 7.55 (Case 24). Cases displayed in Figure 7.72 were computed on a 26x25 grid.

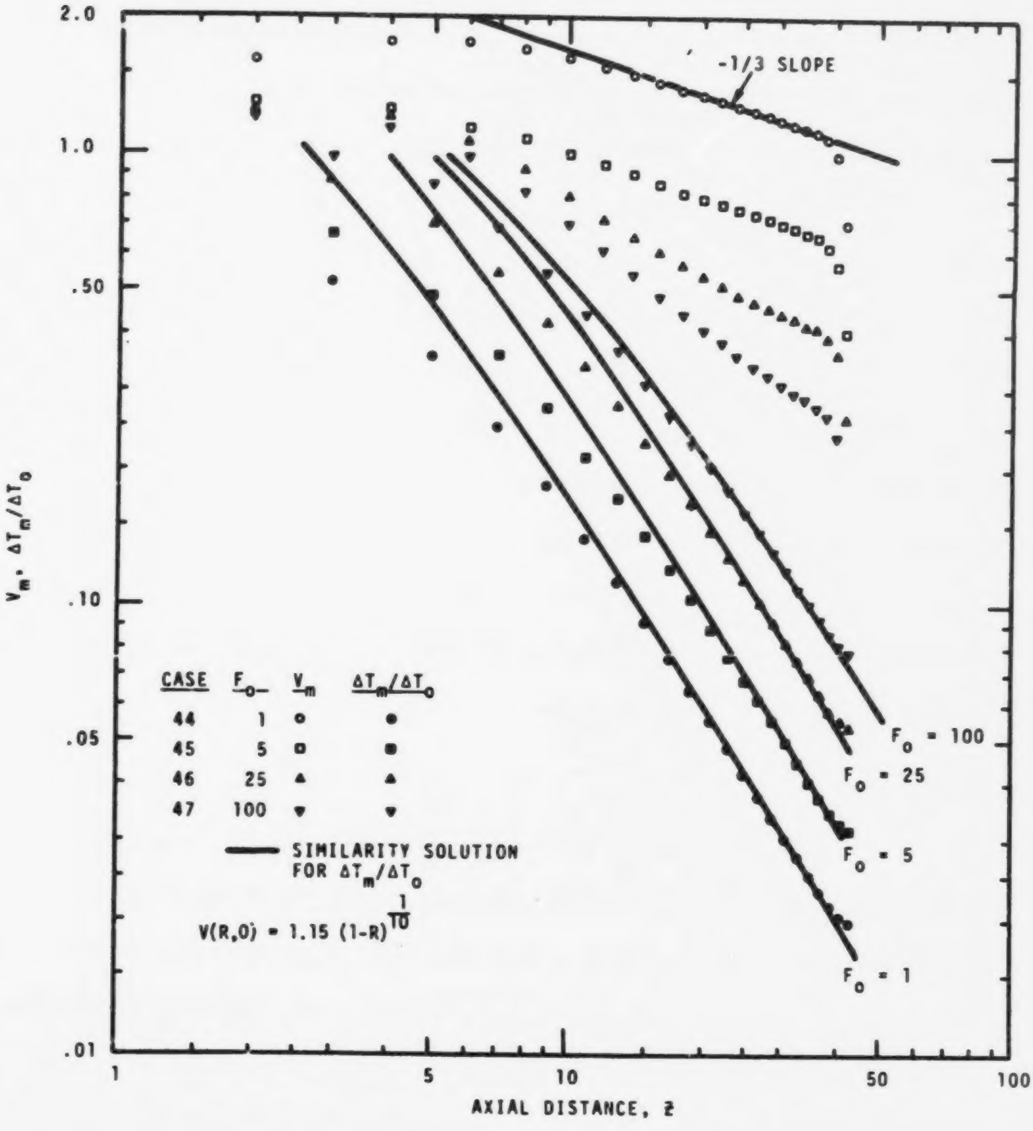

Figure 7.72. Centerline Velocity and Temperature Distribution for 44 Diameter Deep Outfall

For the purpose of comparing results using the two different methods for computing ϵ_r in the core, refer to Figure 7.73, which illustrates the centerline temperature distributions for intermediate water depth cases. A summary of these four cases may be found in Chapter 8, Table 8.1 listed as Cases 48, 49, 50 and 51 for Froude numbers 100, 25, 5 and 1, respectively. Note that Equation (7.68) (Figure 7.73) yields much more rapid deterioration of the centerline temperature than Equation (7.72) (Figure 8.1, Chapter 8).

Results from Figure 8.1 may also be compared to Figure 7.72. Note that for the deep water cases at low Froude number, the centerline temperature distribution again decays more rapidly near the source than for corresponding cases at intermediate depths. This discrepancy is caused by lack of axial finite difference resolution in the core region of the deep water results.

Region III

In the region outside the plume, the value of ϵ_r is set to a reference constant that is descriptive of the ambient conditions. Reasonable variations of this value have been found to have little effect on the circulation patterns or on the plume computed quantities. In fact, several early runs were made letting ϵ_r in the ambient take the same value as computed within the plume. Only slight differences were noted in the plume size when the value of the ambient was set to 1% of the plume interior value.

Most calculations and the present version of the computer program use a "cut-off" point (see Figure 7.66) for ϵ_r at a point just outside

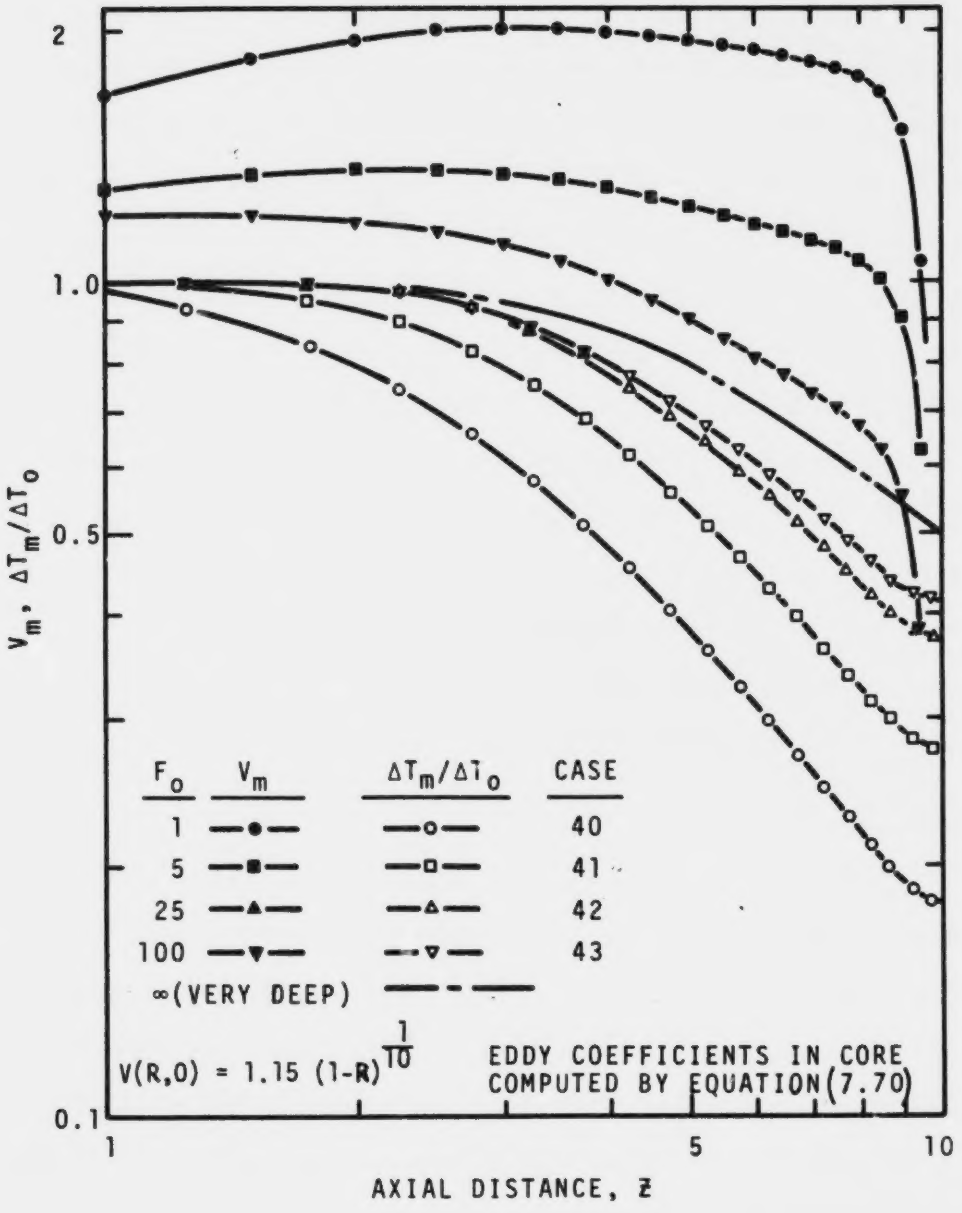

Figure 7.73. Computed Centerline Velocity and Temperature Excess. Cases for 10 Diameter Deep Water.

the plume where radial convective effects dominate radial transport (again radial derivatives in ϵ_r are neglected). The first attempt to establish a radial cut-off was based on Γ (concentration) dropping to 5% of the centerline value. This seemed to be a reasonable criterion but proved to be computationally unacceptable because oscillation of the cut-off point position between nodes, near the plume boundary, dramatically slowed convergence and grossly added to the computation time. The convergence problem was eliminated by extending the cut-off point two nodes beyond the Γ = 5% criterion, but resulted in a "ragged" plume edge, the raggedness being unrelated to flow physics (Figure 7.74). The next step was to preset an envelope in which the plume would always exist and ϵ_r could be held constant at a particular elevation. This envelope extends two to five nodes beyond the Γ = 5% criterion but is computationally very attractive because convergence is significantly speeded with no real loss of accuracy.

Region IV

In the lateral surface spread, the plume boundary is defined by the presence of the circulating or reverse flow field. For a vertical cut-off point, the boundary is extended two nodes below this region of negative radial velocity. The value of ϵ_r is set to the value computed within the vertical rise region and being held radial constant. For all cases run, the convective effects are reasonably large in this region; hence, ϵ_r is of minor importance.

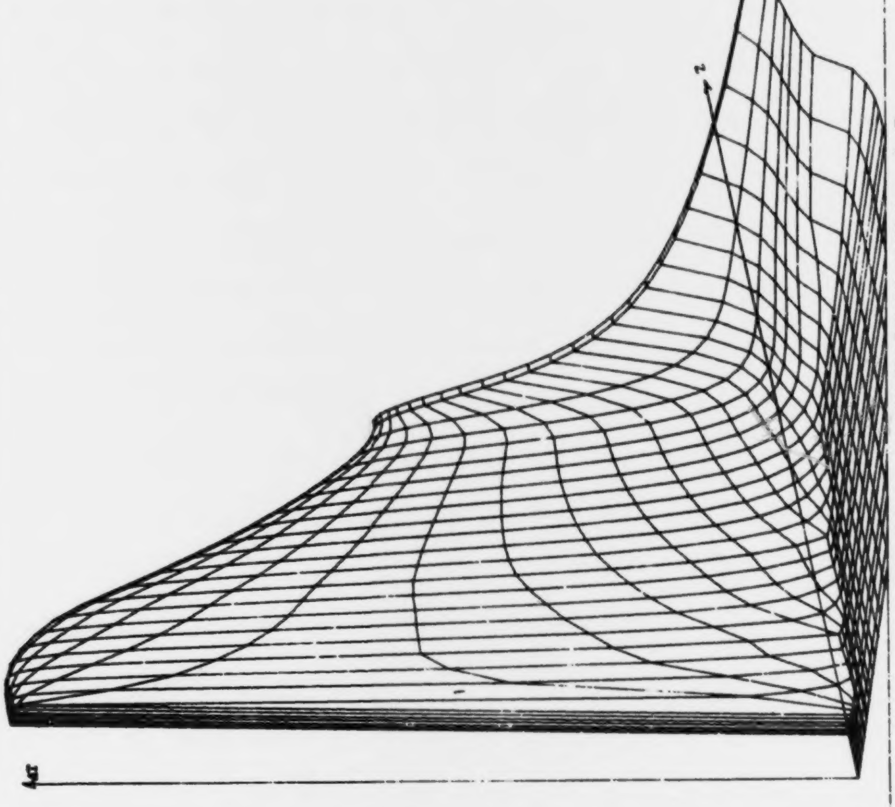

FIGURE 7.74. 3D ILLUSTRATION OF TEMPERATURE FIELD--ΔT

7.2.2 The Vertical Transport Coefficient, ε_z

Referring to Figure 7.66, the unique regions of vertical eddy diffusion computation are identical to those of the radial component. However, it is generally true that for the present model only one of the coefficients, ε_r and ε_z, will be of major importance in a given region. For instance, in Regions I and II, ε_r was found to play a major role in computing the plume dynamics, whereas, for all intents and purposes, ε_z may be ignored. This statement is proved by numerical experiment (Case 10, Figure 7.11) where ε_z was set to ε_r in the mixing zone. Only minor differences were noted between Case 10, and Case 6 where ε_z was set to a constant value of .001. From our knowledge of jet induced turbulence we expect that point-wise, ε_r and ε_z should be nearly the same in Regions I and II. (cf. Hinze [40]). Some differences may be noted near the surface where larger vertical mixing scales are suppressed.

The fact that vertical mixing is of little importance in Regions I and II may be ascertained on theoretical grounds by comparing the order of magnitude of the various vertical transport terms in the Equations of motion (3.67). Although the details are not presented here, one finds that vertical convection dominates vertical diffusions in these regions, an expected result, except near the surface where the two transport mechanisms may play equally important roles.

Hence, we may dispatch concern for ε_z in Regions I and II remote from the surface, without further investigation. However, numerical experiments have shown that ε_z is very important in Region IV and there is, nevertheless, incentive for extending the vertical cut-off to the plume centerline to overlap that portion of Region II.

Region III

The vertical transport coefficient associated with Region III is that of the ambient sea, and as such, ε_z depends on water depth, currents, sea state and ambient stratification. Extensive work has been carried out by the Oceanographic community to determine ε_z as influenced by the above mentioned variables. Summaries and discussions of this work may be found in work by Koh and Fan [52], and Wada [107].

The presence of vertical stratification can dramatically impede vertical mixing, whereas shear force tends to enhance this mixing. Hence, the vertical mixing coefficient must depend on, in some fashion, the relative importance of the stabilizing effect of stratification and the destabilizing forces of shear flow. The local Richardson number, RI, relates the relative importance of these forces through the ratio

$$RI = \frac{\text{stabilizing forces}}{\text{destabilizing forces}} \quad ,$$

$$RI = - \frac{\frac{g}{\rho}\frac{d\rho}{dz}}{\left(\frac{dU}{dZ}\right)^2} \quad . \qquad (7.73)$$

In terms of the dimensionless quantities defined in this manuscript,

$$RI = \frac{-1}{2F_o} \cdot \frac{\frac{d\Delta_1}{dZ}}{\left(\frac{dU}{dZ}\right)^2} \quad . \tag{7.74}$$

If RI < 0, the flow is obviously unstable. Various researchers have proposed methods for computing ε_z using a Richardson number correlation. The most notable of the efforts are summarized in Table 7.5. Note that in this discussion we are speaking of a general vertical eddy transport coefficient with no distinction between the transport of material, heat or momentum. Since any correlation for general application is at best a rough approximation, we are assuming that the vertical Prandtl (or Schmidt) number is unity.

The various correlations given in Table 7.5 are essentially Richardson number modifications of the neutral diffusion coefficient ε_{z_o}. Thus, the first task lies in determining ε_{z_o} for a neutral ambient (RI=0). Kent and Pritchard [51] give one such correlation for the wave induced component, for the James river estuary, as

$$\varepsilon_{z_o} = .01d \left(1 - \frac{d}{L}\right) \frac{H}{T} \; e^{-2\pi d/\ell} \tag{7.75}$$

where

d = distance from the surface,

L = depth of the water body,

H = wave height,

T = wave period, and

ℓ = wave length.

For a well mixed surface layer only, Golubeva [33] and Isayeva

TABLE 7.5. CORRELATION OF THE VERTICAL DIFFUSION COEFFICIENT ϵ_z WITH THE LOCAL RICHARDSON NUMBER, RI (extracted from Koh and Fan [52])

Note: $\epsilon_{z_o} = \epsilon_z$ at RI = 0, i.e., the neutral case, β: proportionality constant; varies from case to case.

Rossby and Montgomery (1935)*	$\epsilon_z = \epsilon_{z_o} (1 + \beta \, RI)^{-1}$	
Rossby and Montgomery (1935)*	$\epsilon_z = \epsilon_{z_o} (1 + \beta \, RI)^{-2}$	
Holzman (1943)*	$\epsilon_z = \epsilon_{z_o} (1 - \beta \, RI)$	$RI \leq \frac{1}{\beta}$
Yamamoto (1959)*	$\epsilon_z = \epsilon_{z_o} (1 - \beta \, RI)^{1/2}$	$RI \leq \frac{1}{\beta}$
Mamayev (1958)*	$\epsilon_z = \epsilon_{z_o} e^{-\beta \, RI}$	
Munk and Anderson (1948)**	$\epsilon_z = \epsilon_{z_o} (1 + \beta \, RI)^{-3/2}$	

$\beta = 3.33$ based upon data by Jacobsen (1913) and Taylor (1931)

*As given by Okubo (1962)

**As given by Bowden (1962)

and Isayev [47] give

$$\epsilon_{zs} = .02 \frac{H^2}{T} \quad . \tag{7.76}$$

Figure 7.75 (extracted from Reference [52]) illustrates the relationship between ϵ_{zs} and the local sea state.

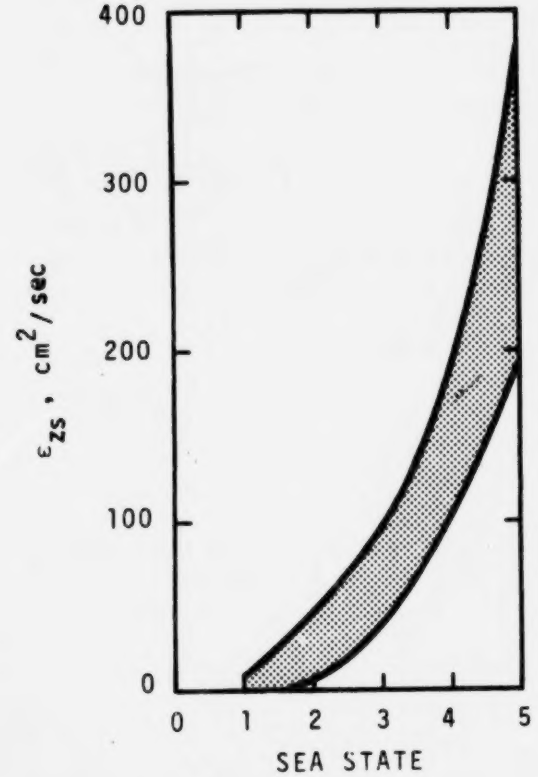

Figure 7.75. Dependence of ϵ_z on Sea State

For the case of tidal currents, Wada [107] gives

$$\epsilon_{z_o} = \frac{K^2 U_s \sqrt{d}\, z}{L\sqrt{L} \log \dfrac{\sqrt{L} + \sqrt{L-L_o}}{\sqrt{L} - \sqrt{L-L_o}}} \tag{7.77}$$

where K is the Karman constant, U_s is the surface current, L_o is the scale of the bottom roughness. Where both components, tidal currents and wind waves, are acting, Wada gives

$$\varepsilon_{z_o} = \frac{K^2 (d+L_o)^2 \, Z2}{L^2} \quad \frac{\sqrt{L} \, U_s}{\gamma \sqrt{d + L_o} \, Z} + \frac{8H}{T} e^{-2\pi d/\ell} \qquad (7.78)$$

Various measured values of $\rho\varepsilon_z$ are given in Table 7.6 (extracted from Reference [107]).

In the absence of ambient currents Harremoes [36] gives

$$\varepsilon_z = \frac{5 \times 10^{-3}}{\rho_o} \left(- \frac{d\rho/\rho_o}{dz} \right)^{-2/3} \text{ cm}^2/\text{sec} \qquad (7.79)$$

where z is in meters. This correlation was obtained off the coast of Denmark. Koh and Fan have obtained the relationship

$$\varepsilon_z = - \frac{10^{-4}}{\frac{d\rho/\rho_o}{dz}} \text{ cm}^2/\text{sec} \qquad (7.80)$$

where again z is in meters. Data used in obtaining this result is displayed in Figure 7.76.

Any estimate of ε_z or ε_{z_o} in the ambient sea has questionable accuracy. At best, these correlations, and measurements for that matter, are accurate only for the observed conditions, conditions which may change drastically with time and location. Aside from this complication, just how the researcher deduced the transport coefficient value from physical measurements may shadow the validity of results

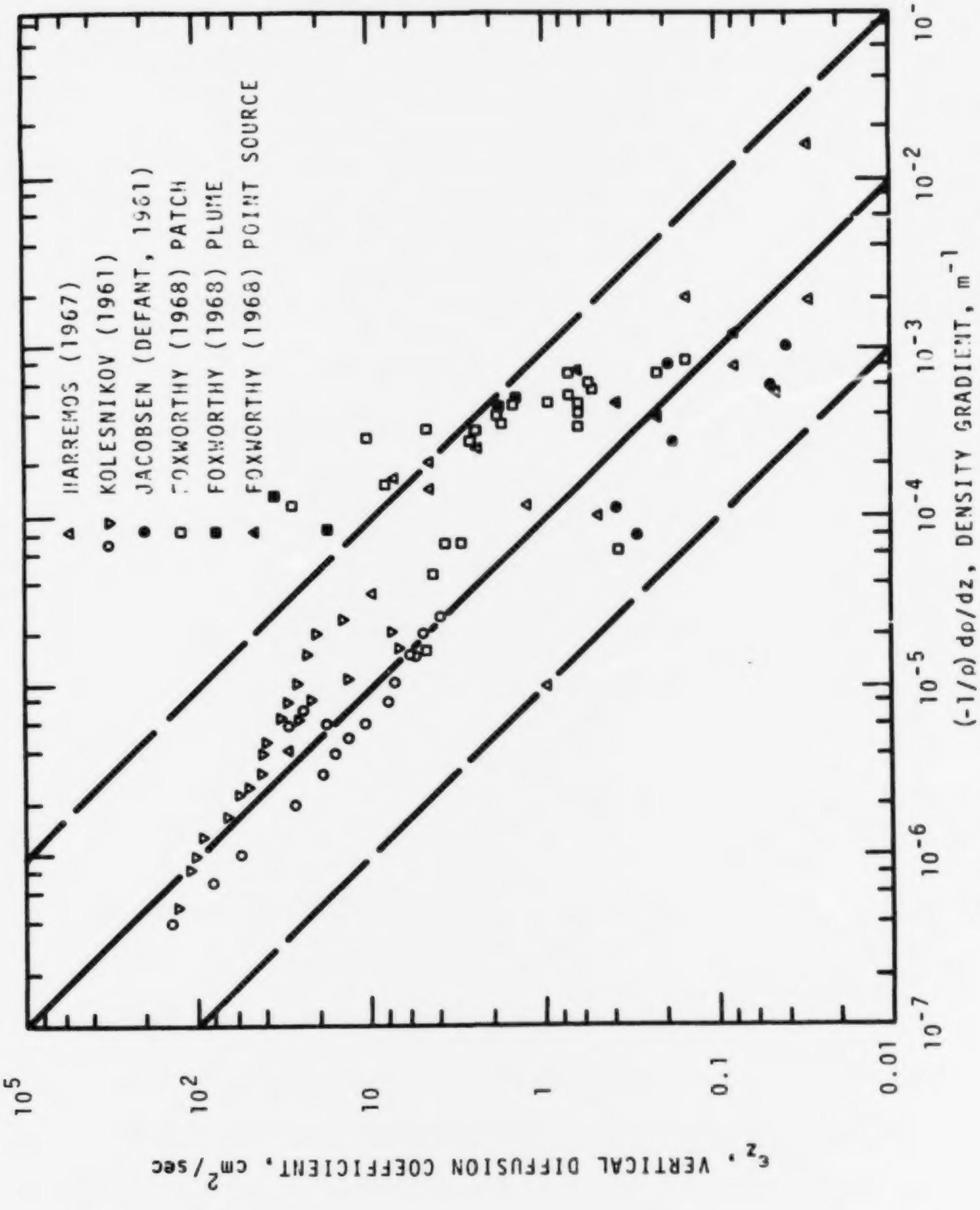

Figure 7.76. Correlation of ε_z with Density Gradient

TABLE 7.6. VALUES OF VERTICAL EDDY VISCOSITIES IN THE SEA

Current or Sea Region	Layer	$\rho\epsilon_z$ in g/cm/sec	$\rho\epsilon_z$ Derived From	Reference
All oceans	Surface	a) $\rho\epsilon_z = 1.02W^3$ (W 6m/sec) $= 4.3W^2$ (W 6m/sec)	Thickness of upper homogeneous layer (wind currents)	Thorade, 1914 Eckman, 1905
North Siberian Shelf	0 to 60m	75-260	Tidal currents	Sverdrup, 1926
North Siberian Shelf	0 to 60m	10-400	Tiual currents	Fjeldstad, 1936
North Siberian Shelf	0 to 22m	b) $385(\frac{Z+0.1}{22.1})^{3/4}$	Wind currents	Fjeldstad, 1929
Schultz Grund	0 to 15m	1.9-3.8		Jacobson, 1913
Caspian Sea	0 to 100m	0-224		Stochman, 1936
North Sea	0 to 31m	75-1720	Strong tidal currents	Thorade, 1928
Danish Waters	0 to 15m	c)1.9-3.8	All currents	Jacobson, 1928
Kuroshio	0 to 200m	d)680-7500	All currents	Suda, 1936
Japan Sea	0 to 200m	150-1460	All currents	Suda, 1936
off San Diego	Near the sea bottom	e) 93-(z+0.02)	Tidal currents	Revelle & Fleming

a) W = wind velocity in m/sec
b) z = distance from sea bottom in meters
c) Very great stability
d) Very strong currents
e) z = distance from sea bottom in meters

and the application to numerical modeling. Generally, these coefficients are deduced from concentration measurements and back-calculated through an analytical diffusion equation. Hence, the values are valid only for the diffusion equation used to calculate them in the first place. Just how appropriate these values are as they enter into more elaborate numerical computation is open to question in this author's opinion. It is felt that the determination of ambient diffusion coefficients is an area that needs extensive research.

In the present computer model for Region III diffusion coefficients, various of the models discussed above were tried. Very little difference was noted in the Region III circulation patterns in any case. Influence on the plume was noted only when the value of ε_z was unrealistically large, in which case the flow dynamics took on the characteristics of a creeping flow. For this reason ε_z was set to a value on the order of 10^{-4} to 10^{-3} ft^2/sec in Region III for succeeding computation, a value corresponding to moderate stratification, low sea state, and low ambient current.

Region IV

In modeling the plume lateral spread, the vertical turbulence component is of utmost importance. As the plume encounters the surface and begins the radial surface spread, plume induced turbulence dominates the mixing phenomena. At increased radial distance, the induced turbulence decays and is suppressed by stratification. Generation of turbulent energy by virtue of the lateral shear flow is also declining because of smaller velocity gradients. At some larger radial distance the field of turbulence will be dominated by ambient effects such as sea state.

We have just discussed the ambient contribution to ε_z and indicated rough methods for such calculation. The plume induced turbulence in the zone of initial spread (or the transition zone) is the important feature of Region IV. Unfortunately there is very little data available in the literature which is directly applicable to the problem of turbulence modeling in this zone.

From a theoretical point of view, we assume that Prandtl's second hypothesis holds, or that

$$\varepsilon_{z_o} = C_1 \ell_2 u_{max} \tag{7.81}$$

for the neutrally buoyant case. We also expect that a Richardson number modification of Equation (7.81) would suffice for the case of a spreading thermal layer, of the form

$$\varepsilon_z = C_1 \ell_z u_{max} f(RI) \tag{7.82}$$

For the neutrally buoyant situation we may gain some insight as to how the produce $\ell_z u_{max}$ behaves by assuming the flow can be approximated by a radial jet similarity solution. The appropriate similarity equations for a radial jet following the methods devised by Morton, et al. [60] for a vertical jet, are

Continuity:

$$\frac{d}{dr}(u_m r \tau) = \alpha \tau u_m \tag{7.83}$$

Radial momentum:

$$\frac{d}{dr}\left(u_m^2\, r\tau\right) = 0. \qquad (7.84)$$

In the above equation a "top-hat" velocity profile has been assumed, where u_m is the mean radial velocity, τ is the characteristic thickness of the jet and α is the usual entrainment constant. The use of the top-hat velocity profile is entirely satisfactory for purposes here, since we are only interested in the relative behavior of τ and u_m, which is insensitive to the similarity profile used.

Solving these equations, one finds

$$u_m r = \text{constant} \qquad (7.85)$$

and

$$u_m^2 r\tau = \text{constant} \qquad (7.86)$$

Hence,

$$(u_m r)(u_m \tau) = \text{constant},$$

and

$$u_m \tau = \text{constant}. \qquad (7.87)$$

Equation (7.87) reveals that if the velocity field is approximately similar then the eddy coefficient ϵ_z must be constant in view of Prandtl's second hypothesis (a result identical to the axisymmetric jet). Hence

$$\epsilon_{z_0} = C_1 \ell_z u_{max} = C_1 \cdot \text{Constant} \qquad (7.88)$$

The remaining problem lies in evaluation of C_1 and $(\ell_z u_{max})$.

In the present work, C_1 is assumed to take the value .0256 as in the case of the axisymmetric flow region.

The quantity $\ell_z u_{max}$ was treated by four different methods during numerical experiments as listed below.

Method 1:

Compute the value of ℓ_z from the local velocity profile based on the distance from the level of maximum lateral velocity to the level where lateral velocity is 1/2 the maximum value. That is,

$$\ell_z = z_{1/2}.$$

This method is identical to that used to compute FR, but in the instance of lateral flow was found to be unsatisfactory because of numerical instability. All attempts to compute FZ_o, where

$$FZ_o = Z_{1/2}U_{max}, \qquad (7.89)$$

iteratively from local information were found to be unstable and the method was abandoned.

Method 2:

Use a constant value of $Z_{1/2}$ based on the value of $R_{1/2}$ at the point of lateral spread. This method proved to yield diffusivities which were too large.

Method 3:

Use a constant value of $FZ_o = Z_{1/2}\ U_{max}$ where $Z_{1/2}$ and U_{max} for the entire system are computed in the vertical plane where the maximum lateral velocity occurs. This method, based on the insight given by the similarity solution, also yielded diffusivities which were too large. This method was applied only to cases having buoyancy; hence, the failure may have been due to an inappropriate Richardson number modification of FZ_o.

Method 4:

Use the method given immediately above, except scale the result by the local ratio (U_{max}): $(U_{max})_{system}$. As in the two methods immediately above, this calculation proved to be numerically stable under all conditions once a reasonably realistic lateral velocity distribution was established. But, unlike the above methods, local diffusivities are computed which give more realistic velocity fields. Hence,

$$RE_{ZO} = RE_{z(ref)}/FZ_o \tag{7.90}$$

and

$$FZ_o = Z_{1/2}\, U_{max}$$

where $Z_{1/2}$ is calculated at the system maximum lateral velocity and U_{max} is the local maximum lateral velocity. The subscript o again indicates the condition of neutral buoyancy.

To account for local stratification, the local Richardson number model due to Mamayev (cf. Reference [108]) was employed,

$$\varepsilon_z = \varepsilon_{z_o}\, e^{-\beta RI} \tag{7.91}$$

where RI is again the local Richardson number as defined by Equation (7.76) and β is an empirical constant. Wada [108] used Equation (7.91) in his study of planar thermal outfalls discharging horizontally, but used a constant value of ε_{zo}.

Although there is no data known to the author relating point eddy diffusivities to the point Richardson number in turbulent jets, data has been obtained which relates the entrainment of such flow to the overall Richardson number (cf. Ellison and Turner [25]). Stolzenbach and Harleman [94] have illustrated that the data of Ellison and Turner may be adequately represented by the form,

$$\frac{\alpha_z}{\alpha_{z_0}} = e^{-5RI'} \qquad (7.92)$$

where α_z and α_{z_0} are the entrainment coefficients for buoyant and neutral spreading surface flows, respectively, and RI' is the gross Richardson number. Stolzenbach also illustrates the relationship between eddy viscosity and entrainment as

$$\frac{\varepsilon_z}{\varepsilon_{z_0}} = \frac{\alpha_z}{\alpha_{z_0}} \quad .$$

Thus, based upon the data of Ellison and Turner, and the functional relationship, Equation (7.92), derived from this data, the Manayev Equation (7.91) is apparently a credible method for modifying point-wise neutral eddy diffusion coefficients for application in laterally spreading buoyant plumes. In the computer program, we use the form,

$$\varepsilon_z = \varepsilon_{z_{ambient}} + \varepsilon_{z_0} e^{-\beta RI} \qquad (7.93)$$

The computer program is also set up to use the various other models given in Table 7.5. These models have not been used owing primarily to lack of appropriate information concerning the empirical constant β.

The value of β (for Equation 7.93) used by Wada [108] was .8 for momentum diffusivity and .4 for heat diffusivity based on ambient conditions. According to work done by Stolzenbach this value should be appreciably higher for plume flow. Computations using various values of β for the present work are illustrated in Chapter 8.

In the present work, another form of ϵ_z has been used, primarily for starting solutions where Equation (7.93) results in numerical instability. This form is given by the equation

$$\epsilon_z = \epsilon_{z_{ref}} e^{-(Ad)^2} \tag{7.94}$$

where d is depth or distance from the surface. The result is a Gaussian depth decay of eddy momentum diffusivity from a surface reference value. Equation (7.94) is used in computation merely as a computational aid and is abandoned in favor of Equation (7.93) once reasonable velocity and temperature profiles are established, or a numerically stable situation is attained.

7.3 Numerical Stability and Convergence

During the course of this investigation various experiments were performed dealing with solution stability and convergence. For each case run, at least five node points were monitored for convergence rates of U, V and Γ. Additionally, the program computes the maximum change of ψ, Ω, and Δ_1 throughout the system at selected iterations, and an overall Γ balance error is computed at the end of each run. Liebmann relaxation factors were employed to each of the equations for ψ, Ω, Δ_1, and Γ to either accelerate or decelerate solutions.

7.3.1 Numerical Stability

To define what is meant by numerical stability in this manuscript, we take the opposite view--that of numerical instability. The reasoning for this view is that it is entirely possible that the system of buoyant fluid may have physical instabilities which are not divergent. The solution which we are trying to attain may, in fact, be physically unsteady, and may never be attained by steady flow methods. Since the Gauss-Seidel method with under/over-relaxation is not unlike certain transient methods (see Appendix E), continued iteration may reveal a cyclic behavior of the computations. This situation cannot be termed a numerical instability. It merely illustrates the inability of steady flow techniques to simulate transitory flow physics.

To demonstrate this idea, the computer program was set to a different task, that of predicting the flow field past the end of a cylinder contained in a larger pipe. From experiments we know that, at low Reynolds numbers, streamlines past the end simply are distorted toward the centerline, much as the case of irrotational flow (Figure 7.77-A). At much higher Reynolds numbers, vortex shedding from the end of the cylinder will occur and the flow field is termed unsteady although patterns may be repeated in time or in a cyclic fashion (Figure 7.77-B).

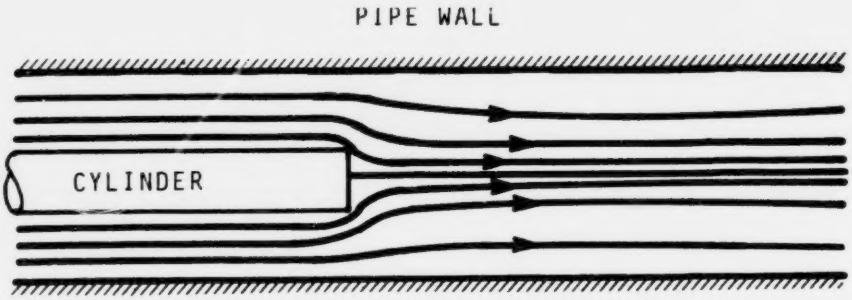
PIPE WALL
CYLINDER

A. LOW REYNOLDS NUMBER (CREEPING FLOW)

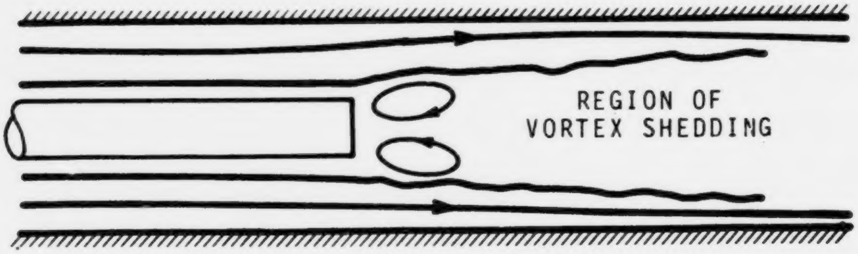
REGION OF
VORTEX SHEDDING

B. HIGH REYNOLDS NUMBER

Figure 7.77. Observation of Flow Patterns Past the End of a Cylinder

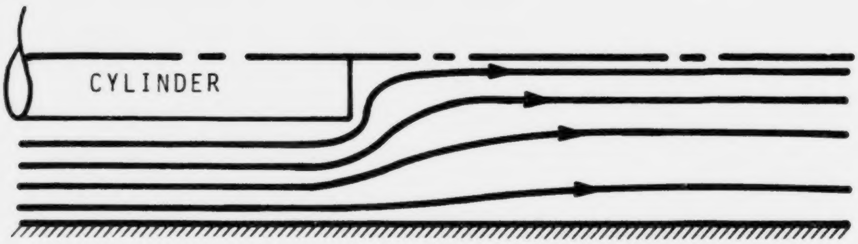

A. LOW REYNOLDS NUMBER (CREEPING FLOW)

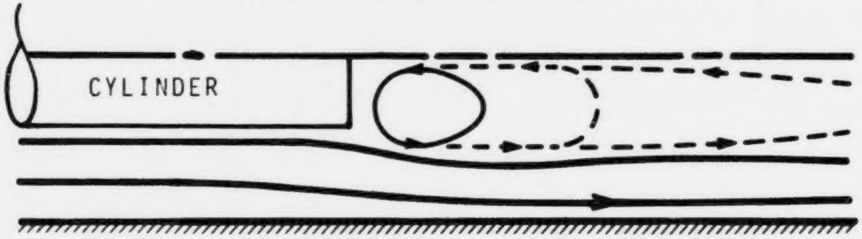

B. HIGH REYNOLDS NUMBER

Figure 7.78. Computed Flow Patterns Past the End of a Cylinder

We expect that the steady flow computer program would converge to a steady solution at low Reynolds number, and, in fact, this was the result as illustrated in Figure 7.78-A. At a high Reynolds number, however, a converged solution could not be attained. Computed quantities demonstrated quite the same behavior that one would expect from a transient solution to this problem. Generally, as computation proceeded, a recirculation pattern formed behind the cylinder, grew by elongation, and collapsed to nearly circular form, and elongated again (see Figure 7.78-B). This process occurred repeatedly as computation continued. Although it is impossible to quantify the physics from these results, it is reassuring to know that the numerical technique will reveal the presence of a physical instability, or unsteady flow, and not converge to an erroneous steady solution.

Thus, it is entirely possible to have non-converging (although not diverging) solutions that are not associated with numerical instability. Hence, we define numerical instability as that situation which upon repeated iteration leads to increasingly divergent and physically ridiculous results.

As a general observation, involving perhaps a hundred or more computer runs of various duration, the numerical techniques used were found to be unconditionally numerically stable provided that:

- All Liebmann acceleration factors were less than unity,
- All eddy diffusion coefficients were constant, or the velocity field at the beginning of computation has at least reasonable similarity to the final solution.

These observations are a result of flows having Reynolds numbers from 0 to infinity and a variety of other testing conditions. Based on these numerous experiments, difficulties encountered by other authors, the accuracy outlined in Section 7.1, and comments made by Spalding [91], the present difference formulations and grid system used is extremely attractive.

At an early date in this investigation it was discovered that solutions invariably became unstable if the acceleration factor, L_T, for the Ω and Δ_1 transport equations was greater than unity. However, the value $L_E = 1.6$ was used for the stream function, Ψ, elliptic equation without difficulty. Later, it was discovered that under some flow condition, the value of L_E also needed to be less than unity to avoid instability. For cases involving constant eddy coefficients, only the transport equations needed to be decelerated. After these initial investigations, the general rule used was to decelerate all equations or set L_E and $L_T < 1.0$. The general form of the decelerated solutions is

$$\Gamma_p^{n+1} = \Gamma_p^n + L(\Gamma_p' - \Gamma_p^n) \qquad (7.95)$$

where the subscript p indicates the nodal point in question, n is the n^{th} iteration and Γ_p' is the result of the n+1 unaccelerated Gauss-Seidel iteration.

A value

$$L_E = L_T = .999 \qquad (7.96)$$

was found to be satisfactory for nearly all cases. In a few instances of very shallow water and non-linear ε_r and ε_z, values as low as L_T = .80 were used. In all cases, the acceleration factor is applied as soon as Γ' is computed at a node.

No attempt of a theoretical analysis of stability will be presented here since the presence of non-linear eddy coefficients negate meaningful analysis and the case of constant diffusion coefficients has been presented by various authors, [7,111], at least for time dependent problems. Some insight to stability of steady state computations is given in Appendix A. Further insight into this question may be gained by the analysis given in Appendix D which compares the Gauss-Seidel iteration technique to an appropriate (similar) transient solution.

It was, perhaps, propitious that a superior grid system was devised at the outset of this study (see Figures 5.3 and 5.4). In a recent publication, Spalding [91] points out that making vorticity adjustments in a cluster of five adjacent points and the stream function at the central point has a striking effect on divergence removal for reasons unknown. Unlike the grid system to which Spalding refers where vorticity and the stream function are computed at the same space points, the present grid system is staggered. The vorticity values which interact as a source for the stream function elliptic equation is averaged from the four adjacent neighbor points, which is closely akin to the method referred to by Spalding and may be responsible in part for the seemingly inherent stability of the present method.

Another aspect of the present computational technique is that linear gradients are always used for flux terms whether on the boundary or in the interior, by the use of fictitious boundary cells. Spalding again points out that higher order methods for treating boundary conditions may in fact lead to less accurate results due to violation of reciprocity and conservation principles at boundaries. In the present method, through the use of the correct conservative difference equations and fictitious boundary cells, quantities are identically conserved. This feature may also contribute to the success of the technique in avoiding instabilities propagated from system boundaries.

7.3.2 Convergence

The question of solution convergence has been partially answered in the preceding section. It is obvious that solutions which are numerically unstable will not converge. On the other hand, it is also possible that a solution which is numerically stable will not converge as demonstrated in the example of flow past the end of a cylinder at high Reynolds number (Section 7.3.1).

The condition for convergence used in this work is defined by

$$\left| \frac{f_p^{n+1} - f_p^n}{f_p^{n+1}} \right| \simeq \delta_f \tag{7.97}$$

where δ_f is the convergence criterion for the quantity f. The subscript p again indicates the nodal point in question and n is the nth iteration. The condition for δ_f approaching zero is not a sufficient condition to guarantee solution accuracy, however, since the numerical procedure may in fact converge to an erroneous solution. The method used in this work to decrease the probability of erroneous solutions was to check the continuity of matter by evaluating net flux of matter at the system boundaries and selected interior planes. This check is subsequently referred to as the Γ-balance error ($\delta\Gamma$), Γ referring to a conservative constituent. This quantity is effectively given as a surface integral for the system in the form of

$$\delta\Gamma = \left\{ \frac{\int_{S_T} \Gamma(\vec{V}\cdot\hat{n})\, dS + \int_{S_T} (-\nabla\epsilon_\Gamma \Gamma)\cdot\hat{n}\, dS}{\int_{S_{in}} \Gamma(\vec{V}\cdot\hat{n})\, dS + \int_{S_{in}} (-\nabla\epsilon_\Gamma \Gamma)\cdot\hat{n}\, dS} \right\} 100\% \qquad (7.98)$$

where S_T represents a vertical plane in the flow field and S_{in} is a radial plane at the inflow boundary extending to R_0. Equation (7.98) gives $\delta\Gamma$ as a percent error of the system inflow.

Typical results showed the Γ-balance error to be on the order of 1%.

General observation of the various numerical experiments illustrated the following:

- The convergence rate decreased significantly with increased grid size.
- The stream function distribution converged with respect to δ_ψ more rapidly than vorticity and buoyancy (or Γ).

- Vorticity was the slowest to converge and also the most erratic.
- Convergence of all quantities near the outfall was much more rapid than in the far field. Thus, sizable errors in the far field did not influence the validity of solutions near the outfall.
- The relative magnitude of buoyant forces compared to inertial forces played a significant role in the rate of convergence. Highly buoyant effluents (low F_0) converged much slower than pure inertial flows.
- Runs made with constant eddy diffusivities converged much more rapidly than those runs using variable coefficients.
- One inner iteration (stream function elliptic equation) was sufficient. Increasing the number of inner iterations served to aggravate the convergence rate.
- Deeply stratified cases (as opposed to surface layer stratification) significantly aggravated the convergence rate. This item is discussed further in Chapter 8.
- Neglecting derivaties of ϵ_z in the transport equations led to Γ-balance errors on the order of 10-20% where variable ϵ_z was employed.
- Beginning a solution from an irrotational flow solution as opposed to zero velocity everywhere, appeared to have no particular advantage, and in some instances tested, actually slowed convergence.

Most computer runs were initialized from a restart tape generated by a previous case. There was considerable economy in this action since a solution would need to be started from a zero initial velocity distribution (or irrotational distribution) only when the grid layout was changed. Unfortunately. from another aspect however, not many solutions beginning at iteration number one and ending at convergence are available for comparison. To illustrate the convergence behavior, some of the computational aspects will be compared for identical grid layouts. This information is displayed in Tables 7.7, 7.8 and 7.9 for grid layouts of (JxK) 40x33, 31x34, and 26x25, respectively.

The four cases cited in Table 7.7 constitute the worst lot as far as convergence lethargy is concerned. The starting run was the momentum jet case which took 800 iteration cycles to converge properly. All succeeding cases used the momentum jet solution as initializing information. Of these succeeding cases, the run for $F_o = 1$ (buoyancy dominated) was the most reluctant to converge. Convergence lethargy in this lot is laid chiefly to grid size although there is some suspicion that cell aspect ratio and position of the inflow-outflow boundary also have some effect. Figure 7.79 shows the convergence history of Ψ, Δ_1 and Ω for the 40x30 grid layout. This illustrates the behavior of δ_{max} for these variables where again the momentum jet is used as a starting solution (first 800 iterations) for the succeeding runs $F_o = 46$ and $F_o = 1$. As noted previously, δ_{max} is the maximum relative change in the entire system and does not always occur

TABLE 7.7 CONVERGENCE BEHAVIOR, 40x33 GRID

	Starting Case	Succeeding Cases		
		A	B	C
$\Delta \xi$	.12591	.12591	.12591	.12591
ΔZ	2.0	2.0	2.0	2.0
F_o	∞	46*	1.0*	1000*
Start Variable ε_r and ε_Z, Iterations	75	801	801	801
Total Iterations	800	1100	1400	1200
Incremental Iterations	800	300	600	400
Γ - Balance Error	- .1281	.734	- .4641	- .9133
δ_{max} Stream Function	1.195×10^{-4}	6.571×10^{-5}	2.92×10^{-5}	6.989×10^{-5}
at Node	37,10	20,37	14,32	37,9
δ_{max} Vorticity	7.221×10^{-3}	3.191×10^{-3}	1.466×10^{-3}	9.422×10^{-3}
at Node	32,6	26,5	37,12	32,6
δ_{max} Buoyancy Parameter	3.210×10^{-3}	7.380×10^{-4}	3.345×10^{-4}	1.508×10^{-3}
at Node	37,2	2,33	2,33	37,2

*Indicates variable changed in restart case.

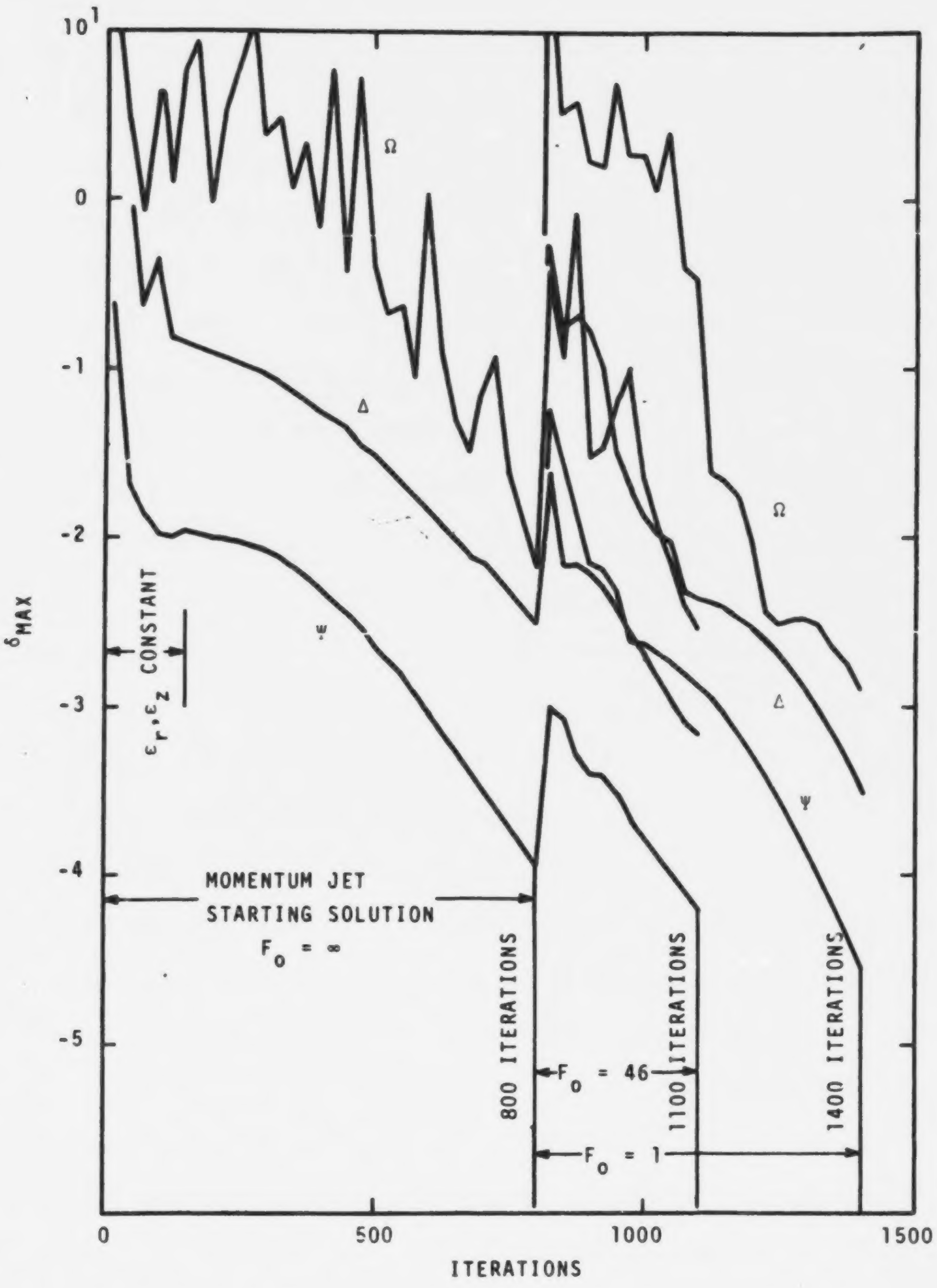

Figure 7.79. Convergence Behavior, 40x33 Grid

at the same cell. Figure 7.80 illustrates the convergence history of the starting solution for V at nodes (2,20) and (2,30) and Γ at node (10,33).

Table 7.8 illustrates similar data for a 31x34 grid layout. Convergence in this lot is rather slow also. Note that the values for δ_{max} are considerably larger in this lot than in the lot given in Table 7.7, although the Γ-balance error is about the same. The explanation is that δ_{max} gives a relative change, and these changes are occurring where the absolute value of the quantity is very small. For instance, the maximum relative change of vorticity in the starting case is .1595, whereas the value of vorticity at this point is -9.76×10^{-6} (the maximum value in the flow field is 2.944). Figure 7.81 shows convergence history of selected data.

Table 7.9 illustrates the convergence characteristics for the 26x25 grid. Note that each case is not finely converged with respect to δ_{max}, whereas the Γ-balance error is less than 1% in all cases. Thus, this table illustrates that the system may be reasonably well converged with regard to absolute quantities although relative changes in part of the system may be comparatively large. Also, only 150 iterations were required to obtain each solution using the starting run initialization.

For this case, the primary concern was plume centerline conditions. Changes of velocity and temperature were occurring only in the fourth and fifth significant figures along the centerline, indicating that computation time may be saved by using a regional

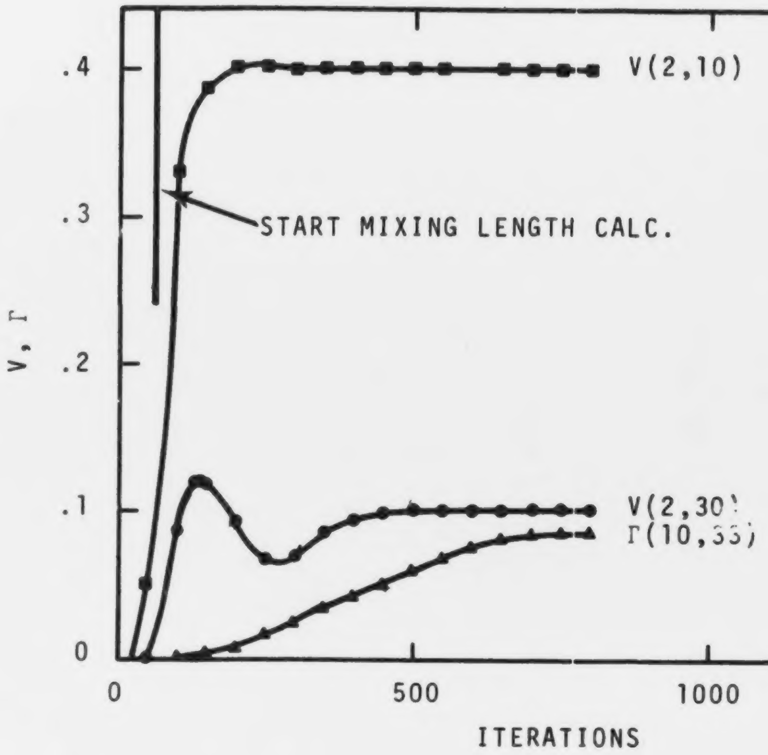

Figure 7.80. Convergence History of V and Γ at Selected Cells, Momentum Jet, 40x33 Grid

TABLE 7.8 CONVERGENCE BEHAVIOR, 31x34 GRID

	Starting Case	Succeeding Cases	
		A	
$\Delta\xi$	.14690	.14690	
ΔZ	.2	.175*	
F_o	51	105*	
Start Variable	150	601	
ϵ_r and ϵ_Z Iterations			
Total Iterations	600	900	
Incremental Iterations	600	300	
Γ-Balance Error	- .4381	.2778	
δ_{max}, Stream Function	1.350×10^{-3}	1.115×10^{-3}	
at Node	28,25	26,12	
δ_{max}, Vorticity	1.595×10^{-1}	1.455×10^{-1}	
at Node	23,24	23,23	
δ_{max}, Buoyancy Parameter	2.918×10^{-2}	4.126×10^{-2}	
at Node	20,5	30,13	

*Indicate changed variable

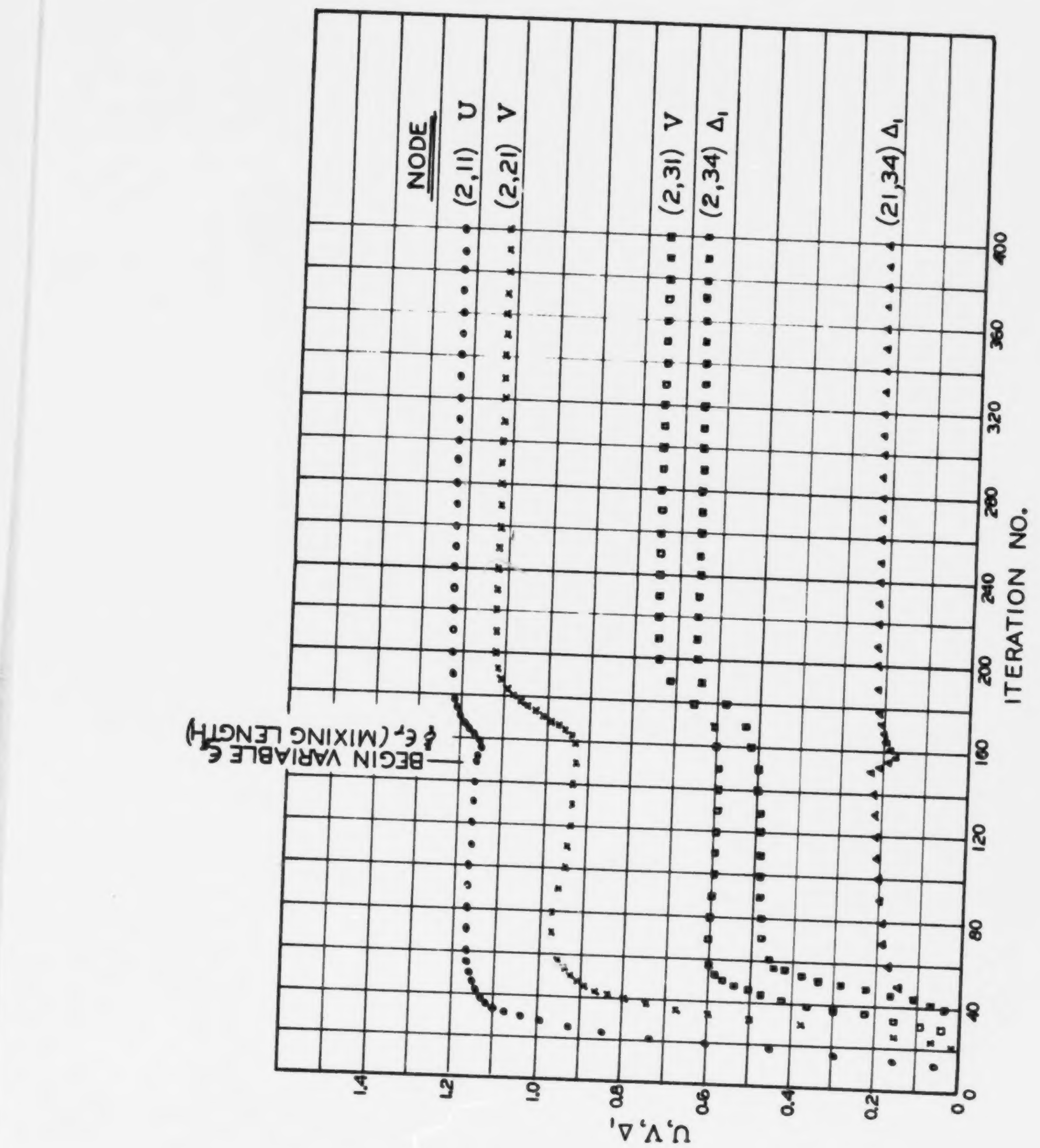

Figure 7.81. Convergence History of U, V and Δ_1 at Selected Cells 31x34 Grid

TABLE 7.9 CONVERGENCE BEHAVIOR, 26x25 GRID

	Starting Case	Succeeding Cases		
		A	B	C
$\Delta\xi$	.14690	.14690	.12591*	.14690*
ΔZ	.50	.50	.50	.50
F_o	1.0	5.0*	25.0*	100*
Start Variable ε_r and ε_z Iterations	100	400	600	800
Total Iterations	400	550	600	750
Incremental Iterations	400	150	150	150
Γ-Balance Error	.8035	.3700	- .9936	- .3203
δ_{max}, Stream Function at Node	1.644×10^{-4} (24,9)	1.011×10^{-3} (24,10)	2.135×10^{-3} (24,12)	2.210×10^{-3} (24,11)
δ_{max}, Vorticity at Node	1.776×10^{-3} (20,14)	9.350^{-2} (20,20)	5.345×10^{-2} (22,20)	5.435×10^{-1} (22,17)
δ_{max}, Buoyancy Parmater at Node	1.976×10^{-3} (24,6)	4.683×10^{-2} (21,20)	4.850×10^{-2} (24,3)	3.440×10^{-2} (24,5)

*Indicates changed variable.

convergence criterion. In the computer program one has some control over this criterion by applying the convergence check only out to a set radius.

As a final illustration of numerical convergence behavior, Figure 7.82 shows the iteration history of V and Δ_1 at one cell for Case 2 (see Table 7.1). The significance of this plot is that the velocity initialization is the irrotational flow solution (for the other cases cited, U and V are zero everywhere except the inflow boundary). Note that velocity V shows considerable oscillation.

The theoretical development of difference equations in this manuscript is based on Equations (5.8) for vorticity, Equations (5.9) for the transport of buoyancy and equations similar to (5.9) for the transport of materials. These equations make no allowance for contributions, or more accurately, corrections, issuing from variable eddy diffusivities. In the instance of Equation (5.9), these corrections may be made rather straightforwardly by adding the terms

$$\left(\frac{\partial \Delta_1}{\partial_r}\right)\left(\frac{\partial \varepsilon_{\gamma r}}{\partial_r}\right) + \left(\frac{\partial \Delta_1}{\partial Z}\right)\left(\frac{\partial \varepsilon_{\gamma Z}}{\partial Z}\right) \quad .$$

However, in Equation (5.8) the appropriate correction terms add considerable complication as noted by comparing Equations (3.80) and (3.81). Fortunately not all of the terms involving derivatives of ε_r and ε_z need to be incorporated into the numerical model either because they are zero in accordance with assumptions concerning the eddy coefficient model, or transported quantities are minute where

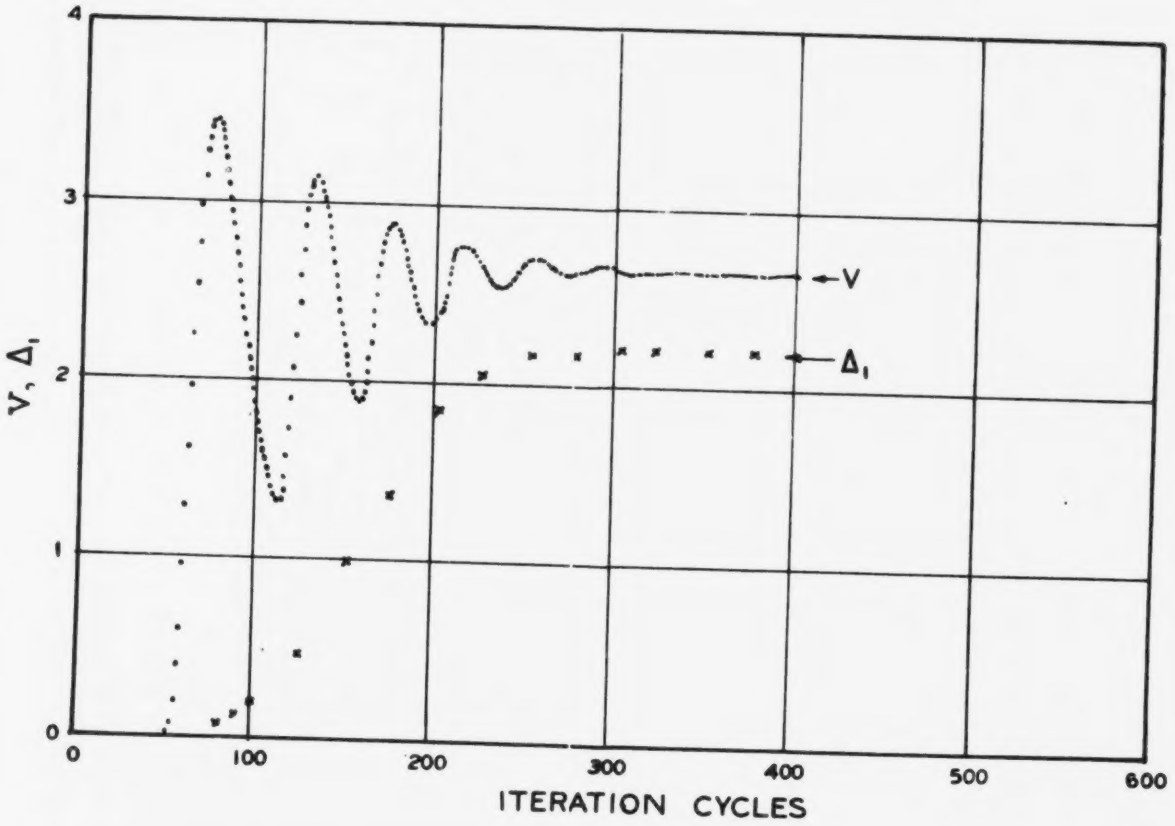

Figure 7.82. Iteration History for One Cell of Case 2

the variations occur. For instance, we may neglect all terms involving $\partial\varepsilon_r/\partial r$ since ε_r is constant where diffusion is important, and convective terms dominate the transport where step changes in ε_r occur. Likewise, other order-of-magnitude approximations may be made. Having eliminated these second order factors one is left with the correction terms for vorticity of:

$$\left\{\frac{1}{RE_Z} \quad 2\,\frac{\partial FZ}{\partial Z} \cdot \frac{\partial^2 U}{\partial Z^2} + \frac{\partial U}{\partial Z} \cdot \frac{\partial^2 FZ}{\partial Z^2}\right\}$$

where FZ is again the vertical eddy diffusion multiplier (cf. Section 7.2).

Similar approximation for Equation (5.9) yields the correction term,

$$\frac{1}{RE_Z PR_Z} \quad \frac{\partial FZ}{\partial Z} \cdot \frac{\partial \Delta_1}{\partial Z}$$

with a similar correction for Γ transport.

The importance of these terms was ascertained by the system Γ-balance. Without the corrections, the Γ-balance error ran as high as 20%. For the same conditions, addition of the correction terms reduced the error to less than 1%.

Before closing the subject of convergence, the author wishes to note that in all cases run where the transport equations were decelerated and turbulence modeling did not lead to numerical instability, the stream function convergence was extremely well behaved. This behavior was obtained by iterating only once on the Ψ elliptic equation; additional iterations were noted to aggravate the convergence of

Ψ as well as the transported quantities Ω, Δ_1 and Γ. It is entirely possible that the system would have converged equally well if even fewer Ψ iterations were performed, that is, iteration on Ψ only once for every two, three or perhaps five outer iterations. This facet was not investigated in the present study, but such experimentation could yield fruitful results in terms of computer time.

CHAPTER 8

NUMERICAL EXPERIMENTS FOR SHALLOW WATER CASES

Material presented in this chapter deals with application of the numerical techniques discussed earlier in shallow water situations. All computer runs presented here are for cases where the assumed water depth is ten or less port diameters above the outfall discharge. The techniques used are identical to those applied for the verification studies presented in the previous chapter.

Unlike cases in Chapter 7, however, applicable data are not available except for one case where surface temperature field data are available. Hence, we rely substantially on the verification study as an indicator of the validity of the computational techniques. Table 8.1 summarizes the cases to be discussed and illustrated in this chapter; those listed are only a portion of the total shallow water computer runs made during the course of the present research. Nonetheless, these cases are typical and space limitations preclude further illustrations.

8.1 Modeling the Vertical Eddy Diffusivity Multiplier, FZ

In the region of the lateral surface spread of shallow water plumes, modeling the vertical component of the pointwise eddy diffusivity plays an important role in determining the flow behavior. Considerable effort was devoted to this subject in Section 7.2.2; the computational methods used to obtain results presented in this chapter will be briefly reviewed.

TABLE 8.1 SUMMARY OF SHALLOW WATER CASES

Case No.	Grid Size	$\Delta\xi$	ΔƵ	Depth Ƶ	R_∞	F_o	D ft	V_o ft/sec	Boundary Type*	ΔT_o °C	σ_{tr} (amb)	Stratification**
48	26x25	.14690	.5	10	19.66	100	10	10.15	2,N=10	18.12	27.98	None
49	26x25	.14690	.5	10	19.66	25	10	5.075	2,N=10	18.12	27.98	None
50	26x25	.14690	.5	10	19.66	5	10	2.270	2,N=10	18.12	27.98	None
51	26x25	.14690	.5	10	19.66	1	10	1.015	2,N=10	18.12	27.98	None
52	26x25	.12591	.25	5	11.62	100	10	10.15	2,N=10	18.12	27.98	None
53	26x25	.12591	.25	5	11.62	25	10	5.075	2,N=10	18.12	27.98	None
54	26x25	.12591	.25	5	11.62	5	10	2.270	2,N=10	18.12	27.98	None
55	26x25	.12591	.25	5	11.62	1	10	1.015	2,N=10	18.12	27.98	None
56	31x34	.14690	.20	5.6	41.00	51	14	7.25	2,N=7	8.33	18.01	None
57	31x34	.14690	.20	5.6	41.00	51	14	7.25	2,N=7	8.33	18.01	None
58	31x34	.14690	.175	4.97	41.00	105	16	11.10	2,N=7	8.33	18.01	None
59	31x34	.14690	.175	4.97	41.00	105	16	11.10	2,N=7	8.33	18.01	None
60	30x26	.14690	.40	8.4	35.40	45	10	7.00	4	11.10	27.78	None
61	30x26	.14690	.40	8.4	35.40	45	10	7.00	4	11.10	24.78	2 °C
62	30x26	.14690	.40	8.4	35.40	45	10	7.00	4	11.10	24.78	3 °C
63	30x26	.14690	.40	8.4	35.40	45	10	7.00	4	11.10	24.78	4 °C
64	30x26	.14690	.40	8.4	35.40	45	10	7.00	4	11.10	24.78	5 °C
65	30x26	.14690	.40	8.4	35.40	45	10	7.00	4	11.10	24.78	5 °C
66	29x20	.12591	.15	1.42	16.97	.111	21	.574	2,N=10	13.80	25.57	None

* See Table 7.1

** Stratification extends somewhat deeper than in Case 63.

The general form of the vertical diffusion coefficient is

$$\varepsilon_z = \varepsilon_{z_{\text{ambient}}} + \varepsilon_{z_{\text{plume}}} \tag{8.1}$$

In the region of plume flow the ambient contribution will be insignificant; hence,

$$\varepsilon_z \simeq \varepsilon_{z_{\text{plume}}} \; . \tag{8.2}$$

The plume generated turbulence is a function of both mean flow character and thermal character.

Recall from Section 7.2.2,

$$\varepsilon_z = \varepsilon_{z_o} f(RI), \tag{8.3}$$

where ε_{z_o} is the vertical diffusion coefficient for neutrally buoyant conditions and f is a function of the point Richardson number, RI. Likewise, the vertical component multiplier, FZ, may be expressed as

$$FZ = FZ_o f(RI), \tag{8.4}$$

where FZ_o is the neutral buoyancy multiplier. The model for FZ_o may be expressed as (See Section 7.2.2)

$$FZ_o = Z_{1/2} (U_{max} - U_{min}) \; , \tag{8.5}$$

where $Z_{1/2}$ is the radial plume half-depth, and the radial velocity difference,

$$U_{max} - U_{min} = U_{max} \; ,$$

since $U_{min} \simeq 0$. Then

$$FZ_o = Z_{1/2} U_{max} . \tag{8.6}$$

If we followed the same method used for computing the radial multiplier,

$$FR = R_{1/2}\, V_{max}, \qquad (8.7)$$

$Z_{1/2}$ and V_{max} would be computed iteratively and pointwise to establish FZ_0 (Method 1, Section 7.2.2). However, all attempts to calculate FZ_0 based on local values of $Z_{1/2}$ and U_{max} led to numerical instability. Exactly why this condition persisted, especially in view of excellent success with Equation (8.7), was never ascertained. After several numerical experiments and correctional efforts without success, it was decided to stabilize the computation by restricting the computed value of the plume half-depth, $Z_{1/2}$, since this value seemed to exhibit the most unstable character in previous experiments. This decision led to Methods 2, 3 and 4, described in Section 7.2.2.

Method 2 used $Z_{1/2}$ based on $R_{1/2}$ computed at the elevation of lateral flow. $Z_{1/2}$ was then held constant for that iteration but the local value of U_{max} was used. This method led to eddy diffusion coefficients which were quite large and a correspondingly unrealistic flow field; hence, the method was quickly abandoned.

Method 3 computed a constant value of FZ_0 to be applied everywhere in the lateral plume spread. The value of FZ_0 in this method was set by computing $Z_{1/2}$ at the radial position corresponding to the maximum radial velocity; the value of U_{max} at this point along with $Z_{1/2}$ was used in Equation (8.6). Results from this method are presented in Section 8.4. Again, this method yielded diffusivities of excessive magnitude.

However, experimentation with this method was carried out, in every case, in conjunction with thermal flows (as opposed to neutrally buoyant conditions). It is possible that the Richardson number modifier, f(RI), was inaccurate.

Finally, the most realistic results were obtained by Method 4 which in principle uses the technique of computing $Z_{1/2}$ of Method 3, but bases U_{max} on the local value. This method was found to be always stable once the general, but approximate, flow patterns were established.

Table 7.5 summarizes several models for f(RI); however, the Mamayev correlation has been employed exclusively in this work which has the form,

$$f(RI) = e^{-\beta RI}, \qquad (8.8)$$

where β is an empirical constant.

The value of β to be used presents an additional uncertainty in computing FZ. Wada [108] used the value $\beta = .8$. However, Stolzenbach [94], based on the data of Ellison and Turner [25], suggests the value $\beta \simeq 5.0$ when using the gross Richardson number. We have used values ranging from .4 to 2.0 in this work (Table 8.2).

Table 8.2 below summarizes the computation of FZ for results presented in this chapter.

TABLE 8.2 SUMMARY OF FZ COMPUTATION

Case	Method	β
48-55	4	1.0
56	3	.4
57	3	.8
58	3	1.0
59	4	1.0
60-65	4	.8
66	4	2.0

Actual computation of FZ proceeds as follows: (sequence of operations for one outer iteration).

Based on the computed values of U, V and Δ_1 for the present iteration:

- Compute the array of local Richardson numbers,

$$RI(J,K) = -\frac{1}{2F_o}\frac{d\Delta_1}{dZ} \Big/ \left(\frac{dV}{dZ}\right)^2\Bigg|_{J,K},$$

- Scan the U array to establish the maximum value of U and the corresponding index, J.
- Compute the plume half-depth, $Z_{1/2}$, at index J.
- Use this value of $Z_{1/2}$ to compute

  $$FZ_o(J,K) = Z_{1/2}\, U_{max}$$

  where U_{max} takes on different values at each radial grid point.
- Compute

  $$FZ(J,K) = FZ_o(J,K)\, e^{-\beta RI(J,K)}$$

- Use the above value of FZ in computing transported quantities for the next iteration.

8.2 Results for Homogeneous Receiving Water 10 Port Diameters Deep

Results for plumes issuing in homogeneous receiving water at a depth of ten port diameters are reported as Cases 48 through 51. For these cases, the initial temperature excess is 18.12 ^{0}C and the value of sigma-t for both the effluent and reference ambient is 27.98. Each case represents a different densimetric Froude number as indicated in Table 8.1. Changes in the Froude number were effected by varying the effluent velocity. All initial velocity profiles are assumed to be turbulent and follow a profile given by Equation (7.17) with the exponent equal to 1/10. The port diameter is held constant at 10 feet and the lateral spread is computed out to about 10 port diameters.

Centerline distributions of velocity and temperature excess are illustrated in Figure 8.1 for all four cases. Note that the plume accelerates for low Froude numbers (F_0 = 1,5), but for Froude numbers of 25 and above, very little acceleration is noted even though turbulent mixing (as a function of distance from the port) is decreased (temperature excess curves). Velocity of the lateral surface spread is illustrated in Figure 8.2 for these same cases. Maximum velocity in each case occurs at radial distance between 1.5 and 2.0 diameters. In the highly buoyant Case 51, the maximum lateral velocity is nearly as great as the initial velocity. Note that these results are normalized to the average effluent velocity; hence, for F_0 = 1 the maximum lateral velocity is about 1 fps, whereas for F_0 = 1, the corresponding velocity is about 3.5 fps. Vertical profiles of lateral velocity for

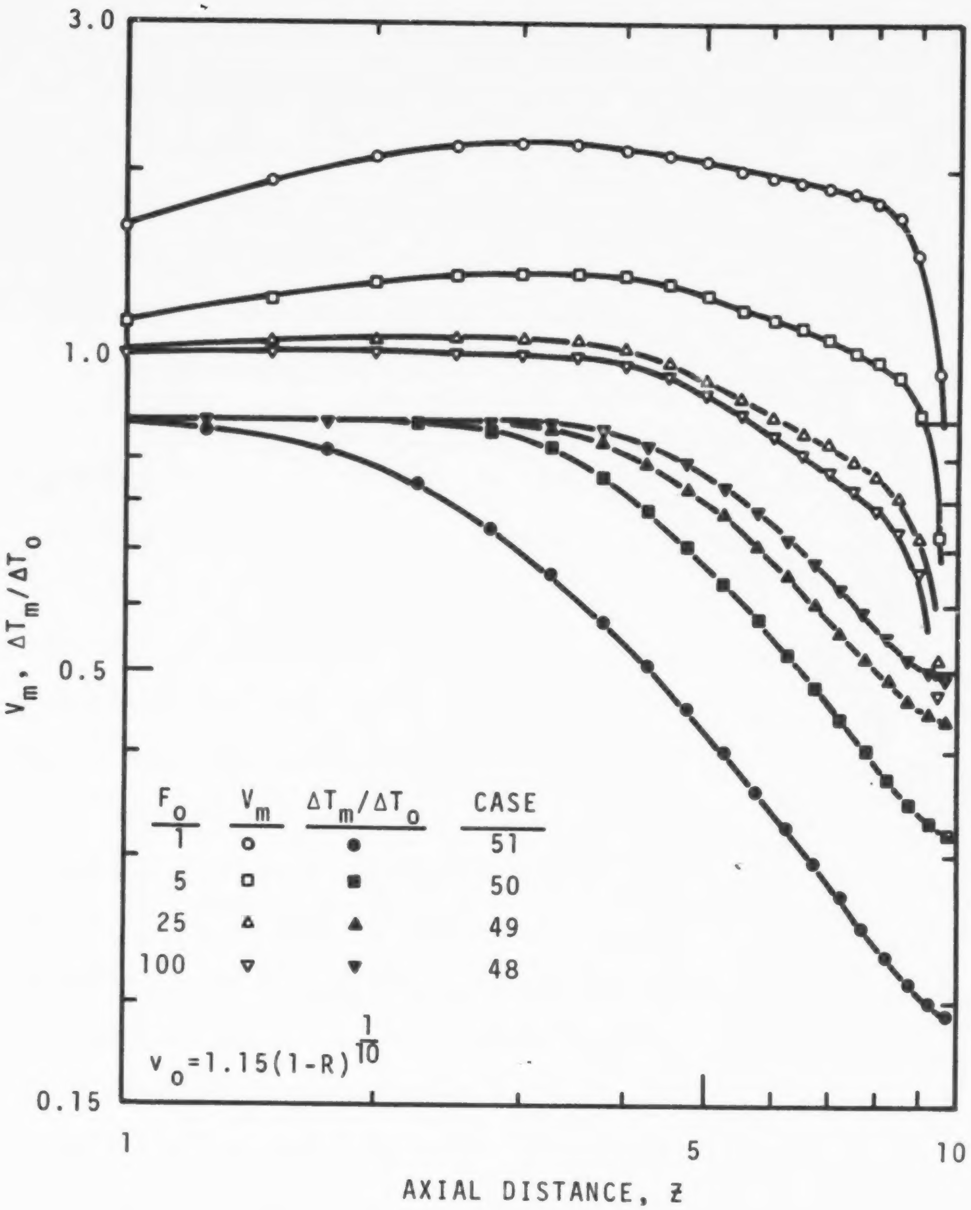

Figure 8.1. Computed Centerline Velocity and Temperature Excess for Intermediate Depth, Cases 48 Through 51 (10 diameters deep)

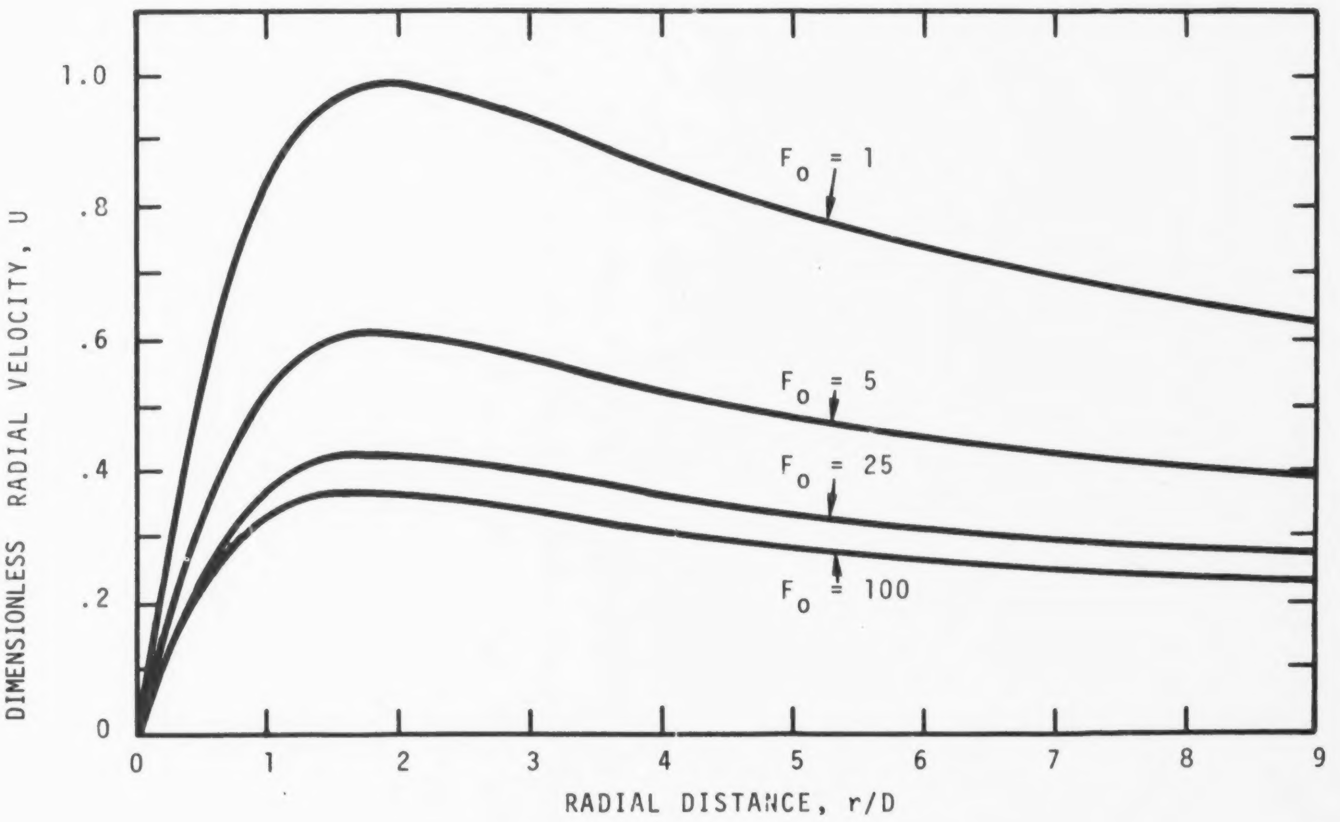

Figure 8.2. Surface Distribution of Radial Velocity, Cases 48 Through 51 (see Table 8.1)

Case 50 are illustrated in Figure 8.3.

Comparison of the radial velocity profiles are illustrated by Figures 8.4 and 8.5. Figure 8.4 is for a radial position of r/D=1.9, which corresponds approximately to the position of maximum velocity in all four cases. This figure also illustrates that radial entrainment occurs below the depth of about 10.5 (1.5 diameters from the surface) for these cases. At 7.32 diameters (Figure 8.5) the spreading surface layer is slightly thinner.

The small cross-hatched rectangle shown in Figure 8.5 illustrates the variation of the spreading depth for these cases. Greater penetration is noted at Froude number 100; F_o = 1 shows the least penetration.

The distributions of temperature excess at the surface ($\Delta T_s/\Delta T_o$) are illustrated by Figure 8.6. Vertical profiles of excess temperature ($\Delta T_s/\Delta T_o$) for Cases 48 and 50 are shown in Figure 8.7 (A and B). Note that the temperature profiles penetrate slightly deeper than the velocity profiles and indicate some minor recirculation of the heated water takes place.

A complete set of contour plots and three-dimensional illustrations for the stream lines, temperature and vorticity for Cases 48 through 51 are given in Figures 8.8 through 8.32.

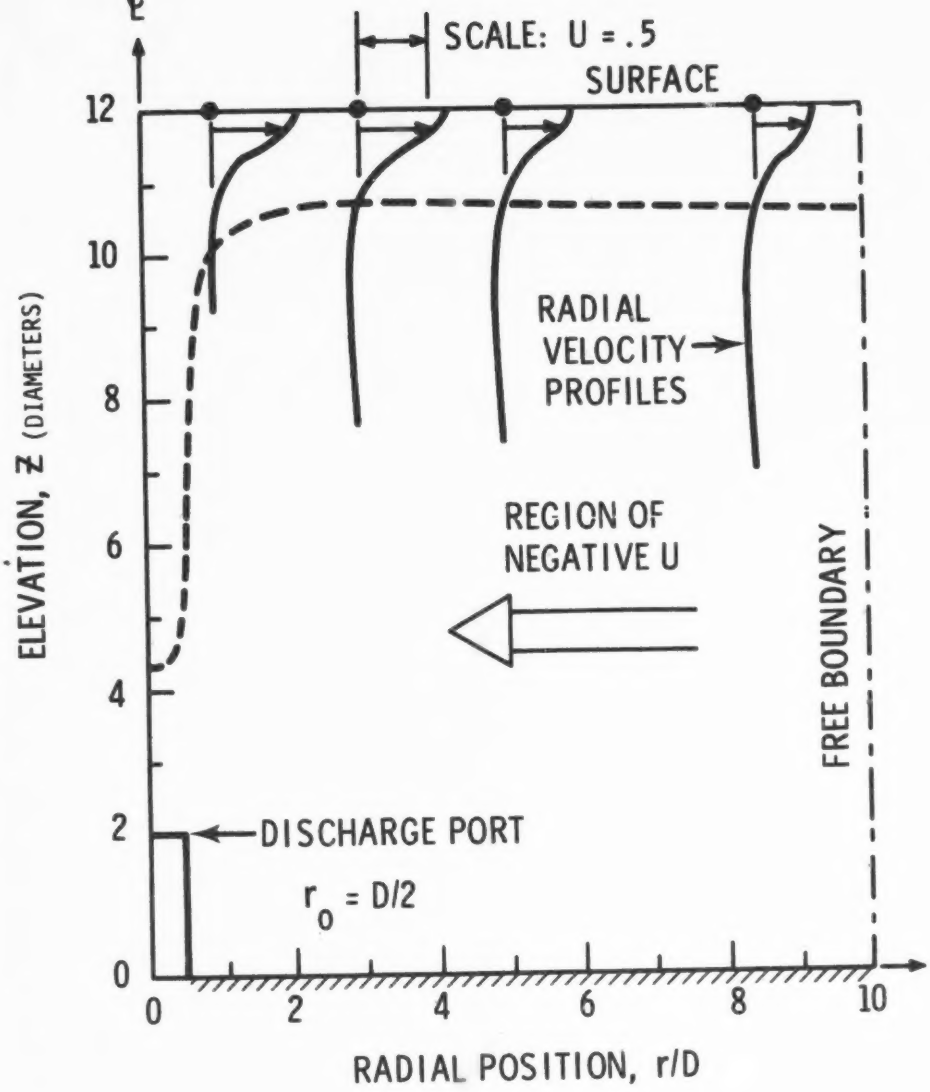

Figure 8.3. Distributions of Radial Velocity Case 50

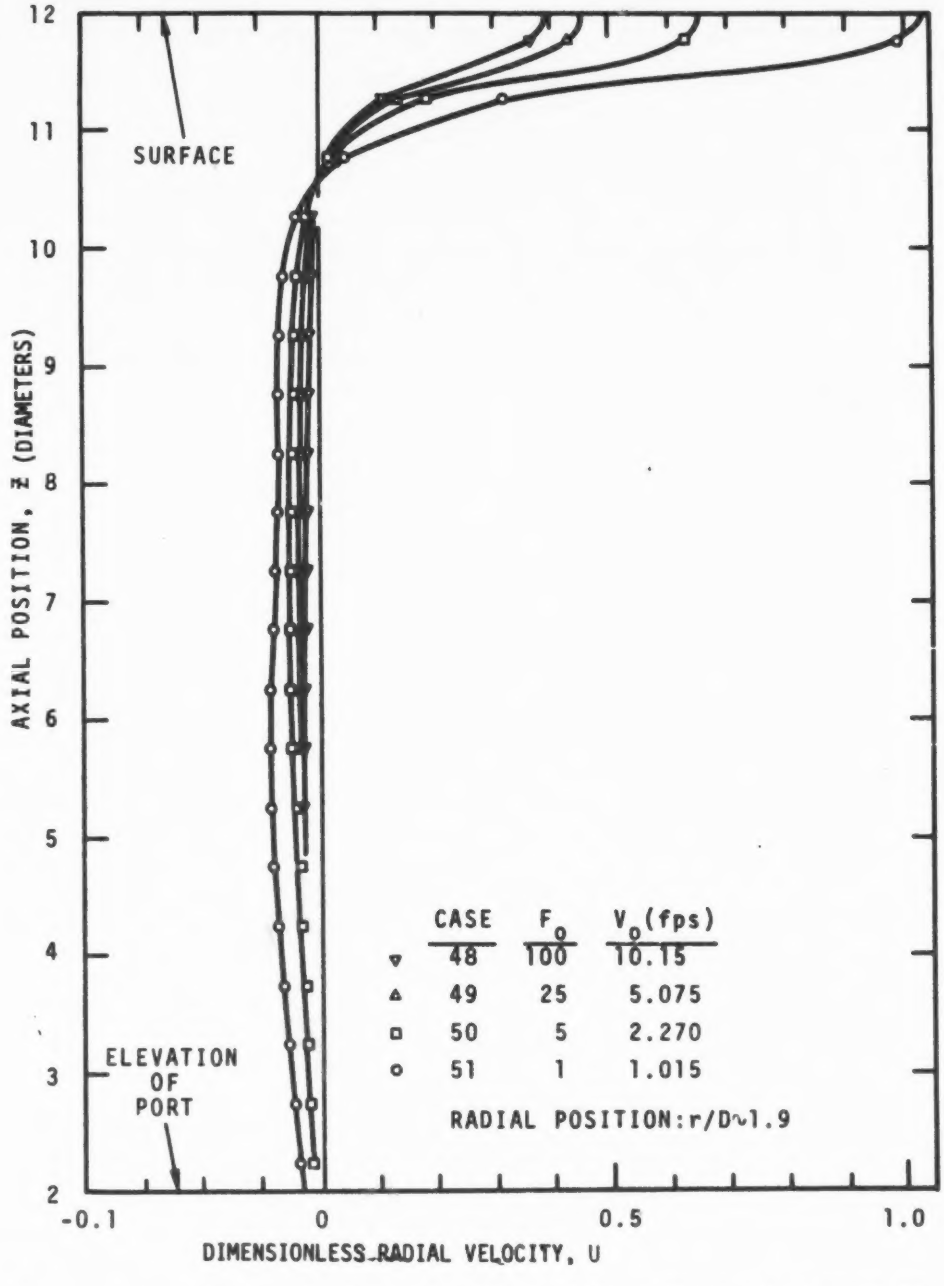

Figure 8.4. Maximum Radial Velocity Profiles, Cases 48 Through 51

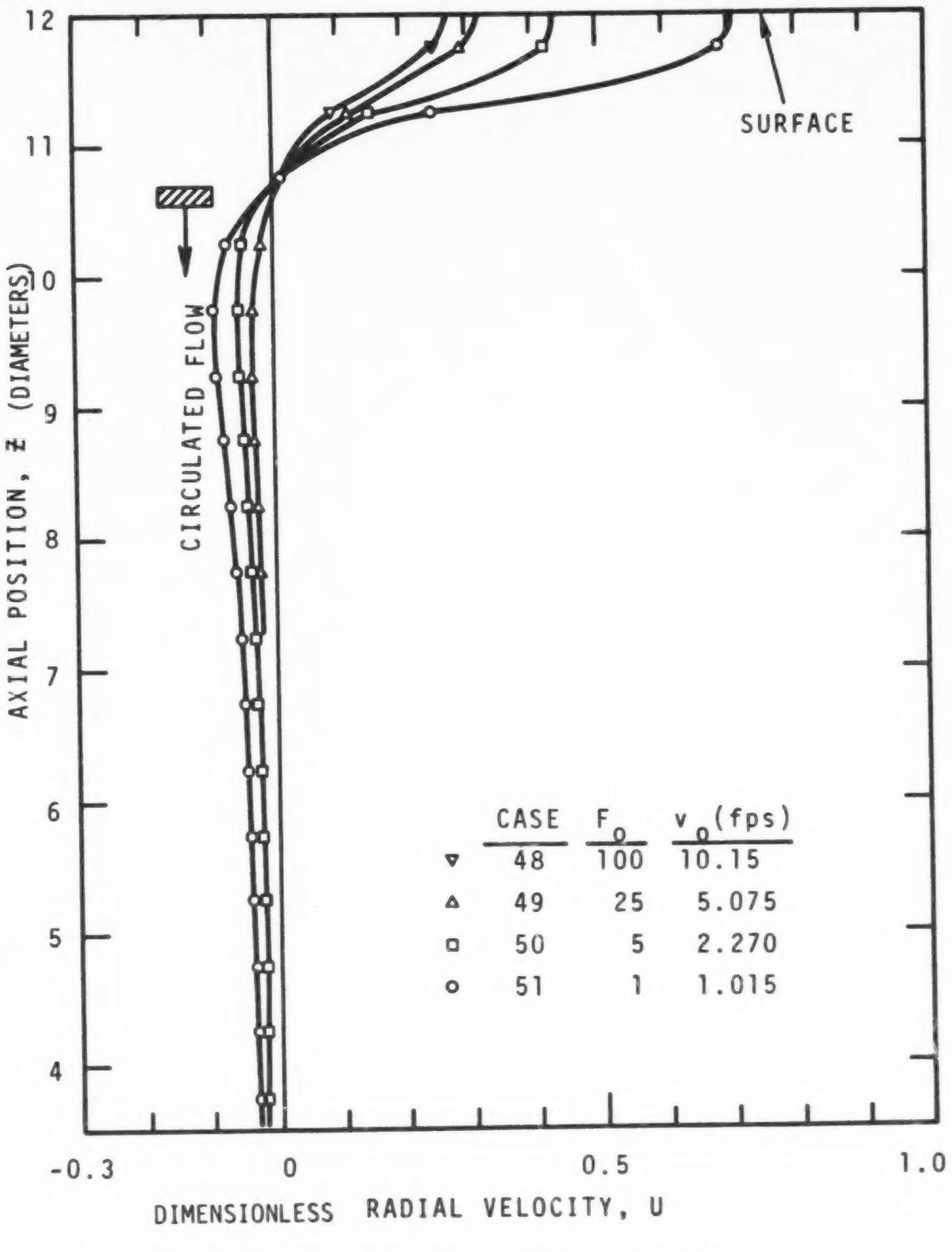

Figure 8.5. Radial Velocity Profiles at r/D=7.32, Cases 48 Through 51

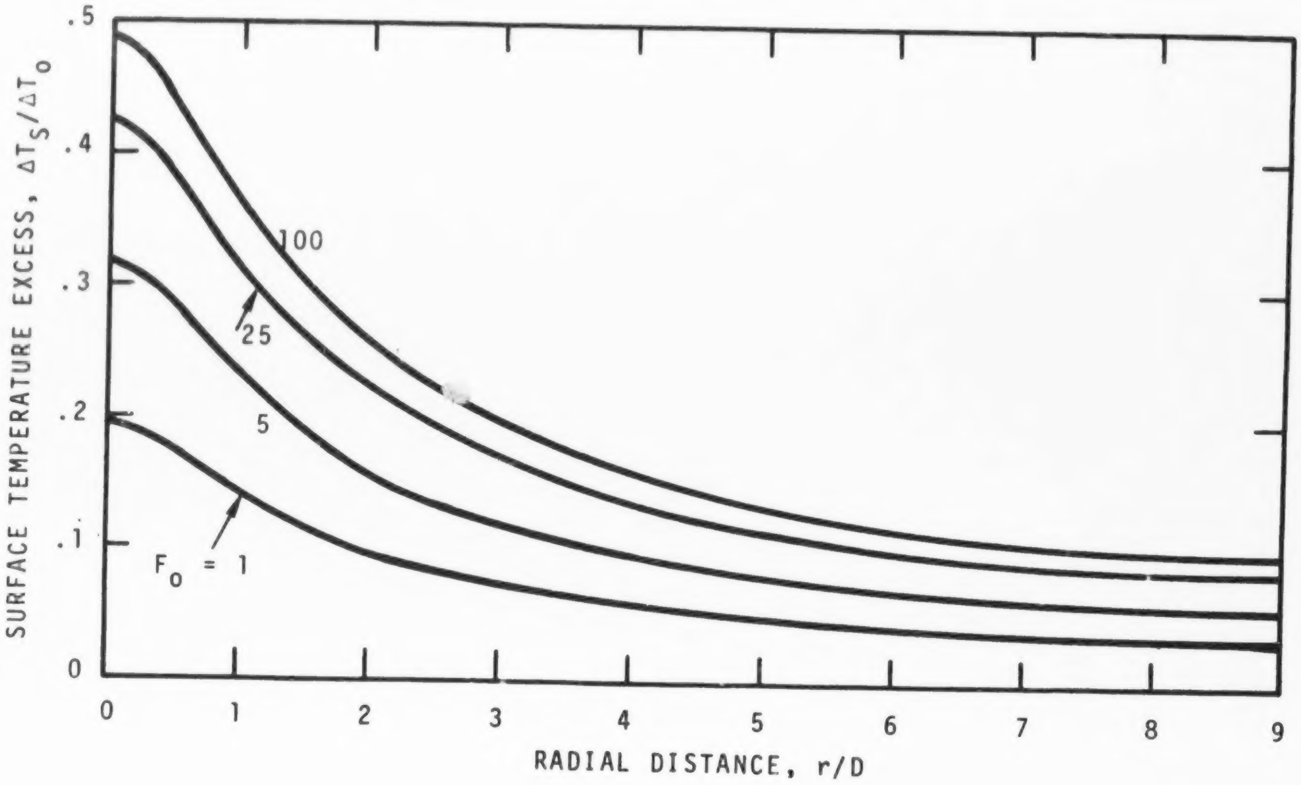

Figure 8.6. Surface Temperature Excess Distribution Cases 48 Through 51 (See Table 8.1)

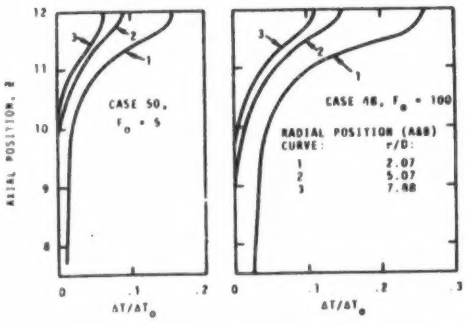

FIGURE 8.7 . VERTICAL TEMPERATURE EXCESS DISTRIBUTIONS FOR VARIOUS RADIAL POSITIONS. CASES 48 & 50.

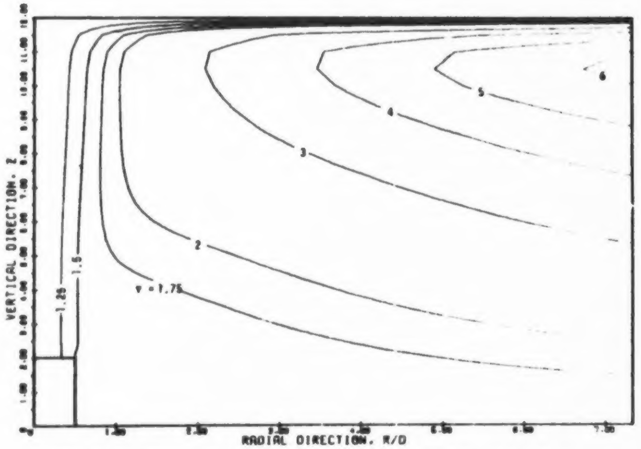

FIGURE 8.8. STREAMLINES FOR CASE 48 - BUOYANT DISCHARGE, FO = 100

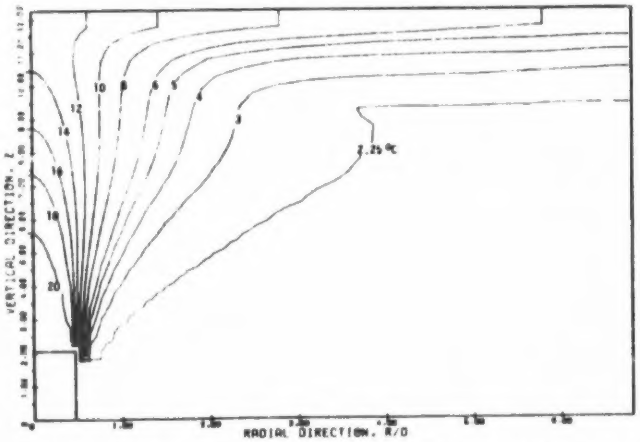

FIGURE 8.9. ISOTHERMS FOR CASE 48 - BUOYANT DISCHARGE, FO = 100

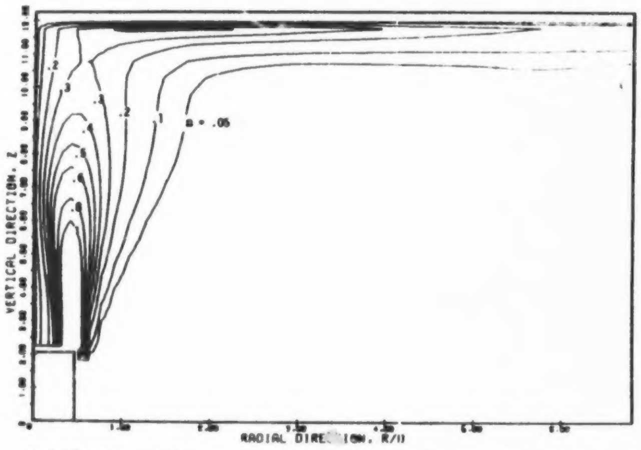

FIGURE 8.10. VORTICITY LEVEL LINES FOR CASE 48 - BUOYANT DISCHARGE, FO = 100

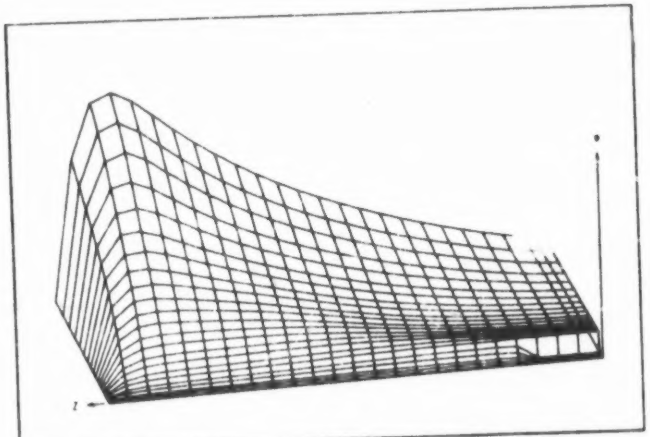

FIGURE 8.11. 3D ILLUSTRATION OF STREAM FUNCTION -- PSI. CASE NO. 48

INTERMEDIATE WATER OUTFALL. SURFACE 10 DIAMETERS ABOVE PORT. FD=100

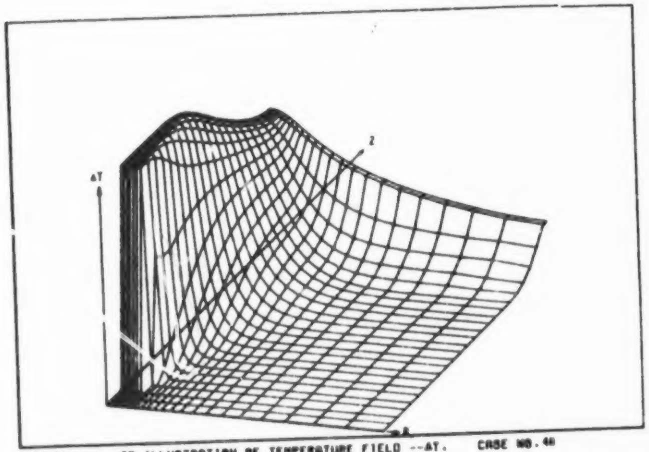

FIGURE 8.12. 3D ILLUSTRATION OF TEMPERATURE FIELD --ΔT. CASE NO. 48

INTERMEDIATE WATER OUTFALL. SURFACE 10 DIAMETERS ABOVE PORT. FD=100

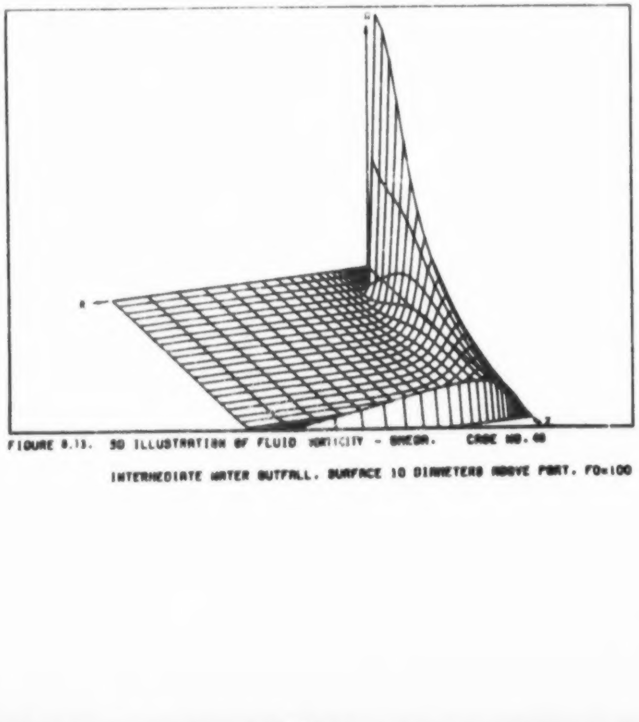

FIGURE 8.13. 3D ILLUSTRATION OF FLUID VORTICITY - OMEGA. CASE NO. 48

INTERMEDIATE WATER OUTFALL. SURFACE 10 DIAMETERS ABOVE PORT. FD=100

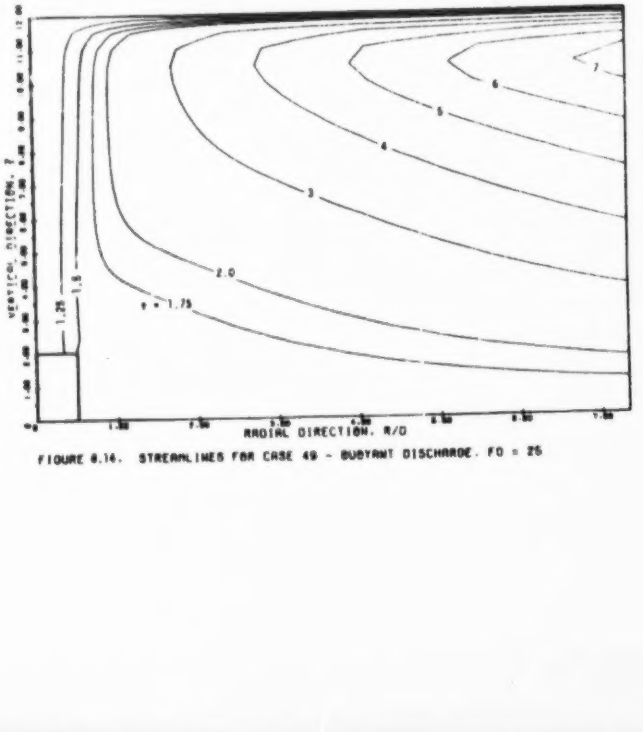

FIGURE 8.14. STREAMLINES FOR CASE 49 - BUOYANT DISCHARGE. FD = 25

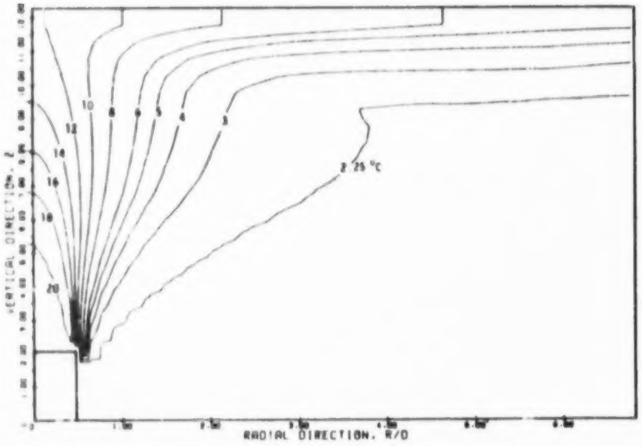

FIGURE 8.15. ISOTHERMS FOR CASE 49 - BUOYANT DISCHARGE, FO = 25

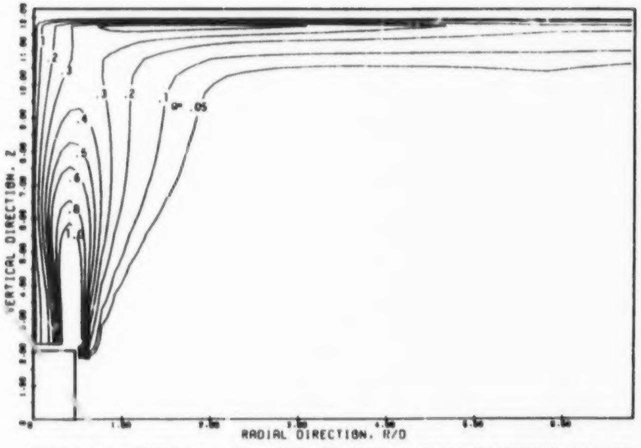

FIGURE 8.16 VORTICITY LEVEL LINES FOR CASE 49 - BUOYANT DISCHARGE, FO = 25

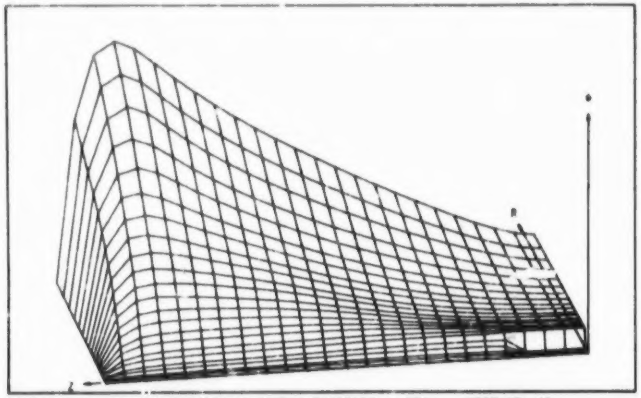

FIGURE 8.17. 3D ILLUSTRATION OF STREAM FUNCTION -- PSI. CASE NO. 49

INTERMEDIATE WATER OUTFALL, SURFACE 10 DIAMETERS ABOVE PORT, FO =25

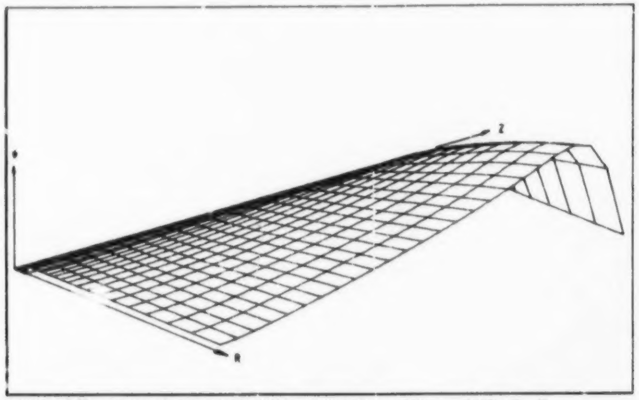

FIGURE 8.18. 3D ILLUSTRATION OF STREAM FUNCTION -- PSI. CASE NO. 49

INTERMEDIATE WATER OUTFALL, SURFACE 10 DIAMETERS ABOVE PORT, FO =25

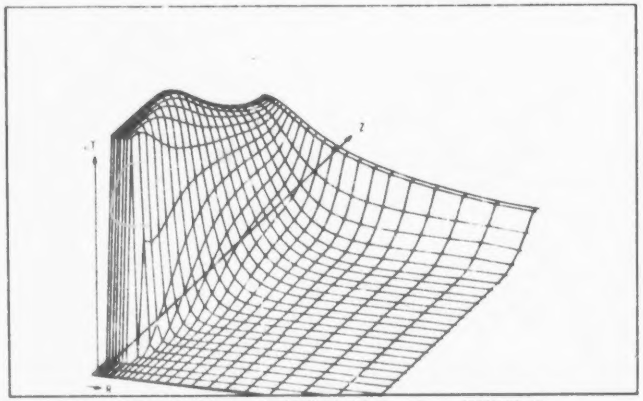

FIGURE 8.19. 3D ILLUSTRATION OF TEMPERATURE FIELD --ΔT. CASE NO. 49

INTERMEDIATE WATER OUTFALL. SURFACE 10 DIAMETERS ABOVE PORT. FD =25

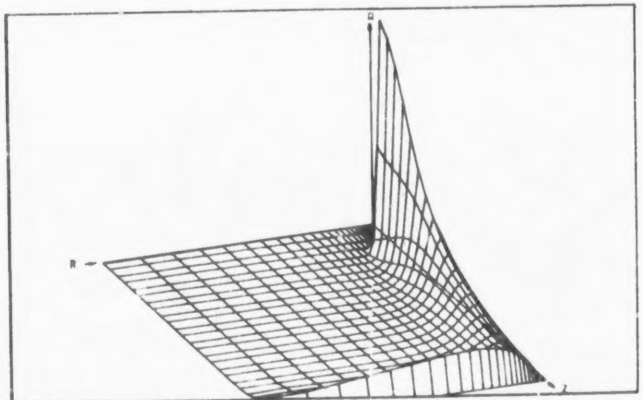

FIGURE 8.20. 3D ILLUSTRATION OF FLUID VORTICITY - OMEGA. CASE NO. 49

INTERMEDIATE WATER OUTFALL. SURFACE 10 DIAMETERS ABOVE PORT. FD =25

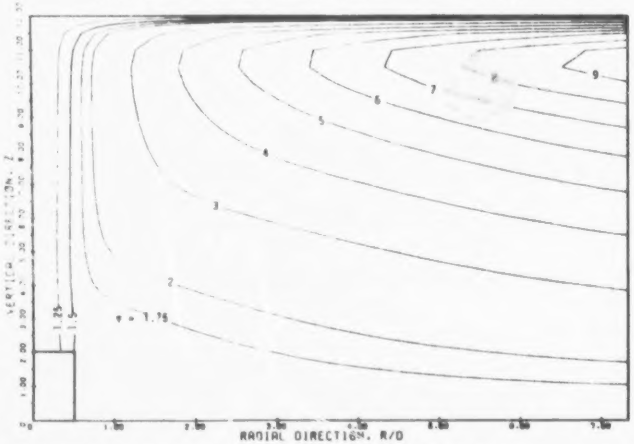

FIGURE 8.21. STREAMLINES FOR CASE 50 - BUOYANT DISCHARGE. FD = 5

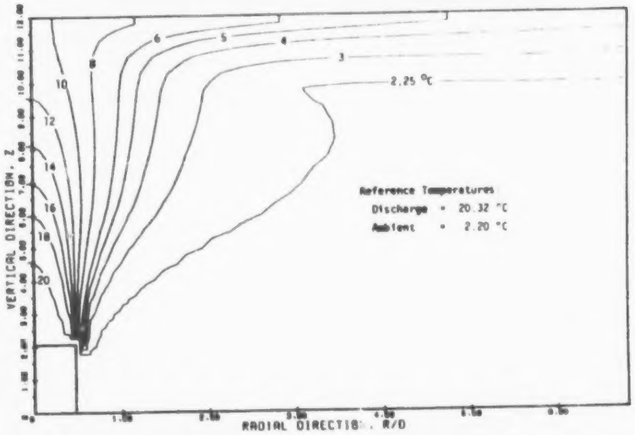

FIGURE 8.22. ISOTHERMS FOR CASE 50 - BUOYANT DISCHARGE. FD = 5

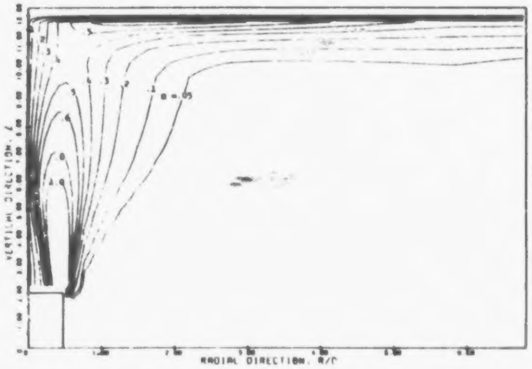

FIGURE 8.23 VORTICITY LEVEL LINES FOR CASE 50 - BUOYANT DISCHARGE, FD = 5

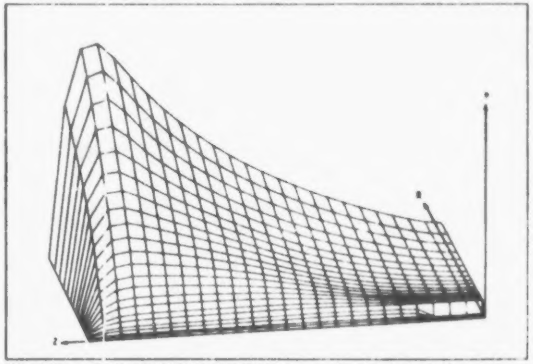

FIGURE 8.24. 3D ILLUSTRATION OF STREAM FUNCTION - PSI. CASE NO 50

INTERMEDIATE WATER OUTFALL, SURFACE 10 DIAMETERS ABOVE PORT, FD = 5

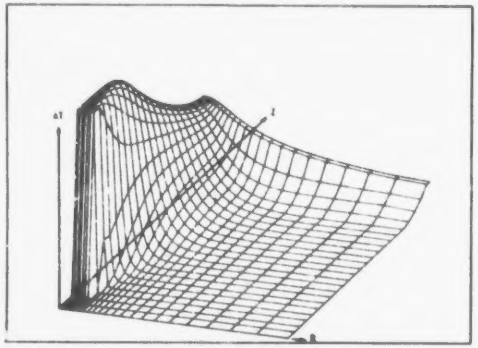

FIGURE 8.25. 3D ILLUSTRATION OF TEMPERATURE FIELD -- ΔT. CASE NO. 50

INTERMEDIATE WATER OUTFALL, SURFACE 10 DIAMETERS ABOVE PORT, FD = 5

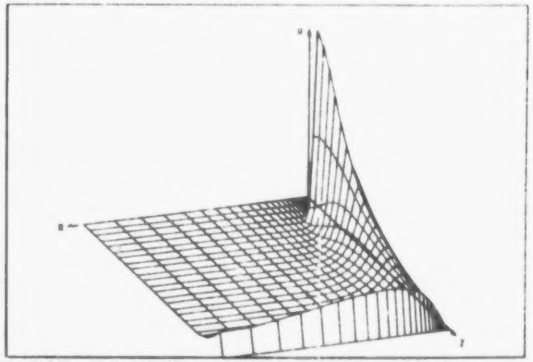

FIGURE 8.26. 3D ILLUSTRATION OF FLUID VORTICITY - OMEGA. CASE NO. 50

INTERMEDIATE WATER OUTFALL, SURFACE 10 DIAMETERS ABOVE PORT, FD = 5

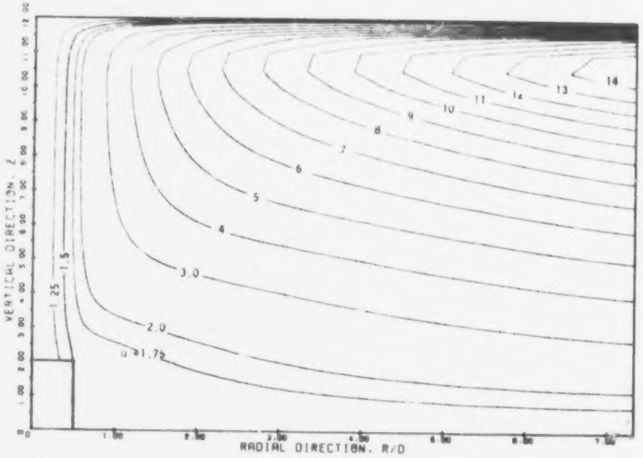

FIGURE 8.27. STREAMLINES FOR CASE 51 - BUOYANT DISCHARGE, FO = 1

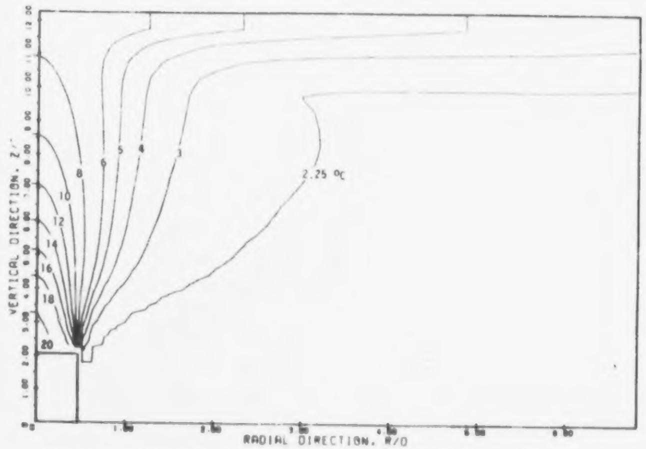

FIGURE 8.28. ISOTHERMS FOR CASE 51 - BUOYANT DISCHARGE, FO = 1

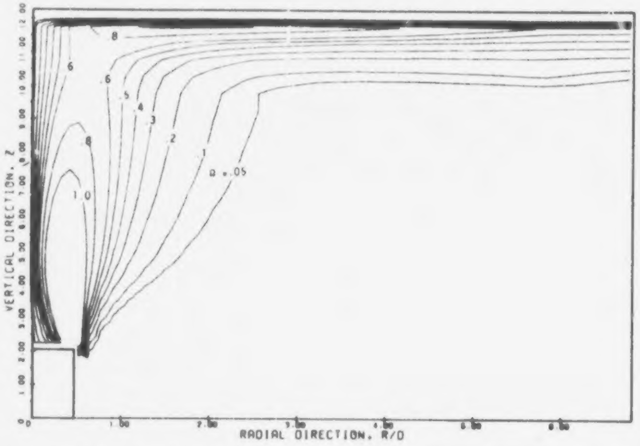

FIGURE 8.29. VORTICITY LEVEL LINES FOR CASE 51 - BUOYANT DISCHARGE, FO = 1

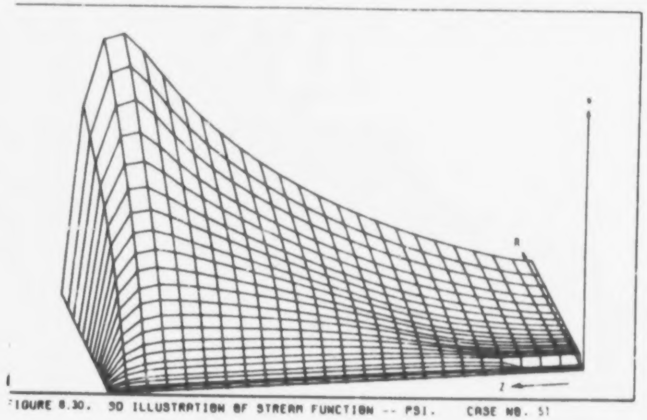

FIGURE 8.30. 3D ILLUSTRATION OF STREAM FUNCTION -- PSI. CASE NO. 51

INTERMEDIATE WATER OUTFALL, SURFACE 10 DIAMETERS ABOVE PORT, FO = 1

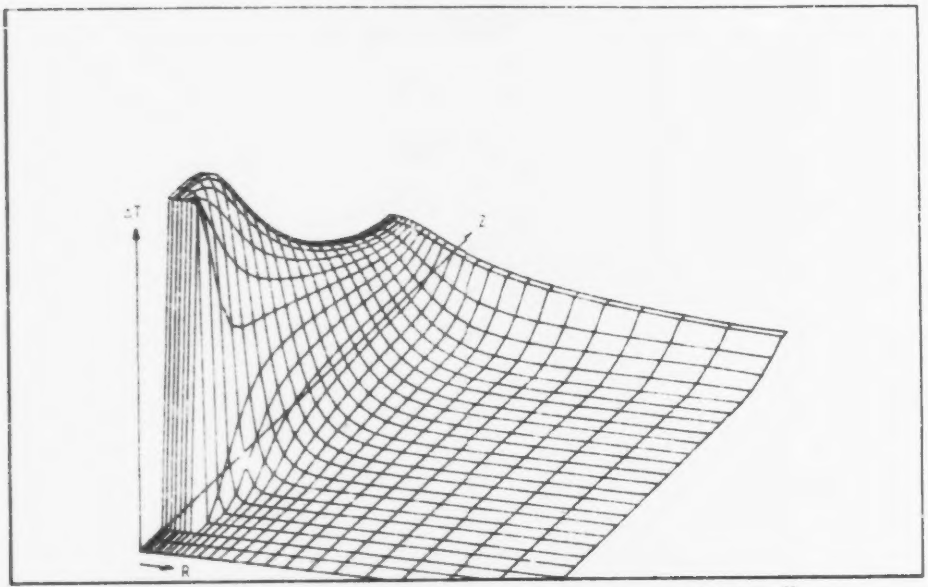

FIGURE 8.31. 3D ILLUSTRATION OF TEMPERATURE FIELD --ΔT. CASE NO. 51

INTERMEDIATE WATER OUTFALL. SURFACE 10 DIAMETERS ABOVE PORT. FO = 1

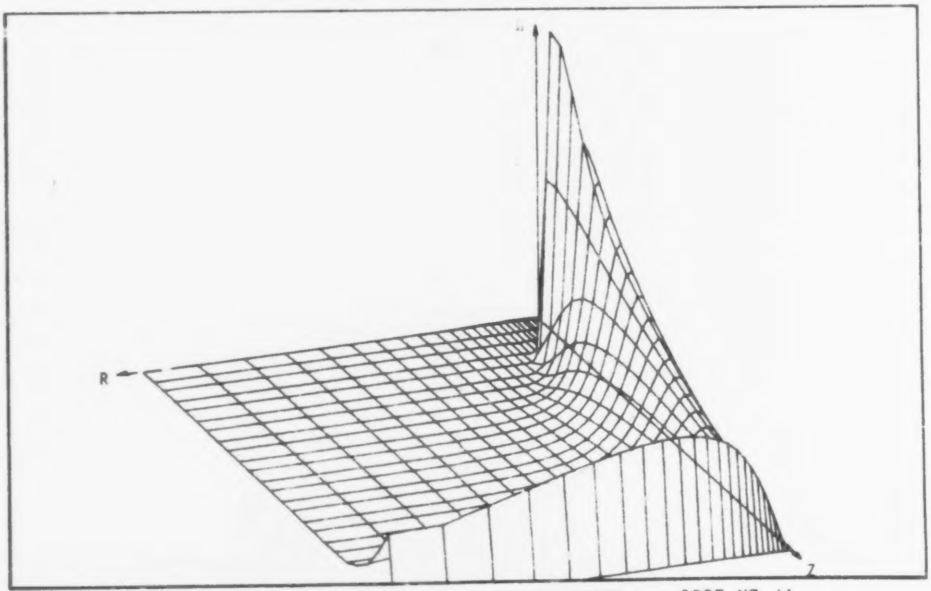

FIGURE 8.32. 3D ILLUSTRATION OF FLUID VORTICITY - OMEGA. CASE NO. 51

INTERMEDIATE WATER OUTFALL. SURFACE 10 DIAMETERS ABOVE PORT. FO = 1

8.3 Results for Homogeneous Receiving Water 5 Port Diameters Deep

Results for outfalls issuing to receiving water 5 port diameters deep are given as Cases 52 through 55 for Froude numbers of 100, 25, 5 and 1, respectively (See Table 8.1). All boundary conditions and parameters for these cases correspond to those of similar Froude numbers for the 10 diameter deep cases given in Section 8.2. Actual water depth here is 6 diameters with the outfall port rising one diameter above the bottom.

Centerline distributions of velocity and temperature excess are shown in Figure 8.33 for Cases 52 through 55. As was illustrated by Case 50 and 51, the plume also accelerates for Cases 54 and 55 as a result of dominant buoyant forces. For Froude numbers of 25 and above the centerline velocity remain essentially constant until surface effects are encountered. On comparing Figure 8.1 with 8.33, one notes that at 5 diameters the temperature excess given in Figure 8.33 is slightly higher than for corresponding cases given in Figure 8.1. The decreased dilution is a result of the surface proximity.

The vertical distribution of radial velocity, U, is illustrated by Figure 8.34 for Case 52. The lateral spread is seen to be quite thin (approximately .8 D) at least out to 4 diameters. Figure 8.35 shows that temperature effects somewhat deeper (approximately 1.2 D) and some recirculation of heated water is indicated. At r/D = 1.0, the temperature distribution lies within the rising portion of the plume above $Z \simeq 2.5$ (1.5 above the port) and is not to be interpreted as penetration of the lateral spread.

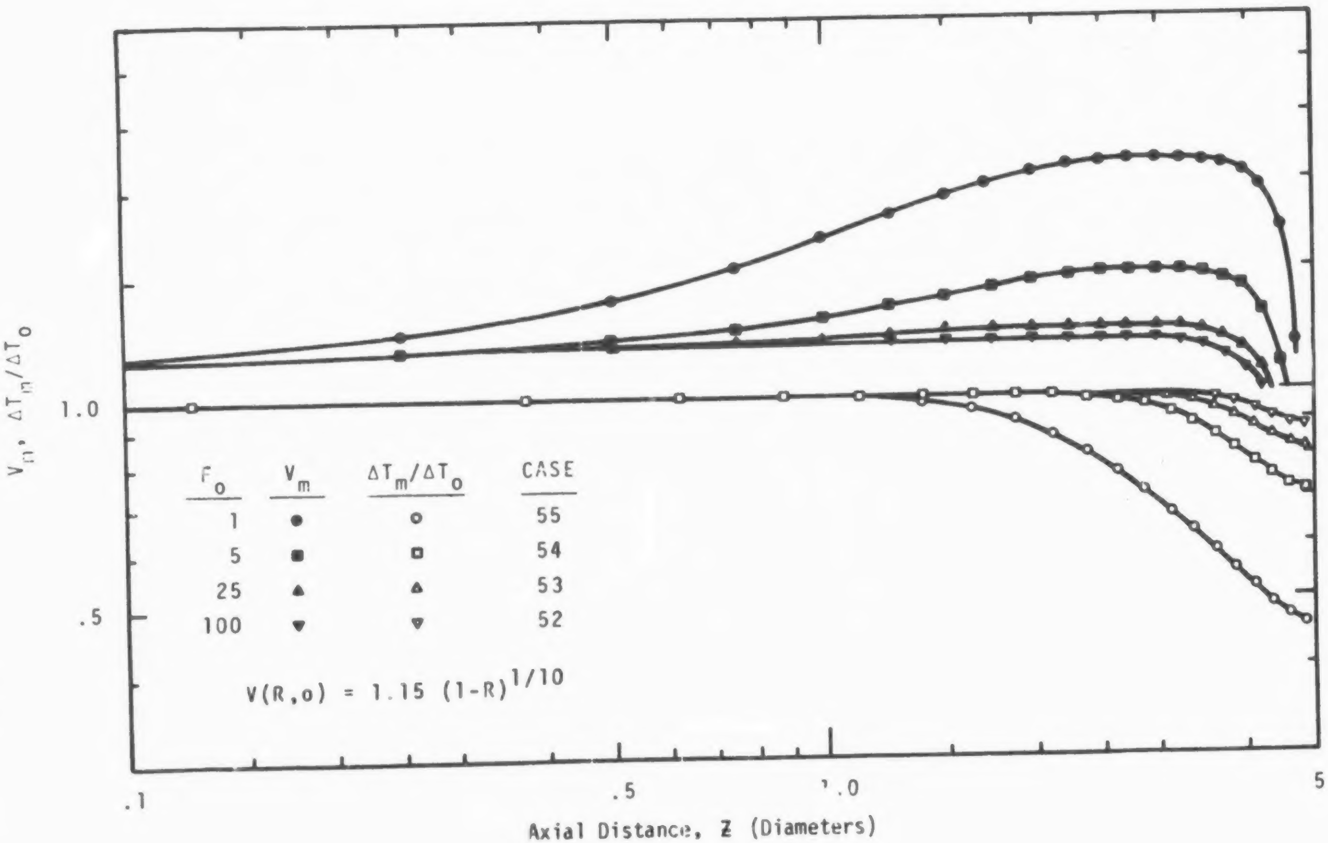

Figure 8.33. Computed Centerline Dimensionless Velocity and Temperature Excess for Shallow Water Cases 52 Through 55 (5 Diameters Deep)

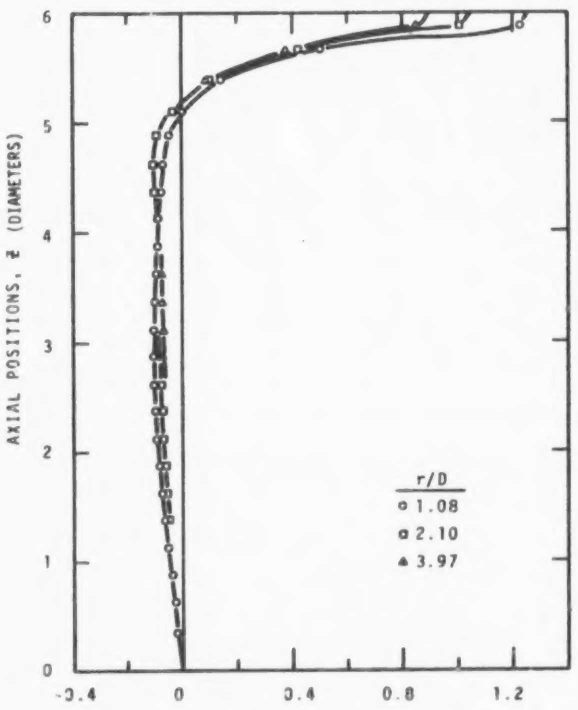

Figure 8.34. Vertical Distribution of Radial Velocity at Various Radial Positions, Case 52

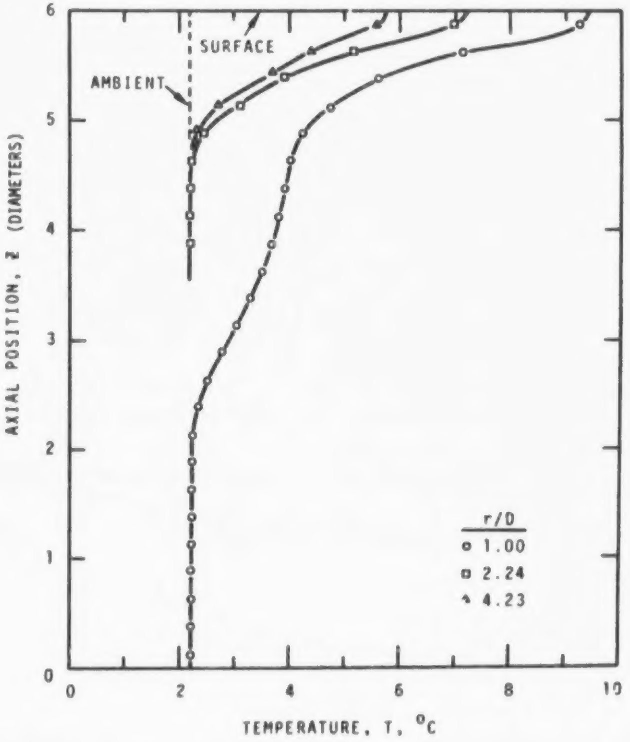

Figure 8.35. Vertical Distribution of Temperature Excess at Various Radial Positions, Case 52

Contour plots and 3-dimensional illustrations of the stream function, temperature and vorticity are given in Figures 8.36 through 8.41.

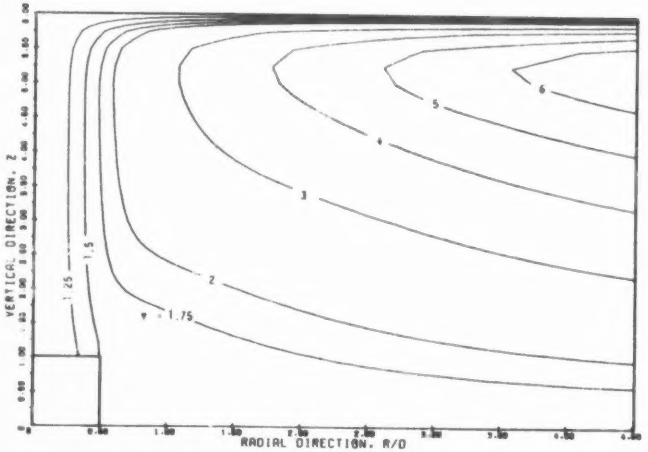

FIGURE 8.36. STREAMLINES FOR CASE 52 - BUOYANT DISCHARGE. FO = 1

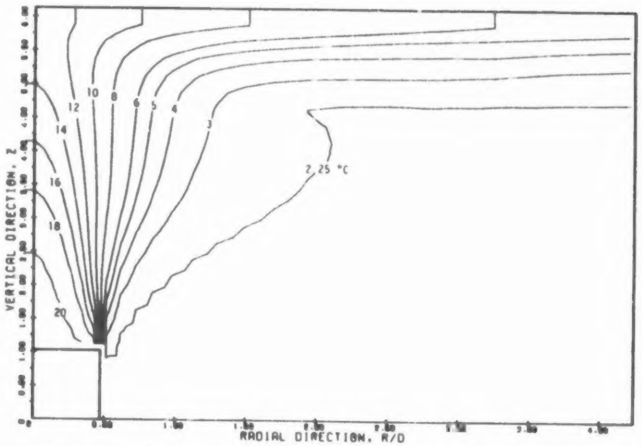

FIGURE 8.37. ISOTHERMS FOR CASE 52 - BUOYANT DISCHARGE. FO = 1

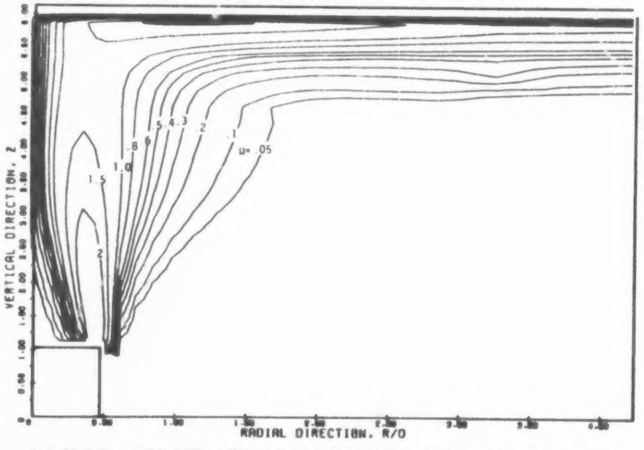

FIGURE 8.38. VORTICITY LEVEL LINES FOR CASE 52 - BUOYANT DISCHARGE. FO = 1

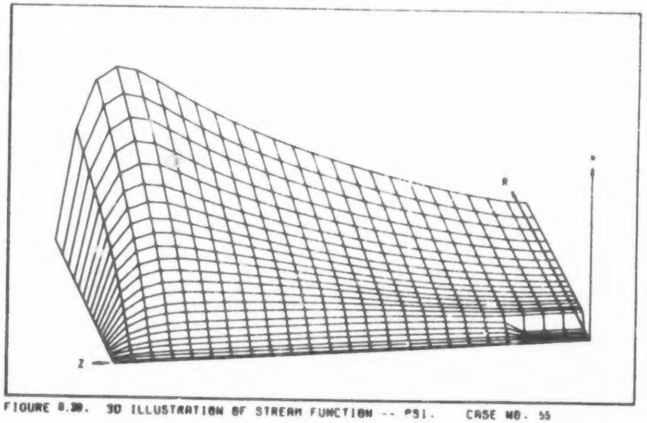

FIGURE 8.39. 3D ILLUSTRATION OF STREAM FUNCTION -- PSI. CASE NO. 55

VERY SHALLOW WATER OUTFALL. SURFACE 5 DIAMETERS ABOVE PORT. FO= 1

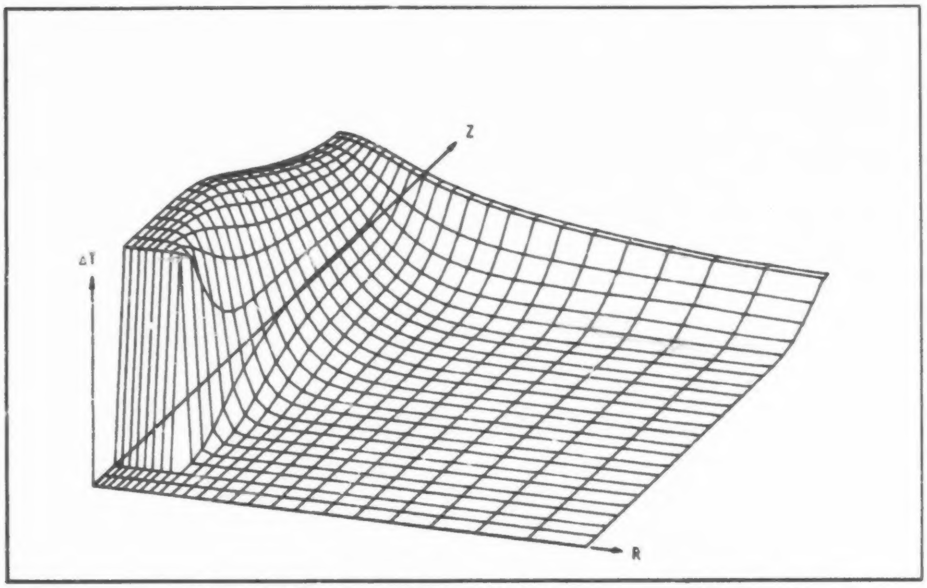

FIGURE 6.40. 3D ILLUSTRATION OF TEMPERATURE FIELD --ΔT. CASE NO. 55

VERY SHALLOW WATER OUTFALL. SURFACE 5 DIAMETERS ABOVE PORT. FO= 1

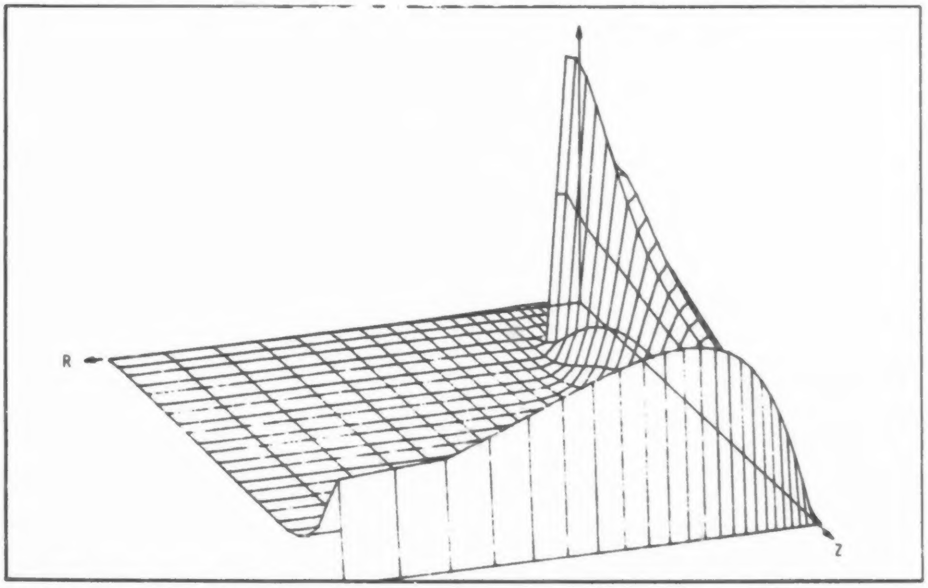

FIGURE 6.41. 3D ILLUSTRATION OF FLUID VORTICITY - OMEGA. CASE NO. 55

VERY SHALLOW WATER OUTFALL. SURFACE 5 DIAMETERS ABOVE PORT. FO= 1

8.4 Results for Two Different Methods of Computing FZ

Cases 56 through 59 are results illustrating the effects of using Methods 3 and 4, and different values of the constant β, for computing the vertical eddy diffusivity multiplier, FZ (refer to Tables 8.1 and 8.2). Cases 56 and 57 are for receiving water 5.6 diameters deep, using Method 3 to compute FZ with Froude number, $F_0 = 51$. Case 58 has $F_0 = 105$, with 4.97 diameter deep water using Method 3. Case 59 is the same as Case 58 except Method 4 is used to compute FZ.

Cases 56 and 57 were run to observe the effect of changing $\beta = .4$ to $\beta = .8$, respectively. Comparative results are not shown, but this change of β did not alter the computed velocity and temperature profile a great deal.

It was observed, however, that computation of FZ_0 by Method 3 resulted in excessive vertical diffusivities. Case 58 also employed Method 3 and exhibited excessive vertical diffusivities (in this Case $\beta = 1.0$). As pointed out in Section 8.2, Stolzenbach suggests the value of $\beta = 5.0$ based on the gross Richardson number; however, values using $\beta > 1.0$ were not tried in these cases. Using the larger value of β could have a major effect on the velocity and thermal distributions computed by the present techniques using Method 3. The use of large β would significantly reduce vertical mixing in the thermal boundary region, but allow substantial vertical exchange within the spreading plume where thermal gradients are expected to be small.

Figure 8.42 shows the comparison of surface spread velocity between Cases 58 and 59. The difference here is not of major importance, but Figures 8.43 and 8.44 illustrate a significant difference in vertical entrainment. Significant differences between streamline patterns is revealed by comparing Figures 8.45 and 8.46. The contours shown in Figure 8.45 (Case 58) are more indicative of creeping flow in the spreading portion of the plume than a high Reynolds number flow (Case 59, Figure 8.46).

The distribution of surface temperature excess is shown in Figure 8.47 for Cases 57, 58 and 59. Case 57 shows lower temperature at the centerline as a result of the port being in deeper water. Case 58 may be compared to Case 59 and exhibits a lower surface temperature (also, refer to Figures 8.48 and 8.49). This result is due to the larger values of vertical mixing employed in the computation of Case 58. Isotherms for Case 59 are illustrated by Figure 8.50.

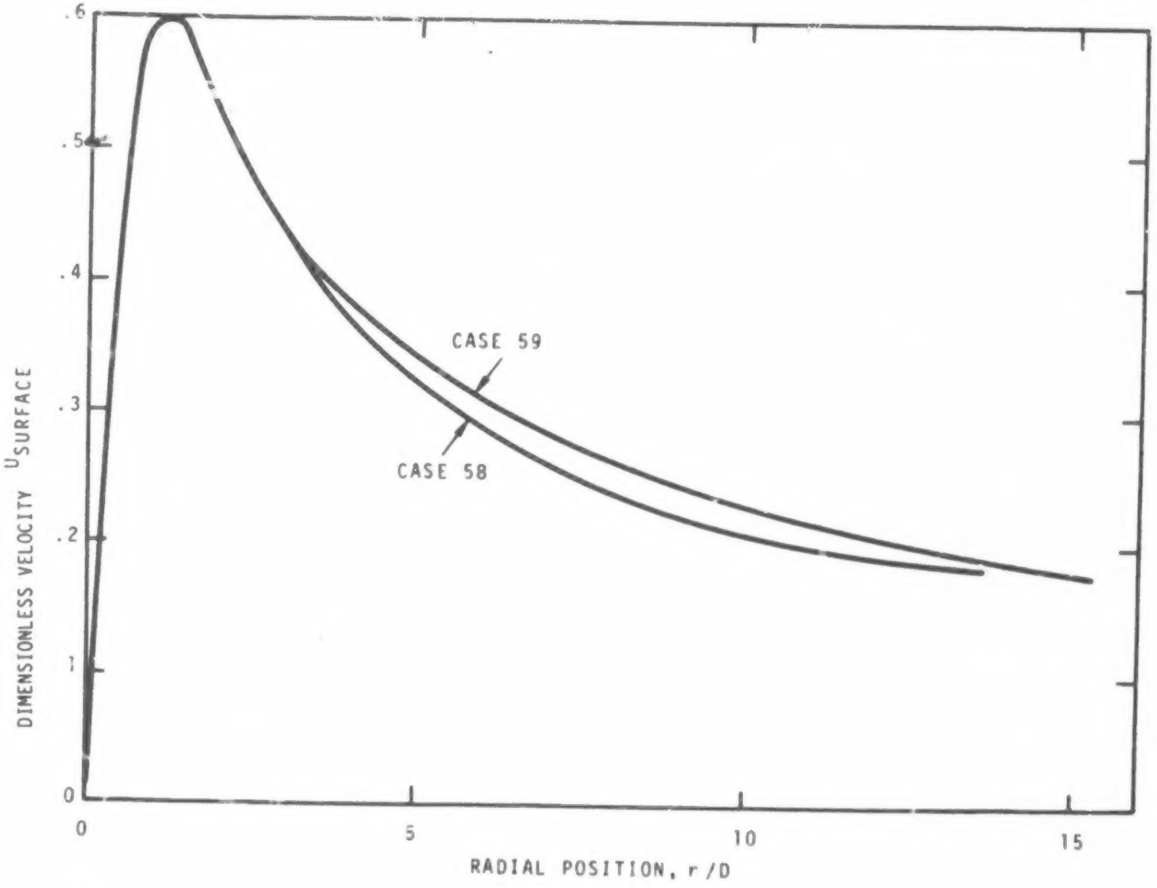

Figure 8.42. Computed Radial Velocity at Surface, Cases 58 and 59

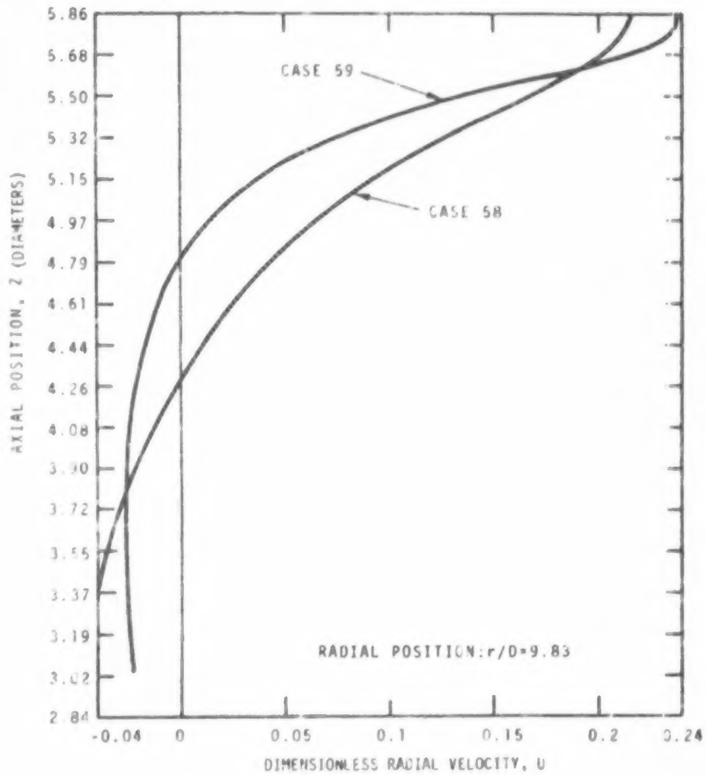

Figure 8.43. Vertical Distribution of Radial Velocity, U.
Cases 58 and 59.

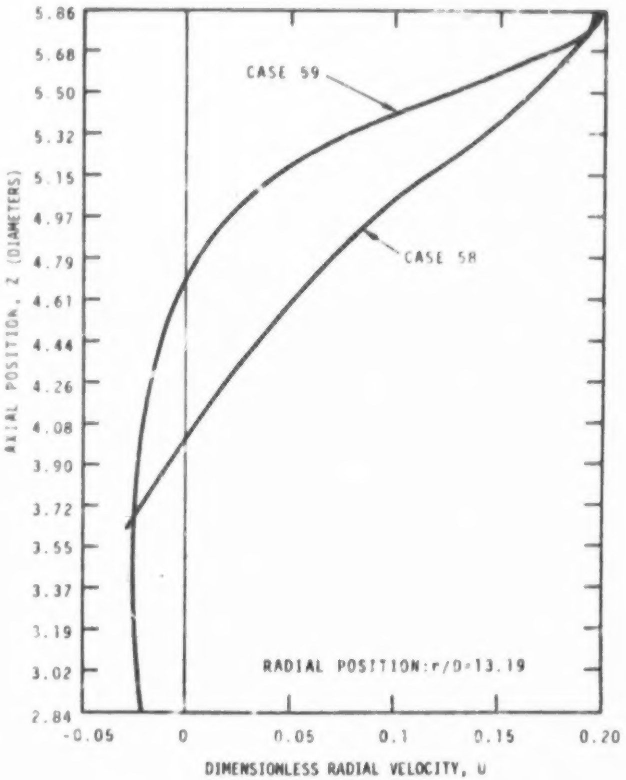

Figure 8.44. Vertical Distribution of Radial Velocity, U.
Case 58 and 59

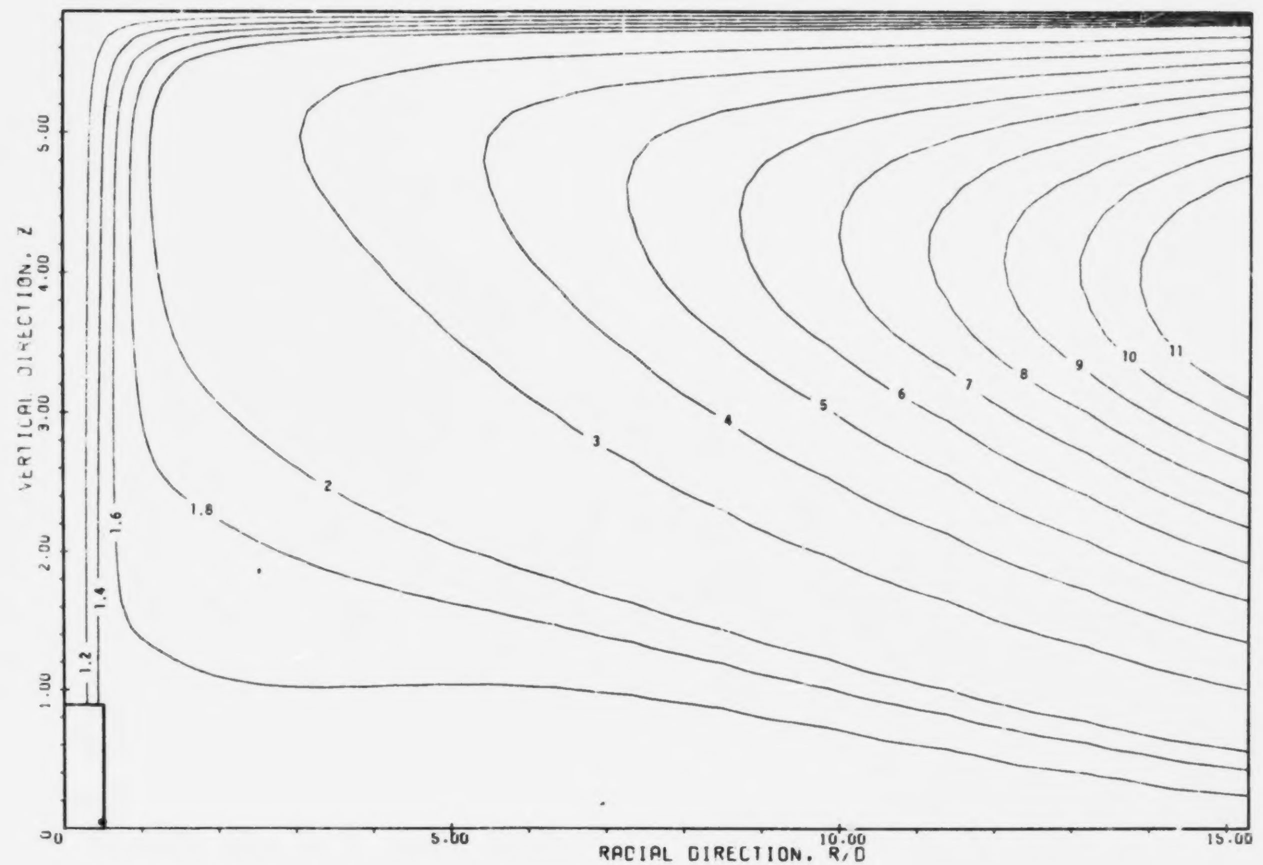

FIGURE 8.45. STREAMLINES FOR AN AXISYMMETRIC, VERTICAL PLUME, CONFINED BY A FREE SURFACE. CASE 58.

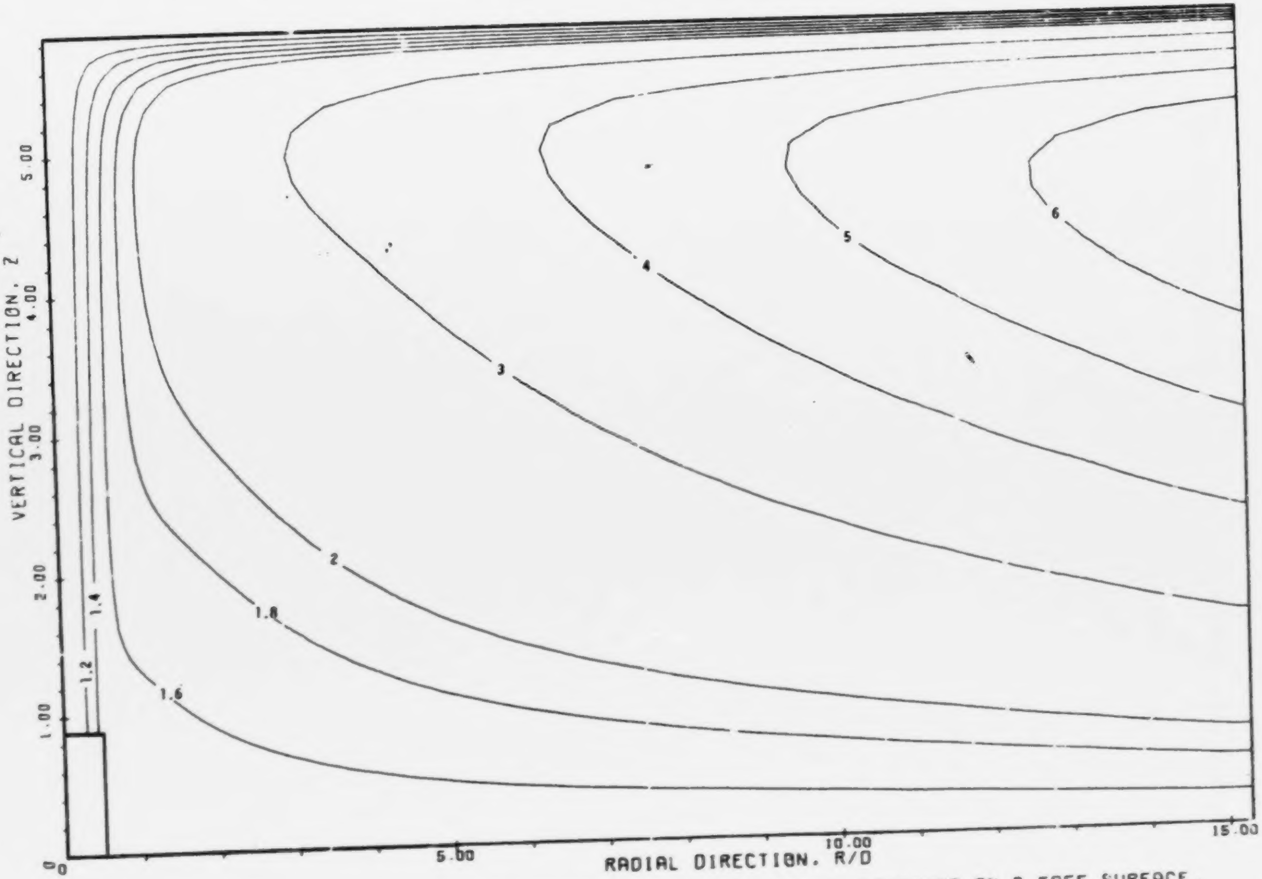

FIGURE 8.46. STREAMLINES FOR AN AXISYMMETRIC. VERTICAL PLUME. CONFINED BY A FREE SURFACE. CASE 59.

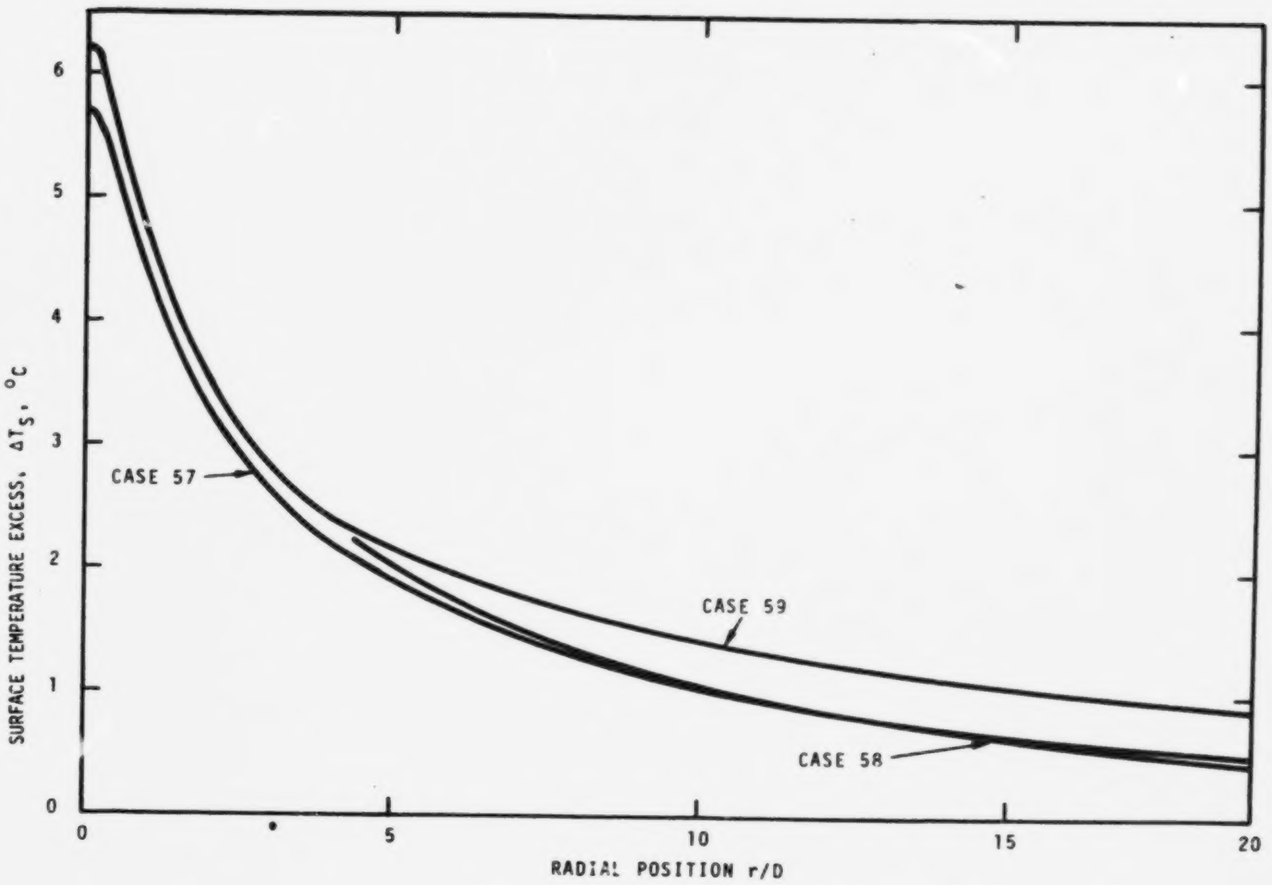

Figure 8.47. Surface Temperature Excess, ΔT_S, Cases 57, 58, and 59

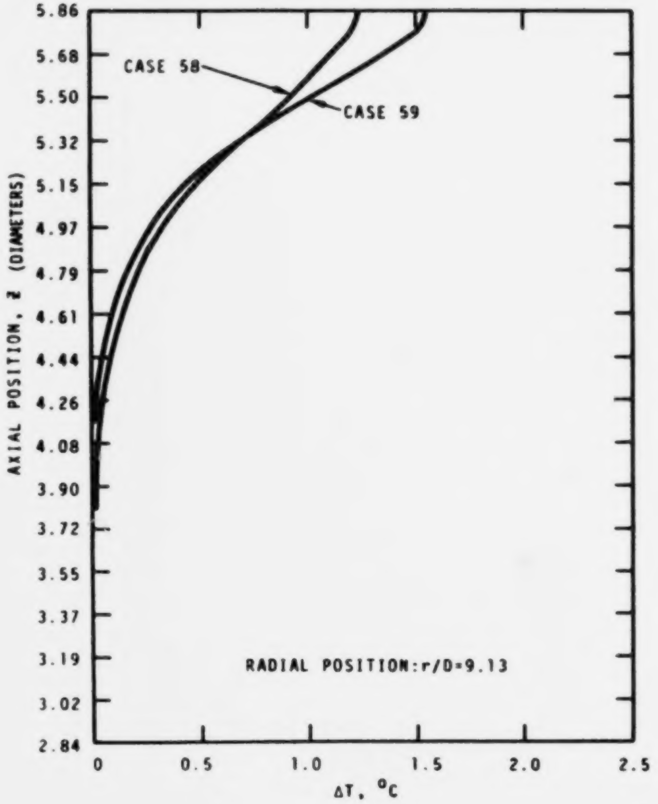

Figure 8.48. Vertical Temperature Excess Distribution. Cases 58 and 59

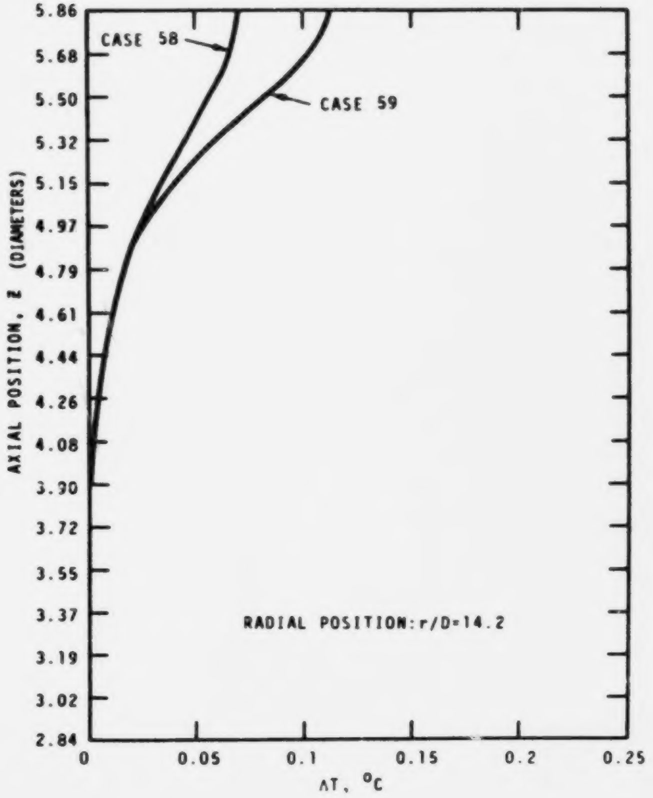

Figure 8.49. Vertical Temperature Excess Distribution. Cases 58 and 59

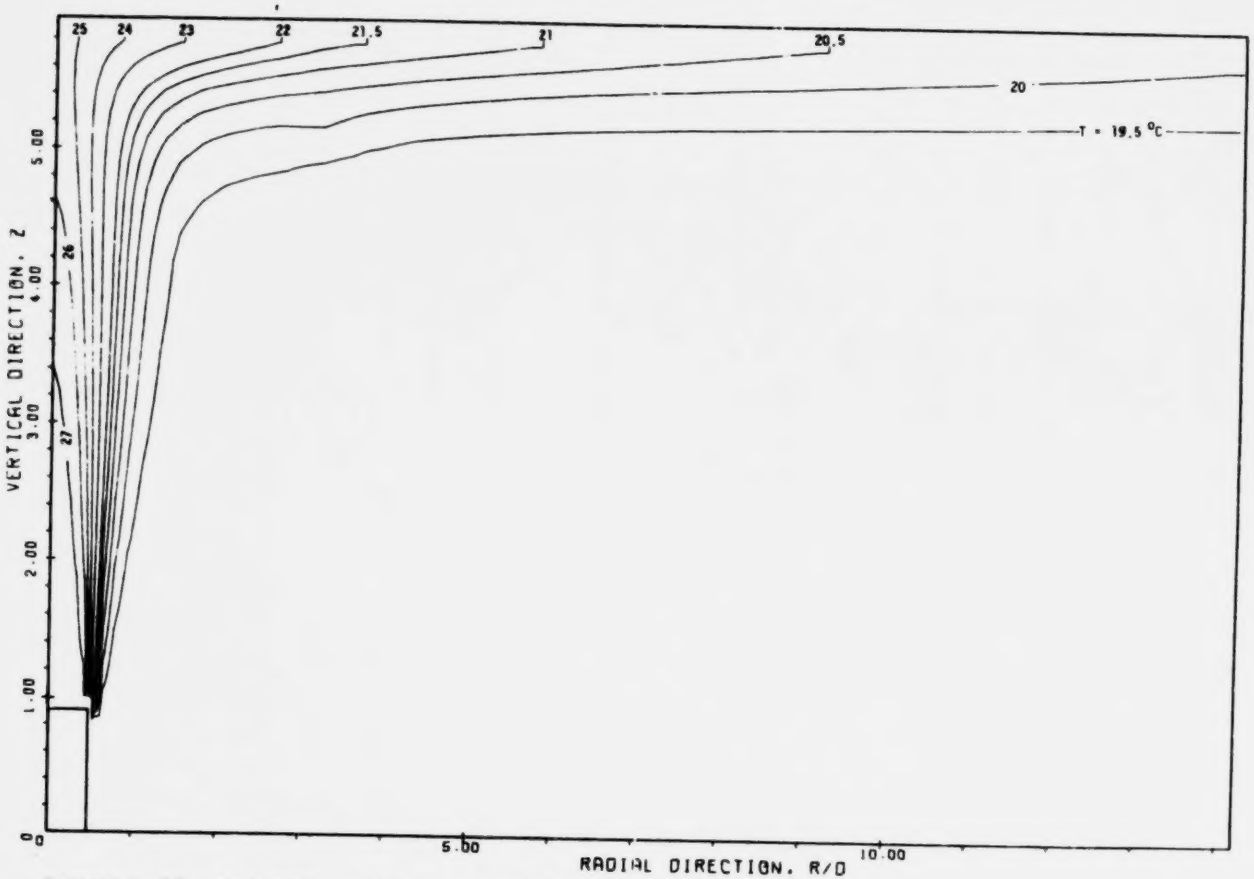

FIGURE 8.50. ISOTHERMS FOR AN AXISYMMETRIC, VERTICAL PLUME, CONFINED BY A FREE SURFACE.
CASE 59.

8.5 Numerical Experiments Involving Ambient Stratification

Results involving the effects of stratification are given by Cases 60 through 65. Case 60 is a base case to be used for comparison and is for a homogeneous ambient. The remaining cases have different degrees of ambient stratification. In all cases the ambient (also, effluent) salinity is constant at 35 ppt, hence the ambient density structure is a function of the temperature distribution alone. In this section, all results use Method 4 to compute F_0 and $\beta = 1.0$. Unlike all previous cases presented in this chapter, the effluent velocity profile is assumed flat.

Figure 8.51 illustrates the assumed ambient density structure for the six cases.

Results for the base Case 60 are illustrated by Figures 8.52 through 8.59. One significant feature of the Case 60 results concern velocity distribution and may be noted in Figures 8.52 and 8.54. Figure 8.52 illustrates that radial velocity profiles for the spreading plume continue to penetrate deeper into the ambient with increasing radial distance from the outfall. For this case, temperature differences are small between the plume flow and ambient as illustrated by Figure 8.53. The upward-distorted streamlines illustrated in Figure 8.54 indicate that there is significant upward entrainment into the plume lateral spread.

The influence of a 2 ^{o}C ambient thermocline situated as shown by Figure 8.51 is illustrated by Figures 8.60 through 8.64. Comparison of Figures 8.62 and 8.54 shows that the presence of the thermocline

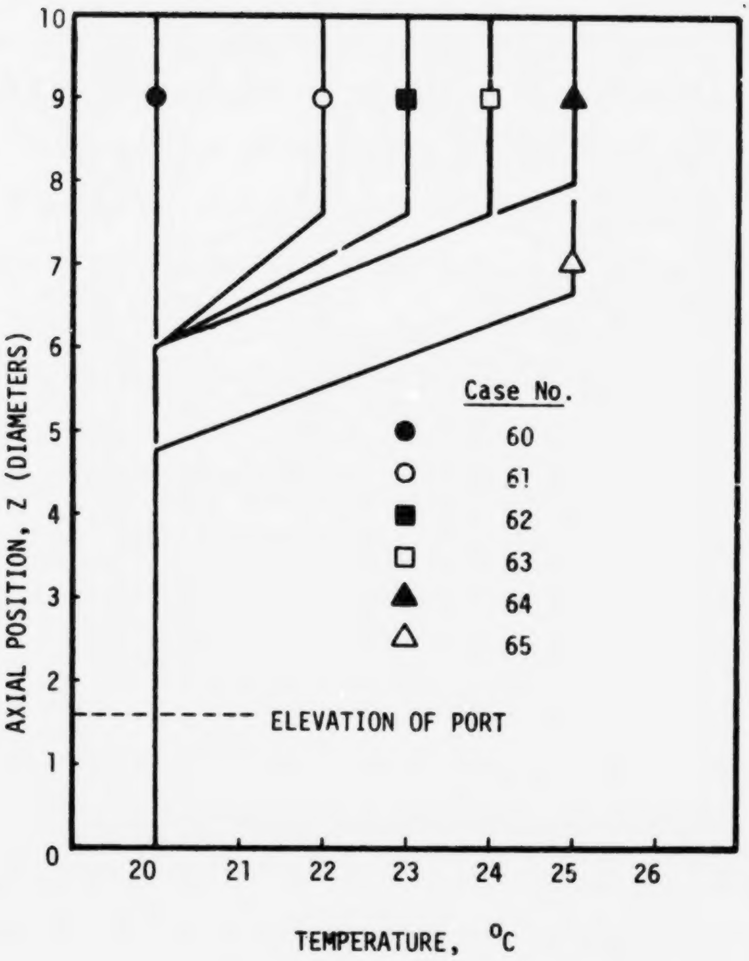

Figure 8.51. Ambient Temperature Profiles for Cases 60 Through 65

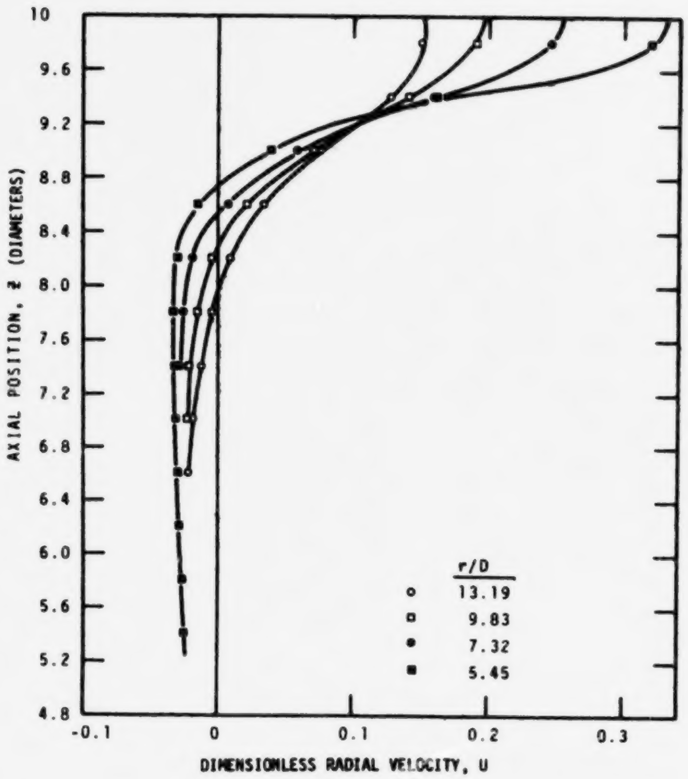

Figure 8.52. Vertical Distribution of Radial Velocity. Case 60

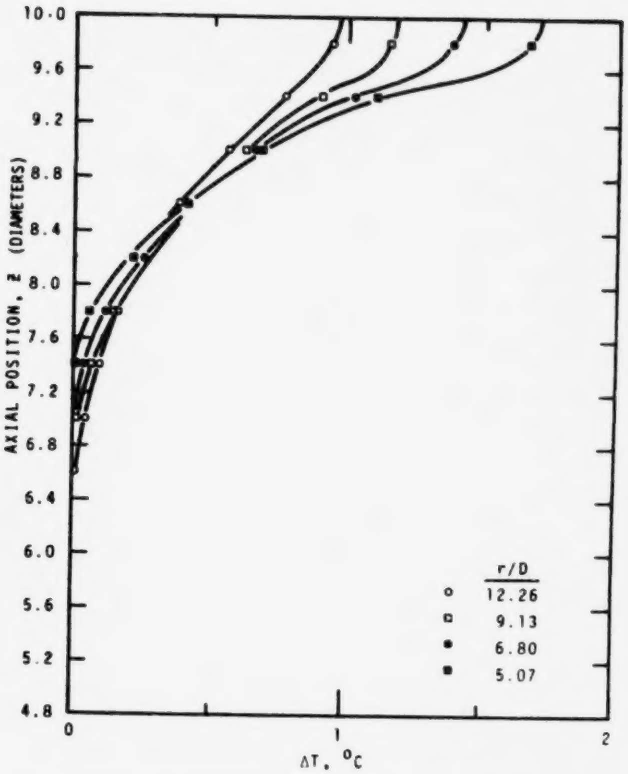

Figure 8.53. Vertical Temperature Excess Distribution. Case 60

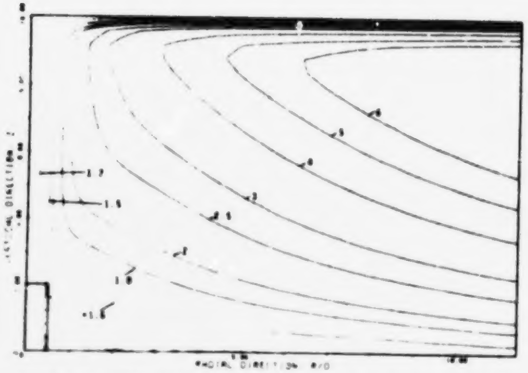

FIGURE 8.54 STREAMLINES FOR AN AXISYMMETRIC, VERTICAL PLUME, CONFINED BY A FREE SURFACE CASE 60 - INTERMEDIATE DEPTH, HOMOGENEOUS AMBIENT, MARAVEY

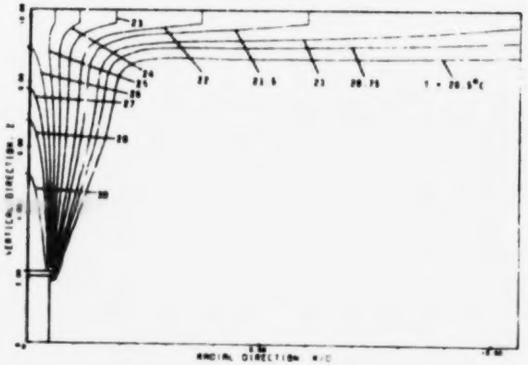

FIGURE 8.55. ISOTHERMS FOR AN AXISYMMETRIC, VERTICAL PLUME, CONFINED BY A FREE SURFACE CASE 60 - INTERMEDIATE DEPTH, HOMOGENEOUS AMBIENT, MARAVEY

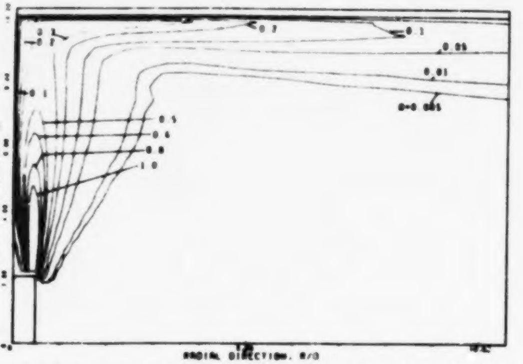

FIGURE 8.56. VORTICITY CONTOURS AXISYMMETRIC, VERTICAL PLUME, CONFINED BY A FREE SURFACE CASE 60 - INTERMEDIATE DEPTH, HOMOGENEOUS AMBIENT, MARAVEY

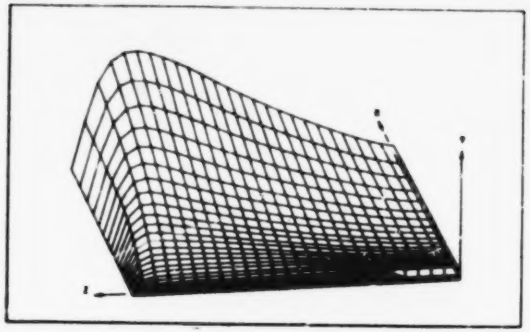

FIGURE 8.57. 3D ILLUSTRATION OF STREAM FUNCTION - PSI. CASE NO. 60

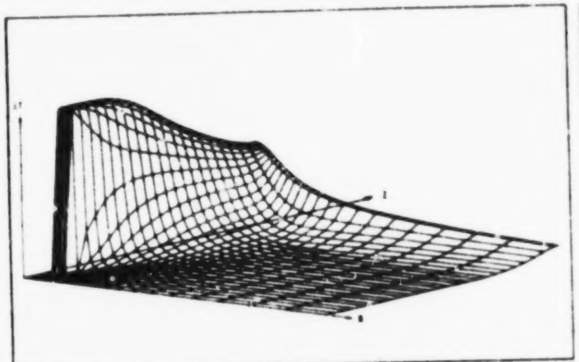

FIGURE 8.58. 3D ILLUSTRATION OF TEMPERATURE FIELD --ΔT. CASE 81.00

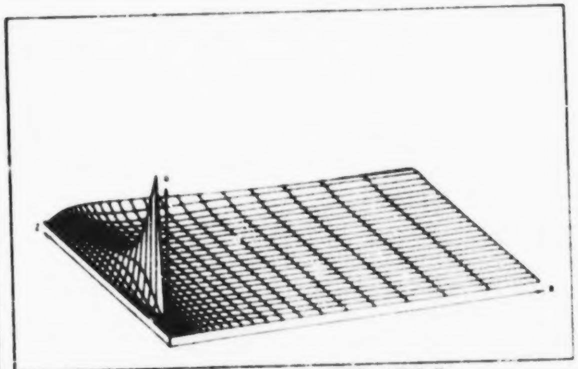

FIGURE 8.59. 3D ILLUSTRATION OF FLUID VORTICITY - OMEGA. CASE 81.00

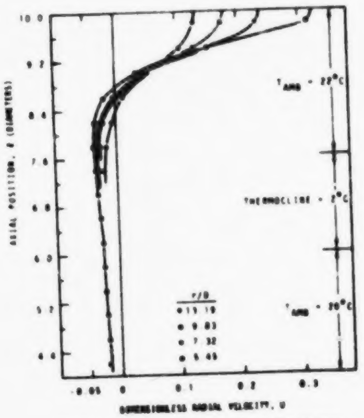

Figure 8.60 Vertical Distribution of Radial Velocity
Case 81

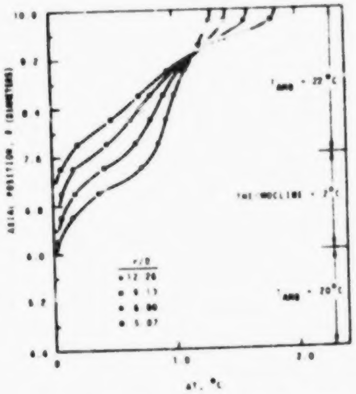

Figure 8.61 Vertical Excess Temperature Distribution
Case 81

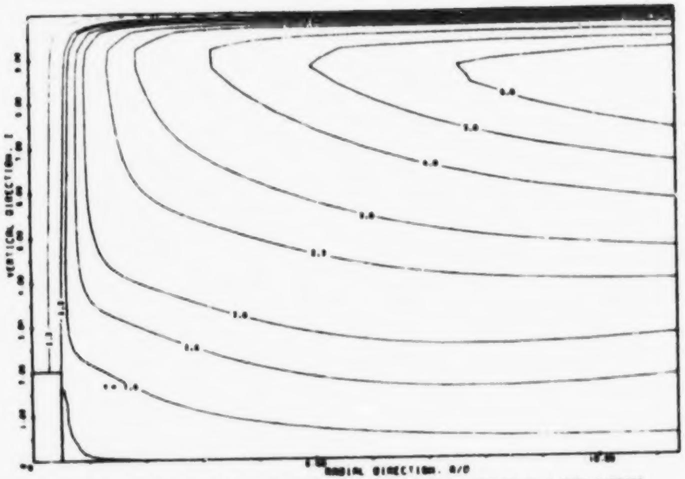

FIGURE 6A2. STREAMLINES FOR AN AXISYMMETRIC, VERTICAL PLUME, CONFINED BY A FREE SURFACE
CASE 61 - INTERMEDIATE DEPTH, WITH 2 DEGREE THERMOCLINE, [illegible]

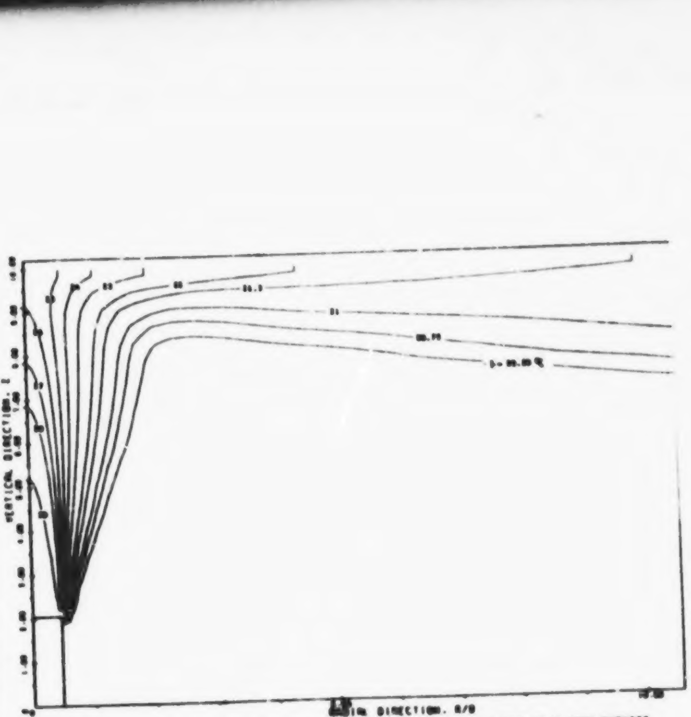

FIGURE 6A3. ISOTHERMS FOR AN AXISYMMETRIC, VERTICAL PLUME, CONFINED BY A FREE SURFACE
CASE 61 - INTERMEDIATE DEPTH, WITH 2 DEGREE THERMOCLINE, [illegible]

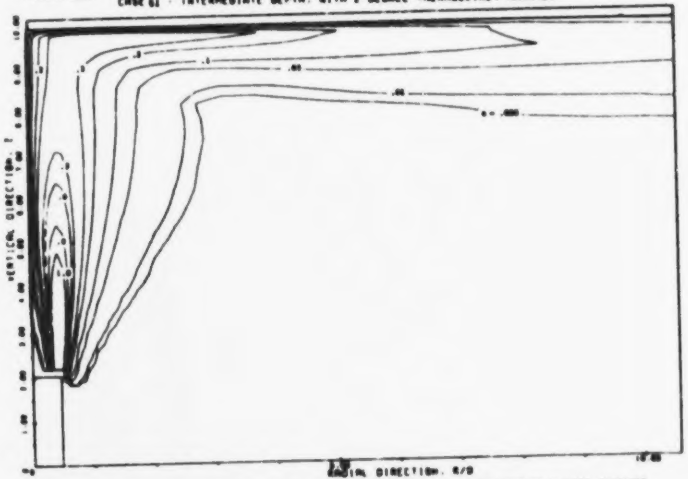

FIGURE 6A4. VORTICITY CONTOUR: AXISYMMETRIC, VERTICAL PLUME, CONFINED BY A FREE SURFACE
CASE 61 - INTERMEDIATE DEPTH, WITH 2 DEGREE THERMOCLINE, [illegible]

causes significant flattening of the streamlines, or reduced vertical entrainment by the spreading plume. This reduction of vertical entrainment is caused by suppression of vertical mixing by the presence of the thermocline. In this case the plume flow spreads above the thermocline. Also, the plume destroys the thermocline in the discharge locale but the "convecting in" of the ambient density structure has a significant effect beginning at distances approximately 5 diameters out. Note the diverging of isotherms in Figure 8.63 and the tendency for the isotherms to attain the ambient condition.

Increasing the magnitude of the thermocline results in further reducing the vertical entrainment and stream line flattening as illustrated by the results of Case 63 (Figures 8.65 through 8.71, respectively). In this case the vertical location of the thermocline is the same as in Case 61, but the magnitude of the thermocline is 4 °C instead of 2 °C.

The effects of a thermocline on the temperature structure are most clearly revealed by Figures 8.66 and 8.67. Also note that out to about 5 diameters the ambient density structure is again completely destroyed by the plume flow. This feature coupled with the upwelling of cooler water from beneath the thermocline results in a phenomenon whereby there is a thermal peak above the outfall, but this peak rapidly deteriorates radially to a temperature which is cooler than the surface (see Figure 8.67). Unlike the base Case 60 where vertical entrainment cools the plume, vertical entrainment warms the

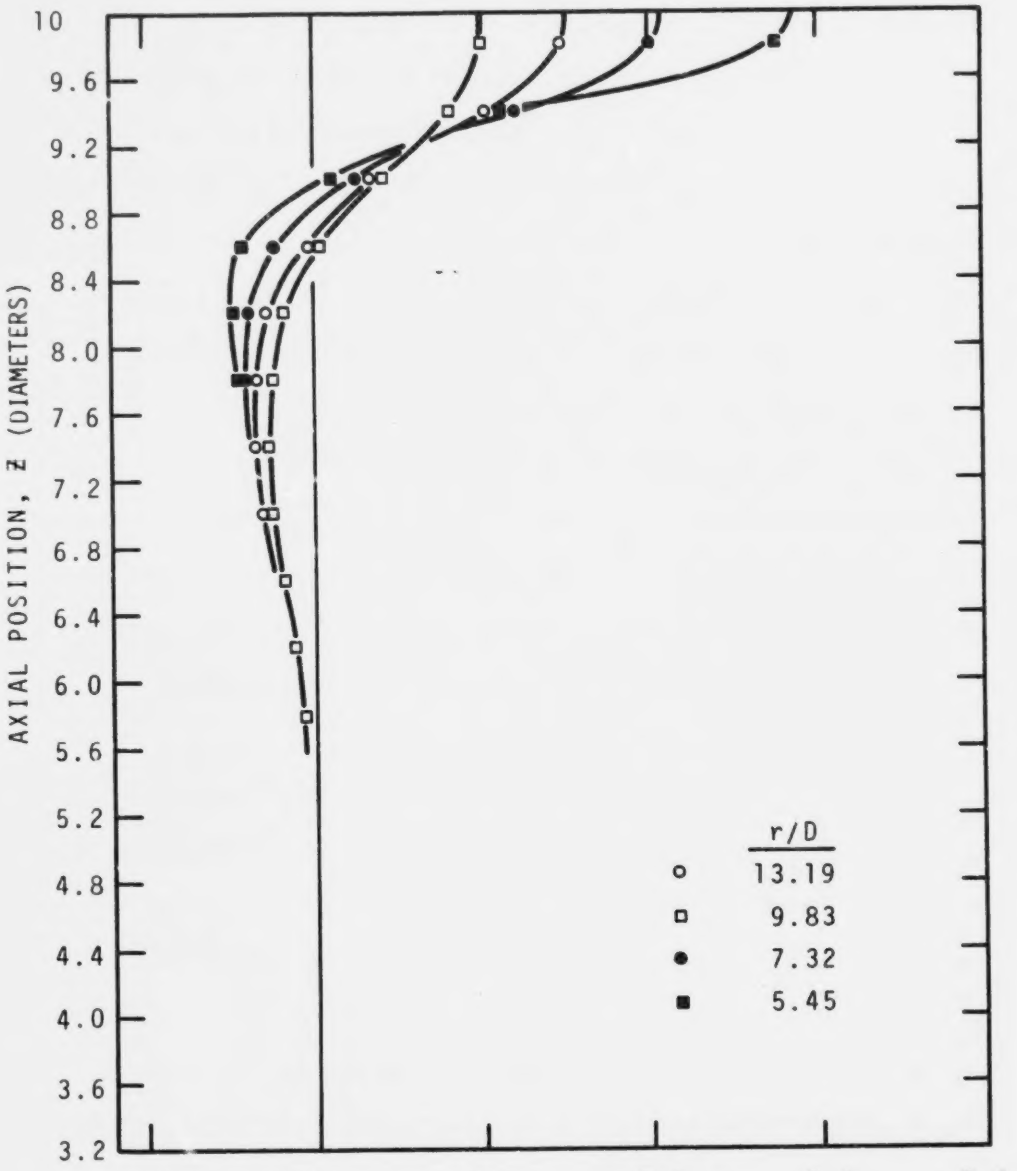

Figure 8.65. Vertical Distribution of Radial Velocity. Case 63

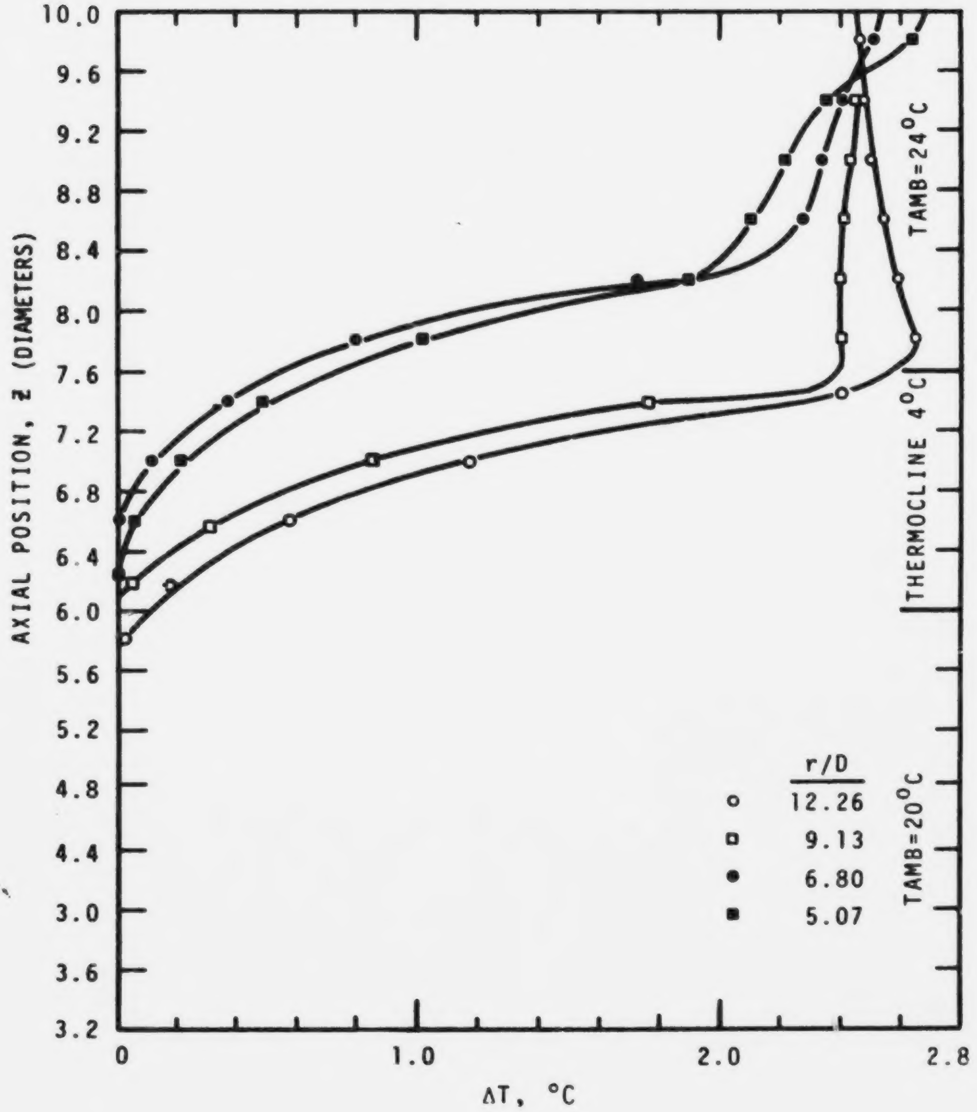

Figure 8.66. Vertical Temperature Excess Distribution. Case 63

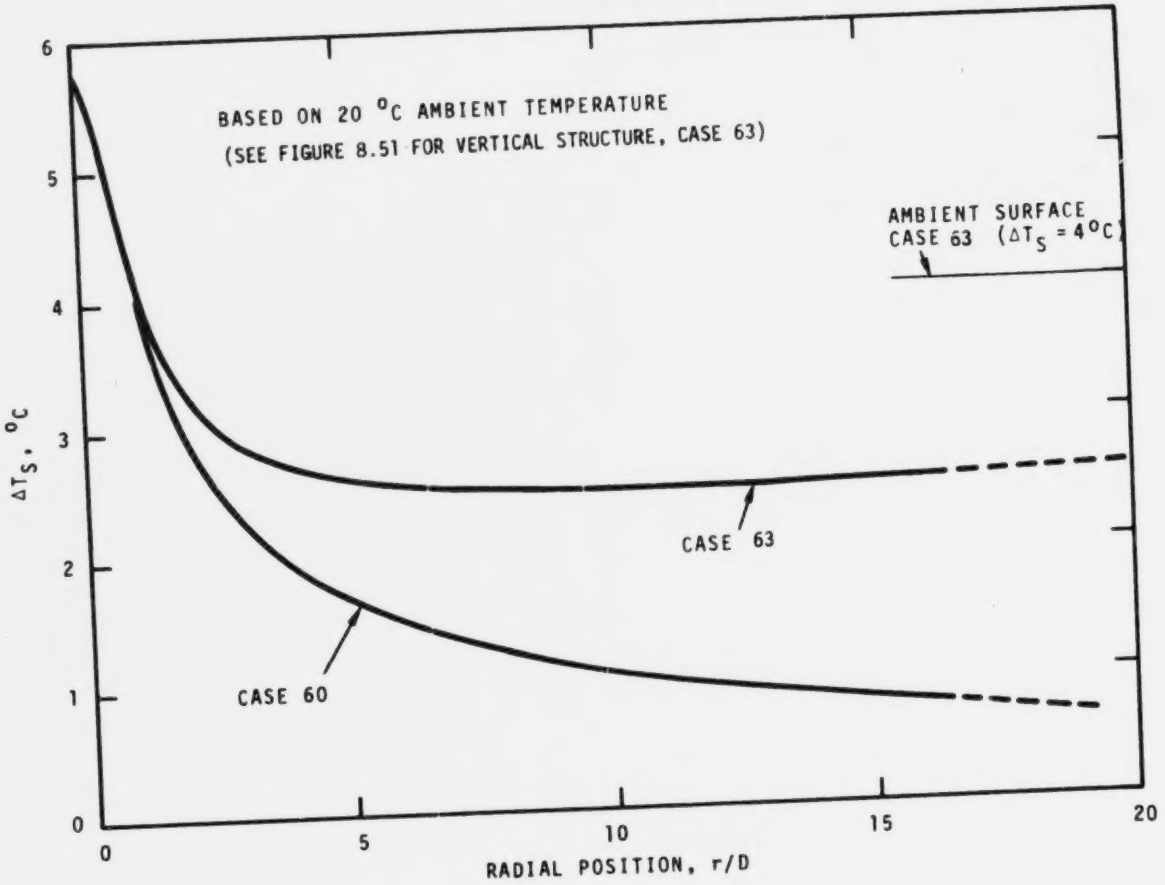

Figure 8.67. Surface Temperature Excess, ΔT_S for Cases 60 and 63

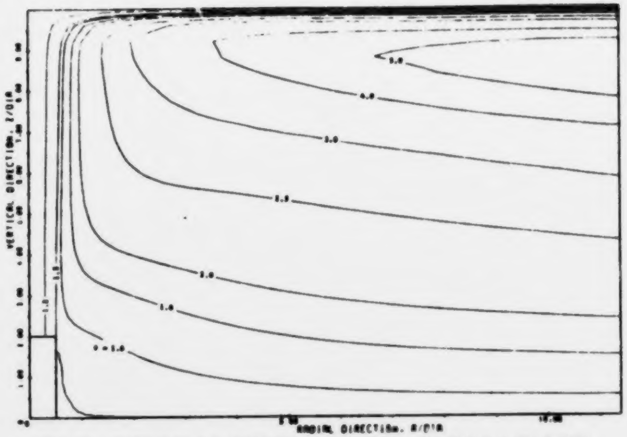

FIGURE 8.68. STREAMLINES FOR AN AXISYMMETRIC, VERTICAL PLUME, CONFINED BY A FREE SURFACE
CASE 63 - INTERMEDIATE DEPTH, WITH 4 DEGREE THERMOCLINE, MAMAYEV

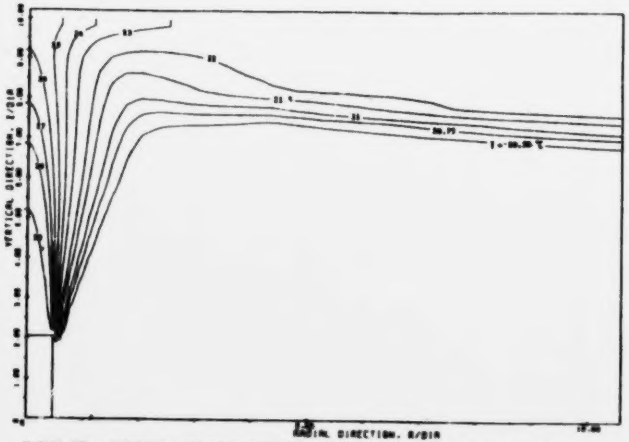

FIGURE 8.69. ISOTHERMS FOR AN AXISYMMETRIC, VERTICAL PLUME, CONFINED BY A FREE SURFACE
CASE 63 - INTERMEDIATE DEPTH, WITH 4 DEGREE THERMOCLINE, MAMAYEV

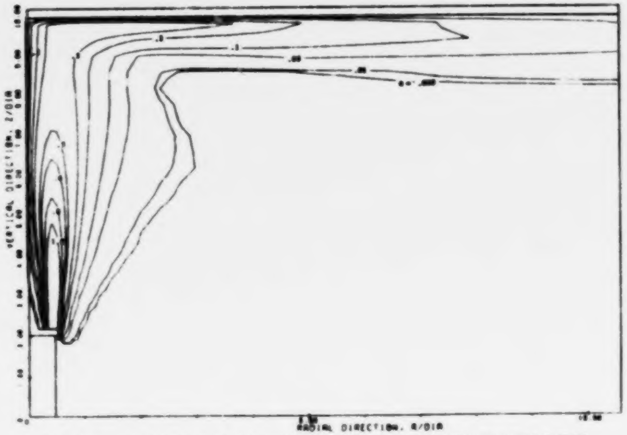

FIGURE 8.70. VORTICITY CONTOURS AXISYMMETRIC, VERTICAL PLUME, CONFINED BY A FREE SURFACE
CASE 63 - INTERMEDIATE DEPTH, WITH 4 DEGREE THERMOCLINE, MAMAYEV

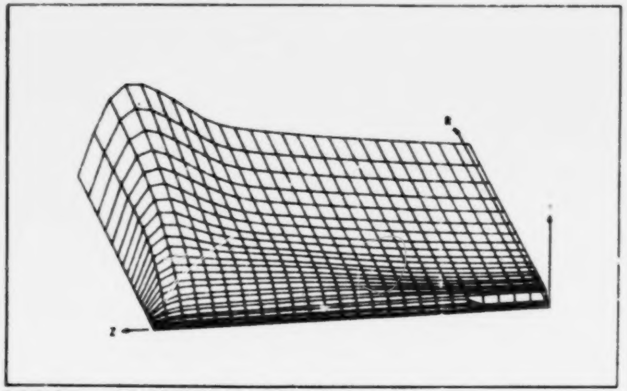

FIGURE 8-71. 3D ILLUSTRATION OF STREAM FUNCTION -- PSI.

CASE 63 - INTERMEDIATE DEPTH, WITH 4 DEGREE THERMOCLINE, MAMAYEV lateral spreading flow since the cooler water is now on the surface in the region of radial spread. This is, of course, a thermally unstable situation, but the configuration is maintained by the flow dynamic forces. This phenomenon is not uncommon and has been observed on several occasions by Eliason [24] through areal infrared photography. We would expect, however, that once dynamic forces are mitigated to the point where buoyant forces (if they still persist) dominate, local upwelling within the lateral spread would occur. Our steady flow computer program cannot reveal these local time dependent effects, but they are indicated by numerical cycling and reluctance to converge. Since the case converged without difficulty, we conclude that the flow field is dynamically stable, at least for the parameters used.

Figures 8.69 and 8.72 again show the thermal effects of "convecting in" or recirculating the ambient thermal structure and the tendency of the thermal distribution to attain the ambient structure.

Figures 8.74 through 8.81 show results for Case 64 where the thermocline is 5 ^{o}C, although the thermal gradient is identical to Case 63 (see Figure 8.51). Comparison with appropriate results of Case 63 snows little influence from this change.

In Case 65 the shape of the thermocline was assumed to be the same as in Case 64 except situated at a somewhat greater depth (Figure 8.51). Figures 8.82 through 8.90 illustrate results for this case. For the problem posed, computation could not be carried out to achieve a steady flow converged solution. Instead numerical

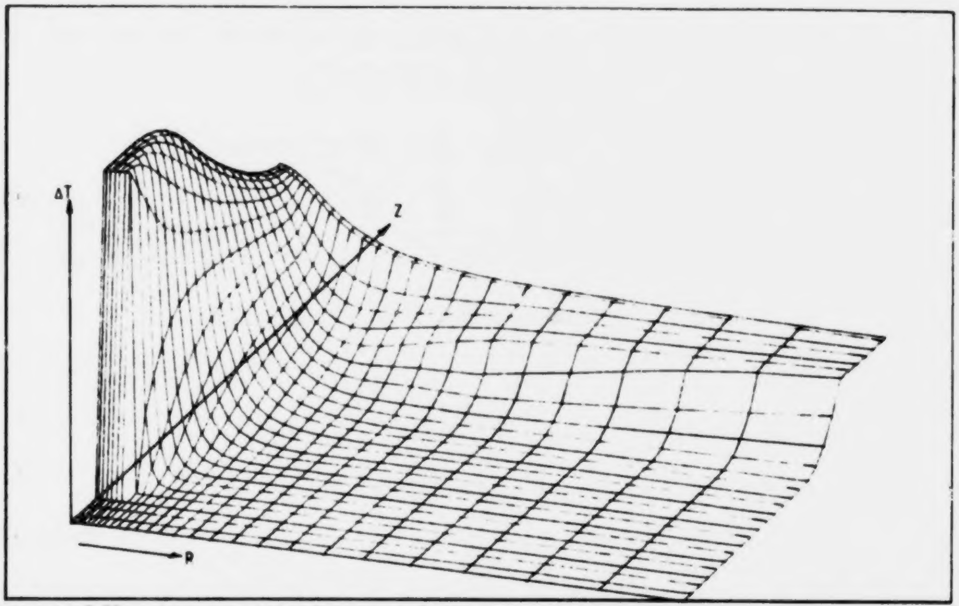

FIGURE 8.72. 3D ILLUSTRATION OF TEMPERATURE FIELD --ΔT.

CASE 63 - INTERMEDIATE DEPTH. WITH 4 DEGREE THERMOCLINE. MAMAYEV

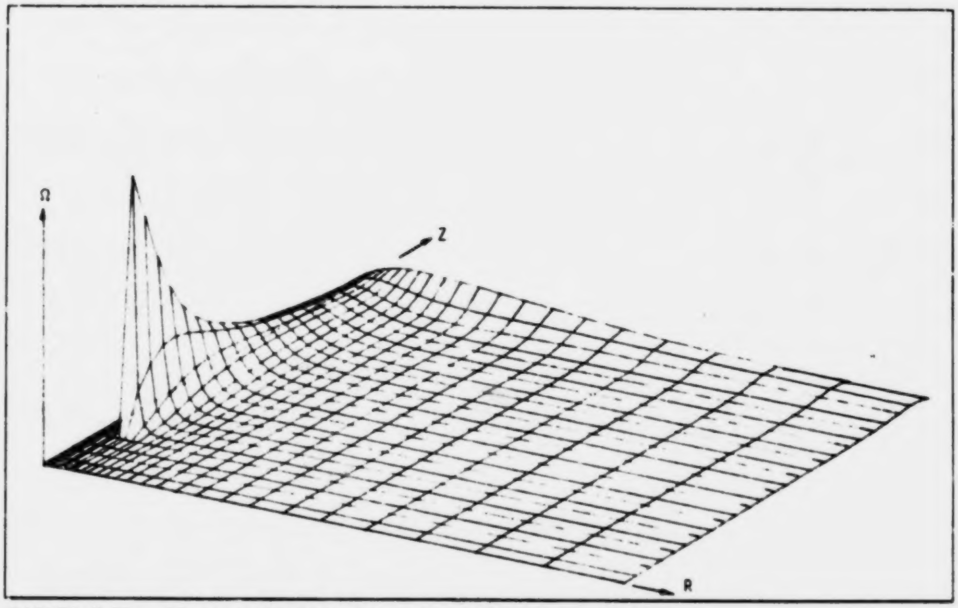

FIGURE 8.73. 3D ILLUSTRATION OF FLUID VORTICTY - OMEGA.

CASE 63 - INTERMEDIATE DEPTH. WITH 4 DEGREE THERMOCLINE. MAMAYEV

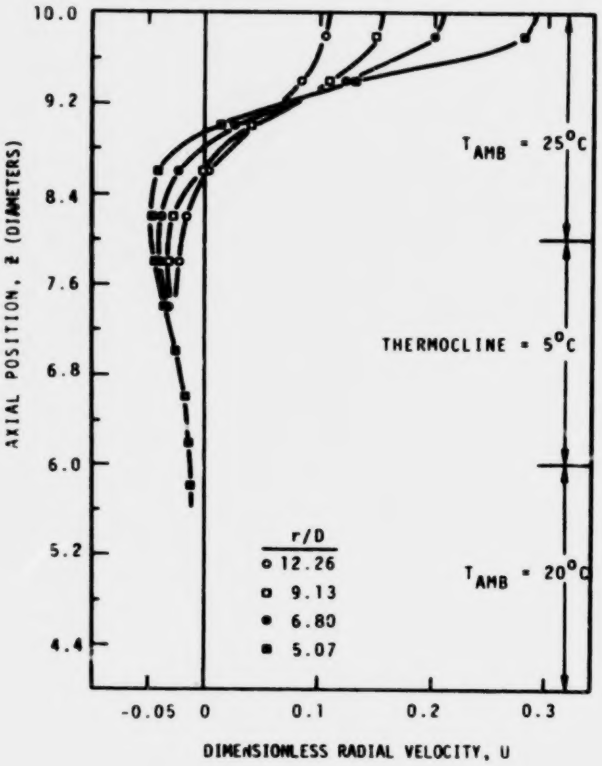

Figure 8.74. Vertical Distribution of Radial Velocity. Case 64

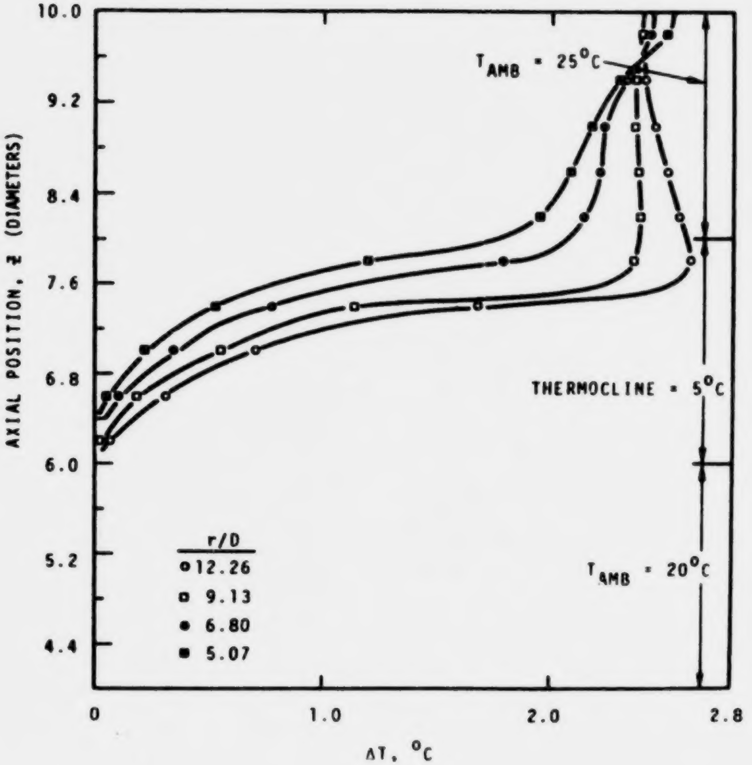

Figure 8.75. Vertical, Excess Temperature Distribution. Case 64.

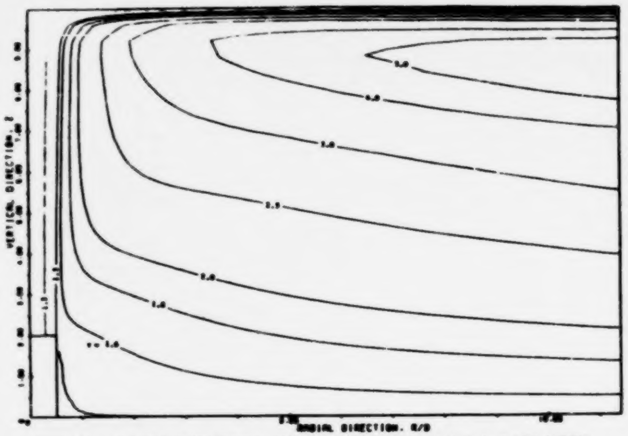

FIGURE 6.76. STREAMLINES FOR AN AXISYMMETRIC, VERTICAL PLUME, CONFINED BY A FREE SURFACE
CASE [illegible] - INTERMEDIATE DEPTH, WITH 5 DEGREE THERMOCLINE, [illegible]

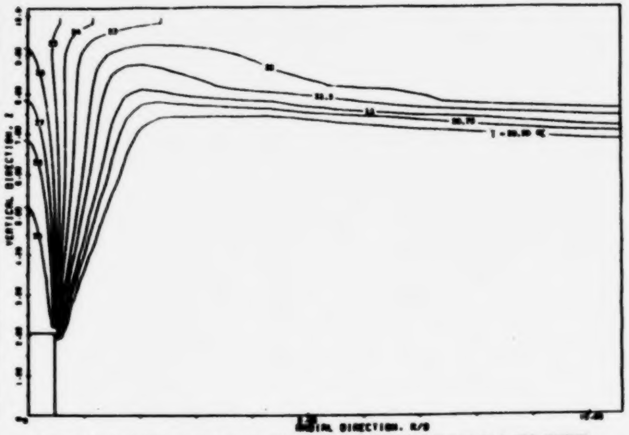

FIGURE 6.77. ISOTHERMS FOR AN AXISYMMETRIC, VERTICAL PLUME, CONFINED BY A FREE SURFACE
CASE [illegible] - INTERMEDIATE DEPTH, WITH 5 DEGREE THERMOCLINE, [illegible]

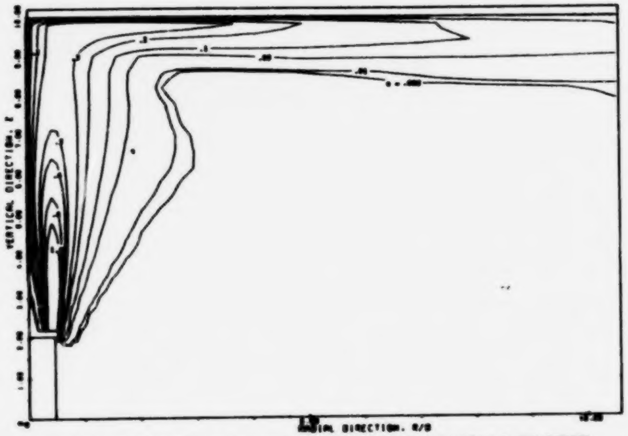

FIGURE 6.78. VORTICITY CONTOURS AXISYMMETRIC, VERTICAL PLUME, CONFINED BY A FREE SURFACE
CASE [illegible] - INTERMEDIATE DEPTH, WITH 5 DEGREE THERMOCLINE, [illegible]

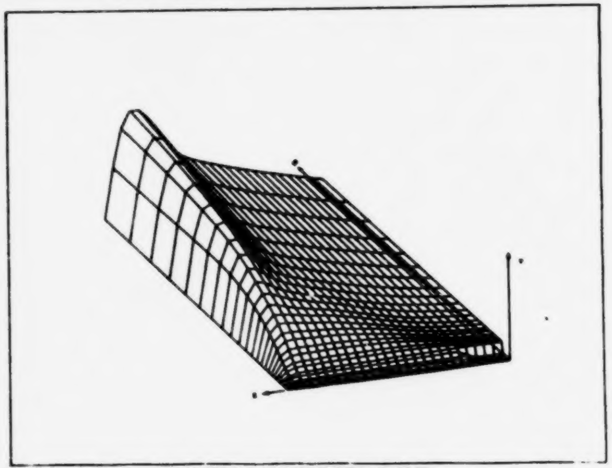

FIGURE 6.79. 3D ILLUSTRATION OF VISCOUS STREAM FUNCTION
CASE [illegible] - INTERMEDIATE DEPTH, WITH 5 DEGREE THERMOCLINE, [illegible]

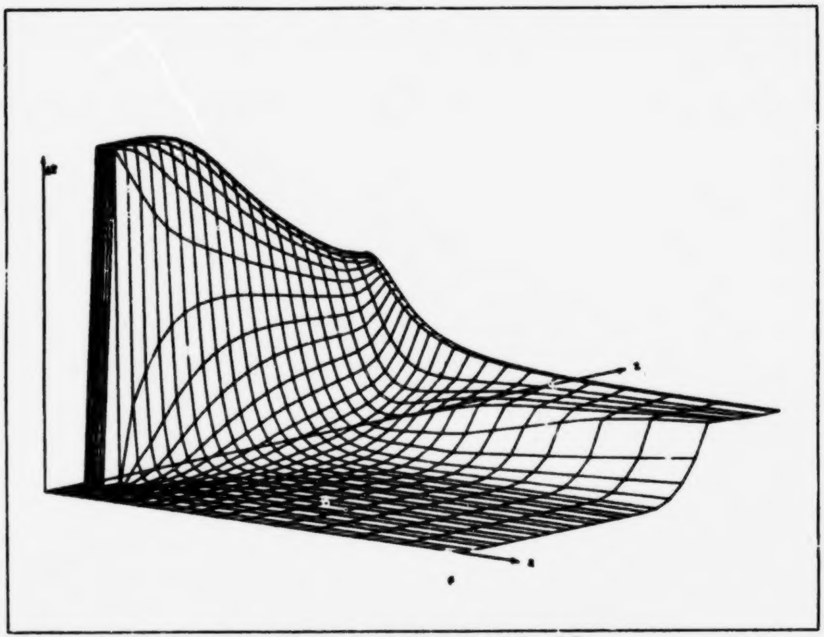

FIGURE 8.80. 3D ILLUSTRATION OF TEMPERATURE FIELD--Δ T
CASE 6A - INTERMEDIATE DEPTH. WITH 5 DEGREE THERMOCLINE. MAMAYEV

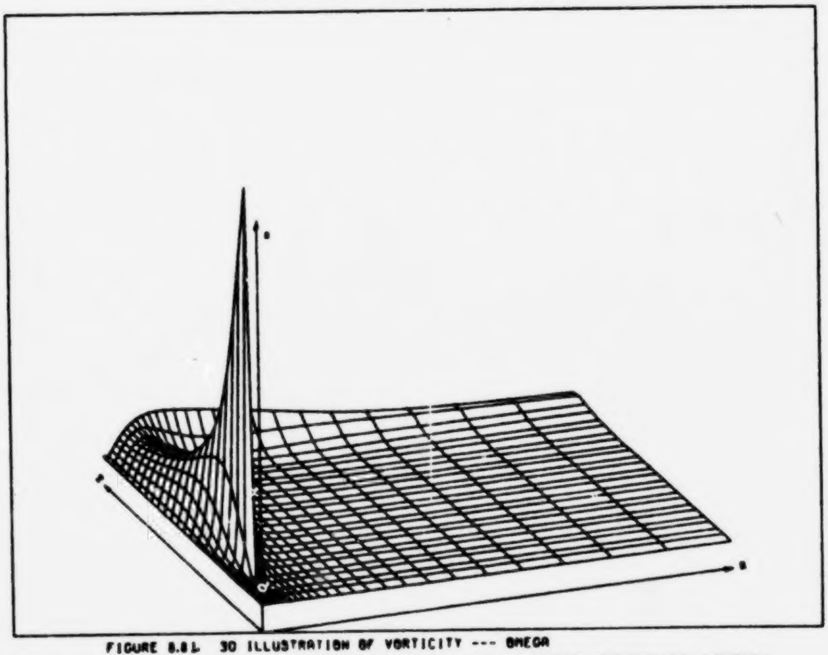

FIGURE 8.81 3D ILLUSTRATION OF VORTICITY --- OMEGA
CASE 6A - INTERMEDIATE DEPTH. WITH 5 DEGREE THERMOCLINE. MAMAYEV

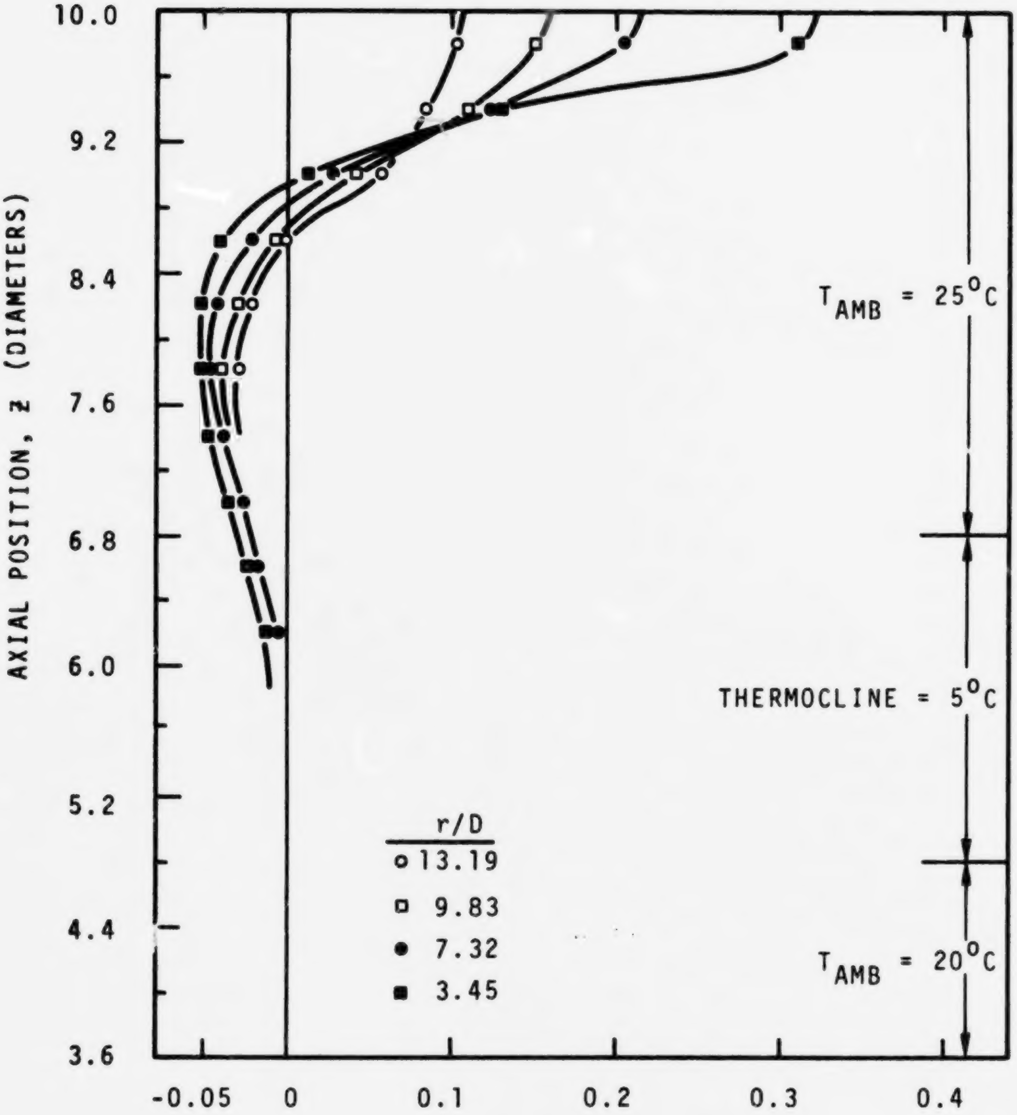

Figure 8.82. Vertical Distribution of Radial Velocity. Case 65

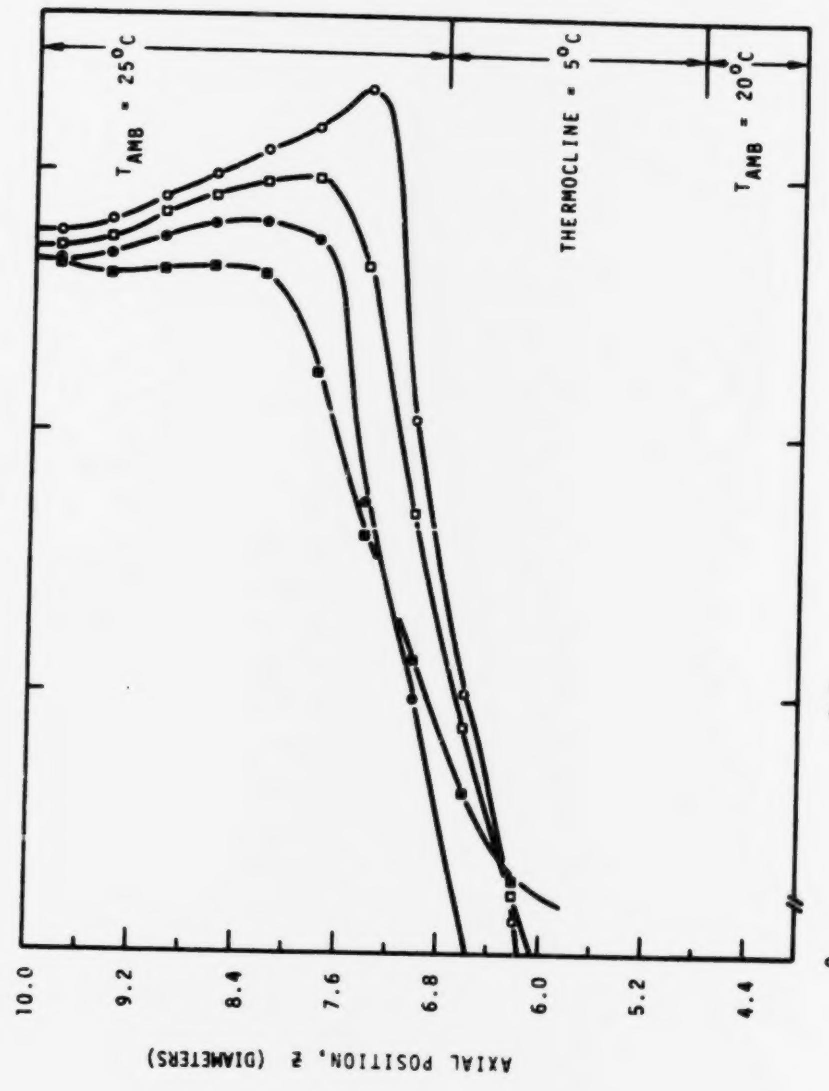

Figure 8.83. Vertical, Excess Temperature Distribution. Case 65

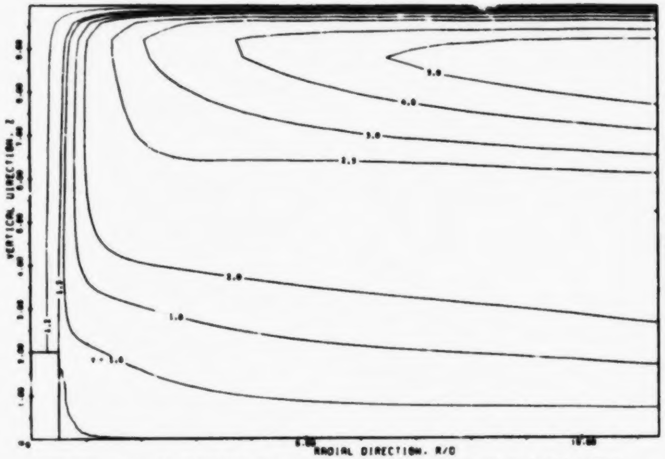

FIGURE 8.84. STREAMLINES FOR AN AXISYMMETRIC, VERTICAL PLUME, CONFINED BY A FREE SURFACE
CASE [illegible] INTERMEDIATE DEPTH, WITH 5 DEGREE THERMOCLINE, MAMAYEV

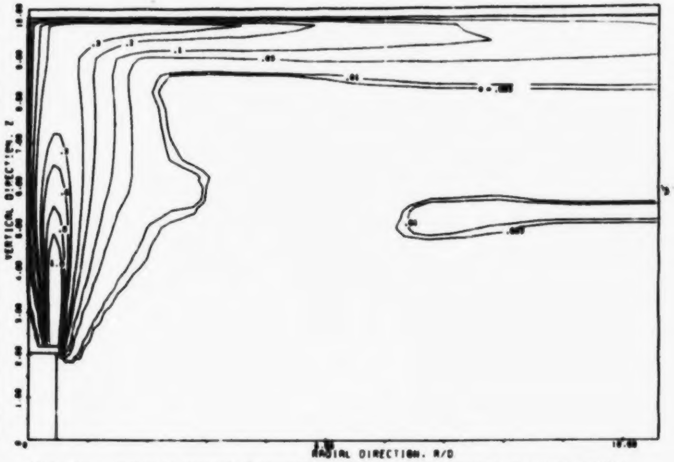

FIGURE 8.85. VORTICITY CONTOURS AXISYMMETRIC, VERTICAL PLUME, CONFINED BY A FREE SURFACE
CASE [illegible]. INTERMEDIATE DEPTH, WITH 5 DEGREE THERMOCLINE, MAMAYEV

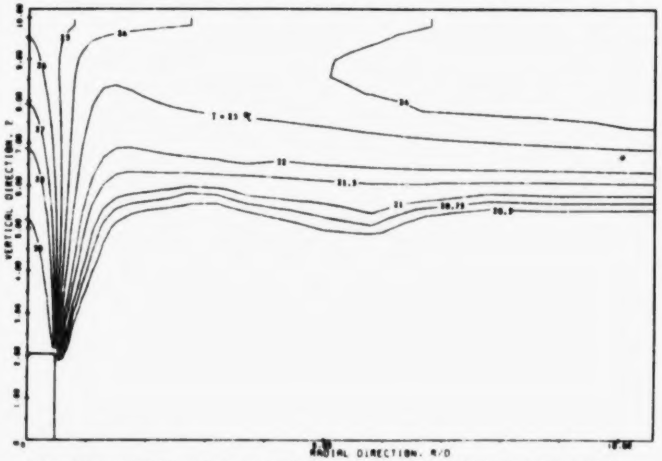

FIGURE 8.86. ISOTHERMS FOR AN AXISYMMETRIC, VERTICAL PLUME, CONFINED BY A FREE SURFACE
CASE [illegible] - INTERMEDIATE DEPTH, WITH 5 DEGREE THERMAL INE. MAMAYEV

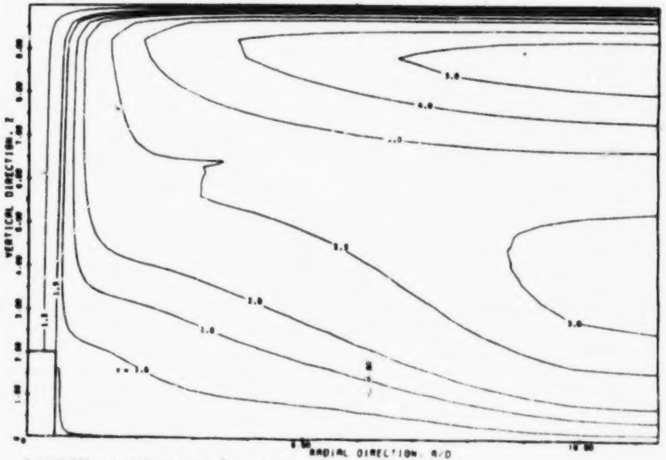

FIGURE 8.87. STREAMLINES FOR AN AXISYMMETRIC, VERTICAL PLUME, CONFINED BY A FREE SURFACE
CASE 65 - INTERMEDIATE DEPTH, CONTINUED ITERATION.

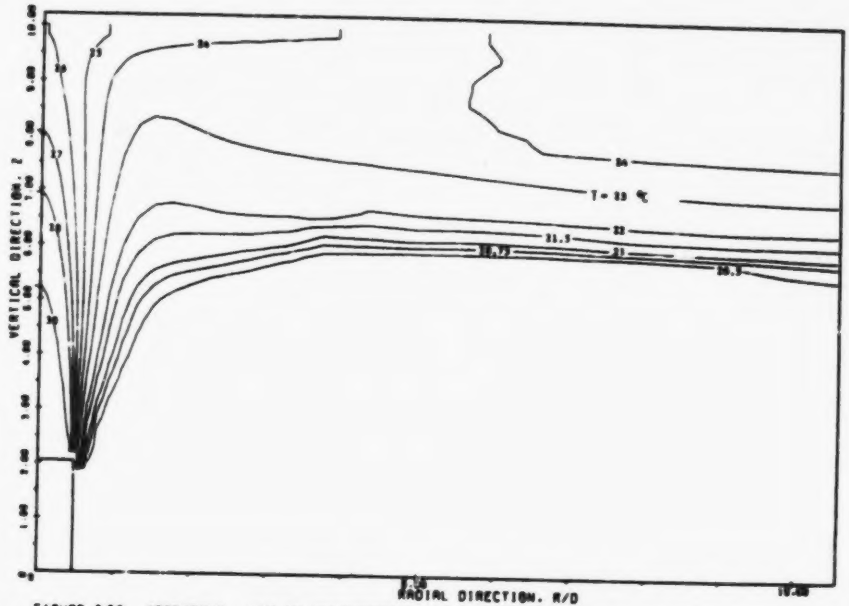

FIGURE 8.88. ISOTHERMS FOR AN AXISYMMETRIC, VERTICAL PLUME, CONFINED BY A FREE SURFACE CASE 65 - INTERMEDIATE DEPTH, CONTINUED ITERATION.

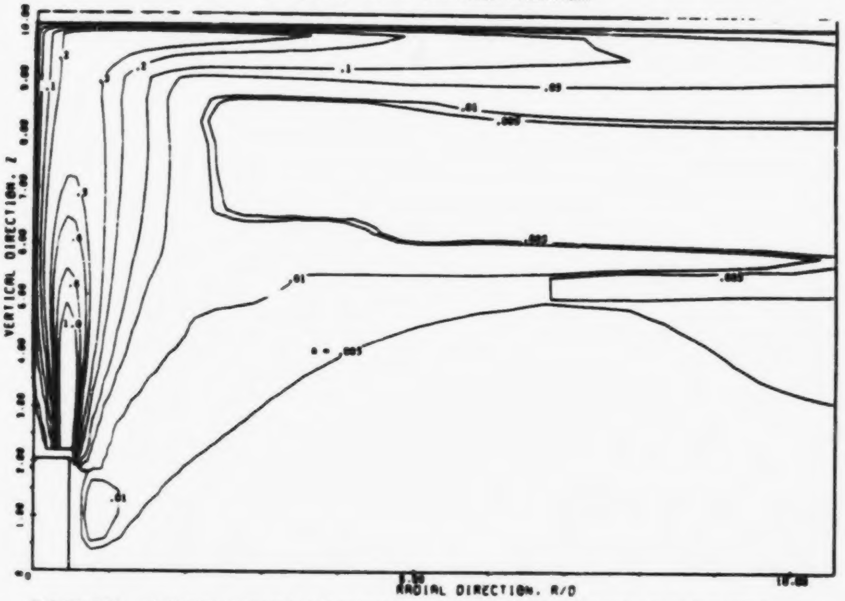

FIGURE 8.89. VORTICITY CONTOURS AXISYMMETRIC, VERTICAL PLUME, CONFINED BY A FREE SURFACE CASE [illegible] - INTERMEDIATE DEPTH, CONTINUED ITERATION.

cycling occurred. Results after 1000 iteration cycles are shown by Figures 8.84 through 8.86. Figures 8.87 through 8.89 reveal results after 300 additional iterations.

Although, the case as posed may not conform to a physically real situation (in particular, the ambient density structure), a thermal instability is suspected which may be either real or perhaps incited by numerical perturbations. Inspecting Figure 8.86 illustrates a large region of cooler water above the thermocline. Continued iteration showed that the ambient isotherms, within the circulating ambient, begin to fluctuate vertically out to about 7 diameters. Further iteration resulted in the development of two recirculating regions: one above the thermocline and the other below (see Figure 8.87). That is, some of the plume flow attempts to spread beneath the thermocline. If the iterative computation is continued, streamline patterns closely resembling those shown in Figure 8.84 will redevelop (single recirculating region).

The investigation of Case 65 was carried out through approximately three cycles of the flow changing from one recirculating region, to two regions and back to one region again. These computations showed neither the tendency for the solution to converge or diverge numerically. It is difficult to derive much incite from steady flow computations possessing such behavior except that a thermal instability is either present or close at hand. A transient computation of the same flow conditions would doubtless reveal similar oscillations during the initial transient, caused by the pulsed plume flow starting condition. However, we would expect the oscillations to damp out with time except if a true thermal instability were present. For our steady flow computation, real conditions may be near to those for a real thermal instability and the nature of the steady flow numerical techniques may be perturbing the solution to a point which prevents a converging result.

It is noteworthy to mention that the solution would diverge numerically with the acceleration factor, L = .999, but displayed the oscillatory nature discussed above with L = .50. Further reduction of L may have eliminated the cycling problem altogether, but would have come at the expense of greatly increased required computer time.

8.6 Discharge at Very Shallow Depth

In concluding the numerical experiments presented in this manuscript, results are illustrated for a large outfall discharging one diameter below the ocean surface (Case 66). This case represents a rather extreme situation, but not unlike several outfalls located off the Southern California Coast. The port diameter is assumed to be 21 feet, the initial densimetric Froude number is 0.111 based on a .574 fps discharge velocity, and initial temperature excess of the effluent is 13.8 ^{O}C with salinity 35 PPt. Computation was carried out laterally to about 10 port diameters.

Figures 8.90 and 8.91 show the spreading velocity and temperature excess at the ocean surface. Note that the maximum surface spreading velocity is about 2.5 times larger than the discharge velocity (2.5 x .574 $\underset{\sim}{}$ 1.4 fps) indicating that the effluent has undergone considerable acceleration caused by buoyancy. Maximum computed velocity occurs about 0.7 diameter from the plume centerline, which is about the edge of the "boil" for a real outfall of these proportions. Figure 8.91 indicates that the plume has undergone only slight cooling on reaching the surface (∿ 3/4 $^{\circ}$C), but cools very rapidly out to about 2 diameters and decreases to about 2 $^{\circ}$C above ambient at 8 diameters.

The radial velocity profiles at selected locations are shown in Figure 8.92 which shows that the plume along with entrained flow, spreads in a fairly shallow sheet at the surface, penetration being less than 0.4 diameter. Temperature profiles (Figure 8.94) penetrate slightly deeper. In fact, the computation shows that plume thermal effects penetrate into the negative flow region, hence there is some indication of plume heat recirculation.

Streamlines, isotherms and level lines of vorticity are illustrated in Figures 8.94, 8.95 and 8.96, respectively. The inward bending of the streamlines (Figure 8.94) above the discharge port indicates considerable acceleration of the effluent. Maximum vorticity for this case occurs near the surface and near the point of maximum lateral spread. This region of high vorticity is also the region where one would expect the edge of the surface boil to occur in a real flow. Three-dimensional surfaces are plotted in Figures 8.97 through 8.101 for the stream function, temperature excess and vorticity.

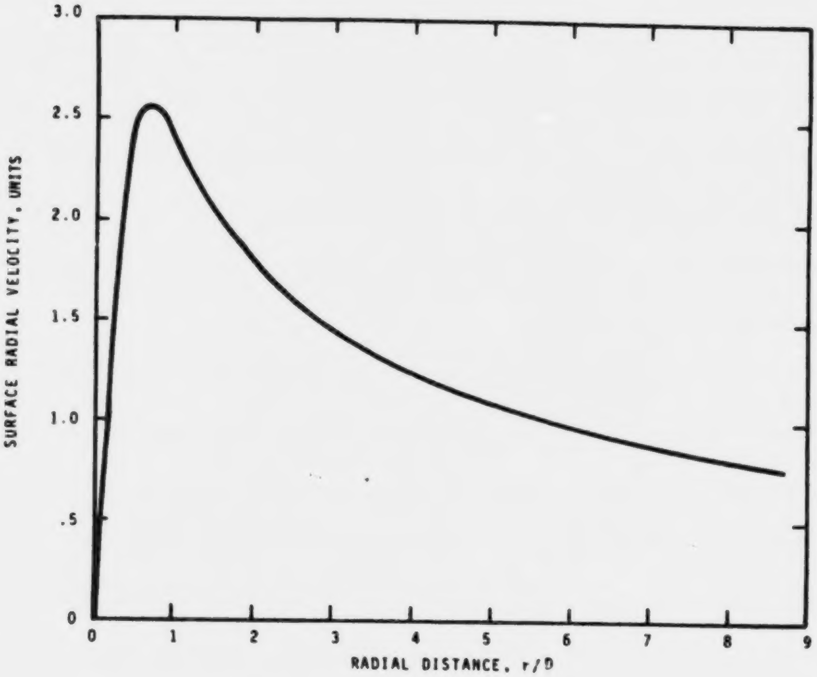

Figure 8.90. Surface Radial Velocity.
Case 66

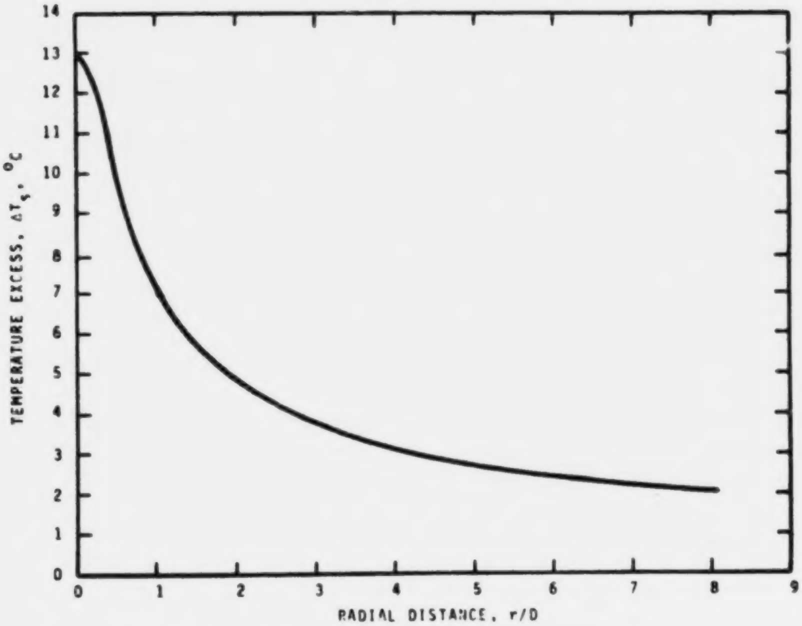

Figure 8.91. Surface Temperature Excess.
Case 66.

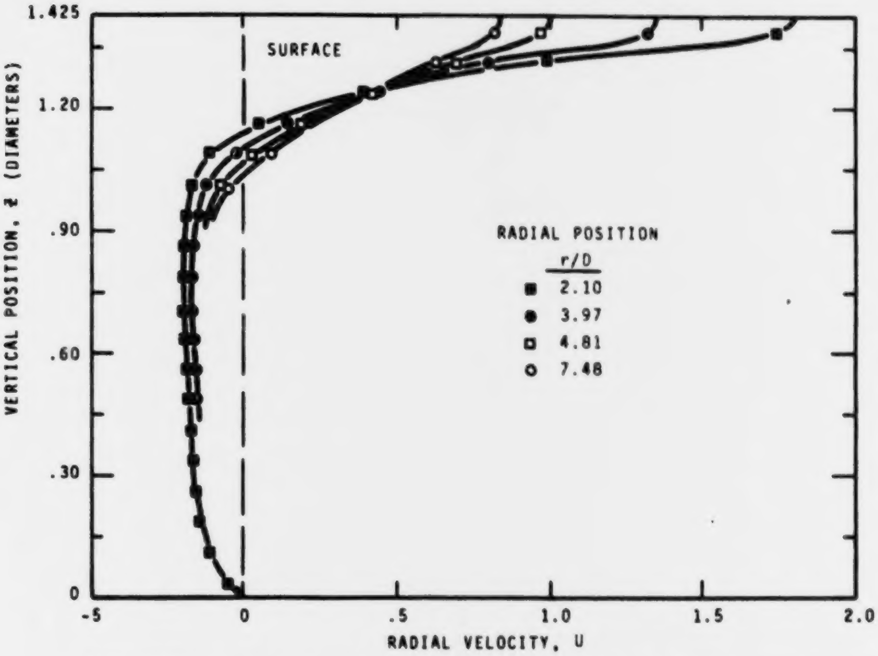

Figure 8.92. Vertical Distribution of Radial Velocity at Various Radial Positions. Case 66

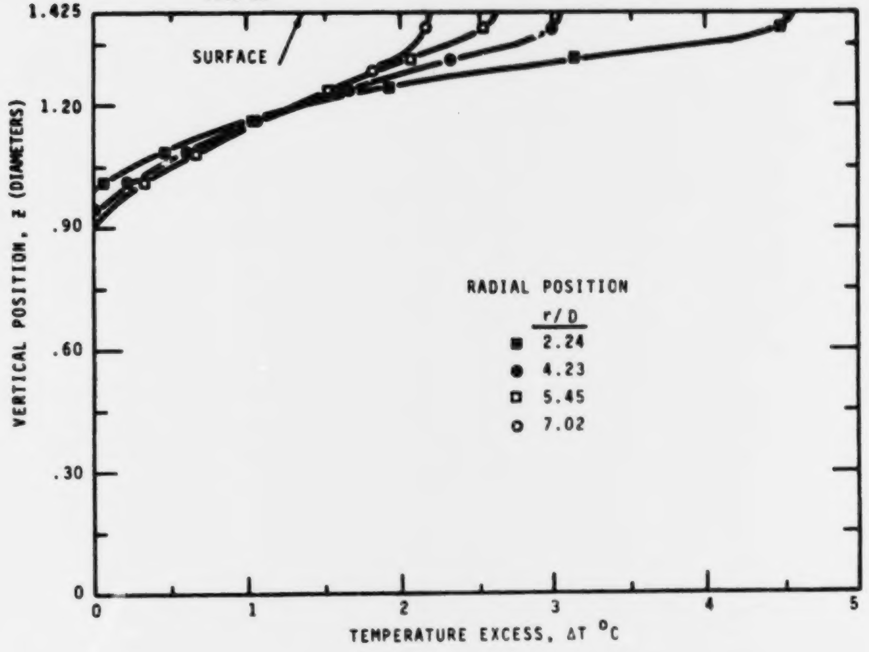

Figure 8.93. Vertical Distribution of Temperature Excess at Various Radial Positions. Case 66

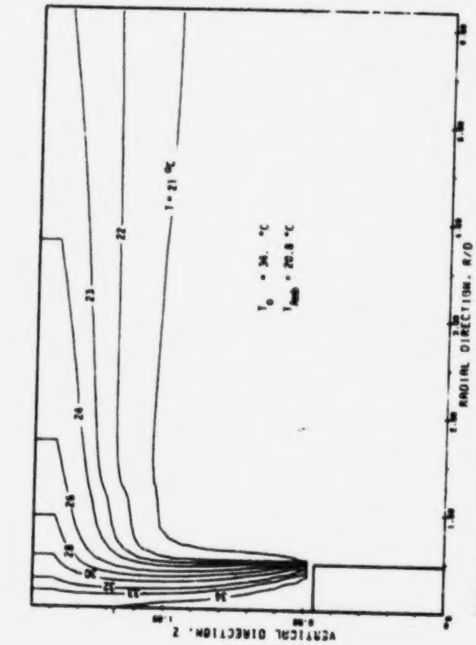

FIGURE 8.95. ISOTHERMS FOR CASE 66 (1.0 DIA DEEP) FO = .111

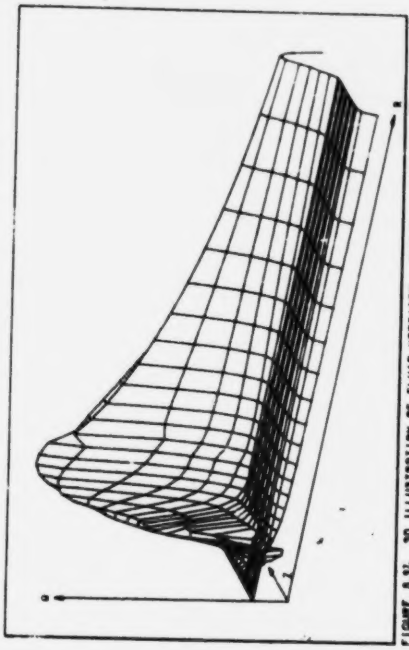

FIGURE 8.97. 3D ILLUSTRATION OF FLUID VORTICITY - OMEGA. CASE NO. 66

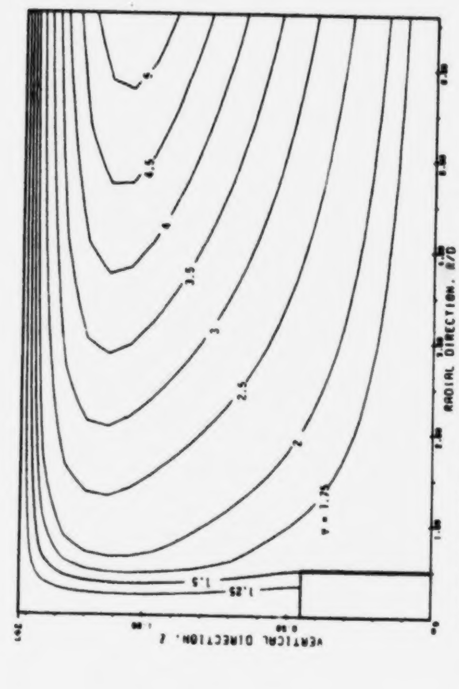

FIGURE 8.94. STREAMLINES FOR CASE 66 (1.0 DIA DEEP) FO = .111

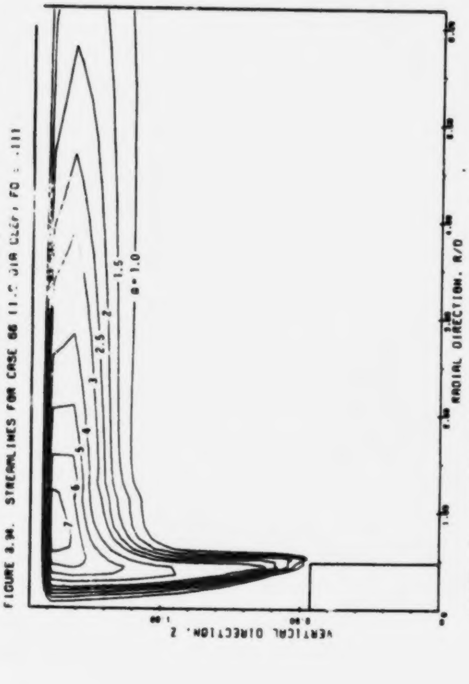

FIGURE 8.96. VORTICITY FOR CASE 66 (1.0 DIA DEEP) FO = .111

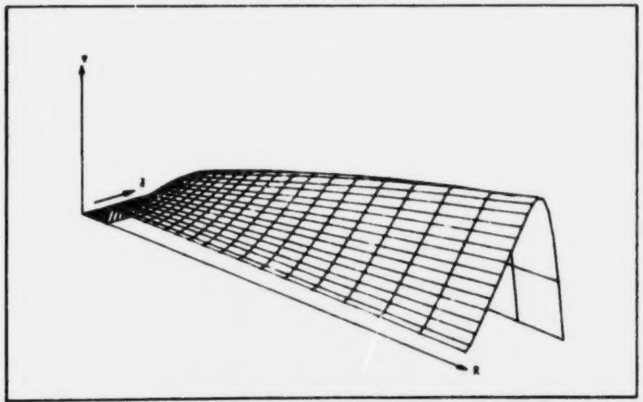

FIGURE 8.98. 3D ILLUSTRATION OF STREAM FUNCTION -- PSI. CASE NO. 66

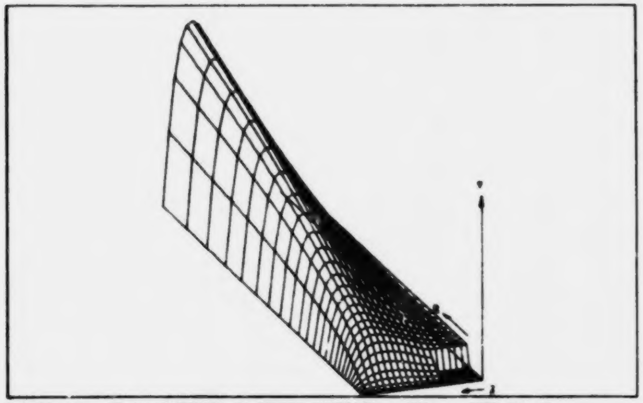

FIGURE 8.99. 3D ILLUSTRATION OF STREAM FUNCTION -- PSI. CASE NO. 66

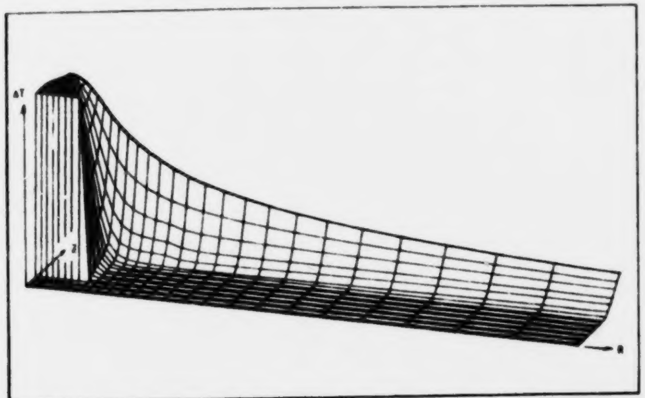

FIGURE 8.100. 3D ILLUSTRATION OF TEMPERATURE FIELD -- T. CASE NO. 66

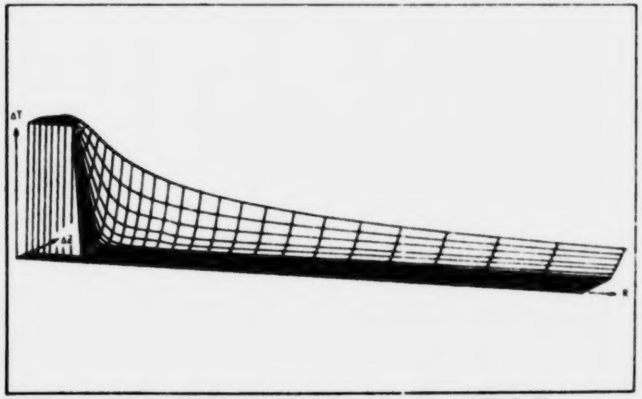

FIGURE 8.101. 3D ILLUSTRATION OF TEMPERATURE FIELD --ΔT. CASE NO. 66

8.7 Comparison with Field Data

At a late-date in this study, the author was able to obtain reliable field data for one shallow water application. This data, obtained for a customer by Battelle-Northwest, is proprietary and details cannot be disclosed. However, the discharge depth is less than one port diameter and the densimetric Froude number is on the order of 2.5.

Figure 8.102 shows a comparison between the computed results and the field measurements. As can be seen, there is reasonably good agreement between data and computation. The computer program predicts surface temperatures which are about 50% high out to about 10 diameters. Temperatures equal to the effluent temperature are predicted at the surface directly over the outfall, whereas the field data indicates an average of about 70% of this value. This discrepancy illustrates that an improved turbulence model is needed for the transition region and perhaps a better representation of the cascading caused by the boil formation. Nonetheless, this result is very encouraging because the computation was performed before the infra-red field data were reduced to temperature information, indicating that at least for very shallow water cases the computer code is a useful predictive device which requires little use of empirical constants.

This result is only one check point and additional field or laboratory data are certainly needed for further verification. Such information could also be used for improvement of the eddy diffusivity model--which is sorely needed.

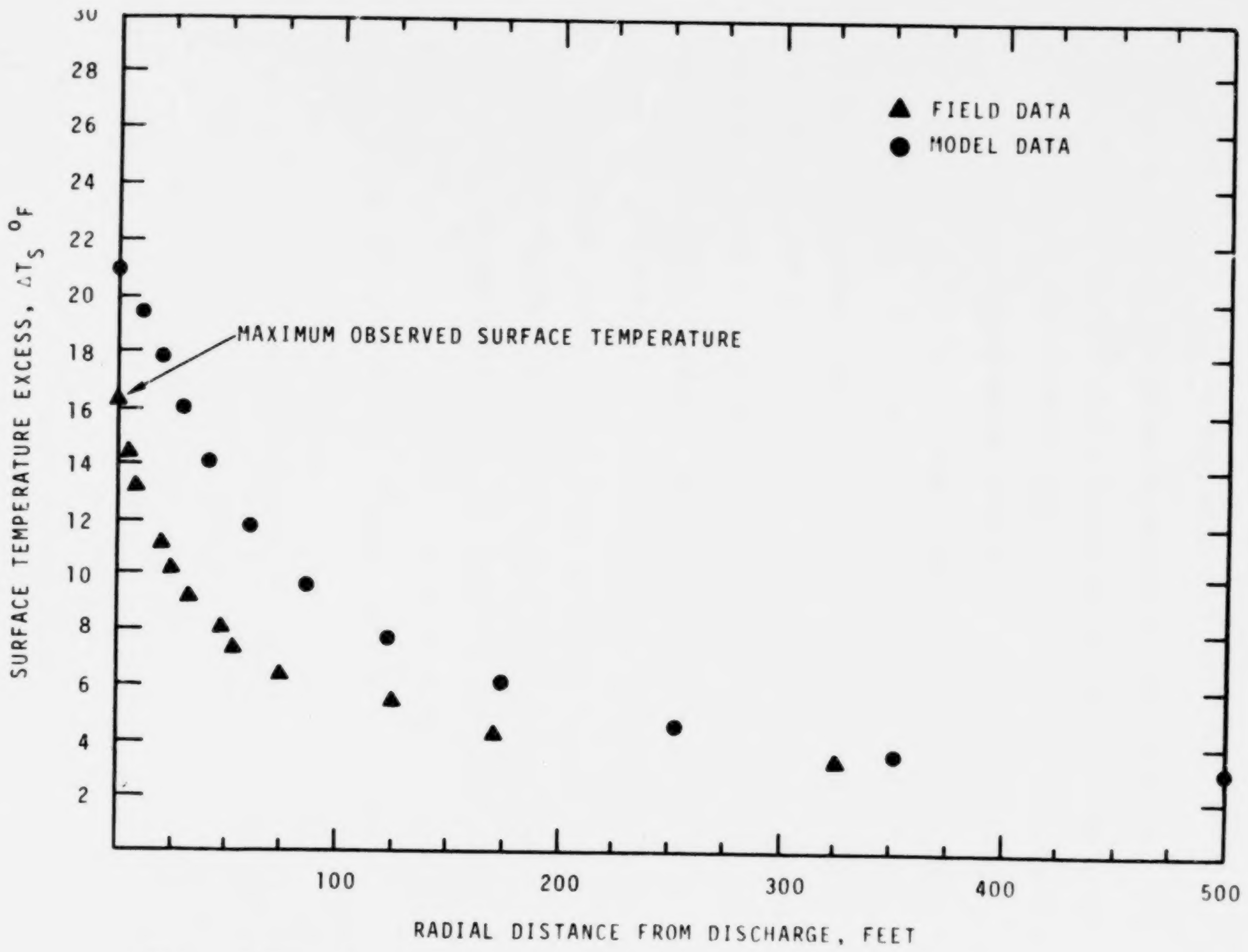

Figure 8.102. Comparison of Computed Surface Temperature with Field Data

CHAPTER 9

CONCLUSIONS

The work contained in this manuscript represents an extensive numerical study of axisymmetric plume flow. Various computational details dealing with practical applications have been investigated along with an extensive verification study comparing numerical results with available published data.

The objective of developing a computer code for general use for vertical plume rise in shallow water and the ensuing lateral spread was not entirely realized. The code developed is more of a research tool than a design tool. The primary reason for this result was the difficulty in modeling turbulent diffusivities. Such models are well established for the vertical rise, but relatively little is known about vertical diffusivities in the lateral spread. Hence, for this and other investigative reasons the computer code suffered through various changes and adaptions during the study; the code listed in Appendix E is one of these later versions.

The more significant conclusions from this study are as follows:

- The steady flow vorticity-stream function technique along with the use of a coupled buoyancy transport equation is an effective and accurate method for computing buoyant plume hydrodynamics up to our ability to model turbulent transport coefficients.
- The iterative use of Prandtl mixing length theory (Prandtl's second hypothesis) is entirely satisfactory

for computing radial eddy transport coefficients in the plume-rise regime. In addition

  - the computations predicted ϵ_r to be essentially constant for a pure initial inertial flow which is also demonstrated by published experimental data.
  - depending on the extent of buoyancy, the computations predicted ϵ_r to vary a great deal with axial position, and that using a constant value of ϵ_r in a buoyant flow can lead to large errors in the computed plume velocity and temperature distributions.

- The iterative use of Prandtl mixing length theory for the vertical eddy transport coefficient was used in this work but was found not to be entirely satisfactory for the plume lateral surface spread. That is, limitations had to be imposed on the maximum size of the computed mixing length to prohibit numerical instability resulting from an unstable mixing length computation. Vertical eddy diffusion was found to have little effect on computed quantities within the plume vertical rise.
- Mixing length theory was found to be entirely unsatisfactory for the circulating (ambient) flow field.
- Solution convergence was slowed dramatically by:
  - Iterative computation of eddy transport coefficient (as opposed to constant values),
  - flow coupled with buoyancy transport (as opposed to a

pure inertial flow),

  - multiple iteration on the stream function elliptic equation between each iteration of the transport equations.

- In addition to the third point mentioned immediately above, in every case tried one psi inner iteration (stream function) per outter iteration (vorticity and buoyancy transport) was found to be satisfactory for convergence. It is strongly suspected that once the approach to convergence for the stream function has become smooth more than one outer iteration per inner iteration would not significantly affect the convergence rate. This action would, however, result in decreased computation time.
- The numerical techniques were found to be stable for every case tried except for the following two instances:
  - over relaxation of the transport equations,
  - use of iteratively computed eddy transport coefficients before reasonable velocity profiles were obtained by using constant coefficients.

It was found that over-relaxation of the vorticity equation always led to a numerical instability for the cases tried. This problem was rectified by using $L_T = .999$. In no case using constant transport coefficients and $L_T \leq .999$, was an instability noted.

The stream function elliptic equation could be over-relaxed in some cases (deep water cases) using $L_E = 1.6$.

However, in the shallow water cases ($Z_S \leq 5$) numerical instabilities were noted using $L_E = 1.6$. Subsequently, $L < 1$ was used with general success.

- Based on results shown in Figure 8.102, it is concluded that the computational methods presented herein can be a very accurate mechanism for computing the surface temperature distribution in the near field of a large, vertical, shallow water coastal thermal outfall. Hence, the primary objective of this study is successfully accomplished.

  The result shown in Figure 8.102 is very encouraging since the computed surface temperature distribution was found to be in excellent agreement with field measurements and the fact that this agreement was obtained without prior knowledge of the field results. However, this is the only case where computation was compared to field data and other situations may reveal discrepancy. Obviously, complete validity of the model can only be ascertained by further comparison with field measurement.

From the results of this study it is generally concluded that the numerical techniques used are a viable and practical method for computing thermal dispersion in confined steady-flow plumes up to our ability to model the plume-generated turbulence. The numerical approach is extremely attractive from the viewpoint that important complexities can be incorporated in the analysis which cannot be accommodated with similarity techniques.Hence, the numerical model, which may be calibrated with field data, will yield reliable computed information and permit a more competent thermal analysis. However, this study has shown that there is indeed a great need for research in turbulence modeling and the application of these models in numerical computation.

BIBLIOGRAPHY

1. Abraham, G. Jet diffusion in stagnant ambient fluid. Delft, Delft Hydraulics Laboratory, 1963. 183 p. (Publication No. 29, series 1, group 14, section 14.42)

2. Abraham, G. Horizontal jets in stagnant fluid of others density. Proceedings of the American Society of Civil Engineers, Journal of the Hydraulics Division 86:1-13. 1960.

3. Abraham, G. Jets with negative buoyancy in homogenous fluid. Journal of Hydraulic Research 4:235-248. 1967.

4. Albertson, M. L., Y. B. Dai, R. A. Jensen, and H. Rouse. Diffusion of submerged jets. Transactions of the American Society of Civil Engineers 115:639-664. 1950.

5. Amsden, A. A. and F. H. Harlow. The SMAC method - a numerical technique for calculating incompressible fluid flows. Los Alamos, Los Alamos Scientific Laboratory. 1970. 85 p. (Document No. LA-4370)

6. Anwar, H. O. Behavior of buoyant jet in calm fluid. Proceedings of the American Society of Civil Engineers, Journal of the Hydraulics Division 97(4):1289-1303. 1969.

7. Aziz, K. A numerical solution of cellular convection. Doctoral dissertation. Houston, Rice University, 1966. 116 numb. leaves. (Microfilm)

8. Baines, Douglas W. Discussion of submerged jets by Albertson et al. Transactions of the American Society of Civil Engineers 115:677-684. 1950.

9. Barakat, H. Transient natural convection flows in closed containers. Doctoral dissertation. Ann Arbor, University of Michigan, 1965. 220 numb. leaves.

10. Batchelor, G. K. An introduction to fluid dynamics. London, Cambridge University Press, 1967. 615 p.

11. Baumgartner, D. J. Vertical jet diffusion in non-linear density stratified fluid. Doctor dissertation. Corvallis, Oregon State University, 1966. 166 numb. leaves.

12. Baumgartner, D. J. and D. S. Trent. Ocean outfall design, part one, literature review and theoretical development. Corvallis, 1970. 129 p. (Federal Water Quality Administration, Environmental Protection Agency)

13. Bird, R. G., W. E. Stewart, and E. N. Lightfoot. Transport phenomena. New York, John Wiley and Son, 1960. 780 p.

14. Bosanqet, C. H., G. Horn and M. W. Thring. The effect of density differences on the path of jets. Proceedings of the Royal Society of London, Ser. A, 263:340-352. 1961.

15. Bradshaw, P. and D. H. Ferriss. Application of a general method of calculating turbulent shear layers. London, Imperial College, 1970. 17 p. (Department of Aeronautics. Report No. 70-06)

16. Brooks, N. H. Conceptual design of submarine outfalls - I. Pasadena, California Institute of Technology, 1969. 19 p.

17. Cederwall, K. Hydraulics of marine water waste disposal. Goteborg Hydraulics Division, Chalmers Institute of Technology, 1968. 273 p. (Publication No. 42)

18. Chou, P. Y. On velocity correlations and solutions of equations of turbulent fluctuations. Quarterly Journal of Applied Mathematics 3(1):38-54. 1945.

19. Chou, P. Y. Pressure flow of turbulent fluid between two infinite parallel planes. Quarterly Journal of Applied Mathematics 3(3):185-197. 1945.

20. Corrsin, S. and M. S. Uberoi. Further experiments on the flow and heat transfer in a heated turbulent jet. Washington, D. C. 1947. 61 p.

21. Crowley, W. P. Numerical advection experiments. Monthly Weather Review 96(1):1-11. 1968.

22. Csanady, G. T. The buoyant motion within a hot gas plume in a horizontal wind. Journal of Fluid Mechanics 22(2):225-239. 1965.

23. Donovan, L. F. Numerical solution of the unsteady Navier-Stokes equations and application to flow in a rectangular cavity with a moving wall. Washington, D. C. 1971. 56 p. (NASA TN D-6312)

24. Eliason, J. R. Battelle-Northwest. Personal communication. Richland, Washington. 1972.

25. Ellison, T. H. and J. S. Turner. Turbulent entrainment in stratified flows. Journal of Fluid Mechanics 6(3):423-448. 1959.

26. Fan, Loh-Nien. Turbulent buoyant jets into stratified or flowing ambient fluids. Pasadena, California Institute of Technology, 1967. 196 p. (W. M. Keck Laboratory of Hydraulics and Water Resources. Report No. KH-R-15)

27. Fan, Loh-Nien and Norman H. Brooks. Numerical solution of turbulent buoyant jet problems. Pasadena, California Institute of Technology, 1969. 94 p. (W. M. Keck Laboratory Hydraulics and Water Resources. Report No. KH-R-18)

28. Fay, J. A., M. Escudier and D. P. Holt. A correlation of field observations of plume rise. Journal of the Air Pollution Control Association 20(6):391-397. 1960.

29. Fox, D. G. Forced plumes in a stratified fluid. Journal of Geophysical Research 75(33):6818-6835. 1970.

30. Frankel, R. J. and J. D. Cummings. Turbulent mixing phenomena of ocean outfalls. Proceedings of the American Society of Civil Engineers. Journal of the Sanitary Engineering Division 91(2):33-59. 1965.

31. Fromm, J. E. Numerical methods for computing non-linear, time dependent, buoyant circulation of air in rooms. IBM Journal of Research and Development 15(3):186-196. 1971.

32. Gaunter, J. W., J. N. B. Livingood and P. Hrycak. Survey of Literature on flow characteristics of a single turbulent jet impinging on a flat plate. Washington, D. C. 1970. 42 p. (NASA TN D-5652)

33. Golubeva, V. N. The formation of the temperature field in a stratified sea, TR. by F. Goodspeed. Bulletin of Academy of Science of the USSR Geophysical Series 5:4670-4671. 1964.

34. Gortler, H. Berechung von aufgaben der freinen turbulenz auf grund eines neuen naherungsansatzes. Zeitschrift Fur Angewandte Mathematik Und Mechanik 22:257-267. 1936.

35. Gosman, A. D. et al. Heat and mass transfer in recirculating flows. London, Academic Press, 1969. 338 p.

36. Harremoes, P. Diffuser design for discharge to a stratified water. Copenhagen, Danish Isotope Center, 1967. 18 p.

37. Hart, W. E. Jet discharge into a fluid with a density gradient. Proceedings of the American Society of Civil Engineers, Journal of the Hydraulics Division 87:171-200. 1961.

38. Hayahsi, T. and N. Shuto. Diffusion of warm water jets discharged horizontally at the water surface. In: Proceedings of the Twelfth Congress of the International Association of Hydraulic Research, Fort Collins, Colorado, 1967. p. 47-59.

39. Hill, M. N. (Editor). The sea. Volume 1. New York Interscience publishers, 1962.

40. Hinze, J. O. Turbulence. New York, McGraw-Hill, 1959. 586 p.

41. Hinze, J. O. and B. G. Van Der Hegge Zijnen. Transfer of heat and matter in the turbulent mixing zone of an axially symmetrical jet. Applied Scientific Research (A) 1:435-461. 1949.

42. Hirasaki, G. J. and J. D. Hellums. Boundary conditions on the vector and scalar potentials in viscous three-dimensional hydrodynamics. Quarterly of Applied Mathematics 28(2):293-296. 1970.

43. Hirst, E. A. Analysis of buoyant jets within the zone of flow establishment. Oak Ridge, Oak Ridge National Laboratory, 1971, 41 p. (Report No. ORNL-TM-3470)

44. Hirst, E. A. Analysis of round turbulent, buoyant jets discharged to flowing stratified ambients. Oak Ridge, Oak Ridge National Laboratory, 1971. 36 p. (Report No. ORNL-4685)

45. Hoult, D. P., J. A. Fay and L. J. Forney. A theory of plume rise compared with field observations. Journal of the Air Pollution Control Association 19(8):585-590. 1969.

46. Hwang, J. D. On numerical solution of the general Navier-Stokes equations for two-layered stratified flows. Doctoral dissertation. Corvallis, Oregon State University, 1968. 134 numb. leaves. (Microfilm)

47. Isayeva, T. and I. L. Isayev. Determination of vertical eddy diffusion in the upper layer of the black sea by a direct method. TR. by Scripta Technica, Inc. Soviet Oceanography Trans. of the Marine Hydrophysical Institute, Academy of Science of the USSR, 1963 series 2:22-24. 1963.

48. Jen, Y., R. L. Wiegel and I. Mobarek. Surface discharge of horizontal warm water jet. Proceedings of the American Society of Civil Engineers, Journal of the Power Division 92(2):1-30. 1966.

49. Keagy, W. R. and A. E. Weller. A study of freely expanding inhomogeneous jets. In: Proceedings of the Heat Transfer and Fluid Mechanics Institute, University of California, Berkeley, June 22-24, 1949. New York, American Society of Mechanical Engineers, p. 89-98. 1949.

50. Keffer, J. F. and W. D. Baines. The round turbulent jet in a crosswind. Journal of Fluid Mechanics 15(4):481-497. 1963.

51. Kent, R. E. and D. W. Pritchard. A test of mixing length theories in a coastal plain estuary. Journal of Marine Research 18(1):62-72. 1959.

52. Koh, R. C. Y., and L. N. Fan. Mathematical models for the prediction of temperature distributions resulting from the discharge of heated water into large bodies of heated water. Washington, D. C. 1970. 219 p. (FWQA Publication No. 16130 DWO10/70, Tetra-Tech Inc.).

53. Larkin, B. K. Some stable explicit difference approximations to the diffusion equation. Math. Computation 18(86):196-202. 1964.

54. Leenderste, J. J. Aspects of a computational model for long period water-wave propagation. Santa Monica, The Rand Corporation. 165 p. 1967. (Document No. RM-5294-PR)

55. Ma, A. S. C. and K. S. Ong. Impulsively started incompressible jet. London, Imperial College, 1970. 28 p. (Department of Mechanical Engineering. Report No. EF/TN/A/28)

56. Manabe, K., Y. Watanabe and A. Wada. Study on recirculation of cooling water of Tsuruga nuclear power station sited on Urazoko Bay. Civil Engineering in Japan 9:156-171. 1966.

57. Masch, F. D. et al. A numerical model for the simulation of tidal hydrodynamics in shallow irregular estuaries. Austin, The University of Texas, 1969. 123 p. (Office of Water Resources Research, D. I. Document No. PB 184834)

58. Morton, B. R. Forced plumes. Journal of Fluid Mechanics 5:151-197. 1959.

59. Morton, B. R. The ascent of turbulent forced plumes in a calm atmosphere. International Journal of Air Pollution 1:184-197. 1959.

60. Morton, B. R., Sir Geoffrey Taylor, and J. S. Turner. Turbulent gravitational convection from maintained and instantaneous sources. Proceedings of the Royal Society of London, Ser. A, 234:1-23. 1956.

61. Muragi, M. P. and H. W. Emmons. Natural convection above fires. Journal of Fluid Mechanics 8(4):611-624. 1960.

62. Murota, A. and K. Muraoka. Turbulent diffusion of the vertically upward jet. In: Proceedings of the Twelfth Congress of the International Association of Hydraulic Research, Fort Collins, Colorado, 1967. p. 60-70.

63. Neuman, G. and W. J. Pierson Jr. Principles of physical oceanography. Engelwood Cliffs, Printice Hall, 1966. 545 p.

64. Okubo, A. Horizontal diffusion from an instantaneous point source due to oceanic turbulence. Baltimore, Johns Hopkins University, 1962. 22 p. (Chesapeake Bay Institute, Tech. Report No. 32)

65. Okubo, A. Fourth report on the rising plume problem in the sea. Baltimore, Johns Hopkins University, 1968. 19 p. (Chesapeake Bay Institute, Reference 68-3)

66. Oregon State University. Department of Civil Engineering. Tidal flats in esturine water quality analysis. Corvallis, 1969. 10 numb. leaves. (Progress Report. Grant No. WP-01385-01 of the Federal Water Quality Administration)

67. Pagnani, B. R. An explicit finite-difference solution for natural convection in air in rectangular enclosures. Doctoral dissertation. Corvallis, Oregon State University, 1968. 176 numb. leaves. (Microfilm)

68. Pai, S. I. and T. Y. Hsieh. Numerical solution of laminar jet mixing with and without free stream. College Park, University of Maryland, 1969. 32 p. (The Institute for Fluid Dynamics and Applied Mathematics. Technical Note BN-627)

69. Patankar, S. V. and D. B. Spalding. A finite-difference procedure for solving the equations of the two-dimensional boundary layer. International Journal of Heat and Mass Transfer 10(10):1389-1412. 1967.

70. Phillips, O. M. The dynamics of the upper ocean. London, Cambridge University Press, 1966. 261 p.

71. Pond, S. Oregon State University. Personal communication. Corvallis, Oregon. 1969.

72. Prandtl, L. Uber die ausgebildete turbulenz. Zeitschrift Fur Angewandte Mathematik Und Mechanik 5:136-139. 1925.

73. Pristly, C. H. B. A working theory of the bent-over plume of hot gas. Quarterly Journal of the Royal Meteorological Society 81:144-157. 1955.

74. Priestly, C. H. B. and K. F. Ball. Continuous convection from an isolated source of heat. Quarterly Journal of the Royal Meteorological Society 81:144-157. 1955.

75. Ramsey, J. W. and R. J. Goldstein. Interaction of a heated jet with a deflecting stream. Transactions of the Americal Society of Mechanical Engineers, Journal of Heat Transfer, Series C, 93(4):365-372. 1971.

76. Rawn, A. M., F. R. Bowerman and N. H. Brooks. Diffusers for disposal of sewage in sea water. Proceedings of the American Society of Civil Engineers, Journal of the Hydraulic Division 86:65-105. 1960.

77. Reichardt, H. Impuls - und warmeaustauch in freier turbulenz. Zeitschrist Fur Angewandte Mathematik Und Mechanik 24:268-272. 1944.

78. Reynolds, O. On the dynamical theory of incompressible viscous fluids and on the determination of the criterion. Philosophical Transactions of the Royal Society, Series A 186:123-164. 1894.

79. Rotta, J. C. Statistische theorie nichthomogener turbulenz. Z. Fur Physik 129:547-572. 1951.

80. Rotta, J. C. Statistische theorie nichthomogener turbulenz. Z. Fur Physik 131:51-77. 1951.

81. Rouse, H., C. S. Yih and H. W. Humphreys. Gravitational convection from a boundary source. Tellus 4:201-210. 1952.

82. Runchal, A. K. and M. Wolfshtein. Numerical integration procedure for the steady state Navier-Stokes equations. Journal of Mechanical Engineering Science 11(5):445-453. 1969.

83. Sami, Sedat. Space correlation in round turbulent jet. Proceedings of the American Society of Civil Engineers, Journal of the Hydraulics Division 97(3):907-917.

84. Schlichting, H. Boundary layer theory, TR. by J. Kerstin. 6th Ed. New York, McGraw-Hill, 647 p. 1968.

85. Schmidt, Wilhelm. Turbulente ausbreiting eines stromes erhitzter lift. Zeitschrift Fur Angewandte Mathematik Und Mechanik 21:265-278, 351-363. 1941.

86. Schmidt, F. H. On the rise of hot plumes in the atmosphere. International Journal of Air and Water Pollution 9:175-198. 1964.

87. Scorer, R. S. The behavior of chimney plumes. International Journal of Air Pollution 1:198-220. 1959.

88. Sharp, J. E. Spread of buoyant jets at the free surface. Proceedings of the American Society of Civil Engineers, Journal of the Hydraulics Division 95(3):811-825. 1967.

89. Sharp, J. J. Unsteady spread of buoyant surface discharge. Proceeding of the American Society of Civil Engineers, Journal of the Hydraulics Division 97(9):1471-1491. 1971.

90. Spalding, D. B. Concentration fluctuations in a round turbulent free jet. Chemical Engineering Science 26:95-107. 1971.

91. Spalding, D. B. Numerical methods in fluid mechanics and heat transfer. London, Imperial College, 1970. 37 p. (Department of Mechanical Engineering. Report No. EF/TN/A/34)

92. Spalding, D. B. Heat and mass transfer in recirculating flows. London, Imperial College, 1968. 28 p. (Department of Mechanical Engineering. Report No. EF/TN/A/8)

93. Spalding, D. B. Mathematical models of turbulent flames. London, Imperial College, 1969. 24 p. (Department of Mechanical Engineering. Report No. BL/TN/B/22)

94. Stolzenbach, K. D. and D. F. Harleman. An analytical and experimental investigation of surface discharges of heated water. Cambridge, Massachusetts Institute of Technology, 1971. 212 p. (Ralph M. Parsons Laboratory for Water Resources and Hydrodynamics. Report No. 135)

95. Stone and Webster Corp. Circulating water discharge system, Shoreham nuclear power station unit 1. Hicksville, Long Island, Long Island Lighting Comp. February 22, 1971.

96. Tamai, N., R. L. Wiegel and G. F. Tornberg. Horizontal surface discharge of warm water jets. Proceeding of the American Society of Civil Engineers, Journal of the Hydraulic Division 95(2)253-276. 1969.

97. Taylor, J. F., H. L. Grimmett and E. W. Comings. Isothermal free jets of air mixing with air. Chemical Engineering Progress 47:175-180. 1951.

98. Tollmien, W. Strahlverbreiterung. Zeitschrift Fur Angewandte Mathematik Und Mechanik 6:468-478. 1926.

99. Tomich, J. Heat and momentum transfer from compressible turbulent jets of hot air impinging normally on a surface. Doctoral dissertation. St. Louis, Washington University, 1967. 216 numb. leaves. (Microfilm)

100. Torrance, K. E. and J. A. Rockett. Numerical study of natural convection in an enclosure with localized heating from below creeping flow to the onset of laminar instability. Journal of Fluid Mechanics 36(1):33-54. 1969.

101. Tulin, M. P. and J. Shwartz. Hydrodynamic aspects of waste discharge. Los Angeles, AIAA 3rd Fluid and Plasma Dynamics Conference, June, 1970. (AIAA Paper No. 70-755)

102. Turner, J. S. Jets and plumes of negative or reversing buoyancy. Journal of Fluid Mechanics 26(4):779-792. 1966.

103. U. S. Navy Hydrographic Office. Tables for sea water density. Washington, D. C. 1952. 265 p. (H. O. Pub. No. 615)

104. Van Sant, J. H. Laminar free convection of heat generating fluids in horizontal pipes. Livermore, Lawrence Radiation Laboratory, 1969. 15 p. (Report No. UCRL-71569)

105. Van Sant, J. H. Lawrence Radiation Laboratory. Personal communication. Corvallis, Oregon. 1969.

106. Wada, Akira. Numerical analysis of distribution flow and thermal diffusion caused by outfall of cooling water. Tokyo, Central Research Institute of Electric Power Industry, 1969. 23 p. (Technical Report:C:67004)

107. Wada, Akira. Effects of winds on a two layered bay. Japan Society of Civil Engineers 9:137-156. 1966.

108. Wada, Akira. Study on recirculation of cooling water of power stations sited on a bay. Japan Society of Civil Engineers 10:143-170. 1967.

109. Welch, J. E., F. H. Harlow, J. P. Shannon and B. J. Daly. The MAC method - a computing technique for solving viscous, incompressible, transient fluid-flow problems involving free surfaces. Los Alamos, Los Alamos Scientific Laboratory, 1965. 146 p. (Document No. LA-3425)

110. Welty, J. R., C. E. Wicks and R. E. Wilson. Fundamentals of momentum, heat and mass transfer. New York, John Wiley and Sons, 1969. 697 p.

111. Wilkes, J. O. and S. W. Churchill. The finite-difference computation of natural convection in a rectangular enclosure. American Institute of Chemical Engineers Journal 12(1):161-166. 1966.

112. Zeller, R. W. Cooling water discharge to Lake Monona. Doctoral dissertation. Madison, University of Wisconsin, 1967. 287 numb. leaves.

113. Zeller, R. W. and R. L. Rulifson. A survey of coastal power plants. Portland, Oregon, 1969. 27 p. (Federal Water Quality Administration Report)

APPENDIX A

CONVECTIVE TRANSPORT DIFFERENCE APPROXIMATION

Differencing the convective terms is the most troublesome aspect of solving transport equations numerically. The mathematical principles for treating these quantities are available, but one must exercise extreme caution when applying these principles or grossly inaccurate solutions will result if not numerical instabilities. When forming difference equations for convective transport, prime consideration must be given to the directional nature of these terms.

A number of papers have been written and studies made concerning numerical convection experiments. Perhaps one of the best studies on higher order methods has been carried out by Crowley [21]. Crowley carried out numerical experiments using a number of difference techniques in solving the "color equation" due to R. Levevier,

$$\frac{\partial \Gamma}{\partial t} + u \frac{\partial \Gamma}{\partial x} + v \frac{\partial \Gamma}{\partial y} = 0 . \tag{A-1}$$

Here Γ is a scalar quantity transported with the flow in a manner such the total derivative is zero along an instantaneous streamline. Crowley refers to Equation (A-1) as the advective form of the Γ transport equation. An alternative way to write Equation (A-1) is

$$\frac{\partial \Gamma}{\partial t} + \frac{\partial u\Gamma}{\partial x} + \frac{\partial v\Gamma}{\partial y} = \Gamma \left(\frac{\partial u}{\partial x} + \frac{\partial v}{\partial y}\right) \tag{A-2}$$

which Crowley refers to as the "conservative" form of the transport equation. By continuity,

$$\frac{\partial u}{\partial x} + \frac{\partial v}{\partial y} = 0. \qquad \text{(A-3)}$$

However, in numerical approximation,

$$\frac{\partial u}{\partial x} + \frac{\partial v}{\partial y} << 1$$

but never zero. For this reason, the right hand side of Equation (A-2) is sometimes included with the analysis in an attempt to reduce accumulating numerical error.

As a point of criticism, in view of transport physics, it is correct to write

$$\frac{\partial \Gamma}{\partial t} + u \frac{\partial \Gamma}{\partial x} + v \frac{\partial \Gamma}{\partial y} + \Gamma \left(\frac{\partial u}{\partial x} + \frac{\partial v}{\partial y}\right) = 0$$

and

$$\frac{\partial \Gamma}{\partial t} + \frac{\partial (u\Gamma)}{\partial x} + \frac{\partial (v\Gamma)}{\partial y} = 0$$

instead of Equations (A-1) and (A-2), respectively.

In the paper cited, Crowley carried out various numerical experiments with first, second and fourth order approximations for Equations (A-1) and (A-2), and the one-dimensional counterpart of these equations. For the one-dimensional tests, he concluded that a second order process using the "conservative" Equation (A-2) was the most accurate. In two dimensions he found that fourth order methods were the most accurate but could not ascertain which equation gave the best results. However, he does recommend that the conservative equation be used.

Reference [66] reports results of numerical experiments concerning the one-dimensional transport equation,

$$\frac{\partial \Gamma}{\partial t} + u \frac{\partial \Gamma}{\partial x} = 0 \qquad \text{(A-4)}$$

Unlike Crowley's work, this work was concerned with the directional nature of u and the proper method for differencing $\partial \Gamma / \partial x$ (forward, backward or central) to minimize numerical error and achieve stable computation.

For these experiments u was assumed positive and steady, with the corresponding explicit difference equation written as:

$$\Gamma_i^{n+1} - \Gamma_i^{n} = \frac{u \Delta t}{\Delta x} \left[(1-\delta_x)(\Gamma_{i-1}^{n} - \Gamma_i^{n}) + \delta_x (\Gamma_i^{n} - \Gamma_{i+1}^{n}) \right] \qquad \text{(A-5)}$$

where the superscript n refers to the nth time step. The parameter δ_x varies from 0 to 1. The following difference techniques are obtained from Equation (A-5) for the corresponding values of δ_x:

$\delta_x = 0$ backwards or upstream method
$\delta_x = .25$ so-called "quarter point" method
$\delta_x = .5$ central method
$\delta_x = 1.0$ forward or downstream method

The results of these numerical experiments are compared with the analytical results for various time steps and total elapsed time, and found that the upstream difference (backward to the direction of flow) gave the superior results.

Note, that in all but the upstream method, downstream quantities, to some extent, are used to establish upstream results. In the case of pure convection these formulations are physically incorrect.

Lelevier (cf. [21]) was evidently the first to introduce the upstream differencing technique. Crowley reports that a great deal of numerical damping results with this method, applied to the "advective" equation, over long integration periods. Nevertheless, the upstream method (also called, unidirectional or one-sided derivative), has been used extensively in solving transport equations. For instance, Van Sant [104] used the "advective" form to solve the vorticity transport equation. Torrance and Rockett [100] solved the "conservative" form of the vorticity equation in this fashion, and Runchal and Wolfshtein [84] used upstream differencing to solve for steady flow vorticity transport in "advective" form. Van Sant [105] stated that he was unable to obtain a solution to the steady flow vorticity equation using central differences.

One trouble with using any method except the upstream method is that truncation and numerical round off can cause serious errors and even destroy the solution through numerical instability. Higher order methods (central difference, for instance) in spite of their purported higher degree of accuracy may be inferior if the direction nature of the flow is not considered. Runchal and Wolfshtein present some clarification of this subject. We will pursue the matter here by formulating convective difference schemes using one-sided and central techniques.

Consider the incompressible steady flow transport equations, with constant eddy coefficients for a conservative scalar quantity Γ in (x,y) coordinates:

$$u \frac{\partial \Gamma}{\partial x} + v \frac{\partial \Gamma}{\partial y} = \frac{1}{N_R N_\Gamma} \left(\frac{\partial^2 \Gamma}{\partial x^2} + \frac{\partial^2 \Gamma}{\partial y^2} \right) \tag{A-6}$$

where N_R is the Reynolds number and

$$N_\Gamma = \frac{\text{momentum diffusivity}}{\Gamma \text{ diffusivity}} .$$

The finite difference grid system (Figure A-1) has constant and equal spacing in the x and y directions.

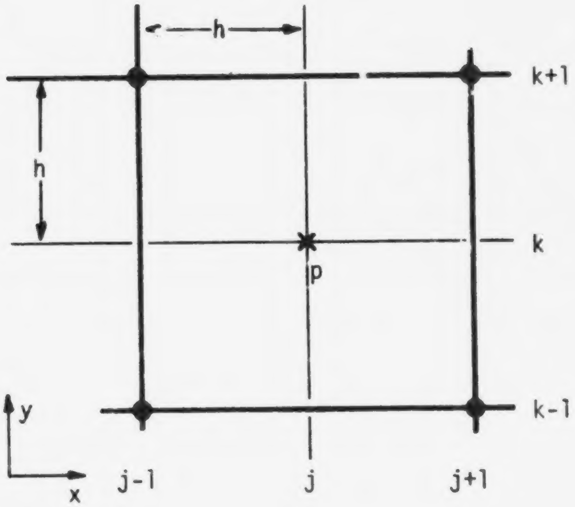

Figure A-1: Finite-Difference Grid System

Suppose we now apply a general difference scheme to the convective terms of Equation (A-6) which, for the time being, disregards the directional sense of the velocity components u and v. Then,

$$u_p \left[(1-\delta_x)(\Gamma_p-\Gamma_{j-1}) + \delta_x (\Gamma_{j+1}-\Gamma_p)\right]$$

$$+ v_p \left[(1-\delta_y)(\Gamma_p-\Gamma_{k-1}) + \delta_y (\Gamma_{k+1}-\Gamma_p)\right]$$

$$= \frac{1}{F} \left[(\Gamma_{j-1}+\Gamma_{j+1}+\Gamma_{k-1}+\Gamma_{k+1}-4\Gamma_p)\right], \qquad \text{(A-7)}$$

where the constant subscript has been suppressed and point (j,k) is replaced by p for convenience. In the above equation, δ_x and δ_y are factors corresponding to difference schemes in the x and y directions. These quantities (δ_x and δ_y) take values of 0, 1/2 and 1 for backward, central, and forward differences, respectively. The quantity F is equal to $N_R N_\Gamma h$. Solving for Γ_p yields

$$\left[(1-2\delta_x)u_p + (1-2\delta_y)v_p + \frac{4}{F}\right] \Gamma_p$$

$$= u_p \left[(1-\delta_x)\Gamma_{j-1}-\delta_x\Gamma_{j+1}\right] + v_p \left[(1-\delta_y)\Gamma_{k-1}-\delta_y\Gamma_{k+1}\right]$$

$$+ \frac{1}{F}\left[(\Gamma_{j-1}+\Gamma_{j+1}+\Gamma_{k-1}+\Gamma_{k-1})\right] \qquad \text{(A-8)}$$

Case 1. Central difference scheme, δ_x and $\delta_y = \frac{1}{2}$.

Equation (A-8) reduces to

$$\Gamma_p = \frac{F}{8}\left[u_p(\Gamma_{j-1}-\Gamma_{j+1}) + v_p(\Gamma_{k-1}-\Gamma_{k+1})\right]$$
$$+ \frac{1}{4}(\Gamma_{j-1}+\Gamma_{j+1}+\Gamma_{k-1}+\Gamma_{k+1}) . \qquad \text{(A-9)}$$

If F is very small, implying a very small Reynolds number (creeping flow) or a very small grid spacing, h, Equation (A-9) will usually converge. However, for large F,

$$\Gamma_p \approx \frac{F}{8}\left[u_p(\Gamma_{j-1}-\Gamma_{j+1}) + v_p(\Gamma_{k-1}-\Gamma_{k+1})\right] \qquad \text{(A-10)}$$

Hence, small errors in the differences are magnified by a large coefficient, F, which will eventually destroy the computation through instability. For this reason the central difference scheme is not desirable for either transient or steady state application for intermediate and large values of F.

Case 2. Forward difference scheme, δ_x and $\delta_y = 1$.

Equation (A-8) reduces to

$$\left[-\frac{F}{4}(u_p+v_p)+1\right]\Gamma_p = -\frac{F}{4}(u_p\Gamma_{j+1}+v_p\Gamma_{k+1})$$
$$+ \frac{1}{4}(\Gamma_{j-1}+\Gamma_{j+1}+\Gamma_{k-1}+\Gamma_{k+1}) . \qquad \text{(A-11)}$$

Equation (A-11) poses additional complications because of the presence of the negative sign in the coefficient multiplying Γ_p. For positive u_p and v_p and

$$\frac{F}{4}(u_p+v_p) \approx 1.$$

Equation (A-11) is unmanageable. For large values of F, the difference scheme becomes

$$\Gamma_p \simeq \frac{1}{u_p+v_p}\left(u_p\Gamma_{j+1}+v_p\Gamma_{k+1}\right). \qquad \text{(A-12)}$$

If either u_p or v_p is positive, this equation is physically incorrect because we would be basing upstream computation on downstream information. On the other hand, if both u_p and v_p are negative, then Equation (A-11) becomes

$$\left[\frac{F}{4}\left(|u_p|+|v_p|\right)+1\right]\Gamma_p = \frac{F}{4}\left(|u_p|\Gamma_{j+1}+|v_p|\Gamma_{k+1}\right)$$

$$+\frac{1}{4}\left(\Gamma_{j-1}+\Gamma_{j+1}+\Gamma_{k-1}+\Gamma_{k+1}\right) \qquad \text{(A-13)}$$

which may be shown to be computationally stable for all values of F and is a preferred scheme. This equation is also physically correct since upstream quantities are used for downstream computation.

Case 3. Backward difference scheme, δ_x and $\delta_y = 0$.

Equation (A-8) reduces to

$$\left[\frac{F}{4}\left(u_p+v_p\right)+1\right]\Gamma_p = \frac{F}{4}\left(u_p\Gamma_{j-1}+v_p\Gamma_{k-1}\right)$$

$$+\frac{1}{4}\left(\Gamma_{j-1}+\Gamma_{j+1}+\Gamma_{k-1}+\Gamma_{k+1}\right) \qquad \text{(A-14)}$$

If velocities u_p and v_p are both positive we have a computationally stable scheme which is posed physically correct. However if either velocity component is negative, we have the same type of situation discussed in Case 2 where the scheme may be unstable and is not posed correctly with regard to transport physics.

Clearly, it is necessary to have a computationally stable and correctly posed difference scheme for all values of F. It is impossible to meet this criterion in a general flow system without cognizance of velocity directional sense and magnitude at each and every boundary and computation point in the difference network. A sound scheme may be obtained by choosing δ_x and δ_y according to the sign of the velocity components. We disregard δ_x and δ_y = 1/2 because of instability at large F.

	u_p		v_p	
	+	-	+	-
δ_x	0	1		
δ_y			0	1

Figure A-2 Values of δ_x and δ_y for a Preferred Difference Scheme

Figure A-2 summarizes the upstream difference method. Since the velocity sign must be checked at each point in order to decide which value of δ_x and δ_y is to be used, an alternate method is formed which is well adapted to computer application. Consider Equation (A-6), specifically the term

$$u_p \left[(1-\delta_x)(r_p-r_{j-1}) - \delta_x (r_p-r_{j+1})\right].$$

Let

$$u_p(1-\delta_x) = \frac{1}{2}\left(|u_p| + u_p\right) = \begin{cases} u_p, \text{if } u_p \text{ is positive} \\ 0, \text{if } u_p \text{ is negative} \end{cases} ,$$

$$u_p\delta_x = \frac{1}{2}\left(|u_p| - u_p\right) = \begin{cases} 0, \text{if } u_p \text{ is positive} \\ u_p, \text{if } u_p \text{ is negative} \end{cases} ;$$

hence,

$$u_p \frac{\partial \Gamma}{\partial x}\bigg|_p = \frac{1}{2\Delta x}\left[\left(|u_p| + u_p\right)\left(\Gamma_p - \Gamma_{j-1}\right) + \left(|u_p| - u_p\right)\left(\Gamma_p - \Gamma_{j+1}\right)\right]$$

which always gives the correct difference regardless of the sign of u_p.

The upstream difference technique applied to Equation (A-8) yields

$$\begin{aligned}\left(|u_p| + |v_p| + \frac{4}{F}\right)\Gamma_p &= \frac{1}{2}\left(|u_p| + u_p\right)\Gamma_{j-1} \\ &+ \frac{1}{2}\left(|u_p| - u_p\right)\Gamma_{j+1} + \frac{1}{2}\left(|v_p| + v_p\right)\Gamma_{k-1} \\ &+ \frac{1}{2}\left(|v_p| - v_p\right)\Gamma_{k+1} + \frac{1}{F}\left[\Gamma_{j-1} + \Gamma_{j+1} + \Gamma_{k-1} + \Gamma_{k+1}\right] . \qquad \text{(A-15)}\end{aligned}$$

Solving for Γ_p yields

$$\Gamma_p = \frac{\frac{F}{2}\left\{\left(|u_p| + u_p\right)\Gamma_{j-1} + \left(|u_p| - u_p\right)\Gamma_{j+1} + \left(|v_p| + v_p\right)\Gamma_{k-1} + \left(|v_p| - v_p\right)\Gamma_{k+1}\right\} + \left(\Gamma_{j+1} + \Gamma_{j-1} + \Gamma_{k+1} + \Gamma_{k-1}\right)}{4 + F\left(|u_p| + |v_p|\right)} \qquad \text{(A-16)}$$

Upstream Differencing for Conservative Forms

Previous discussion of upstream differencing has dealt entirely with convective differences in the "advective" form, $u_j \partial\Gamma/\partial x_j$. However, this form is a result of mathematical manipulation of the correct "conservative" form, $\partial(u_j\Gamma)/\partial x_j$. The conservative form is a direct result of a Γ balance in terms of infinitesimal quantities and is the correct method for proper conservation of a transported quantity in numerical analysis.

Consider the convective balance of Γ in r,z coordinates (Figure A-3).

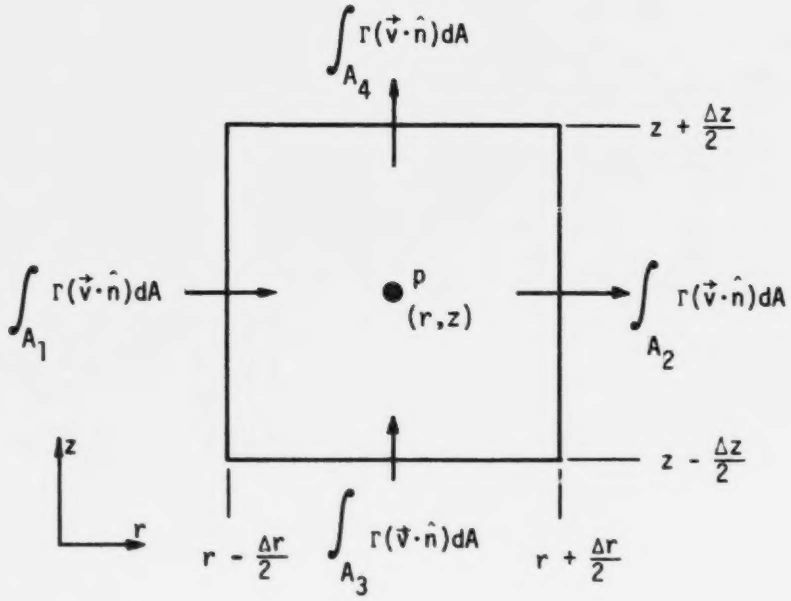
$\int_{A_4} \Gamma(\vec{v}\cdot\hat{n})dA$
$z + \frac{\Delta z}{2}$
$\int_{A_1} \Gamma(\vec{v}\cdot\hat{n})dA$
P
(r,z)
$\int_{A_2} \Gamma(\vec{v}\cdot\hat{n})dA$
$z - \frac{\Delta z}{2}$
z
r
$r - \frac{\Delta r}{2}$
$\int_{A_3} \Gamma(\vec{v}\cdot\hat{n})dA$
$r + \frac{\Delta r}{2}$

Figure A-3 Convective Γ Flux for an Infinitesimal Axisymmetric Volume Element

The steady flow convective balance equation for volume element p is given by

$$\int_{A_T} \Gamma(\vec{v}\cdot\hat{n})dA = \int_{A_1} \Gamma(\vec{v}\cdot\hat{n})dA + \int_{A_2} \Gamma(\vec{v}\cdot\hat{n})dA$$

$$+ \int_{A_3} \Gamma(\vec{v}\cdot\hat{n})dA + \int_{A_4} \Gamma(\vec{v}\cdot\hat{n})dA = 0. \qquad \text{(A-17)}$$

In Equation (A-17) and Figure A-3, A_1, A_2, etc., are element areas corresponding to side 1, 2, etc., and $\hat{n}$ is a unit normal vector, with outward, the positive sense and inward, negative. Like directional sense is used for the boundary velocity vector $\vec{v}$.

Now refer to the grid system shown in Figure A-4. This grid has constant Δr and Δz, and velocities u and v are specified at the cell face, whereas Γ is cell centered at point p (also see Figure A-2). In setting up the difference scheme based on Equation (A-17) we want to:

1) convect into the cell, p, the value of Γ at the upstream neighbor, and
2) convect out of cell p, the value of Γ at p.

Hence, the value of Γ to be used in Equation (A-17) is given by

$$\Gamma = \begin{cases} \Gamma_p, \text{ for } |\vec{v}\cdot\hat{n}| = \vec{v}\cdot\hat{n} \\ \\ \text{value at upstream neighbor for } |\vec{v}\cdot\hat{n}| \neq \vec{v}\cdot\hat{n}. \end{cases} \qquad \text{(A-18)}$$

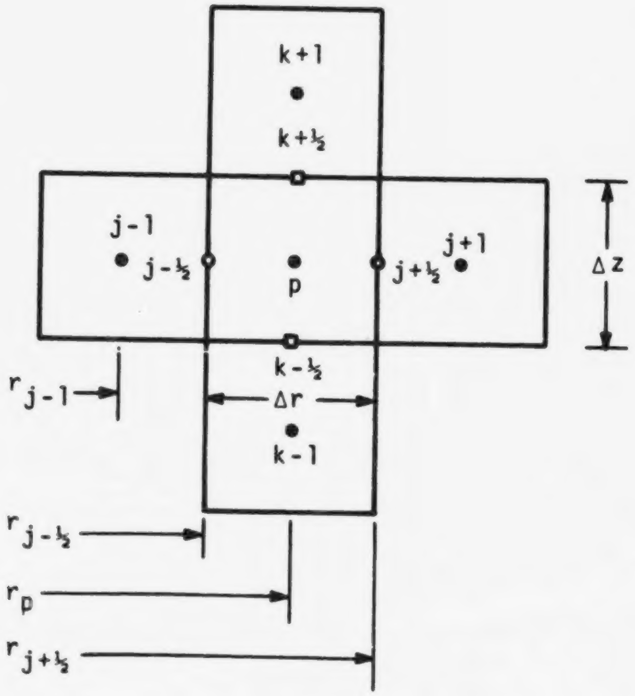
k + 1
k + ½
j - 1
j - ½
p
j + ½
j + 1
Δz
k - ½
Δr
k - 1
r_{j-1}
$r_{j-½}$
r_p
$r_{j+½}$

Figure A-4 Axisymmetric Finite-Difference Cell, p, with the Four Immediate Neighbor Cells

Unlike typical difference schemes, Equation (A-17) provides flexibility of convecting into or out of any cell face. For the element, Equation (A-17) may be written as

$$2\pi\left(r-\frac{\Delta r}{2}\right)\Delta z\Gamma\ (\vec{v}\cdot\hat{n})\Big|_{r-\frac{\Delta r}{2}} + 2\pi\left(r+\frac{\Delta r}{2}\right)\Delta z\Gamma\ (\vec{v}\cdot\hat{n})\Big|_{r+\frac{\Delta r}{2}}$$

$$+\ \pi r\ \Delta r\quad \Gamma(\vec{v}\cdot\hat{n})\Big|_{z-\frac{\Delta z}{2}} + \pi r\ \Delta r\quad \Gamma(\vec{v}\cdot\hat{n})\Big|_{z+\frac{\Delta z}{2}} = 0\,.$$

Dividing by volume ($2\pi r\Delta r\Delta z$) yields

$$\frac{\left(r-\frac{\Delta r}{2}\right)\Gamma(\vec{v}\cdot\hat{n})\Big|_{r-\frac{\Delta r}{2}}}{r\Delta r} + \frac{\left(r+\frac{\Delta r}{2}\right)\Gamma(\vec{v}\cdot\hat{n})\Big|_{r+\frac{\Delta r}{2}}}{r\Delta r}$$

$$+\frac{\Gamma(\vec{v}\cdot\hat{n})\Big|_{z-\frac{\Delta z}{2}}}{\Delta z} + \frac{\Gamma(\vec{v}\cdot\hat{n})\Big|_{z+\frac{\Delta z}{2}}}{\Delta z} = 0. \qquad \text{(A-19)}$$

In accordance with Equation (A-18) and Figure A-4, Equation (A-19) may be expressed as

$$\frac{\frac{1}{2}\, r_{j-1/2}\left\{\Gamma_p(|u_{j-1/2}| - u_{j-1/2}) - \Gamma_{j-1}(|u_{j-1/2}| + u_{j-1/2})\right\}}{r_p\Delta r}$$

$$+\ \frac{\frac{1}{2}\, r_{j+1/2}\left\{\Gamma_p(|u_{j+1/2}| + u_{j+1/2}) - \Gamma_{j+1}(|u_{j+1/2}| - u_{j+1/2})\right\}}{r_p\Delta r}$$

$$+\ \frac{\frac{1}{2}\left\{\Gamma_p\ (|v_{k-1/2}| - v_{k-1/2}) - \Gamma_{k-1}\ (|v_{k-1/2}| + v_{k-1/2})\right\}}{\Delta z}$$

$$+ \frac{\frac{1}{2}\left\{\Gamma_p \left(|v_{k+1/2}| - v_{k+1/2}\right) - \Gamma_{k+1} \left(|v_{k+1/2}| + v_{k+1/2}\right)\right\}}{\Delta z}$$

$$\Longleftrightarrow \left\{\frac{1}{r} \frac{\partial(ru\Gamma)}{\partial r} + \frac{\partial(v\Gamma)}{\partial z}\right\}\Bigg|_p . \tag{A-20}$$

The above form is used throughout in this thesis for convective differences. Vorticity transport has a slightly different form in the convective terms,

$$\frac{\partial u\omega}{\partial r} + \frac{\partial v\omega}{\partial z} ,$$

which amounts to deletion of $r_{j-1/2}$, $r_{j+1/2}$ and r_p in the first two terms of Equation (A-20).

APPENDIX B

FINITE-DIFFERENCES FOR IRREGULAR NODE SPACING

A.1 General

Consider the irregular grid shown in Figure B-1 below.

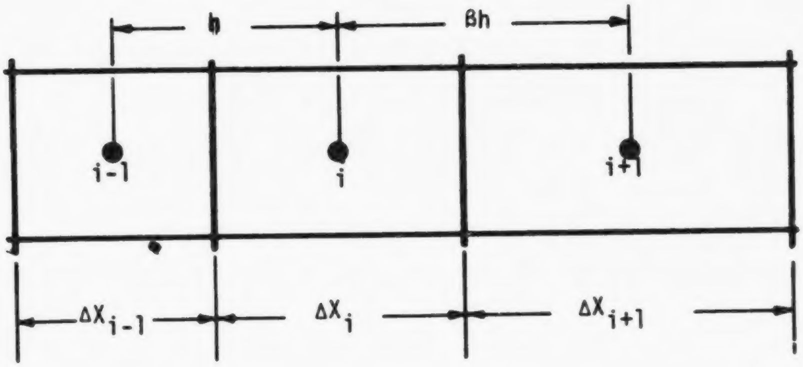

Figure B-1. Irregular Spaced Grid

The width of node i is designated ΔX_i and the nodal points are all cell centered. Finite-difference approximations for the first and second derivatives at node i are developed as follows.

Let,

$$h = \frac{1}{2}(\Delta X_{i-1} + \Delta X_i)$$

and

$$\beta h = \frac{1}{2}(\Delta X_i + \Delta X_{i+1}).$$

Then a Taylor series expansion of a function f about point i is given by the equations:

$$f_{i+1} = f_i + \beta h f_i' + \frac{\beta^2 h^2}{2} f_i'' + \frac{\beta^3 h^3}{6} f_i''' + \frac{\beta^4 h^4}{24} f_i^{IV} \ldots . \qquad \text{(B-1)}$$

and,

$$f_{i-1} = f_i - h f_i' + \frac{h^2}{2} f_i'' - \frac{h^3}{6} f_i''' + \frac{h^4}{24} f_i^{IV} \ldots . \qquad \text{(B-2)}$$

Now, divide Equation (B-1) by β and add the result to Equation (B-2) to obtain the difference approximation for the second derivative of f:

$$\left.\frac{\partial^2 f}{\partial X^2}\right|_i = \frac{2f_{i+1}}{h^2\beta(\beta+1)} + \frac{2f_{i-1}}{h^2(\beta+1)} - \frac{2f_i}{h^2\beta} + (\beta^2-1)\, Oh + Oh^2. \qquad \text{(B-3)}$$

For $\beta = 1$, Equation (B-3) reduces to the familiar central difference form:

$$\left.\frac{\partial^2 f}{\partial X^2}\right|_i = \frac{f_{i+1}+f_{i-1}-2f_i}{h^2} + Oh^2 . \qquad \text{(B-4)}$$

A finite-difference approximation for the first derivative of f at point i may be found by subtracting Equation (B-2) from (B-1), up to and including terms involving f'''. Hence,

$$\left.\frac{\partial f}{\partial X}\right|_i = \frac{f_{i+1}-f_{i-1}}{h(\beta+1)} - (\beta-1)\, Oh + Oh^2. \qquad \text{(B-5)}$$

Again with $\beta = 1$ the familiar central difference form results:

$$\left.\frac{\partial f}{\partial X}\right|_i = \frac{f_{i+1}-f_{i-1}}{2h} + Oh^2 . \qquad \text{(B-6)}$$

Equation (B-5) is a first order approximation of $\frac{\partial f}{\partial X}$. A second order method may be developed by reducing the coefficients of f_i'' to 1 in Equations (B-1) and (B-2). Equation (B-2) is then subtracted from (B-1) to obtain:

$$\left.\frac{\partial f}{\partial X}\right|_i = \frac{1}{(\beta+1)\beta h}\left[f_{i+1}-\beta^2 f_{i-1}\right] + \left[\frac{\beta-1}{\beta h}\right] f_i + \beta O h^2. \qquad \text{(B-7)}$$

Equation (B-7) collapses to (B-6) for $\beta = 1$.

A.2 Computer Application

For computer application, irregular spaced first and second derivatives difference forms are needed for both points (j,k) and (p,q) in the vertical direction (Figure B-2).

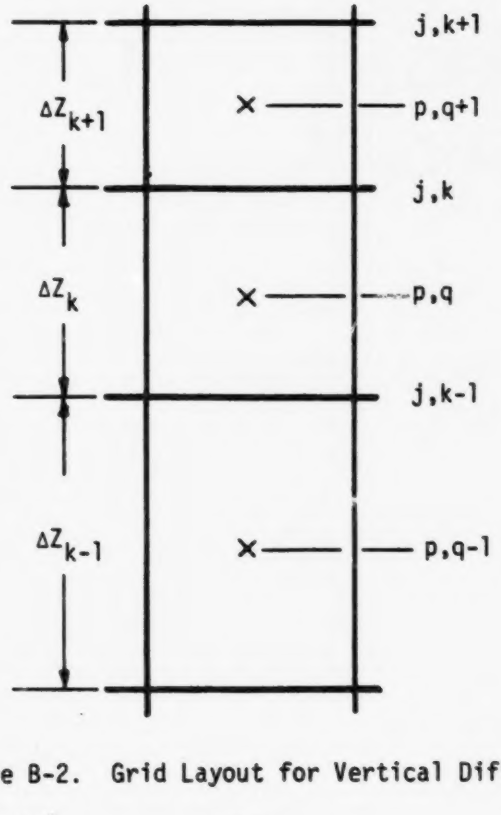

Figure B-2. Grid Layout for Vertical Differences

The following forms are used for differencing a general quantity, F(the subscripts p and j have been suppressed).

Point (j,k)

First derivative of F:

$$\left.\frac{\partial F}{\partial Z}\right|_k = \frac{\Delta Z_k \; F_{k+1}}{\Delta Z_{k+1}(\Delta Z_k+\Delta Z_{k+1})} - \frac{\Delta Z_{k+1} F_{k-1}}{\Delta Z_k(\Delta Z_k+\Delta Z_{k+1})} - \left(\frac{\Delta Z_k-\Delta Z_{k+1}}{\Delta Z_{k+1}\Delta Z_k}\right)F \tag{B-8}$$

Second derivative of F:

$$\left.\frac{\partial^2 F}{\partial Z^2}\right|_k = \frac{F_{k+1}-F_k}{\frac{1}{2}\,\Delta Z_{k+1}(\Delta Z_{k+1}+\Delta Z_k)} - \frac{F_k-F_{k-1}}{\frac{1}{2}\,\Delta Z_k(\Delta Z_{k+1}+\Delta Z_k)} \; . \tag{B-9}$$

Point (p,q)

First derivative of F:

$$\left.\frac{\partial F}{\partial Z}\right|_q = \frac{F_{q+1}}{\Delta Z_{k+1}+\Delta Z_k} - \frac{F_{q-1}}{\Delta Z_{k-1}+\Delta Z_k} - \left[\frac{\Delta Z_{k-1}}{\Delta Z_k+\Delta Z_{k-1}} - \frac{\Delta Z_{k+1}}{\Delta Z_k+\Delta Z_{k+1}}\right]F_q \tag{B-10}$$

Second derivative of F:

$$\left.\frac{\partial^2 F}{\partial Z^2}\right|_q = \frac{F_{q+1}-F_q}{\frac{1}{2}\,\Delta Z_k(\Delta Z_{k+1}+\Delta Z_k)} - \frac{F_q-F_{q-1}}{\frac{1}{2}\,\Delta Z_k(\Delta Z_k+\Delta Z_{k-1})} \; . \tag{B-11}$$

APPENDIX C

COORDINATE TRANSFORMATION

The required partial differential equations are given in Chapter 5 by Equations (5.10) through (5.14) and are restated here for reference.

Stream Function:

$$\frac{\partial^2 \Psi}{\partial R^2} - \frac{1}{R} \frac{\partial \Psi}{\partial R} + \frac{\partial^2 \Psi}{\partial Z^2} = - R\Omega, \qquad (5.10)$$

Vorticity:

$$\frac{\partial}{\partial R} (U\Omega) + \frac{\partial}{\partial Z} (V\Omega) = - \frac{1}{2F_o} \frac{\partial \Delta_1}{\partial R}$$

$$+ \frac{1}{RE_r} \cdot \frac{\partial^2 \Omega}{\partial R^2} + \frac{1}{R} \frac{\partial \Omega}{\partial R} - \frac{\Omega}{R^2} + \frac{1}{RE_z} \cdot \frac{\partial^2 \Omega}{\partial Z^2}, \qquad (5.11)$$

Buoyancy Parameter:

$$\frac{1}{R} \frac{\partial}{\partial R} (RU\Delta_1) + \frac{\partial}{\partial Z} (V\Delta_1)$$

$$= \frac{1}{RE_r PR_z} \cdot \frac{\partial^2 \Delta_1}{\partial R^2} + \frac{1}{R} \frac{\partial \Delta_1}{\partial R} + \frac{1}{RE_z PR_z} \cdot \frac{\partial^2 \Delta_1}{\partial Z^2}, \qquad (5.12)$$

along with

$$U = - \frac{1}{R} \frac{\partial \Psi}{\partial Z}, \qquad (5.13)$$

and

$$V = \frac{1}{R} \frac{\partial \Psi}{\partial R}. \qquad (5.14)$$

These same expressions are given in transformed coordinates by Equations (5.16) through (5.20), respectively. The transformation to ξ coordinates by setting

$$R = \sinh \xi \qquad \text{(C-1)}$$

has the desirable properties mentioned in Section 5.5. Details of the transformation are given in the following discussion.

Consider a quantity F and first and second derivatives of this quantity in R coordinates. The general transformation of these derivatives to ξ coordinates is derived as follows:

$$\frac{dF}{dR} = \frac{dF}{d\xi} \cdot \frac{d\xi}{dR} = G \cdot \qquad \text{(C-2)}$$

Then

$$\frac{d^2F}{dR^2} = \frac{dG}{dR} = \frac{dG}{d\xi} \cdot \frac{d\xi}{dR} = \frac{d}{d\xi}\left[\frac{dF}{d\xi} \cdot \frac{d\xi}{dR}\right] \cdot \frac{d\xi}{dR},$$

or

$$\frac{d^2F}{dF^2} = \left(\frac{d\xi}{dR}\right)^2 \frac{d^2F}{d\xi^2} + \left(\frac{dF}{d\xi}\right)\left(\frac{d\xi}{dR}\right) \frac{d}{d\xi}\left(\frac{d\xi}{dR}\right)$$

Now,

$$\frac{d}{d\xi}\left(\frac{d\xi}{dR}\right) = \frac{dH}{d\xi} = \frac{dH}{dR} \cdot \frac{dR}{d\xi}$$

$$= \frac{dR}{d\xi} \cdot \frac{d^2\xi}{dR^2}.$$

Hence,

$$\frac{d^2F}{dR^2} = \left(\frac{d\xi}{dR}\right)^2 \cdot \frac{d^2F}{d\xi^2} + \left(\frac{d^2\xi}{dR^2}\right) \cdot \frac{dF}{d\xi}. \qquad \text{(C-3)}$$

From Equation (C-1),

$$\frac{d\xi}{dR} = \frac{1}{\cosh \xi} \qquad \text{(C-4)}$$

and

$$\frac{d^2\xi}{dR^2} = \left(\frac{\partial\xi}{\partial R}\right) \frac{\partial}{\partial\xi} \left(\frac{\partial\xi}{\partial R}\right) = - \frac{\tanh \xi}{\cosh^2 \xi} . \qquad \text{(C-5)}$$

Then,

$$\frac{dF}{dR} = \operatorname{sech} \xi \frac{dF}{d\xi} \qquad \text{(C-6)}$$

and

$$\frac{d^2F}{dR^2} = \operatorname{sech}^2 \xi \left(\frac{d^2F}{d\xi^2} - \tanh \xi \frac{\partial F}{\partial \xi}\right) . \qquad \text{(C-7)}$$

Substitution of Equations (C-1),(C-6) and (C-7) into Equations (5.10) through (5.14) yields the transformed set (5.16) through (5.20).

One discomforting feature of non-linear transformations is that small errors are introduced in calculating areas and distances in the transformed coordinates. For instance the distance ΔR in real coordinates is given by

$$\Delta R_A = \sinh (\xi + \Delta\xi) - \sinh (\xi) .$$

In the difference computation,

$$\Delta R_C = \cosh \left(\xi + \frac{\Delta\xi}{2}\right) \Delta\xi .$$

Taking the ratio of these two expression yields, after manipulation of identities:

$$\frac{R_A}{R_C} = \frac{\text{Actual spacing}}{\text{Computed spacing}} = \frac{2}{\Delta\xi} \operatorname{Sinh} \left(\frac{\Delta\xi}{2} \right) . \qquad \text{(C-8)}$$

As Figure C-1 indicates, $\Delta\xi$ should be kept as small as possible.

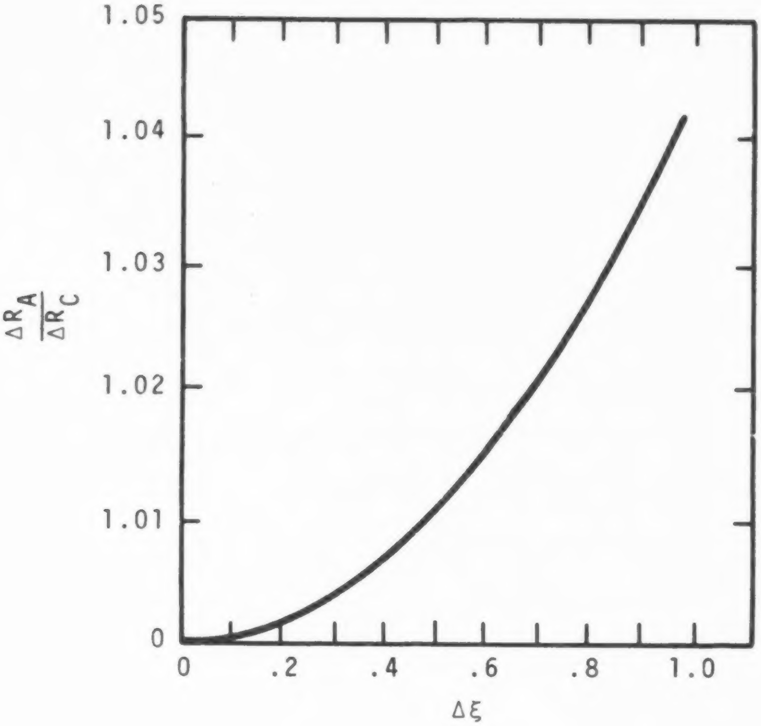

Figure C-1. Ratio of Actual to Computed Node Spacing

APPENDIX D

SOME RELATIONSHIPS BETWEEN TIME DEPENDENT AND STEADY STATE NUMERICAL METHODS IN HEAT TRANSFER AND FLUID FLOW

The general transport equation for a conservative quantity, T, is written in tensor form as:

$$\frac{\partial T}{\partial t} + \frac{\partial U_j T}{\partial x_j} = \frac{\partial}{\partial x_j} \left(a_{\underline{j}} \frac{\partial T}{\partial x_j}\right), \tag{D-1}$$

where the summation convention does not extend over the underscored indices and source and sink terms are negligible. The symbols in the above equations are:

t = time

x_j = jth spatial coordinate

U_j = jth velocity component

a_j = diffusion coefficient along the jth coordinate

For simplicity in this discussion, we will ignore the convective terms, consider a as a constant, and write Equation (D-1) as

$$\frac{\partial T}{\partial t} = a \left(\frac{\partial^2 T}{\partial x_j \, \partial x_j}\right) . \tag{D-2}$$

For steady flow,

$$\frac{\partial^2 T}{\partial x_j \, \partial x_j} = 0. \tag{D-3}$$

The usual technique for solving the above equation is either by Gauss-Seidel or Gauss iteration, where the former is much faster than the latter and, consequently, the most popular technique. In both cases successive over-relaxation (SOR, extrapolated Liebmann method) is employed.

It is the task here to illustrate that certain methods for solving Equations (D-2) and (D-3) above are identical up to the Liebmann extrapolation factor, L, in the steady state technique and the time scale factor, α, in certain time dependent methods.

D.1 Correspondence Between the Classical Explicit and Gauss Methods

The classical explicit and most common method for solving Equation (D-2) is given in difference form for an evenly spaced grid as follows:

$$T_{jk}^{n+1} - T_{jk}^{n} = \alpha \{T_{j-1k}^{n} + T_{j+1k}^{n} + T_{jk-1}^{n} + T_{jk+1}^{n} - 4\, T_{jk}^{n}\}, \quad \text{(D-4)}$$

where $\alpha = \frac{a\Delta t}{\Delta x^2}$.

The superscript n denotes the nth time step. One may rearrange Equation (D-4) to give

$$T_{jk}^{n+1} = \alpha \{T_{j-1k}^{n} + T_{j+1k}^{n} + T_{jk-1}^{n} + T_{jk+1}^{n}\} + (1-4\,\alpha)\, T_{jk}^{n} . \quad \text{(D-5)}$$

Equation (D-5) may be further simplified by letting

$$4T_{jk}^{*n} = T_{j-1k}^{n} + T_{j+1k}^{n} + T_{jk+1}^{n} + T_{jk-1}^{n}$$

So that

$$T_{jk}^{n+1} = 4\,\alpha\, T_{jk}^{*n} + (1-4\,\alpha)\, T_{jk}^{n} . \quad \text{(D-6)}$$

An algorithm for Gauss iteration of Equation (D-3) may be written as

$$T_{jk}^{s+1} = L\ T_{jk}^{*s} + (1-L)\ T_{jk}^{s}, \qquad \text{(D-7)}$$

where s denotes the sth iteration and L is again the Liebmann extrapolation (or SOR) factor. We note that Equations (D-6) and (D-7) are identical insofar as

$$L = 4\,\alpha. \qquad \text{(D-8)}$$

In Equation (D-7), L is greater than 1, but must be less than 2 to prevent solution divergence; that is, for over-relaxation

$$1 \leq L \leq 2.$$

Hence, as a maximum value

$$\frac{4\ a\Delta t}{\Delta x^2} \leq 2, \qquad \frac{a\Delta t}{\Delta x^2} \leq 1/2.$$

which is exactly the explicit method stability criterion.

D.2 Correspondence Between ADEP Transient Methods and the Gauss-Seidel Technique

Alternating direction explicit procedures (ADEP) are relative newcomers to the field of applied numerical analysis. The prototype ADEP was conceived by the Russian mathematician, Saul 'ev, in 1957. Since then other methods have been presented such as those proposed by Larkin [53] and Barakat [9]. These methods, which have been demonstrated to have good accuracy and incredible stability, have basic algorithms identical to the Gauss-Seidel method with SOR.

A. Saul 'ev Method

The Saul 'ev method consists of alternate directional sweeping of the grid system. A forward sweep is written as

$$T^{n+1}_{jk} - T^{n}_{jk} = \alpha \{T^{n+1}_{j-1k} + T^{n+1}_{jk-1} + T^{n}_{j+1\ k} + T^{n}_{jk+1} - 2\ T^{n}_{jk} - 2\ T^{n+1}_{jk}\}. \tag{D-9}$$

Note that there is equal weighting on the n and n+1 time levels. Rearranging Equation (D-9) into the context of Gauss-Seidel iteration with SOR yields

$$(1 + 2\ \alpha)\ T^{n+1}_{jk} = 4\ \alpha\ T^{*n+1}_{jk} + (1-2\ \alpha)\ T^{n}_{jk}$$

where, $$4\ T_{jk}^{*n+1} = T^{n+1}_{j-1k} + T^{n+1}_{jk-1} + T^{n}_{j+1k} + T^{n}_{jk+1}.$$

Hence, $$T^{n+1}_{jk} = \left(\frac{4\ \alpha}{1+2\alpha}\right) T^{*n+1}_{jk} + \left(\frac{1-2\ \alpha}{1+2\ \alpha}\right) T^{n}_{jk}. \tag{D-10}$$

Comparing Equation (D-10) to the Gauss-Seidel algorithm,

$$T^{s+1}_{jk} = L\, T^{*s+1}_{jk} + (1-L)\ T^{s}_{jk}, \tag{D-11}$$

again shows equivalence insofar as

$$L = \frac{4\alpha}{1+2\alpha} \leq 2, \tag{D-12}$$

or

$$L = \frac{4}{2+\frac{1}{\alpha}} \leq 2.$$

Now $$\lim_{\alpha \to \infty} \frac{4}{2+\frac{1}{\alpha}} \to 2;$$

hence, the upper limit of the Liebmann extrapolation constant is satisfied from the standpoint of stability irregardless of the size of the time step, Δt. For $\alpha = .5$,

$$T_{jk}^{n+1} = T_{jk}^{*n+1}$$

which is identical to the Gauss-Seidel method without SOR. For the Saul 'ev method, the next time level computation involves a similar backward sweep.

B. Larkin's ADEP

Larkin's ADEP is actually one of several methods discussed by Larkin in the cited reference. The method here is very similar in the mechanics to the prototype Saul 'ev ADEP, except that the forward and backward sweeps are averaged to form a time level. Larkin's methods yield the same relationship between L and α given in Equation (D-12).

D.3 Further Comparisons Between Larkin's ADEP And The Gauss-Seidel Iterative Technique

Consider the two-dimensional form of Equation (D-1),

$$\frac{\partial T}{\partial t} + \frac{\partial UT}{\partial X} + \frac{\partial VT}{\partial Y} = a\left(\frac{\partial^2 T}{\partial X^2} + \frac{\partial^2 T}{\partial Y^2}\right). \qquad \text{(D-13)}$$

Based on upstream differencing of the convective terms, the forward sweep ADEP finite-difference equation would be,

$$\begin{aligned}
\frac{T_{jk}^{n+1} - T_{jk}^{n}}{\Delta t} &+ \frac{1}{2\Delta X}\left\{\left(|U_{jk}| + U_{jk}\right) T_{jk}^{n+1} - \left(|U_{j-1k}| + U_{j-1k}\right) T_{j-1k}^{n+1}\right. \\
&\qquad \left. + \left(|U_{j-1k}| - U_{j-1k}\right) T_{jk}^{n+1} - \left(|U_{jk}| - U_{jk}\right) T_{j+1k}^{n}\right\} \\
&+ \frac{1}{2\Delta Y}\left\{\left(|V_{jk}| + V_{jk}\right) T_{jk}^{n+1} - \left(|V_{jk-1}| + V_{jk-1}\right) T_{jk-1}^{n+1}\right. \\
&\qquad \left. + \left(|V_{jk-1}| - V_{jk-1}\right) T_{jk}^{n+1} - \left(|V_{jk}| - V_{jk}\right) T_{jk+1}^{n}\right\} \\
&= a\left\{\frac{T_{j-1k}^{n+1} + T_{j+1k}^{n} - T_{jk}^{n} - T_{jk}^{n+1}}{\Delta X^2} + \frac{T_{jk-1}^{n+1} + T_{jk+1}^{n} - T_{jk}^{n} - T_{jk}^{n+1}}{\Delta Y^2}\right\}. \qquad \text{(D-14)}
\end{aligned}$$

Figure D-1 illustrates a finite-difference cell and the relative locations of the quantities T, U, and V.

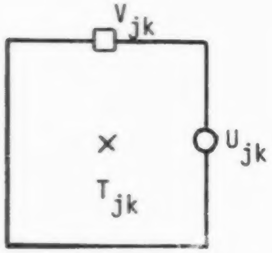

Figure D-1. Finite-Difference Cell

Note that in Equation (D-14) if velocity is negative T_{ij} is evaluated at n, whereas for positive velocity T_{ij} is evaluated at n+1. The backward sweep would use the opposite sense. Also, this convention is not a necessity and other time level evaluation schemes may be used as long as they are computationally explicit.

Solving for T_{jk}^{n+1} yields

$$
\begin{aligned}
&\left\{1 + \frac{\Delta t}{2\Delta X}\left(|U_{jk}| + U_{jk} + |U_{j-1k}| - U_{j-1k}\right)\right. \\
&\qquad \left. + \frac{\Delta t}{2\Delta Y}\left(|V_{jk}| + V_{jk} + |V_{jk-1}| - V_{jk-1}\right) + \frac{a\Delta t}{\Delta X^2} + \frac{a\Delta t}{\Delta Y^2}\right\} T_{jk}^{n+1} \\
&\quad = \left\{\frac{\Delta t}{2\Delta X}\left(|U_{j-1k}| + U_{j-1k}\right) + \frac{a\Delta t}{\Delta X^2}\right\} T_{j-1k}^{n+1} \\
&\quad + \left\{\frac{\Delta t}{2\Delta X}\left(|U_{jk}| - U_{jk}\right) + \frac{a\Delta t}{\Delta X^2}\right\} T_{j+1k}^{n} \\
&\quad + \left\{\frac{\Delta t}{2\Delta Y}\left(|V_{jk-1}| + V_{jk-1}\right) + \frac{a\Delta t}{\Delta Y^2}\right\} T_{jk-1}^{n+1} \\
&\quad + \left\{\frac{\Delta t}{2\Delta Y}\left(|V_{jk}| - V_{jk}\right) + \frac{a\Delta t}{\Delta Y^2}\right\} T_{jk+1}^{n} \\
&\quad + \left\{1 - a\,\Delta t\left[\frac{1}{\Delta X^2} + \frac{1}{\Delta Y^2}\right]\right\} T_{jk}^{n} \qquad \text{(D-15)}
\end{aligned}
$$

For a short hand notation let:

$$C_{jk} = \frac{1}{2\Delta X}\left\{|U_{jk}| + U_{jk} + |U_{j-1k}| - U_{j-1k}\right\}$$

$$+ \frac{1}{2\Delta Y}\left\{|V_{jk}| + V_{jk} + |V_{jk-1}| - V_{jk-1}\right\}$$

$$D_{jk} = a\left\{\frac{1}{\Delta X^2} + \frac{1}{\Delta Y^2}\right\} .$$

Then,

$$\begin{aligned}\left\{1 + \left(C_{jk} + D_{jk}\right)\Delta t\right\} T_{jk}^{n+1} &= \left\{\frac{1}{2\Delta X}\left(|U_{j-1k}| + U_{j-1k}\right) + \frac{a}{\Delta X^2}\right\}\Delta t\ T_{j-1k}^{n+1} \\ &+ \left\{\frac{1}{2\Delta X}\left(|U_{jk}| - U_{jk}\right) + \frac{a}{\Delta X^2}\right\}\Delta t\ T_{j+1k}^{n} \\ &+ \left\{\frac{1}{2\Delta Y}\left(|V_{jk-1}| + V_{jk-1}\right) + \frac{a}{\Delta Y^2}\right\}\Delta t\ T_{jk-1}^{n+1} \\ &+ \left\{\frac{1}{2\Delta Y}\left(|V_{jk}| - V_{jk}\right) + \frac{a}{\Delta Y^2}\right\}\Delta t\ T_{jk+1}^{n} \\ &+ \left(1 - D_{jk}\,\Delta t\right) T_{jk}^{n} \qquad \text{(D-16)}\end{aligned}$$

The Gauss-Seidel scheme yields

$$\left(C_{jk} + 2D_{jk}\right) T^{*s+1}_{jk} = \left\{\frac{1}{2\Delta X}\left(|U_{j-1k}| + U_{j-1k}\right) + \frac{a}{\Delta X^2}\right\} T^{s+1}_{j-1k}$$

$$+ \left\{\frac{1}{2\Delta X}\left(|U_{jk}| - U_{jk}\right) + \frac{a}{\Delta X^2}\right\} T^{s}_{j+1k}$$

$$+ \left\{\frac{1}{2\Delta Y}\left(|V_{jk-1}| - V_{jk-1}\right) + \frac{a}{\Delta Y^2}\right\} T^{s+1}_{jk-1}$$

$$+ \left\{\frac{1}{2\Delta Y}\left(|V_{jk}| - V_{jk}\right) + \frac{a}{\Delta Y^2}\right\} T^{s}_{jk+1} \; . \qquad \text{(D-17)}$$

Substituting Equation (D-17) into (D-16) yields,

$$\left[1 + \left(C_{jk} + D_{jk}\right) \Delta t\right] T^{n+1}_{jk} = \left(C_{jk} + 2D_{jk}\right) \Delta t \; T^{*s+1} + \left(1 - D_{jk}\Delta t\right) T^{n}_{jk}$$

(D-18)

or in terms of iterations s,

$$T^{s+1}_{jk} = \left\{\frac{(C_{jk} + 2D_{jk})\Delta t}{1 + (C_{jk}+D_{jk})\Delta t}\right\} T^{*s+1}_{jk} + \left\{\frac{(1-D_{jk}\Delta t)}{1+(C_{jk}+D_{jk})\Delta t}\right\} T^{s}_{jk} \; . \qquad \text{(D-19)}$$

Comparing to

$$T^{s+1}_{jk} = L \, T^{*s+1}_{jk} + (1-L) \, T^{s}_{jk}$$

Yields

$$L = \frac{(C_{jk} + 2D_{jk})\Delta t}{1+(C_{jk}+D_{jk})\Delta t} \qquad \text{(D-20)}$$

Thus,

$$\lim_{\Delta t \to \infty} \frac{C_{jk} + 2D_{jk}}{\frac{1}{\Delta t} + C_{jk} + D_{jk}} = \frac{C_{jk} + 2D_{jk}}{C_{jk} + D_{jk}} \quad . \tag{D-21}$$

The condition

$$\frac{C_{jk} + 2D_{jk}}{\frac{1}{\Delta t} + C_{jk} + D_{jk}} \leq \delta$$

leads to some restrictions on the over-relaxation factor L.

For the case where convection effects are very small, characteristic of a creeping flow,

$$\frac{2D_{jk}}{\frac{1}{\Delta t} + D_{jk}} \leq \delta \tag{D-22}$$

The question is what values of δ are possible in Equation (D-22).

For $\Delta t \to \infty$, $\delta = 2$ and for $\Delta t \to 0, \delta = 0$.

$\therefore \quad 0 \leq L \leq 2.$

For very high Reynolds number flow, viscous effects become relatively small and

$$\frac{C_{jk}}{\frac{1}{\Delta t} + C_{jk}} \leq \delta$$

for $\Delta t \to \infty$, $\delta \to 1$ and for

$\Delta t = 0$, $\delta = 0$; hence,

$0 \leq L \leq 1$

This preceding analysis indicates that it is impossible to accelerate the Gauss-Seidel technique for flows where viscous effects are negligible. In the general case there will be regions in the flow field where the local Reynolds number will be such that $D_{jk} \simeq 0$. If the condition $0 \leq L \leq 1$ is violated, then an instability will propagate from this local point.

APPENDIX E

LISTING OF SYMJET COMPUTER CODE - UNIVAC 1108 VERSION

```
C*    FOLLOWING ARE THE PROGRAM PARAMETERS AND DIMENSIONS.
C*
COMLST*  FCOPY
       PARAMETER  LJ=42,LK=42
       COMMON     OMEG(LJ,LK),PSI(LJ,LK),DFLT(LJ,LK),UX(LJ,LK),UZ(LJ,LK),
     1            GAM(LJ,LK),SC(LJ,15),R(LJ),X(LJ),RC(LJ),TEMPER(LJ,LK),
     2            RSEA(LK),SZ(LK,20),Z(LK),DZ(LK),FR(LJ,LK),FZ(LJ,LK),
     3            DGRAD(LJ,LK),UGRAD(LJ,LK),PICH(LJ,LK),RB(LK),
     4            R05(LK),TEM(10),XR(LJ),ZC(LK),ISOLN(5,30),N3DPT(5),
     5            DATE(2),TIM(2),TLABEL(12),CONTRL(17)
       COMMON     NOX(LJ),NRITE(15),NODE(6),MON(30),ISOPT(5)
       COMMON     DX,DX2,R0,V0,RER,RFZ,F0,SIGTR,DELTJ,DSIGT,ZB,RRP,
     1            DPMAX,DOMAX,DUMAX,DZC,EZ,SIGTS,VMB,DMB,SIGTB,ZRP,
     2            G,GMB,SALR,SALJ,DSALT,RMIN,EXR,EXS,EXT,BETA,AK1,
     3            SIGTJ,TINT,START,RATIO,GAMEND,ERATIO,VMB1,PLX
       COMMON     NJ,NJJ,NH,NL,NOUT,NPI,IN,OUT,IPMAX,KASE,KT,INMODE,
     1            ITMAX,ITNO,NB,NTTY,NK,NKK,NCR,NPT,NMAD,NX,DZT5,T0,TR,
     2            ITEMP,NED,NEDDY,NOTEMP,JPORT,KPORT,ITNOO,
      REAL        ISOLN
      INTEGER     CUT
      LOGICAL     CONTRL
      END

APDIM*    FCOPY
      PARAMETER  LJ=42,LK=42
      END
C*
C     **********************************************************************
```

```
C      UNIVAC 1108 VERSION
C      *************,**************,*******,*****************************
C*     THIS VERSION OF THE SYMJET PROGRAM HAS BEEN CHECKED-OUT FOR THE
C*     FOLLOWING OPTIONS:
C*
C*         1)    AOUT, OPTION (OUTPUT ARRAYS)
C*                     PSIP,,PSIV,,DELT,,OMEG,,VELV,,VELR,,GAMA,,TEMP,,
C*                     RFAC,,VFAC,,RICH,
C*         2)    PLOT, OPTION(CREATES PLOT ARRAYS FOR SUBSEQUENT
C*                            CONTOURING AND 3-D PLOTS)
C*                     ALL OPTIONS WORK
C*         3)    TERP, OPTION (CALCULATES UNORDERED CONTOUR VALUES)
C*                     ALL OPTIONS WORKED CORRECTLY ON PREVIOUS VERSION,
C*                     BUT HAVE NOT BEEN CHECKED FOR THIS VERSION.
C*         4)    CONT, OPTION (PROGRAM CONTROL)
C*                     BUOY,,TRAN,,TEMP,,MONT,,TAPE,,SAVE,,INVS,,TURB,,
C*                     CENO,,CENI,
C*
C*
C*         INMODE     = 4

C*
C**** NOTE ****
C*
C*     THIS CODE VERSION HAS BEEN DEBUGGED FOR OPTION INMODE = 4 ONLY
C*     WHICH TREATS SHALLOW WATER PLUMES WITH POWER LAW INFLOW VELOCITY
C*     PROFILE.  SOME CHANGES HAVE BEEN MADE ON THE LATERAL DIFFUSIVITY
C*     MODEL SINCE RUNNING OF CASE 66, HENCE RESULTS WILL NOT CHECK
C*     PRECISELY.
C*
C*      SYSTEMS ROUTINES USED BY CODE.
C*
C*               TOY   (F)
C*               DOY   (F)
C*               ETIME (F)
```

```
C*              ETIMEF(F),
C*
C*         WHERE F IS A REAL VARIABLE.
C*         THESE ROUTINES ABOVE MAY BE DUMMIED.
C*      THE FOLLOWING SUBROUTINE MAY BE DUMMIED IF ONLY
C*      THE   OPTION INMODE = 4 IS USED.
C*
C*              GAUSS (LIST)
C*              SIMJET(LIST)
C*              FR     (LIST)
C*              FZ     (LIST)
C*
C
C      ******** PARTIAL LIST OF PROGRAM VARIABLES  ********
C
C      DELT(J,K)  BUOYANCY PARAMETER
C      GAM(J,K)   CONSERVATIVE CONSTITUENT CONCENRATION
C      OMEG(J,K)  VORTICITY
C      PSI(J,K)   STREAM FUNCTION
C      SC(J,M)    RADIAL PROGRAMMING CONSTANTS
C      SZ(L,K)    VERTICAL PROGRAMMING CONSTANTS
C      UX  (J,K)  DIMENSIONLESS VELOCITY AT POINT (X,Z), X-COMPONENT
C      UZ  (J,K)  DIMENSIONLESS VELOCITY AT POINT (X,Z), Z-COMPONENT
C      FR(J,K)    RADIAL EDDY MULTIPLICATION FACTORS-
C                    WHEN NEDDY=0 ,FR(K)=1.178
C                    WHEN NEDDY=1 ,FR(K)=R.5*VMAX,WITH R.5 SPECIFIED
C                    WHEN NEDDY=2 ,FR(K)=R.5*VMAX,WITH R.5 CALC DURING
C                                                EXECUTION OF PROGRAM
C      FZ(J,K)    VERTICAL EDDY MULTIPLICATION FACTORS
C      R(J)       RADIAL DISTANCE TO OUTER CELL SIDE J,K
C      R (J)      RADIAL DISTANCE TO CENTER CELL J,K
C      RSEA(K)    DENSITY STRATIFICATION OF AMBIENT(SIGMA UNITS)
C      X(J)       TRANSFORMED RADIAL DIMENSION TO NODAL POINT

C      DELTJ      DENSITY DIFFERENCE BETWEEN PLUME AT PORT AND REF.AMBIENT
C      DMB        CENTERLINE VALUE OF DELTA AT Z=Z3
```

```
C     DSIGT      VERTICAL DENSITY CHANGE OVER DZ IF CONSTANT(SIGMA UNITS
C     DZ         VERTICAL NODE THICKNESS IF CONSTANT,DELTAZ/DIA
C     DX         WIDTH OF NODE, X-DIRECTION
C     DX2        DX*DX
C     DZ         WIDTH OF NODE, Z-DIRECTION
C     DZ2        DZ*DZ
C     DIAC       DIAMETER OF OUTFALL PORT
C     EZ         VERTICAL EDDY TRANSPORT COEFFICIENT
C     FO         DENSIMETRIC FROUDE NUMBER AT OUTFALL PORT
C     G          LINEAR STRATIFICATION PARAMETER+ SIMILARITY SOLUTION
C     GMB        CENTERLINE GAMMA (GAMM/GAMO) AT Z = ZB
C     R.5        RADIAL DISTANCE TO HALF VELOCITY (MIXING LENGTH APPROX)
C     REK        RADIAL REFERENCE TURBULENT REYNOLDS NUMBER
C     REZ        VERTICAL REFERENCE TURBULENT REYNOLDS NUMBER
C     RRP        RADIAL REFERENCE PRANDTL NUMBER
C     RO         RADIUS OF OUTFALL PORT
C     SALJ       SALINITY OF PLUME AT OUTFALL PORT
C     SALR       SALINITY OF REFERENCE AMBIENT (ASSUMED CONTSTANT WITH Z
C     DSALT      SALR-SALJ
C     SIGTJ      DENSITY OF PLUME AT OUTFALL(SIGMA UNITS)
C     SIGTR      DENSITY OF REFERENCE AMBIENT(SIGMA UNITS)
C     SIGTB      DENS. OF REF. AMBIENT AT Z = ZB (SIGMA UNITS)
C     TLABEL(J)ALPHANUMERIC CASE HEADER ARRAY
C     TLIST(J) ALPHANUMERIC DATA INPUT FOR CERTAIN CONTROLS AS FOLLOWS:
C                 TLIST = AOUT,  SET UP ARRAY WRITER WITH OLIST(I)
C                                OPTIONS.
C                 TLIST = TERP,  INTERPOLATE ARRAYS GIVEN BY ELIST(I)
C                                FINDS ISOLINES OF VALUE ISOLN(K,N) FOR
C                                ARRAY MATCHING ELIST(I), BUT DOES NOT
C                                ORDER CONTOUR POINT(MUST BE HAND PLOT)
C                 TLIST = PLOT:  WRITE TO LUN 8 (MAG TAPE) ARRAYS MATCH-
C                                ING ELIST(I). THIS DATA TO BE SAVED
C                                FOR POSSIBLE FUTURE PLOTTING USING
C                                SPECIAL CONTOUR AND 3-D PLOTTING ROUT-
C                                INES.
```

```
C                    TLIST = CONT,  SET UP PROGRAM LOGICAL CONTROL FROM
C                                   DIRECT(I) DATA.
C
C       VO           CENTERLINE VELOCITY THERMAL PLUME AT SYSTEM IN-BOUNDARY
C       VMB          CENTERLINE VELOCITY (VM/V0) AT Z=ZB
C       ZB           ELEVATION TO GRID BOTTOM PHYSICAL BOUNDARY,Z/DIA
C       ZRP          VERTICAL REFERENCE PRANDTL NUMBER
C
C       IPMAX        MAXIMUM NUMBER OF ITERATIONS FOR PSI ITERATION
C       INMODE       INFLOW BOUNDARY INPUT DATA MODE +
C                        INMODE=0 , INPUT FROM DATA
C                        INMODE=1 , GAUSSIAN-FLOW ESTABLISHMENT ZONE
C                        INMODE=2 , GAUSSIAN-ESTABLISHMENT
C                        INMODE=3 , INPUT CALCULATED FROM SIMILARITY SOLUTION
C                        INMODE=4 , INFLOW DATA AT PORT ORIFICE
C       ITMAX        TOTAL NUMBER OF ITERATIONS
C       ITAPE        SIGNAL FOR CONTINUED ITERATION OF OLD CASE+
C                        ITAPE=0 , NEW CASE
C                        ITAPE=1 , CONTINUE ITERATIONS OF OLD CASE
C       ITEMP        SIGNAL FOR DENSITY OR TEMPERATURE INPUT
C                        ITEMP = 0, SIGMA-T INPUT
C                        ITEMP = 1, TEMPERATURE INPUT
C       KASE         CASE NUMBER
C       KT           SIGNAL FOR TRANSFORM OF LINEAR RADIAL COORDINATES+
C                        KT    = 0, LINEAR RADIAL COORDINATES
C                        KT    = 1, TRANSFORMED ACCORDING TO R=SANH(X)
C       NEDDY        SIGNAL FOR TYPE OF RADIAL EDDY TRANSPORT COEFF CALCULAT
C                        NEDDY=0 , ER = CONSTANT
C                        NEDDY=1 , ER = E0*R.5*VMAX,PRIOR SPECIFICATION OF R.
C                        NEDDY=2 , ER = E0*R.5*VMAX,RUNNING CALCULATION OF R.
C       NED          NUMBER OF ITERATIONS PERFORMED AT ER=E0*1.178 BEFORE
C                        RUNNING MIXING LENGTH CALCULATIONS
C                        USED WHEN NEDDY = 2
C       NCR          RADIAL CONVERGEN E RANGE
C       NJ           NUMBER OF NODES, RADIAL DIRECTION
```

```
C     NJJ          NJ-1
C     NK           NUMBER OF NODES, VERTICAL DIRECTION
C     NKK          NK-1
C     NL          NJ+1
C     NH          NK+1
C     NOX(J)       NUMBERING FOR OUTPUT HEADING, SET IN MAIN PROGRAM
C     NOUT         NUMBER OF ITERATIONS FOR LINE PRINTER OUTPUT
C     NMAD        SIGNAL TO CALL RICHARDSON MODIFIER ROUTINE
C                   NMAD  = 0, DONOT CALL
C                   NMAD  = 1-6  SEE SUPROUTINE RCHMOD
C     NTTY         NUMBER OF ITERATIONS FOR CALCULATION MONITORING OUTPUT
C                     NPT =1 , CALL PLAPAK
C     NPI          NUMBER OF ITERATIONS ON STREAM FUNCTION IN MAIN COMP
C     NRITE(J)     SIGNAL TO CALL OUTPUT OF SPECIFIC DATA
C     NX          MAXIMUM VALUE OF INDEX J FOR PLOTTING
C     OLIST(J)     CHARACTER DATA INPUT SIGNAL OUTPUT ARRAYS DESIRED
C                  OPLIST(J) MATCHES IMBEDDED DATA OLIST(J)
C                  TO SET VALUE OF NRITE(J)
C                     OLIST(1) = PSIP, WRITE POTENTIAL FLOW STREAM FUNCT
C                     OLIST(2) = PSIV, WRITE VISCOUS FLOW STREM FUNCT.
C                     OLIST(3) = DELT, WRITE DENSITY DISPARITY
C                     OLIST(4) = OMEG, WRITE VORTICITY
C                     OLIST(5) = VELV, WRITE VERTICAL VELOCITY
C                     OLIST(6) = VELR, WRITE RADIAL VELOCITY
C                     OLIST(7) = GAMA, WRITE GAMMA CONSTITUENT
C                     OLIST(8) = TEMP, WRITE TEMPERATURES
C                     OLIST(9) = NDEL, WRITE NORMALIZED DENS. DISP.
C                     OLIST(10)= NVEL, WRITE NORMALIZED VERT. VELOCITY
C                     OLIST(11)= NTEM, WRITE NORMALIZED TEMPERATURE
C                     OLIST(12)= RFAC, WRITE RADIAL EDDY FACTORS
C                     OLIST(13)= VFAC, WRITE VERTICAL EDDY FACTORS
C                     OLIST(14)= RICH, WRITE RICHARDSON NUMBERS
C                     OLIST(15)= BLANK AT PRESENT
C     DIRECT(I)  LOGICAL CHARACTER DATA FOR PROGRAM CONTROL
C                 READ IN UNDER TLIST OPTION CONT..
```

```
C
C        DIRECT(1) = BUOY,:  BUOYANCY COUPLED FLOW.
C                            CONTRL(1) = .TRUE.
C                  BLANK     MOMENTUM FLOW ONLY, NO BUOYANCY
C                            CONTRL(1) = .FALSE.
C        DIRECT(2) = UNCP,:  NO BUOYANT INTERACTION, BUT BOTH
C                            TEMPERATURE AND SALINITY OR
C                            CONCENTRATION ARE COMPUTED.
C                            CONTRL(2) = .TRUE.
C        DIRECT(3) = GRAD,:  AMBIENT STRATIFICATION
C                            CONTRL(3) = .TRUE.
C                  BLANK     IF HOMOGENEOUS AMBIENT
C                            CONTRL(3) = .FALSE.
C        DIRECT(4) = TRAN,:  TRANSFORM RADIAL COORDINATE
C                            ACCORDING TO  R = SINH(XI)
C                            CONTRL(4) = .TRUE.
C                  BLANK     FOR LINEAR RADIAL COORDINATES,
C                            CONTRL(4) = .FALSE.
C        DIRECT(5) = TEMP,:  FLUID STATE INPUT DATA TO BE
C                            GIVEN IN TERMS OF TEMPERATURE
C                            (DEG. C OR F) AND SALINITY (PPT)
C                            IF TEMP, OPTION USED WITH INPUT
C                            IN DEGREES C, THEN CENT, OPTION
C                            MUST ALSO BE USED.
C                            CONTRL(5) = .TRUE.
C                  BLANK     FLUID STATE GIVEN IN TERMS OF
C                            SIGMA-T AND SALINITY.
C                            CONTRL(5) = .FALSE.
C        DIRECT(6) = MONT,: MONITOR INFORMATION TO BE PRINTED
C                            AT EACH ITERATION.
C                            CONTRL(6) = .TRUE.
C                  BLANK     DO NOT MONITOR.
C        DIRECT(7) = NPCH,:  PUNCH RESTART DATA TO CARDS
C                            CONTRL(7) = .TRUE.
C                  BLANK     DO NOT PUNCH
```

```
C              DIRECT(8) = TAPE.:  INITIALIZE ARRAYS FROM RESTART
C                                  DATA FILE OR TAPE. MUST EQUIP OR
C                                  ASSIGN LUN 7.
C                                  CONTRL(8) = .TRUE.
C                          BLANK   DO NOT READ RESTART DATA FILE
C              DIRECT(9) = SAVE.:  SAVE ARRAYS FOR RESTART FILE, OR
C                                  PLOT FILE. MUST EQUIP OR ASSIGN
C                                  CONTRL(9) = .TRUE.
C                          BLANK   DO NOT SAVE
C              DIRECT(10)= INVS.:  PERFORM INVISCID FLOW COMPUTATIO
C                                  FOR CASE INITIALIZATION
C                                  CONTRL(10)= .TRUE.
C                          BLANK   NO INVISCID COMPUTATION
C              DIRECT(11)= TURB.:  COMPUTE AMBIENT TURBULENCE AND/O
C                                  CONSIDER DERIVATIVES OF THE EDDY
C                                  TRANSPORT TERMS.
C                                  CONTRL(11)= .TRUE.
C              DIRECT(12)= CENT.:  TEMPERATURE INPUT DATA SPECIFIED
C                                  IN DEGREES CENTIGRADE.
C                                  CONTRL(12)= .TRUE.
C                          BLANK   TEMPERATURE INPUT DATA SPECIFIED
C                                  IN DEGREES FAHRENHEIT.
C              DIRECT(13)= CENO.:  TEMPERATURE OUTPUT RESULTS
C                                  SPECIFIED IN DEGREES CENTIGRADE
C                                  CONTRL(13)= .TRUE.
C                          BLANK   TEMPERATURE OUTPUT RESULTS
C                                  SPECIFIED IN DEGREES FAHRENHEIT.
C
C              UNUSED CONTRL OPTIONS : CL14.,CL15.,CL16.,CL17.,
C
C
C   IN        CARD READER  LOGICAL UNIT
C   OUT       LINE PRINTER LOGICAL UNIT
C
C
```

```
 DIMENSION  OLIST(15),DLIST(15),PLIST(5),ELIST(5),RLIST(5)
 DIMENSION  OPTION(4),DATA(15),CLIST(17),DIRECT(17)
 INCLUDE    COMLST,LIST
 DATA(DLIST(I),I=1,15)/5HPSIP,,5HPSIV,,5HDELT,,5HOMEG,,5HVELV,,
1           5HVELP,,5HGAMA,,5HTEMP,,5HNDEL,,5HNVEL,,
1           5HNTEM,,5HRFAC,,5HVFAC,,5HRICH,,5H     /
 DATA(ELIST(I),I=1,5)/5HPSIV,,5HDELT,,5HGAMA,,5HTEMP,,5HOMEG,/
 DATA(OPTION(I),I=1,4)/5HAOUT,,5HPLOT,,5HTERP,,5HCONT,/
 DATA(DIRECT(I),I=1,17)/5HBUOY,,5HUNCP,,5HGRAD,,5HTRAN,,5HTEMP,,
1           5HMONT,,5HNPCH,,5HTAPE,,5HSAVE,,5HINVS,,5HTURB,,
2           5HCENI,,5HCENO,,5HCL14,,5HCL15,,5HCL16,,5HCL17,/
 CALL ETIME
 CALL TOD(TIM)
 CALL DOY(DATE)
 OUT      = 6
 IN       = 5
 GAMEND   = .9
 EXT      = 1.6
 KPLOT    = 0
 DO   4 I = 1,11
4 CONTRL(I)= .FALSE.
5 READ(IN,1002) TLABEL
 READ(IN,1000) KASE,NJ,NK,INMODE,NPI,IPMAX,NCR,NX
 IF(NPI.EQ.0) NPI = 1
 IF(IPMAX.EQ.0) IPMAX = 100
 IF(NCR.EQ.0) NCR = NJ-1
 IF(NX.EQ.0) NX = NJ-1
 IF(KASE.EQ.0) STOP
 WRITE(OUT,1004) TLABEL,DATE,TIM
 READ(IN,1000) NOUT,NTTY,ITMAX,NEDDY,NED
6 READ(IN,1001) TLIST,DATA
 IF(TLIST.EQ.OPTION(1)) GO TO 7
 IF(TLIST.EQ.OPTION(2)) GO TO 9
 IF(TLIST.EQ.OPTION(3)) GO TO 11
 IF(TLIST.EQ.OPTION(4)) GO TO 13
```

```
   GO TO 15
 7 DO  8 I = 1,15
 8 OLIST(I) = DATA(I)
   GO TO 6
 9 DO  10 I = 1,5
10 RLIST(I) = DATA(I)
   KPLOT    = 1
   GO TO 6
11 DO  12 I = 1,5
12 PLIST(I) = DATA(I)
   GO TO 6
13 DO  14 I = 1,17
14 CLIST(I) = DATA(I)
   GO TO 6
15 NJJ       = NJ-1
   NKK       = NK-1
   NH        = NK+1
   NL        = NJ+1
   JPORT     = 1
   KPORT     = 1
   NB        = 1
   ITERS     = IPMAX
   ITNOO     = 0
   ITNO      = 0
   DO  18 M  = 1,NL
18 NOX(M)    = M
   DO  20 J  = 1,NJ
   DO  20 K  = 1,NK
   PSI(J,K)  = 1.
   DELT(J,K)= 0.
   OMEG(J,K)= 0.
   FZ(J,K)    = 1.
   FR(J,K)   = 1.178
   UX(J,K)   = 0.
   UZ(J,K)   = 0.
```

```
      RICH(J,K)= 0.
      UGRAD(J,K)= 0.
      DGRAD(J,K)= 0.
   20 CONTINUE
      DO  30 N = 1,3
      K         = (N-1)*10
      MON(K+1)  = 2
      MON(K+2)  = NK/3
      MON(K+3)  = 2
      MON(K+4)  = 2*MON(K+2)
      MON(K+5)  = 2
      MON(K+6)  = NK
      MON(K+7)  = NJ/2
      MON(K+8)  = NK
      MON(K+9)  = NJ-1
      MON(K+10)= NK
   30 CONTINUE
      DO 100 I = 1,15
      DO 100 J = 1,15
      IF(DLIST(I).EQ.OLIST(J)) NRITE(J) = I
  100 CONTINUE
      DO 105 I = 1,5
      DO 105 J = 1,5
      IF(ELIST(I).EQ.RLIST(J)) N3DPT(J) = I
      IF(ELIST(I).EQ.PLIST(J)) ISOPT(J) = I
  105 CONTINUE
      DO 107 I = 1,17
      DO 107 J = 1,17
      IF(DIRECT(I).EQ.CLIST(J)) CONTRL(I) = .TRUE.
  107 CONTINUE
      IF(KPLOT.EQ.1.AND..NOT.CONTRL(9)) GO TO 160
      KT        = 0
      ITEMP     = 0
      IF(CONTRL(4)) KT = 1
      IF(CONTRL(5)) ITEMP = 1
      CALL INPUT
      CALL READY
      CALL PLABAK
      CALL ETIMEF(START)
      WRITE(OUT,1003) START
      IF(CONTRL(10)) CALL STREAM(ITERS,0)
      EXT       = EXS
      CALL SSCOMP
      DO 110 I = 1,5
      IF(ISOPT(I).NE.0) GO TO 120
  110 CONTINUE
      GO TO 150
  120 CALL INTERP
  150 CONTINUE
      GO TO 5
  160 WRITE(OUT,1005)
      STOP
 1000 FORMAT(14I5)
 1001 FORMAT(16A5)
 1002 FORMAT(12A6)
 1003 FORMAT(////
     1 35H     $ $ $ $ $ $ $ $ $ $ $ $ $ $ $        /
     2/26H     PROGRAM SET-UP TIME = F5.2, 5H SEC /
     3/35H     $ $ $ $ $ $ $ $ $ $ $ $ $ $ $                ////)
 1004 FORMAT(///12A6,5X4A6)
 1005 FORMAT(//@      YOU CAN NOT SAVE A PLOT FILE WITHOUT ASSIGNING A SA
     *VE FILE TO LUN 86/@     EITHER DELETE PLOT FILE CALL OR EQUIP LUN
     *86/@     RUN ABORTED - - TRY AGAIN@)
      END


      SUBROUTINE INPUT
      DIMENSION  DATA(10)
      INCLUDE    COMLST,LIST
```

Reproduced from best available copy.

```
      IF(.NOT.CONTRL(8)) GO TO 10
      READ(7) ITNO,OMEG,DELT,UX,UZ,PSI,GAM
      ITNOO     = ITNO
      REWIND 7
      NR        = 0
   10 READ(IN,1000) DATA,JI,KI,NI
      NI        = NI + 1
      GO TO (100,20,30,40,60,60,60,60,70,70,70,80),NI
   20 DIA       = DATA(1)
      DX        = DATA(2)
      DZC       = DATA(3)
      ZB        = DATA(4)
      V0        = DATA(5)
      JPORT     = DATA(6)+.01
      KPORT     = DATA(7)+.01
      IF(DATA(8).EQ.0.) VMB = 1.
      IF(DATA(9).EQ.0.) DMB = 1.
      IF(DATA(10).EQ.0.) GMB = 1.
      R0        = .5*DIA
      IF(DZC.EQ.0) GO TO 10
      DO  25 K = 1,NH
   25 DZ(K)     = DZC*2.
      GO TO 10
   30 TBOT      = DATA(3)
      T0        = DATA(1)
      TR        = DATA(3)
      IF(CONTRL(12)) GO TO 32
      IF(ITEMP.EQ.0) GO TO 32
      DATA(1)   = 5./9.*(DATA(1)-32.)
      DATA(2)   = 5./9.*(DATA(2)-32.)
      DATA(3)   = 5./9.*(DATA(3)-32.)
   32 CONTINUE
      DATA(1)   = SIGMAT(DATA(6),DATA(1),ITEMP)
      DATA(2)   = SIGMAT(DATA(5) ,DATA(2),ITEMP)
      DATA(3)   = SIGMAT(DATA(5) ,DATA(3),ITEMP)
      SIGTJ    = DATA(1)
      SIGTR    = DATA(2)
      SIGTB    = DATA(3)
      DSIGT    = DATA(4)
      SALR     = DATA(5)
      SALJ     = DATA(6)
      EXS      = DATA(7)
      EXR      = DATA(8)
      IF(EXS.EQ.0.) EXS = .999
      IF(EXR.EQ.0.) EXR = .999
      DSALT    = SALR-SALJ
      DELTJ    = SIGTR-SIGTJ
      RSEA(1)  = TBOT
      IF(CONTRL(5)) GO TO 10
      TO = TEMP(SALJ,SIGTJ)
      TR = TEMP(SALR,SIGTR)
      TO = 1.8*TO+32.
      TR = 1.8*TR+32.
      GO TO 10
   40 NMAX     = DATA(1) +.01
      BETA     = DATA(2)
      PLX      = DATA(3)
      RRP      = DATA(4)
      ZRP      = DATA(5)
      EZ       = DATA(6)
      ERATIO   = DATA(7)
      IF(PLX.EQ.0.) PLX = 10.
      IF(ERATIO.EQ.0.) ERATIO = .01
      IF(EZ.EQ.0.) EZ = .1
      IF(RRP.EQ.0.) RRP = 1./.714
      IF(ZRP.EQ.0.) ZRP = 1./.714
   45 CONTINUE
      GO TO 10
   60 DO  65 I = JI,KI
      KAT      = N-JI+1
```

Reproduced from best available copy.

```
      IF(NI.EQ.5) UZ (N,1 )  = DATA(KAT)
      IF(NI.EQ.6) DELT(N,1 ) = DATA(KAT)
      IF(NI.EQ.7) RSEA(N)    = DATA(KAT)
      IF(NI.EQ.8) DZ(N)      = DATA(KAT)*2.
   65 CONTINUE
      IF(NI.EQ.5) NB = KI
      GO TO 10
   70 JI        = (NI-9)*10+1
      KI        = JI+9
      DO  75 N  = JI,KI
      KAT       = N-JI+1
      MON(N)    = DATA(KAT)+.0001
   75 CONTINUE
      GO TO 10
   80 NN        = JI-1
      DO  85 N  = 1,10
      NA        = NN+N
      ISOLN(KI,NA)= DATA(N)
   85 CONTINUE
      GO TO 10
 1000 FORMAT(10F5.0,3I5)
  100 RETURN
      END


      SUBROUTINE READY
      INCLUDE     COMLST,LIST
      NOTEMP    = 1
      IF(KPORT.EQ.0) KPORT= 1
      IF(INMODE.EQ.4.AND.CONTRL(4)) DX = .88137359/(JPORT-1)
      RER       = 39.
      REZ       = R0*V0/EZ
      Z(1)      = ZB
      ZC(1)     = Z(1)-.25*DZ(1)
```

Reproduced from best available copy.

```
      ZPORT     = 0.
      DO   5 K = 2,NH
      IF(K.LE.KPORT) ZPORT = ZPORT+.5*DZ(K)
      Z(K)      = Z(K-1)+DZ(K)*.5
      ZC(K)     = Z(K)-.25*DZ(K)
      RB(K)     = 1.5+ZC(K)-ZPORT
    5 CONTINUE
      DZTOT     = Z(NK)-ZB
      IF(INMODE.EQ.4) DZTOT = Z(NK)-ZPORT
      DZT5      = DZTOT*.5
      IF(DSIGT.EQ.0) GO TO 15
      RSEA(1)   = SIGTR
      DO  10 K = 2,NH
      RSEA(K)   = RSEA(K-1)+DSIGT*DZ(K)/(Z(NK)-ZB)*.5
   10 CONTINUE
   15 DO  20 K = 1,NH
      IF(.NOT.CONTRL(12).AND.ITEMP.NE.0) RSEA(K) = 5./9.*(RSEA(K)-32.)
      IF(.NOT.CONTRL(3)) RSEA(K) = SIGTR
      IF(CONTRL(3)) RSEA(K) = SIGMAT(SALR,RSEA(K),ITEMP)
      RSEA(K)   = RSEA(K)+1000.
   20 CONTINUE
      DX2       = DX*DX
      F0        = V0*V0/(DELTJ/(SIGTJ+1000.)*2.*P0*32.2)
      IF(DELTJ.EQ.0.) F0 =0.
      DO  50 K = 2,NH
      DELT(NL,K)= (SIGTR+1000.-(RSEA(K)+RSEA(K-1))*.5)/DELTJ
      GAM(NL,K)= 0.
      IF(.NOT.CONTRL(11)) GO TO 50
      Z1        = (Z(NK)-Z(K)+.25*DZ(K))*2.
      ED1       = (RSEA(K)-RSEA(K-1))/(RSEA(1)*R0*DZ(K)*.3048)
      IF(ED1.EQ.0.) ED1=-1.E-4
      IF(.NOT.CONTRL(3)) ED1 = -1.E-4
      ED        = -1.E-7/ED1
      FZ(1,K)   = ED/EZ
      FZ(NL,K) = FZ(1,K)
      AK1        = .5*DZTOT*SQRT(.689)/(Z(NK)-ZR)
      DO  40 J = 2,NJ
      FZ(J,K)    = EXP(-(AK1*Z1)**2)+FZ(1,K)
   40 CONTINUE
   50 CONTINUE
      IF(KPORT.LE.1.OR.CONTRL(11)) GO TO 60
      DO  55 J = 1,NL
      DO  55 K = 1,NH
      FZ(J,K) = .0001
   55 CONTINUE
   60 CONTINUE
      G          = ABS((SIGTB-SIGTR)/ZB)/DELTJ
      IF(ZB.EQ.0) G = 0.
      DZ(NH)     = DZ(NK)
C
C     SET-UP FOR Z-DIRECTION CONSTANTS
C
      DO  70 K = 2,NK
      SZ(K,1)    = 2./REZ*(1./(DZ(K+1)+DZ(K))+1./(DZ(K-1)+DZ(K)))/DZ(K)
      SZ(K,2)   = 2./REZ*(1./(DZ(K)+DZ(K-1))/DZ(K))
      SZ(K,3)   = 2./REZ*(1./(DZ(K+1)+DZ(K))/DZ(K))
      SZ(K,4)   = 1./(2.*DZ(K))
      SZ(K,5)   = SZ(K,1)*ZRP
      SZ(K,6)   = SZ(K,2)*ZRP
      SZ(K,7)   = SZ(K,3)*ZRP
      SZ(K,8) = 2./(DZ(K)*DZ(K+1))
      SZ(K,9) = 2./(DZ(K)*(DZ(K)+DZ(K+1)))
      SZ(K,10) = 2./(DZ(K+1)*(DZ(K)+DZ(K+1)))
      SZ(K,11) = SZ(K,8)/4.
      SZ(K,12) = DZ(K)/(DZ(K)+DZ(K+1))
      SZ(K,13) = SZ(K,4)/F0
      SZ(K,14) = 1./(DZ(K)+DZ(K-1))
      SZ(K,15) = 1./(DZ(K)+DZ(K+1))
      SZ(K,16) = DZ(K-1)*SZ(K,14)-DZ(K+1)*SZ(K,15)
   70 CONTINUE
```

```
C
C     SET-UP FOR R-DIRECTION CONSTANTS
C
      R(1)       = 0.
      XX         = 0.
      X(1)       = -.5*DX
      XR(1)      = 0.
      DO  80 J = 2,NL
      X(J)       = X(J-1)+DX
      IF(J.EQ.2) X(1) = 0.
      XX         = XX+DX
      XR(J)      = XX
      RC(J)      = SANH(X(J),KT)
      R(J)       = SANH(XX,KT)
      CONC       = .5*DX*(R(J)*KT/CASH(XX,KT)+CASH(XX,KT)/R(J))
      SC1        = 1./((CASH(X(J),KT)*DX)**2)/RER
      SC2        = .5*DX/(CASH(X(J),KT)*RC(J))
      SC(J,1)    = SCI*(2.+DX2*(CASH(X(J),KT)/RC(J))**2)
      SC(J,2)    = SCI*(1.-SC2)
      SC(J,3)    = SCI*(1.+SC2)
      SC(J,4)    = 1./(CASH(X(J),KT)*2.*DX)
      SC(J,6)    = 2.*RRP*SCI
      SC(J,5)    = SC(J,4)/(2.*F0)
      SC(J,7)    = SC(J,4) *R(J-1)/RC(J)
      SC(J,8)    = SC(J,4) *R(J  )/RC(J)
      SC(J,9)    = RRP*SC(J,2)
      SC(J,10)   = RRP*SC(J,3)
      SC(J,11)   = 2./((CASH(XX,KT)*DX)**2)
      SC(J,12)   = SC(J,11)*(1.+CONC)*.5
      SC(J,13)   = SC(J,11)*(1.-CONC)*.5
      SC(J,14)   = 1./(RC(J)*CASH(X(J),KT)*DX)
      IF(CONTRL(2)) SC(J,5) = 0.
      IF(.NOT.CONTRL(1)) SC(J,5)= 0.
   80 CONTINUE
      RC(1)      = -RC(2)
      DO  90 J = 1,NL
      DO  90 K = 1,NH
      IF(FB(K).LT.RC(J).OR.K.LT.KPORT) FR(J,K) = ERATIO
   90 CONTINUE
      IF(INMODE.NE.0) GO TO 150
      DO 100 J = 2,NJ
      PSI(J,1) = PSI(J-1,1) + UZ(J,1)*RC(J)*CASH(X(J),KT)*DX
  100 CONTINUE
  150 IF(INMODE.EQ.3) CALL SIMJET (NCD,ZB,DZ(1),G,F0,VMB,VMB1,AMB,DMB)
      IF(INMODE.EQ.1) CALL GAUSS(1)
      IF(INMODE.EQ.2.OR.INMODE.EQ.3) CALL GAUSS(2)
      UZ(1,1)  = UZ(2,1)
      IF(INMODE.NE.4) GO TO 200
      DO 160 J = 1,JPORT
      DELT(J,KPORT)= 1.0
      GAM(J,KPORT) = 1.0
      IF(J.EQ.1) GO TO 160
      UZ(J,KPORT)   = (PLX+1)*(2*PLY+1)/(2*PLX*PLX)*(1.-RC(J))**(1./PLX)
      PSI(J,KPORT)  = PSI(J-1,KPORT)+RC(J)*CASH(X(J),KT)*DX*UZ(J,KPORT)
  160 CONTINUE
      PSIB      = PSI(JPORT,KPORT)
      UZ(1,KPORT)   = UZ(2,KPORT)
      DO 170 K = 1,KPORT
  170 PSI(JPORT,K)= PSIB
      DO 180 J = JPORT,NJ
      PSI(J,1) = PSIB
  180 CONTINUE
      NB        = JPORT
  200 CONTINUE
      RETURN
      END


      SUBROUTINE  PLABAK
      INCLUDE     COMLST,LIST
      DATA/DF/1HF/CF/1HC/
      TU        = DF
      IF(CONTPL(12)) TU = CF
      EPR       = 1./KRP
      EPZ       = 1./ZRP
      WRITE(OUT,1001) KASE
      WRITE(OUT,1002) NJ,NK,DX,RO,VO,FO,TU,TU,TU,TR,SALJ,SALR,SIGTJ,
     1                SIGTR,KER,REZ,PLX,UZ(2,KPORT)
      WRITE(OUT,1007) NMAD,KPORT,JPORT,NEDDY,EXS,BETA,AK1
    5 WRITE(OUT,1010) DATE,TIM,(NOX(K),K=1,8)
      DO 140 J = 1,NJ
      WRITE(OUT,1012) J,X(J),RC(J),R(J),(SC(J,L),L=1,8)
  140 CONTINUE
      WRITE(OUT,1010) DATE,TIM,(NOX(K),K=9,15)
      DO 145 J = 1,NJ
      WRITE(OUT,1012) J,X(J),RC(J),R(J),(SC(J,L),L=9,15)
  145 CONTINUE
      WRITE(OUT,1013)
      WRITE(OUT,1014) DATE,TIM,(NOX(K),K=1,8)
      DO 150 K = 1,NH
  150 WRITE(OUT,1012) K,DZ(K),ZC(K),Z(K),(SZ(K,L),L=1,8)
      WRITE(OUT,1014) DATE,TIM,(NOX(K),K=9,16)
      DO 155 K = 1,NH
      WRITE(OUT,1012) K,DZ(K),ZC(K),Z(K),(SZ(K,L),L=9,16)
  155 CONTINUE
      WRITE(OUT,1016) DATE,TIM,(NOX(K),K= 17,20)
      DO 165 K = 1,NH
      WRITE(OUT,1006) K,DZ(K),ZC(K),Z(K),(SZ(K,L),L=17,20),DELT(NL,K),
     1          RSEA(K)
  165 CONTINUE
      WRITE(OUT,1003) ZB,FO,G,VMB,GMB,DMB
      WRITE(OUT,1004)
  190 DO 200 J = 1,NJ
      L         = KPORT
      WRITE(OUT,1005) PSI(J,L),UZ(J,L),UX(J,L),DELT(J,L),GAM(J,L)
  200 CONTINUF
1
 1001 FORMAT(/// 40H     PARAMETERS FOR THERMAL PLUME CASE    I3)
 1002 FORMAT(///
     1/55H     NUMBER OF RADIAL NODFS (X-DIRECTION)    - - - - - - - I7
     3/55H     NUMBER OF VERTICAL NODES (Z-DIRECTION) - - - - - - - I7
     4/55H     RADIAL NODE THICKNESS (X-DIRECTION), DX- - - - - - - F13.5
     6/55H     PLUME OUTFALL PORT RADIUS (X-COORD), R0- - - - - - - F13.5
     7/55H     PLUME OUTFALL PORT VELOCITY,FT/SEC),    - - - - - - - F13.5
     8/55H     DENSIMETRIC FROUDE NO. AT OUTFALL PORT(V0**2)  - - F13.5
     A/5X@TEMPERATURE OF REFERENCE AMBIENT(DEG. WA1, @) - - - - -@F13.5
     9/5X@TEMPERATURE OF EFFLUENT,(DEG. WA1, @) - - - - - - - - -@F13.5
     B/55H     SALINITY OF EFFLUENT, PARTS/THOUSAND - - - - - - - - F13.5
     C/55H     SALINITY OF REFERENCE AMBIENT, PARTS/THOUSAND  - - F13.5
     D/55H     SIGMA-T  OF EFFLUENT - - - - - - - - - - - - - - - - F13.5
     E/55H     SIGMA-T  OF REFERENCE AMBIENT  - - - - - - - - - - - F13.5
     F/55H     RADIAL REFERENCE REYNOLDS NUMBER - - - - - - - - - - F13.5
     G/55H     VERTICAL REFERENCE REYNOLDS NUMBER - - - - - - - - - F13.5
     H/55H     INFLOW POWER-LAW VELOCITY PROFILE EXPONENT - - - - F13.5
     I/55H     CENTERLINE VELOCITY AT OUTFALL PORT, V/V0  - - - - F13.5)
 1007 FORMAT(
     1 55H     TYPE OF RICHARDSON NUMBER MODIFICATION(0 = NONE) - I7
     2/55H     GRID POINT AT INFLOW BOUNDARY, KPORT - - - - - - - - I7
     3/55H     GRID POINT AT INFLOW BOUNDARY, JPORT - - - - - - - - I7
     4/55H     TYPE OF EDDY DIFFUSIVITY COMPUTATION - - - - - - - - I7
     5/55H     OUTER LOOP ACCELERATION FACTOR - - - - - - - - - - - F13.5
     6/55H     VALUE OF CONSTANT, BETA  - - - - - - - - - - - - - - F13.5
     7/55H     VALUE OF CONSTANT, AK1   - - - - - - - - - - - - - - F13.5
     8///)
 1003 FORMAT(1H1 //@     INFLOW BOUNDARY CENTERLINE VALUES @/
     */53H     ELEVATION OF GRID BOUNDARY(PORT DIAMS)    ,ZB  = F9.3
     1/53H     DENSIMETRIC FROUDE NUMBER AT OUTFALL PORT,F0  = F9.3
     2/53H     STRATIFICATION PARAMETER                  ,G   = F11.5
     3/53H     CENTERLINE VELOCITY                       ,VMB = F9.3
     4/53H     CENTERLINE VALUE OF GAMMA-CONSTIULNT     ,GMB = F9.3
     5/53H     CENTERLINE VALUE OF BUOYANCY PARAMETER   ,DMB = F9.3)
 1004 FORMAT(//@      RADIAL DISTRIBUTIONS @/
     1/8X65HPSI        VERT VELO    RAD VELO      DELT          GAMMA
     2        //)
 1005 FORMAT(1P6(E13.3,1X))
 1006 FORMAT(I3,F7.2,2F10.3,1P5E11.3,E13.5)
 1010 FORMAT(1H1,@    DATE @2A6,@ TIME @2A6/
     1 60H      COMPUTED CONSTANTS FOR RADIAL DIFFERENCES - -SC(J,L)    //
     2 30H   J   X(J)        R/R0       R(J)      ,8(I6,5X)/)
 1012 FORMAT(I3,F7.2,2F10.2,1P6E11.3)
 1013 FORMAT(/)
 1014 FORMAT(1H1,@    DATE @2A6,@ TIME @2A6/
     1 60H      COMPUTED CONSTANTS FOR VERTICAL DIFFERENCES - -SZ(K,L) //
     2 30H   K   DZ(K)      Z/D0      Z(K)      ,8(I6,5X)/)
 1016 FORMAT(1H1,@    DATE @2A6,@ TIME @2A6/
     1 60H      COMPUTED CONSTANTS FOR VERTICAL DIFFERENCES - -SZ(K,L)//
     2 30H   K   DZ(K)      Z/D0      Z(K)      ,4(I6,5X) ,
     3 30H DELT(NL,K)     KSEA(K)
      RETURN
      END


      SUBROUTINE  STREAM (IT,NSKIP)
C     SUBROUTINE CALCULATES THE TWO  DIMENSIONAL  STREAM FUNCTION, PSI(J
      INCLUDE    COMLST,LIST
      OMEGA3= 0.
   10 DO 120 I = 1,II
      DPMAX    = 0.
C     SET OUT-BOUNDARY STREAM FUNCTION FOR NEXT ITERATION CYCLE
      DO  20 K = 2,NKK
      PSI(NJ,K)= 2.*PSI(NJ-1,K)-PSI(NJ-2,K)
   20 CONTINUE
      DO 100 J = 2, NJJ
```

Reproduced from
best available copy.

```
      A1        = SC(J,11)
      A2        = SC(J,12)
      A3        = SC(J,13)
      DO 100 K = 2,NK
      IF(J.LE.JPORT.AND.K.LE.KPORT) GO TO 100
      CON       = A1+SZ(K,8)
      PSIO      = PSI(J,K)
      IF(NSKIP.EQ.0) GO TO 50
      OMEGA1    = .5*(OMEG(J+1,K)+OMEG(J,K))
      OMEGA2    = .5*(OMEG(J+1,K+1)+OMEG(J,K+1))
   45 CONTINUE
      OMEGA3    = OMEGA1+SZ(K,12)*(OMEGA2-OMEGA1)
   50 PSI(J,K) = (A2*PSI(J-1,K)+A3*PSI(J+1,K) +
     1            SZ(K,9)*PSI(J,K-1)+SZ(K,10)*PSI(J,K+1)+OMEGA3
     2            *R(J))/CON
      DEL       = ABS((PSIO-PSI(J,K))/PSI(J,K))
      IF(J.GT.NCR)  GO TO 95
      DPMAX = AMAX1(DPMAX,DEL)
      IF(DPMAX.GT.DEL) GO TO 95
      NODE(5)   = J
      NODE(6)   = K
   95 PSI(J,K) = PSIO+EXT *(PSI(J,K)-PSIO)
  100 CONTINUE
      IF(DPMAX.LE..0005) GO TO 130
  120 CONTINUE
  130 IF(NSKIP.EQ.1) GO TO 150
      ITNC      = I
C     CALCULATE VELOCITY FIELD
  150 DO 250 J = 2,NJ
      A4        = SC(J,14)
      DO 250 K= 2,NK
      IF(J.LT.JPORT.AND.K.LT.KPORT) GO TO 250
      UX(J,K)   = -(PSI(J,K)-PSI(J,K-1))/(R(J)*DZ(K))
      UZ(J,K)   = (PSI(J,K)-PSI(J-1,K))*A4
      IF(J.EQ.2) UZ(1,K) = UZ(2,K)
      IF(K.EQ.NK) UX(J,NH) = UX(J,NK)
      IF(K.EQ.2.AND.INMODE.EQ.4) UX(J,1) = -UX(J,2)
      IF(K.EQ.2.AND.INMODE.NE.4.AND.J.GT.NB) UX(J,1) = UX(J,2)
  250 CONTINUE
      CALL ETIMEF(TIME)
  270 IF(NSKIP.NE.0) RETURN
      TINT      = TIME-START
      IF(NSKIP.EQ.0) CALL OUTPUT(0)
      RETURN
 1000 FORMAT(I5,E12.3)
      END


      SUBROUTINE  SSCOMP
      INCLUDE     COMLST,LIST
      DIMENSION  TDELT(LJ),AMON(15)
      DATA/DF/1HF/DC/1HC/
      GZCON     = ZRP/REZ
      DOMEG     = 0.
      DDELT     = 0.
      DGAM      = 0.
C
      NV        = 2
      DELT(JPORT,KPORT) = DELT(JPORT+1,KPORT)
      GAM (JPORT,KPORT) = GAM (JPORT+1,KPORT)
      IF(INMODE.EQ.4) NV = 3
      MASK      = 0
      NSTART    = JPORT+1
      N2        = ITMAX
      ITNO      = ITNOO
      ITERS     = NPI
      N1        = 1
      IF(.NOT.CONTRL(8)) GO TO 15
      N1        = ITNO+1
      ITMAX     = ITNO+ITMAX
      N2        = ITMAX
      NED       = NED + ITNO
      IF(NED.GT.ITNO.OR.NEDDY.EQ.0) GO TO 15
      CALL EDDY(NEDDY)
   15 CALL ETIMEF(START)
      DO 800 L = N1,N2
      ITNO      = L
      DDMAX     = 0.
      IF(.NOT.CONTRL(1).AND..NOT.CONTRL(2)) GO TO 290
      DO 200 J = 2,NJ
      DO 200 K = 2,NK
      IF(INMODE.NE.4) GO TO 20
      IF(J.LE.JPORT.AND.K.LE.KPORT) GO TO 200
      MASK      = 0
      IF(J.EQ.JPORT.AND.K.EQ.KPORT+1) MASK = 1
   20 A1        = SC(J,7)
      A2        = SC(J,8)
      A3        = SC(J,9)*FR(J,K-1)
      A4        = SC(J,10)*FR(J,K-1)
      A5        = SC(J,6)*FR(J,K-1)
      UPOS1     = ABS(UX(J-1,K)) + UX(J-1,K)
      UPOS2     = ABS(UX(J,K))   + UX(J,K)
      UNEG1     = ABS(UX(J-1,K)) - UX(J-1,K)
      UNEG2     = ABS(UX(J,K))   - UX(J,K)
      VPOS1     = ABS(UZ(J,K-1)) + UZ(J,K-1)
      VPOS2     = ABS(UZ(J,K))   + UZ(J,K)
      VNEG1     = ABS(UZ(J,K-1)) - UZ(J,K-1)
      VNEG2     = ABS(UZ(J,K))   -UZ(J,K)
      IF(CONTRL(11).OR.NEDDY.EQ.4) GO TO 30
      GO TO 50
   30 DM1       = SZ(K,14)
      DP1       = SZ(K,15)
      DC0       = SZ(K,16)
      DFZ       = DP1*FZ(J,K+1)-DM1*FZ(J,K-1)-DC0*FZ(J,K)
      DGAM       = GZCON*DFZ*(DP1*GAM(J,K+1)-DM1*GAM(J,K-1)-DCO*GAM(J,K))
      DGRAD(J,K)     = DP1*DELT(J,K+1)-DM1*DELT(J,K-1)-DCO*DELT(J,K)
      DDELT      = GZCON*DFZ*DGRAD(J,K)
   50 CONTINUE
      BO         = FZ(J,K)*SZ(K,5)
      B1         = 1./(BO+A1*UNEG1+A2*UPOS2+SZ(K,4)*(VPOS2+VNEG1)+A5)
      AJ1        = (A1*UPOS1+A3)
      AJ2        = (A2*UNEG2+A4)
      AK1        = (SZ(K,4)*VPOS1+SZ(K,6)*FZ(J,K))
      AK2        = (SZ(K,4)*VNEG2+SZ(K,7)*FZ(J,K))
      DJ1        = AJ1*DELT(J-1,K)
      DJ2        = AJ2*DELT(J+1,K)
      DJ3        = AK1*(DELT(J,K-1)*(1-MASK)+MASK)
      DJ4        = AK2*DELT(J,K+1)
      GJ1        = AJ1*GAM(J-1,K)
      GJ2        = AJ2*GAM(J+1,K)
      GJ3        = AK1*(GAM(J,K-1)*(1-MASK)+MASK)
      GJ4        = AK2*GAM(J,K+1)
      GAMO       = GAM(J,K)
      DELTO      = DELT(J,K)
      DELT(J,K)= (DJ1+DJ2+DJ3+DJ4+DDELT)*B1
      GAM (J,K)= (GJ1+GJ2+GJ3+GJ4+DGAM)*B1
      DEL        = ABS((DELT(J,K)-DELTO)/DELT(J,K))
      IF(J.GT.NCR) GO TO 195
      DDMAX      = AMAX1(DDMAX,DEL)
      IF(DDMAX.GT.DEL) GO TO 195
      NODE(1)    = J
      NODE(2)    = K
  195 DELT(J,K)= DELTO+EXR*(DELT(J,K)-DELTO)
      GAM(J,K)   = GAMO+EXR*(GAM(J,K)-GAMO)
  200 CONTINUE
C     SET BOUNDARY VALUES FOR DELTA(J,K)
      DO 230 J = 2,NJ
      GAM(J,NH)= GAM(J,NK)
      DELT(J,NH)= DELT(J,NK)
      IF(J.LT.NP) GO TO 230
      DELT(J,1)= DELT(J,2)
      GAM(J,1) = GAM(J,2)
  230 CONTINUE
      IF(INMODE.NE.4) GO TO 250
      DO 240 K = 2,KPORT
      DELT(JPORT,K) = DELT(JPORT+1,K)
      GAM(JPORT,K)  = GAM(JPORT+1,K)
  240 CONTINUE
  250 CONTINUE
      DO 260 K = 1,NK
      DELT(1,K)= DELT(2,K)
      GAM(1,K) = GAM(2,K)
  260 CONTINUE
  290 DOMAX     = 0.
      DO 300 J = 2,NJ
      DO 300 K = NV,NK
      IF(J.LE.JPORT.AND.K.LE.KPORT+1) GO TO 300
      IF(J.EQ.JPORT+1. AND.K.LE.KPORT) GO TO 300
      A1        = SC(J,1)*FR(J,K-1)
      A2        = SC(J,2)*FR(J,K-1)
      A3        = SC(J,3)*FR(J,K-1)
      A4        = SC(J,4)
      A5        = SC(J,5)
      UPOS1     = ABS(UX(J-1,K)) + UX(J-1,K)
      UPOS2     = ABS(UX(J,K))   + UX(J,K)
      UNEG1     = ABS(UX(J-1,K)) - UX(J-1,K)
      UNEG2     = ABS(UX(J,K))   - UX(J,K)
      VPOS1     = ABS(UZ(J,K-1)) + UZ(J,K-1)
      VPOS2     = ABS(UZ(J,K))   + UZ(J,K)
      VNEG1     = ABS(UZ(J,K-1)) - UZ(J,K-1)
      VNEG2     = ABS(UZ(J,K))   - UZ(J,K)
      IF(CONTRL(11).OR.NEDDY.EQ.4) GO TO 291
      GO TO 293
  291 UM1       = .5*(UX(J,K-1)+UX(J-1,K-1))
```

```
                  = .5*(UX(J,K+1)+UX(J-1,K+1))
      UP1         = .5*(UX(J,K   )+UX(J-1,K   ))
      UCO         = SZ(K,15)*FZ(J,K+1)-SZ(K,14)*FZ(J,K-1)-SZ(K,16)*FZ(J,K)
      DFZ         = SZ(K,15)*UP1-SZ(K,14)*UM1-SZ(K,16)*UCO
      UGRAD(J,K)       = SZ(K,15)*(SZ(K,3)*(UP1-UCO)-SZ(K,2)*(UCO-UM1))
      DOMEG       = 2.*DFZ*(SZ(K,3)*(FZ(J,K+1)-FZ(J,K))-SZ(K,2)*(FZ(J,K)-
      SOMEG       = DOMEG+(SZ(K,3)*(FZ(J,K+1)-FZ(J,K))-SZ(K,2)*(FZ(J,K)-
                    FZ(J,K-1)))*UGRAD(J,K)
     1
  293 CONTINUE
      BO          = FZ(J,K)*SZ(K,1)
      B1          = 1./(BO+A1+A4*(UPOS2+UNEG1)+SZ(K,4)*(VPOS2+VNEG1))
      AJ1         = (A2+A4*(UPOS1))*OMEG(J-1,K)
      AJ2         = (A3+A4*(UNEG2))*OMEG(J+1,K)
      AK1         = (FZ(J,K)*SZ(K,2)+SZ(K,4)*VPOS1)*OMEG(J,K-1)
      AK2         = (FZ(J,K)*SZ(K,3)+SZ(K,4)*VNEG2)*OMEG(J,K+1)
      ADELT       = -A5*(DELT(J+1,K)-DELT(J-1,K))
      IF(J.EQ.NJ) ADELT = 0.
      OMEGO       = OMEG(J,K)
      OMEG(J,K)= (AJ1+AJ2+AK1+AK2+ADELT+DOMEG)*B1
      DEL         = ABS((OMEG(J,K)-OMEGO)/OMEG(J,K))
      IF(J.GT.NCR) GO TO 295
      DOMAX       = AMAX1(DOMAX,DEL)
      IF(DOMAX.GT.DEL) GO TO 295
      NODE(3)    = J
      NODE(4)    = K
  295 OMEG(J,K)= OMEGO+EXR*(OMEG(J,K)-OMEGO)
  300 CONTINUE
      CALL STREAM(ITERS,1)
      SET CENTERLINE AND OUT BOUNDARY VORTICITY
C     DO 310 K = 2,NK
      OMEG(NL,K)       = 0.
      OMEG(1,K) = -OMEG(2,K)
  310 CONTINUE
      SET SURFACE BOUNDARY  VORTICITY
C     DO 320 J = 2,NJ
  320 OMEG(J,NH)          = -OMEG(J,NK)
```

```
C     SET BOTTOM BOUNDARY VORTICITY
      IF(INMODE.EQ.4) GO TO 350
C     SET SLIP BOUNDARY
      DO 330 J = NB,NJ
      OMEG(J,1)= -OMEG(J,2)
  330 CONTINUE
C     SET INFLOW BOUNDARY VORTICITY
      VORT2    = 1./DZ(KPORT+1)
      DO 340 J = 2,NB
      DUZ      = .25*VORT2*(UX(J,3)+UX(J-1,3)-UX(J,1)-UX(J-1,1))
      DVR      = .5*(UZ(J+1,2)+UZ(J+1,1)-UZ(J-1,2)-UZ(J-1,1))*SC(J,4)
      OMEG(J,2)= DUZ-DVR
      OMEG(J,1)= 0.
C         OMEG(J,1) FOR J LESS THAN NB  DOES NOT ENTER IN CALCULATIONS
  340 CONTINUE
      GO TO 400
  350 CONTINUE
C     SET NO-SLIP  BOTTOM BOUNDARY
      NSTART   = JPORT+1
      DO 360 J = NSTART,NJ
      DUZ      = .25*(UX(J,3)+UX(J-1,3)-UX(J,1)-UX(J-1,1))/DZ(2)
      DVR      = .5*(UZ(J+1,2)-UZ(J-1,2))/(RC(J+1)-RC(J-1))
      OMEG(J,2)= DUZ-DVR
  360 CONTINUE
C     SET PORT SIDE NO-SLIP BOUNDARY
      DO 370 K = 2,KPORT
      UKP1     = .5*(UX(JPORT,K+1)+UX(JPORT+1,K+1))
      UKM1     = .5*(UX(JPORT,K-1)+UX(JPORT+1,K-1))
      UKC      = .5*(UX(JPORT,K  )+UX(JPORT+1,K  ))
      DUZ      =  SZ(K,15)*UKP1-SZ(K,14)*UKM1-SZ(K,16)*UKC
      DVR      = .5*(UZ(JPORT+2,K)+UZ(JPORT+2,K-1)+UZ(JPORT+1,K)+
     1           UZ(JPORT+1,K-1))/(RC(JPORT+2)-RC(JPORT))
      OMEG(JPORT+1,K) = DUZ-DVR
  370 CONTINUE
C     SET INFLOW BOUNDARY VORTICITY
```

```
      DO 380 J = 2,JPORT
      DVR        = (UZ(J+1,KPORT)-UZ(J-1,KPORT))/(RC(J+1)-RC(J-1))
      DVR        = .5*DVR
      IF(J.EQ.JPORT)
     1            DVR = .5 *(UZ(J+1 ,KPORT)-UZ(J,KPORT))/(RC(J+1)-RC(J))
      DVR        = DVR+.5*(UZ(J+1,KPORT +1)-UZ(J-1,KPORT+1))
     1            /(RC(J+1)-RC(J-1))
      U2         = .25*(UX(J,KPORT+2)+UX(J-1,KPORT+2)+UX(J,KPORT+1)
     1            +UX(J-1,KPORT+1))
      DUZ        = U2/DZ(KPORT+1)
      OMEG(J,KPORT+1) = DUZ-DVR
  380 CONTINUE
  400 CONTINUE
      DELT(1,NH)      = DELT(2,NK)
      GAM (1,NH)      = GAM (2,NK)
      IF(.NOT.CONTRL(6)) GO TO 410
      JK         = 0
      DO 405 KK = 1,10,2
      L1         = MON(KK)
      L2         = MON(KK+1)
      L3         = MON(KK+10)
      L4         = MON(KK+11)
      L5         = MON(KK+20)
      L6         = MON(KK+21)
      JK         = JK+1
      AMON(JK)        = UZ(L1,L2)
      AMON(JK+5)      = UX(L3,L4)
      AMON(JK+10)     =DELT(L5,L6)
  405 CONTINUE
      WRITE(OUT,1006) ITNO,(AMON(KK),KK=1,15)
  410 CONTINUE
      IF(NEDDY.EQ.0.OR.NEDDY.GE.5) GO TO 750
      IF(NED.GE.L) GO TO 750
      CALL EDDY(NEDDY)
  750 IF(MOD(L,NOUT).EQ.0) CALL OUTPUT (1)
```

```
      IF(MOD(L,NTTY).EQ.0) CALL OUTPUT (2)
  800 CONTINUE
      IF(INMODE.EQ.4) TEMPER(JPORT,KPORT)=TEMPER(JPORT-1,KPORT)
      IF(.NOT.CONTRL(9)) GO TO 880
      WRITE(8) ITNO,OMEG,DELT,UX,UZ,PSI,GAM
      N3DPTS    = 0
      DO 810 J = 1,5
      IF(N3DPT(J).EQ.0) GO TO 810
      N3DPTS    = N3DPTS+1
  810 CONTINUE
      NZ        = NK
      IF(N3DPTS.EQ.0) GO TO 830
      WRITE(8) KASE,DATE,TIM,TLABEL,N3DPTS,JPORT,KPORT,NX,NZ
      DO 820 J = 1,5
      L         = N3DPT(J)
      IF(L.EQ.0) GO TO 820
      IF(L.EQ.1) WRITE(8) L,(R (N),N=1,NX),(Z (N),N=1,NZ),
     1                    ((PSI (N,M),N=1,NX),M=1,NZ)
      IF(L.EQ.2) WRITE(8) L,(RC(N),N=1,NX),(ZC(N),N=2,NH),
     1                    ((DELT(N,M),N=1,NX),M=2,NH)
      IF(L.EQ.3) WRITE(8) L,(RC(N),N=1,NX),(ZC(N),N=2,NH),
     1                    ((GAM (N,M),N=1,NX),M=2,NH)
      IF(L.EQ.4) WRITE(8) L,(RC(N),N=1,NX),(ZC(N),N=2,NH),
     1                  ((TEMPER(N,M),N=1,NX),M=2,NH)
      IF(L.EQ.5) WRITE(8) L,(RC(N),N=1,NX),(ZC(N),N=2,NH),
     1                    ((OMEG(N,M),N=1,NX),M=2,NH)
      LL        = L
      IF(L.EQ.1) WRITE(OUT,1004) LL
      IF(L.EQ.2) WRITE(OUT,1005) LL
      IF(L.EQ.3) WRITE(OUT,1006) LL
      IF(L.EQ.4) WRITE(OUT,1007) LL
      IF(L.EQ.5) WRITE(OUT,1008) LL
  820 CONTINUE
  830 CONTINUE
      WRITE(OUT,1003) N3DPTS,NX,NZ
      IF(TEMPER(2,NK)-TEMPER(NL,NK).LT..1) GO TO 860
      IF(CONTRL(13)) WRITE(OUT,1001) RC
      IF(.NOT.CONTRL(13)) WRITE(OUT,1001) DF
      DO 850 J = 1,80
      TDELT(J) = TEMPER(NL,NK)+J
      IF(TDELT(J).LT.TEMPER(2,NK)) GO TO 850
      LAST      = J-1
      GO TO 855
  850 CONTINUE
  855 DO 870 L = 1,LAST
      DO 860 J = 2,NJ
      IF(TEMPER(J,NK).GT.TDELT(L)) GO TO 860
      RAD       = (RC(J-1)+(TDELT(L)-TEMPER(J-1,NK))/(TEMPER(J,NK)
     1            -TEMPER(J-1,NK))*(RC(J)-RC(J-1)))*R0
      AREA      = 3.141*RAD*RAD
      WRITE(OUT,1002) L,AREA,RAD
      GO TO 870
  860 CONTINUE
  870 CONTINUE
C*    GAMA SUM CONVERGENCE CHECK
  880 WRITE(OUT,1010)
      GAMIN     = 2.*(PSI(JPORT,KPORT)-1.)
      NSTART    = JPORT+5
      DO 900 J = NSTART,NJ,3
      NCR       = J
      GAMC      = 2.*R(NCR)*RHP/(RER*(RC(NCR+1)-RC(NCR)))
      GAMCON    = 0.
      GAMDIF    = 0.
      DO 895 K = 1,NK
      UFACE     = UX(NCR,K)
      IF(UFACE.GT.0.)GAMCON=GAMCON+2.*R(NCR)*DZ(K)*GAM(NCR,K)*UFACE
      IF(UFACE.LT.0.)GAMCON=GAMCON+2.*R(NCR)*DZ(K)*GAM(NCR+1,K)*UFACE
      GAMDIF    = GAMC*FR(NCR,K)*DZ(K)*(GAM(NCR,K)-GAM(NCR+1,K))+GAMDIF
  895 CONTINUE
      GAMCON    = 100.*GAMCON/GAMIN
      GAMDIF    = 100.*GAMDIF/GAMIN
      GAMSUM    = GAMCON+GAMDIF
      GAMERR    = GAMSUM-100.
      WRITE(OUT,1011) J,GAMCON,GAMDIF,GAMERR
  900 CONTINUE
      RETURN
 1000 FORMAT(I6,4X15(F6.4,2X))
 1001 FORMAT(//30H      SURFACE ISOTHERM DATA      //            RADIUS OF
     1/15H       DEGREES ,A1,35H        AREA IN              ISOTHERM, FEET
     2/60H      ABOVE AND       SQ. FEET
     3/)
 1002 FORMAT(I10,2(10XF10.1))
 1003 FORMAT(///5XI5, @ THREE-D PLOT RECORDS WRITTEN ON TAPE@/
     1          @            SET PLOT PARAMETERS NJ = @I3,@ NK = @I3)
 1004 FORMAT(@ STREAM FUNCTION RECORD WRITTEN TO TAPE - RECORD NO    @I3)
 1005 FORMAT(@ BUOYANCY PARAMETER RECORD WRITTEN TO TAPE - RECORD NO@I3)
 1006 FORMAT(@ GAMMA-CONSTITUENT RECORD WRITTEN TO TAPE - RECORD NO @I3)
 1007 FORMAT(@ TEMPERATURE RECORD WRITTEN TO TAPE - RECORD NO       @I3)
 1008 FORMAT(@ VORTICITY RECORD WRITTEN TO TAPE - RECORD NO         @I3)
 1010 FORMAT(1H1,//@      GAMMA-CONSTITUENT BALANCE ERROR    @ ///
     1    @      NET CONVECTIVE        NET DIFFUSIVE         GAMMA BALANCE
     2@/ @      OUTFLOW, PERCENT     OUTFLOW, PERCENT      ERROR, PERCEN
     3T@/@  J@)
 1011 FORMAT(I5,3(5X,F10.4,5X))
      END


      SUBROUTINE EDDY(M)
      INCLUDE     COMLST,LIST
      DIMENSION  RCORE(LK),R5(LK),KR(LJ)
      RATIO      = REZ/REP
      VEDC       = .015
      GO TO (10,20,120,20,20,500,500),M
C*    CALCULATE RADIAL EDDY FACTORS USING PRESCRIBED MIXING LENGTH
```

```
   10 DO  15 K = 2,NK
      VMAX      = .5*(UZ(2,K)-UZ(2,K-1))
      FR(J,K-1)= .180*(Z(K)-.25*UZ(K))*VMAX
   15 CONTINUF
   20 CONTINUE
C*    CALCULATE RADIAL EDDY FACTORS BASED ON A RUNNING CALC. OF MIXING L
C*    BASE LENGTH OF POTENTIAL CORE ON PERCENT GAMMA DECREASE AT CENTERL
      IF(INMODE.LT.4) GO TO 40
      DO  25 K = KPORT,NH
      IF(GAM(2,K).LT.GAMEND) GO TO 30
   25 CONTINUE
      IF(MOD(ITNO,NOUT).EQ.0) WRITE(OUT,1000)
   30 KCORE     = K
      ZCORE     = Z(K)-Z(KPORT)
   40 CONTINUF
      DO 100 K = KPORT,NKK
      IF(N.EQ.1) GO TO 60
      VMAX      = UZ(2,K)
      V50       = .50*VMAX
      V05       = .05*VMAX
      RCORE(K) = 0.
      DO  50 J = 3,NJJ
      IF(V50.GT.UZ(J,K)) GO TO 45
      N50       = J
   45 IF(V05.GT.UZ(J,K)) GO TO 55
      N05       = J
   50 CONTINUF
   55 CONTINUE
C*    CALCULATE PLUME GEOMETRY AT LEVEL K
      IF(K.LT.KCORE) RCORE(K) = AMAX1(0.,(1.-(Z(K)-Z(KPORT))/ZCORE))
      R5(K)     = 1.
      IF(K.LT.KCORE) GO TO 60
      R5(K)     = RC(N50)+(UZ(N50,K)-V50)/(UZ(N50,K)-UZ(N50+1,K))*
     1            (RC(N50+1)-RC(N50))
   60 R05(K)    = RC(N05)+(UZ(N05,K)-V05)/(UZ(N05,K)-UZ(N05+1,K))*
```

```
     1             (RC(N05+1)-RC(N05))
  70 CONTINUE
     IF(M.EQ.1) GO TO 100
     DO  90 J = 2,NJ
     IF(M.EQ.2) GO TO 75
     FR(J,K)  = FRATIO
     IF(RB(K).LT.RC(J-1)) GO TO 100
  75 CONTINUE
     FR(J,K)  = (RS(K)-RCORE(K))*VMAX
     IF(K.EQ.KPORT) GO TO 90
     FR(J,K-1)= .5*(FR(J,K-1)+FR(J,K))
  90 CONTINUE
 100 CONTINUE
     IF(M.EQ.1 .OR.M.EQ.2) GO TO 400
C*   CALCULATE VERTICAL EDDY FACTORS FZ(J,K) IN SURFACE SPREAD
 120 CONTINUE
     DO 140 K = KPORT,NK
     DO 130 J = 2,NJ
     IF(RC(J-1).GT.RB(K)) GO TO 140
     FZ(J,K)  = RATIO*FR(J,K-1)
 130 CONTINUE
 140 CONTINUE
C*   CALCULATE VERTICAL EDDY FACTORS FOR LATERAL FLOW BASED ON LENGTH Z
     UMAX     = 0.
     DO 145 J = 2,NJ
     IF(UMAX.GT.UX(J,NK)) GO TO 145
     UMAX     = UX(J,NK)
     JMAX     = J
 145 CONTINUE
     DO 152 K = 1,NK
     IF(UX(JMAX,K).LT..5*UMAX) GO TO 152
     ZLEN     = Z(NK)-ZC(K-1)-(.5*UMAX-UX(JMAX,K-1))/
    1           (UX(JMAX,K)-UX(JMAX,K-1))*(ZC(K)-ZC(K-1))
     IF(ZLEN.GT.DZT5) ZLEN = DZT5
     GO TO 153
  152 CONTINUE
  153 CONTINUE
      FZC       = VFOC*ZLEN*UMAX*REZ*2.
      DO 200 J = 2,NJ
      DO 150 K = 1,NH
      UAVE      = .5*(UX(J-1,K)+UX(J,K))
      IF(UAVE.LT.0.) KB(J) = K
  150 CONTINUE
      DO 160 K = 2,NK
      IF(RC(J-1).LE.RB(K).AND.K.GT.KPORT) GO TO 155
      FZ(J,K)   = FZ(NL,K)
      IF(K+2.LT.KB(J).OR.K.LE.NK/2) GO TO 160
      IF(J.NE.NJ) FR(J,K-1) = FR(2,K-1)
      FZ(J,K) = FZ(J,K) + FZC*UX(J,NK)/UMAX
  155 IF(NMAD.EQ.0) GO TO 160
C*    MODIFY BY RICHARDSON NUMBER MODEL (IN LATERAL PLUME SPREAD ONLY)
      RICHNO    = +.5/F0*DGRAD(J,K)/(UGRAD(J,K)**2)
      IF(RICHNO.LT.0.) RICHNO = 0
      RICH(J,K)= RICHNO
      IF(RICHNO.GT.15.) RICHNO = 15.
      FZ(J,K)   = FZ(J,K)*RCHMOD(NMAD,RICHNO,BETA)
  160 CONTINUE
      FZ(J,1)   = FZ(J,2)
      FZ(J,NH)  = FZ(J,NK)
  200 CONTINUE
  400 IF(MOD(ITNO,NOUT).NE.0) RETURN
      WRITE(OUT,1001) ITNO
      DO 450 K = 2,NK
      KN        = NK+2-K
      D1        = .5*RCORE(KN)
      D2        = .5*R5(KN)
      D3        = .5*R05(KN)
      D4        = .5*RB(KN)
      WRITE(OUT,1002) KN,Z(KN),D1,D2,D3,D4
  450 CONTINUE
```

```
 500 RETURN
1000 FORMAT(1H1//@      PLUME CORE EXTENDS TO SURFACE @
    1/             @      CORE ASSUMED TO END AT K = NH FOR PURPOSES OF E
    2DY CALCULATION, FR(J,K-1) @ )
1001 FORMAT(//   @      PLUME LATERAL SECTION GEOMETRY, ITERATION NO. @
    1I5//@     K        Z/D      RCORE/D    RHALF/D    RBOUND/D     PB/D @)
1002 FORMAT(I10,F8.2,2X4(F9.3,2X))
     END


     SUBROUTINE OUTPUT(MODE)
     INCLUDE      COMLST,LIST
     IF(MODE.NE.2) GO TO 10
     WRITE(OUT,1000) ITNO,NPI,DPMAX,NODE(5),NODE(6),
    1              DUMAX,NODE(3),NODE(4),DVMAX,NODE(1),NODE(2)
     DO    5 J = 1,NJ
     DO     5 K = 1,NK
     IF(UZ(J,K).LE.0.)GO TO 5
     WRITE(OUT,1003)
     ISTOP      = 99999
     GO TO 10
   5 CONTINUE
     WRITE(OUT,1002) (MON(KK),KK= 1,70)
     RETURN
  10 CALL ETIMEF(TIME)
     IF(MODE.EQ.0) WRITE(OUT,1001) ITNO,DPMAX,ITNO,TINT
     TINT        = (TIME-START)/NOUT
     DO 100 J = 1,15
     L           = NPITE(J)
     IF(L.EQ.6) NOTEMP =0
     IF(L.EQ.0) GO TO 100
     IF(MODE.EQ.1) GO TO 90
     IF(L.EQ.1) CALL APOUT(L,Z, R,PSI,
    1                    42HSTREAM FUNCTION - IRROTATIONAL FLOW          )
```

```
      IF(MODE.EQ.0) GO TO 100
   90 IF(L.EQ.2) CALL AROUT(L,Z,R,PSI,
                      42HSTREAM FUNCTION - VISCOUS FLOW
     1                                                              )
      IF(L.EQ.3) CALL AROUT(L,ZC,RC,DELT,
                      42HBUOYANCY PARAMETER - DELT
     1                                                              )
      IF(L.EQ.4) CALL AROUT(L,ZC,RC,OMEG,
                      42HVORTICITY - OMEG
     1                                                              )
      IF(L.EQ.5) CALL AROUT(L,Z,RC,UZ,
                      42HVERTICAL VELOCITY COMPONENT - UZ
     1                                                              )
      IF(L.EQ.6) CALL AROUT(L,ZC, R,UX,
                      42HRADIAL VELOCITY COMPONENT - UX
     1                                                              )
      IF(L.EQ.7) CALL AROUT(L,ZC,RC,GAM,
                      42HGAMMA-CONSTITUENT
     1                                                              )
      IF(.NOT.CONTRL(13)) GO TO 92
      IF(L.EQ.8) CALL AROUT(L,ZC,RC,DELT,
                      42HTEMPERATURE, DEGREES CENTIGRADE
     1                                                              )
      GO TO 94
   92 IF(L.EQ.8) CALL AROUT(L,ZC,RC,DELT,
                      42HTEMPERATURE, DEGREES FAHRENHEIT
     1                                                              )
   94 CONTINUE
      IF(L.EQ.9) CALL AROUT(L,ZC,RC,DELT,
                      42HNORMALIZED BUOYANCY PARAMETER
     1                                                              )
      IF(L.EQ.10)CALL AROUT(L,Z,RC,UZ,
                      42HNORMALIZED VERTICAL VELOCITY COMPONENT
     1                                                              )
      IF(L.EQ.11)CALL AROUT(L,ZC,RC,DELT,
                      42HNORMALIZED TEMPERATURE DISTRIBUTION
     1                                                              )
      IF(L.EQ.12)CALL AROUT(L,ZC,RC,FR,
                      42HRADIAL EDDY MIXING FACTORS
     1                                                              )
      IF(L.EQ.13)CALL AROUT(L,ZC,RC,FZ,
                      42HVERTICAL EDDY MIXING FACTORS
     1                                                              )
      IF(L.EQ.14)CALL AROUT(L,ZC,RC,RICH,
                      42HRICHARDSON NUMBERS
     1                                                              )
      IF(L.EQ.15)GO TO 100
  100 CONTINUE
      IF(ISTOP.EQ.99999) STOP
      CALL ETIMEF(START)
      RETURN
 1000 FORMAT(1H1       26H     RESULTS FOR ITER. NO.     I5/
     1/ 35H     NO. OF PSI ITERATIONS- - - - -      I7,10X4HNODE
     2/ 35H     MAX CHANGE IN PSI  - - - - - - -     1PE10.3
     *,7H       (I2,1H.,I2,1H)
     3/ 35H     MAX CHANGE IN OMEG - - - - - - -     E10.3
     *,7H       (I2,1H.,I2,1H)
     4/ 35H     MAX CHANGE IN DELT - - - - - - -     E10.3
     *,7H       (I2,1H.,I2,1H)   )
 1001 FORMAT(1H1 45H      STREAM FUNCTION RESULTS FOR ITERATION       I5/
     1/           30H      MAXIMUM RELATIVE ERROR IS    1PE12.3/
     2/           23H      TIME REQUIRED FOR I3,14H ITERATIONS = F6.2,
     35H SEC         ///)
 1002 FORMAT(/    10H ITERATION
     1 40H.......... VERTICAL VELOCITY ...........
     2 40H*********. RADIAL VELOCITY **************
     3 40H.......... BUOYANCY PARAMETER ...........
     4/10H  NUMBER     15(2H (I2,1H,I2,1H))//)
 1003 FORMAT( ///@      THIS CASE IS APPARENTLY UNSTABLE, RUN ABORTED @)
      END


      SUBROUTINE AROUT(N,VCOORD,RCOORD,ARNAME,LABEL)
      INCLUDE     COMLST,LIST
      DIMENSION   ARNAME(LJ,LK),ANORM(LK),LABEL(7),HCOORD(LJ),VCOORD(LK)
      DIMENSION   RCOORD(LJ)
      REAL        LABEL
      DO  10 J = 1,NL
      HCOORD(J) = .5*RCOORD(J)
   10 CONTINUE
      N2         = 0
   60 N1         = N2+1
      N2         = N1+9
      IF(N2.GT.NL)N2=NL
      WRITE(OUT,1000) DATE,TIM,LABEL,ITNO,TINT
      WRITE(OUT,1004)
      WRITE(OUT,1001) (NOX(K),K=N1,N2)
   65 WRITE(OUT,1002) (HCOORD(K),K = N1,N2)
   70 DO 200 K = 1,NH
      KN       = NH-K+1
      IF(N.EQ.8.OR.N.EQ.11) GO TO 160
      IF(N.NE.9.AND.N.NE.10) GO TO 150
      AMAX     = ARNAME(2,KN)
      IF(ARNAME(3,KN).GT.AMAX) AMAX=ARNAME(3,KN)
      DO 100 J = N1,N2
  100 ANORM(J) = ARNAME(J,KN)/AMAX
      WRITE(OUT,1003) KN,VCOORD(KN),(ANORM(J),J=N1,N2)
      GO TO 200
  150 WRITE(OUT,1003) KN,VCOORD(KN),(ARNAME(J,KN),J=N1,N2)
      GO TO 200
C     COMPUTE ABSOLUTE DENSITY AND SALINITY
  160 DO 165 J = N1,N2
      SAL         = SALR-GAM(J,KN)*DSALT
      SIGT        = SIGTR-ARNAME(J,KN)*DELTJ
C     COMPUTE TEMPERATURE FROM DENSITY AND SALINITY
      TEMPER(J,KN)   = TEMP(SAL,SIGT)
      IF(.NOT.CONTRL(13)) TEMPER(J,KN) = 1.8*TEMPER(J,KN)+32.
  165 CONTINUE
      TMAX        = TEMPER(2,KN)
      IF(N.EQ.11) GO TO 170
  167 WRITE(OUT,1003) KN,VCOORD(KN),(TEMPER(J,KN),J=N1,N2)
      GO TO 200
  170 DO 175 J = N1,N2
  175 ANORM(J) = TEMPER(J,KN)/TMAX
      WRITE(OUT,1003) KN,VCOORD(KN),(ANORM(J),J=N1,N2)
  200 CONTINUE
      IF(N2.NE.NL) GO TO 60
 1000 FORMAT(1H1,@     DATE @2A6,@  TIME @2A6/
   1            5X7A6,@      ITERATION NUMBER    @ ,I5,
   1 25H        COMPUTATION SPEED = F6.3,15H SEC/ITERATION          )
1001 FORMAT(/17X3HJ =  10(I8,3X))
1002 FORMAT(12X@RCOORD =@,10(F9.2,2X)/12X@ZCOORD@)
1003 FORMAT( 5H K = I2, 5H  Z = F6.2,2X1P10E11.3)
1004 FORMAT(@      COORDINATES GIVEN IN PORT DIAMETERS, Z/D OR R/D @)
     END


     FUNCTION SIGMAT(SAL,T,N)
     IF(N.EQ.0) GO TO 10
     SIGO       = (((6.8E-6*SAL)-4.82E-4)*SAL+.8149)*SAL-.093
     B          = 1.E-6*T*((.01667*T-.0164)*T+18.03)
     A          = .001*T*((.0010843*T-.09818)*T+4.7867)
     SUMT       = (T-3.98)*(T-3.98)*(T+283.)/(503.57*(T+67.26))
     SIGMAT     = (SIGO+.1324)*(1.-A+B*(SIGO-.1324))-SUMT
     RETURN
  10 SIGMAT     = T
     RETURN
     END


     FUNCTION     TEMP(SALT,SIGMA)
C****************NEWTON RAPHSON METHOD FOR CALCULATING TEMP.
C****************FROM SALINITY AND REFERENCE DENSITY
     ERROR      = .01
     T          = 20.
     SIGO       = -.093+.8149*SALT-.000482*SALT*SALT
     SIGO       = SIGO+6.8E-6*SALT*SALT*SALT
     DO 100   I = 1,50
     TSQD       = T*T
     TQBD       = TSQD*T
     F          = SIGMAT(SALT,T,1)-SIGMA
     DSUMT      = (215.74*(T-3.98)**2)/(503.570*(T+67.26)**2)
```

```
      DSUMT       = DSUMT-2*(T-3.98)*(T+283.)/(503.570*(T+67.26),
      DA          = .001*(4.7867-.19637*T+.0032529*TSQD)
      DB          = 1.E-6*(18.03-1.6328*T+.05*TSQD)
      DF          = (SIGO+.1324)*(-DA+DB*(SIGO-.1324))+DSUMT
      T1          = T-F/DF
      ER          = T1-T
      ER         = ABS(ER)
      T           = T1
      IF(ER.LT.ERROR)GO TO 150
  100 CONTINUE
  150 TEMP        = T
      RETURN
      END


      FUNCTION   RCHMOD(M,RICH,BETA)
C     CHOOSE BETA CONSTANT FOR APPROPRIATE MODEL AT INPUT
      GO TO (10,20,30,40,50,60),M
C* 10 ROSSBY AND MONTGOMERY  (1935)
   10 RCHMOD    = 1./(1.+BETA*RICH)
      RETURN
C* 20 ROSSBY AND MONTGOMERY (1935)
   20 RCHMOD    = 1./(1.+BETA*RICH)**2
      RETURN
C* 30 HOLZMAN (1935)
   30 RCHMOD    = AMAX1(0.,1.-BETA*RICH)
      RETURN
C* 40 YAMAMOTO (1959)
   40 RCHMOD    = SQRT(AMAX1(0.,1.-BETA*RICH))
      RETURN
C* 50 MAMAYEV (1958)
   50 RCHMOD    = EXP(-BETA*RICH)
      RETURN
C* 60 MUNK AND ANDERSON (1948)
```

```
60 RCHMOD    = (1.+BETA*RICH)**1.5
   RETURN
   END


   SUBROUTINE ISOGEN(Z,R,PSI,ISOLN,L,NJ,NK,LABEL)
   INCLUDE      ARDIM,LIST
   DIMENSION    Z(LK),R(LJ),PSI(LJ,LK),ISOLN(5,30),LABEL(6)
   DIMENSION    XP(200),ZP(200),ROOT(3)
   REAL         LABEL,ISOLN
   INTEGER      OUT
   OUT       = 6
   WRITE(OUT,1000) LABEL
   JN        = 2
   KN        = 2
   IF(L.EQ.1) KN = 1
   IF(L.EQ.1) JN = 1
   NOLINE    = 0
   DO  3 I = 1,30
   IF(ISOLN(L,I).EQ.0) GO TO 3
   NOLINE    = NOLINE+1
 3 CONTINUE
   DO 900 NI = 1,NOLINE
   PSIC      = ISOLN(L,NI)
   KOUNT     = 0
   DO 85 J=JN,NJ
   K         = 1
 5 IF(PSI(J,K)-PSIC      )10,20,30
10 K=K+1
   IF(K.GT.NK)GO TO 85
   IF(PSI(J,K)-PSIC      )10,20,40
30 K=K+1
   IF(K.GT.NK)GO TO 85
   IF(PSI(J,K)-PSIC      )40,20,30
```

```
C     ********* INTERPOLATION *********
   40 M=K-1
C     $$$$$$$$$ QUADRATIC INTERPOLATION $$$$$$$$$
C     EQUATION FOR INTERPOLATION IS OF FORM Y = AX**2+BX+D
      IF((NK-K)-1)43,43,41
   41 IF((K-1)-1)45,45,42
   42 IF((PSIC     -PSI(J,M))/(PSI(J,K)-PSI(J,M))-0.5)43,45,45
C     ML CORRESPONDS TO I-1
C     MM CORRESPONDS TO I
C     MH CORRESPONDS TO I+1
C     BRANCH TO 43--USE POINTS K-2,K-1,AND K FOR THE
C     QUADRATIC INTERPOLATION
   43 ML=K-2
      MM=K-1
      MH=K
      GO TO 44
C     BRANCH TO 45--USE POINTS K-1,K, AND K+1 FOR THE
C     QUADRATIC INTERPOLATION
   45 ML=K-1
      MM=K
      MH=K+1
   44 DENOM=(Z(MM)**2-Z(ML)**2)*(Z(MH)-Z(MM))-(Z(MH)**2-Z(MM)**2)
     1*(Z(MM)-Z(ML))
      ANUM=(PSI(J,MM)-PSI(J,ML))*(Z(MH)-Z(MM))-(PSI(J,MH)-PSI(J,MM))
     1*(Z(MM)-Z(ML))
      BNUM=(PSI(J,MH)-PSI(J,MM))*(Z(MM)**2-Z(ML)**2)-(PSI(J,MM)
     1-PSI(J,ML))*(Z(MH)**2-Z(MM)**2)
      AA = ANUM/DENOM
      BB = BNUM/DENOM
      D=PSI(J,MM)-AA*Z(MM)**2-BB*Z(MM)
      TERM=SQRT(BB**2-4.*AA*(D-PSIC))
      ROOT(1)=(-BB+TERM)/(2.*AA)
      ROOT(2)=(-BB-TERM)/(2.*AA)
      DO 57 I=1,2
      IF(MM.EQ.K)GO TO 61
      IF(ROOT(I).LT.Z(MH).AND.ROOT(I).GT.Z(MM))GO TO 60
      IF(ROOT(I).LT.Z(MM).AND.ROOT(I).GT.Z(MH))GO TO 60
      GO TO 54
61    IF(ROOT(I).LT.Z(MM).AND.ROOT(I).GT.Z(ML))GO TO 60
      IF(ROOT(I).LT.Z(ML).AND.ROOT(I).GT.Z(MM))GO TO 60
54    IF(I.EQ.2)PRINT 55
   55 FORMAT(@0@,@ERROR IN PROGRAM FOR COMPUTING RZ(J,N)@,
     1@BY QUADRATIC INTERPOLATION@)
   57 CONTINUE
      IF(I.EQ.2)GO TO 825
   60 ZP(KOUNT+1) = ROOT(I)
      GO TO 80
   20 ZP(KOUNT+1) = Z(K)
   80 KOUNT     = KOUNT + 1
      XP(KOUNT)= XCOORD(K(J))
      GO TO 5
   85 CONTINUE
      DO 185 K=KN,NK
      J        = 1
   90 IF(PSI(J,K)-PSIC      )100,200,300
  100 J=J+1
      IF(J.GT.NJ)GO TO 185
      IF(PSI(J,K)-PSIC      )100,200,400
  300 J=J+1
      IF(J.GT.NJ)GO TO 185
      IF(PSI(J,K)-PSIC      )400,200,300
C     ********* INTERPOLATION *********
  400 M=J-1
C     $$$$$$$$ QUADRATIC INTERPOLATION $$$$$$$$
      IF((NJ-J)-1)430,430,410
  410 IF((J-1)-1)450,450,420
 420  IF((PSIC      -PSI(M,K))/(PSI(J,K)-PSI(M,K))-0.5)430,450,440
C     ML CORRESPONDS TO I-1
C     MM CORRESPONDS TO I
C     MH CORRESPONDS TO I+1
```

```
C     BRANCH TO 430--USE POINTS J-2,J-1,AND J FOR THE
C     QUADRATIC INTERPOLATION
  430 ML=J-2
      MM=J-1
      MH=J
      GO TO 440
C     BRANCH TO 450--USE POINTS J-1,J, AND J+1 FOR THE
C     QUADRATIC INTERPOLATION
  450 ML=J-1
      MM=J
      MH=J+1
  440 DENOM=(R(MM)**2-R(ML)**2)*(R(MH)-R(MM))-(R(MH)**2-R(MM)**2)
     1*(R(MM)-R(ML))
      ANUM=(PSI(MM,K)-PSI(ML,K))*(R(MH)-R(MM))-(PSI(MH,K)-PSI(MM,K))
     1*(R(MM)-R(ML))
      BNUM=(PSI(MH,K)-PSI(MM,K))*(R(MM)**2-R(ML)**2)-(PSI(MM,K)
     1-PSI(ML,K))*(R(MH)**2-R(MM)**2)
      AA = ANUM/DENOM
      BB = BNUM/DENOM
      D=PSI(MM,K)-AA*R(MM)**2-BB*R(MM)
      TERM=SQRT(BB**2-4.*AA*(D-PSIC))
      ROOT(1)=(-BB+TERM)/(2.*AA)
      ROOT(2)=(-BB-TERM)/(2.*AA)
      DO 570 I=1,2
      IF(MM.EQ.J)GO TO 610
      IF(ROOT(I).LT.R(MH).AND.ROOT(I).GT.R(MM))GO TO 615
      IF(ROOT(I).LT.R(MM).AND.ROOT(I).GT.R(MH))GO TO 615
      GO TO 540
  610 IF(ROOT(I).LT.R(MM).AND.ROOT(I).GT.R(ML))GO TO 615
      IF(ROOT(I).LT.R(ML).AND.ROOT(I).GT.R(MM))GO TO 615
  540 IF(I.EQ.2) WRITE(6,555) KOUNT
  555 FORMAT(@U@,@ERROR IN PROGRAM FOR COMPUTING XP(@I2,@+1)@
     1@BY QUADRATIC INTERPOLATION@)
  570 CONTINUE
      IF(I.EQ.2)GO TO 825
```

```
615 XP(KOUNT+1) = XCOORD(ROOT(I))
    GO TO 800
200 XP(KOUNT+1) = XCOORD(R(J))
800 KOUNT = KOUNT+1
    ZP(KOUNT) = Z(K)
    GO TO 90
185 CONTINUE
    WRITE(OUT,1001) NI,PSIC,KOUNT
    WRITE(OUT,1002)
    DO 500 KK= 1,KOUNT,10
    KT        = ABS(KK-1)
    KS        = KT+10
    IF(KS.GE.KOUNT) KS = KOUNT
    WRITE(OUT,1003) KT,(XP(KR),KR = KK,KS)
    WRITE(OUT,1004) (ZP(KR),KR = KK,KS)
 500 CONTINUE
 900 CONTINUE
    WRITE(OUT,1005) NJ,NK
 825 RETURN
1000 FORMAT(1H1//5X6A6)
1001 FORMAT(/@     DATA FOR ISOLINE NUMBER @I2,@ AT VALUF @F10.4,@ - @
    1I3,@ DATA POINTS LOCATED@)
                                                          5    @,
1002 FORMAT(/  @0       1          2          3          4          10    @)
   1          @       6          7          8          9
1003 FORMAT(I3,2X10(F8.2,2X))
1004 FORMAT(5X10(F8.2,2X))
1005 FORMAT(//@ *****SET PLOT PARAMETERS, NJ=@,I3,@ NK=@I3,@ *****@)
     END


     SUBROUTINE INTERP
     INCLUDE    COMLST,LIST
     DO 100 J = 1,5
     L        = ISOPT(J)
```

```
      IF(L.EQ.0) GO TO 100
      IF(L.EQ.1) CALL ISOGEN(Z,XR,PSI,ISOLN,L,NJ,NK,
     1           36HVISCOUS STREAMLINES                 )
      IF(L.EQ.2) CALL ISOGEN(ZC,X,DELT,ISOLN,L,NJ,NK,
     1           36HBUOYANCY PARAMETER ISOLINES, ISOPYCS )
      IF(L.EQ.3) CALL ISOGEN(ZC,X,GAM,ISOLN,L,NJ,NK,
     1           36HSALINITY ISOLINES,PARTS PER THOUSAND )
      IF(L.EQ.4) CALL ISOGEN(ZC,X,TEMPER,ISOLN,L,NJ,NK,
     1           36HTEMPERATURE CONTOURS, DEG CENTIGRADE )
  100 CONTINUE
      RETURN
      END


      SUBROUTINE GAUSS(N)
      INCLUDE    COMLST,LIST
      DIMENSION  PSB(LJ)
C
      DELB     = (SIGTR-SIGTB)/DELTJ
      ZR       = 2.*ZB
      ZP       = ZR-DZ(2)*.5
      ZR1      = 2.*(ZB-DZ(2))
      PSB(1)   = PSI(1,1)
      IF(N.NE.1) GO TO 100
      RMIND    = 1.-ZP/8.
      RMIN     = 1.-ZR/9.
      RMIN1    = 1.-ZR1/9.
      C        = 1./9.
      C1       = 1./8.
      DO  10 J = 2,NJ
      UZ(J,1)  = 1.0
      UB       = 1.
      IF(RC(J).GE.RMIN) UZ(J,1) = EXP(-40.5*(C+(RC(J)-1.)/ZR)**2)
      IF(RC(J).GE.RMIN1) UB = EXP(-40.5*(C+(RC(J)-1.)/ZR1)**2)
      IF(UZ(J,1).LE..01) UZ(J,1) = 0.
      IF(UB.LE..01) UB = 0.
      PSI(J,1) = PSI(J-1,1)+UZ(J,1)*RC(J)*CASH(X(J),KT)*DX
      PSB(J)   = PSB(J-1)+UB*RC(J)*CASH(X(J),KT)*DX
   10 CONTINUE
      DO  50 J = 2,NJ
      DELT(J,1)= 1.0
      IF(RC(J).GE.RMIND) DELT(J,1) = EXP(-32.*(C1+(RC(J)-1.)/ZP)**2)
      IF(DELT(J,1).LE..01) DELT(J,1) = 0.
      GAM(J,1) = DELT(J,1)
   50 CONTINUE
      GO TO 120
  100 DO 110 J = 2,NJ
      UZ(J,1)   = EXP(-92.*(RC(J)/ZR)**2)*VMB
       UB         = EXP(-92.*(RC(J)/ZR1)**2)*VMB1
      IF((UZ(J,1)/VMB).LE..01) UZ(J,1) = 0.
       IF(UB/VMB1.LE..01) UB = 0.
      PSI(J,1) = PSI(J-1,1)+UZ(J,1)*RC(J)*CASH(X(J),KT)*DX
       PSB(J)    = PSB(J-1)+UB*RC(J)*CASH(X(J),KT)*DX
      EXPART    = EXP(-68.*(RC(J)/ZP)**2)
      IF(EXPART.LE..01) EXPART = 0.
      DELT(J,1)= EXPART*DMB+DELB
      GAM(J,1) = EXPART*GMB
  110 CONTINUE
  120 DO 150 J = 2,NJ
      IF(UZ(J,1).GT.0.) GO TO 150
      NB        = J
      JPORT     = J
       GO TO 160
  150 CONTINUE
  160 DO 170 J = 1,NB
      UX(J,1)   = -(PSI(J,1)-PSB(J))/([illegible](J)*DZ(2))
  170 CONTINUE
      RETURN
      END
      SUBROUTINE SIMJET(NCD,ZB,DZM,T,F0,VMB,VMB1,GMB,DMB)
C     SUBROUTINE OBTAINS SIMILARITY SOLUTION FOR VERTICAL PLUME
      DIMENSION  A(4),AE(4),AR(4),DZ1(4),N1(4)
      AK        = 84.
      A(1)      = 0.
      A(2)      = .5
      A(3)      = .5
      A(4)      = 1.
      FRACT     = 1./6.
      EX1       = 1./3.
      DELZ      = .5*DZM
      ZB3       = ZB
      ZB2       = ZB-.25*DZM
      ZB1       = ZB-DELZ
C     FIND LENGTH FOR FLOW ESTABLISHMENT
      ZO        = 5.
      DO  10 K  = 1,10
      ZE        = 5.57/((1.42/F0*ZO+1)**.5)
      DEL       = ABS((ZE-ZO)/ZE)
      IF(DEL.LE..0001) GO TO 15
   10 CONTINUE
   15 IF(NCD.EQ.0) GO TO  30
      EB1       = (4./ZE)**3+3./32./F0*(ZB1**2-ZE**2)
      EB2       = (4./ZE)**3+3./32./F0*(ZB2**2-ZE**2)
      EB3       = (4./ZE)**3+3./32./F0*(ZB3**3-ZE**2)
      VMB1      = EB1**EX1*AK**.5/ZB1
      SB        = .245*ZB2*EB2**EX1
      VMB       = EB3**EX1*AK**.5/ZB3
      DMB       = 1./SB
      GMB       = DMB
      RETURN
   30 DZ1(1)    = INT(ZE+1.)-ZE
```

```
      DZ1(2)    = .1
      DZ1(3)    = DELZ/10.
      DZ1(4)    = DZ1(3)
      N1(1)     = 1
      N1(2)     = 10.*(ZB1-ZE)
      N1(3)     = 5
      N1(4)     = 5
      E         = (4./ZE)**3
      R         = .25
      Z         = ZE
      DO 200 L = 1,4
      DZ        = DZ1(L)
      NSTEPS    = N1(L)
      DO 100 J = 1,NSTEPS
      DO  50 K = 1,4
      AE(K)     = DZ*FE(A(K)*DZ+Z,A(K)*AE(K-1)+E,A(K)*AR(K-1)+R,F0)
      AR(K)     =DZ*FR(A(K)*DZ+Z,A(K)*AE(K-1)+E,A(K)*AR(K-1)+R,T)
   50 CONTINUE
      Z         = Z+DZ
      E         = E+FRACT*(AE(1)+2.*(AE(2)+AE(3))+AE(4))
      R         = R+FRACT*(AR(1)+2.*(AR(2)+AR(3))+AR(4))
  100 CONTINUE
      IF(L.NE.3) GO TO 150
      DMB       = 16.*R/(E**EX1*Z)
      GMB       = 1./(.245*Z*E**EX1)
      GO TO 160
  150 IF(L.EQ.1) GO TO 160
      VMB       = E**EX1*AK**.5/Z
      IF(L.EQ.2) VMB1 = VMB
  160 CONTINUE
  200 CONTINUE
      RETURN
      END
      FUNCTION  MOD(N,M)
C     RETURNS ZERO WHENEVER N IS EVENLY DIVISIBLE BY M
      MOD       = N-(N/M)*M
      END


      FUNCTION  SANH(X,N)
      SANH      = .5*(EXP(X)-EXP(-X))
      IF(N.EQ.0) SANH=X
      END


      FUNCTION  CASH(X,N)
      CASH      = .5*(EXP(X)+EXP(-X))
      IF(N.EQ.0) CASH=1.
      END


      FUNCTION XCOORD(X)
      XCOORD    = .5*SINH(X)
      RETURN
      END


      FUNCTION   FR(Z,E,R,T)
      FR        = -.109*E**(1./3.)*T*Z
      RETURN
      END
```

```
FUNCTION    FE(Z,E,R,F0)
FE        = .75*Z*R/F0
RETURN
END
```

*U.S. GOVERNMENT PRINTING OFFICE:1973 514-153/238 1-3